

Ions in Polymers

Adi Eisenberg, EDITOR

McGill University

Based on a symposium
sponsored by the
Division of Polymer Chemistry
at the 176th Meeting of the
American Chemical Society,
Miami Beach, Florida,
September 11–15, 1978.

ADVANCES IN CHEMISTRY SERIES


187

AMERICAN CHEMICAL SOCIETY

WASHINGTON, D. C.

1980



Library of Congress  Data

Ions in polymers.

(Advances in chemistry series; 187 ISSN 0065-2393)

Includes bibliographies and index.

1. Ionomers—Congresses.

I. Eisenberg, Adi. II. American Chemical Society.
Division of Polymer Chemistry. III. Series.

QD1.A355 [QD382.I45] 540s [547.8'404572]
80-19321

ISBN 0-8412-0482-9 ADCSAJ 187 1-376 1980

Copyright © 1980

American Chemical Society

All Rights Reserved. The appearance of the code at the bottom of the first page of each article in this volume indicates the copyright owner's consent that reprographic copies of the article may be made for personal or internal use or for the personal or internal use of specific clients. This consent is given on the condition, however, that the copier pay the stated per copy fee through the Copyright Clearance Center, Inc. for copying beyond that permitted by Sections 107 or 108 of the U.S. Copyright Law. This consent does not extend to copying or transmission by any means—graphic or electronic—for any other purpose, such as for general distribution, for advertising or promotional purposes, for creating new collective works, for resale, or for information storage and retrieval systems.

The citation of trade names and/or names of manufacturers in this publication is not to be construed as an endorsement or as approval by ACS of the commercial products or services referenced herein; nor should the mere reference herein to any drawing, specification, chemical process, or other data be regarded as a license or as a conveyance of any right or permission, to the holder, reader, or any other person or corporation, to manufacture, reproduce, use, or sell any patented invention or copyrighted work that may in any way be related thereto.

PRINTED IN THE UNITED STATES OF AMERICA

American Chemical
Society Library
1155 16th St. N. W.
Washington, D. C. 20036

Advances in Chemistry Series

M. Joan Comstock, *Series Editor*

Advisory Board

David L. Allara

Kenneth B. Bischoff

Donald G. Crosby

Donald D. Dollberg

Robert E. Feeney

Jack Halpern

Brian M. Harney

Robert A. Hofstader

W. Jeffrey Howe

James D. Idol, Jr.

James P. Lodge

Leon Petrakis

F. Sherwood Rowland

Alan C. Sartorelli

Raymond B. Seymour

Gunter Zweig

FOREWORD

ADVANCES IN CHEMISTRY SERIES was founded in 1949 by the American Chemical Society as an outlet for symposia and collections of data in special areas of topical interest that could not be accommodated in the Society's journals. It provides a medium for symposia that would otherwise be fragmented, their papers distributed among several journals or not published at all. Papers are reviewed critically according to ACS editorial standards and receive the careful attention and processing characteristic of ACS publications. Volumes in the ADVANCES IN CHEMISTRY SERIES maintain the integrity of the symposia on which they are based; however, verbatim reproductions of previously published papers are not accepted. Papers may include reports of research as well as reviews since symposia may embrace both types of presentation.

PREFACE

Ionic interactions in macromolecules represent simultaneously one of the oldest and one of the most recent areas of activity in modern polymer science. While on the one hand polyelectrolyte solution studies have been pursued in a host of laboratories for decades, the study of the bulk properties of ionomers dates back hardly more than ten years ago—as a matter of fact the word “ionomer” came into common use only about a decade ago with the advent of the first commercial material of this type based on ethylene. Since that time, that aspect of the field has grown profoundly, both in regard to bulk investigations as well as studies in nonaqueous solutions, as is evidenced by the periodic symposia in the field, the recently initiated Gordon Conference, and the appearance of two books dealing primarily with bulk properties.

This volume contains the majority of the papers presented at an ACS symposium on Ion-Containing Polymers. The papers highlight several of the trends that had become evident in the past; paralleling these trends, the papers are grouped, somewhat arbitrarily, into six sections.

The first section comprises the hydrocarbons containing sulfonic acids or salts as pendant groups (and includes the exciting new family of sulfonated EPDM's). The next section is devoted to the perfluoro-sulfonate ionomers (another new and promising material being explored for a host of applications). The third section contains chapters describing new materials or applications, while the fourth and fifth sections are devoted to an exploration of physical properties in bulk and in solution, respectively. In the last section, the final chapter describes one of the many biological polymers that contain ionic groups, specifically heparin.

While these chapters provide only a small sampling of the activity in the field, the range of topics covered here clearly reflects the enormous area within the discipline, ranging all the way from synthetic organic materials in the bulk to naturally occurring macromolecules in solution. There is every indication that the high level of interest is continuing, notably in regard to industrial research, as evidenced particularly by the explosive growth of the recent patent literature. One can thus look

forward to a continuing high level of activity in this area, in both industrial and academic laboratories, and to the appearance of new products and new applications based on this research.

Finally, it is with deep regret that we note the untimely passing of two distinguished scientists and friends who participated in this symposium.

Dr. Henry S. Makowski died September 30, 1979 at the age of 48. He obtained his PhD in organic chemistry from the University of Notre Dame in 1955 and shortly thereafter joined the Exxon Research and Engineering Company. At the time of his death he was a senior research associate with the Polymer Science Group of the Corporate Research Science Laboratory. During his career Hank was active in the areas of Ziegler cationic and anionic polymerization, the development of curable ethylene- α -olefin copolymers, and the elucidation of the vulcanization chemistry of EPDM. Hank authored 37 publications and was the holder of 35 U.S. patents. In recent years he was very active in the area of ionic polymers, specifically sulfonated EPDM and polystyrene, and he was chairman-elect of the 1981 Gordon Conference on Ion-Containing Polymers. In addition to his scientific talents, Hank was well-known among his colleagues for his wit and humor and was frequently called upon to serve as host, toastmaster, and MC. He is survived by his wife, Patricia, and three children, Noel, Mark, and Matthew.

Dr. Sid Cutler died suddenly on December 3, 1978 at the age of 34, only three months after returning home from this symposium. He received his PhD at Aberdeen University in 1975 working with P. Meares, and in October of that year, joined the Imperial Chemical Industries where he was employed at the Mond Division until his death. His work concentrated on ion-exchange membranes and, most recently, the Nafions. He is survived by his wife, Pat, and two children, April and Sid.

McGill University
Montreal, Canada

November 26, 1979

ADI EISENBERG

Synthesis and Properties of Sulfonated EPDM

H. S. MAKOWSKI, R. D. LUNDBERG, L. WESTERMAN, and J. BOCK

Corporate Research Laboratories, Exxon Research and Engineering Company,
Linden, NJ 07036

Metal sulfonate groups were introduced into an ethylene-propylene-diene monomer terpolymer (EPDM) via reaction of its residual unsaturation with acetyl sulfate, followed by neutralization of the resultant polymeric sulfonic acid with metal acetates. The composition, structure, and molecular weight of the EPDM and the sulfonate content, cation borne by the sulfonate group, and metal acetate concentration of the ionomer were found to substantially affect the rheological and mechanical properties of the ionomer. Through the proper selection of EPDM backbone, EPDM molecular weight, and sulfonate content, and through the use of the zinc cation, it was possible to prepare EPDM-based ionomers with excellent mechanical properties and with the lowest possible melt viscosities. Although formulations derived from these zinc sulfonate-containing EPDM's possess melt viscosities that are higher than desirable for facile processability, in many respects they are truly thermo-plastic elastomers.

The presence of small amounts of ionic groups in hydrocarbon polymers exerts a profound effect on their physical properties (1,2). The polymers are effectively cross-linked through the association of these ionic groups forming multiplets or higher order associations described as "domains." These associations can be thermally relaxed to a greater or lesser extent depending on the composition of the ionic domains. In elastomeric systems, if the degree of ionic association at processing temperatures is sufficiently reduced to permit adequate melt flow, then the ion-containing elastomer is a thermoplastic elastomer.

Carboxylate-containing elastomers and the effects of the free acid and metal carboxylate groups on elastomer properties have been studied

0-8412-0482-9/80/33-187-003\$05.00/0
© 1980 American Chemical Society

rather extensively (1, 2, 3, 4). However, reports on carboxylate-containing ethylene-propylene-diene monomer terpolymers (EPDM) are very limited (5, 6).

When compared at the same functional groups level with the same cation and backbone molecular weight, it was shown that carboxylated polystyrene (C-PS) and sulfonated polystyrene (S-PS) differ markedly in both solution and physical properties (7). On the basis of these studies it was concluded that sulfonated ionomers are more strongly and more highly associated than the corresponding carboxylate ionomers. Because sulfonates exert such a large effect on polymer properties it might be expected that only modest levels of sulfonate groups in rubbers, such as EPDM, would result in a sufficient number of ionic cross-links for the enhancement of mechanical properties. And yet it might be hoped that these ionic associations would be relaxed sufficiently at elevated processing temperatures for melt processability.

The preparation of elastomeric hydrocarbon polymers containing low levels of sulfonic acid is a relatively recent development (8, 9). The neutralization of the polymeric sulfonic acid to the corresponding metal sulfonate results in a strongly and highly associated system.

This paper describes (a) the synthesis of metal sulfonate-containing EPDM elastomers via sulfonation through the residual unsaturation and the neutralization of the resultant sulfonic acids, and (b) the effects of molecular weight, composition, and structure on the physical properties of the resultant ionomer.

Experimental

Starting EPDM's. The general properties of the starting EPDM's are given in Table I. Vistalon 2504 (V-2504) from the Exxon Chemical Company was used as received and was also thermally and shear degraded with an extruder to a 20 Mooney viscosity product (ML, 1 + 8, 212°F) designated CR-2504. Both of these materials were fully amorphous. A higher ethylene content EPDM designated as CR-709A was similarly generated through extruder breakdown. The EPDM's designated by E-55 and E-70 were synthesized directly, and both possessed a Mooney viscosity of about 20. All of the EPDM's contained 5-ethylidene-2-norbornene (ENB) as the third monomer.

Table I. Description

	<i>V-2504</i>	<i>CR-2504</i>
Source	commercial	extruder breakdown
Ethylene content (wt %)	52	52
Mooney viscosity (212°F)	40	20
ENB content (wt %)	5	5

Sulfonation Reagents. Although the SO_3 complexes of triethyl phosphate, dioxane, and tetrahydrofuran are effective in introducing sulfonic acid groups into EPDM (8), all the sulfonations reported herein were effected with acetyl sulfate (9, 10). Acetyl sulfate can be generated from a variety of combinations of reagents, e.g., SO_3 and acetic acid. However, this reagent is generated most conveniently from acetic anhydride and concentrated sulfuric acid.

The reagent acetyl sulfate for these studies was generated in two ways. In one case acetic anhydride and concentrated sulfuric acid were mixed at a temperature below 0°C , the thick solution warmed to about 10°C , and the preformed neat reagent added to the EPDM solution (cement). In the second case, the acetyl sulfate was generated in situ, i.e., acetic anhydride was added to the EPDM cement and then the concentrated sulfuric acid was dripped in. With the polymers previously described and according to the following procedures, results with the preformed and the in situ reagents were fully equivalent.

The acetyl sulfate was generated from at least 1.6 mol of acetic anhydride per mol of concentrated sulfuric acid.

Sulfonation of EPDM. EPDM was dissolved in an aliphatic hydrocarbon, generally hexane or heptane, at a concentration of from 50 to 100 g/L. The sulfonation reagent was added at room temperature and after 30 min sulfonation was terminated through the addition of an alcohol, generally isopropanol or methanol. At this point Antioxidant 2246 [2,2'-methylene-bis(4-methyl-6-tert butyl phenol)] was added, and the polymeric sulfonic acid was isolated through the solvent flashing of the resultant cement in boiling water (steam stripping). The resultant polymeric mass was pulverized and washed with water in a Waring blender. The crumb was filtered and then dewatered by banding on a rubber mill at about 120°F to a water level of 2–5%, or was dried in a laboratory Aeromatic fluid bed dryer at 70°C to a water level of about 0.2%. The acid content of the sulfonated EPDM was determined through the titration of a sample dissolved in 95 toluene/5 methanol with 0.1N NaOH in absolute ethanol to an alizarin–thymophthalein end point. Sulfur content was determined via Dieter sulfur analysis (ASTM D1552). The coincidence of the titration and sulfur values, illustrated in Figure 1, indicates that each sulfur corresponds to a sulfonic acid moiety.

Neutralization of Sulfonated EPDM. Neutralization of the polymeric sulfonic acid was accomplished in two ways:

1. *Direct Neutralization.* After sulfonation the resultant cement was treated with an alcohol, a water–alcohol solution, or an aqueous solution of metal hydroxide or acetate.

of Starting EPDM's

<i>CR-709A</i>	<i>E-55</i>	<i>E-70</i>
extruder breakdown	direct synthesis	direct synthesis
68	55	70
20	17	20
7.5	4.4	4.7

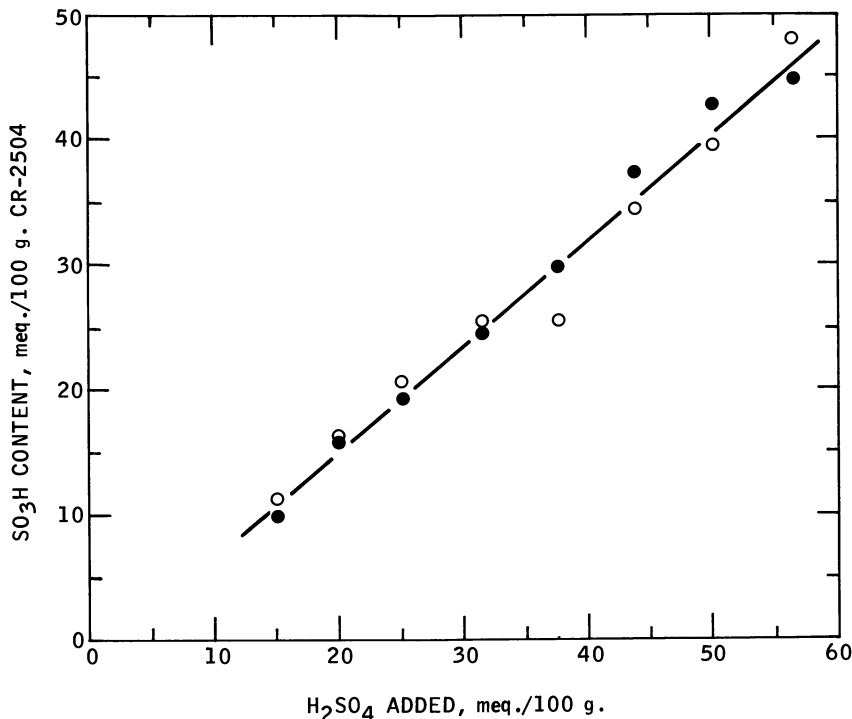


Figure 1. Sulfonation of CR-2504 with *in situ* acetyl sulfate in heptane: (●) sulfuryl analysis; (○) titration. (Acetic anhydride = 1.62; polymer concentration = 100 g/L; temperature = 25°C; time = 30 min).

After 30 min of agitation and the addition of the antioxidant, the neutralized sulfonated EPDM was isolated by solvent flashing in boiling water. The wet crumb was dried either on a rubber mill at about 220°F or in a laboratory Aeromatic fluid bed dryer at 100°C.

2. *Neutralization of the Isolated Polymeric Acid.* The isolated polymeric acid was redissolved in a mixture of toluene/methanol or hexane/alcohol at a concentration of 50 to 100 g/L. Neutralization was effected through the addition of a solution of metal acetate in water or water/methanol. The neutralized polymer was isolated as described previously.

Neutralization with Various Levels of Zinc Acetate. A sulfonated CR-2504 containing about 33 meq sulfonic acid/100 g of sulfonated polymer was dissolved in hexane and 3 vol % methanol at a concentration of 100 g/L. Zinc acetate was added as a water/methanol solution at zinc acetate levels ranging from 0.5 to 6.0 equiv/equiv of sulfonic acid. The polymers were isolated as described previously. Zinc analyses were obtained on all products, and the data are given in Table II. Essentially all of the zinc that was added to the polymer was retained after workup.

**Table II. Zinc Acetate Neutralization of Sulfonated CR-2504—
Effect of Zinc Acetate Concentration**

Zinc Acetate Added (<i>meq Zn/mmol SO₃H</i>)	Wt % Zn		Retention of Zinc Acetate (%)
	Theor.	Obtained	
0.50	0.52	0.56	97
0.75	0.78	0.80	100
1.00	1.04	1.07	100
1.25	1.29	1.30	100
1.50	1.53	1.51	100
1.75	1.78	1.75	100
2.00	2.02	2.13	100
2.50	2.49	2.45	98
3.00	2.95	3.00	100
4.00	3.82	3.75	98
5.00	4.66	4.23	89
6.00	5.45	5.23	95

Rheological and Tensile Properties. Melt rheological measurements were made on an Instron Capillary Rheometer (0.993" L × 0.05014" D) at a temperature of 200°C and at various shear rates corresponding to crosshead speeds of from 0.005 in./min to 20 in./min. Measurements were also made with an Instron TM Model (0.05034" D × 1.0074" L) at 200°C and at various shear rates corresponding to crosshead speeds of from 0.006 in./min to 10 in./min.

Melt index was determined at 190°C and at either 250 psi or 476 psi (ASTM 1238-70).

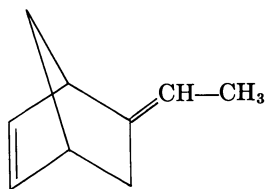
Tensile strengths were determined on microdumbbells from about 20-mil thick compression-molded films with an Instron table model instrument at the rate of 2 in./min.

Water Absorption. Compression-molded pads about 20–30 mils thick were placed in jars containing distilled water, which in turn were placed in ovens at 50°C. Periodically the samples were removed, the excess water blotted off, and the treated specimen weighed. The specimen was then returned to the jar and oven for longer term data.

Results and Discussion

The reaction of simple olefins with SO₃ and SO₃ complexes and derivatives has been demonstrated to yield allylic and vinylic sulfonic acids, hydroxysulfonic acids, and other neutral products (10). The product distribution is a function of olefin type, sulfonation reagent, solvent, and reaction conditions.

The introduction of sulfonate groups into EPDM occurs via an electrophilic attack of the sulfonation reagent on the unsaturation in EPDM. Many termonomers can be copolymerized with ethylene and propylene to produce EPDM's with a variety of residual olefinic types (11). All of the EPDM's in this study were produced from ENB. Since the incorporation of ENB into the polymer chain during copolymerization



ENB

with ethylene and propylene occurs through the endocyclic double bond, the residual unsaturation is the somewhat strained, highly substituted exocyclic double bond. This ethylidene norbornane moiety as well as any highly substituted olefin sulfonates rapidly and reproducibly with acetyl sulfate at room temperature. With careful reagent preparation the conversion of reagent is essentially quantitative when the impurities in the starting EPDM are accounted for.

Figure 1 illustrates the effect of acetyl sulfate concentration on sulfonate incorporation into CR-2504. The acetyl sulfate reagent was generated in situ from acetic anhydride and concentrated sulfuric acid. Sulfonate content varied linearly with reagent concentration up to the unsaturation level of the CR-2504 sample (50 mmol/100 g EPDM). Over this range of sulfonation level reagent conversion was about 80%. Similar results were obtained when preformed neat acetyl sulfate was used as the reagent. Sulfonate contents derived from sulfur analysis and titration data were closely coincident indicating that each sulfur is part of a sulfonic acid or easily hydrolyzed sulfonate group.

Compared to the metal salts the free polymeric acids are not highly or strongly associated. In fact, they can be dissolved in aliphatic and aromatic hydrocarbons in the absence of a polar cosolvent. The free acids tend to possess low strength and to be less stable thermally. In order to obtain useful products the free acids must be converted to their corresponding metal or ammonium sulfonates.

When the polymer acids are treated with metallic bases the bulk and solution properties of the neutralized products are changed markedly. In bulk the neutralized products behave as if they are covalently cross-linked. In fact, they are not covalently cross-linked since they are soluble in mixtures of hydrocarbon and polar solvents (12). Nevertheless, their solution behaviors are so significantly different from those of the base polymers and the polymeric sulfonic acids that effective neutralization is not a simple operation. If solutions containing the free polymeric sulfonic acid are treated with an aqueous solution of neutralizing agent, a gel results which prevents effective neutralization and processing. The metal sulfonates are solubilized through the inclusion of a polar cosolvent such

as methanol or isopropanol. Many metallic bases, such as the metal acetates, possess good solubility in water while some are soluble in methanol or methanol/water mixtures. In the absence of water the metal sulfonates are generally readily soluble in mixtures of an aliphatic hydrocarbon and an alcohol, and the solutions are relatively fluid. Up to the point of polymer precipitation, the higher the alcohol concentration the lower the solution viscosity. The addition of even small amounts of water exerts a tremendous effect on the viscosity of the neutralized solution, or cement. Thus, in most neutralization processes it is important to use the minimum amount of water required for solution of the neutralizing agent and the maximum amount of alcohol permissible.

The descriptions of the EPDM's used in this study are given in Table I. These materials varied primarily with respect to Mooney viscosity, which is a measure of molecular weight, and with regard to ethylene content. Since CR-2504 was generated through the extruder breakdown of V-2504 these two materials possessed identical compositions and monomer distributions and varied only in molecular weight or Mooney viscosity. CR-709A, a higher ethylene-content EPDM, was also generated through the extruder breakdown of a higher Mooney viscosity material. E-55 and E-70, by contrast, were prepared directly from the same catalyst system and were similar in Mooney viscosity but different in ethylene content. All of the base EPDM's contained ENB levels corresponding to 40–50 mmol unsaturation/100 g of EPDM.

The EPDM specifications in Table I fail to differentiate between molecular weight distribution and monomer distribution. Indeed EPDM's possessing the same composition and Mooney viscosity can be substantially different. Different transition metal catalyst systems can produce EPDM's with different molecular weight distributions, different ethylene distributions, and different unsaturation distributions. These differences in distributions can exert rather substantial effects on sulfonated-EPDM properties. Higher ethylene-content EPDM's can manifest polyethylenic crystallinity depending on the monomer reactivity ratios for the specific catalyst system. Since the incorporation of sulfonate groups into EPDM occurs by way of the residual unsaturation, and not through reaction with the saturated backbone, the sulfonate distribution depends on the distribution of the unsaturation along the EPDM backbone. It is clear, then, that EPDM composition, structure, and molecular weight distribution could be expected to affect ionomer properties.

The effect of sulfonate content on melt viscosity is illustrated in Figure 2 for four different EPDM's having approximately the same Mooney viscosity (20). The data are given for the zinc salts. A substantial association began to manifest itself at about 10–15 meq sulfonate/100

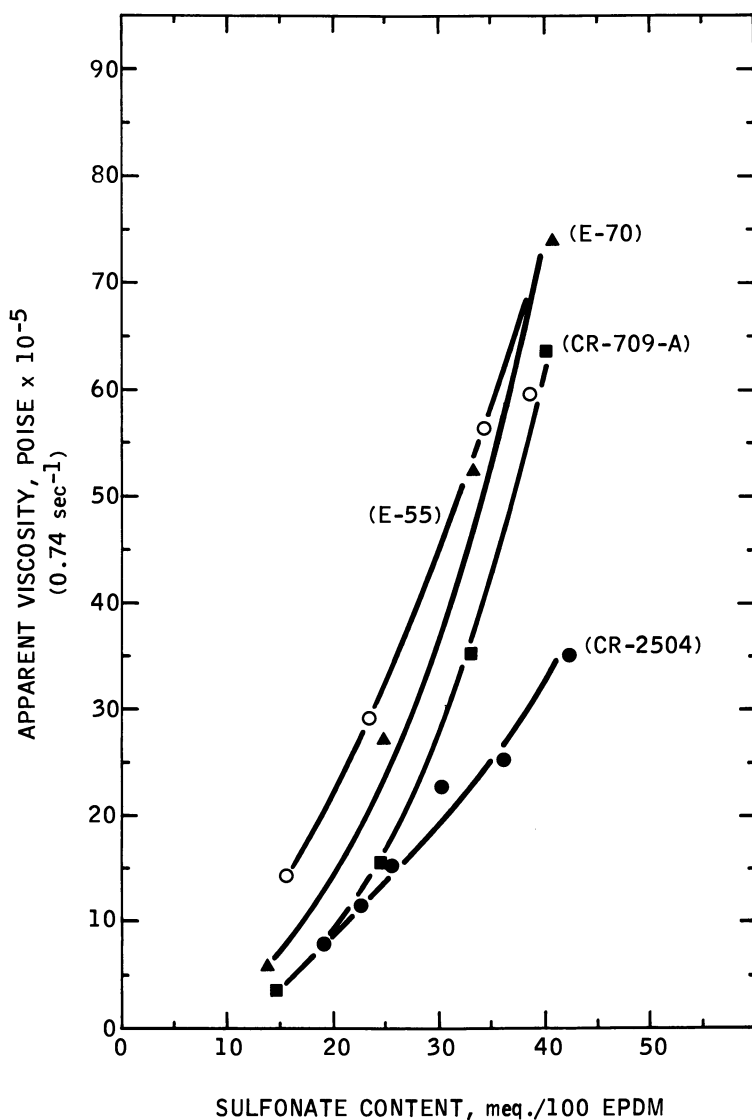


Figure 2. Effect of sulfonate content on melt viscosity at 200°C and 0.74 sec⁻¹ (metal cation: zinc)

g of polymer. As sulfonate content was increased to about 40 meq, marked increases in melt viscosity were obtained. These large viscosities were achieved at very low sulfonate levels, corresponding to about 1 mol %.

If the EPDM's possessed the same molecular weight, molecular weight distribution, and unsaturation distribution, all the melt viscosity data would be expected to fall on the same line. Three materials, derived from E-70, E-55, and CR-709A, behaved similarly but showed some differences. These differences can be attributed largely to differences in molecular weight. The behavior of the CR-2504 system deviated from the behaviors of the other three systems rather substantially. It is not likely that this deviation is explicable on the basis of molecular weight differences. This deviation is interpreted as resulting from a less even distribution of sulfonate groups along the CR-2504 backbone so that the sulfonate groups are used less effectively in network formation.

The effect of sulfonate content on room temperature tensile strength is illustrated in Figure 3 for the same family of zinc sulfonate-containing EPDM's. Here, as in the case of melt viscosity, strength began to develop for the amorphous polymers as a result of ionic association at about 10–15 meq sulfonate/100 g of polymer. Striking tensile properties were obtained at 30 meq sulfonate, which corresponds to about 1 mol % sulfonate. Rather substantial differences in tensile properties were obtained with the different base polymers. E-70 developed significantly higher strengths, which is directly attributable to the presence of polyethylenic crystallinity in this high ethylene copolymer. The high strength obtained is the result of a combination of crystallinity and ionic association effects. E-55 and CR-709A behaved similarly. Neither appeared to manifest any polyethylenic crystallinity even though CR-709A possessed a rather high ethylene content. Increases in tensile strength for these two systems are the result of ionic associations only because these two copolymers are essentially amorphous. The CR-2504, which also is a fully amorphous copolymer, deviated again from the behaviors of the other amorphous copolymers. These results closely paralleled the melt viscosity results and are explicable on the basis of a less even distribution of sulfonate groups within CR-2504.

The effect of sulfonate content on modulus and elongation is illustrated in Figure 4 for zinc sulfonate-containing CR-2504. As expected, elongation decreased with increasing sulfonate content. Since tensile strength increased with increasing sulfonate content (cf. Figure 3), and elongation decreased, the modulus must increase rather substantially, and in fact it did.

The composition and structure of the base EPDM and the sulfonate content of the metal sulfonate-containing EPDM exert substantial effects on the mechanical and flow properties of ionomers. The systems discussed to this point have all contained zinc sulfonate groups. In terms of melt flow the zinc cation is the cation of choice. The metal cation borne by

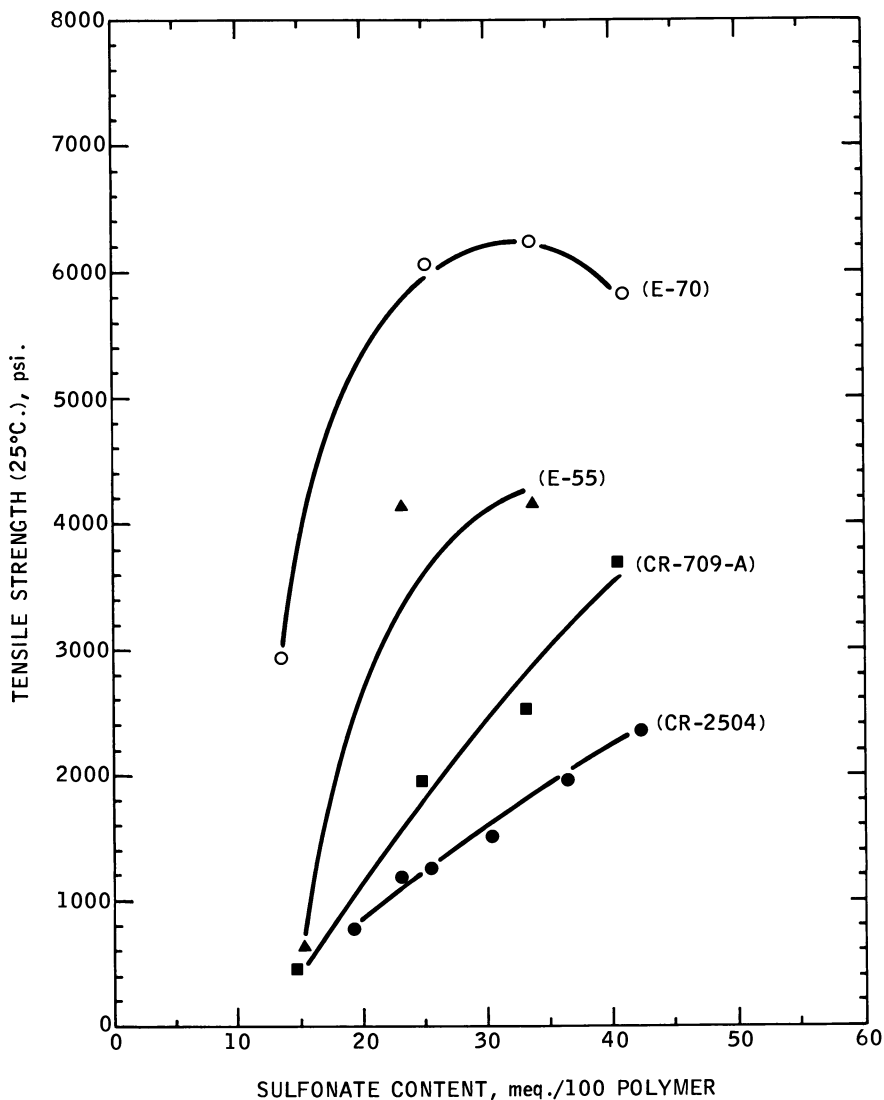


Figure 3. Effect of sulfonate content and EPDM on tensile strength at 25°C (metal cation: zinc)

the sulfonate group can have a profound influence on ionomer properties. A comparison of the flow and mechanical properties of the metal sulfonates from nine different cations is given in Table III. The metal sulfonate-containing EPDM's were prepared from the same CR-2504 sulfonic acid by neutralization with the corresponding acetates. Hence, the comparison is strictly one of cations.

In terms of melt viscosity, the Hg cation resulted in such a high melt viscosity that a coherent strand did not emanate from the capillary rheometer at the lowest shear rate (0.88 sec^{-1}). Six cations, Mg, Ca, Co, Li, Ba, and Na, gave very high and virtually identical melt viscosities. All of these materials were melt-fractured at the shear rate of the viscosity measurement (0.88 sec^{-1}). This lack of distinction in cation type is most likely attributable to the departure of these highly viscous materials from laminar flow. Nevertheless, it is quite clear that these materials are very

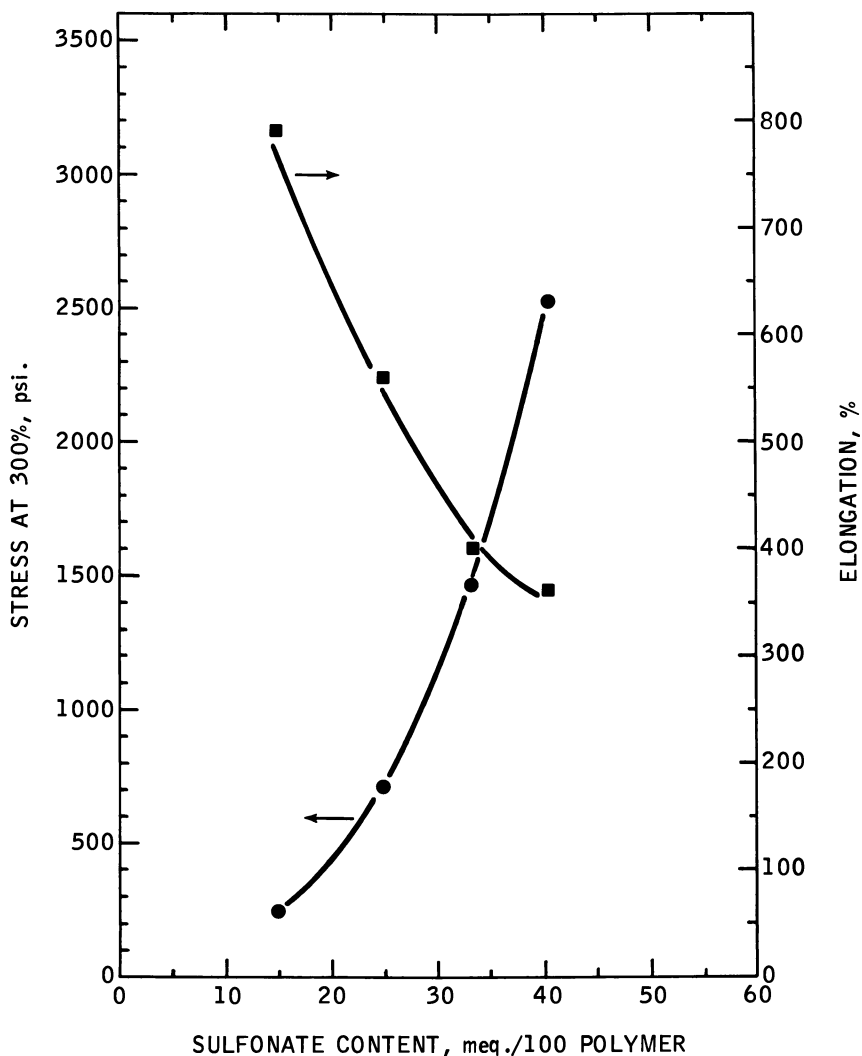


Figure 4. Effect of sulfonate content on modulus and elongation at 25°C

Table III. Effect of Cation

<i>Metal</i>	<i>Apparent Viscosity^b</i> (poise $\times 10^{-5}$)	<i>Melt Fracture at Shear Rate</i> (sec ⁻¹)	<i>Melt Index</i> (190°C, 478 psi, g/10 min)
Hg	—	—	disintegrated
Mg	55.0	< 0.88	0
Ca	53.2	< 0.88	0
Co	52.3	< 0.88	0
Li	51.5	< 0.88	0
Ba	50.8	< 0.88	0
Na	50.6	< 0.88	0
Pb	32.8	88	0.1
Zn	12.0	147	0.75

^a Base polymer: CR-2504. Sulfonate content: 31 meq/100 EPDM. Dissolved 100 g of free acid in 1000 mL hexane-150 mL isopropanol; neutralized with 90 meq acetate in 25 mL water.

^b At 200°C and 0.88 sec⁻¹.

highly and strongly associated. Yet these strong associations are achieved at sulfonate levels of perhaps one in every 200 backbone carbon atoms. A considerably lower melt viscosity was achieved with the Pb cation, and the lowest melt viscosity was achieved with the Zn cation. Not only were these two systems lower in melt viscosity, but they also melt-fractured at higher shear rates. Thus, the Pb and Zn systems appear to be less strongly associated than those containing the other cations.

The melt index data corresponded to the melt viscosity data. No flow was obtained with any of the cations except for Pb and Zn, and the highest melt flow rate was obtained with the Zn cation.

The high degrees of ionic association in these various metal sulfonate-containing EPDM's are also manifested in their low elongations. These low elongations make a large contribution to the lowering of the tensile strength. Those systems with the higher elongations, notably the Zn and Pb systems, gave the highest tensile strengths.

The composition and structure of EPDM and the composition of the ionomer affect the mechanical and flow properties of the ionomer. Another parameter that affects ionomer properties is the concentration of metal acetate, specifically zinc acetate, present in the neutralized sulfonated EPDM. This is illustrated in Figure 5, where the melt viscosity of zinc sulfonate CR-2504 is plotted as a function of zinc acetate concentration. Zinc acetate was added to a cement of the polymeric acid, and the resultant neutralized polymer was isolated through the solvent flashing of the cement. Essentially all of the zinc acetate that was added to the polymeric free acid was retained by the polymer (cf. Table II).

on Flow and Physical Properties^a

Room Temperature		70°C	
Tensile Strength (psi)	Elongation (%)	Tensile Strength (psi)	Elongation (%)
—	—	—	—
320	70	150	40
410	90	170	40
1180	290	450	160
760	320	250	130
340	70	150	30
960	350	270	110
1680	480	320	350
1480	400	270	450

Figure 5 shows that increasing the zinc acetate concentration decreased melt viscosity by a factor of two. In other copolymer systems even more substantial changes have been obtained.

The effects of zinc acetate on melt viscosity can be interpreted as a plasticization of the ionic associations by the zinc acetate, thereby lowering apparent molecular weight, and hence melt viscosity. It can also be considered that disulfonates, $-\text{SO}_3-\text{Zn}-\text{O}_3\text{S}-$, are converted to less strongly associating monosulfonates, $-\text{SO}_3-\text{Zn}-\text{OOC}-\text{CH}_3$, at higher zinc acetate concentrations. It might be reasonable to expect that both phenomena are occurring.

The molecular weight of the EPDM might be expected to affect the flow properties of the ionomer and perhaps even its mechanical properties. Some effects of molecular weight on melt viscosity were seen in earlier data (cf. Figure 2). In Table IV a comparison is made between the properties of zinc sulfonate-containing EPDM's which are identical in all respects except with regard to Mooney viscosity, or molecular weight. V-2504, a commercial material having a Mooney viscosity of 40, was extruder degraded to a material having a Mooney viscosity of 20 to provide the base polymers for this study. The materials were compared at two sulfonate levels. The doubling of the Mooney viscosity from 20 to 40 did result in a modest decrease in melt flow; however, a more substantial reduction in melt flow was obtained when the sulfonate content was approximately doubled from a level of about 22 meq sulfonate/100 g of polymer. It should be pointed out that most commercial rubbers possess Mooney viscosities significantly higher than 40. It is expected

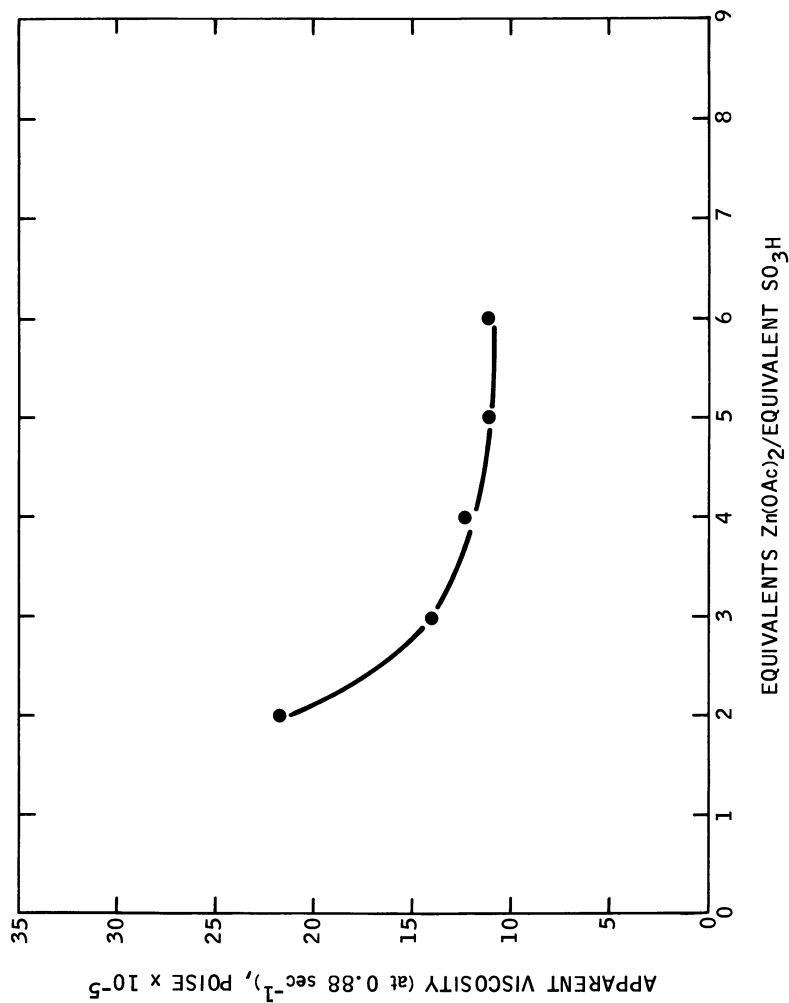


Figure 5. Effect of $Zn(OAc)_2$ concentration on rheology of nonplasticized gums (sulfonic acid: 33 meq $SO_3H/100$ EPDM; base polymer: CR-2504)

Table IV. Effect of Mooney Viscosity and Sulfonate Content on Melt Viscosity and Tensile Properties^a

Mooney viscosity (ML, 1 + 8, 212°F)	20	20	40	40
Sulfonate content (meq/100 g polymer)	22.3	46.7	22.9	48.4
Melt index (190°C, 250 psi, g/10 min)	0.61	0.04	0.18	0.005
At 25°C				
tensile strength (psi)	970	2960	390	2260
elongation (%)	630	470	740	390
At 70°C				
tensile strength (psi)	80	490	70	590
elongation (%)	410	420	275	300

^a Base polymer: V-2504.

that much higher Mooney viscosities will result in a considerable reduction in melt flow. The tensile properties of the zinc sulfonate-containing EPDM's were not affected over the 20–40 Mooney range. It is possible to reduce Mooney viscosity even further without substantial loss of mechanical properties. But, of course, more substantial increases in melt viscosity are obtained with further increases in Mooney viscosity. Thus, in order to obtain the best assemblage of ionomer properties it is desirable to keep the molecular weight of the base polymer low.

When highly ionic groups are placed along a hydrocarbon polymer backbone it is expected that the interaction with polar molecules, such as water, would be enhanced. It is further expected that the response to water would be a function of the cation borne by the sulfonate group. The effect of water as a function of cation type is illustrated in Figure 6. The metal sulfonate EPDM's used in these water absorption studies are described in Table III. The incorporation of sulfonate groups into EPDM did indeed enhance the polymers' sensitivity to water, and the water absorption was a function of cation type. The order of water sensitivity as a function of cation type was approximately the order expected, with the exception of the barium cation, which was the most water sensitive. However, the two cations that provided the lowest melt viscosities and among the best mechanical properties, viz. the Pb and Zn cations, also were the least water sensitive. So the cation is important in determining not only the rheological and mechanical properties but also the response of the system to water.

In summary, it has been shown that profound changes in the properties of EPDM can be made through the introduction of metal sulfonate groups. Relatively low sulfonate levels, approximately 20–30 meq sul-

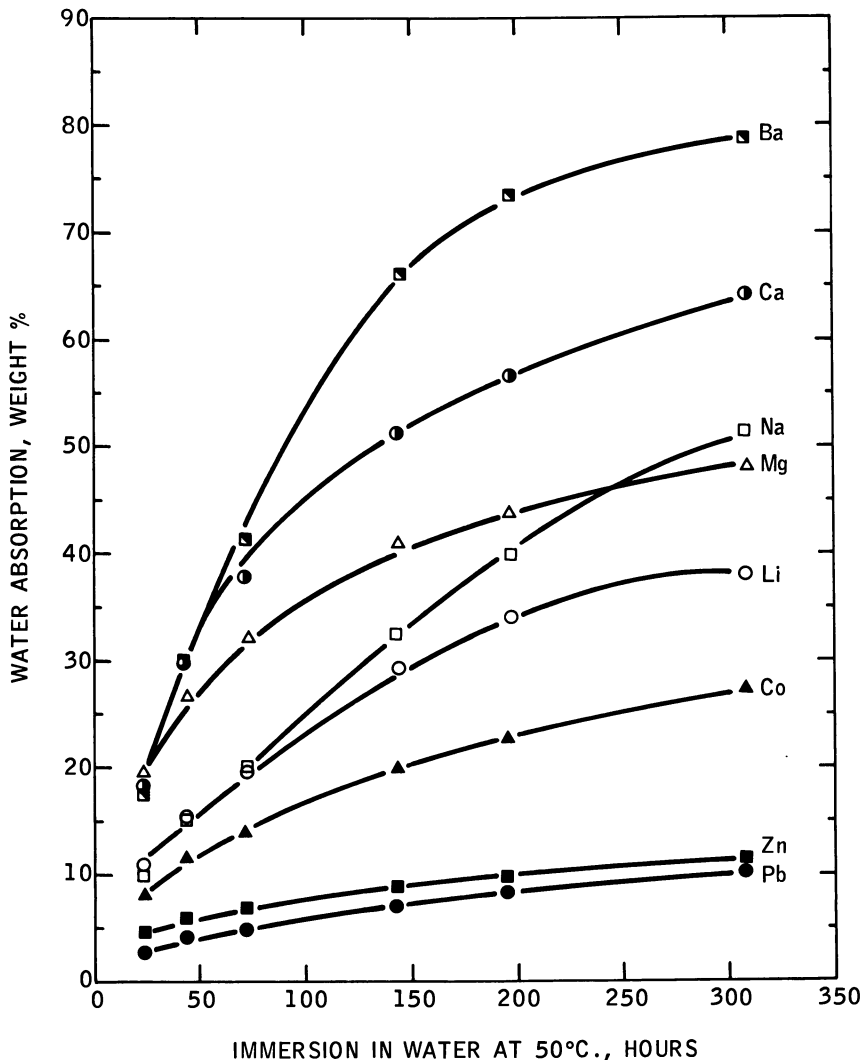


Figure 6. Effect of cation on water absorption

fonate/100 g polymer, produce ionomers with excellent mechanical properties. Highly intractible systems occur with higher molecular weight polymers, at higher sulfonate contents, and with most metal cations. However, it is possible through the proper selection of EPDM backbone and molecular weight, sulfonate content, and through the use of the Zn cation, to prepare polymers with outstanding mechanical properties and with the lowest possible melt viscosities. In many respects this zinc sulfonate-containing EPDM is a truly thermoelastic system.

On the other hand, even when these systems are formulated with filler and extender oils, melt viscosities are generally still too high for injection molding and many extrusion operations. Such are the strengths and associative powers of metal sulfonate groups that it is desirable, and even necessary, to further reduce melt viscosity. This can be accomplished through the use of nonfugitive additives which interact with, or plasticize, the ionic associations, or domains, to reduce the degree of ionic association and thereby improve melt flow. These ionic domain plasticizers are described in another chapter (13).

Acknowledgment

The massive and expert technical assistance of Joseph A. Sissano is gratefully acknowledged.

Literature Cited

1. Eisenberg, A.; King, M. "Ion-Containing Polymers"; Academic: New York, 1977.
2. Holliday, L. Ed. "Ionic Polymers"; Wiley: New York, 1975.
3. Otocka, E. P. *Macromolecular Science-Rev. Macromol. Chem.* **1971**, C5(2), 275.
4. Brown, H. P. *Rubber Chem. Technol.* **1975**, 35(5), 1347.
5. Amass, A. J.; Duck, E. W.; Hawkins, J. R.; Locke, J. M. *Eur. Polym. J.* **1972**, 8, 781.
6. Rees, R. W.; Reinhardt, H. G. U.S. Patent 3 997 487, 1976; to E. I. duPont de Nemours and Company.
7. Lundberg, R. D.; Makowski, H. S., chapter 2 in this book.
8. Canter, N. H. U.S. Patent 3 642 728, 1972; to Esso Research & Engineering Company.
9. O'Farrell, C. P.; Serniuk, G. E. U.S. Patent 3 836 511, 1974; to Esso Research & Engineering Company.
10. Gilbert, E. E. "Sulfonation and Related Reactions;" Interscience: New York, 1965.
11. Baldwin, F. P.; van Strate, G. *Rubber Chem. Technol.* **1972**, 45, 709.
12. Lundberg, R. D. *Polym. Prepr., Am. Chem. Soc., Div. Polym. Chem.* **1978**, 19(1), 455.
13. Makowski, H. S.; Lundberg, R. D., chapter 3 in this book.

RECEIVED October 16, 1978.

A Comparison of Sulfonate and Carboxylate Ionomers

R. D. LUNDBERG and H. S. MAKOWSKI

Corporate Research Laboratories, Exxon Research and Engineering Company,
Linden, NJ 07036

A comparison of metal carboxylate and metal sulfonate ionomers based on identical polystyrene backbones was conducted, showing a substantial difference between these two ionomers. Sodium carboxylated and sodium sulfonated polystyrenes were synthesized containing 0.3–5.0 mol % ionic functionality. The softening behavior of the metal sulfonate ionomer suggests that strong ionic association persists to temperatures of 50°–100°C above that of the corresponding carboxylate ionomer. Similarly, the melt viscosities of the sulfonate ionomers at a given level of functionality are two to three orders of magnitude greater than those of the carboxylate analogues. Similar differences are observed in the solution behavior of these two ionomers. These results are attributable to greater polarization in the sulfonate ionomers, thereby providing stronger ionic association.

The substantial published literature dealing with ionomers (1–5) has been directed mainly toward carboxylate-based systems. Only limited work (6, 7, 8) has been directed toward other types of ionomers such as phosphonates, sulfonates, and other systems, although MacKnight and coworkers (9, 10, 11) have recently published some studies dealing with the effect of various types of ionomers pendant to a polypentenamer backbone. In our laboratories a significant effort has been directed primarily toward metal sulfonate ionomers. Based on the published information relating to carboxylate-based ionomers (1–5), it appears that there are many similarities between those and the sulfonate ionomers. However, there are also very significant differences in these technologies (6, 7, 8), but an adequate distinction has not been made between carboxylate and

sulfonate ionomers to quantify them. It is the purpose of this publication to describe some preliminary studies comparing these two ionomer systems in order to highlight the major similarities and differences.

To be informative, it is desirable that the comparisons of these two different technologies be based on identical polymer backbones, having identical molecular weights, and having comparable levels of ionic functionality present. In addition, it is the purpose of these studies to make such comparisons with the same metal cation and thereby quantify, insofar as possible, the nature of the ionic interactions that exist. To do this, ionomers were prepared based on a polystyrene (PS) hydrocarbon backbone into which the ionic functionality was incorporated. PS was selected as the backbone because of the relative ease of functionalization and the relative freedom of side reactions during the sulfonation or carboxylation reactions. The polymers prepared were designed to come as close as possible in terms of ionic functionality for both sulfonate and carboxylate ionomers over a range of ionic contents.

Experimental

The routes to sulfonated and carboxylated polystyrenes are illustrated in Figure 1. The specific experimental approaches are provided in the following sections.

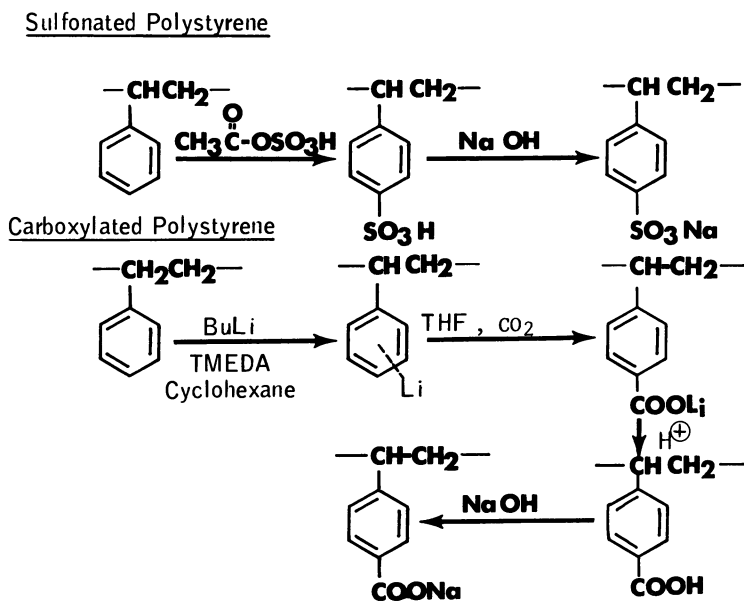


Figure 1. Synthesis of sulfonated and carboxylated polymers

Sulfonated Polystyrene (S-PS). The preparation of S-PS has been described in detail in Ref. 6. The following procedure was generally followed: 104 g of PS (Styron 666 manufactured by Dow Chemical Company) were dissolved in 490 mL of 1,2-dichloroethane. The solution was heated to 50°C, and the requisite amount of acetyl sulfate was added, in this case, 30 mL of 0.996M acetyl sulfate (29.9 meq). The solution was stirred for 60 min at 50°C, and the reaction was terminated by the addition of 25 mL of methanol. Sufficient sodium hydroxide (diluted with methanol) was added to neutralize all acid present. The polymer solution was precipitated into a substantial excess of methanol with vigorous agitation, followed by filtration and washing with methanol. The product was then vacuum dried. Analyses were conducted for sulfur and sodium. The level of sulfonate incorporated was determined by sulfur analysis.

A commercial PS (Styron 666 produced by Dow Chemical Company—52 g, 0.5 mol of styrene) was dissolved in sodium-dried cyclohexane at 60°C at a concentration of 100 g/L in clean, dry glassware under an atmosphere of nitrogen. *N,N,N',N'*-tetramethylethylenediamine (TMEDA), which was dried over calcium hydride, was added, followed by an equimolar quantity of *n*-butyllithium in hexane. Within 30 min a very tight gel formed which separated from most of the cyclohexane. After decanting the separated cyclohexane solution, the resultant gel was redissolved in 1600 mL of sodium-dried tetrahydrofuran (THF) and then transferred to a dropping funnel in a dry box. The THF solution of lithiated PS was then added to 1000 mL of THF through which about 300 g of dried CO₂ were bubbled. After complete addition and 30 min additional stirring, the reaction mixture was deactivated with 200 mL of methanol and acidified with an excess of concentrated hydrochloric acid. The carboxylated polystyrene (C-PS) was isolated through solvent flashing of the resultant reaction product in boiling water. The polymer was washed and pulverized with water in a Waring blender and the resultant fine solid filtered and dried in a vacuum oven at 80°C. The dried solid contained about 20 ppm lithium.

Fifty grams of the C-PS were dissolved in 475 mL of toluene and 25 mL of methanol. The solution was titrated with 1.0M NaOH in ethanol to an alizarin-thymolphthalein end point and then filtered through Celite. The sodium C-PS was isolated through solvent flashing, washing the resultant solid with water and methanol in a Waring blender, filtering, and drying.

Results and Discussion

Effect of Functionalization on the Backbone Polymer Molecular Weight. It is important that the functionalization of PS's in the experimental section be demonstrated to have no substantial effect on backbone polymer molecular weight in order for the comparisons that follow to have the desired significance. The PS used in these studies has an intrinsic viscosity of about 0.7 in xylene solvent or in xylene/methanol mixed solvent systems. It is a basic assumption of these studies that if

the carboxylated and sulfonated polymers prepared with this PS are shown to have very similar reduced or intrinsic viscosities in the same solvent systems when most of the ionic associations have been eliminated, then it can be reasonably inferred that the backbone molecular weight of these polymers has not been altered significantly during the functionalization processes.

In the case of the C-PS, the free acid form of the carboxylate can be compared directly with the PS control using reduced viscosity measurements. A comparison of the acid form of the C-PS with PS in terms of polymer reduced viscosity vs. polymer concentration is illustrated in Figure 2. It is seen that in a mixed solvent system comprised of methanol and xylene, with methanol being present in 5 and 10 vol %, that the C-PS at a level of about 1/2-2 mol % free acid content has a reduced and an intrinsic viscosity very similar to the starting PS (i.e., within about 10%). It would be expected that the presence of the carboxylic acid groups on the polymer would affect the intrinsic viscosity to some degree; however, the differences between the PS carboxylic acid and the PS control are not marked. Therefore, it can be inferred that the carboxylation process, when conducted at the indicated range on the PS backbone, does not substantially alter the degree of polymerization of the PS.

In the case of S-PS, there was some question as to whether the stability of the free sulfonic acid would permit a direct comparison of the reduced viscosity measurements. Therefore, comparisons were made with the neutralized salts (Figure 3). It has been noted in previous reports (13) that the use of methanol with xylene at about 10 vol % markedly reduces the ionic association of sulfonated polymers when they are present at low concentrations. Therefore, a comparison of the reduced viscosity behavior as a function of polymer concentration in that mixed solvent system is illustrated in Figure 3. Here it is evident that the PS has a reduced viscosity of about 0.7. The sulfonated polymers, however, at a sulfonated functionality of about 0.3 and 1.7 mol % are shown to have very similar intrinsic viscosity behavior. In the case of the sulfonated systems, it is observed that the intrinsic viscosity extrapolation provides values slightly below that of the PS. It is inferred, for reasons that follow, that these lower values are not the result of a decreased degree of polymerization of the PS backbone, but are attributable to a contraction of the polymer coil in dilute solution relative to PS. At any rate, the values of the S-PS under conditions which have markedly reduced ionic associations are such that there is relatively little change in the polymer backbone from that of the PS. Other evidence by gel permeation chromatography has supported the contention that the backbone molecular weight changes are negligible during sulfonation of PS under the conditions of these experiments.

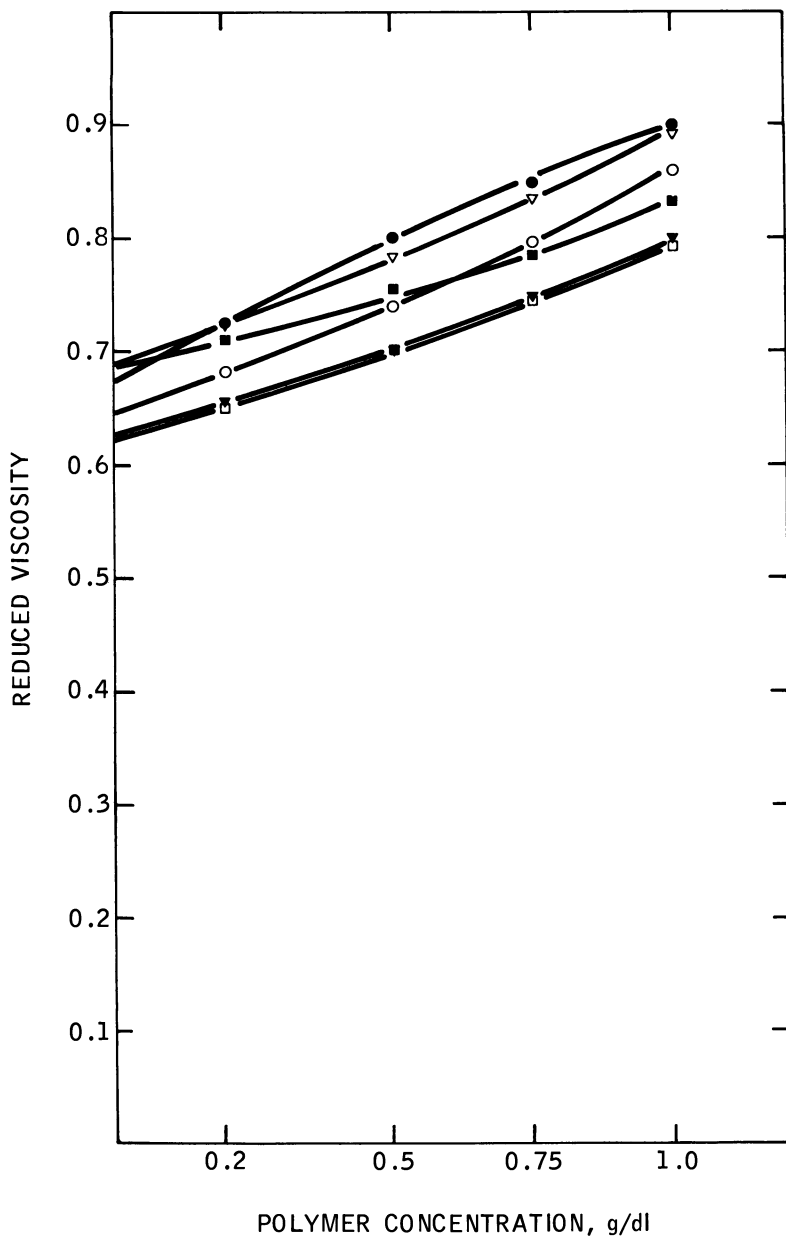


Figure 2. Reduced viscosity-concentration relations for PS and C-PS: (●) PS 5% MeOH/xylene; (▽) C-PS, 0.48%, acid, 5% MeOH/xylene; (□) C-PS, 1.9%, acid, 5% MeOH/xylene; (■) PS 10% MeOH/xylene; (○) C-PS, 0.48%, acid, 10% MeOH/xylene; (▼) C-PS, 1.9%, acid, 10% MeOH/xylene

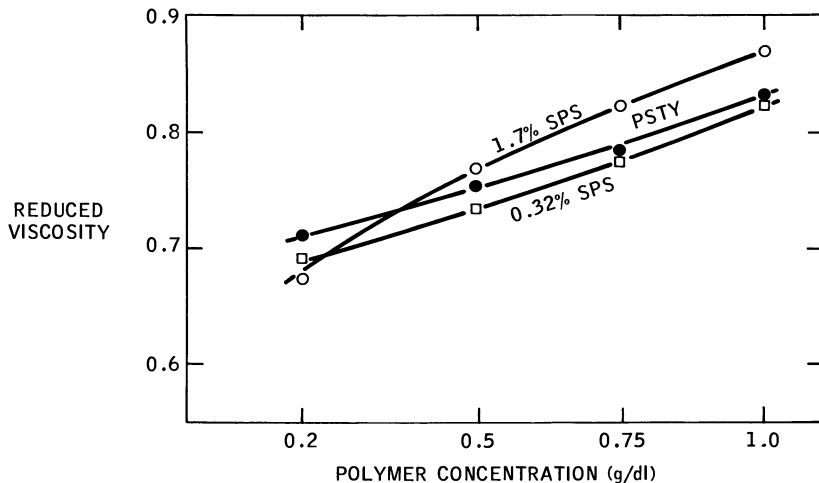


Figure 3. Reduced viscosity-concentration relation in methanol/xylene (10/90): (●) PS; (□) S-PS, 0.32%; (○) S-PS, 1.7%

Therefore, we can conclude that any comparisons done with the C-PS and S-PS of these studies illustrate the ionic interactions and the differences therein, and are not attributable to any significant differences in the backbone degree of polymerization.

Softening Behavior. The softening behavior of the PS control, a sodium C-PS, and a sodium S-PS are illustrated in Figure 4. These softening curves were obtained on materials that were compression molded. Both ionomers contained about 5 mol % ionic functionality and at that level are extremely difficult to melt process. Compression molding can be effected at temperatures of 250°C for the S-PS and 200°C for C-PS, provided that the molding is effected over a sufficiently long time to permit the viscous flow processes to occur. A Du Pont Thermo Mechanical Analyzer was used (10°C/min) under the same conditions for all three materials.

Under the conditions of this qualitative measurement the following observations can be made. The carboxylate ionomer displays a modest increase in the glass transition (T_g) compared with PS, but more significantly, it exhibits a plateau to temperatures greater than 150°C before a gradual softening is observed. This plateau is clearly attributable to the ionic associations persisting above the backbone T_g in this system.

However, in the case of the sulfonated ionomer it is seen that while the T_g is again increased above that of PS, the plateau attributable to ionic associations persists to temperatures some 75° to 100°C higher than that for the carboxylate ionomer. Similar but less dramatic differences between S-PS and C-PS are seen at lower functional levels (12).

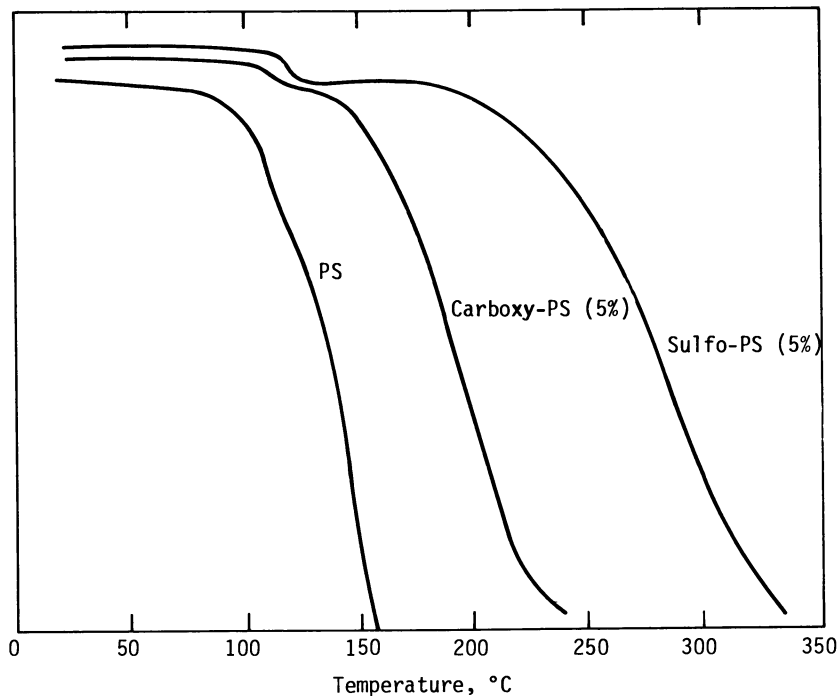


Figure 4. A comparison of the softening behaviors via TMA of PS, C-PS, and S-PS (load 10 g; heating rate: 10°C/min)

Rheological Behavior. A series of several S-PS and C-PS ionomers were characterized with respect to their melt viscosity at 220°C. The results are summarized in Figure 5. These measurements were made in a specially modified melt index rheometer capable of measuring very viscous materials. The unmodified PS was observed to possess a melt viscosity of about 4000 poise under the conditions of these measurements (a constant shear stress of $\tau = 2.05 \times 10^5$ dyn/cm² with capillary of 1.0 in. length \times 0.05 in. diameter). The sodium C-PS containing about 2 mol % functional level is seen to possess a viscosity of about 4×10^5 poise and a melt viscosity that increases with carboxylate content. However, in the case of the sodium sulfonate ionomer it is seen that at a comparable level of functionality the melt viscosity is higher by a factor of 1000 or so. These measurements clearly demonstrate a stronger ionic association for the sodium sulfonate ionomers compared with the carboxylates over the range of functionalities studied.

Solution Viscosity Behavior of Carboxylate and Sulfonate Ionomers. The solution behavior of sulfonated polymers has been described in some detail in a previous publication (13). It was shown in that study that

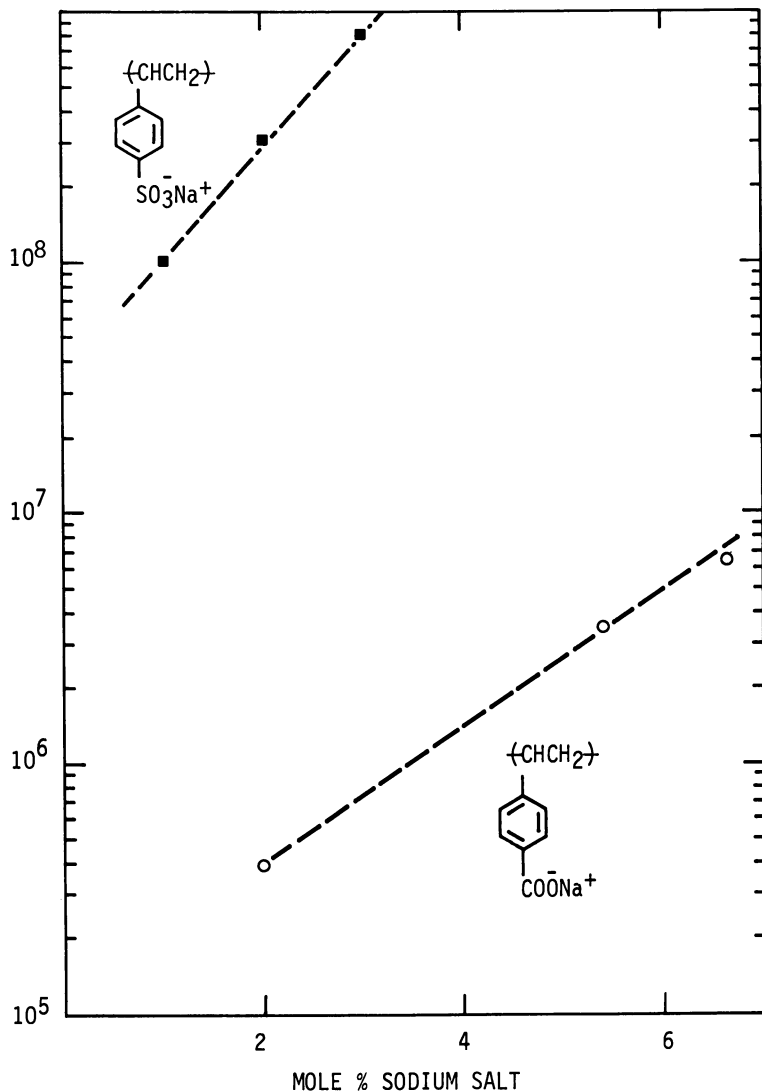


Figure 5. Melt viscosity of lightly sulfonated PS compared with lightly carboxylated PS, Na^+ salts (viscosity (poise) at 220°C)

sulfonated ionomers could be examined in solution under conditions which dramatically reduced the degree of ionic association by the addition of an appropriate polar cosolvent. In the absence of such cosolvents these polymers do not dissolve in hydrocarbon solvents at functional levels greater than 1 mol %. If a suitable cosolvent such as an alcohol or an amine is added (at levels of 1–10 vol %), then these polymers

dissolve readily. This behavior has been interpreted as a consequence of a preferential solvation of the ionic groups by the polar cosolvent, which helps diminish the ionic association (13). The use of various types and levels of cosolvents provides some insight into the differences between the carboxylates and sulfonates.

The solution viscosities of these two ionomers at a very low level of functionality are shown in Figure 6 as a function of hexanol cosolvent. At high cosolvent contents all polymers exhibit similar solution viscosities, but as the alcohol level is diminished, there is a marked increase in solution viscosity for S-PS, but only a modest change for C-PS. It is important to note that this behavior is not similar to that of a poly-

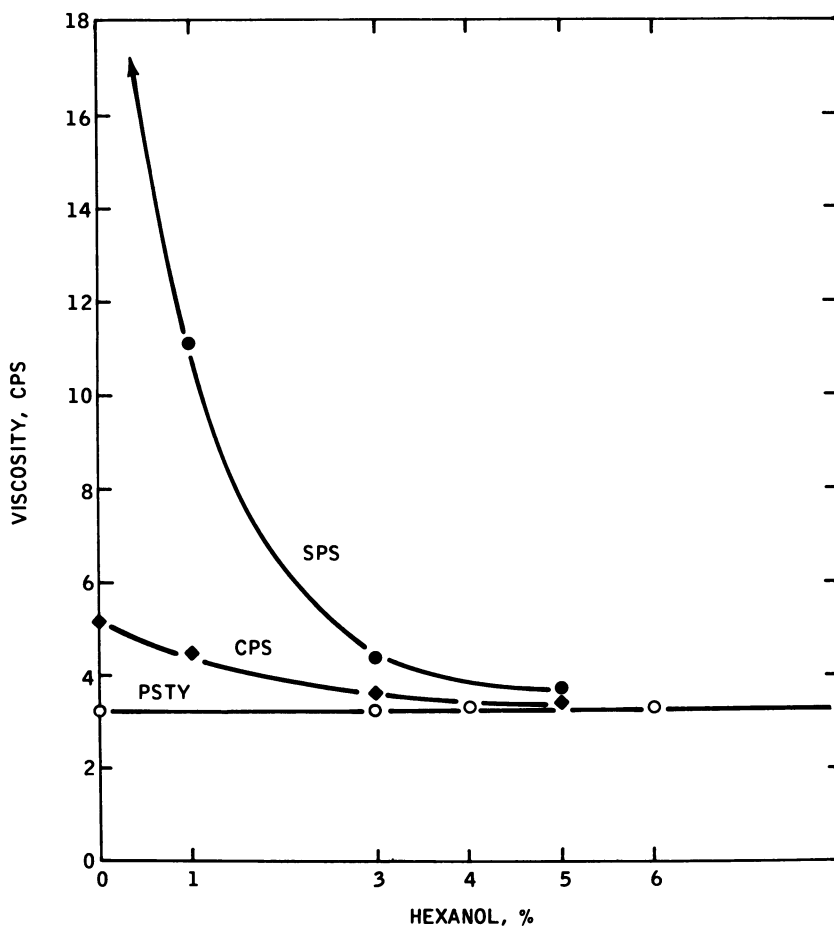


Figure 6. Solution viscosity of lightly sulfonated and carboxylated PS's as a function of cosolvent. Viscosity vs. hexanol level: (●) 0.32 mol% S-PS; (◆) 0.48 mol% C-PS; (○) PS; 3% concentration in hexanol/xylene.

electrolyte in aqueous solution, but is considered a result of the aggregation of ionic groups. Further evidence on this point can be established by examination of reduced viscosity behavior.

If both the carboxylate and the sulfonate are dissolved in a suitable solvent system, the reduced viscosities are readily obtained as a function of polymer concentration. The sodium S-PS's and sodium C-PS's were examined in a solvent system comprised of xylene and hexanol (95/5). The polymer-reduced viscosities are shown in Figure 7 as a function of concentration at two levels of ionic group functionality. At the low level, the carboxylate and the sulfonate ionomers exhibit viscosity concentration relationships very similar to that of the PS control. This would suggest that the level of ionic interaction is sufficiently low so as not to perturb the viscosity behavior significantly. In the case of the higher ionic group functionality, it is observed that both the sulfonate and carboxylate ionomers have very similar intrinsic viscosities based on these data, i.e., about 0.4. However, as polymer concentration is increased, it is observed that the sulfonate ionomer has a marked concentration dependence for the reduced viscosity, while the carboxylate system is rather insensitive. It is known from other work (13) that hexanol as a cosolvent is relatively poor compared with other alcohols and therefore, it is not surprising that the sulfonate analog at sufficiently high concentration exhibits marked upward curvature. This is presumed to arise from the increased interaction between sulfonate groups on different polymer molecules, which results in the higher viscosity with increasing polymer concentration. It is significant that the C-PS does not show the same dependence of reduced viscosity on concentration.

The influence of a stronger cosolvent, such as methanol, is shown in Figure 8 with the 5% methanol-95% xylene solvent pair. It is noted that under these conditions the behavior of the S-PS and C-PS at a low level of functionality is not significantly changed, nor would one expect it to be changed because of the low level of ionic interactions in these systems. However, at the higher functionality levels it is observed that the intrinsic viscosity of S-PS is significantly higher, and the pronounced upward curvature is absent. Thus the presence of 5% methanol markedly reduces the level of ionic interactions in the case of the 1.7% S-PS. In the case of the 1.9% C-PS, little difference is obtained in either the intrinsic viscosity or the slope as a function of polymer concentration.

The effect of higher levels of methanol cosolvent (10 vol %) on these polymers is shown in Figure 9. At this level of methanol, the 1.7% S-PS values are very similar to those of the PS control, although there are some differences that are still not fully understood. Nevertheless, under these conditions methanol reduces the level of ionic associations in

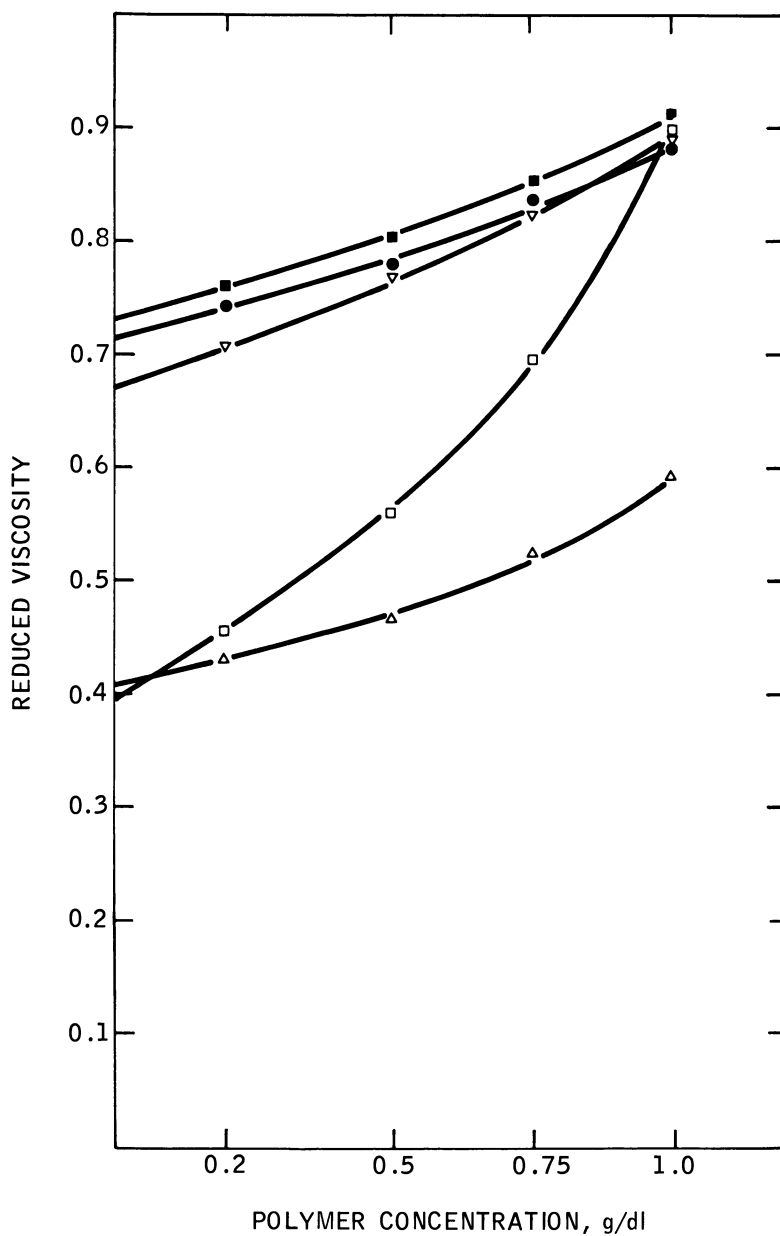


Figure 7. Reduced viscosity-concentration relations for PS, C-PS, and S-PS in hexanol/xylene (5% Hexanol/xylene): (●) PS; (▽) S-PS 0.32%; (□) S-PS 1.7%; (■) C-PS 0.48%; (△) C-PS 1.9%.

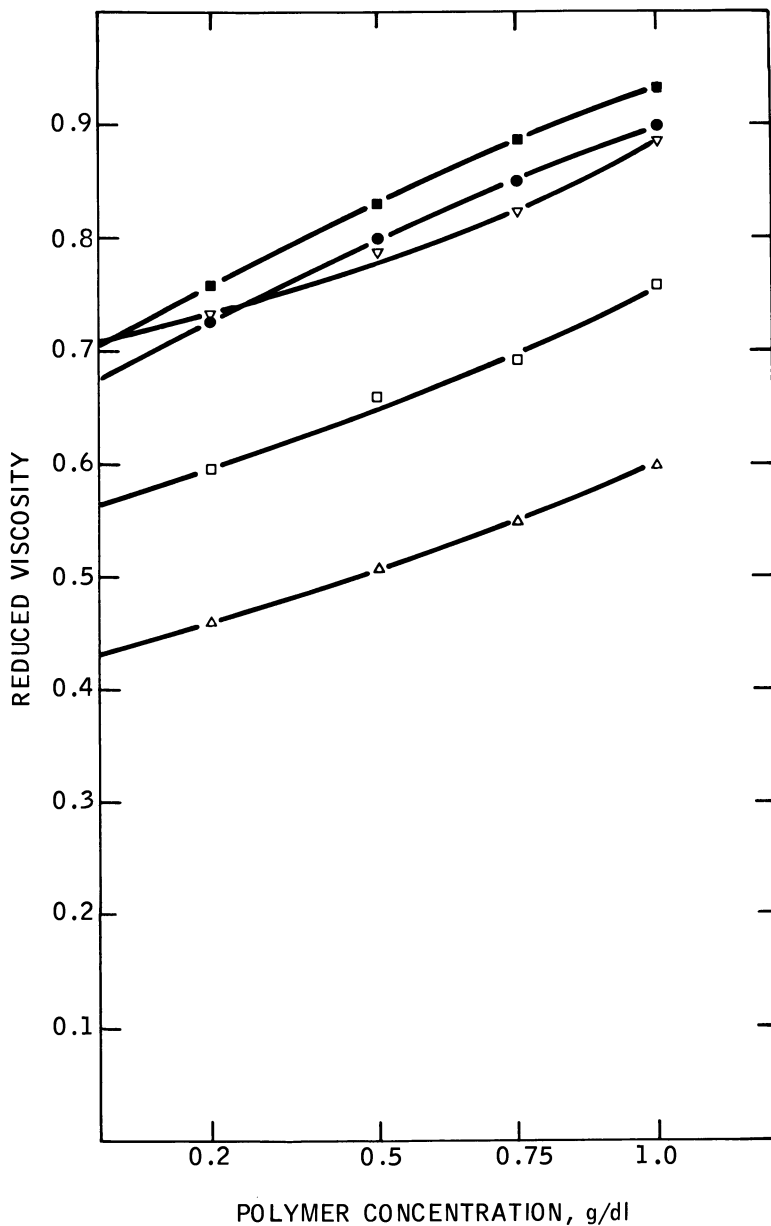


Figure 8. Reduced viscosity-concentration relations for PS, C-PS, and S-PS in methanol/xylene (5% MeOH/xylene: (●) PS; (▽) S-PS 0.32%; (□) S-PS 1.7%; (■) C-PS 0.48%; (△) C-PS 1.9%)

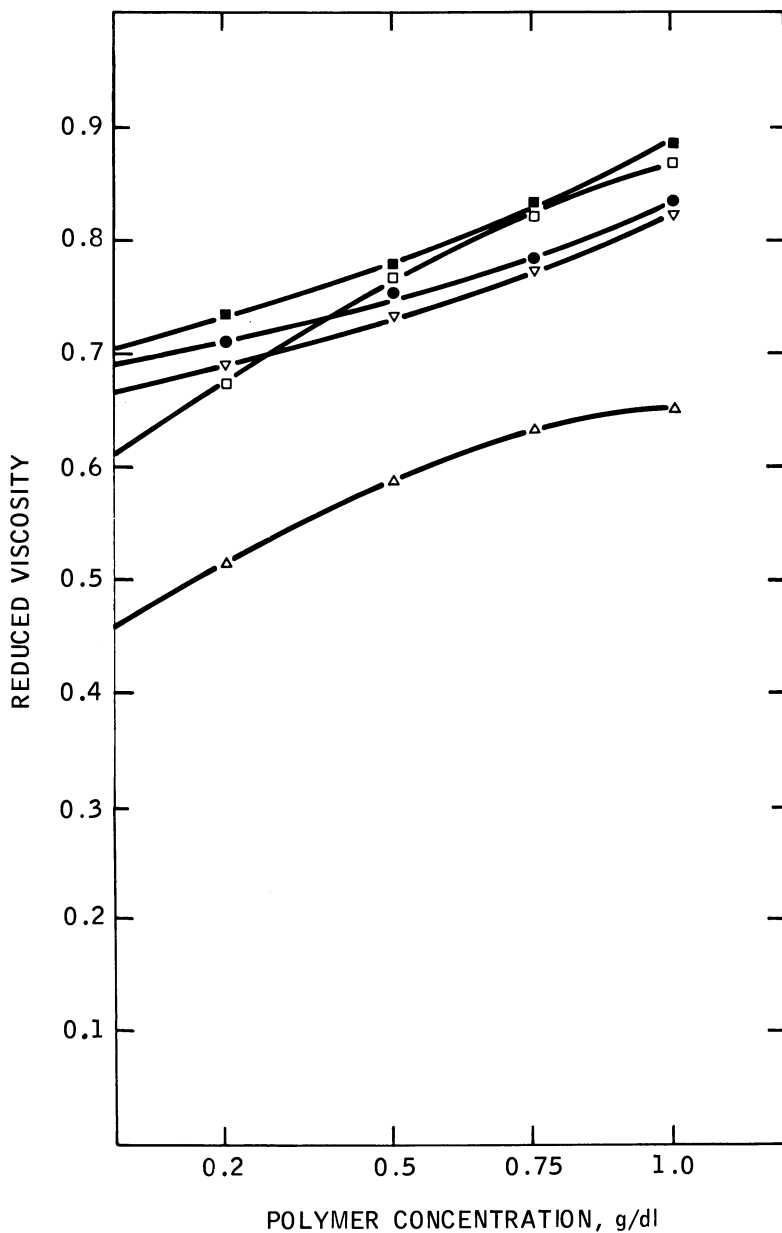


Figure 9. Reduced viscosity-polymer concentration relations for PS, C-PS, and S-PS in methanol/xylene (10/90) (10% MeOH/xylene: (●) PS; (▽) S-PS 0.32%; (□) S-PS 1.7%; (■) C-PS 0.48%; (△) C-PS 1.9%)

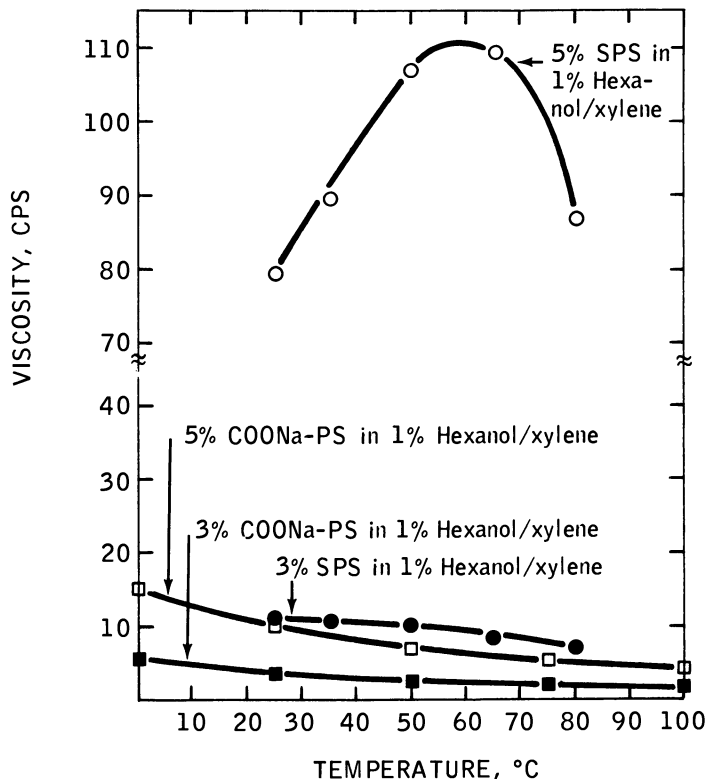


Figure 10. Solution viscosity-temperature relation of S-PS and C-PS at low functional group levels (S-PS = 0.32 mol % sulfonate; C-PS = 0.48 mol % carboxylate)

the sulfonated ionomer. However, in the case of C-PS, again the intrinsic viscosity is not changed substantially, and only modest changes in the slopes of these curves occur.

In summary, one can interpret these dilute solution viscosity results as indicative of a stronger interaction between sulfonate groups at higher polymer concentrations than for the carboxylate ionomers. This behavior is consistent with the bulk and melt rheological observations of these two ionomers. It is also interesting to note that the sulfonate ionomers appear more sensitive to the type and level of cosolvent present than do the carboxylate ionomers. These results suggest that the higher polarity of the sulfonate ionomer makes it much more responsive to the nature of the cosolvent and the degree of interaction that takes place. The intrinsic viscosity of both ionomers strongly suggests that there is a substantial amount of intramolecular association under dilute polymer conditions where intermolecular association has been minimized. Therefore, as the polymer concentration is increased, a transition from intramolecular inter-

action to intermolecular interaction is observed. The consequences of this transition are especially pronounced in the case of the sulfonate system.

Effect of Temperature on the Solution Behavior of Carboxylate and Sulfonate Ionomers. Based on the results above, a substantial difference in the solution behavior of carboxylate and sulfonate ionomers might be expected as a function of temperature. Figure 10 illustrates the effect of temperature on the solution viscosity of carboxylated and sulfonated ionomers at very low sulfonate and carboxylate content. At low polymer concentrations it is seen that the sulfonate system manifests a higher viscosity level in 1% hexanol/xylene solution. This is consistent with the dilute solution viscosity behavior. More importantly, at high polymer concentrations it is seen from Figure 10 that the 5% S-PS curve actually goes through a maximum, while the carboxylate system decreases monotonically. These results are apparently attributable to the weaker ionic association in the carboxylate case as compared to the sulfonate system.

Conclusions

Based on the results in this study and those reported previously it is concluded that the sulfonate ionomers, when compared to carboxylate ionomers under conditions as similar as possible, possess much stronger ionic associations than the corresponding carboxylates. Furthermore, this ionic association persists to higher temperatures and to a much greater degree under all conditions where it has been examined; that is, in the bulk at elevated temperatures, in the melt, and finally, in dilute solution. It is suggested that the observed sulfonate ionomer interactions occur as a result of a much greater degree of polarity obtained with the sulfonate ionomer as contrasted with the carboxylate system.

These differences in sulfonate and carboxylate associations are believed to be important factors in potential applications involving these ionomers, such as thermoplastic elastomers (8), elastic foams (14), solution applications (13), and related uses (6).

Acknowledgments

We gratefully acknowledge J. A. Sissano and R. R. Phillips for their experimental assistance in sample preparation and in making many of the measurements reported herein. The assistance of Dr. Lowell Westerman in conducting some of the rheological measurements and the helpful discussions of W. J. MacKnight are also appreciated.

Literature Cited

1. Eisenberg, A.; King, M. "Ion-Containing Polymers"; Academic: New York, 1977.
2. Holliday, L., Ed. "Ionic Polymers"; Wiley: New York, 1975.

3. Otocka, E. P. *Macromolecular Science-Rev. Macromol. Chem.* **1971**, *C5*(2), 275.
4. Brown, H. P. *Rubber Chem. Technol.* **1975**, *35*(5), 1347.
5. Rees, R. W.; Reinhardt, H. G. U.S. Patent 3 997 487, 1976; to E. I. du Pont de Nemours and Company.
6. Makowski, H. S.; Lundberg, R. D.; Singhal, G. S. U.S. Patent 3 870 841, 1975; to Exxon Research and Engineering Company.
7. Canter, N. H. U.S. Patent 3 642 728, 1974; to Esso Research and Engineering Company.
8. Makowski, H. S.; Lundberg, R. D., chapter 3 in this book.
9. Sanui, K.; Lenz, R. W.; MacKnight, W. J. *J. Polym. Sci., Polym. Chem. Ed.* **1974**, *12*, 1965.
10. Azuma, C.; MacKnight, W. J. *J. Polym. Sci., Polym. Chem. Ed.* **1978**, *15*, 547.
11. Rahrig, D. C.; MacKnight, W. J. *Polym. Prepr., Am. Chem. Soc., Div. Polym. Chem.* **1978**, *19*(2), 314.
12. Lundberg, R. D.; Makowski, H. S., unpublished results.
13. Lundberg, R. D. *Polym. Prepr., Am. Chem. Soc., Div. Polym. Chem.* **1978**, *19*(1), 455.
14. Brenner, D.; Lundberg, R. D. *ChemTech* **1977**, *7*(12), 748.

RECEIVED October 16, 1978.

Plasticization of Metal Sulfonate-Containing EPDM with Stearic Acid Derivatives

H. S. MAKOWSKI and R. D. LUNDBERG

Corporate Research Laboratories, Exxon Research and Engineering Company,
Linden, NJ 07036

Metal sulfonate-containing ethylene-propylene-diolefin terpolymers (EPDM) were plasticized with stearic acid and derivatives for the reduction of the melt viscosities of these ionomers through interaction with the very strong ionic associations. Substantial improvements in melt flow were achieved with stearic acid and the zinc, lead, and ammonium stearates, while other metal stearates were ineffective. Zinc stearate and lead stearate not only markedly improved melt flow but, remarkably, also enhanced the mechanical properties of the plasticized systems. These unique additives were fully compatible with the EPDM ionomers and provided thermoelastic systems with excellent physical properties and ready processability.

The introduction of relatively low levels of metal sulfonate groups into ethylene-propylene-diolefin terpolymers (EPDM) yields ionomers with extremely high melt viscosities (1). These high melt viscosities are attributable to the very strong associations of metal sulfonate groups (2). Through a suitable choice of EPDM composition and molecular weight, ionomer sulfonate content, and cation borne by the sulfonate group, it is possible to obtain metal sulfonate-containing EPDM's with excellent mechanical properties and sufficiently low melt viscosities for compression molding (a low shear rate operation). Such materials, after formulation with fillers and extender oils, still do not possess sufficiently low melt viscosities for easy injection molding and extrusion operations.

It is possible to add agents to metal sulfonate-containing EPDM to reduce melt viscosity and to improve melt processability. Canter and Buckley (3) were the first to preferentially plasticize metal sulfonate-

containing EPDM's. These plasticizers were postulated to interact with the ionic groups, thereby reducing the degree of ionic association, decreasing apparent molecular weight, and reducing melt viscosity. Because these plasticizers were to interact with and solvate ionic groups it was necessary that they possess some polar functionality.

There are a large number of compounds which could function as plasticizers for ionic associations. When the plasticized products are to be processed at elevated temperatures the plasticizers must be nonvolatile or of low vapor pressure. It is also desirable that the plasticizers be fully compatible and that they not adversely affect the mechanical and chemical properties of the ionomer.

This chapter describes the effects of various stearates on the rheological, mechanical, and chemical properties of metal sulfonate-containing EPDM's.

Experimental

The base EPDM used in these studies, CR-2504, was derived from the extruder breakdown of Vistalon 2504 (Exxon Chemical Company). Vistalon 2504 contains about 50 wt % ethylene and 5 wt % 5-ethylidene-2-norbornene (ENB) and has a Mooney viscosity (ML, 1 + 8, 100°C) of about 40. The CR-2504 had a Mooney viscosity of about 20.

Sulfonation procedures, neutralization methods, analytical testing, and physical testing procedures have been described earlier (1).

Stearate plasticizers were added to metal sulfonate-containing EPDM's by dissolving the unplasticized gums in 95% toluene/5% methanol at a concentration of 100 g/L, dissolving or dispersing the stearate therein, and flashing the solvent from the resulting cement in boiling water. The resultant wet polymeric mass was washed and pulverized in a Waring blender, and the wet crumb was filtered and dried on a hot rubber mill.

Results and Discussion

Metal sulfonate-containing EPDM's are not soluble in hydrocarbon solvents alone; however, they do dissolve in combinations of a major amount of hydrocarbon and a minor amount of polar cosolvent, for example, an alcohol (4). Thus the ion-dipole interactions can be solvated, or plasticized, and thereby reduce the level of ionic cross-linking to a level where solution occurs. In the unplasticized melt metal sulfonate-containing EPDM's can possess extremely high melt viscosities at even low sulfonate levels. Thus while the incorporation of metal sulfonate groups results in physically cross-linked systems with a good assemblage of mechanical properties, the ionic interactions are so strong as to preclude ready melt processability. In the development of a thermoplastic elastomer from sulfonated EPDM the problem is not that metal sulfonates do not associate strongly enough, but that they associate too strongly. Still it is possible, through proper choice of EPDM structure, composition,

molecular weight, sulfonate content of the ionomer, and cation borne by the sulfonate group, to substantially reduce melt viscosity; however, even in these best instances melt viscosity is still too high for ready processability. To convert metal sulfonate-containing EPDM's into useful thermoplastic elastomers it is necessary that the ionic interactions be abated (plasticized) to reduce melt viscosity. The plasticization of ionic associations requires compounds which are nonfugitive under conditions of processing and testing. In this regard, the saturated fatty acids, such as myristic, palmitic, and stearic acids and their derivatives, are relatively nonvolatile at 190°–200°C, a temperature range suitable for processing and for capillary melt extrusion characterization. These fatty acids satisfy the basic requirements for an ionic domain plasticizer, that is, that it contain a polar group and that it be nonfugitive.

The effect of stearic acid upon the melt index of metal sulfonate-containing EPDM is illustrated in Figure 1. Stearic acid was added to the zinc, magnesium, and barium salts of sulfonated CR-2504 containing about 33 meq sulfonate/100 g of polymer. The stearic acid was added at levels of 30, 60, and 90 mmol/100 g polymer (approximately 10, 20, and 30 parts, respectively, per 100 parts of polymer). The incorporation of stearic acid converted essentially intractible systems with no melt flow to materials with a high degree of flow. The zinc salt responded most readily to the plasticization, followed by the magnesium salt, and then the barium salt. This order of melt flow behavior corresponds to the order of the strengths of the ionic associations, that is, barium sulfonates are the most strongly, and zinc sulfonates the least strongly, associated. Rather substantial quantities of stearic acid were required to effect more major changes in melt flow; however, with suitable compositional adjustments only lower stearic acid levels are required. The stearic acid was compatible with the ionomer up to about 10 parts/100 of polymer, but slow exudation (blooming) of stearic acid occurred at higher levels. The blooming rate was low enough so that physical testing of stearic acid-plasticized samples could be effected well before significant amounts of stearic acid could be lost to blooming.

It might be expected that plasticized systems showing improved melt flow would consequently exhibit a loss in mechanical properties. Figure 2 illustrates the effect of stearic acid on room temperature tensile strength. The tensile strength of the zinc sulfonate ionomer showed little change with stearic acid concentration. On the other hand, the barium and magnesium sulfonates exhibited improvements in tensile properties. These improvements were obtained primarily as a result of increased elongations over those of the highly intractible unplasticized gums. Thus, stearic acid appears to improve tensile properties. Certainly there appears to be no deleterious effect.

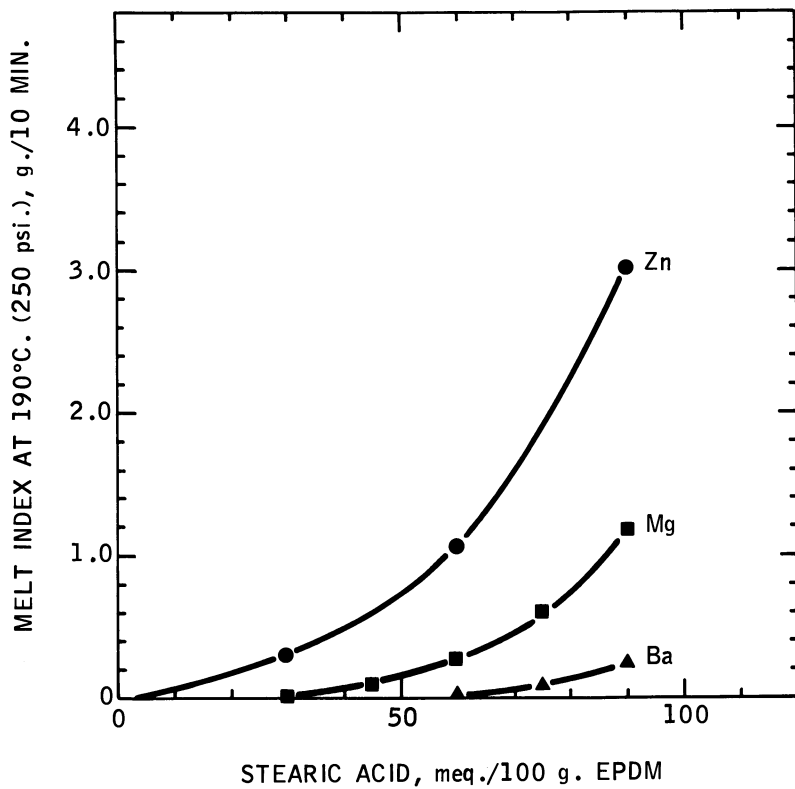


Figure 1. Effect of stearic acid on melt index of metal sulfonate CR-2504 (base polymer—CR-2504; sulfonate content—33 meq/100 polymer)

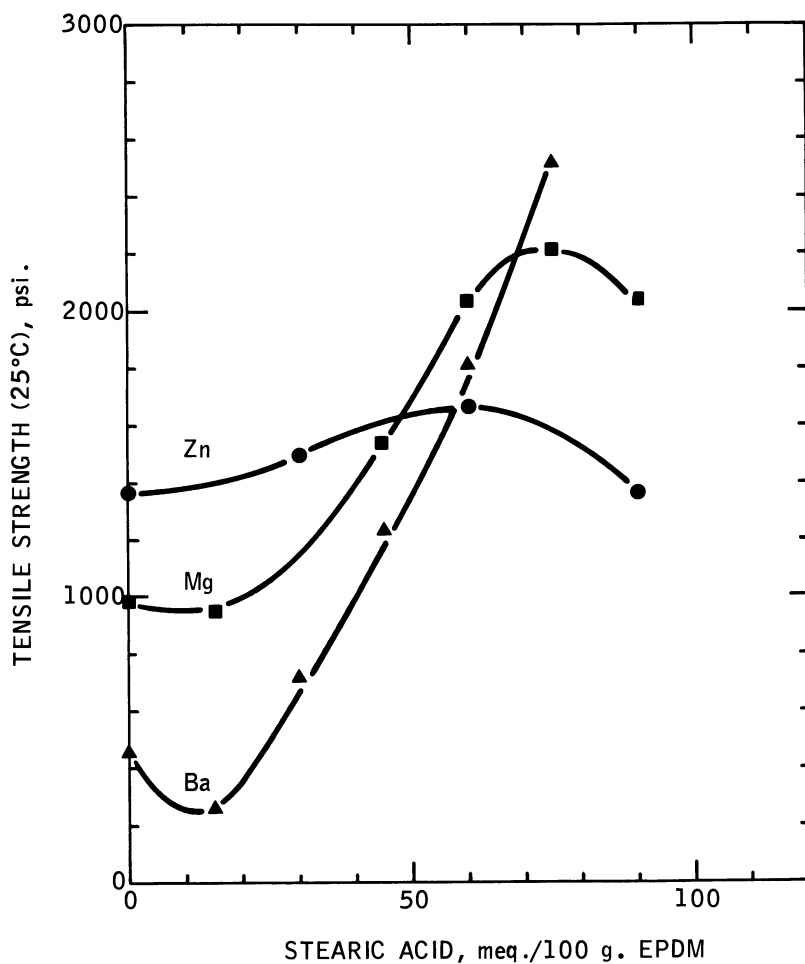


Figure 2. Effect of stearic acid on the 25°C-tensile strength of metal sulfonate CR-2504 (base polymer—CR-2504; sulfonate content—33 meq/100 polymer)

Although stearic acid was beneficial to tensile strength at room temperature it exerted a deleterious effect at a 70°C-testing temperature, as illustrated in Figure 3. Substantial reductions in tensile strength were obtained at this elevated temperature. At the higher stearic acid levels the plasticized systems possessed hardly any strength. Thus, although stearic acid is indeed an excellent flow improver and provides for ready melt processability, a penalty is paid with the mechanical properties. Certainly it would be desirable to avoid this loss in mechanical properties.

Three metal stearates, the zinc, barium, and magnesium stearates, were examined with the barium, magnesium, and zinc sulfonate-containing EPDM's. The effects of these stearates on the melt flow and tensile properties are given in Table I. Stearic acid is included for comparison. The plasticizers were added to the ionomers at a level of 30 parts/100 of polymer. Neither the magnesium nor the barium stearate improved the melt flow of the magnesium, barium, or zinc sulfonate-containing EPDM's. In fact, it appeared that these two metal stearates showed an antiplasticizing effect in the zinc sulfonate EPDM. On the other hand, zinc stearate was highly effective in increasing melt flow—almost as good as stearic acid. Of the four materials examined as melt flow improvers two were, and two were not.

It has already been shown that stearic acid exerts a generally deleterious effect on mechanical properties, and the results in Table I further corroborate this. The barium and magnesium stearates appeared

Table I. Effects of Metal Counterion and Metal Stearates

<i>Metal Sulfonate</i>	<i>Plasticizer</i>	<i>Room Temperature</i>	
		<i>Tensile Strength (psi)</i>	<i>Elongation (%)</i>
Ba	none	450	100
Ba	BaSt ₂	—	—
Ba	MgSt ₂	770	230
Ba	ZnSt ₂	2050	470
Ba	StCOOH	1290	590
Mg	none	980	210
Mg	BaSt ₂	870	310
Mg	MgSt ₂	870	205
Mg	ZnSt ₂	3530	520
Mg	StCOOH	2040	560
Zn	none	1480	400
Zn	BaSt ₂	1920	410
Zn	MgSt ₂	2570	490
Zn	ZnSt ₂	3040	460

* Base polymer—CR-2504; sulfonate content—33 meq/100 g polymer.

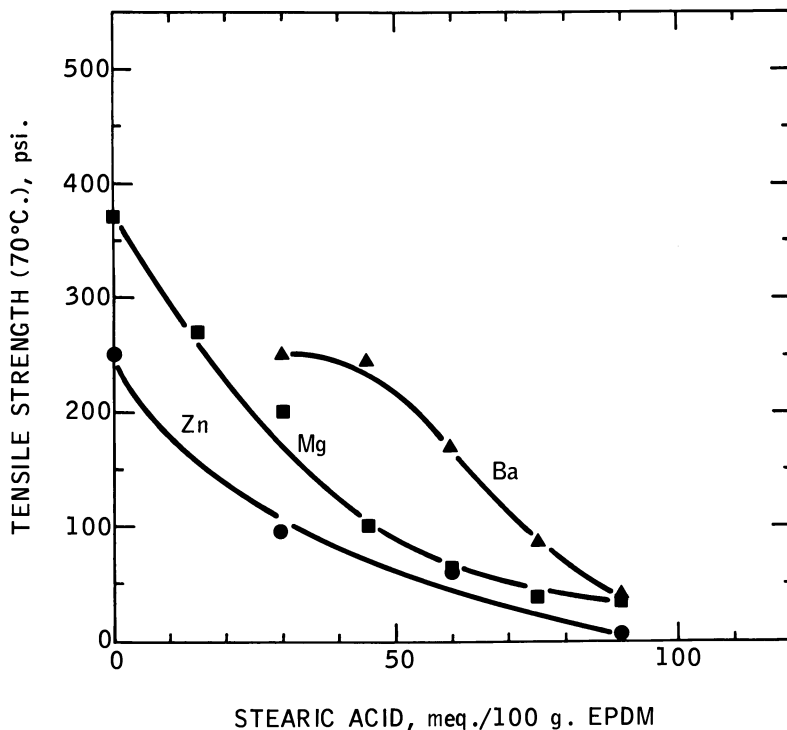


Figure 3. Effect of stearic acid on the 70°C-tensile strength of metal sulfonate CR-2504 (base polymer—CR-2504; sulfonate content—33 meq/100 polymer)

on Flow and Tensile Properties of EPDM Ionomers^a

70°C		
Tensile Strength (psi)	Elongation (%)	Melt Index (190°C, 250 psi, g/10 min)
40	40	0
340	110	0.01
610	410	0.6
40	> 800	1.0
370	75	0
320	140	0.02
300	85	0.02
840	470	1.9
40	> 800	4.0
270	450	0.2
960	370	0.04
690	370	0.05
1150	750	8.2

to improve the tensile properties of the zinc sulfonate EPDM but exerted little improvement on the barium and magnesium sulfonate EPDM's. Zinc stearate on the other hand produced remarkable increases in tensile strengths in all of the metal sulfonate systems, and the best tensile properties were generated from a zinc stearate-plasticized zinc sulfonate EPDM. The zinc stearate-plasticized gums were essentially transparent and apparently fully compatible. No blooming of zinc stearate has been observed in systems containing 60 parts, and higher, of zinc stearate.

Zinc stearate provides a rather remarkable result. It markedly enhances the melt flow of metal sulfonate ionomers while simultaneously improving the mechanical properties of the resultant system.

The effect of zinc stearate concentration on the melt flow of zinc, magnesium, and barium sulfonate-containing CR-2504 is shown in Figure 4. These results parallel those obtained with stearic acid plasticizer (cf. Table I). The zinc sulfonate EPDM responded most readily to zinc stearate plasticization. Although the melt flows of the magnesium and

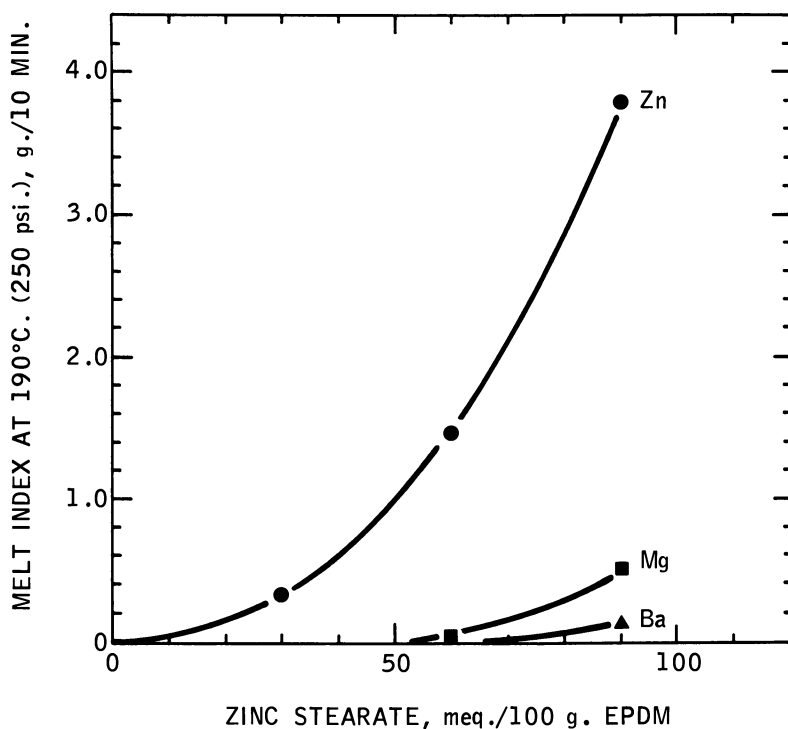


Figure 4. Effect of zinc stearate on the melt index of metal sulfonate CR-2504 (base polymer—CR-2504; sulfonate content—33 meq/100 polymer)

barium sulfonate EPDM's were significantly improved, zinc stearate appeared to be a slightly less effective melt flow improver than stearic acid for these ionomers.

The effect of zinc stearate concentration on the room temperature tensile properties of the zinc, barium, and magnesium ionomers is illustrated in Figure 5. Whereas stearic acid showed little or modest improve-

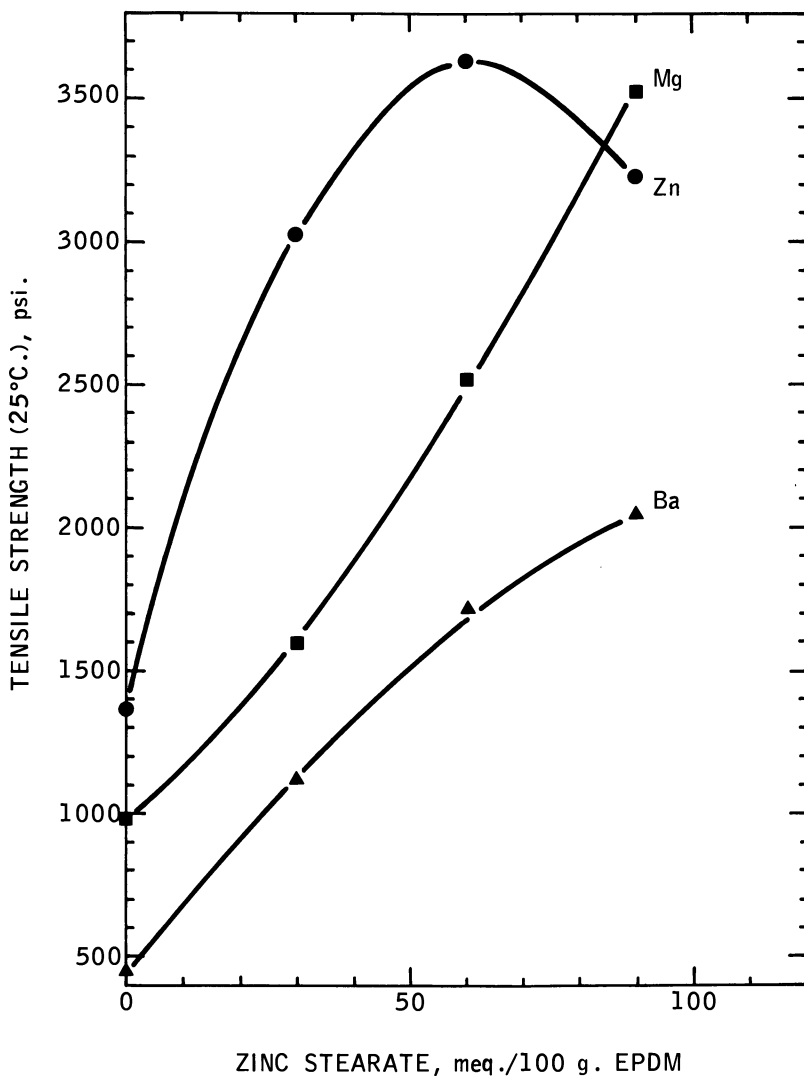


Figure 5. Effect of zinc stearate on the 25°C-tensile strength of metal sulfonate CR-2504 (base polymer—CR-2504; sulfonate content—33 meq/100 polymer)

ments in tensile strength, zinc stearate effected substantial improvements in all cases. Over this concentration range the zinc sulfonate ionomer improved tensile strength the most. Figure 6 illustrates that these improvements in tensile properties were still manifested at 70°C. Quite substantial improvements were obtained for every cation, but again, the best response was obtained with the zinc sulfonate ionomer. The improvements in tensile properties were primarily the result of increased elongations and not of increased moduli. Moduli remained essentially constant over this range of zinc stearate concentration.

The zinc stearate plasticization of a larger number of metal sulfonate-containing EPDM's is shown in Table II. The incorporation of 90 meq of zinc stearate/100 g polymer resulted in large reductions in melt viscosity and substantial increases in the shear rates at which melt fracture occurred. In addition, substantial improvements in tensile strength at room temperature and 70°C were obtained. The low viscosities were manifested in much improved melt flow. The improved tractability of the plasticized ionomers was reflected in much higher elongation, which was largely responsible for the improved tensile strength. Thus, zinc stearate functions as both a melt viscosity improver and a mechanical property enhancer for all metal sulfonate-containing EPDM's.

The plasticizing effects of a larger number of metal stearates on the zinc sulfonate ionomer were examined, and the results are given in Table III in terms of flow and mechanical properties. Lead stearate, zinc stearate, and ammonium stearate significantly improved melt flow along with the stearic acid control. The barium, magnesium, sodium, lithium, and calcium stearates showed little, if any, improvement in melt flow. Of the four melt flow improvers, both stearic acid and ammonium stearate exerted deleterious effects on tensile properties. Only the zinc and lead stearates substantially improved tensile properties. Thus, while zinc stearate is not unique, the number of fatty acid derivatives that improve both melt flow and mechanical properties is limited.

It was noted earlier that the incorporation of metal sulfonate groups into EPDM resulted in enhanced water sensitivity. The response of the ionomer to water pick-up was a function of the metal cation borne by the sulfonate group (1). The incorporation of zinc stearate plasticizer into EPDM ionomers resulted in marked reductions in water absorption, and this is illustrated in Figure 7. In the absence of zinc stearate water absorptions of 30–80% were obtained for most cations while the lead and zinc cations absorbed about 10%. Zinc stearate markedly reduced water absorption for all metal cations. However, the zinc and lead cations yielded the lowest water absorptions.

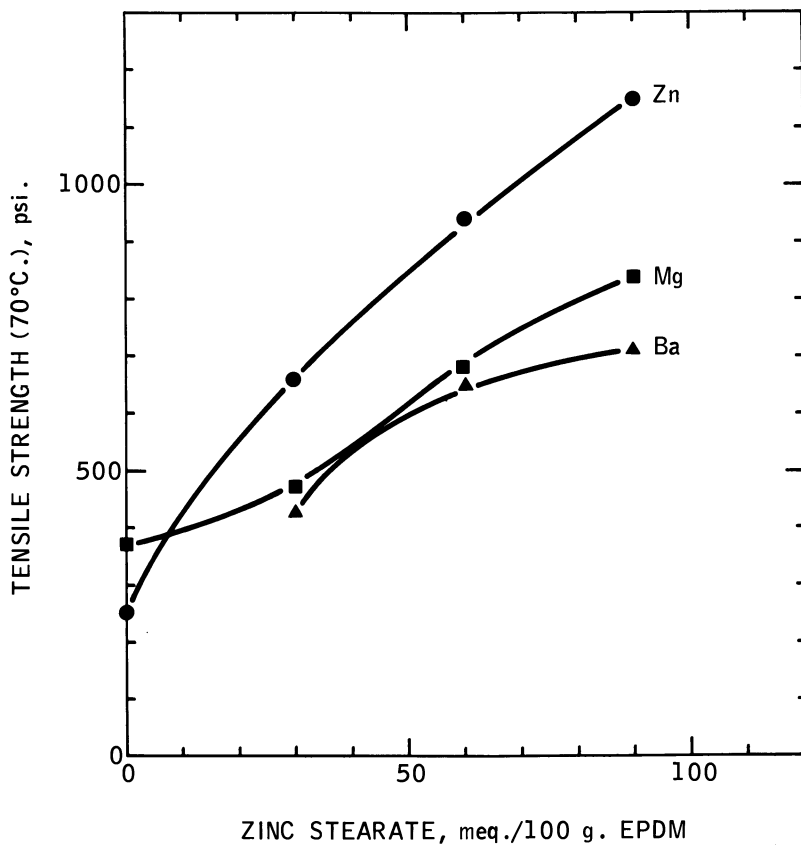


Figure 6. Effect of zinc stearate on the 70°C-tensile strength of metal sulfonate CR-2504 (base polymer—CR-2504; sulfonate content—33 meq/100 polymer)

Table II. Effect of Cation and Zinc

<i>Metal</i>	<i>Apparent Viscosity^b</i> (poise $\times 10^{-5}$)	<i>Melt Fracture at Shear Rate</i> (sec^{-1})	<i>Melt Index</i> (190°C, 478 psi, g/10 min)
<i>Unplasticized</i>			
Hg	—	—	disintegrated
Mg	55.0	< 0.88	0
Ca	53.2	< 0.88	0
Co	52.3	< 0.88	0
Li	51.5	< 0.88	0
Ba	50.8	< 0.88	0
Na	50.6	< 0.88	0
Pb	32.8	88	0.1
Zn	12.0	147	0.75
<i>Plasticized^c</i>			
Hg	12.7	29	2.2
Mg	5.7	1469	2.1
Ca	6.0	294	2.4
Co	6.1	1469	2.2
Li	3.4	1469	7.4
Ba	10.7	88	1.0
Na	5.0	294	4.5
Pb	3.0	> 1469	10.2
Zn	1.5	> 1469	16.8

^a Base polymer—CR-2504; sulfonate content—31 meq/100 g EPDM; dissolved 100 g of free acid in 1000 mL hexane—150 mL isopropanol; neutralized with 90 meq acetate in 25 mL water.

Table III. Effect of Various Metal

<i>Stearate Plasticizer</i>	<i>Room Temperature</i>	
	<i>Tensile Strength (psi)</i>	<i>Elongation (%)</i>
Ba	1920	410
Mg	2570	490
Na	1460	480
Li	1635	510
Ca	1220	530
Pb	3255	480
Zn	3040	460
NH ₄	2100	570
StCOOH	1495	590

^a Base polymer—CR-2504; sulfonate content—33 meq/100 g EPDM.

Stearate on Flow and Physical Properties^a

<i>Room Temperature</i>		<i>70°C</i>	
<i>Tensile Strength (psi)</i>	<i>Elongation (%)</i>	<i>Tensile Strength (psi)</i>	<i>Elongation (%)</i>
<i>Unplasticized</i>			
—	—	—	—
320	70	150	40
410	90	170	40
1180	290	450	160
760	320	250	130
340	70	150	30
960	350	270	110
1680	480	320	350
1480	400	270	450
<i>Plasticized^c</i>			
400	160	170	90
2130	510	610	390
1900	470	590	360
2020	490	570	400
1970	480	460	440
1710	480	540	340
1690	500	430	420
2312	460	740	610
2470	480	770	580

^b At 200°C and 0.88 sec⁻¹.^c With 90 meq of zinc stearate/100 g of polymer.**Stearates on Zinc Sulfonate Gums^a**

<i>70°C</i>		<i>Melt Index (190°C, g/10 min)</i>	
<i>Tensile Strength (psi)</i>	<i>Elongation (%)</i>	<i>at 250 psi</i>	<i>at 476 psi</i>
960	370	—	0.04
690	370	—	0.05
360	200	0.04	0.14
275	360	0.07	0.27
510	410	—	0.37
665	670	0.83	3.11
1150	750	2.09	8.21
70	> 800	2.29	10.48
15	> 800	3.02	11.73

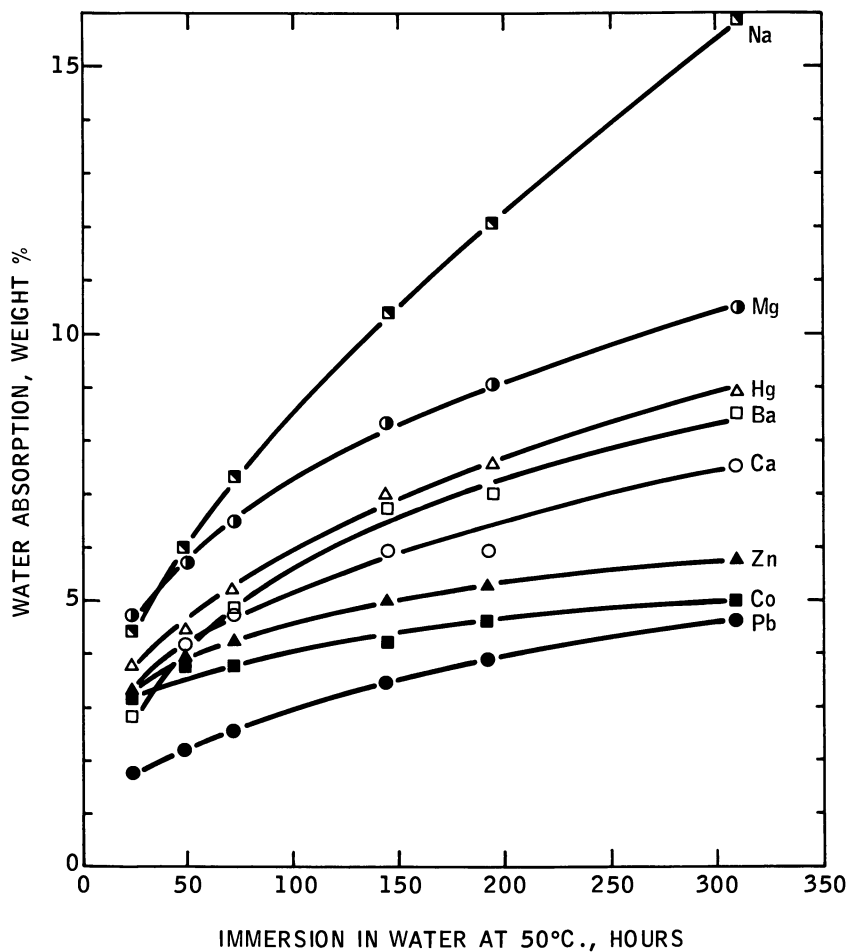


Figure 7. Effect of cation and zinc stearate on water absorption (base polymer—CR-2504; sulfonate content—31 meq/100 g EPDM; zinc stearate—90 meq/100 g EPDM)

In summary, it is possible to prepare metal sulfonate-containing EPDM's with good mechanical properties. Most systems possess very high melt viscosities, and those with the best flow properties are still borderline in usefulness. These melt viscosities can be reduced to useful levels through the use of nonfugitive additives, such as fatty acid derivatives. There are among these additives unique materials, such as zinc stearate, that not only dramatically improve flow but also unexpectedly improve physical properties. These unique additives are highly compatible with EPDM ionomers in the sense that there is no blooming. The question of the mechanism of tensile enhancement is important and interesting. Studies toward this end will be the subject of future publications.

Acknowledgment

The authors are indebted to J. A. Sissano, M. A. Grossman, and M. Vieira for their fine efforts, expert assistance, and good cheer.

Literature Cited

1. Makowski, H. S.; Lundberg, R. D.; Westerman, L.; Bock, J., chapter 1 in this book.
2. Lundberg, R. D.; Makowski, H. S., chapter 2 in this book.
3. Canter, N. H.; Buckley, D. J., Sr. U.S. Patent 3 847 854, 1974, Esso Research & Engineering Company.
4. Lundberg, R. D. *Polym. Prepr., Am. Chem. Soc., Div. Polym. Chem.* **1978**, *19*(1), 455.

RECEIVED October 16, 1978.

Effect of Counterion Structure on Ionomer Properties: Quaternary Phosphonium Counterions in Sulfonated EPDM

DOUGLAS BRENNER and ALEXIS A. OSWALD

Exxon Research and Engineering Company, Linden, NJ 07036

The effect of the structure of quaternary phosphonium counterions on the physical properties of an ethylene-propylene-diene monomer elastomer containing about 1 mol % sulfonation was studied. These quaternary counterions have an essentially full positive charge on the heteroatom so covalent interactions with anions are minimal, and the substituents can be varied over a wide range so that systematic studies of the effect of counterion structure can be made. Tensile strength decreased and melt-flow rate increased with increasing length of n-alkyl substituents. Substituent atoms near the central charged atom had a greater effect on physical properties than atoms farther out on a chain. Some ionomers containing divalent quaternary counterions were stronger and some were weaker than those containing corresponding monovalent quaternary ions. The sensitivity of some of these polymers to water uptake also was studied briefly.

The type of counterion used in an ion-containing polymer can have a substantial effect on the physical properties of the material. Many studies have been made in the past comparing the properties of metal- or ammonium-neutralized ionomers: two recent books on ion-containing polymers present a comprehensive review of the literature (1, 2). There is a wealth of information comparing different metal counterions in neutralized or partially neutralized ethylene-carboxylic acid copolymers. Rees and Vaughan studied the melt flow and tensile properties of

0-8412-0482-9/80/33-187-053\$05.00/0
© 1980 American Chemical Society

ethylene-acrylic acid copolymers partially neutralized with a variety of different metal counterions (3,4). Properties tended to depend more strongly on the degree of neutralization than on the metallic counterion used. Bonotto and Bonner also examined partially neutralized ethylene-acrylic acid copolymers, and among other studies, compared the effect of monovalent vs. divalent counterions (5). The samples with monovalent and divalent types of counterions did not show major differences in their melt-flow rates at 190°C. On the other hand, in studies by Fitzgerald and Nielsen on metal-neutralized styrene-methacrylic acid copolymers, major differences were found in the stress relaxation of samples containing the divalent counterion barium as compared with sodium (6). Eisenberg and collaborators have studied a number of ion-containing polymers including carboxylated polyethylene and carboxylated polystyrene copolymers (7,8,9,10). It was found that changes in the glass transition temperatures (T_g 's) of many of the materials could be related to the ratio of the valence of the counterion and the separation between cation and anion. Eisenberg also has made extensive investigations of the effect of different counterions on viscoelastic properties of carboxylated polyethylene and carboxylated polystyrene ionomers. Other polymer systems in which Eisenberg et al. have studied the effect of various metal counterions include polyphosphates and polysilicates, where correlations between T_g 's and the ratio of charge to interion distance also have been made (11,12). Rees examined some amine-neutralized ethylene-methacrylic acid copolymers and found that the amines were not as efficient as the metal ions in physically cross-linking the systems (13). For example, there was a relatively small effect on melt flow at 190°C. MacKnight et al. also have studied counterion effects in ethylene-methacrylic acid copolymer systems and, in particular, have investigated dynamic mechanical properties of these materials (14,15).

Ion-containing polymers with ammonium groups have been studied in several different polymer systems. A wide range of cationic polyelectrolytes containing quaternary ammonium cations either in or covalently appended to the polymer chains has been reviewed by Hoover (16). Many of these materials are water soluble. A type of cationic quaternary ammonium-containing polymer in which the quaternary ammonium groups are an integral part of the backbone chain has been investigated extensively by Rembaum et al. (17,18). In these studies the effect of the lengths of the hydrocarbon connecting chains on the T_g of these polymers was measured.

The effect of a variety of counterions in a carboxylated elastomer has been studied by Brown (19,20). Both divalent and monovalent metal counterions were investigated in a carboxylated butadiene-acrylonitrile copolymer system. The properties obtained depended on the particular

counterion used and it was difficult to make generalizations; however, divalent ions appeared to be more effective in raising the modulus of the rubbers than monovalent ones. Some amine-neutralized carboxylated rubbers also were studied by Brown; they tended to exhibit substantial creep. Upon heating, these nonquaternary ammonium salt linkages formed amide linkages. Cooper has studied the melt-flow and stress-relaxation characteristics of copolymers of butadiene and acrylic or methacrylic acid neutralized to various degrees with different divalent metal cations. Significant differences were noted depending on which divalent cation was used (21). A divalent quaternary ammonium cation was included in these studies and was found to give properties similar to the divalent metal ions. Dolgoplosk has studied the mechanical properties of a variety of divalent counterions in a butadiene-styrene-methacrylic acid copolymer (22). These elastomers were neutralized with divalent metal oxides or hydroxides. Substantial differences in properties as a function of counterion were noted. In addition, there were appreciable differences depending on whether the oxide or hydroxide form of the neutralizing reagent was used. Apparently these latter differences were the result of different degrees of reaction completion. Although there is a large body of work on the effect of various counterions on carboxylated polymers, Holliday has observed in his review of ionic polymers that it is difficult to make generalizations about the magnitude and effect of ion type and valency on the melt flow of the ionomers (1).

Recently there has been considerable work on metal-neutralized sulfonated elastomers (23, 24, 25). The effect of various monovalent and divalent cations on physical properties of sulfonated ethylene-propylene-diene monomers (EPDM's) has been investigated and large differences have been found in both melt-flow rates and tensile properties, depending on the cation used.

A problem in interpreting the effect of different counterions on the mechanical properties of ionic polymers is the difficulty in evaluating how cation-anion interactions are changing from counterion to counterion. For example, metal counterions differ in ionicity as well as in size and valence, and they can have a partially covalent character. In contrast, quaternary phosphonium ions have a number of desirable characteristics that make them particularly attractive as model systems for the study of counterion effects. They have an essentially full positive charge on the heteroatom so partially covalent interactions, fractional charge transfer between the counterion and anion, and hydrogen bonding do not come into play. Furthermore, with quaternary ions there is no possibility of the tautomerism that can occur with nonquaternary ammonium or phosphonium counterions.

An important characteristic of quaternary phosphonium ions is that the substituents can be varied systematically over a wide range. Studies can then be made of such variables as substituent chain length, steric hindrance around the central charged atom, total amount of hydrocarbon present in the substituents, aromaticity and polarity of substituents, etc. (26). The effect of these substituent changes on the structure of the ionic associations that link ionomeric molecules as well as the resultant physical properties can be investigated. In addition, divalent and higher polyvalent quaternary ions of various structures can be prepared and can be either intercompared or compared with monovalent structures. For the polyvalent quaternary counterions, changes in the structure(s) of the chain(s) connecting the charged heteroatoms can be studied also. As compared with quaternary ammonium ions, the quaternary phosphonium ions generally exhibit higher thermal stability; and, there are some bulky groups that can be substituted readily onto phosphorus but not onto nitrogen. The four substituents in quaternary phosphonium ions limit how close anions can approach the charged heteroatom. The bulkier the substituents (especially in the immediate vicinity of the central charged atom) the more restricted is access to the central atom. This is in contrast to most metal ions that have no covalently attached substituents to restrict access of anions or polar molecules to their surfaces. Because of the large alkyl groups attached to most of the quaternary cations in this study, most of the ionic groupings in these ionomers probably contain only a few (perhaps only two) ion pairs. (With very highly crowded quaternary counterions, charge separation might even become a significant process in the breaking of cross-linkages.)

This chapter describes the effects of various quaternary phosphonium counterions on the melt-flow and tensile properties of a hydrocarbon elastomeric ionomer system. The ionomer is a sulfonated EPDM with roughly 1 mol % sulfonate groups. Quaternary phosphonium ions having a wide range of different alkyl structures were investigated. Comparisons were made between short- and long-chain alkyl substituents, different numbers of long-chain substituents on the phosphorus, and monovalent and polyvalent quaternary counterions. These comparisons show that the structure of the quaternary counterion has a very strong influence on the tensile and melt-flow properties of the elastomeric ionomer. An additional parameter studied briefly is the effect of water absorption on the physical properties of ionomers containing quaternary counterions.

Experimental

The sulfonated EPDM ionomers were prepared by neutralizing the free acid form of the polymer in solution with the specified quaternary phosphonium hydroxide. The free acid form of the sulfonated EPDM was prepared from a commercial EPDM—Vistalon 2504 manufactured by

Exxon Chemical Company. This EPDM has a Mooney viscosity ML(1 + 8 min) of about 42 at 100°C, an ethylene content of about 52 wt %, and an ethylidene norbornene content of about 5 wt %. The EPDM was sulfonated to a free acid form using acetyl sulfate in a manner similar to that described in U.S. Patent 3,836,511 (24, 27); it was then steam-stripped and dried on a two-roll mill at a temperature between 40° and 70°C. The free acid was stored under dry ice until used. The sulfonate content was determined by titration with thymol blue (1 g of thymol blue/L of ethanol, using the green to blue color change) just prior to neutralization, and is expressed as meq of acidity/100 g of polymer. The quaternary phosphonium hydroxides used were formed from the corresponding chlorides or bromides in an ion-exchange column. The tetrabutyl phosphonium chloride was manufactured by the Cincinnati Milacron Company; the other quaternary phosphonium halides were synthesized using the general methods described in Ref. 28, 29, and 30. Unless otherwise indicated, the substituents of the various quaternary phosphonium ions are all linear and unbranched.

The free acid form of the sulfonated EPDM is somewhat unstable, and is affected by drying procedures and conditions of storage. For these reasons intercomparisons ordinarily were restricted to samples derived from the same batch of free acid and neutralized on the same day. (Nevertheless, samples from different batches containing the same counterion had roughly comparable properties.) In the neutralization procedure the free acid form of the sulfonated polymer was dissolved in a mixture of 95% toluene and 5% methanol. Portions of the resulting solution were neutralized fully at room temperature with solutions of the various quaternary hydroxides. The neutralized sulfonated polymers were recovered from solution by either steam-stripping or by precipitation in methanol. Samples were dried in vacuum at 50°C for 3 days. For each ionomer sample, test pads of about 0.6 mm thickness were compression-molded at 160°C, using a 2-min preheat of the material and 2 min under pressure. At least 1 day was allowed to elapse after molding before the samples were tested. The samples were stored in dry air in the dark prior to testing. Microtensile dumbbells having a test region 2.54 mm in width and about 12.7 mm in length were cut from the pads, and tensile measurements were made on an Instron TM table model apparatus at a pulling speed of 51 mm/min. For the measurements at elevated temperatures a 3-min waiting period in the test oven was used prior to pulling to enable the samples to equilibrate thermally. Most of the tensile measurements were made at 100°C because these properties were expected to depend more on the ionic interactions and less on imperfections and fabricating techniques at this temperature than at room temperature. Melt-flow rate measurements were made using the melt index instrument described in ASTM D 1238, at 190°C and a 12.5-kg load. Flow rates were measured electronically as probe displacement per minute and these results were converted to g/10 min using a conversion factor.

Results and Discussion

Data on the 100°C tensile properties of a sulfonated EPDM neutralized with various quaternary tetralkyl phosphonium ions are presented in

Table I. Tensile Properties at 100°C of a Sulfonated EPDM^a Neutralized with Quaternary Phosphonium Ions

Sample No.	Quaternary Phosphonium Ion	Tensile Strength ^b (KPa)	Initial Modulus (KPa)
1	(CH ₃)P ⁺ (C ₂ H ₅) ₃	540	1700
2	(CH ₃)P ⁺ (C ₆ H ₁₃) ₃	300	1100
3	(CH ₃)P ⁺ (C ₈ H ₁₇) ₃	290	970
4	(CH ₃)P ⁺ (C ₁₂ H ₂₅) ₃	260	940
5	(C ₁₈ H ₃₇)P ⁺ (C ₂ H ₅) ₃	300	1000
6	(C ₂₂ H ₄₅)P ⁺ (C ₂ H ₅) ₃	290	1000

^a Before neutralization—31 meq of acid/100 g.

^b Maximum tensile strength, not strength at break since the samples yielded.

Table I. These data demonstrate the effect of increasing the *n*-alkyl chain lengths of substituents of a quaternary counterion. Two series of chain length changes are shown in Table I. The first series consists of Samples 1, 2, 3, and 4, where a methyl substituent is held constant and the other three equal-length chains increase from 2 to 12 carbons in three steps. The decrease in tensile strength and modulus with increased chain length is evident. Of particular interest is the substantial decrease in tensile properties when the three equal-length chains increase from 2 to 6 carbons, as contrasted to the quite modest property changes when the chain lengths increase from 6 to 8 and then to 12 carbons in Samples 2, 3, and 4 of Table I. This indicates that the atoms of the chain that are closest to the central charged (phosphorus) atom are most important in determining the properties of the materials. Presumably these chain atoms are most effective in preventing close approach of anions because of their limited ability to move aside. This also suggests that substituents with branched or other bulky structures attached near the central charged atom will have a greater effect on physical properties than straight chain structures. On the other hand, atoms that are farther out on a chain have greater freedom of movement so they can move aside more readily to accommodate anions that are attracted to the central charged atom. However, the resultant restrictions on chain movement will decrease entropy.

Samples 1, 5, and 6 in Table I illustrate a different series of chain-length increases. In this case the three ethyl substituents remain constant and the fourth substituent changes from methyl to octadecyl and then to behenyl. The relatively small effect on tensile properties of carbon atoms far out on the chain is again evident in comparing Samples 5 and 6.

Table II presents another group of quaternary tetralkyl phosphonium counterions that were used to neutralize a different batch of sulfonated EPDM. In this table melt-flow as well as tensile data are included. The

samples in Table II illustrate again the decrease in tensile properties as the chain length of *n*-alkyl substituents increases; also, an accompanying increase in melt-flow rate (improved processability) is observed. The effect of increasing the number of long-chain substituents is illustrated in Table II with Samples 8, 9, and 10. This series of samples shows the effect of an increase in the number of long (18-carbon) chains from zero to two while keeping the remaining short chains of constant (2-carbon) length. Each increase in the number of long-chain substituents causes a major weakening of the physical properties. The addition of the second long chain has a substantially greater impact than did addition of the first long chain—especially on the melt-flow rate. This difference in impact is probably caused by the particularly crowded condition around the central charged atom after addition of the second long chain. That is, while the presence of one long chain increases crowding and reduces access of anions to the charged central atom of the quaternary ion, the second long chain even further diminishes what space is still available near the central atom. This results in a much higher degree of steric hindrance in the region near the central atom as well as making the close approach of anions much less favorable entropically. Of course, the magnitude of the effects of adding long chains will depend strongly on the lengths of the short chains originally present and on the lengths of the added long chains. Increasing the lengths of the original short chains will tend to diminish the effect of the added chain lengths.

A number of systematic comparisons can be made with the data of Table II as follows (in terms of sample numbers): 8 to 7, 8 to 13, 11 to 9 to 14, and 12 to 13. All of these comparisons support the concepts discussed previously. Of particular interest is the change from Sample

Table II. Physical Properties of a Sulfonated EPDM^a Neutralized with Various Quaternary Phosphonium Ions

Sample No.	Quaternary Phosphonium Ion	Tensile Properties (100°C)		Melt-Flow Rate (150°C, 12.5 kg, g/10 min)
		Strength ^b (KPa)	Initial Modulus (KPa)	
7	(C ₄ H ₉) ₄ P ⁺	300	1000	0.090
8	(C ₂ H ₅) ₄ P ⁺	520	1500	0.014
9	(C ₂ H ₅) ₃ P ⁺ C ₁₈ H ₃₇	390	1250	0.030
10	(C ₂ H ₅) ₂ P ⁺ (C ₁₈ H ₃₇) ₂	180	700	0.22
11	(CH ₃) ₃ P ⁺ C ₁₈ H ₃₇	550	1500	0.010
12	(C ₈ H ₁₇) ₃ P ⁺ CH ₃	310	1100	0.080
13	(C ₈ H ₁₇) ₃ P ⁺ C ₂ H ₅	210	900	0.10
14	[(CH ₃) ₂ CHCH ₂] ₃ P ⁺ C ₁₈ H ₃₇	185	750	0.20

^a Before neutralization—21 meq of acid/100 g.

^b Maximum tensile strength, not strength at break since the samples yielded.

12 to 13 where only a single carbon atom out of a total of 25 was added. However, it was added in a crucial position close to the central charged atom, so it has a major effect on limiting the close approach of anions to the charged atom. These comparisons make it clear that the total amount of hydrocarbon in the substituents (or the molecular weight of the quaternary counterion) is not a reliable indicator of the physical properties to be expected from a counterion. A comparison between Samples 7 and 11 in Table II also illustrates this point particularly well. Although the counterion of Sample 11 has a larger total amount of hydrocarbon in the substituents, this material is much stronger and has a far lower melt-flow rate than Sample 7.

In considering the effect of the counterion on the physical properties of an ionomer, it should be emphasized that the strength of an ionic cross-linkage depends not only on the structure of a single counterion, but also on the interaction between counterion-anion ion pairs (or even more complex groupings). Thus, the anion from a first ion pair, in attempting to closely approach the cation of a second ion pair, must contend not only with the substituents of that quaternary ion, but also with the anion in that second ion pair. At the same time, this second anion is trying to minimize its distance from its own associated counterion, and thereby is also dragging its covalently attached polymer backbone chain close to the central charged atom. In addition, the first anion must contend with the substituents of its quaternary counterion in the first ion pair to which it is closely held as well as with its appended polymer backbone chain which it must drag along. This greatly crowded situation is especially severe for the ionomer systems described in this chapter since the sulfonate group is a large anion and is attached to the polymer backbone chain through a bulky ethylidene norbornene-derived structure.

Tables I and II dealt only with monovalent quaternary counterions; Table III compares some divalent quaternary counterions with monovalent counterions. In Table III, the free acid sulfonated EPDM used to prepare Sample 15 was from a different preparation than that used for the other samples of this table. However, samples having the same counterion that were prepared from these two different batches of free acid had roughly comparable properties, so semiquantitative comparisons are justified. The first point to note in Table III is that one of the divalent counterion samples, 16, containing the tetradecamethylene bistritylphosphonium ion, has greater tensile properties and a lower melt-flow rate than any of the three monovalent samples. The other divalent sample, 15, containing the ethylene bistritylphosphonium ion, has much lower tensile properties as well as a much higher melt-flow rate than any of the monovalent samples. That is, one of the samples containing a divalent counterion (Sample 16) is much tougher than any of the monovalent samples in

Table III. Comparison of Divalent and Monovalent Quaternary Phosphonium Counterions in a Sulfonated EPDM^a

Sample No.	Quaternary Phosphonium Ion	Tensile Properties (100°C)		Melt-Flow Rate (150°C, 12.5 kg, g/10 min)
		Maximum Strength (KPa)	Initial Modulus (KPa)	
12	(C ₈ H ₁₇) ₃ P ⁺ CH ₃	310	1100	0.080
15	(C ₈ H ₁₇) ₃ P ⁺ CH ₂ CH ₂ P ⁺ (C ₈ H ₁₇) ₃	160 ^b	560 ^b	0.25 ^b
8	(C ₂ H ₅) ₃ P ⁺ C ₂ H ₅	520	1500	0.014
16	(C ₂ H ₅) ₃ P ⁺ (CH ₂) ₁₄ P ⁺ (C ₂ H ₅) ₃	700	1700	0.003
9	(C ₂ H ₅) ₃ P ⁺ C ₁₈ H ₃₇	390	1250	0.030

^a Before neutralization acid contents were as follows: Samples 12, 8, 16, and 9—21 meq/100 g; Sample 15—28 meq/100 g.

^b A different sample of free acid was used to prepare Sample 15; see superscript (a) above for its acid content.

Table III, while the sample containing the other divalent counterion (Sample 15) is much weaker. Therefore, blanket statements about the relative strength of ionomer samples neutralized with divalent or monovalent counterions cannot be made; rather, more detailed considerations are necessary. Polyvalent and monovalent counterions can be compared more meaningfully by considering polyvalent quaternary counterions made by attaching two or more monovalent quaternary counterions. In particular, monovalent counterion structures corresponding to a given polyvalent quaternary ion can be defined as those structures produced by breaking the chain connecting two charged atoms of the polyvalent ion as near as possible to its middle, and terminating the resulting radicals with hydrogen atoms. Applying this definition, Sample 12 contains the monovalent methyltrioctylphosphonium counterion corresponding to the divalent ethylene bistrioctylphosphonium counterion of Sample 15 in Table III. In this comparison of corresponding structures, it is seen from Table III that the divalent counterion yields a far weaker material than the corresponding monovalent counterion. Apparently this weakness is caused by the short connecting chain between the two phosphorus atoms; it forces the six relatively long (8-carbon) substituents from the two parts of the divalent ion to remain in close proximity in the region around the two connected central atoms. This causes severe crowding and steric hindrance in the vicinity of these charged atoms. In addition, it apparently limits the closeness of approach of anions to the charged atoms to a substantially greater degree than did the substituents of the corresponding monovalent ion.

Sample 16 contains the other divalent quaternary phosphonium counterion in Table III, the tetradecamethylene bistriethylphosphonium

ion; the corresponding monovalent ion would be the triethylheptylphosphonium ion. This material was not available; however, data for a sample containing the tetraethylphosphonium counterion are given in Table III. From the previous discussion it is clear that a sample containing a given alkyl-substituted quaternary counterion will be stronger than a sample containing the same quaternary counterion with one or more of the alkyl substituents lengthened. Therefore, the sample containing the tetraethylphosphonium counterion (Sample 8) will be substantially stronger than a sample containing the triethylheptylphosphonium counterion. So, by comparing Samples 16 and 8 it is clear that the divalent Sample 16 containing the tetradecamethylene bistriethylphosphonium counterion would be far stronger and have a much lower melt-flow rate than the material containing the triethylheptylphosphonium counterion. This result, when considered in view of the previous divalent-monovalent comparison, suggests that once the connecting chain of a divalent ion becomes sufficiently long, the groups of substituents from the different charged central atoms are no longer constrained to remain close, steric hindrance is reduced and the divalent sample is substantially stronger than the sample containing the corresponding monovalent counterion. The stronger physical cross-linkages for the divalent counterions probably occur primarily because a single counterion-anion ion pair cannot leave an ionic cross-linkage (assuming monovalent anions such as in the sulfonate case) because of the covalently bonded connecting chain between the two charged heteroatoms. Relaxation of a cross-linkage can occur by the divalent counterion leaving a cross-link region with a single anion; however, in this case charge separation occurs which requires high energy. Relaxation also can occur if two (or more) counterions with their four anions (attached to their polymer chains) come together, and the divalent counterions exchange one (and only one) anion partner before separating again. There may be an activation energy for this exchange process if it requires movement of an anion away from the sterically crowded vicinity of its polyvalent counterion before it can be replaced by another ion. In any case, the more restricted and complicated mode of flow for systems containing polyvalent counterions (with sufficiently long connecting chains) will tend to decrease melt-flow rates as compared to a system with the corresponding monovalent counterion. However, it should be cautioned that if potentially ionic impurities are present in a material, some polyvalent counterions might be converted into monovalent groupings.

These results indicate that it is possible for an ionomer containing a selected monovalent quaternary counterion to be stronger than an ionomer containing one of its corresponding divalent counterions, but at the same time be weaker than another. This is because a monovalent ion can have several radically different corresponding divalent ions depending on which

substituent is used in forming the divalent ion. For example, whereas the divalent ethylene bistriethylphosphonium counterion of the weak Sample 15 of Table III is a corresponding structure to the monovalent methyltriethylphosphonium ion of Sample 12, the other divalent ion that corresponds to Sample 12 is the hexadecamethylene bismethyldioctylphosphonium ion $(C_8H_{17})_2CH_3P^+(CH_2)_{16}P^+CH_3(C_8H_{17})_2$. This latter divalent counterion would be expected to give a much stronger material than Sample 12.

Table IV presents room-temperature tensile properties of some sulfonated EPDM's neutralized with both monovalent and divalent quaternary phosphonium ions. A wide range of properties is obtained with both types of ions. The relative order of strengths and stiffnesses of the samples containing the various quaternary counterions at room temperature is similar to that observed in the previous tensile data at 100°C in Tables I, II, and III. The tensile strengths for the stronger materials in Table IV are roughly 20 times the strengths at 100°C; however, the two weakest materials, Samples 19 and 20, are less than ten times as strong at room temperature than at 100°C. The tensile measurements at 100°C were preferred because the properties were expected to be more representative of the characters of the quaternary counterions and less dependent on sample perfection and, possibly, crystallinity (though, the EPDM used, Vistalon 2504, is not thought to have significant crystallinity). In addition to the quaternary phosphonium-neutralized samples in Table IV, a sodium-neutralized sample is included for comparison. The 100% modulus of the sodium-neutralized sample is higher than that for any of the quaternary phosphonium-neutralized samples in Table IV. At room temperature the tensile strength of the sodium-neutralized sample is low; however, this is not because the material is inherently weak, but because

Table IV. Tensile Properties at Room Temperature for Sulfonated EPDM's^a Neutralized with Various Quaternary Phosphonium Ions

Sample No.	Quaternary Phosphonium Ion	Tensile Strength (KPa)	Elongation (%)	100% Modulus (KPa)
12	$(C_8H_{17})_3P^+CH_3$	5900	620	1100
11	$(CH_3)_3P^+C_{18}H_{37}$	14500	585	1600
16	$(C_2H_5)_3P^+(CH_2)_{14}P^+(C_2H_5)_3$	13800	575	1650
18	$(C_2H_5)_3P^+C_{18}H_{37}$	8400	700	1400
20	$(C_8H_{17})_3P^+CH_2CH_2P^+(C_8H_{17})_3$	1100	820	700
19	$[(CH_3)_2CHCH_2]_3P^+C_{18}H_{37}$	700	> 1,000	690
21	Na ⁺	6200	200	3200

^a Before neutralization acid contents were as follows: Samples 12, 11, 16, and 21—21 meq/100 g; Samples 18, 19, and 20—28 meq/100 g.

Table V. Effect of Water Uptake on a Sulfonated EPDM^a Neutralized with a Quaternary Phosphonium Ion

Sample No.	Quaternary Phosphonium Ion	Treatment of Sample	Water Uptake ^b (Wt %)	Tensile Strength ^c (100°C, KPa)
17	(C ₂ H ₅) ₃ P ⁺ C ₁₈ H ₃₇	original dry ^d	0	290
		in water 23°C, 1 day	3.9	410
		in water 23°C, 12 days	8.1	520
		redried ^e	-0.2	250

^a Before neutralization—28 meq of acid/100 g.

^b During 3-min preheat in tensile test oven samples lost about one half of the absorbed water.

^c Maximum tensile strength, not strength at break since the samples yielded.

^d Dried in vacuum 3 days at 48°C.

^e Redried in vacuum 3 days at 47°C.

it is so intractable that it does not mold well, resulting in breakage at very low elongation. The poor processability is indicated by the poor melt-flow rate (190°C and 12.5 kg loading) which was too low to measure (less than 0.0004 g/10 min). At elevated temperatures the sodium-neutralized sample has better tensile strength than most quaternary phosphonium-neutralized samples.

The absorption of water by sulfonated EPDM causes a decrease in tensile properties for some quaternary phosphonium counterions, while with others, increases in tensile properties have been observed. Table V shows data for a triethyloctadecylphosphonium counterion; it is seen that water uptake is accompanied by substantially increased tensile strength. To check that the water uptake was not causing irreversible changes, the sample was redried and tensile strength measured after the water exposure. Recovery was approximately to the original dry value. A number of studies involving metal counterions have shown that the presence of water in an ionomer weakens the ionic cross-linkages (5, 31). However, for low concentrations where the water does not constitute a mobile continuous phase, there seems to be no fundamental requirement that water must have a weakening effect. For example, for isolated, electrostatically bonded positive and negative ions, the addition of a small molecule having a dipole moment can increase the energy required to remove either of the charged ions from the association. As another example, the presence of water molecules in some hydrated crystals results in highly stable, rigid structures.

Conclusions

The structures of quaternary phosphonium counterions have a major impact on the physical properties of sulfonated EPDM elastomeric iono-

mers. The tensile properties decrease and the melt-flow increases with increasing length of *n*-alkyl substituents and with an increasing number of higher-alkyl substituents on the phosphorus. Substituent atoms near the central charged atom have a greater effect on physical properties than atoms farther out on the chain. Apparently this is attributable to their greater contribution to the steric crowding around the central charged atom of the quaternary counterion. The relative strengths of divalent and monovalent counterions of corresponding structure depend on the specific structures involved. A long connecting chain in a diphosphonium counterion results in a relatively strong ionomer. Water uptake can strengthen as well as weaken a sulfonated EPDM ionomer depending on the structure of the quaternary counterion.

Acknowledgments

The authors gratefully acknowledge the assistance of M. S. Beam and T. G. Jermansen in the laboratory work. H. S. Makowski and N. G. Thame kindly provided the free acid sulfonated polymers.

Literature Cited

1. "Ionic Polymers"; Holliday, L., Ed.; Applied Science Publishers: London, 1975.
2. Eisenberg, A.; King, M. "Ion-Containing Polymers"; Academic: New York, 1977.
3. Rees, R. W.; Vaughan, D. J. *Polym. Prepr. Am. Chem. Soc., Div. Polym. Chem.* **1965**, *6*, 287.
4. *Ibid.*, p. 296.
5. Bonotto, S.; Bonner, E. F. *Macromolecules* **1968**, *1*, 510.
6. Fitzgerald, W. E.; Nielsen, L. E. *Proc. R. Soc. (London)* **1964**, *A282*, 137.
7. Eisenberg, A.; Takahashi, K. *J. Non-Cryst. Solids* **1970**, *3*, 279.
8. Navratil, M.; Eisenberg, A. *Macromolecules* **1974**, *7*, 84.
9. Matsuura, H.; Eisenberg, A. *J. Polym. Sci., Polym. Phys. Ed.* **1976**, *14*, 773.
10. Eisenberg, A.; Matsuura, H.; Yokoyama, T. *J. Polym. Sci., Polym. Phys. Ed.* **1971**, *9*, 2131.
11. Eisenberg, A.; Farb, H.; Cool, L. G. *J. Polym. Sci., Polym. Phys. Ed.* **1966**, *4*, 855.
12. Eisenberg, A. *Adv. Polym. Sci.* **1967**, *5*, 59.
13. Rees, R. W. *Polym. Prepr. Am. Chem. Soc., Div. Polym. Chem.* **1973**, *14*, 796.
14. MacKnight, W. J.; Kajiyama, T.; McKenna, L. *Polym. Eng. Sci.* **1968**, *8*, 267.
15. Phillips, P. J.; MacKnight, W. J. *J. Polym. Sci., Polym. Phys. Ed.* **1970**, *8*, 727.
16. Hoover, M. F. *Polym. Prepr. Am. Chem. Soc., Div. Polym. Chem.* **1969**, *10*, 908.
17. Rembaum, A.; Baumgartner, W.; Eisenberg, A. *J. Polym. Sci., Polym. Lett. Ed.* **1968**, *6*, 159.
18. Hadek, V.; Noguchi, H.; Rembaum, A. *Polym. Prepr. Am. Chem. Soc., Div. Polym. Chem.* **1971**, *12*, 90.
19. Brown, H. P. *Rubber Chem. Tech.* **1957**, *30*, 1347.

20. Brown, H. P. *Rubber Chem. Tech.* **1963**, *36*, 931.
21. Cooper, W. *J. Polym. Sci.* **1958**, *28*, 195.
22. Dolgoplosk, B. A.; Tinyakova, E. I.; Reikh, V. N.; Zhuravleva, T. G.; Belonovskaya, G. P. *Rubber Chem. Tech.* **1959**, *32*, 321.
23. Brenner, D.; Lundberg, R. D. *J. Cell. Plast.* **1977**, *13*, 270.
24. Makowski, H. S.; Lundberg, R. D.; Westerman, L.; Bock, J. *Polym. Prepr. Am. Chem. Soc., Div. Polym. Chem.* **1978**, *19*, 2.
25. Lundberg, R. D.; Makowski, H. S. *Polym. Prepr. Am. Chem. Soc., Div. Polym. Chem.* **1978**, *19*, 2.
26. Brenner, D.; Oswald, A. A. U. S. Patent 4 102 876, 1978.
27. O'Farrell, C. P.; Serniuk, G. E. U. S. Patent 3 836 511, 1974.
28. "Organic Phosphorus Compounds"; Kosolapoff, G. M., Maier, L., Eds.; Wiley: New York, 1972; Vol. 2.
29. Kosolapoff, G. M. "Organic Phosphorus Compounds"; Wiley: New York, 1950.
30. Oswald, A. A. U. S. Patent 3 998 754, 1976.
31. Longworth, R.; Vaughan, D. J. *Polym. Prepr. Am. Chem. Soc., Div. Polym. Chem.* **1968**, *9*, 525.

RECEIVED October 16, 1978.

The Dual Plasticization of Sulfonated Polystyrene Ionomer

R. D. LUNDBERG, H. S. MAKOWSKI, and L. WESTERMAN

Corporate Pioneering Research, Exxon Research and Engineering Company,
P.O. Box 45, Linden, NJ 07036

A series of lightly sulfonated polystyrene ionomers was prepared with levels of sulfonic acid ranging from about 1 to 5 mol %. When neutralized with metal salts the resulting ionomers are strongly physically cross-linked at sulfonate contents greater than 1 mol %. While the sulfonated polystyrene ionomers possess extremely high melt viscosities, the incorporation of suitable polar plasticizers markedly lowers the melt viscosities by selectively relaxing the ionic associations. Alternatively, plasticizers that primarily solvate the polystyrene backbone provide a flexible sulfonated polystyrene not unlike plasticized polyvinylchloride. Those factors affecting the physical properties of the resultant plasticized sulfonated polystyrenes include the sulfonate level, the neutralizing metal cation, and the type and level of plasticizer used.

Previous studies have shown that the introduction of metal carboxylate groups into a thermoplastic, such as polystyrene (PS), provides strong ionic associations that result in phase-separated polymer systems (1). An alternate approach to PS-based ionomers is via PS sulfonation and neutralization of the polymer sulfonic acid (2,3). Other studies (4) have shown that sulfonated-based ionomers possess a degree of ionic aggregation that appears stronger and more persistent to higher temperatures than that observed for carboxylate ionomers. This study is concerned with the preparation of PS-based sulfonate ionomers, and a description of how the strong ionic interactions can be diminished by appropriate plasticization approaches. In addition, it will be shown that

the polymer backbone can be selectively plasticized, relatively independently of the ionic groups. Finally, it will be shown that by effectively combining both plasticization approaches, a flexible polymer composition similar to plasticized polyvinyl chloride (PVC) can be prepared.

Experimental

The preparation of sulfonated polystyrene (S-PS) has been described in other publications and in issued U.S. patents (2, 3). The melt viscosities described were measured in a melt index rheometer especially equipped to measure very high melt viscosities under conditions of constant shear stress (generally $\tau = 2.1 \times 10^5$ dyn/cm² at 220°C, or 1.1×10^5 dyn/cm² at 250°C).

In those cases where plasticizers were added, this was generally effected by adding polymer and plasticizers to toluene/alcohol mixtures, evaporating the solvent, and finally drying the plasticized polymer at 80°C under vacuum. Alternately, the polymer-plasticizer mixture could be prepared by direct addition of the plasticizer to the powdered base resin. Stress-strain measurements were made on microdumbbells obtained from compression-molded pads of .020 mil thickness. Tensile measurements were conducted at strain rates of 1000%/min.

Results and Discussion

The melt viscosity of the S-PS, in this case as the sodium salt, markedly depends on the degree of neutralization. Figure 1 illustrates the dependence of melt viscosity on the level of neutralization for one sample of polymer sulfonic acid. In this case the melt viscosity measurements were conducted at 250°C, and it is seen that the melt viscosity increases monotonically from about 0 to 90% neutralization. In this region the data are consistent with those reported previously for ethylene-acrylic acid copolymers and their corresponding sodium salts (5). However, in the region of 95–100% neutralization, it is seen that there is a marked rise in the melt viscosity. Based on these and other data, it is apparent that the melt viscosity of fully neutralized S-PS is extremely high. These samples have been shown to be free of covalent cross-linking since they are completely soluble in suitable mixed solvents (6). Therefore, the high melt viscosity of these sulfonate ionomers is a consequence of the strong ionic association of these materials (2, 3, 4).

The general characteristics of these lightly sulfonated PS's containing from about 1 to 5 mol % sodium sulfonate can be summarized as follows. These systems can be compression molded with difficulty at temperatures greater than or equal to 250°C. The resulting molded plaques are clear, brittle, and not markedly different from PS at ambient temperatures. However, an examination of the stiffness modulus as a function of temperature shows marked differences from that of PS as shown in Figure 2. These measurements were conducted on a sample of S-PS containing 2.5 mol % sodium sulfonate using a rheovibron at a frequency of 11 Hz.

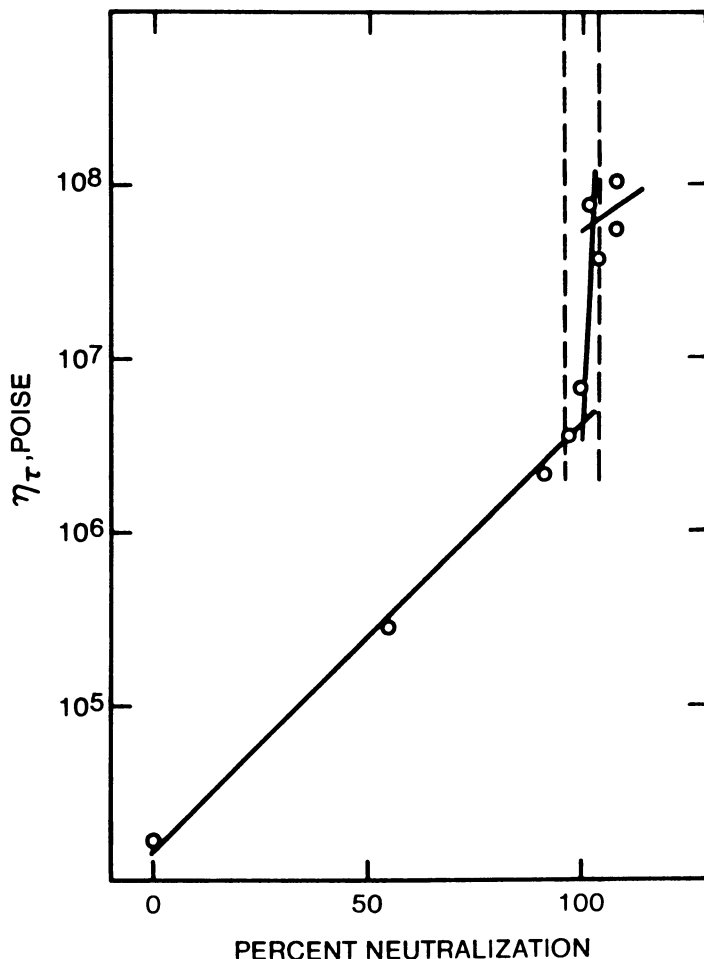


Figure 1. Melt viscosity of S-PS as a function of % neutralization (average meq NaOH to reach endpoint: ± 0.004 or 1.5%; melt index rheometer: 250°C; $-\text{SO}_3\text{Na}$ content: 2.5 mol %)

It is evident that under these conditions a significant increase in the glass transition of the polymer backbone over that of PS is observed, but more importantly, a substantial rubbery plateau is observed which extends to temperatures above 250°C. Clearly this rubbery plateau can be attributed exclusively to ionic association. The magnitude of the increase in glass transition and the actual modulus of the plateau depends on the level of metal sulfonate groups incorporated in the PS chain.

The melt viscosities of these systems are sufficiently high that the conventional melt processing techniques are not viable at metal sulfonate levels above about 1 mol %. Therefore, studies were conducted using various types of diluents or plasticizers to lower the melt viscosities. The

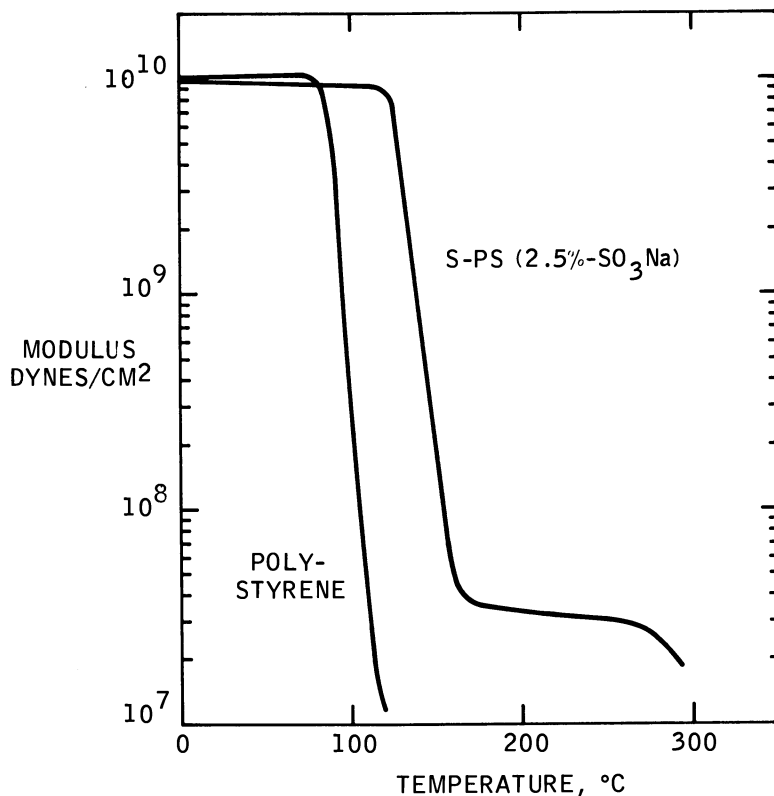


Figure 2. Modulus-temperature relationship for PS and S-PS

effect of diluents on polymer viscosity has been well explored. The viscosity of conventional polymers is lowered by the incorporation of a diluent; this is assumed to arise as a result of the increase in free volume and from the decrease in polymer segment concentration attributable to dilution. This increase in free volume is accompanied by a depression in the glass transition temperature of the mixture. Based on these concepts, it is possible through theory to predict the amount of viscosity lowering that will occur by adding a diluent to a given polymer (7). However, in the case of ionically cross-linked polymers such as sodium salts of lightly sulfonated PS, there is an additional complicating feature caused by intermolecular interactions between the sodium sulfonate groups.

Therefore, one can expect two types of plasticizing action; the more conventional type known in the prior art where a viscosity reduction arises from free volume effects (backbone plasticizers) and a second that acts ideally by diminishing the interchain association of the ionic groups on the polymer chain (ionic domain plasticizers). One would

expect this latter class of plasticizers to be much more effective in viscosity depression for ionomers than the former class. The melt viscosities of a series of plasticized PS's were measured in order to differentiate quantitatively these two plasticizing modes.

Diocetyl phthalate (DOP) was used as a representative of the class of backbone plasticizers and glycerol as a plasticizer for ionic groups. Both systems were studied with S-PS (sodium salt) as the base polymer in which the base resin had a sodium sulfonate content of 1.78 mol %. Various quantities of the two aforementioned diluents were added to this resin.

The results of viscosity measurements made at 220°C on these polymer-diluent mixtures are shown in Figure 3, where the viscosity measured at a constant shear stress is plotted against the weight fraction

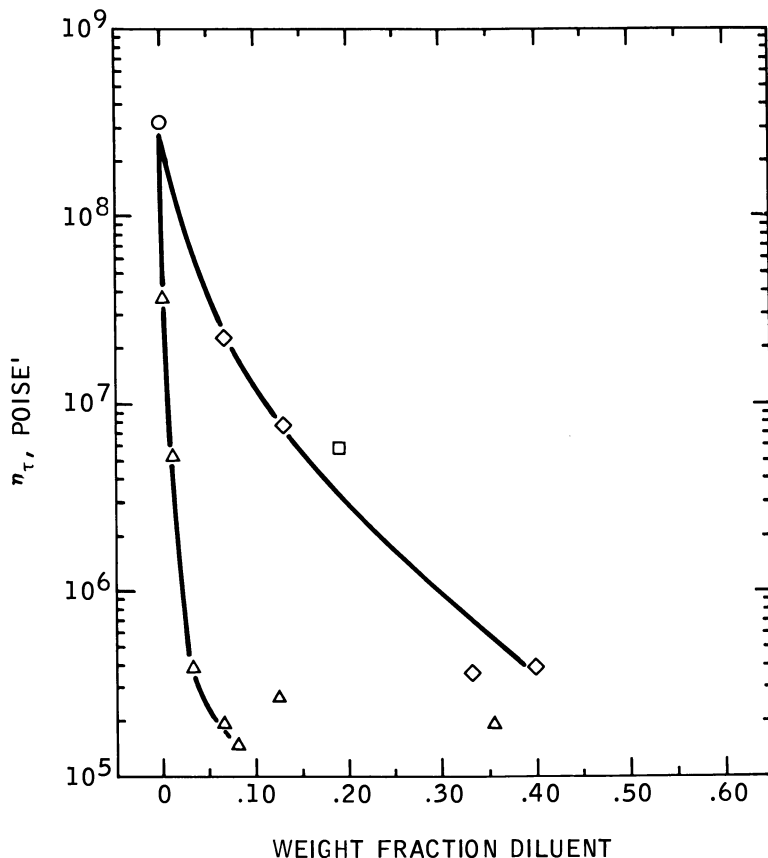


Figure 3. Melt viscosity as a function of weight fraction of diluent (melt index rheometer data at 220°C; $\tau = 2.05 \times 10^5 \text{ dyn/cm}^2$; 1" L \times 0.05" D capacity; $-\text{SO}_3\text{Na}$ content = 1.78 mol %. (○) base resin; (◇) base resin + DOP; (□) base resin + DEP; (△) base resin + glycerol.

of the diluent added to the base resin. It is seen that the viscosity for the base resin is extremely high (3.2×10^8 poise). Upon the addition of DOP the viscosity is seen to drop off, reaching a level of about 4×10^5 poise at 40 wt % DOP. In contrast, only 3.5 wt % glycerol is required to drop the viscosity to the same extent. Although glycerol is very effective in reducing the viscosity of the base resin, its effect terminates in the vicinity of about 10 wt %, presumably because of the incompatibility of glycerol with the polymer above this level.

Clearly, the behavior of glycerol is different from that of a conventional plasticizer (DOP) and not in accord with published theory (7). As a further demonstration of the different action of these two types of plasticizers the effect of plasticizer level on the PS glass transition was measured using differential scanning calorimetry (DSC) as shown in Figure 4. In these experiments, a series of plasticized S-PS samples with a single base resin (sodium sulfonate level of 1.78 mol %) was prepared containing DOP or glycerol at various levels. The glass transitions (DSC at $10^\circ\text{C}/\text{min}$) and the melt viscosities were measured at 220°C . By plotting the log of melt viscosity vs. polymer glass transition two essentially linear relationships are obtained. It is readily apparent that the DOP-plasticized samples exhibit a marked decrease in glass transition with a relatively moderate decrease in melt viscosity. However, in the case of the glycerol-plasticized systems, the glass transition reflective of the polymer backbone is decreased from about 118°C to about 100°C , while the melt viscosity decreases by a factor of nearly 10^4 . The reduction of the glass transition with glycerol as plasticizer is good evidence that the ionic associations have been markedly reduced, thereby resulting in a T_g similar to that of PS. It is clear from these data that DOP is solvating the polymer backbone while glycerol, having virtually no plasticizing effect on the polymer backbone, primarily affects the ionic associations.

Based on this analysis one would expect plasticizers of different polarity to display varying degrees of effectiveness in plasticizing the backbone or the ionic associations. The effect of several representative plasticizers (DOP, dibutyl phthalate (DBP), and glycerol) on a different sample of S-PS is shown in Table I.

It is seen that DOP is modestly effective in lowering melt viscosity, but very effective in lowering the glass transition. Glycerol, as expected, is very effective in lowering melt viscosity, but has little effect on the glass transition. DBP, on the other hand, is moderately effective in lowering both melt viscosity and the glass transition.

It should now be possible, in principle, to plasticize S-PS having an appropriate metal sulfonate level to achieve a flexible thermoplastic composition similar to plasticized PVC. Previous attempts to do this with PS have led essentially to a viscous fluid of little strength attributable to the lack of a physical network to hold the system together. Some years ago

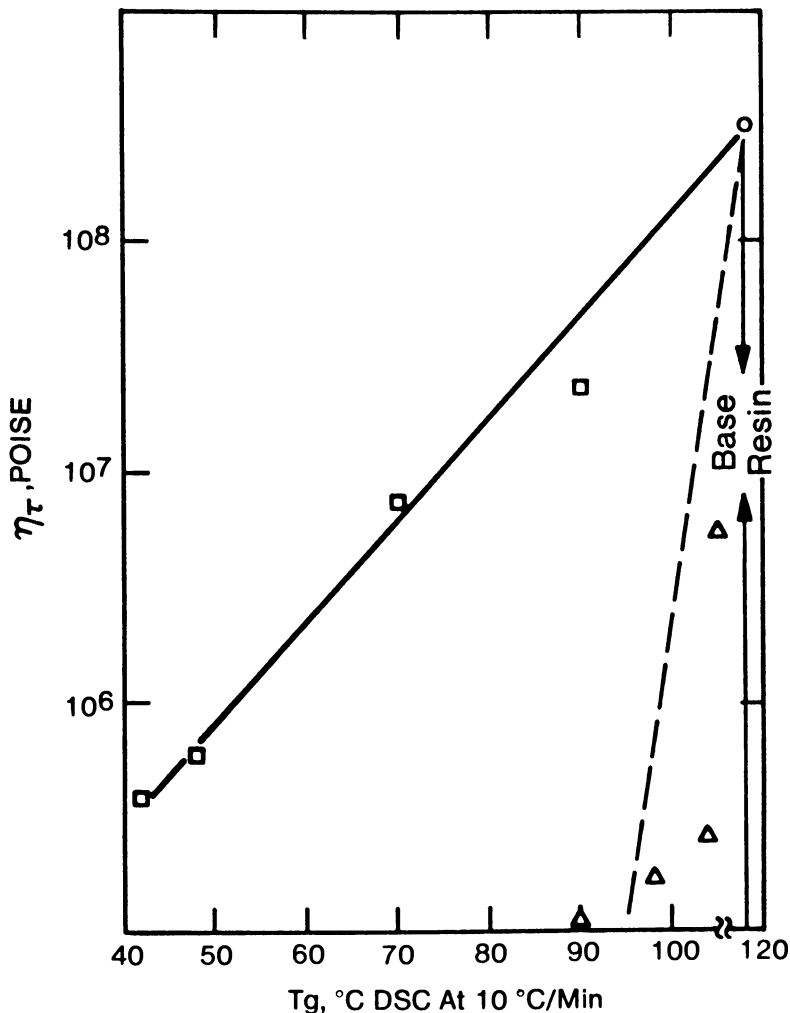


Figure 4. Melt viscosity-glass transition relationships for plasticized S-PS (1.78 mol %) samples based on various levels of DOP and glycerol ($\tau = 2 \times 10^5$ dyn/cm²; 220°C; 1" × 0.05" capillary; (□) DOP; (Δ) glycerol)

Erdi and Morawetz (8) attempted to overcome this problem by incorporating ionic groups into PS in the form of metal carboxylate-containing comonomers. When they plasticized the PS phase in these systems, they observed only a very weak physically bonded network of no substantial strength. However, the availability of these metal-sulfonated ionomers coupled with the inherently stronger associations of the metal sulfonates offer a more attractive system to test this hypothesis. Therefore, plasticized S-PS samples of varying sulfonate level were blended with DOP

Table I. Experimental and Predicted Viscosity Values for PS Sodium Sulfonate-Diluent Mixtures^a

Diluent	Wt Fraction Polymer	Vol Fraction Polymer (220°C)	T _g (°C)	Predicted ^d (Poise)	Measured (Poise)
None	1.0000	1.0000	116	—	6.4 × 10 ⁸
DOP ^b	0.7143	0.6885	-7.5	1.8 × 10 ⁵	1.6 × 10 ⁵
DOP ^c	0.7143	0.6885	-11.0	1.7 × 10 ⁵	1.1 × 10 ⁵
DBP ^c	0.7692	0.7545	20	6.1 × 10 ⁵	1.4 × 10 ⁴
DBP ^c	0.8333	0.8217	31	1.5 × 10 ⁶	1.0 × 10 ⁵
DBP ^c	0.9090	0.9020	52	6.0 × 10 ⁶	9.4 × 10 ⁵
Glycerol ^b	0.9091	0.9178	106	1.3 × 10 ⁸	2.5 × 10 ⁵

^a At 220°C and $\tau = 4.1 \times 10^5$ dyn/cm²; base resin = 1.48 mol % SO₃ Na.

^b Prepared by dissolving both diluent and polymer in benzene-methanol followed by evaporation.

^c Prepared by adding diluent directly to polymer, blending, and milling.

^d Calculation based on Ref. 10.

and DBP, compression molded, and stress-strain characteristics determined, as shown in Figure 5. For comparison the stress-strain characteristics of plasticized PVC are shown as well. It is seen that the stress-strain characteristics are quite similar for the samples shown. While the plasticization of S-PS with phthalate plasticizers can result in a flexible composition similar in some respects to plasticized PVC, there are significant differences. For example, S-PS at sufficiently high sulfonate levels and a strongly associating cation can create such a tight ionic network that only relatively low levels of a nonpolar backbone plasticizer

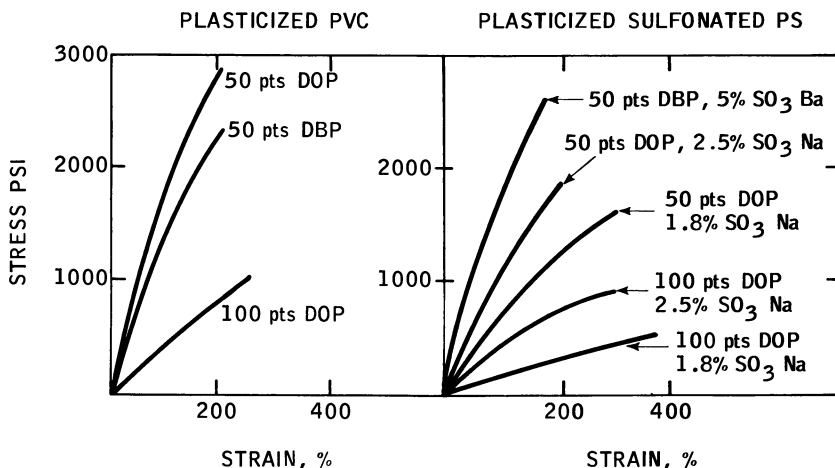


Figure 5. Stress-strain relationships for plasticized PVC and S-PS

(such as DOP) can be accommodated. Under these circumstances plasticizer exudation can be observed.

The data thus far have shown that S-PS can be plasticized effectively with respect to backbone and ionic domain plasticizers. By appropriate choice of the plasticizer type either the PS backbone or the ionic domains can be plasticized preferentially. By appropriate control of the metal sulfonate content and the polarity of the plasticizer used, flexible S-PS compositions possessing useful tensile properties are feasible. While this approach has substantial merit, it is apparent that simply increasing the level of a phthalate plasticizer to improve melt flow results in a substantial decrease in useful tensile properties. It would be desirable to use a given level of backbone plasticizer and adjust the melt flow of the entire composition by independently plasticizing the ionic domains. One approach to achieve this objective has been described in the plasticization of ionic groups in metal-sulfonated ethylene propylene terpolymers (9). In those systems, the incorporation of metal carboxylates as plasticizers can improve both flow behavior and tensile properties. It is of interest to determine if this class of plasticizers can be combined with the phthalate plasticizers used for the S-PS backbone to provide an improved balance of flow behavior and tensile properties for S-PS's.

Therefore, plasticized compositions using DOP and zinc stearate at various levels were prepared by melt blending, and their tensile properties and flow behavior are shown in Table II. It is seen that the addition of zinc stearate at modest levels (5 and 10 pph) markedly improves melt flow as measured by melt index. Furthermore, this improvement in flow is achieved without a loss in tensile properties; in fact, a modest improvement is noted. For comparison, the unplasticized, unsulfonated PS exhibited a melt index of 30 under these conditions. Therefore, a combi-

Table II. Effect of Combined Plasticizers (DOP and Zinc Stearate) on Zinc S-PS Properties and Flow Behavior^a

DOP (Parts/100 Polymer)	Zn(St) ₂ (Parts/100 Polymer)	Room Temperature Tensile Properties		Melt Index (190°C, 250 psi, g/10 min)
		100% Modulus (psi)	Tensile (psi)	
50	0	860	1220	3.3
50	5	870	1310	7.5
50	10	1020	1330	28.1
75	0	300	860	10.8
75	5	320	910	26.4
75	10	385	890	53.1

^a 4 mol % zinc sulfonate S-PS.

nation of a backbone plasticizer for S-PS and a suitable ionic domain plasticizer can give rise to a product possessing flow behavior surpassing that of the base resin, yet retaining a strong physical network at ambient temperatures. These results are consistent with those reported for sulfonated elastomers (9) and with the concept that plasticizers can preferentially plasticize the metal sulfonate groups or the polymer backbone in S-PS depending on the plasticizer polarity.

Conclusions

This study has shown that the strong physical cross-links in lightly sulfonated PS can be controlled by the use of suitable polar plasticizers. At the same time the PS backbone can be plasticized independently. By appropriate control of the backbone plasticizer, the ionic group plasticizer, the sulfonate level, and the cation, a family of flexible sulfonated plastics can be prepared possessing acceptable flow and tensile properties. Such flexible compositions are similar in some respects to plasticized PVC.

Acknowledgments

We gratefully acknowledge the help of J. A. Sissano in preparing the sulfonated polymers and the help of R. R. Phillips, M. A. Grossman, and M. Vieira in characterizing these materials.

Literature Cited

1. Eisenberg, A.; King, M. "Ion-Containing Polymers"; Academic: New York; 1977.
2. Lundberg, R. D.; Makowski, H. S.; Westerman, L. U.S. Patent 4 014 847, 1977, to Exxon Research and Engineering Company.
3. Makowski, H. S.; Lundberg, R. D.; Singhal, G. S. U.S. Patent 3 870 841, 1975, to Exxon Research and Engineering Company.
4. Lundberg, R. D.; Makowski, H. S., chapter 2 in this book.
5. Clampitt, B. H. *J. Macromol. Sci., Chem.* **1971**, *5*(8), 1317.
6. Lundberg, R. D. *Polym. Prepr. Am. Chem. Soc., Div. Polym. Chem.* **1978**, *19*(1), 455.
7. Kelley, F. N.; Bueche, F. *J. Polym. Sci.* **1961**, *50*, 549.
8. Erdi, N. A.; Morawetz, H. *J. Colloid Sci.* **1964**, *19*, 708.
9. Makowski, H. S.; Lundberg, R. D., chapter 3 in this book.
10. Bueche, F. "Physical Properties of Polymers"; Interscience: New York, 1962; pp. 116-120.

RECEIVED October 16, 1978.

Thermal and Dynamic Mechanical Properties of Sulfonated Polypentenamers

D. RAHRIG and W. J. MAC KNIGHT

Polymer Science and Engineering, Materials Research Laboratory,
University of Massachusetts, Amherst, MA 01003

A series of sulfonated polypentenamers containing from 1.9 to 17.6 mol % pendant groups in the form of sodium salts was studied by differential scanning calorimetry (DSC) and dynamic mechanical techniques. The composition dependencies of the glass transition temperatures (T_g 's) measured by DSC show typical random copolymer behavior at low levels of sulfonation but deviate significantly from this behavior above 10 mol %. The dynamic mechanical results exhibit an ionic-phase relaxation α that is believed to originate within ionic clusters. The fact that the α relaxation is only present in samples sulfonated above 10 mol % is taken as evidence, along with the T_g behavior, that clustering occurs only above a critical sulfonate concentration of 10 mol % or two sulfonate groups per 100 backbone carbon atoms.

It is usually not possible to alter the nature or concentration of salt groups without significantly affecting such variables as molecular weight, molecular weight distribution, and monomer sequencing, since most ionomers are prepared by copolymerization reactions. This factor presents a serious obstacle to a meaningful study of the effects of the nature and concentration of salt groups on the properties of ionomeric materials. One method of avoiding this drawback is to prepare materials by postpolymerization reactions on a common precursor. It is this concept that has led to our continuing investigation of the properties of modified polypentenamers (PP's).

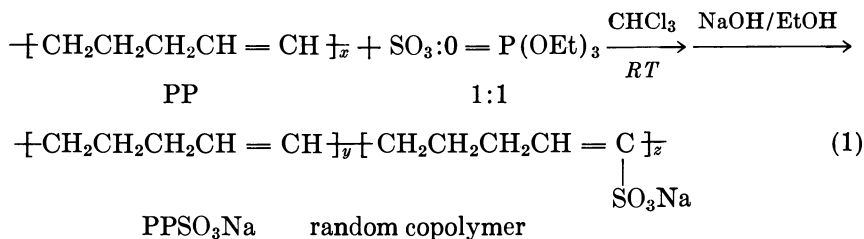
We reported previously the modification of a PP by phosphonylation (1) and by the addition of thioglycolate side groups (2), and exam-

ined the thermal and dynamic mechanical properties of the neutralized derivatives of these systems (3, 4). Recently we were able to extend this series by preparing sulfonated PP's free of covalent cross-links, in the form of sodium salts (5). In this study we used thermal and dynamic mechanical techniques to investigate a range of the sulfonated materials containing up to four sulfonate groups per 100 backbone carbon atoms. This pendant group content is nearly twice that present in the previously studied PP derivatives.

The dynamic mechanical results of this study are consistent in many ways with the behavior observed for the phosphonylated and thioglycolate-substituted PP's. In each case the temperature of the glass-rubber relaxation is altered considerably by the presence of pendant groups, and in each case the salt forms display an extended pseudoplateau region, indicating some form of cross-linking. However, unlike the previous PP systems studied, the dynamic mechanical results for the sulfonated PP's provide strong evidence for the existence of ionic clusters (6,7) through the presence of an ionic-phase relaxation. In addition, the dynamic mechanical results combined with the differential scanning calorimetry (DSC) results suggest a critical level of sulfonation at which clustering becomes detectable.

Experimental

Materials. The starting PP was kindly provided by the Goodyear Tire and Rubber Company. It contains 82% trans and 17% cis double bonds with fewer than 1% vinyl side groups. The molecular weight averages are $\bar{M}_n = 172,000$ and $\bar{M}_w = 470,000$. The PP was sulfonated using a 1:1 complex of sulfur trioxide with triethyl phosphate in chloroform at room temperature. The sulfonated material was neutralized by precipitating the reaction mixture into a 0.25M solution of NaOH in ethanol. This reaction is described in detail elsewhere (5) and is summarized as follows:



To prevent covalent cross-linking with aging, these materials were stabilized with hydroquinone. Characterization data for the samples investigated are collected in Table I.

The sulfonated PP's were compression molded into films suitable

Table I. Characterization Data for Sulfonated PP's

Sample	% Sulfonation	% Neutralization	T_g ($^{\circ}\text{C}$)
PPSO ₃ Na(2)	1.9	89	-95
PPSO ₃ Na(5)	6.7	72	-85
PPSO ₃ Na(10)	10.8	73	-72
PPSO ₃ Na(15)	14.3	78	-38
PPSO ₃ Na(20)	17.6	74	+31

for dynamic mechanical and DSC measurements. Film preparation was carried out by pressing at 130°–140°C and 10,000 psi for 20 min under nitrogen. The resulting films were stored in a desiccator under vacuum at room temperature in the absence of light until use.

Water-saturated samples were prepared by storing film samples overnight in distilled water at room temperature. Water uptake in these samples was not observed to increase significantly after 4 hr. The rate of water uptake was not measured.

Measurements. DSC measurements were carried out on a Perkin-Elmer Model DSC II. The scanning speed was 20°C/min in all cases, and cyclohexane and indium were used as standards. The temperature range scanned was -120°–100°C.

Dynamic mechanical measurements were carried out on a Vibron Dynamic Viscoelastometer, Model DDV-II (Toyo Measuring Instruments Co.). The temperature range was -160°–200°C and the frequencies used were 3.5, 11, and 110 Hz. Samples were heated at a rate of 1°–2°C/min under dry nitrogen.

Results

The DSC results for three of the sulfonated PP samples are displayed in Figure 1. Sample PPSO₃Na(2) exhibits a very distinct glass transition at -95°C, followed by an exotherm that is centered around -65°C and an endotherm that appears around 11°C. The DSC traces of the remaining sulfonated PP samples display neither an exotherm nor an endotherm, though all of these samples display readily observable glass transitions. The glass transitions detected by DSC for these materials become broadened and increase in temperature as the degree of sulfonation increases. This trend is demonstrated in the scans shown in going from sample PPSO₃Na(5), with a relatively narrow glass transition centered at -85°C, to the most highly sulfonated material in this study, sample PPSO₃Na(20), which displays a glass transition spread over several decades of temperature centered at 31°C. A summary of the DSC-determined T_g 's is given in Table I. When these T_g 's are plotted against the mol % sulfonation determined by elemental analysis, the plot in Figure 2 is obtained. For low levels of sulfonation this plot demonstrates a linear relationship with slightly positive slope, but above 10 mol % sulfonation the DSC-determined T_g 's differ significantly from such linear behavior.

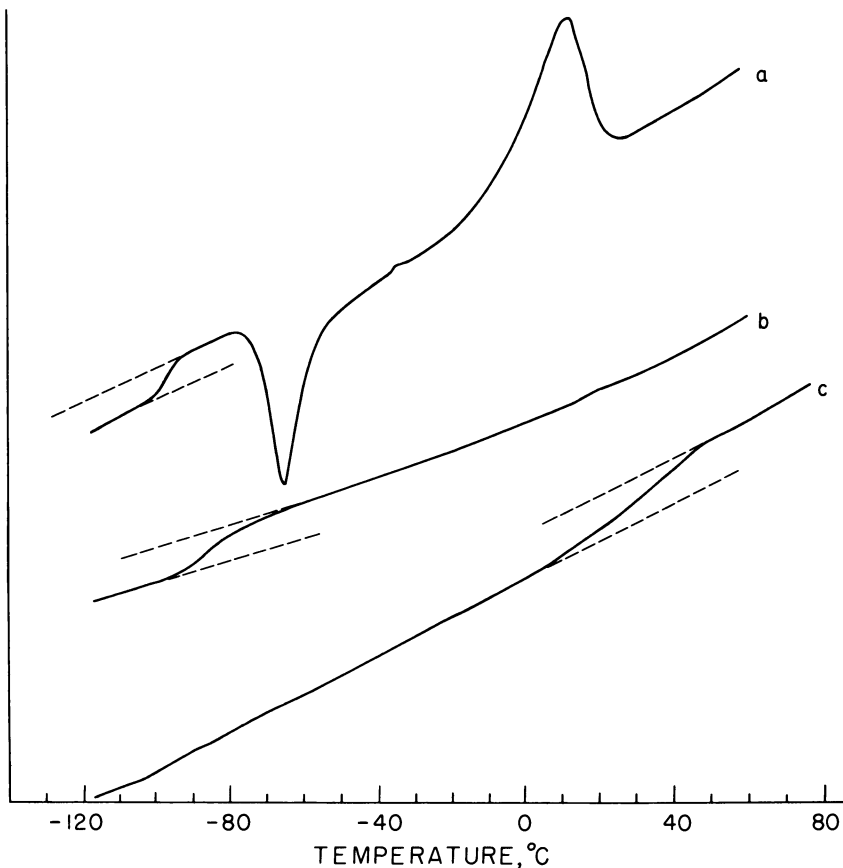


Figure 1. DSC scans recorded at $20^{\circ}\text{C}/\text{min}$ for (a) sample $\text{PPSO}_3\text{Na}(2)$; (b) sample $\text{PPSO}_3\text{Na}(5)$; and (c) sample $\text{PPSO}_3\text{Na}(20)$

Figures 3–6 represent the temperature dependencies of the tensile storage and loss moduli (E' and E'') at 11 Hz for the sulfonated PP's. The E'' behavior of sample $\text{PPSO}_3\text{Na}(2)$ shown in Figure 3 displays three relaxation regions. These three relaxations are labeled α , β , and γ in order of decreasing temperature. Sample $\text{PPSO}_3\text{Na}(5)$ exhibits only two relaxations, a β relaxation at -72°C and a γ relaxation centered around -130°C . As shown in Figure 4, the α relaxation is absent in the E'' plot of sample $\text{PPSO}_3\text{Na}(5)$, but is present around 0°C for sample $\text{PPSO}_3\text{Na}(10)$. In addition, sample $\text{PPSO}_3\text{Na}(10)$ displays a β relaxation at -49°C and a γ relaxation at -120°C . Figures 5 and 6 show the dynamic mechanical responses of both dry and water-saturated samples of materials $\text{PPSO}_3\text{Na}(15)$ and $\text{PPSO}_3\text{Na}(20)$, respectively. In this context “dry” means the sample was stored in a desiccator under vacuum and only exposed to atmospheric moisture, while “water-saturated”

means the sample was allowed to stand submerged in distilled water at room temperature until it reached a constant weight. The dynamic mechanical spectra of the PPSO_3Na (15) samples given in Figure 5 show that the dry material displays three relaxations, with the α occurring at 25°C , the β at -35°C , and the γ at -123°C . The water-saturated sample absorbed 72% of its dry weight in water, corresponding to roughly 23 water molecules per sulfonate group. It is seen in Figure 5 that the α relaxation is not observable when the material is saturated with water, but the β and γ relaxations remain at the same temperatures as for the dried samples. Also very noticeable in the dynamic mechanical behavior of sample PPSO_3Na (15) is the fact that the tensile storage modulus decreases rapidly at the temperature of the β relaxation for the water-

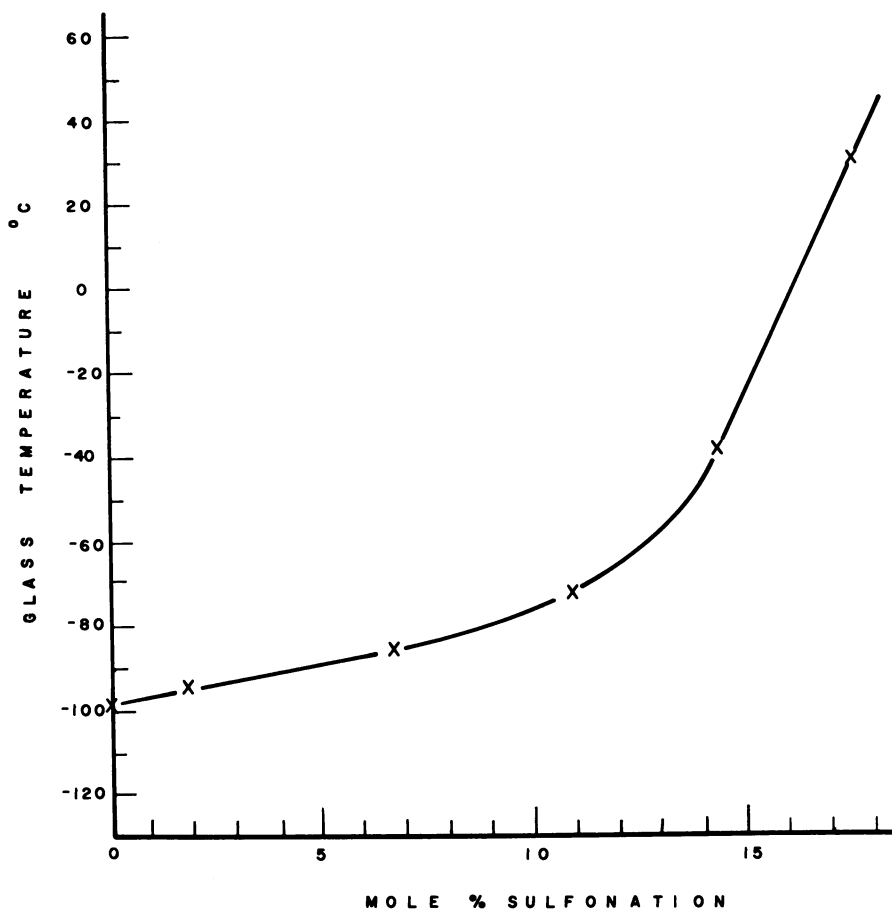


Figure 2. Composition dependence of the DSC-determined T_g 's for the sulfonated PP's

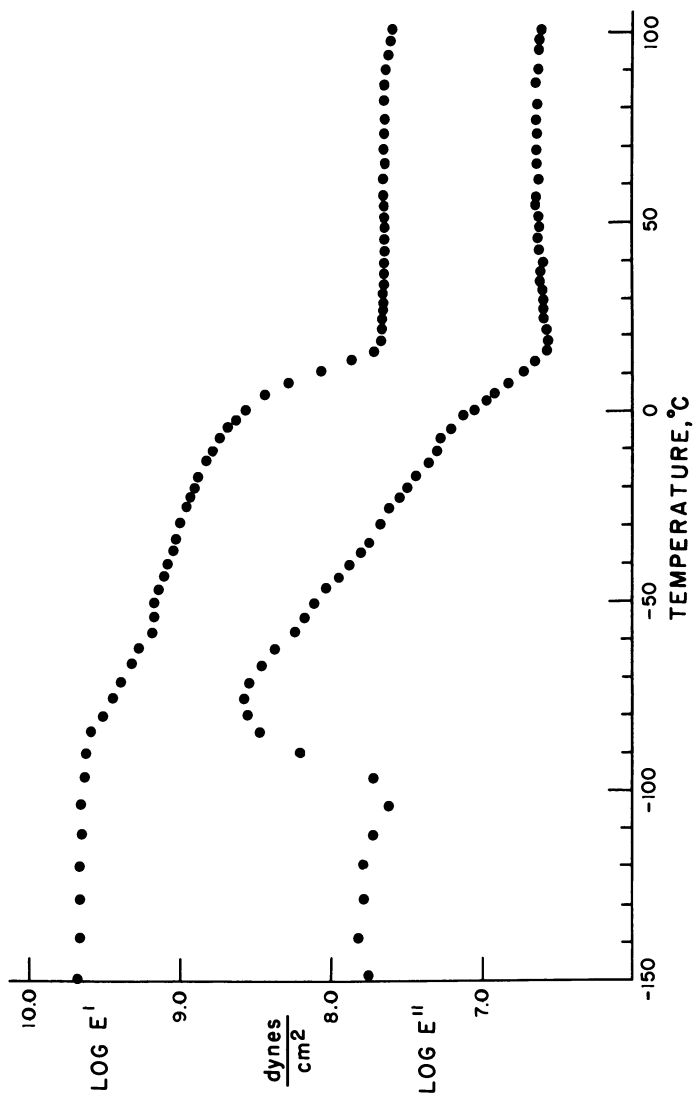


Figure 3. Temperature dependencies of E' and E'' at 11 Hz for sample PPSO₃Na(2)

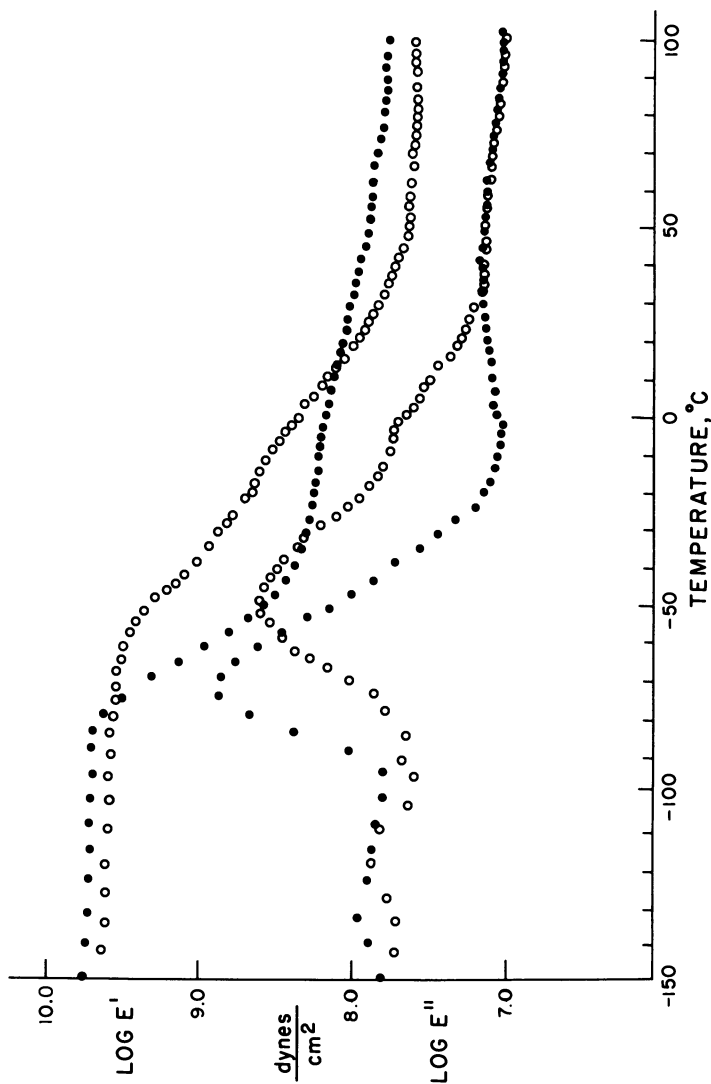


Figure 4. Temperature dependencies of E' and E'' at 11 Hz for samples PPSO₃Na(5) (●) and PPSO₃Na(10) (○)

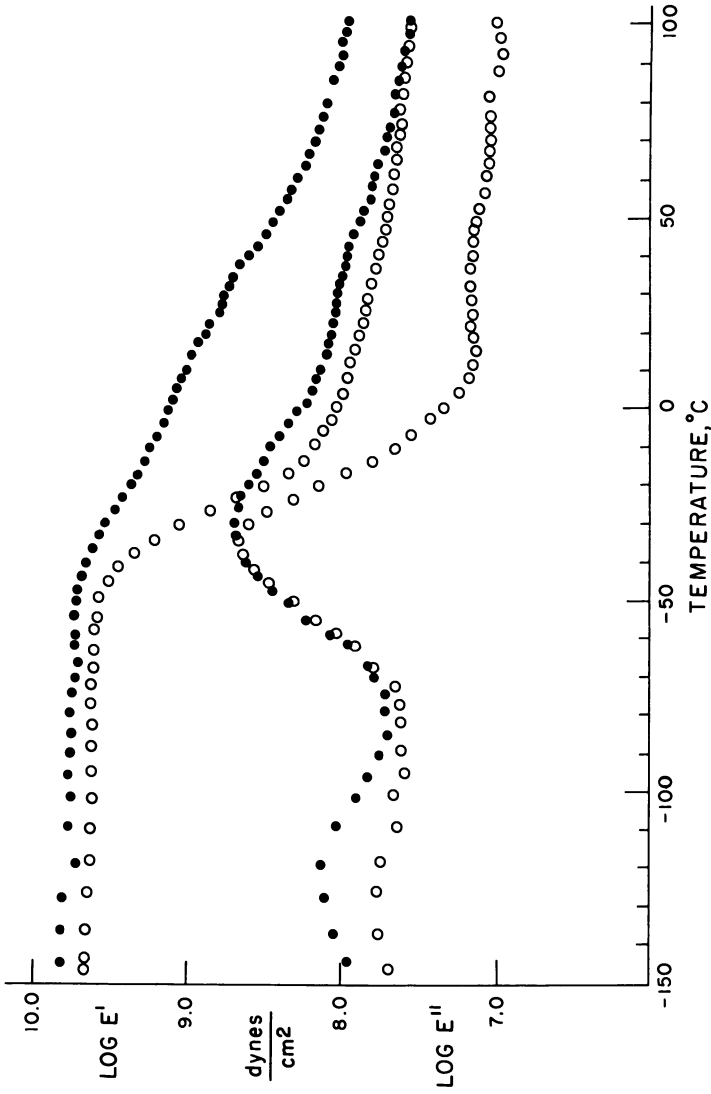


Figure 5. Temperature dependencies of E' and E'' at 11 Hz for dry (●) and water-saturated (○) samples of PPSO₃Na(15)

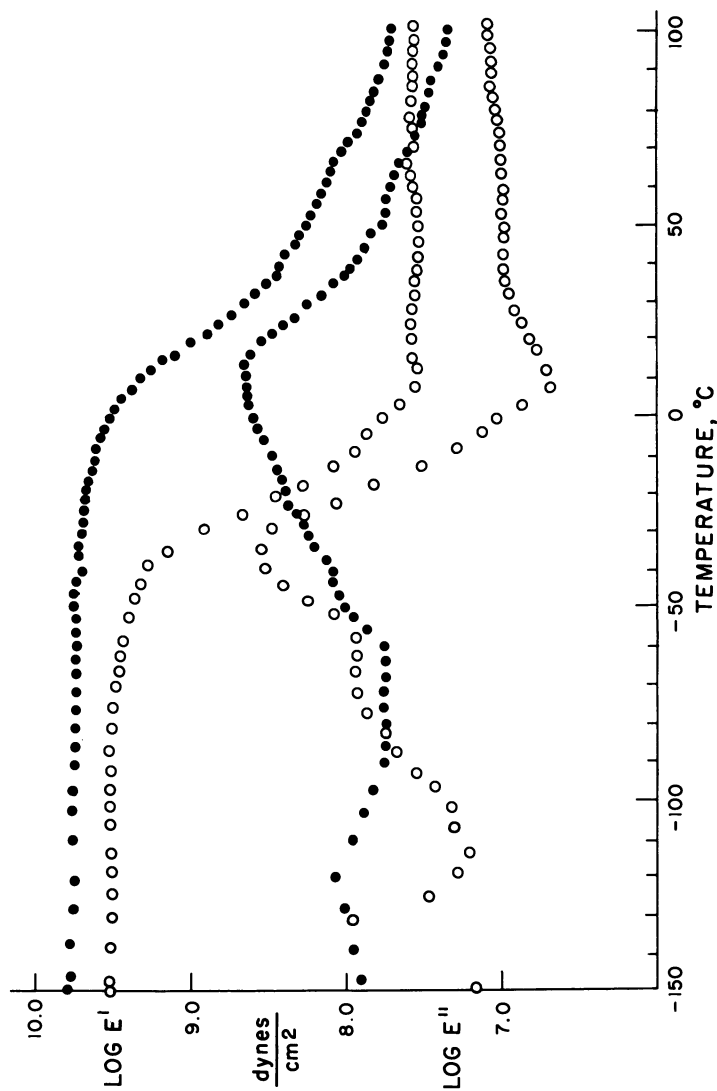


Figure 6. Temperature dependencies of E' and E'' at 11 Hz for dry (●) and water-saturated (○) samples of PPSO₃Na(20)

saturated case. However, it decreases much more gradually and in two steps for the dry sample, with these two steps coinciding with the temperatures of the β and α relaxations. For sample PPSO₃Na(20) Figure 6 shows α , β , and γ relaxations for both the dry and water-saturated cases. The E'' plot for the dry material demonstrates that at this level of sulfonation the α relaxation occurring at 12°C is the dominant relaxation mechanism; the β relaxation is reduced in magnitude relative to the less highly sulfonated samples studied, and appears almost as a shoulder on the α relaxation peak. The tensile storage modulus shows virtually no change at the temperature of the β relaxation, but decreases rapidly at the temperature of the α relaxation. At this level of sulfonation the material absorbed 84% of its initial weight when submerged overnight in distilled water. This, as in sample PPSO₃Na(15), corresponds to roughly 23 molecules of water per sulfonate group. The dynamic mechanical behavior of the water-saturated sample as shown in Figure 6 displays an 80°C decrease in the temperature of the α relaxation, from 12°C for the dry sample to -68°C for the water-treated material. At the same time the temperature of the β relaxation remains unaffected, though its magnitude is observed to increase slightly. The γ relaxation becomes narrower and decreases slightly in temperature with water uptake. The tensile storage modulus exhibits a catastrophic decrease in conjunction with the β relaxation at -35°C, rather than at the temperature of the α relaxation as it does in the dry materials. A summary of the temperatures at which each of the relaxations is observed to occur at 11 Hz for the materials investigated in this work is compiled in Table II.

Discussion

The behavior of sample PPSO₃Na(2) when studied by DSC can be explained readily by the fact that PP's containing a high content of trans double bonds are known to form trans double bond-containing crystals (4, 8). Since these crystals have a melting point below room temperature,

Table II. Temperatures* of Relaxations in Sulfonated PP's (°C at 11 Hz)

Sample	$\alpha(E'')$	$\beta(E'')$	$\gamma(E'')$
PPSO ₃ Na(2)	-8	-77	-130
PPSO ₃ Na(5)	—	-72	-130
PPSO ₃ Na(10)	0	-49	-120
PPSO ₃ Na(15)	25	-35	-123
PPSO ₃ Na(20)	12	-35	-120
PPSO ₃ Na(15);H ₂ O	—	-36	-123
PPSO ₃ Na(20);H ₂ O	-68	-35	-134

* All temperatures have error bounds of $\pm 3^\circ\text{C}$.

the rapid cooling used in the DSC experiment ($\sim 320^\circ\text{C}/\text{min}$) quenches the sample and inhibits crystal formation during the cooling cycle. Upon heating the sample at a rate of $20^\circ\text{C}/\text{min}$ starting from -120°C , crystals form once the temperature of the materials is adequately above T_g . The formation of these trans double bond-containing crystals accounts for the exotherm seen at -65°C , while the endotherm present at 11°C results from the melting of such crystals. Therefore, it is seen in this study that at 1.9 mol % sulfonation, the concentration of pendant sulfonate groups is not high enough to completely disrupt the formation of crystals. However, at 6.3 mol % sulfonation and above, the pendant group concentration is sufficient to suppress crystallization.

The plot of T_g vs. mol % sulfonation shown in Figure 2 is unusual with respect to typical copolymers, but has been observed previously in ion-containing copolymers (9, 10). Matsuura and Eisenberg have reported that for ethyl acrylate-based ionomers, the T_g increases linearly with the concentration of salt groups at low concentrations of such groups, but eventually begins to deviate substantially from this typical copolymer-type behavior by rising sharply. Furthermore, it was observed that the concentration of salt groups at which the T_g begins to deviate from the typical copolymer-type linearity is the same concentration at which the time-temperature superposition of viscoelastic behavior is observed to break down. Since such nonsuperposability is taken as evidence for ion clustering (11, 12), this seems to suggest that the deviation of T_g from typical copolymer behavior correlates with the critical concentration of salt groups necessary for the formation of microphase-separated domains. If such is the case, the plot of T_g vs. mol % sulfonation shown in Figure 2 indicates the presence of ionic clusters in PP's sulfonated above a level of roughly 10 mol %.

The dynamic mechanical properties of the sulfonated PP's combine with the DSC results to give a much clearer idea of the transition behavior of these materials. However, a discussion of the dynamic mechanical behavior of these derivatives is best understood by examining each relaxation region individually.

α Relaxation. As shown in the results section of this chapter, the α relaxation is present in sample $\text{PPSO}_3\text{Na}(2)$, disappears for sample $\text{PPSO}_3\text{Na}(5)$, but then reappears in sample $\text{PPSO}_3\text{Na}(10)$ and is present in all samples sulfonated above 10 mol %. In addition, for samples sulfonated above 10 mol % the magnitude of the α relaxation increases as the degree of sulfonation increases. In view of the DSC results for these materials and dynamic mechanical studies on PP's with other pendant groups (3, 4), it is concluded that the origin of the α relaxation in sample $\text{PPSO}_3\text{Na}(2)$ differs from that for the more highly substituted materials. For PP's with a high content of trans double bonds that are

either unsubstituted or only substituted to a low degree, an α relaxation is present owing to the melting of the trans double bond-containing crystals. Since sample PPSO₃Na(2) is known from the DSC results to crystallize, it seems likely that the α relaxation for this materials is attributable to the melting of these crystals. The absence of an α relaxation in PPSO₃Na(5), which is known from DSC to be noncrystalline, tends to verify this assignment.

The concentration of sulfonate groups at which the DSC-determined T_g 's begin to deviate from typical copolymer behavior corresponds with the concentration of sulfonate groups at which the mechanical α relaxation reappears. The fact that the magnitude of the α relaxation increases as the degree of sulfonation increases suggests that it is related to a separate ionic phase. This postulate is reinforced further by the fact that the α relaxation is "plasticized" or decreases substantially in temperature when the sulfonated PP samples are saturated with water. If a separate ionic phase, such as the proposed ionic clusters (6, 7), is present in these materials one would expect water to migrate to this phase and avoid the hydrocarbon matrix. Such behavior would result in a preferential plasticization of ionic-phase relaxations with little or no effect on hydrocarbon relaxations. This is exactly the type of phenomenon observed in these samples if the α relaxation is assigned to the ionic phase and the β relaxation to the amorphous hydrocarbon matrix. This leads to the conclusion that the α relaxation observed in samples sulfonated above 10 mol % is in fact attributable to a relaxation mechanism that occurs in a separate ionic phase and is evidence for the presence of ionic clusters in the sulfonated PP's. Moreover, the dependence of the ionic-phase α relaxation on sulfonate concentration suggests that ionic clusters occur only above a critical concentration of roughly 10-mol % sulfonation. This conclusion is consistent with the interpretation given for the T_g behavior of these materials.

β Relaxation. The β relaxation is believed to be created by the microbrownian segmental motion that accompanies the glass transition of the amorphous hydrocarbon matrix. The manner in which the β relaxation magnitude changes as the sulfonate concentration changes suggests its amorphous hydrocarbon-phase origin. For sample PPSO₃Na(2), which is slightly crystalline, the magnitude of the β relaxation is less than that of the completely amorphous sample PPSO₃Na(5). For samples PPSO₃Na(10), PPSO₃Na(15), and PPSO₃Na(20), the magnitude of the β relaxation decreases as the degree of sulfonation increases, attributable to the increasing volume of material present in the ionic phase. The large decrease in storage modulus accompanying the β relaxation further indicates that it arises from the glass-to-rubber transition. However, the most conclusive evidence is the correlation that exists between the DSC-

determined T_g 's and the β relaxation temperatures. With the exception of sample PPSO₃Na(20), this correlation is good. In the case of sample PPSO₃Na(20), it is possible that the second-order transition observed by DSC corresponds to the dominant α relaxation of the ionic phase rather than the glass transition of the amorphous hydrocarbon phase.

γ Relaxation. All of the sulfonated PP's display a well-defined mechanical γ relaxation. It has long been known that three or more CH₂ units in sequence are necessary for the appearance of a γ relaxation (13), and it has been proposed that a crankshaft motion of the three methylene groups between the double bonds, based on the mechanism of Boyd and Breitling (14), can account for the γ process observed in unsubstituted PP's (15, 16). It seems likely that this same mechanism explains the mechanical γ relaxation observed for the sulfonated materials. The fact that the phosphonate- (3), thioglycolate- (4), and cyano- (17) substituted PP's exhibit identical behavior in this region further reinforces the proposal that the γ relaxation mechanism involves segments of the polymer chain other than the pendant groups.

Conclusions

The dynamic mechanical and DSC results for sulfonated PP's combine to give strong evidence for the existence of ionic clusters in these materials. In addition they suggest that these clusters are only present above a critical sulfonate concentration of 10 mol %. These conclusions are based on the existence of an ionic-phase α relaxation for materials sulfonated above 10% and the deviation of the T_g vs. % sulfonation plot from typical copolymer-type behavior at this same concentration.

Acknowledgments

The authors are grateful to the National Science Foundation under Grant DMR 75-06916 and to the donors of the Petroleum Research Fund of the American Chemical Society for partial support of this research. The use of the facilities of the Materials Research Laboratory at the University of Massachusetts is also gratefully acknowledged.

Literature Cited

1. Azuma, C.; MacKnight, W. J. *J. Polym. Sci., Polym. Chem. Ed.* **1977**, *15*, 547.
2. Sanui, K.; Lenz, R. W.; MacKnight, W. J. *J. Polym. Sci., Polym. Chem. Ed.* **1974**, *12*, 1965.
3. Rahrig, D.; Azuma, C.; MacKnight, W. J. *J. Polym. Sci., Polym. Phys. Ed.* **1978**, *16*, 59.
4. Sanui, K.; MacKnight, W. J. *Br. Polym. J.* **1976**, *8*, 22.
5. Rahrig, D.; MacKnight, W. J.; Lenz, R. W. *Macromolecules* **1979**, *12*, 195.

6. MacKnight, W. J.; Taggart, W. P.; Stein, R. S. *J. Polym. Sci., Polym. Symp.* **1974**, *45*, 113.
7. Eisenberg, A.; King, M. "Ion-Containing Polymers"; Stein, R. S., Ed.; Academic: New York; 1977.
8. Tucker, H.; Minchak, R. J.; Macey, J. H. *Polym. Eng. Sci.* **1975**, *15*, 360.
9. Matsuura, H.; Eisenberg, A. *J. Polym. Sci., Polym. Phys. Ed.* **1976**, *14*, 1201.
10. Noshay, A.; Robeson, L. M. *J. Appl. Polym. Sci.* **1976**, *20*, 1885.
11. Eisenberg, A.; Navratil, M. *Macromolecules* **1973**, *6*, 604.
12. Eisenberg, A.; Navratil, M. *Macromolecules* **1974**, *7*, 84.
13. McCrum, N. G.; Read, B. E.; Williams, G. "Anelastic and Dielectric Effects in Polymeric Solids"; Wiley: New York, 1967; Chapter 10.
14. Boyd, R. H.; Breitling, S. M. *Macromolecules* **1974**, *7*, 855.
15. Sanui, K.; MacKnight, W. J.; Lenz, R. W. *Macromolecules* **1974**, *7*, 101.
16. Earnest, Jr., T. R.; MacKnight, W. J. *Macromolecules* **1977**, *10*, 206.
17. Neumann, R.; Sanui, K.; MacKnight, W. J. *Macromolecules* **1975**, *8*, 665.

RECEIVED November 20, 1978.

Thermal, Dynamic Mechanical, and Dielectric Properties of Hydrogenated, Sulfonated Polypentenamers

D. RAHRIG and W. J. MAC KNIGHT

Polymer Science and Engineering, Materials Research Laboratory,
University of Massachusetts, Amherst, MA 01003

Hydrogenated, sulfonated polypentenamers containing from 2.9 to 19.1 mol % pendant groups in the form of sodium salts were examined by differential scanning calorimetry (DSC) and dynamic mechanical and dielectric relaxation techniques. DSC results display two endotherms and provide evidence of a room-temperature annealing phenomenon. Four relaxations, α , β , γ' , and γ , in order of decreasing temperature, are observed dynamic mechanically. The α relaxation is composite in origin but appears to arise partially from an ionic-phase mechanism which suggests the existence of ionic clusters. The β relaxation is related to the glass transition and is affected by the crystalline content. Large increases in ϵ' and $\tan \delta_\epsilon$ accompany the dielectric results. A dielectric α relaxation displays behavior that parallels that of the mechanical α peak.

We have reported previously the sulfonation of a polypentenamer (PP) under reaction conditions that preclude the formation of covalent cross-links (1). The sulfonated materials are isolated in the form of sodium salts to give ion-containing elastomers. The thermal and dynamic mechanical properties of the sulfonated PP's indicate the existence of phase-separated ionic clusters above a sulfonate concentration of roughly 10 mol % (2). It has been shown (1) that the unsaturation in the sulfonated PP's can be removed by a diimide hydrogenation reaction to yield a material that is essentially linear polyethylene with pendant sulfonate groups. In this manner the effect of backbone crystallinity on

the ability of an ion-containing polymer to form phase-separated domains can be investigated.

By conducting a study on sulfonated PP's and their hydrogenated derivatives, it is possible to look at materials that have identical chain backbones. As a result, such complications as variations in molecular weight, molecular weight distribution, and monomer sequencing can be eliminated. In this study we have used thermal, dynamic mechanical, and dielectric relaxation techniques to investigate four series of hydrogenated, sulfonated PP's. The level of sulfonation present in these systems ranges from 2.9 to 19.1 mol %. By varying the sulfonate concentrations and thermal histories of the samples in this study, much can be learned about the origins of the various relaxations that these materials display. The results of this investigation can then be compared with the results of previous investigations carried out in this laboratory on the properties of phosphonylated (3) and thioglycolate-substituted (4) PP's. This comparison will yield a better understanding of the effects of the nature and concentration of pendant ionic groups on the behavior of ion-containing polymers.

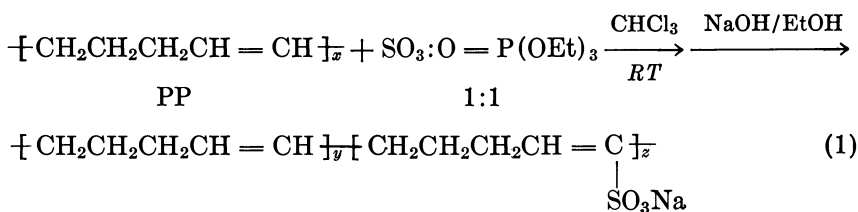
The desired comparisons of this study are obscured somewhat by three factors. The first and most serious of these is the fact that elemental analysis of the hydrogenated, sulfonated PP's indicates the presence of nitrogen in these materials. While the weight percent of nitrogen is low, its exact origin cannot be determined. It is found that the amount of nitrogen present increases as the degree of sulfonation increases. This suggests that the nitrogen results either from a side reaction during the hydrogenation step which is aided by the pendant sulfonate groups or from dimethyl formamide (DMF), the solvent used in the hydrogenation reaction, which is "bound" to the polar polymer. A second drawback is the fact that the degree of ionization in these materials varies from a low of 64% to a high of 100%. A third factor is that the sulfonate salts pendant to the hydrogenated-PP backbone have a propensity to absorb water from the atmosphere. As a result the materials investigated in this study are not completely dry but do hold some water.

The dynamic mechanical results of this study demonstrate that backbone crystallinity plays an important role in the properties of these materials. Moreover, it is observed that thermal history affects the properties of the materials investigated in a more complex manner than can be explained by simple changes in the degree of crystallinity. At low levels of sulfonation the materials generally behave very much like linear polyethylene, but this behavior is modified significantly as the level of sulfonation is increased. Evidence is clearly present for the existence of an ionic-phase relaxation that supports the proposed model for micro-phase-separated domains (5, 6, 7). However, owing to the effects of crystallinity the concentration at which the ionic-phase relaxation first

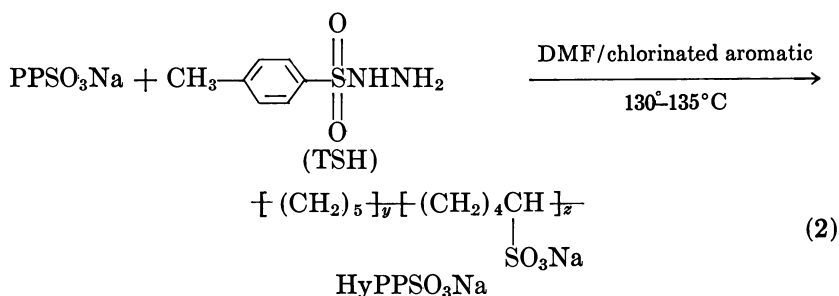
occurs cannot be determined unambiguously. While the dielectric results are consistent with the conclusions drawn from the dynamic mechanical investigation, the known presence of impurities in these systems and the occurrence of an undetermined interfacial phenomenon prohibit a rigorous interpretation of the data obtained in the dielectric experiments.

Experimental

Materials. The starting PP was kindly provided by the Goodyear Tire and Rubber Company. It contains 82% trans and 17% cis double bonds with fewer than 1% vinyl side groups. The molecular weight averages are $\overline{M}_n = 172,000$ and $\overline{M}_w = 470,000$. The PP was sulfonated using a 1:1 complex of sulfur trioxide to triethyl phosphate in chloroform at room temperature. The sulfonated material was neutralized by precipitating the reaction mixture into a 0.25M solution of NaOH in ethanol. The unsaturated product was then stabilized with hydroquinone, dried, put into solution using a mixed solvent system of DMF with a chlorinated aromatic (either chlorobenzene or 1,2,4-trichlorobenzene), and treated with *p*-toluenesulfonyl hydrazide (TSH). The reaction scheme is detailed elsewhere (1) and summarized below:



random copolymer



Characterization data for the samples investigated in this study are collected in Table I.

The hydrogenated, sulfonated PP's were compression molded into films suitable for differential scanning calorimetry (DSC), dynamic mechanical, and dielectric measurements. Films were prepared by pre-heating at 140°-145°C for 5 min and then pressing at 140°-145°C and 20,000 lb for 5 min. Annealed samples were prepared by placing air-cooled films between two metal platens and storing them in a vacuum oven at 80°C for 3 days. The platens were necessary to prevent the films

Table I. Characterization Data for Hydrogenated, Sulfonated PP's

<i>Sample</i>	<i>Mol % Sulfonation</i>	<i>% Neutralization</i>	<i>Wt % Nitrogen</i>
HyPPSO ₃ Na (2)	2.9	66	0.37
HyPPSO ₃ Na (5)	6.3	84	1.02
HyPPSO ₃ Na (10)	9.4	> 100	1.54
HyPPSO ₃ Na (20)	19.1	64	3.48

from becoming fluted during the annealing process. Quenched materials were prepared by submerging the films in a dry ice-isopropanol bath immediately after they were removed from the press. The resulting quenched and annealed films were stored in a desiccator under vacuum at room temperature and in the absence of light until use.

Water-saturated samples were prepared by storing film samples overnight in distilled water at room temperature. The rate of water uptake was not measured.

Measurements. DSC measurements were carried out on a Perkin-Elmer instrument, Model DSC II. The scanning speed was 20°C/min in all cases, and indium was used as a standard. The temperature range scanned was -50°-180°C. The peak temperature of the melting endotherm was taken as the melting point of the polymer crystals.

Dynamic mechanical measurements were carried out on a Vibron dynamic viscoelastometer, Model DDV-II (Toyo Measuring Instruments Co.). The temperature range was from -160° to 150°C and the frequencies used were 3.5, 11, and 110 Hz. Samples were heated at a rate of 1°-2°C/min under dry nitrogen.

Dielectric measurements were carried out using a General Radio Corporation capacitance-measuring assembly of the transformer-ratio-arm bridge type (Model 1620 A), in conjunction with a three-terminal cell (Balsbaugh type LD-3) having 53-mm diameter electrodes. Capacitance and $\tan \delta_\epsilon$ measurements were carried out at 0.1, 1, 10, and 100 kHz over a temperature range of -160°-100°C. Low-temperature variation was achieved by cooling the cell with liquid nitrogen and then regulating the flow of dry, chilled nitrogen gas through the cell. Heating above room temperature was achieved with a heating element regulated by two variacs, and was accompanied by a steady flow of dry nitrogen through the sample chamber. The temperature was increased at a rate of 1°-2°C/min throughout the experiment. DC resistance measurements were made using a General Radio megohmmeter, Type 1852A. To prevent the films from sticking to the electrode surface, one side was covered with a thin layer of aluminum foil.

Results

Differential Scanning Calorimetry. The DSC traces obtained at a scan rate of 20°C/min for the hydrogenated, sulfonated PP's are somewhat unique in that two distinct endotherms are present in all of the samples. Figure 1 shows the DSC behavior of the quenched HyPPSO₃Na samples. From this figure it can be seen that the low-temperature endotherm occurs between 55° and 60°C for each sample and increases in

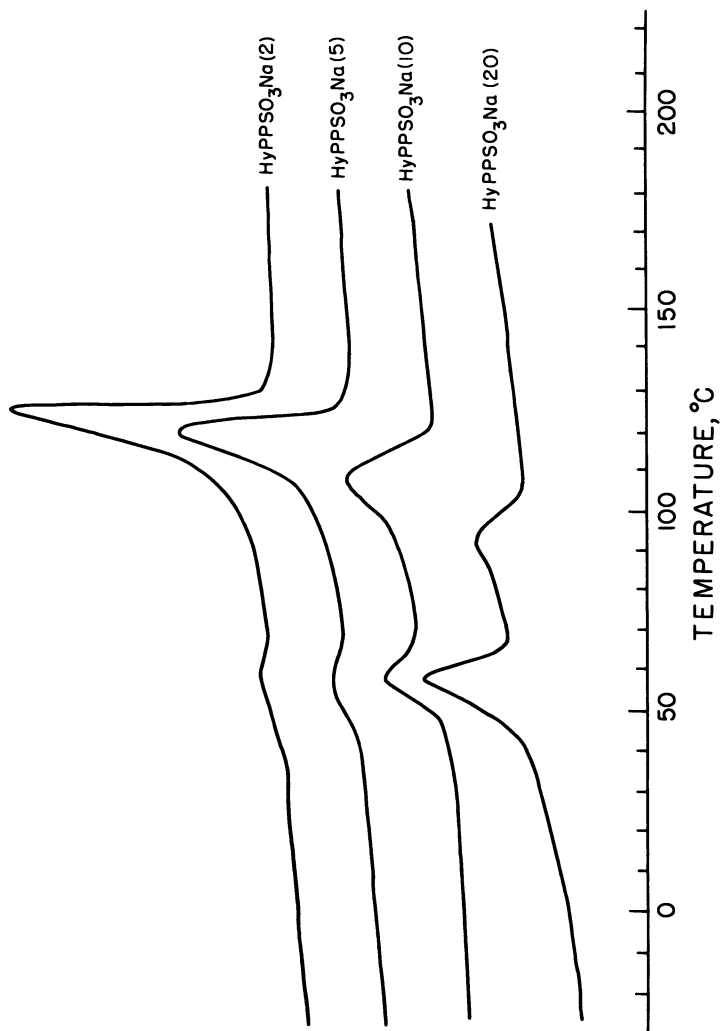


Figure 1. DSC results for quenched films of HyPPSO₃Na

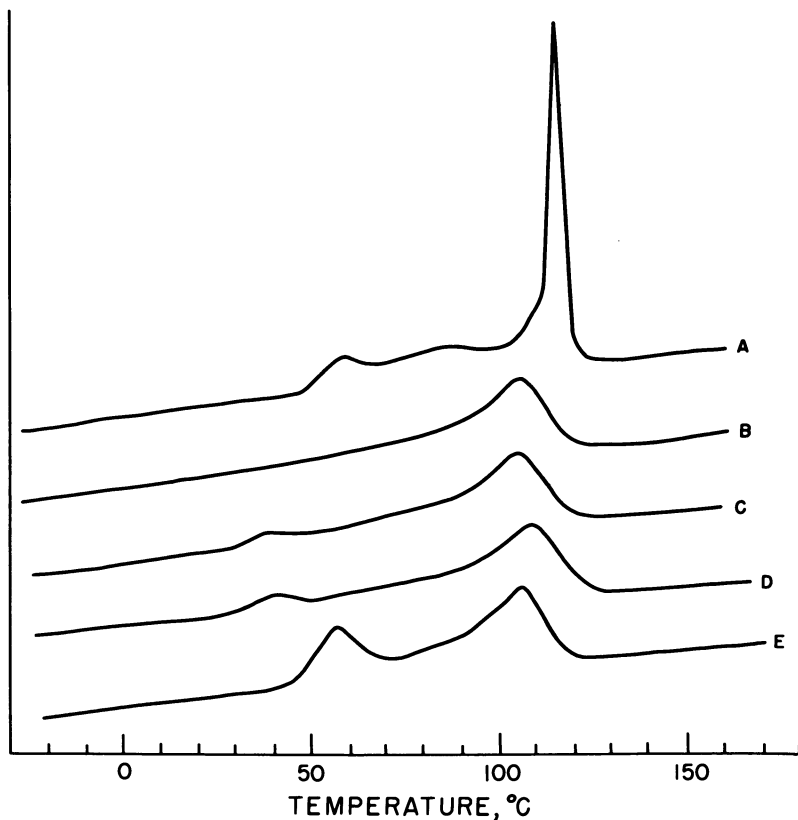


Figure 2. DSC results for HyPPSO₃Na(10) films with the following thermal histories: (A) annealed 3 days at 80°C and stored 30 days at room temperature; (B) quenched and immediately observed; (C) annealed 1/2 hr at 25°C; (D) annealed 1 hr at 25°C; (E) quenched and stored at room temperature for 30 days.

magnitude as the degree of sulfonation increases. The higher-temperature endotherm, on the other hand, decreases in both magnitude and temperature as the level of sulfonation increases. The existence of a second, low-temperature endotherm in the DSC curves of ethylene-based ionomers has been observed previously (8) and has been related to a room-temperature annealing phenomenon. As a result, the effect of room-temperature annealing on the DSC behavior of Sample HyPPSO₃-Na(10) was investigated. The results are shown in Figure 2. It is clear from these data that increasing the time a sample is maintained at room temperature causes a resulting increase in the magnitude of the endotherm that occurs around 55°C. However, no significant change takes place in the higher-temperature endotherm.

Table 2 lists the weight percent crystallinities determined for the samples in this study. These represent the ratio of $\Delta H_t/\Delta H_u$, where ΔH_t is the experimental enthalpy of fusion and ΔH_u the enthalpy of fusion for the hypothetical 100% crystalline polymer. Since the samples in this study display two endotherms, ΔH_t is based on the entire area enclosed by the two peaks, including the area between the two peaks, since the DSC curve does not return to the original baseline over this portion of the scan. Owing to the bulkiness of the sulfonate group, it is assumed that these groups are excluded completely from the crystalline phase. As a result, the value of ΔH_u determined by the polymer-diluent technique for fully hydrogenated PP's, evaluated as 59 cal/g (9), was used. While this value is appropriate for an unsubstituted, fully hydrogenated-PP crystal of infinite thickness, it might be reduced if the crystals are small. In addition, while the sulfonate groups may be excluded from the crystal lattice, their presence at the crystalline surface may distort the crystal lattice and thereby reduce ΔH_u further. However, in spite of these drawbacks the DSC results seem to give a good relative determination of the crystallinity present in these systems.

Dynamic Mechanical Measurements. The dynamic mechanical results for both quenched and annealed samples of the four materials investigated are presented in the form of E' and E'' plots against temperature in Figures 3–6. These figures show the presence of four relaxation regions (α , β , γ' , and γ in order of decreasing temperature) in each of the samples examined. The labeling of these relaxations is based on the nomenclature used for polyethylene. For Sample HyPPSO₃Na(2) shown in Figure 3 it is seen that the temperature and magnitude of the α relaxation increase with annealing, while the β and γ relaxations demonstrate virtually no change associated with the thermal history. The

Table II. Wt % Crystallinities and Melting Points of HyPPSO₃Na Films for Rheovibron and Dielectric Studies

Sample	Mechanical		Dielectric	
	Wt % Crystallinity	T_m (°C) ^a	Wt % Crystallinity	T_m (°C) ^a
HyPPSO ₃ Na(2)A	54	127	54	126
HyPPSO ₃ Na(2)Q	47	122	39	124
HyPPSO ₃ Na(5)A	52	120	46	119
HyPPSO ₃ Na(5)Q	37	120	32	118
HyPPSO ₃ Na(10)A	34	115	27	116
HyPPSO ₃ Na(10)Q	22	107	21	107
HyPPSO ₃ Na(20)A	13	96	4	96
HyPPSO ₃ Na(20)Q	9	97	—	—

^a Taken as the point where the melting endotherm displays maximum excursion from the baseline in the DSC scan.

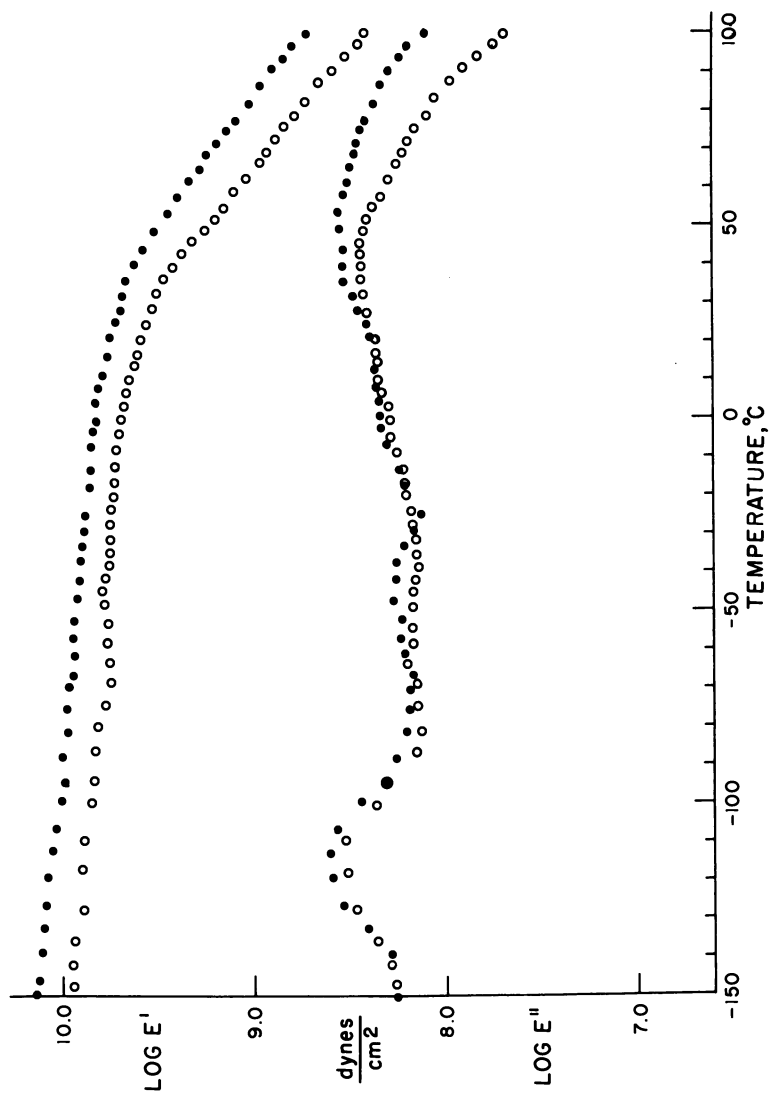


Figure 3. Dynamic mechanical results for HyPFO₃Na(2) at 11 Hz: (●) annealed; (○) quenched

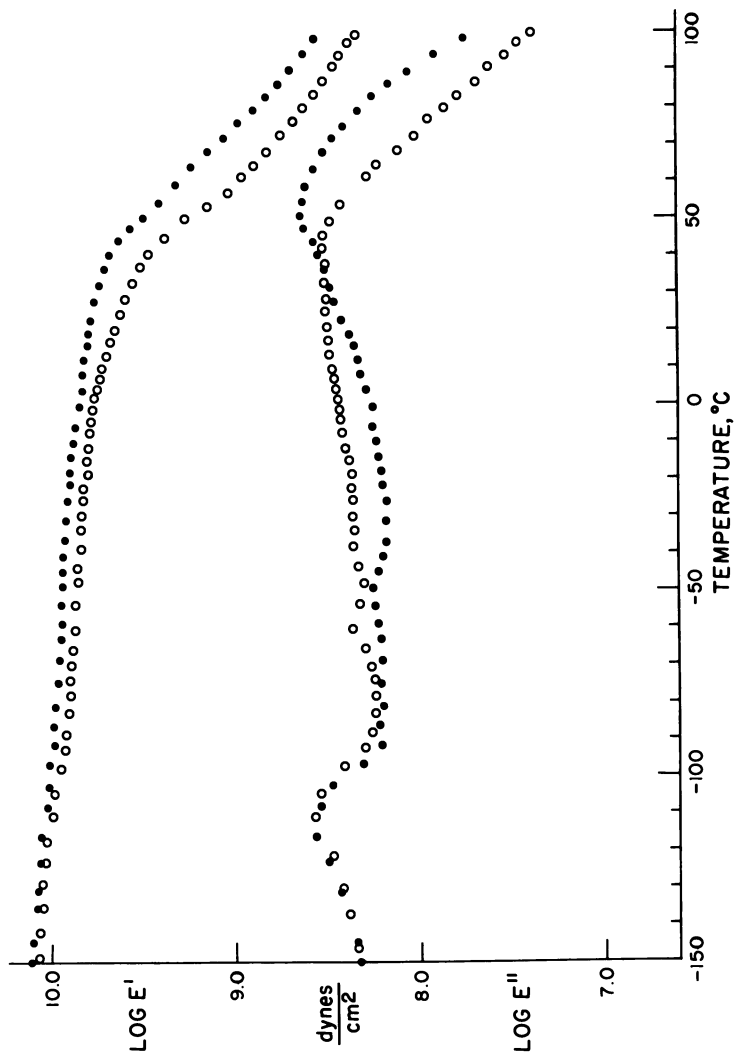


Figure 4. Dynamic mechanical results for HyPPO₃Na(5) at 11 Hz: (●) annealed; (○) quenched

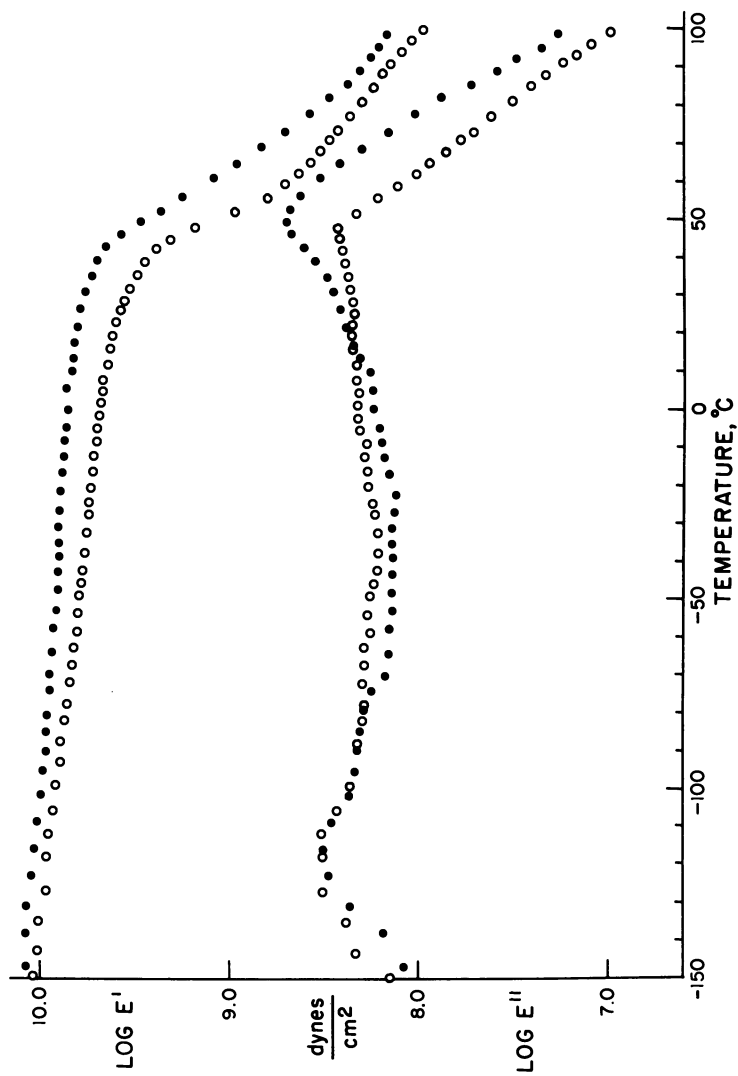


Figure 5. Dynamic mechanical results for HyPPO₃Na(10) at 11 Hz: (●) annealed; (○) quenched

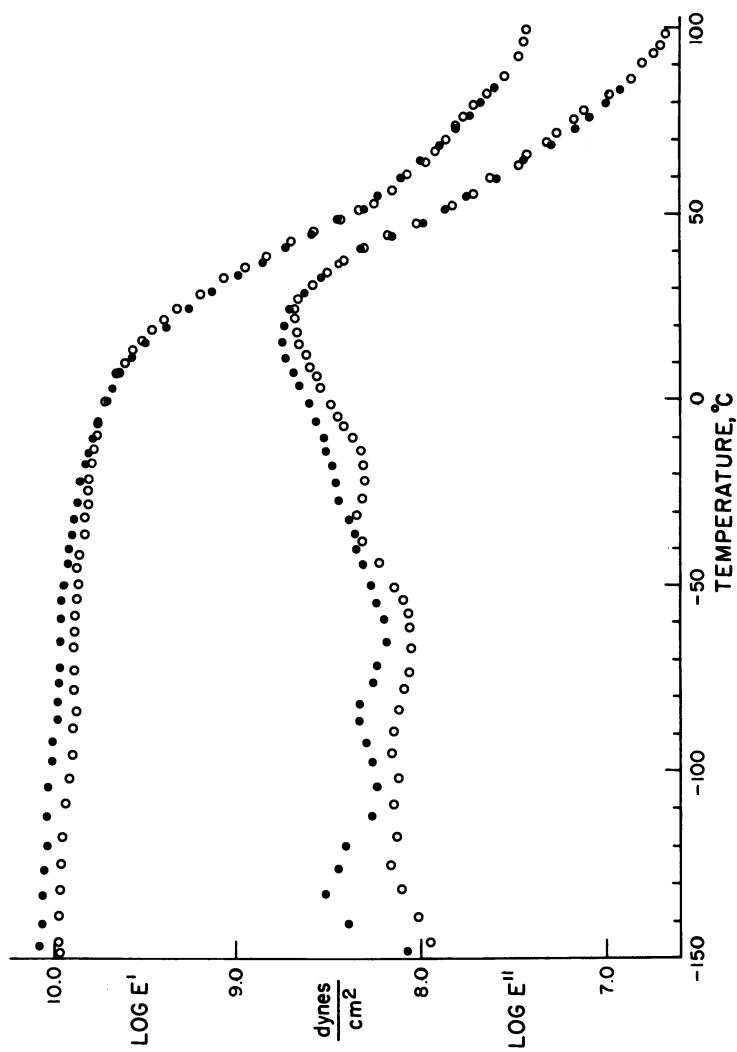


Figure 6. Dynamic mechanical results for HyPPO₃Na(20) at 11 Hz: (●) annealed; (○) quenched

relaxation labeled γ' does appear somewhat larger for the annealed case than for the quenched sample. Samples HyPPSO₃Na(5) and HyPPSO₃-Na(10) react identically to their changing thermal histories. The α relaxation is observed to increase in both magnitude and temperature on annealing, while the β and γ' relaxations remain relatively unchanged with respect to temperature, though somewhat greater in magnitude in going from the annealed to the quenched case. The thermal history of both samples has essentially no effect on the behavior of the α relaxation. A discussion of the effect of thermal history on the behavior of Sample HyPPSO₃Na(20) must be prefaced by noting that the annealing temperature of 80°C used in this study is very close to the melting temperature observed by DSC for this material. Therefore the change in crystallinity between the quenched and annealed samples is quite small, as shown in Table II. Nonetheless Figure 6 demonstrates the fact that the α relaxation increases somewhat in magnitude while decreasing just slightly in temperature with annealing. The β relaxation, which is distinct in the quenched case, merges with the α relaxation peak to become virtually indistinguishable in the annealed sample. Both the γ' and γ relaxations increase in magnitude on annealing, while displaying no change in position. A summary of the relaxation temperatures determined for these samples at 11 Hz is given in Table III. From this table it can be seen that the temperatures of both the α and γ' relaxations clearly decrease as the degree of sulfonation is increased. For both the quenched and annealed cases the β relaxation is seen to increase in temperature on going from Sample HyPPSO₃Na(2) to Sample HyPPSO₃-Na(5), but then drop as the degree of sulfonation is increased above the level found in Sample HyPPSO₃Na(5). The temperature of the γ relaxation displays no significant change with variations in the sulfonation level.

The effect of water on the dynamic mechanical behavior of a hydrogenated, sulfonated PP is displayed in Figure 7 for a quenched film of Sample HyPPSO₃Na(20). The sample labeled "dry" had been stored in

Table III. Temperatures^a of Mechanical Relaxations in Hydrogenated, Sulfonated PP's (°C at 11 Hz)

Sample	γ	γ'	β	$\alpha (E'')$	$\alpha (\tan \delta)$
HyPP	-115	—	-3	80	100
HyPPSO ₃ Na(2) A	-115	-45	20	60	95
HyPPSO ₃ Na(5) A	-113	-50	30	55	80
HyPPSO ₃ Na(10) A	-115	-80	15	50	68
HyPPSO ₃ Na(20) A	-133	-83	-20	15	45
HyPPSO ₃ Na(2) Q	-133	-60	10	43	80
HyPPSO ₃ Na(5) Q	-110	-60	12	43	62
HyPPSO ₃ Na(10) Q	-120	-65	0	46	55
HyPPSO ₃ Na(20) Q	-120	-90	-33	25	45

^a All temperatures have error bounds of $\pm 3^\circ\text{C}$.

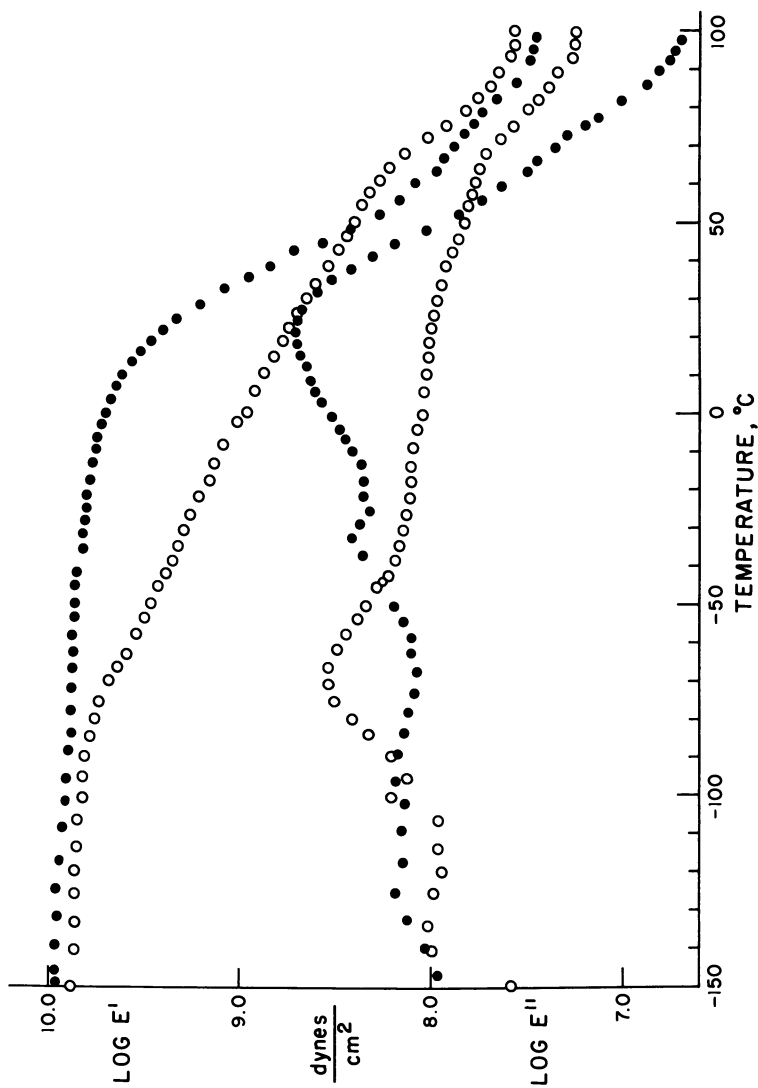


Figure 7. Effect of water on the dynamic mechanical results for a quenched film of HyPPSO₃Na(20) at 11 Hz: (●) dry; (○) water saturated

a desiccator under vacuum at room temperature until studied and had been exposed only to the moisture in the air. The water-plasticized sample, on the other hand, had been stored overnight in a beaker of distilled water at room temperature. This process resulted in a water uptake equivalent to 43% of the initial weight of the sample, which corresponds to roughly 11 water molecules per sulfonate group. It can be seen in Figure 7 that the α relaxation, which is the dominant relaxation mechanism in this material, is shifted from a temperature of 25°C for the dry sample to -70°C for the water-plasticized sample. This result parallels the behavior seen previously in water studies on the unhydrogenated, sulfonated PP's (2).

The α relaxation region undergoes significant changes as the degree of sulfonation is increased. This is best demonstrated in the plot of $\tan \delta$ vs. temperature given in Figure 8 for annealed films of the four materials studied. The magnitude of the α relaxation peak is seen to increase steadily with increasing sulfonation, while its position clearly decreases in temperature. Figure 9 shows the $\tan \delta$ vs. temperature behavior of both quenched and annealed films of Sample HyPPSO₃Na(10). Thermal history alters the behavior of the α relaxation in a different fashion than does the level of sulfonation. While increasing the level of sulfonation causes the magnitude of the α relaxation to increase with a corresponding temperature decrease, annealing causes both magnitude and temperature to increase. The α relaxation temperatures determined from $\tan \delta$ measurements are included in Table III.

Dielectric Measurements. Dielectric measurements on the hydrogenated, sulfonated PP's suffer from several drawbacks. Among these are the fact that (1) these materials are known to possess some absorbed water; (2) they contain a small amount of nitrogen in an undetermined form; and (3) they are heterogeneous in that they contain both an amorphous and a crystalline phase as well as an apparent ionic phase. A comparative plot of $\tan \delta_\epsilon$ values against temperature for three of the samples is displayed in Figure 10. It is seen that the behavior of the observed relaxation, which we have labeled α , correlates well with the behavior of the mechanical α relaxation. Both are found to increase in magnitude and decrease in temperature as the degree of sulfonation increases. For Sample HyPPSO₃Na(2) the $\tan \delta_\epsilon$ vs. temperature plot does not display a relaxation maximum in this region, though the magnitude of $\tan \delta_\epsilon$ does increase continuously above -40°C and reaches a value of 0.15 at 100°C. However, the $\tan \delta_\epsilon$ values measured for Samples HyPPSO₃Na(5), (10), and (20) are extremely large and clearly continue to increase sharply above the relaxation region. Correcting for dc conductivity results in only a moderate decrease in the $\tan \delta_\epsilon$ values. It appears that the α relaxation is superimposed on some other phenomenon occurring in these materials, obscuring the dielectric relaxation studies.

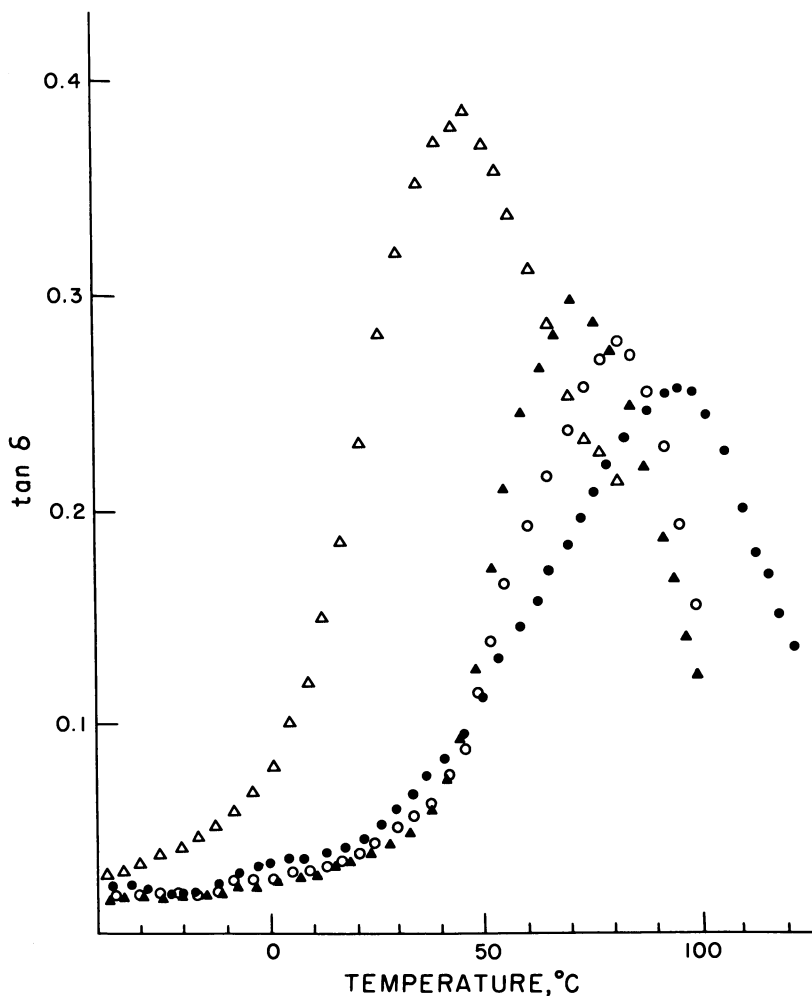


Figure 8. Comparative $\tan \delta$ results for annealed HyPPSO_3Na films in the region of the α relaxation: (●) $\text{HyPPSO}_3\text{Na}(2)$; (○) $\text{HyPPSO}_3\text{Na}(5)$; (▲) $\text{HyPPSO}_3\text{Na}(10)$; (△) $\text{HyPPSO}_3\text{Na}(20)$

The behavior of the $\tan \delta_\epsilon$ below 0°C for all four of the materials investigated is displayed in Figure 11. A low-temperature dielectric relaxation centered between -70° and -80°C appears to exist in these systems. This relaxation is labeled β . The magnitude of the β relaxation clearly increases as the degree of sulfonation increases. For the more highly sulfonated samples the β relaxation appears as a low-temperature shoulder on the much larger α relaxation, but in all cases the β relaxation is distinguishable. No evidence for any dielectric relaxations other than the α and β is present in these materials.

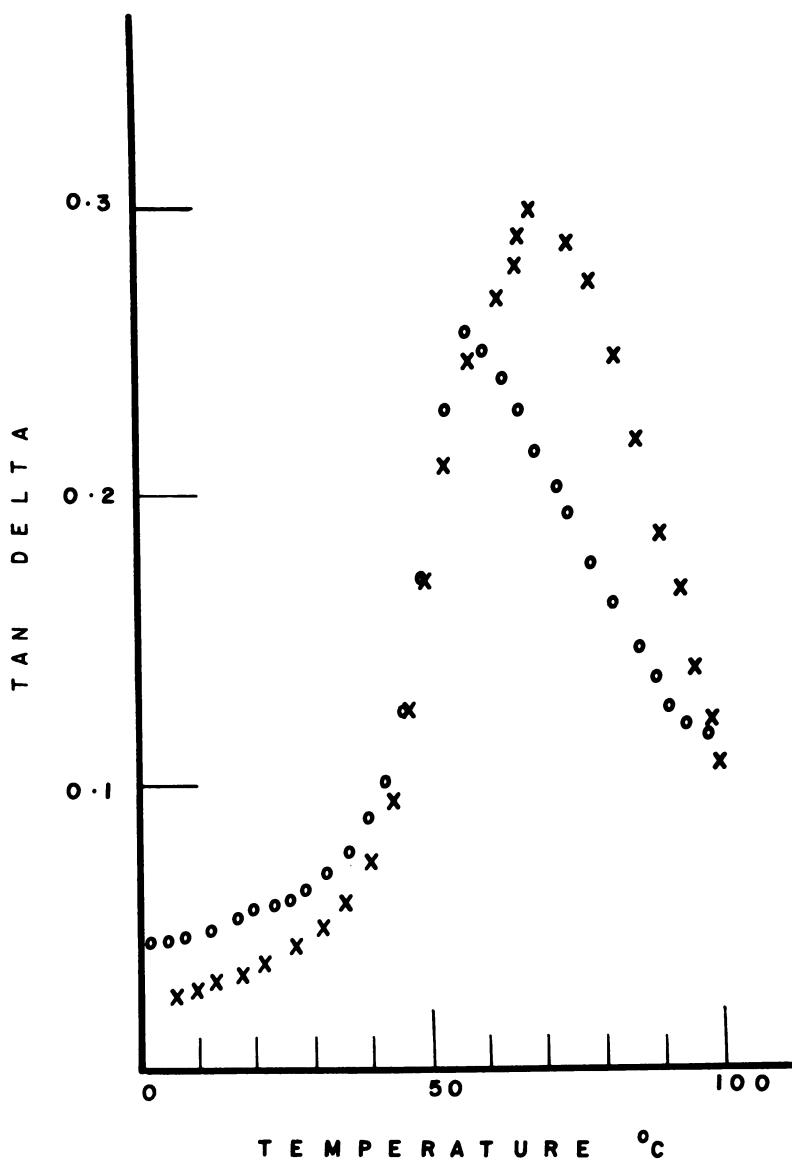


Figure 9. The $\tan \delta$ results for Sample HyPPSO₃Na(10): (x) annealed; (o) quenched

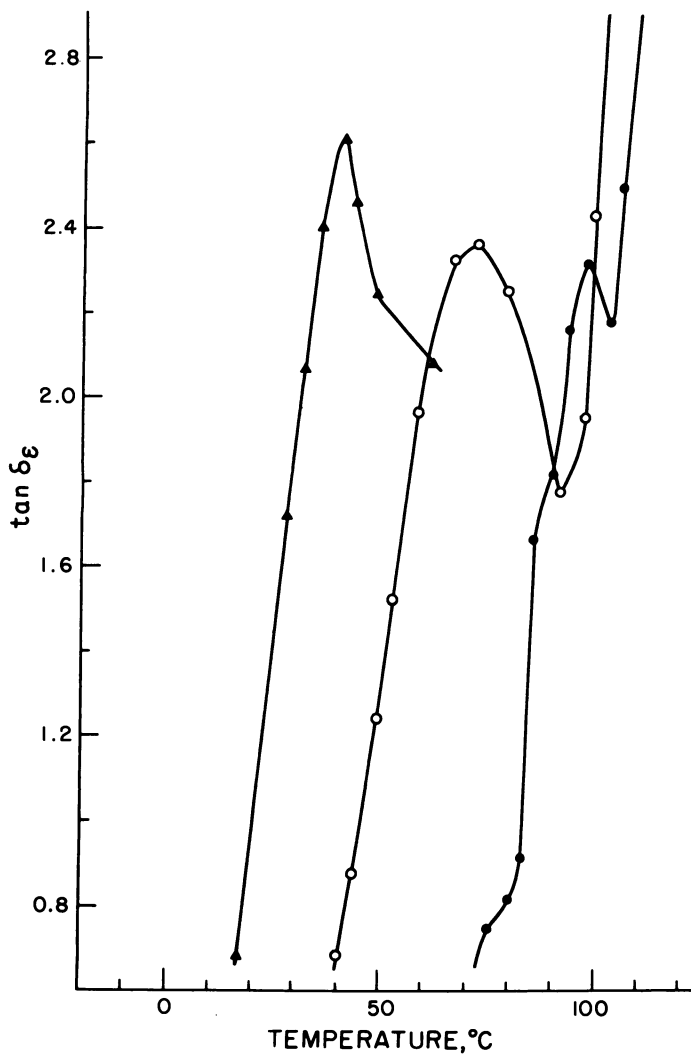


Figure 10. The $\tan \delta_\epsilon$ behavior for annealed HyPPO₃Na materials in the region of the α relaxation: (●) HyPPO₃Na(5); (○) HyPPO₃Na(10); (▲) HyPPO₃Na(20)

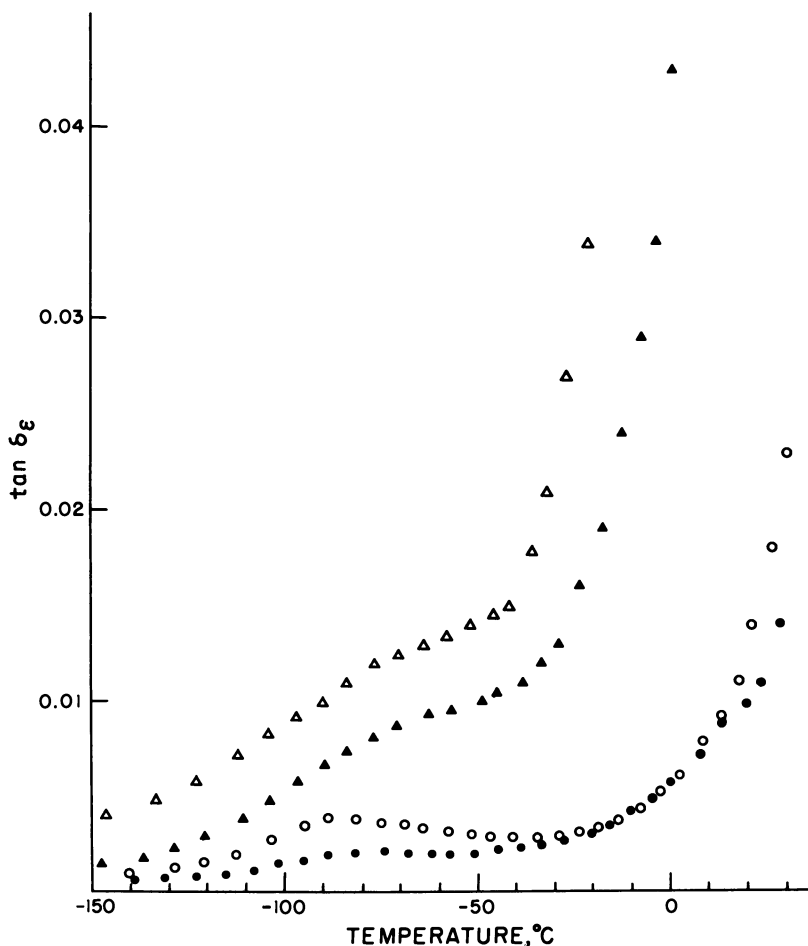


Figure 11. The $\tan \delta_\epsilon$ behavior for annealed HyPPO_3Na materials at low temperatures: (●) $\text{HyPPO}_3\text{Na}(2)$; (○) $\text{HyPPO}_3\text{Na}(5)$; (▲) $\text{HyPPO}_3\text{Na}(10)$; (△) $\text{HyPPO}_3\text{Na}(20)$

While the $\tan \delta_\epsilon$ values measured for the materials in this study are unusually large, the dielectric constants measured likewise increase tremendously in the region of the α relaxation. Figure 12 shows the temperature dependence of ϵ' at 0.1 kHz for an annealed film of Sample $\text{HyPPO}_3\text{Na}(10)$. The value of ϵ' for this material increases so rapidly that the figure was prepared by plotting $\log \epsilon'$ against temperature. Such a large change in the ϵ' value cannot be accounted for by a simple orientational dielectric relaxation mechanism. Similar ϵ' behavior was seen for Samples $\text{HyPPO}_3\text{Na}(5)$ and $\text{HyPPO}_3\text{Na}(20)$.

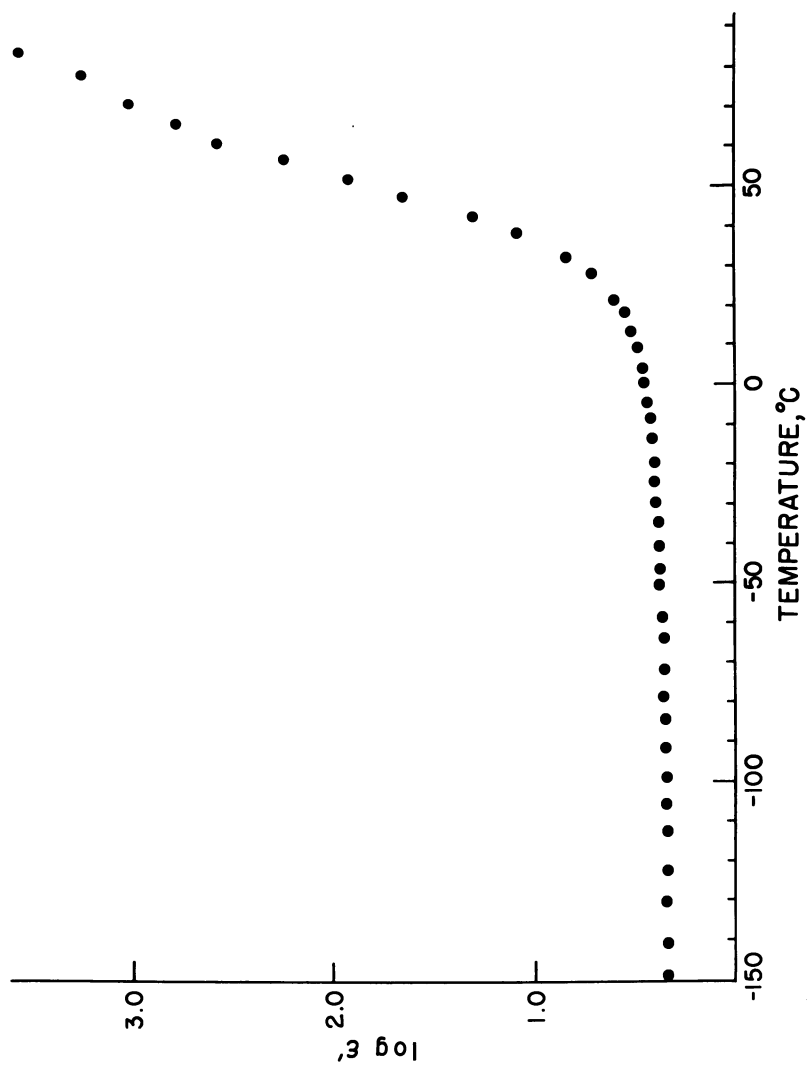


Figure 12. Temperature dependence of $\log \epsilon'$ for an annealed film of Sample HyPPSO₃Na(10)

Discussion

Thermal Properties. The results of the DSC experiments on the HyPPSO₃Na systems display both a high-temperature and a lower-temperature endotherm for all samples investigated. The nature of the high-temperature peak is unaffected by annealing at room temperature for long periods of time. However, annealing at 80°C for three days causes this high-temperature endotherm to increase in both magnitude and temperature, and become significantly sharpened. While the high-temperature endotherm is independent of effects occurring at room temperature, the lower-temperature peak exists only when the material has been maintained at ambient conditions for a moderate period of time. The magnitude of this endotherm is related both to the amount of time a sample spends at room temperature and to the level of sulfonation. Its temperature is independent of composition, but it does appear to be a function of the time maintained at room temperature.

According to Flory (10) the dependence of the equilibrium melting point on the concentration of crystallizable units in a random copolymer should be given by the equation

$$1/T_m - 1/T_m^\circ = -(R/\Delta H_u) \ln N_A \quad (3)$$

where T_m is the melting point of the copolymer, T_m° that of the crystalline homopolymer, N_A the mole fraction of crystallizable units in the copolymer, and ΔH_u the heat of fusion per mole of homopolymer repeat unit. A plot of $1/T_m$ vs. $-\ln N_A$ for annealed films of the HyPPSO₃Na copolymers is given in Figure 13, where T_m is taken as the temperature at which the high-melting endotherm displays maximum excursion from the baseline. It is seen that a straight line results and that the intercept gives a T_m° value of 132.5°C. This agrees well with the T_m of 131°C determined experimentally for the completely hydrogenated PP (9). The slope yields a ΔH_u value of 347 cal/mol of $-\text{CH}_2-$, which is less than half of the ΔH_u value of 802 cal/mol of $-\text{CH}_2-$ determined by the polymer-diluent technique for fully saturated PP. However, it is commonly seen for polymers that the ΔH_u value determined by the copolymer method is less than that determined by the diluent method (11). This discrepancy is generally attributed to both the inability to measure the equilibrium melting point in such systems and the inability to achieve equilibrium conditions during the crystallization process. It is seen then that the position of the high-temperature endotherm depends qualitatively on composition in the manner predicted by theory for random copolymers. Its failure to comply quantitatively with theory is typical of most copolymer systems.

Marx and Cooper have demonstrated that in ethylene-based ionomers, the ease of forming a low-temperature melting peak in the DSC

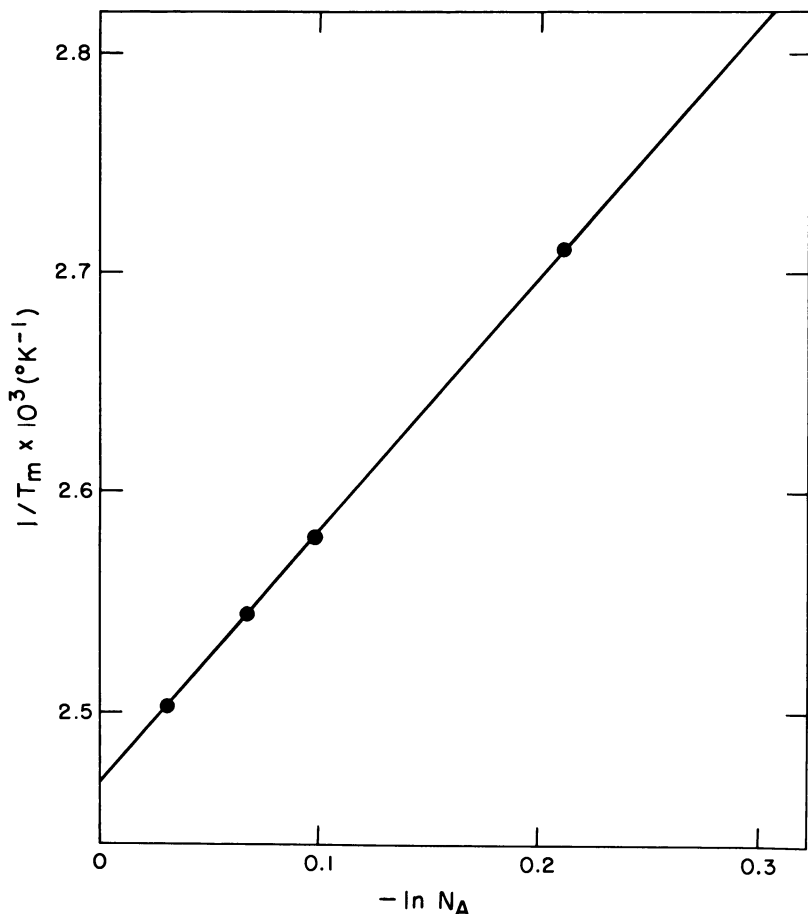


Figure 13. Plot of $1/T_m$ vs. $-\ln N_A$ for annealed films of hydrogenated, sulfonated PP's ($1/T_m - 1/T_m^\circ = (-R/\Delta H_\mu) \ln N_A$; $\Delta H_\mu = 347 \text{ cal/mol } (-CH_2-)$; $T_m^\circ = 132.5^\circ\text{C}$)

scan by annealing at room temperature increases slightly in going from low-density polyethylene to ethylene-methacrylic acid copolymers, but is augmented dramatically when the methacrylic acid units are neutralized to sodium salts (8). Since the acid and salt groups are assumed to be excluded from the crystal lattice, Marx and Cooper suggest that the distance between the noncrystallizable repeat units in each chain segment is the maximum lamellar thickness into which that chain segment can fit. They propose that long, uninterrupted runs of ethylene repeat units give rise to the crystals that melt at the higher temperatures while crystallites composed of short, imperfect polyethylene segments between more closely spaced acid or salt groups result in the lower-melting crys-

tals. However, this does not explain the reason for discrete endotherms as opposed to one quite broad melting peak, nor does it address the question of why the effect is more distinct for the ion-containing systems than for the ethylene-methacrylic acid copolymers.

It has been shown that in ethylene-methacrylic acid copolymers, the supercooling required before crystallization occurs increases as the acid groups are neutralized (12, 13). This phenomenon has been attributed to the increase in melt viscosity, which has been shown to be significantly higher in ionomers than in ethylene-methacrylic acid copolymers or in unsubstituted polyethylene (14). If the changes in supercooling and melt viscosity are considered along with the ideas proposed by Marx and Cooper, an explanation for the thermal behavior of the HyPPSO₃Na systems can be proposed. The longer, uninterrupted runs of polyethylene repeat units crystallize on cooling to yield the higher-melting crystals. The average length of such runs, and therefore the resulting lamellar thickness, decreases as the level of sulfonation increases. This explains the dependence of the high-temperature endotherm position on composition. High local viscosity causes the shorter polyethylene segments between closely spaced pendant groups to refrain from crystallizing initially on quenching. When the samples are annealed at 80°C for three days, the annealing temperature causes all but the longest polyolefin sequences to melt. However, when the samples are stored at room temperature for reasonable periods of time these smaller polyethylene segments gradually crystallize. The size of these secondary crystals is so small, though, that their lamellar thickness is undisturbed by increased levels of substitution. This explains the failure of the lower-temperature endotherm to display a temperature dependence on composition. Annealing at room temperature results in thickening of the small lamellae, which accounts for the slight increase in the melting point of the small crystals after several days at room temperature. The increased magnitude of the low-temperature endotherm with increasing sulfonation simply reflects the greater number of short ethylene sequences as the number of pendant groups is raised.

Since the lower-melting crystallites are assumed to be in the form of chain-folded lamellae, a first approximation of the thickness expected for these lamellae can be obtained from the equation

$$T_m = T_m^\circ (1 - 2\sigma_e/l\Delta H_u) \quad (4)$$

where T_m is the measured melting temperature, T_m° the melting point of an infinitely thick crystal, σ_e the surface free energy, l the lamellar thickness, and ΔH_u the heat of fusion. This equation has been derived in several crystallization theories including those of Lauritzen and Hoffman (15), Frank and Tosi (16), and Sanchez and DiMarzio (17). Using

values of the variables determined for polyethylene, the lamellar thickness of those crystallites melting at 57°C is calculated to be between 35 and 42 Å, depending on which values of σ_e , T_m° , and ΔH_u are used. Since the polyethylene unit cell displays a spacing of 2.53 Å along the fiber axis, and since this unit-cell distance incorporates two methylene groups (18), the lamellar thickness determined using this equation corresponds to between 27 and 33 methylene groups. Obviously the average spacing between sulfonated groups will depend on the degree of sulfonation for the HyPPSO₃Na materials, but from synthetic work it is known that sulfonation occurs preferentially across the cis double bonds (1). If successive cis bonds are sulfonated, then the average distance between the sulfonate groups should be roughly six repeat units, based on the cis/trans ratio of the starting PP. For the hydrogenated derivatives this corresponds to 28–30 methylene groups. It would appear from these rough calculations, then, that the polyethylene segments between the more closely spaced pendant groups are long enough to account for the lower-melting crystals.

The fact that crystals can be formed and annealed at room temperature in these systems can also be cited as evidence that the glass transition temperature (T_g) of these materials is sufficiently below room temperature. If the amorphous material were glassy at room temperature, there could not be sufficient large-scale motion to allow the formation of such crystals. This information can be applied in the interpretation of the dynamic mechanical relaxations as will be seen. No indication of a glass-to-rubber relaxation was found in the DSC scans of these materials.

Dynamic Mechanical Properties. Hydrogenation of sulfonated PP's to give a crystallizable backbone results in significant changes in the dynamic mechanical properties of the materials. When the unsaturated linkages are converted to methylene groups, the rather clear-cut behavior of the ion-containing elastomers is transformed to a much more complex behavior affected by such variables as thermal history and degree of crystallinity. As a result, the dynamic mechanical behavior of the HyPPSO₃Na materials should be examined in the light of previous studies on polyethylene, ethylene-based ionomers, and hydrogenated PP's as well as unsaturated, sulfonated PP's. This is best accomplished by analyzing each relaxation region independently as is done in the following discussion.

α RELAXATION. The α relaxation in polyethylene (19), hydrogenated PP's (20, 21), and ethylene-based copolymers (22) is found to depend on the presence of polyethylene crystals. This relaxation generally is accepted as being composite in nature, arising from both an interlamellar slip process (23, 24) and intracrystalline motion involving the simultaneous rotation and translation of chains within the crystal (25). For hydrogenated PP's, three partially merged α peaks are observed in the samples

with a sufficient level of crystallinity. All three of these peaks display a general increase in both magnitude and temperature with increasing crystallinity (20).

The behavior of the α relaxation is more complex for the HyPPSO₃Na materials. At any fixed level of sulfonation, annealing succeeds in increasing the temperature and magnitude of the α process. However, as the level of sulfonation is increased, the magnitude of the α relaxation peak also increases, despite the fact that crystallinity drops significantly in this direction. In addition it is observed that while the magnitude of the α peak increases with increasing sulfonation, the temperature decreases correspondingly. Such behavior indicates that this α mechanism differs from that detected in polyethylene. It is proposed that the α relaxation observed in the HyPPSO₃Na materials results from the superposition of two distinct processes. The one process is the composite α relaxation process normally observed in polyethylene-based systems of sufficient crystallinity. As the crystallinity of the materials studied decreases, the contribution of this complex process to the α peak also decreases. Accompanying this crystallinity-related process, though, is another relaxation mechanism originating in a separate ionic phase. It has been suggested previously (26, 27) that a relaxation reflecting motion in ionic clusters or domains should occur in ionomer systems and, in the case of monovalent salts, should appear in the temperature range of 50°–100°C. Such a relaxation has been observed in ethylene–methacrylic acid- and ethylene–acrylic acid-based ionomers (28, 29, 30, 31), in phosphonylated low-density polyethylene (32), and in the sodium salts of hydrogenated, thioglycolate-substituted PP's (4). Evidence in this study suggests that a similar process contributed greatly to the α relaxation observed in the HyPPSO₃Na systems.

The proposal that the α relaxation is attributable in part to a relaxation mechanism occurring in microphase-separated ionic clusters is based on several factors. The fact that the α peak increases in magnitude with increasing sulfonation indicates that this relaxation is related either to the behavior of an ionic-phase or an amorphous-phase mechanism, since crystallinity decreases as the sulfonation level is raised. However, the trend of the α peak to increase in magnitude and temperature with annealing contradicts the assignment of this peak to an amorphous-phase origin. Previous small-angle x-ray work on ethylene–acrylic acid-based ionomers (33) suggests that annealing either increases or alters the morphology of phase-separated ionic clusters. Therefore the annealing behavior of the α relaxation is consistent with the ionic-phase assignment. However, the strongest support for the proposed assignment is found in the water studies conducted on these materials. If a separate ionic phase is present in the systems studied, one would expect water to migrate to the ionic clusters and avoid the more hydrophobic amorphous and crys-

talline hydrocarbon regions. As Figure 7 shows for the quenched film of Sample HyPPSO₃Na(20), the dominant α relaxation is shifted downward almost 95°C when the material is saturated with water. This demonstrates the significant plasticizing effect that water has on the α relaxation mechanism, and reinforces the assignment of the α relaxation to an ionic-phase origin.

The trend of the α relaxation to decrease in temperature with increasing sulfonation is related to the hydrophilicity of these materials. As the level of sulfonation is raised, the ability of the materials to absorb water from the air also is raised. Though attempts were made to keep these systems reasonably free from water, stringent drying procedures were not used nor were extraordinary handling precautions taken to prevent the samples from having normal contact with the atmosphere as they were being prepared for dynamic mechanical testing. As the water study on these materials demonstrates, moisture can reduce the temperature of the α relaxation significantly. Thus it would appear that the varying amounts of water absorbed by the HyPPSO₃Na materials from the atmosphere account for the decreasing temperature of the α relaxation with increasing sulfonation.

β RELAXATION. The mechanism that accounts for the β relaxation in polyethylene has been a matter of controversy for years (19, 34, 35). Studies on hydrogenated PP's (17, 18) have concluded that this relaxation is attributable to the microbrownian segmental motion accompanying the glass transition, and propose that the T_g is very dependent on crystallinity. Succeeding studies on substituted, hydrogenated PP's have likewise associated the observed β relaxations with motions accompanying the glass transition (3, 4, 36). In view of this background and the fact that the β relaxation in the HyPPSO₃Na materials appears to increase in magnitude as the degree of crystallinity decreases, the assignment of this relaxation to the glass-to-rubber transition seems reasonable.

The glass transition in a material of the type examined in this study is affected by several factors. On the basis of simple copolymer-type arguments (37, 38) one would expect the glass temperature to increase as the extent of sulfonation is increased. However, recent studies on ionomer systems demonstrate that the onset of clustering can cause a much more dramatic rise in T_g than can be explained on the basis of copolymer effects alone (2, 39, 40). Varying the level of sulfonation and thermal history alters the degree of crystallinity, which also affects the T_g in polymers of this type. The complex interaction of these variables then, must determine the behavior of the β relaxation if it is assigned correctly.

A view of the β relaxation temperatures given in Table III suggests that they are very dependent on the crystallinities of the samples studied. In every case the T_β was higher in the annealed film than in the quenched

film having the same sulfonation level. Superimposed on the crystalline contribution to the β relaxation temperature is the copolymer effect. Between Samples HyPPSO₃Na(2) and HyPPSO₃Na(5) it appears that the effect of the additional sulfonate groups outweighs the effect of the slight decrease in crystallinity. This causes higher β relaxation temperatures in the HyPPSO₃Na(5) material for both the quenched and annealed cases. However, above 6.3% sulfonation, it is seen that the temperature of the β relaxation is dominated by the effect of the decreasing crystallinity, as increasing sulfonation results in lower T_{β} values. Owing to the multiphase nature of these materials, no clear-cut effect of cluster formation on the β relaxation temperature is discernible.

The fact that the materials in this study exhibit a room-temperature crystallization process was suggested as evidence that the glass transition of these systems is below ambient temperatures. However, the β relaxation temperatures recorded in Table III are, in some cases, quite close to room temperature. This apparent contradiction results from the fact that the β relaxation is related not to a true amorphous-phase glass transition but to the apparent glass transition of a semicrystalline system, where T_g is altered significantly by the degree of crystallinity. From basic copolymer arguments alone, for example, one would expect the T_g of Sample HyPPSO₃Na(20) to be higher than that of Sample HyPPSO₃Na(2). However, such behavior is not displayed by the β relaxations of these materials because of the role that crystallinity plays in increasing the apparent T_g . Thus while the T_g 's of these materials would be considerably below room temperature if they were completely amorphous, crystallinity causes the values to be increased. The crystals that form at room temperature then increase the apparent T_g 's determined as the β relaxation temperatures.

γ' RELAXATION. Unlike the other dynamic mechanical relaxations observed in this study, the γ' relaxation does not have an analog in the dynamic mechanical behavior of polyethylene, hydrogenated PP's, or other ionomer systems. In addition, it displays no definite trends in changing temperature or magnitude as the level of sulfonation and thermal history are altered. Coupled with the fact that these systems are known to contain water as well as nitrogen, it is not possible to assign this relaxation to any specific phase or mechanism. Additional studies are necessary before this task can be approached adequately.

γ RELAXATION. The previous publications on hydrogenated PP's (20, 21) and their derivatives bearing pendant ionic groups (3, 4, 36) all have concluded that the γ relaxation is a secondary relaxation of composite nature, involving both an amorphous and crystalline component. The results of this investigation suggest no reason to disagree with these conclusions. Therefore the γ relaxation observed in the dynamic mechanical spectra of the HyPPSO₃Na materials is believed to arise from the same

mechanisms. The amorphous contribution is envisioned as resulting from a crankshaft motion with three bonds between the stem bonds of the crankshaft (after the Boyd–Breitling proposal (41)), while the crystalline contribution is believed to result from motion around defects within the crystals (25, 42).

Dielectric Properties. The extremely large increases in $\tan \delta_\epsilon$ and ϵ' values accompanying increases in temperature dominate the results of the dielectric experiments. Since these materials are known to possess some absorbed water and to contain a small amount of nitrogen in an undetermined form, the potential for both impurity ionic conduction and space-charge localization at the electrodes exists. In addition the dynamic mechanical results suggest the presence of a separate ionic phase in these systems, so the possibility of Maxwell–Wagner absorption is real as well (43, 44, 45). Independent measurement of dc conductivity was carried out, and the resulting correction of ϵ'' values demonstrated that this factor was making only a minor contribution to the overall dielectric loss measured, besides which ϵ' values should be unaffected by dc conductivity. These factors combine to suggest that while impurity ionic conduction is playing a role in the dielectric behavior of these materials, it is not the most significant component. However, drawing a distinction between interfacial polarization which occurs either at the electrodes or on an occluded phase is not readily accomplished. As a result, the source of the phenomenon observed in these systems cannot be determined absolutely. It is known though, that the Maxwell–Wagner effect will cause ϵ' values to increase only by a factor of about 2–4 if the occluded phase is spherical (46, 47); therefore attempts to explain the observed behavior via the Maxwell–Wagner concept must assume that the domains are nonspherical.

From Figure 10 it appears that a dipolar relaxation labeled α is superimposed on the phenomenon we have just discussed. The behavior of this α peak correlates well with the behavior of the dynamic mechanical α relaxation since it increases in magnitude and decreases in temperature with increasing sulfonation. The presence of this peak in the dielectric spectra of these materials and its behavior as a function of sulfonate concentration are consistent with the assignment of the mechanical α relaxation to an ionic-phase mechanism. However, it is not possible to cite this dielectric peak as proof of the mechanical assignment; the known presence of ionic impurities in these systems and the unknown origin of the large increases in $\tan \delta_\epsilon$ and ϵ' dictate that the dielectric results be interpreted with caution.

On the basis of similar arguments, an assignment of the dielectric β peak is not suggested. The magnitude of the $\tan \delta_\epsilon$ values in the region of the β peak, the fact that the magnitude of this peak appears to increase roughly in proportion to the increase in sulfonate groups, and the fact

that the temperature of this peak remains relatively constant combine to suggest that it does arise from an actual dipolar relaxation. This peak is in the same temperature range as the unassigned mechanical γ' relaxation, which might imply some relationship between the two. However the data are not sufficient to propose a mechanism for this apparent dielectric relaxation or a relationship between it and the mechanical γ' process.

Conclusions

The DSC results for HyPPSO₃Na materials demonstrate the existence of low-melting crystals that form when these polymers are maintained at room temperature. The volume fraction of such crystals increases as the degree of sulfonation is increased, but the melting temperature is unaffected by the level of sulfonation. The higher-melting crystallites qualitatively obey the Flory equation for melting-point depression in random copolymers.

The α relaxation observed by dynamic mechanical techniques is attributable in part to an ionic-phase mechanism. The existence of this relaxation is suggested as evidence for the presence of phase-separated clusters in these materials. The temperature at which the β relaxation occurs is found to result from the complex interaction of crystallinity and ionic group concentration.

The high-temperature phenomenon present in the dielectric results for these materials is believed to arise from an interfacial effect either at the electrodes or on an occluded phase. No assignment is made for the origins of the α and β relaxations observed dielectrically.

Acknowledgments

The authors are grateful to the National Science Foundation under Grant DMR 75-06916 and to the donors of the Petroleum Research Fund of the American Chemical Society for partial support of this research. The use of the facilities of the Materials Research Laboratory at the University of Massachusetts is also gratefully acknowledged.

Literature Cited

1. Rahrig, D.; MacKnight, W. J.; Lenz, R. W. *Macromolecules* **1979**, *12*, 195.
2. Rahrig, D.; MacKnight, W. J. Chapter 6 in this book.
3. Rahrig, D.; Azuma, C.; MacKnight, W. J. *J. Polym. Sci., Polym. Phys. Ed.* **1978**, *16*, 59.
4. Sanui, K.; MacKnight, W. J. *Br. Polym. J.* **1976**, *8*, 22.
5. Eisenberg, A.; King, M. "Ion-Containing Polymers"; Stein, R. S., Ed.; Academic: New York, 1977.

6. Eisenberg, A. *Macromolecules* 1970, 3, 147.
7. MacKnight, W. J.; Taggart, W. P.; Stein, R. S. *J. Polym. Sci., Polym. Symp.* 1974, 45, 113.
8. Marx, C. L.; Cooper, S. L. *J. Macromol. Sci., Phys.* 1974, B9(1), 19.
9. Sanui, K.; MacKnight, W. J.; Lenz, R. W. *J. Polym. Sci., Polym. Lett. Ed.* 1973, B11, 427.
10. Flory, P. J. *J. Chem. Phys.* 1949, 17, 223.
11. Mandelkern, L. *Rubber Chem. Technol.* 1959, 32, 1392.
12. MacKnight, W. J.; McKenna, L. W.; Read, B. E. *J. Appl. Phys.* 1967, 38, 4208.
13. MacKnight, W. J.; Kajiyama, T.; McKenna, L. W. *Polym. Eng. Sci.* 1968, 8, 267.
14. Earnest, Jr., T. R.; MacKnight, W. J. *Polym. Prepr., Am. Chem. Soc., Div. Polym. Chem.* 1977, 18(2), 391.
15. Lauritzen, Jr., J. I.; Hoffman, J. D. *J. Res. Nat. Bur. Stand., Sect. A* 1960, 64, 73.
16. Frank, F. C.; Tosi, M. *Proc. R. Soc. London, Ser. A* 1961, 263, 323.
17. Sanchez, I. C.; DiMarzio, E. A. *Macromolecules* 1971, 4, 677.
18. Meares, P. "Polymers, Structure and Bulk Properties"; Van Nostrand Reinhold Company: London, 1965; Chapter 4.
19. McCrum, N. G.; Read, B. E.; Williams, G. "Anelastic and Dielectric Effects in Polymeric Solids"; Wiley: New York, 1967; Chapter 10.
20. Sanui, K.; MacKnight, W. J.; Lenz, R. W. *Macromolecules* 1974, 7, 101.
21. Earnest, Jr., T. R.; MacKnight, W. J. *Macromolecules* 1977, 10, 206.
22. Schmieder, K.; Wolf, K. *Kolloid-Z.* 1953, 134, 149.
23. Hoffman, J. D.; Williams, G.; Passaglia, E. *J. Polym. Sci., Polym. Symp.* 1966, 14, 173.
24. Boyd, R. H. *Polym. Prepr., Am. Chem. Soc., Div. Polym. Chem.* 1976, 17(2), 125.
25. Hoffman, J. D.; Williams, G.; Passaglia, E. *J. Polym. Sci., Polym. Symp.* 1966, 15, 10.
26. Read, B. E.; Carter, E. M.; Connor, T. M.; MacKnight, W. J. *Br. Polym. J.* 1969, 1, 123.
27. Phillips, P. J.; MacKnight, W. J. *J. Polym. Sci., Polym. Chem. Ed.* 1970, A2(8), 727.
28. MacKnight, W. J.; McKenna, L. W.; Read, B. E. *J. Appl. Phys.* 1967, 38, 4208.
29. Longworth, R.; Vaughan, D. J. *Nature* 1968, 218, 85.
30. Otocka, E. P.; Kwei, T. K. *Macromolecules* 1968, 1, 244.
31. Otocka, E. P.; Kwei, T. K. *Macromolecules* 1968, 1, 401.
32. Phillips, P. J.; Emerson, F. A.; MacKnight, W. J. *Macromolecules* 1970, 3, 767.
33. Taggart, W. P., Ph.D. Thesis, University of Massachusetts, Amherst, MA, 1973.
34. Stehling, F. C.; Mandelkern, L. *Macromolecules* 1970, 3, 242.
35. Illers, K. H. *Kolloid. Z. Z. Polym.* 1972, 250, 426.
36. Neumann, R.; Sanui, K.; MacKnight, W. J. *Macromolecules* 1975, 8, 665.
37. Wood, L. A. *J. Polym. Sci.* 1958, 28, 319.
38. Gordon, M.; Taylor, J. S. *J. Appl. Chem.* 1952, 2, 493.
39. Matsuura, H.; Eisenberg, A. *J. Polym. Sci., Polym. Phys. Ed.* 1976, 14, 1201.
40. Noshay, A.; Robeson, L. M. *J. Appl. Polym. Sci.* 1976, 20, 1885.
41. Boyd, R. H.; Breitling, S. M. *Macromolecules* 1974, 7, 855.
42. Crissman, J. M.; Passaglia, E. *J. Appl. Phys.* 1971, 42, 4636.
43. Hill, N. E.; Vaughn, W. E.; Price, A. H.; Davies, M. "Dielectric Properties and Molecular Behavior"; Van Nostrand Reinhold Company: London, 1969; Chapter 5.

44. Daniel, V. V. "Dielectric Relaxation"; Academic: New York, 1967; Chapter 14.
45. Phillips, P. J.; Emerson, F. A.; MacKnight, W. J. *Macromolecules* **1970**, *3*, 771.
46. Sillars, R. W. *J. Inst. Electr. Eng.* **1937**, *80*, 378.
47. North, A. M.; Reid, J. C.; Shortall, J. B. *Eur. Polym. J.* **1969**, *5*, 565.

RECEIVED November 20, 1978.

Theoretical Model for the Structures of Ionomers: Application to Nafion Materials

K. A. MAURITZ and C. J. HORA

Diamond Shamrock Corporation, T. R. Evans Research Center, P.O. Box 348, Painesville, OH 44077

A. J. HOPFINGER

Department of Macromolecular Science, Case Western Reserve University, Cleveland, OH 44106

A general formalism is presented to describe the structural organization of ionomers under different physicochemical conditions. The theory is applied specifically to Nafion. Resultant predicted properties are compared with experimental findings. Preliminary application of the predicted ionomeric molecular structure of Nafion to modeling ion transport through Nafion chlor-alkali separators is discussed and evaluated.

Considerable progress has been made in the solution theory of poly-electrolytes. However, for the condensed-phase analogs of poly-electrolytes, ionomers, this is not the case. Eisenberg (1) has put forth an initial theory of ionomer structure that contains conceptual formalisms of general use. His theory has been consulted extensively in the work reported here. Ponomarev and Ionova (2) have attempted to construct a sophisticated statistical mechanical model to describe the thermodynamics of ionomers. Recently, Gierke (3) has described a theory of ion transport in the Nafion ionomer based on a specific molecular organization.

To be complete, three physicochemical states of the ionomeric material need to be considered in a structural theory: (a) dry; (b) in aqueous solution; and (c) in aqueous solution containing mobile ions. There is increasing evidence (4) that the amount of water present in the ionomer can influence structural, mechanical, and thermodynamic properties. Thus these latter two states must be viewed as possessing substates that depend on water content.

0-8412-0482-9/80/33-187-123\$05.50/0
© 1980 American Chemical Society

Obviously, considering only aqueous solution is a limitation. However, this is the solvent of interest in most ionomer applications. Ionomers, irrespective of physicochemical state, tend to phase separate. That is, the polar groups, along with associated solvent and ions (if present), cluster together to the exclusion of the nonpolar units. This molecular picture is the one that emerges from the detailed studies of a relatively limited number of ionic polymers. All of these are hydrocarbon-based materials and include polyethylene (5–13), polystyrene (14–19), polybutadiene (20, 21), and some polar polymers containing low molecular weight salts (22). In all cases the bound ionic species was a carboxyl group. One should keep in mind that the degree and morphology of the phase-separated material will depend on the relative amounts of polar and nonpolar units. Most ionomers are excessively rich in nonpolar material. Uptake of water by polar groups tends to equalize the quantity of polar and nonpolar phases.

Readers not familiar with polymer science and/or statistical thermodynamics probably should have the following reference books in hand when reading this chapter: *Textbook of Polymer Science*, F. W. Billmeyer, Jr., John Wiley, New York (1971) and *Introduction to Statistical Thermodynamics*, T. Hill, Addison-Wesley, Reading, Mass. (1960).

The goal of the work reported here was to devise a theory that predicts the polar/nonpolar phase separation as a favorable thermodynamic process. In addition, the effects of each of the physicochemical forms on the thermodynamic and structural characteristics of the biphasic material were sought. The current molecular model was not developed to predict mechanical or thermal behavior of ionomers. Hence, properties like glass transition and melt temperatures, storage, and shear moduli cannot be determined from the current model. We must also stress that this modeling work is still in its infancy. As such, it has used several tenuous assumptions that must be tested. The formalism is a start, but not the end, to devising a comprehensive treatment of ionomeric structure.

A pseudo-quantitative application of the theoretical formalism has been made for Nafion. The values for the requisite molecular parameters were estimated from a combination of experimental bulk thermodynamic data and molecular structure calculations using both molecular and quantum mechanics (23, 24). A constraint was imposed in the development of the structural formalism. The model was constructed so that the predicted structural information could be used in a computer simulation of ion transport through an ionomer, that is, modeling the ionomer as a permselective membrane.

The model has the capacity to:

1. demonstrate biphasic separation as a favorable thermodynamic process in ionomers. The interrelationship be-

- tween competing interactions necessary for polar cluster formation can be identified explicitly on the molecular level.
2. predict water absorption and density behavior as a function of equivalent weight and solution molarity for Nafion that is in good agreement with experimental findings. More significantly, the model makes it possible to trace the molecular origins of the interactions giving rise to the macroscopic behavior. Thus interrelationships between, for example, equivalent weight and number of water molecules in clusters can be established correspondingly.
 3. support implicitly (by the prediction of current efficiency as a function of caustic concentration, which is in agreement with experiments for Nafion as a chlor-alkali separator) the reasonableness of the predicted molecular structure organization of Nafion, which is assumed to be qualitatively representative of many ionomers.

Theory

General Mechanism of Cluster Formation. We begin by restricting ourselves to an equilibrium representation of ionomer structure. Then, on a time-average basis, the polar groups on the ionomer sidechains are able to "see" one another through their dipolar interactions. From Monte Carlo simulation calculations we were able to show that the configurational dipole-dipole interaction free energy for unrestricted dipolar motion has the empirical form

$$F = C \ln (n_c - 1) \quad (1)$$

where C is a constant characteristic of (a) lifetime of the dipoles; (b) strength of the dipoles; and (c) dielectric medium. The n_c corresponds to the number of interacting dipoles.

In the ionomer, mutual localization of polar groups through their dipolar behavior necessitates expansion and contraction of the associated polymer chains. If we assume this process is random to the extent that chain expansions and contractions are equal in number, then the elastic deformation energy per dipole is

$$W = \frac{3kT}{2 \langle h^2 \rangle} (\Delta d^2) \quad (2)$$

where T is temperature, Δd the average chain expansion/contraction, and $\langle h^2 \rangle$ the mean square end-to-end chain dimension. Equation 2 is valid strictly for a Gaussian chain. However, we can extend its utility by defining Δd in terms of the physicochemical state of the ionomer and by generalizing the definition of $\langle h^2 \rangle$ to

$$\langle h^2 \rangle = N \left[\left(\frac{n-1}{2} \right) l \right]^\Delta \frac{1 - \cos \alpha_0}{1 + \cos \alpha_0} \quad (3)$$

- N = the number of monomer units/chain;
 n = the number of CX_2 — units/monomer backbone chain;
 l = trans distance for the CCC backbone groups;
 α_0 = the CCC backbone valence bond angle;
 Δ = chain ordering parameter; fixed = 2 for a random distribution of chain segments in space.

Recently, we came to doubt the applicability of Equation 3, especially to ionomers having perfluoro backbones. In the case of ionomers having linear hydrocarbon backbones, an all-trans chain geometry is the lowest energy conformation. In addition, some polyethylene-like crystallinity is suggested (5-13). Nevertheless, other conformational states are possible as can be seen in a conformational energy map for polymethylene shown in Figure 1. For a perfluoro material the all-trans conformation is energetically unreasonable as shown in Figure 2, a plot of conformational energy vs. the torsional angle θ between adjacent $-CF_2-$ units. Also, the trans state is energetically unfavorable for both backbone $C-C$ bond rotations adjacent to the ionomeric sidechain. Thus we might

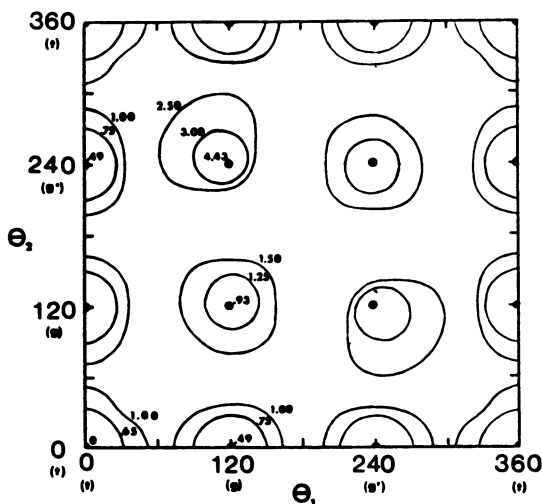
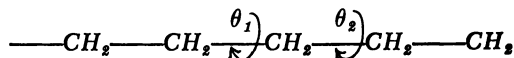
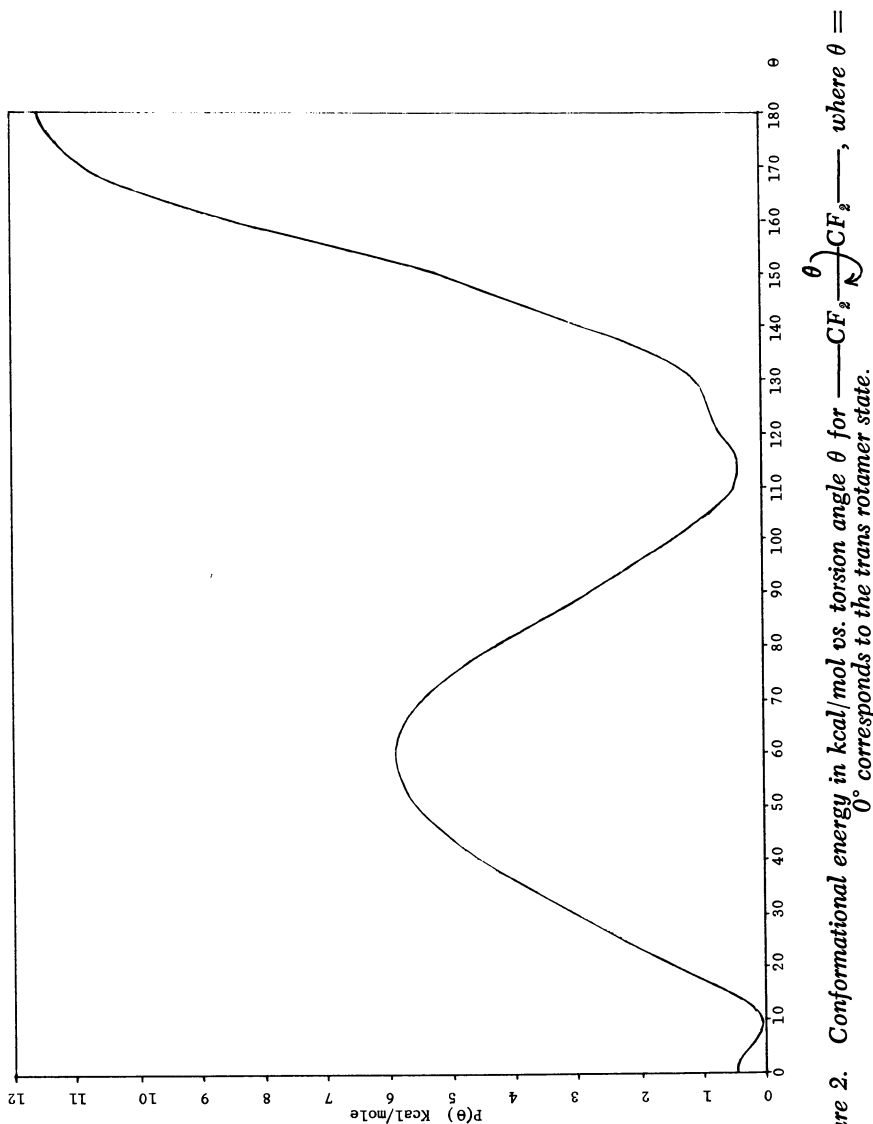


Figure 1. Second nearest neighbor conformational energy map for polymethylene:



The energy contours are in kcal/mol with the all-trans conformation ($\theta_1 = 0^\circ$ and $\theta_2 = 0^\circ$) being the global energy minimum.



expect $\langle h^2 \rangle$ in an ionomer to be different from that predicted by Equation 3. In addition, the mathematical form of the equation may be wrong irrespective of the assignment of Δ . We hope to overcome these difficulties by doing extended conformational analyses from which we can estimate the probability of each h^2 . By integration averaging over the set of h^2 and corresponding probabilities, we should be able to determine $\langle h^2 \rangle$ values to use in Equation 2. Tacticity and the even/oddness of the number of backbone $\text{—CX}_2\text{—}$ spacers in a monomer unit may also be important to $\langle h^2 \rangle$, depending, primarily, on the length and physicochemical state of the sidechain.

We stress that the correct determination of $\langle h^2 \rangle$ is essential to our model; $\langle h^2 \rangle$ is highly responsible for dictating cluster size.

In the most simple representation, the size of a cluster, in terms of n_c , could be found by solving

$$F = W + T\Delta S(n_c) \quad (4)$$

where $\Delta S(n_c)$ is the change in the entropy of the ionomer attributable to clustering. This term can reasonably be equated to the loss in the configurational entropy of a typical chain because of clustering, which when normalized to a per dipole scale is,

$$\Delta S(n_c) = - \left(\frac{n_c}{N} \right) R \ln [N!(N - n_c)!] \quad (5)$$

where $N = (\text{chain molecular weight})/(\text{monomer molecular weight})$. The right-hand side of Equation 5 can be simplified using Stirling's approximation. In practice, additional structure and energy terms must be considered for each physicochemical state. We now discuss the physicochemical states in this regard.

Dry State. The sidechain polar groups, neutral or charged, serve as the dipoles. The only additional energy term that needs to be added to Equation 4 is a destabilizing term on the right to account for the surface tension between the cluster and nonpolar phases. Equation 4 then takes the form,

$$F + \epsilon r^2(n_c) = W + T\Delta S(n_c) \quad (6)$$

where $r(n_c)$ is the radius of the cluster and $\epsilon = 4\pi\epsilon_0$ (where ϵ_0 is the surface energy per unit area).

In Aqueous Solution. When the ionomer is placed in aqueous solution, water molecules diffuse into the ionomer and hydrate about polar groups. Depending on the history of the ionomeric material as well as

the relative rates of aqueous diffusion and cluster formation, clusters may or may not form. We have considered the case in which clusters are not formed prior to solvating. In this situation we first must consider the polar group-hydrate structure which is termed a hydration shell. Again, the size of the hydration shell is postulated to result from a free energy balance. Polar group-water interactions coupled with water-water intra-hydration shell interactions are balanced against the elastic deformation energy needed to move chains out of the way of the growing hydration shell. In addition, a surface tension term again must be included to account for the aqueous-nonpolar interface generated by the growing hydration shell. The general form of this energy balance is

$$K_e(r_h(n_h)^m - r_p^m) + \epsilon' r_h^2 = n_b A_1 + (n_h - n_b) A_o \quad (7)$$

where the first term on the left is a generalized, spherically symmetric deformation energy in which K_e is the elastic force constant, $r_h(n_h)$ the radius of the hydration shell for n_h water molecules in that shell, and r_p the unsolvated radius of the polar sidechain unit. The second term on the left is the interfacial surface tension term with ϵ' being the water-nonpolar surface tension energy. The first term on the right is the free energy of hydration of the polar sidechain unit with n_b being the effective number of first-layer hydrating water molecules, and A_1 the average free energy of hydration per water molecule. The second term on the right is free energy gain attributable to water-water hydration shell interactions with A_o being the average free energy of interaction per water molecule.

For the assumed temporal basis, the hydration shells now come together through dipolar interactions to form a hydrated cluster. The form of Equation 6 can be used once a term is added on the left to account for a potential loss of free energy owing to the expulsion of water molecules from overlapping hydration shells. However, this loss in energy can be compensated by interhydration shell water-water interactions and a net decrease in the total water-nonpolar interfacial area. In total, Equation 6 now becomes

$$F' + \epsilon' r^2(n_c) + O(n_c, n_h, F') = W' + T\Delta S(n_c) + O'(n_c, n_h, A_o) \quad (8)$$

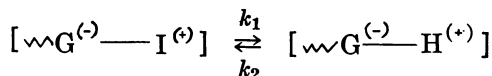
where the expulsion overlap function is of the form

$$O(n_c, n_h, F') = \phi_1 \Delta R^2(n_c, n_h, F') r_h(n_c) + \phi_2 \Delta R^3(n_c, n_h, F') \quad (9)$$

in which ϕ_1 and ϕ_2 are molecular constants characteristic of groups present, and ΔR is the radial overlap distance of two hydration shells. $O'(n_c, n_h, A_o)$, the interhydration water-water energy term, has the same form in Equation 9, but with different ϕ 's which depend on A_o .

The primes associated with F and W in Equation 8 are to remind one that the numerical forms of these expressions differ from those of Equation 6. The effective dipole of a hydration shell is now attributable to the sidechain group (irrespective of neutral or charged form) plus the net dipolar arrangement of the water molecules. Hence F' is different from F . The elastic work W' requires moving hydration shells plus polymer chains. Thus W' is not equal to W .

Aqueous Solution Containing Ions. We will assume for



where $\text{W}G^{(-)}$ is the anionic form of the polar sidechain unit and $I^{(+)}$ is the mobile solution cation, that $k_2 > k_1$. Under these conditions the size of the polar clusters can be found by solving Equation 8. However, the numerical constants in the equation will be different from those of the purely aqueous solution situation. Now the effective hydration shell dipole also will depend on the type of mobile cation and its solution concentration. The size of the ion-dipole hydration shell also will be altered by the presence of the solution cation. It must be stressed that $[\text{W}G^{(-)}\text{---}I^{(+)}$] is not considered to be a rigid form possessing a discrete bond length. Rather, on a time-average basis this dipolar assembly is realized as a significant state of the system.

In this regard a current flaw in our structural model centers on our inability to describe changes in the average location of ions in a cluster as a function of water content. Mauritz and Lowry (4) have evidence that the sodium ions in Nafion ionomers become increasingly mobile as water content increases. In addition, water not directly involved in hydration to the ions behaves much like bulk water. Mauritz and Lowry (4) are developing a correction to the cluster theory of our current model. It is built around a four-state ion-counterion hydration model, motivated in large part by the multistep mechanism for the dissociation of ion pairs in electrolytic solutions (25, 26). The four states of the ionic-hydrate associations are depicted in Figure 3. These states are classified as: (1) completely dissociated hydrated ion pairs; (2) ion pairs at the contact of undisturbed primary hydration shells; (3) outer sphere complexes; and (4) inner sphere complexes. The molecular energetics of the revised theory are underway. However, at this time it appears that clusters having high water content will adopt structures that can be described as inverse micelles. That is, the bound anionic sites project from the nonpolar phase into a sea of water containing the mobile cations. This picture of a cluster is similar to that proposed by Gierke (3).

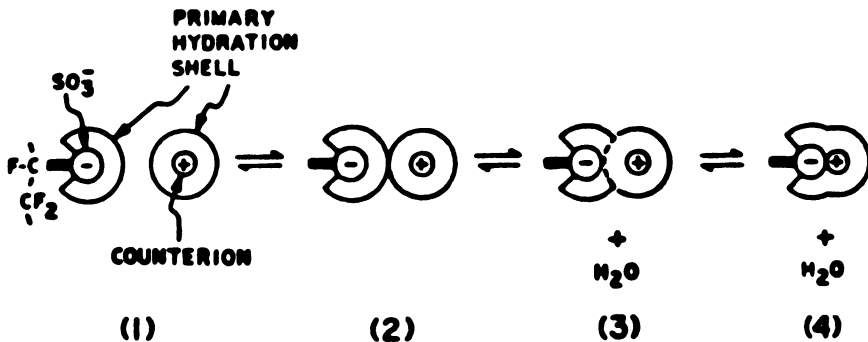
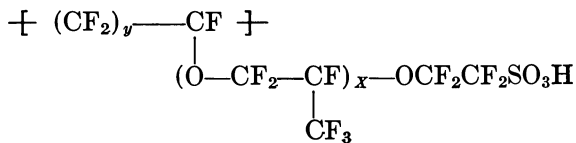


Figure 3. Four-state model of the hydration-mediated dissociation equilibrium between solvated counterions (4)

Application to Nafion

Qualitative Molecular Structure. The general theory has been applied to Nafion ionomers whose general repeat structure is given as:



In Figures 4a–4d are representations of the molecular organization of the dry and hydrated structures for Nafion as postulated in the theory.

Theory for Nafion. To apply the general theory quantitatively it is necessary to express explicitly the relationships between r_h and n_h , r_c and n_c , and the force constant K_c . A four-parameter model ($K_c, \rho_1, \rho_2, \rho_3$) was formulated to accomplish this goal. First, we define three packing factors: ρ_1 , ρ_2 , and ρ_3 as: ρ_1 = packing factor for water molecules in a purely aqueous hydration shell; ρ_2 = packing factor for water molecules in hydration shells containing a cation, for example, ion–dipole hydration shells; and ρ_3 = packing factor of hydration shells in a cluster.

When this four-parameter constraint is selected to describe the structural organization of Nafion the general formalism as represented by Equation 8 becomes:

$$|F_{n_c} + \phi_T| = (\langle W \rangle + O_{n_c} + T\Delta S(n_c)) (n_c - 1) \quad (10)$$

for which the following library of functions and the Glossary of Symbols at the end of the chapter uniquely specify Equation 10:

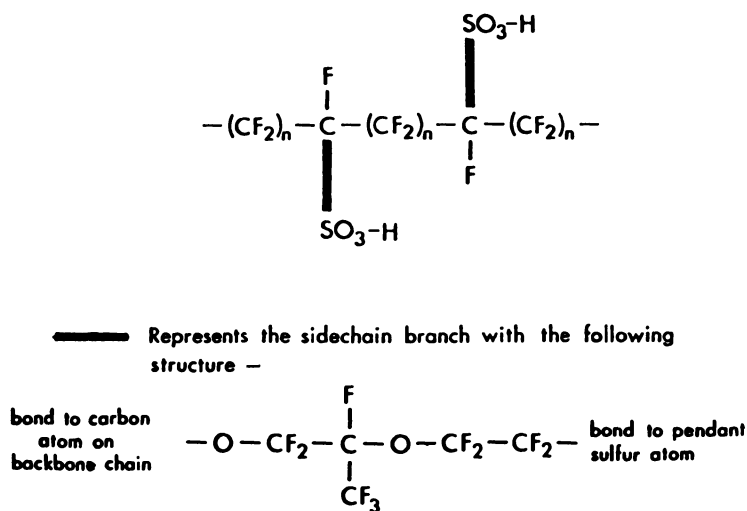


Figure 4a. Schematic of individual Nafion chain structure: dry—sulfonic acid form

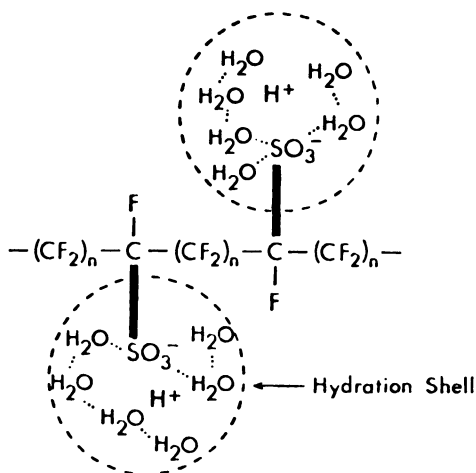


Figure 4b. Schematic of individual Nafion chain structure: wet—sulfonic acid form

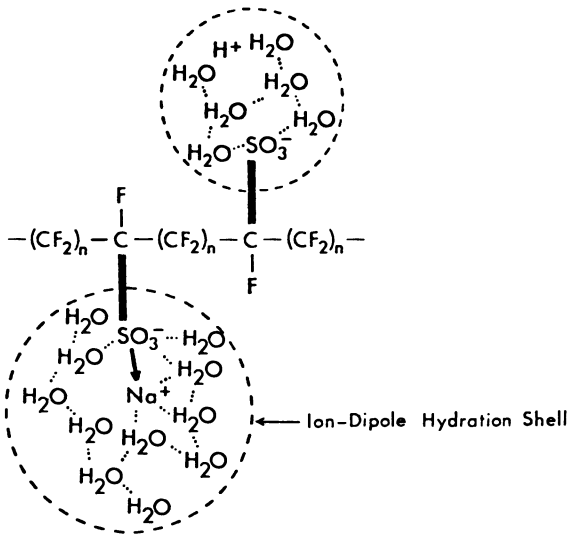


Figure 4c. Schematic of individual Nafion chain structure: wet—ion-dipole formation

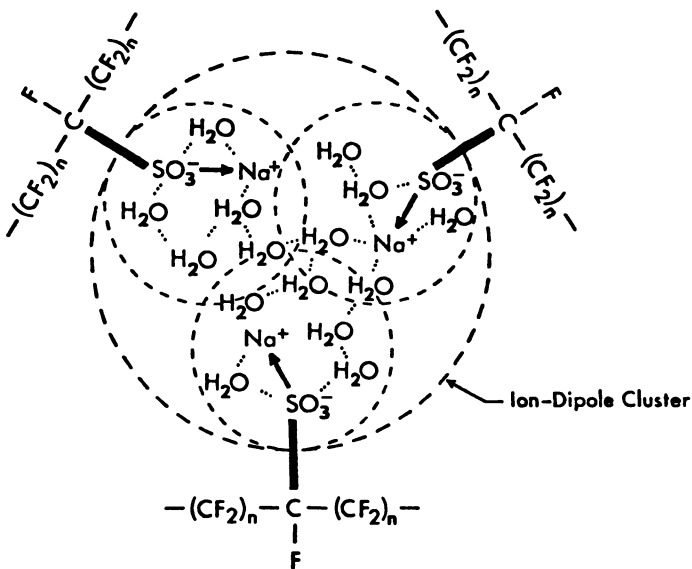


Figure 4d. Schematic of individual Nafion chain structure: wet—ion-dipole cluster formation

$$I. \quad \langle W \rangle = \frac{3kT}{\langle 2h^2 \rangle} \left[\Delta R + \frac{1}{2} (R - 4r_{id}) \right]^2 \quad (11)$$

where the equilibrium distance between hydration shells prior to cluster formation is

$$R = \left[\tau \left(\left\{ \frac{4}{3} \pi r_w^3 \left[\Phi \left(\frac{n_{id}}{\rho_2} - \frac{n_h}{\rho_1} \right) + \frac{n_h}{\rho_1} \right] + \frac{4}{3} \pi r_{Na^+}^3 + \langle V_d \rangle \right\} \right)^{1/3} \right]$$

where $\Phi = 1$ (normally) and

$$n_h = \rho_1 \left[\frac{(r_h^3 - r_{SO_3^-}^3)}{r_{wh}} \right]$$

in which r_h is the solution of

$$2\pi K_e (r_h^4 - r_{SO_3^-}^4) = 2k|A_o| + m_o|A_1|$$

The number of water molecules in an ion-dipole hydration shell is,

$$n_{id} = \rho_2 \left[\frac{r_{id}^3 - r_{SO_3^-}^3 - r_{Na^+}^3}{r_w^3} \right]$$

in which the radius of the ion-dipole hydration shell is the solution of,

$$2\pi K_e r_{id}^4 - \left[\frac{2\rho_2|A_o|}{r_w^3} \right] r_{id}^3 = 2\pi K_e r_h^4 - \left[\frac{2\rho_1|A_o|}{r_w^3} \right] r_h^3 - \left[\frac{2(\rho_2 - \rho_1)|A_o|}{r_w^3} \right] r_{SO_3^-}^3 - \left[\frac{2\rho_2|A_o|}{r_w^3} \right] r_{Na^+}^3 + |A_2| + m_1|A_3| - m_o|A_1|$$

Lastly in specifying $\langle W_T \rangle$,

$$\tau = \frac{\langle V_o \rangle}{V_d}$$

where V_d can be expressed in terms of the number of monomer CF_2 -units, n , as

$$V_d = \frac{4\pi}{3} [(n + 6)r_c^3 + (2n + 11)r_f^3 + r_s^3 + 5r_o^3]$$

and

$$\langle V_o \rangle \equiv \frac{\langle M_o \rangle}{\rho_o} = \frac{\text{average monomer molecular weight}}{\text{dry density of ionomer}}$$

$$\text{II. } O_{n_c} = \left[\frac{3\mu\Delta A_4}{16r_w^3} \right] (\Delta R)^2 \left(r_{id} - \frac{1}{6} \Delta R \right) (n_c - 1) \quad (12)$$

III. $T\Delta S(n_c)$ is the same as given in Equation 5.

IV. F_{n_c} is the same as given in Equation 1.

$$\text{V. } \phi_T = \frac{A_o}{2} n_h N_h + \left[A_s - \frac{A_o}{2} \right] (1 - \chi) N_c N_h, \quad (13)$$

in which

$$N_c = \rho_3 \left\{ \frac{n_h}{\rho_3} - \left[\left(\frac{n_h}{\rho_3} \right)^{1/3} - 2 \right]^3 \right\}$$

and

$$N_h = \rho_2 \left[\frac{r_{id}^3 - (r_{id} - 2r_w)^3}{r_w^3} \right]$$

Lastly, Equation 10 contains two unknowns, n_c and ΔR . However, in addition to satisfying Equation 10, the solution must be that which minimizes the free energy. In other words,

$$\frac{\partial G}{\partial(\Delta R)} = 0 \quad \text{and} \quad \frac{\partial G}{\partial n_c} = 0 \quad (14)$$

where

$$G = F_{n_c} + \phi_T + (\langle W \rangle + O_{n_c} + T\Delta S(n_c)) (n_c - 1)$$

Thus of all the solutions to Equation 10 in n_c and ΔR we select the n_c^* and ΔR^* which minimize the free energy of the system.

The elastic force constant K_e is set equal to the functional form of the bulk elastic modulus (27) and normalized as the fourth parameter of the model. The remaining parameters were estimated using molecular and quantum mechanical calculations (*see* the Glossary of Symbols).

Experimental Calibration. A trial-and-error procedure was used to calibrate the model, for example, to define ρ_1 , ρ_2 , ρ_3 , and K_e . The molecular parameters for sodium cations are given in the Glossary of Symbols. Figure 5 contains plots of water absorption for the sulfonic acid form of Nafion in contact with water as a function of ionomer equivalent weight. Both experimentally measured (27) and theoretically predicted water absorption-equivalent weight curves are presented. Admittedly, the theoretical curve deviates from the experimental data, especially at increasing equivalent weights. However, in the range of major commercial interest (that is, equiv wt = 1000–1200), the agreement between theory and experiment is quite good ($\pm 6\%$).

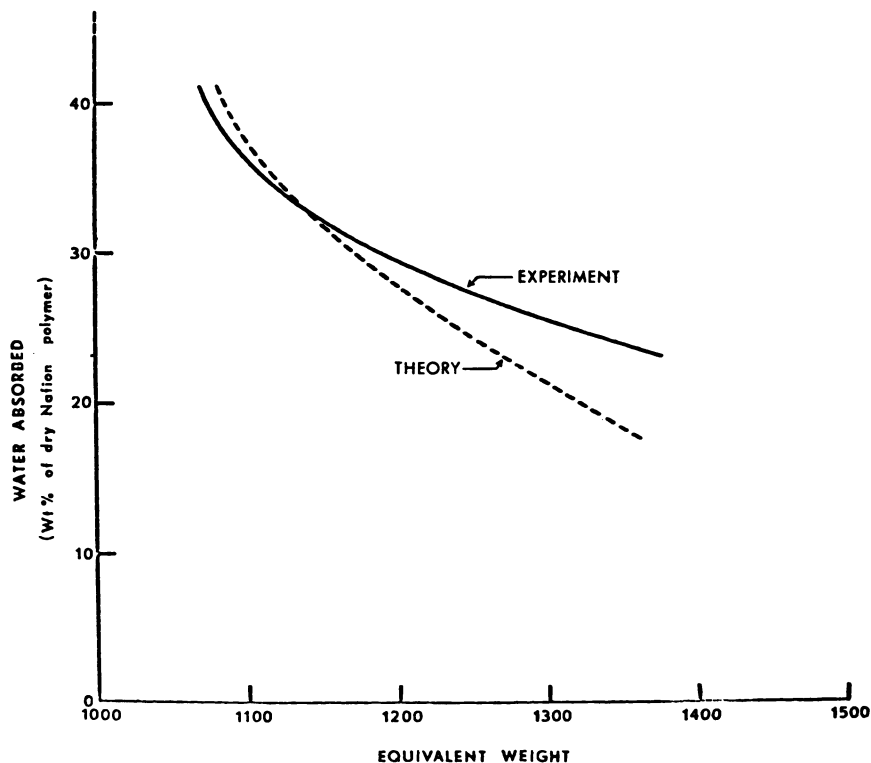


Figure 5. Comparison of experimentally measured and theoretically predicted water absorption vs. equivalent weight for standard Nafion

Plots of water absorption and wet density of the sodium sulfonate form of the ionomer as a function of the solution molarity of sodium ions are shown, respectively, in Figures 6 and 7 for 1100- and 1200-equiv wt materials. As with Figure 5, both theoretical predictions and experimental data are presented in these latter figures to demonstrate the ability of the calibrated model to describe quantitatively the equilibrium solution behavior of standard Nafion ionomers.

As demonstrated by the results presented in Figures 5-7, the model does a fairly good job of describing the equilibrium density and water absorption properties of Nafions. The single most important study supporting the basic cluster structure in Nafion is that of Yeo and Eisenberg (28). They found a small-angle x-ray peak in the Nafion-cesium complex at a Bragg distance of 51 Å (the equiv wt of the sample material was reported to be 1365). The presence of this peak must be attributed to the existence of large scattering centers (the ion clusters) in the polymer. This combination of experimental and theoretical data lead us to conclude that the conceptual picture of Nafion is probably

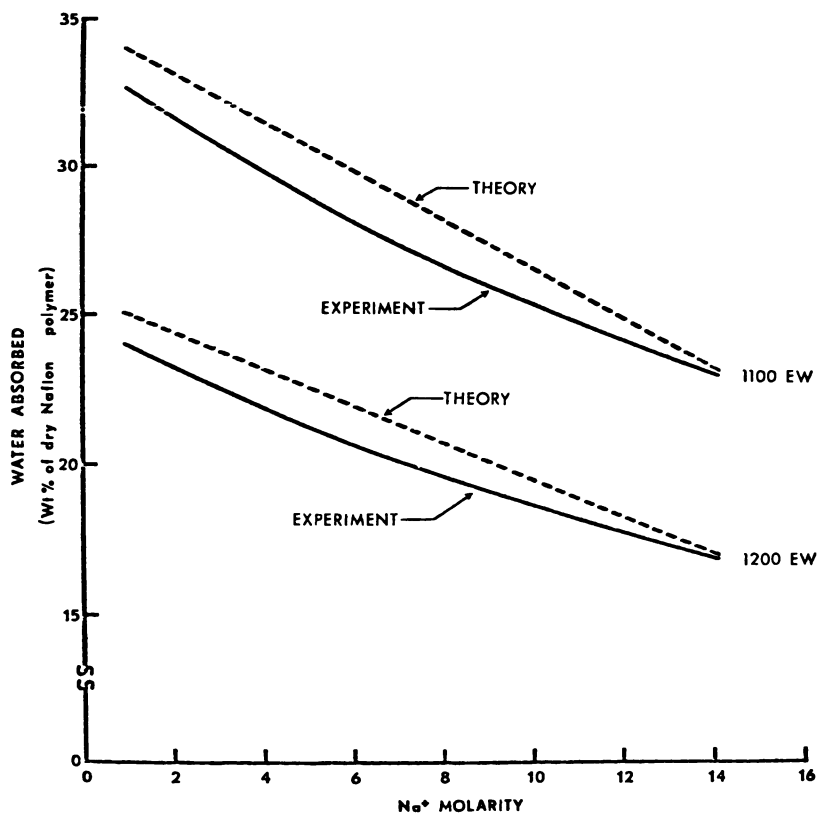


Figure 6. Comparison of experimentally measured and theoretically predicted water absorption vs. Na^+ molarity for standard Nafion in the sodium sulfonate form

correct. In addition, quantitative application of the conceptual theory leads to reasonably well-predicted macroscopic properties.

Prediction of Molecular Organization. It is possible to make a predictive description of molecular organization in the ionomeric material using the calibrated model. In particular, we conclude this section by reporting the effect of the external solution ion concentration on the size of the hydration shell cluster. In Figure 8 we plotted the number of water molecules per ion-dipole hydration shell ($n_h=N$) as a function of n (which is proportional to the equivalent weight) for three different sodium ion concentrations. It can be seen that the water retained in an ion-dipole hydration shell of a cluster increases slowly with increasing ion concentration, and drops off rapidly, in a roughly linear fashion, with increasing n (equiv wt) for all three ionic concentrations. From this we conclude that n (equiv wt) of the polymer (that is, more generally,

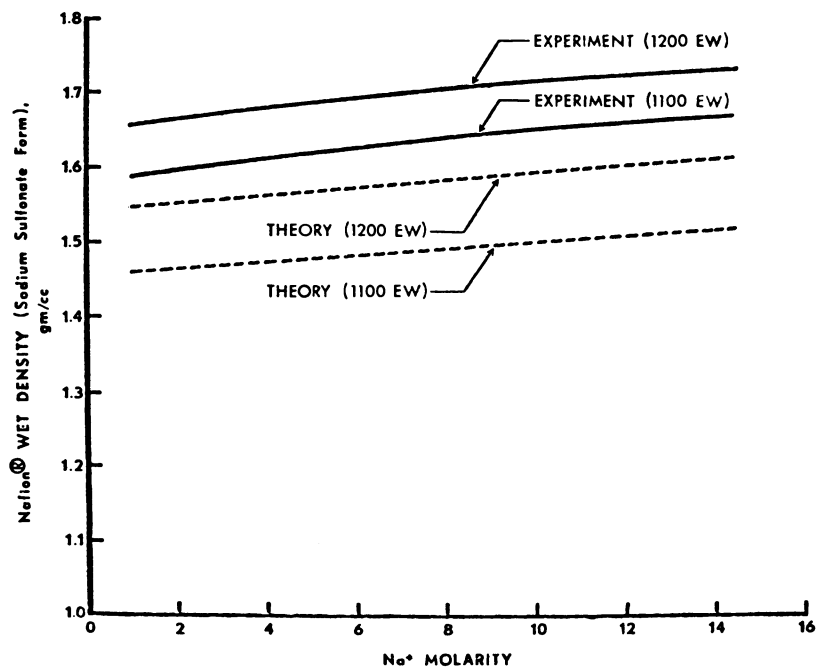


Figure 7. Comparison of experimentally measured and theoretically predicted membrane wet density vs. Na^+ molarity for standard Nafion in the sodium sulfonate form

polymer structure) plays a more crucial role in water domain formation than does external ionic concentration. This is an important observation in regard to the design of Nafion membrane separators.

Ion Transport through Nafion. In the case of Nafion, any structural model that is developed probably will be applied to describe ion transport behavior through the material. Gierke (3) has proposed that for a series of spherically symmetric clusters connected by small transport tubes, as shown in Figure 9, absolute reaction rate theory can be used to describe the flux of ions through the membrane. The potential is based on electrostatic and diffusion interactions. He has shown that such a cluster-network model works well in predicting current efficiency vs. equivalent weight (*see* Figure 10).

We are attempting to computer model ion transport through Nafions by generating sample membrane cubes. These cubes contain the structures determined from our theory of ionomer structure. Once a sample cube is generated, we computer simulate the migration of solvated anions (OH^-) and cations (Na^+) through the membrane sample cube under the potential of an applied field. Electrostatic and diffusion interactions are computed with respect to the explicit structure of the sample

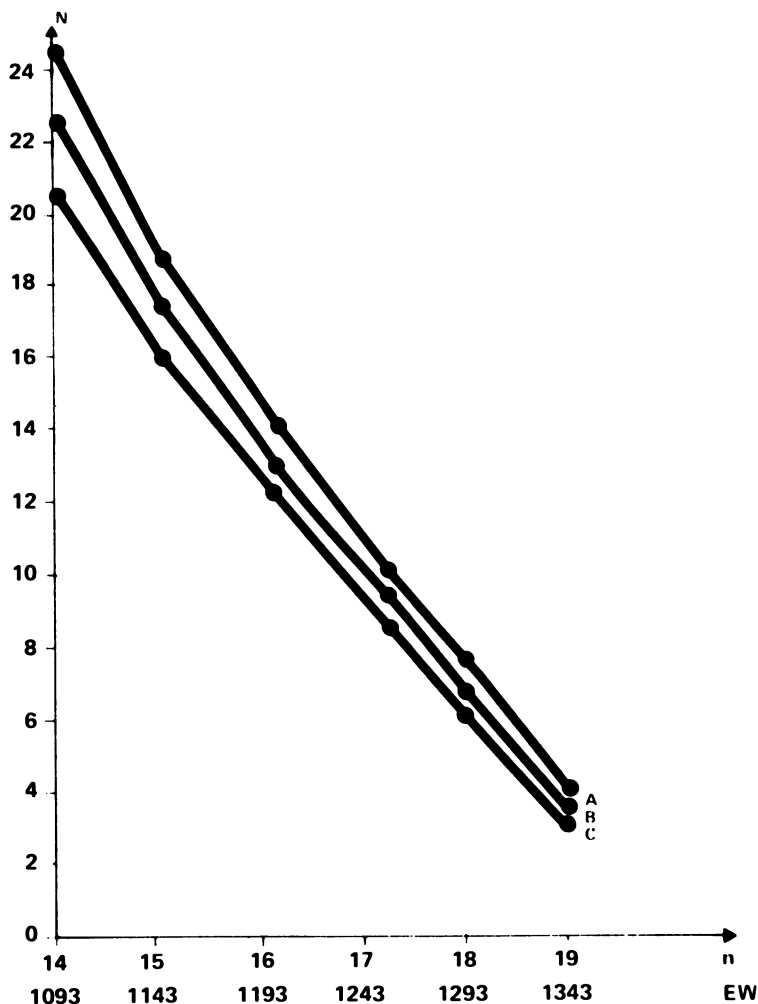


Figure 8. N vs. n (equiv wt) for three different external aqueous- Na^+ concentrations

membrane cube. A pictorial representation of this transport model is shown in Figure 11. Such calculations are costly in that many simulated ion transportations must be considered for each of many sample cubes before a reliable measure of current efficiency can be obtained.

Preliminary current efficiency vs. caustic concentration profiles using this transport model are shown in Figure 12. The prediction of a current efficiency "hump" at high caustic concentration, as seen experimentally, is, according to our model, attributable largely to a minimization of the electrostatic free energy of the dynamic intramembrane (anion-cation)

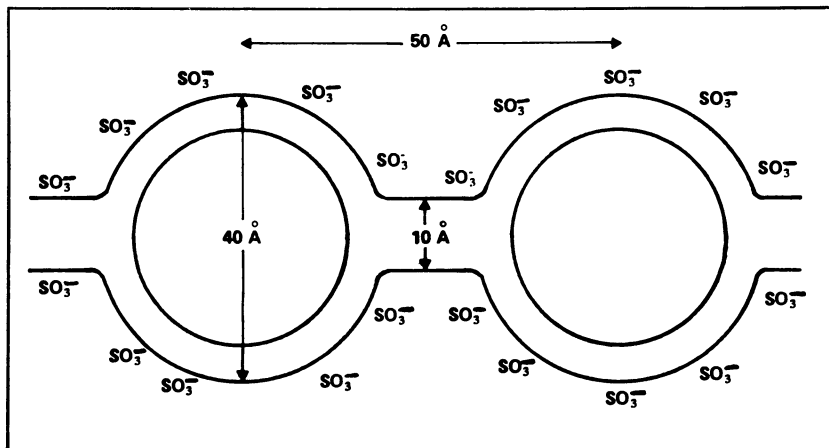


Figure 9. Cluster-network model proposed by Gierke (3)

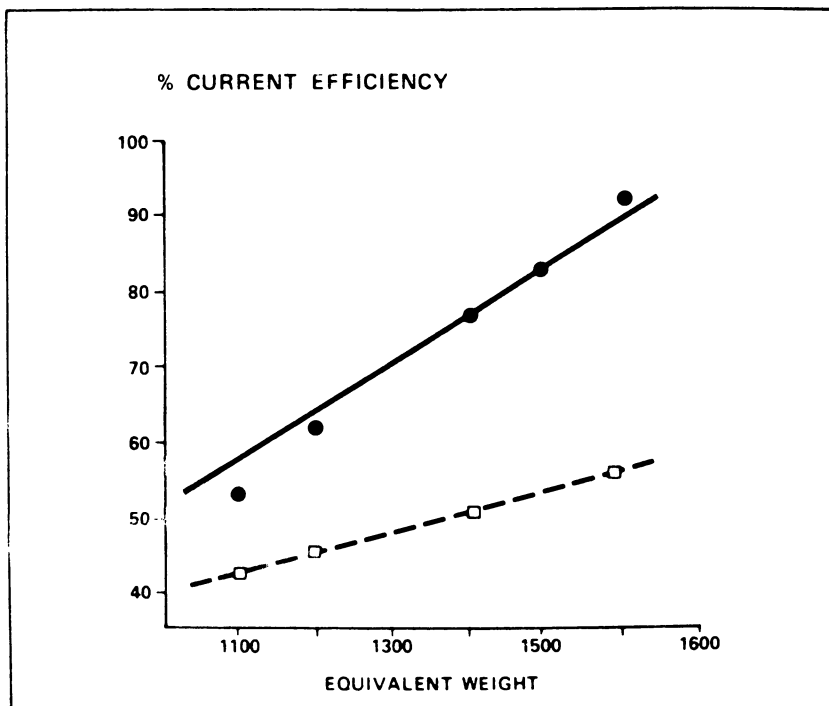


Figure 10. Current efficiency vs. equivalent weight (3) (●) cluster-network model; (□) Donnan Equilibrium; (—) experimental (G. Munn)

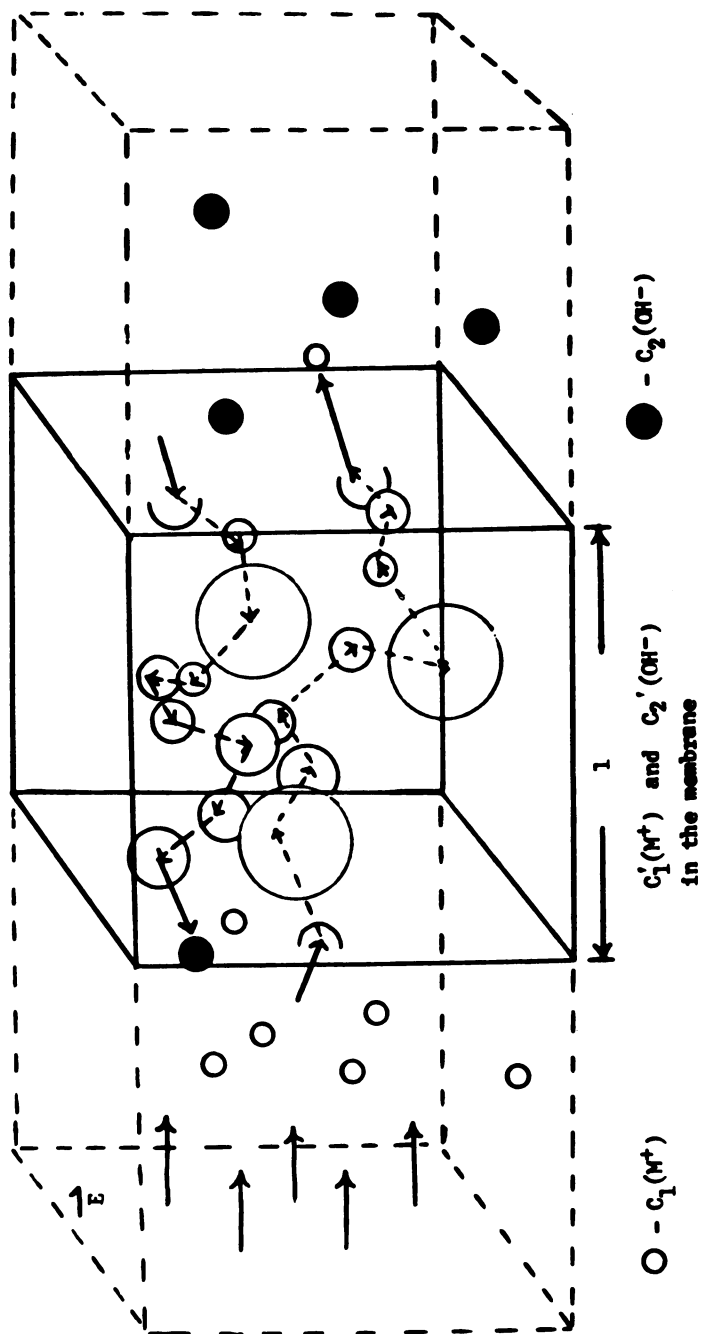


Figure 11. Schematic of the computer simulation of ion transport through a sample membrane cube. Monte Carlo modeling considers: N = unique sample cubes; M = unique ion transport simulations per cube.

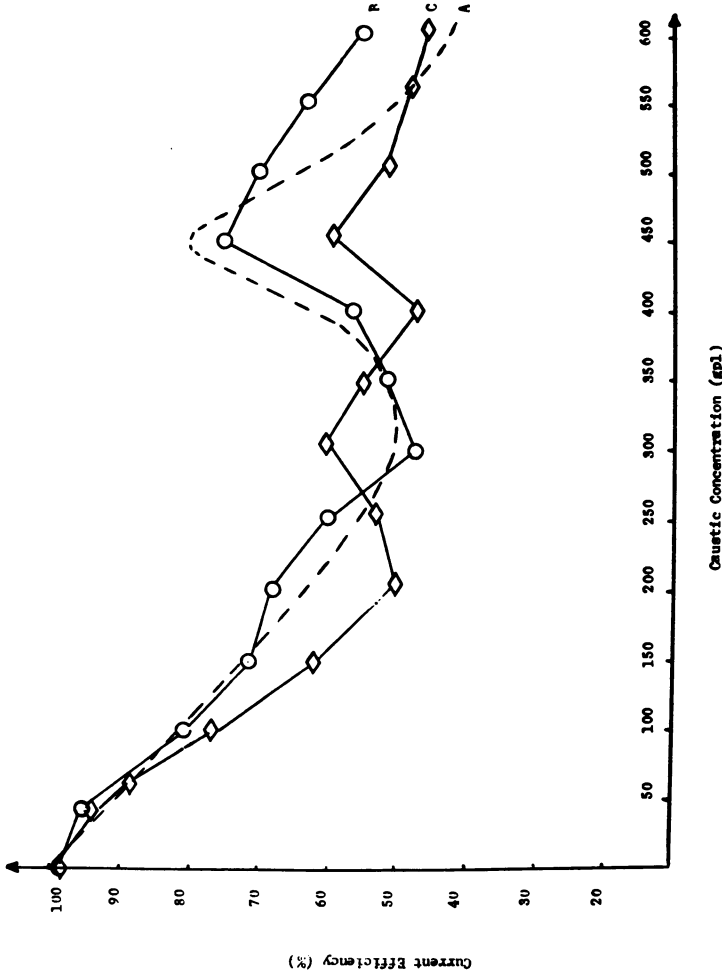


Figure 12. Current efficiency vs. caustic concentration as observed experimentally and predicted by computer simulation for some Nafion separators. (The experimental curve is based on data collected as part of U.S. Patent 3,773,634). N = 5; M = 10; brine strength = 200 gpl; T = 85°C. (A) composite experimental curve (1100 equiv wt); (B) calculated curve for 1143 equiv wt; (C) calculated curve for 1011 equiv wt.

system. Figure 12 has been included in this chapter as additional, but indirect, support for the reasonableness of the predicted molecular structure organization in Nafion. Presumably, if the resultant theoretical structural organization was wrong, we should not expect to predict correctly current efficiency of sodium ion transport through a model Nafion sample as a function of caustic concentration.

Acknowledgments

A. J. Hopfinger was a Sloan Research Fellow during the time this work was done, and would like to thank Diamond Shamrock Corporation and his collaborators at Diamond for making this investigation possible. All of the authors gratefully acknowledge the contributions of Martin Turk of Diamond Shamrock in transforming the theory into a computer software product.

Glossary of Symbols

- K_e = elastic force constant, functional form Ref. 27 ($[3.971 - 12.185$
(equiv wt/1000) + 14.255 (equiv wt/1000)² - 7.439 (equiv
wt/1000)³ + 1.467 (equiv wt/1000)⁴] (kcal/Å⁴mol))
- ρ_o = "dry" density (1.98 g/cc)
- r_C = van der Waal's radius of the carbon atom (1.5 Å)
- r_F = van der Waal's radius of the fluorine atom (1.4 Å)
- r_S = van der Waal's radius of the sulfur atom (1.8 Å)
- r_O = van der Waal's radius of the oxygen atom (1.35 Å)
- $r_{SO_3^-}$ = radius of SO_3^- group (2.4 Å)
- A_o = formation free energy of a H_2O-H_2O bond (-1.8 kcal/mol)
- m_o = number of H_2O molecules directly interacting with the SO_3^-
group (4)
- A_1 = formation free energy of a $H_2O-SO_3^-$ bond (-18.8 kcal/mol)
- r_w = radius of H_2O molecule (1.85 Å)
- A_2 = free energy of formation of $(SO_3^-Na^+)$ dipole (-48.3 kcal/mol)
- m_1 = number of Na^+-H_2O bonds formed per ion-dipole (1)
- A_3 = free energy of formation of Na^+-H_2O bond (-13.8 kcal/mol)
- l = trans distance for the CCC backbone groups (2.30 Å)
- α_o = the CCC backbone angle (112°)
- μ = the average number of nearest neighbors surrounding an id-
hydration shell in a cluster (6)
- ΔA_4 = the free energy change resulting from the removal of a water
molecule from an id-hydration shell (2.6 kcal/mol)
- χ = fraction of surface water molecules contained in hydration shells
on the outer surface of a cluster (0.1)

C_1 = a constant which is characteristic of the dipoles and dielectric of the organic medium (-56 kcal/mol)

A_5 = the H_2O - CF_2 interfacial free energy (1.06 kcal/mol)

ρ_1 = packing factor of H_2O molecules in the hydration shell (.74)

ρ_2 = packing factor of H_2O molecules in the id-hydration shell (.30)

ρ_3 = packing factor of id-hydration shells in the cluster (1.50)

Literature Cited

1. Eisenberg, A. *Macromolecules* 1970, 3, 147.
2. Ponomarev, O. A.; Ionova, I. A. *Vysokomol. Soedin., Ser. A* 1974, 16, 1023.
3. Gierke, T. D. "Ionic Clustering in Nafion Perfluorosulfonic Acid Membranes and Its Relationship to Hydroxyl Rejection and Chlor-Alkali Current Efficiency", presented at the 152nd National Meeting, the Electrochemical Society, Atlanta, GA, October, 1977.
4. Mauritz, K. A.; Lowry, S. R. *Polym. Prepr., Am. Chem. Soc., Div. Polym. Chem.* 1978, 19(2), 336.
5. Rees, R. W.; Vaughan, D. J. *Polym. Prepr., Am. Chem. Soc., Div. Polym. Chem.* 1965, 6, 296.
6. Ward, T. C.; Tobolsky, A. V. *J. Appl. Polym. Sci.* 1967, 11, 2403.
7. Otocka, E. P.; Kwei, T. K. *Macromolecules* 1968, 1, 401.
8. Bonotto, S.; Bonner, E. F. *Polym. Prepr., Am. Chem. Soc., Div. Polym. Chem.* 1968, 9, 537.
9. MacKnight, W. J.; McKenna, L. W.; Read, B. E. *J. Appl. Phys.* 1967, 38, 4208.
10. Phillips, P. J.; MacKnight, W. J. *J. Polym. Sci., Polym. Phys. Ed.* 1970, 8, 727.
11. Sakamoto, K.; MacKnight, W. J.; Porter, R. S. *J. Polym. Sci., Polym. Phys. Ed.* 1970, 8, 277.
12. Rafikov, S. R., et al. *Vysokomol. Soedin. Ser. A* 1973, 15, 1974.
13. Marx, C. L.; Cooper, S. L. *J. Macromol. Sci., Phys.* 1974, 9, 19.
14. Fitzgerald, W. E.; Nielsen, L. E. *Proc. R. Soc. London, Ser. A* 1964, 282(1388), 137.
15. Erdi, N. Z.; Morawetz, H. *J. Colloid Sci.* 1964, 19, 708.
16. Eisenberg, A.; Navratil, M. *J. Polym. Sci., Polym. Lett. Ed.* 1972, 10, 537.
17. Eisenberg, A.; Navratil, M. *Macromolecules* 1973, 6, 604.
18. *Ibid.*, 7, 84.
19. *Ibid.*, p. 90.
20. Otocka, E. P.; Eirich, F. R. *J. Polym. Sci., Polym. Symp., Part A2* 1968, 6, 921.
21. *Ibid.*, p. 933.
22. Moacanin, J.; Cuddihy, E. F. *J. Polym. Sci., Polym. Symp.* 1966, 14, 313.
23. Hopfinger, A. J. "Conformational Properties of Macromolecules"; Academic: New York, 1973.
24. Segal, G. A., Ed. *Mod. Theor. Chem.* 1977, 7-8.
25. Diebler, H.; Eigen, M. *Z. Phys. Chem. (Frankfurt Am. Main)* 1959, 20, 299.
26. Eigen, M.; Tamm, K. *Z. Elektrochem.* 1962, 66, 93, 197.
27. Grot, W. G. F.; Munn, G. E.; Walmsley, P. N. "Perfluorinated Ion Exchange Membranes", presented at the 141st National Meeting, The Electrochemical Society, Houston, TX, May, 1972.
28. Yeo, S. C.; Eisenberg, A. *Polym. Prepr., Am. Chem. Soc., Div. Polym. Chem.* 1975, 16(2), 104.

RECEIVED October 25, 1978.

Transport Phenomena and Morphology Changes Associated with Nafion 390 Cation-Exchange Membranes

S. G. CUTLER

ICI Ltd, Mond Division, Research and Development Department, P. O. Box 7, Winnington, Northwich, Cheshire, England CW8 4DJ

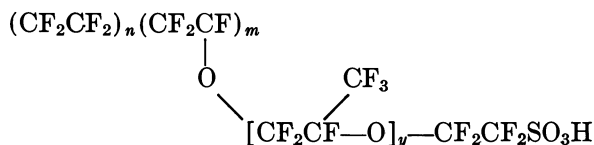
Electrolysis, for the production of alkali and chlorine, using Nafion 390 (a perfluoro sulfonic acid cation-exchange membrane) as a cell separator is described. The current efficiency of the membrane increases with the applied electrical field gradient. However, membrane transport phenomena at high current density (0.5 amps cm^{-2}) are unstable and the selectivity decreases over a period of several days. The use of low-angle x-ray diffraction and electron transmission microscopy indicate that this decrease in selectivity correlates with a dramatic transition in membrane morphology, resulting in a thermodynamically more stable expanded form. The hydrated membrane as supplied contains ion clusters of about 50 Å in diameter; in the expanded form, which involves gross molecular rearrangement, ion clusters are as large as 100 Å.

The discovery of the ion-exchange properties of phenol formaldehyde resins in 1935 by Adams and Holmes (1) led to the synthesis of the first high capacity ion-exchangers. This discovery, coupled with subsequent advances in polymer science and technology, led to the availability of many types of hydrocarbon-based ion-exchange membranes in the early 1950's. This era also witnessed the emergence of numerous patents on the use of ion-exchange membranes in various electrochemical processes that were of industrial significance. Of particular interest to the chlor-alkali industry was the use of cation-exchange membranes as cell separators in brine and water electrolysis. A diagram of such a cell is

shown in Figure 1. A saturated sodium chloride solution is fed to the anode compartment where chloride ions are oxidized to chlorine gas, while water is reduced at the cathode to yield hydroxyl ions and hydrogen gas.

To restore electroneutrality, sodium ions are transported selectively in the electrochemical field gradient across the cation-exchange membrane from the anode to the cathode chamber. Ideally the membrane should be 100% cation permselective, therefore excluding any hydroxyl ion transport; but in practice this is not the case and current efficiencies are always less than 100%. This current inefficiency is represented by the reaction of hydroxyl ions with chlorine. Patent applications for this method of chlor-alkali production appeared as early as 1949 (2).

The advent of Du Pont's inert perfluorosulfonic acid membranes, Nafion, in the late 1960's made chlor-alkali production in a membrane cell a realistic possibility. The basic structure of Du Pont's fluoro ionomer is shown



Copolymers of the type shown can be fabricated into large sheets and are characterized by their equivalent weight, that is, the weight in grams of polymer in the acid form required to neutralize one equivalent of base.

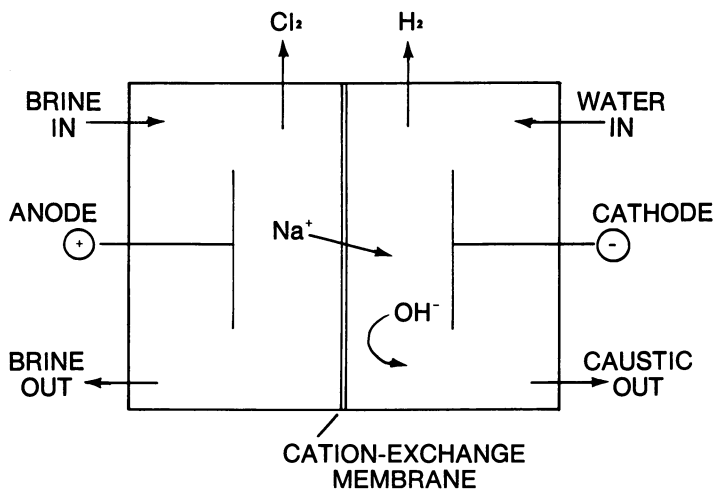


Figure 1. Cation-exchange membrane

The work described relates to the study of transport phenomena and morphology changes associated with Nafion 390 when used in an electrochemical cell. This membrane is a laminate of two equivalent weights of copolymer, 1500 and 1100, supported by a rayon/PTFE mesh. When installed in a cell, the 1500 equiv wt faces the cathode compartment.

A rigorous interpretation of transport phenomena associated with Nafion 390 during electrolysis is not possible, since no adequate theory exists for systems so far from equilibrium and under such high applied forces. In addition, a further complicating factor is that observed transport phenomena result from the combined effects of both membranes in the laminate.

However, as in the theory of irreversible thermodynamics (3, 4), each flux J across the membrane may depend on every applied force X . Thus the flux of species i across the membrane may be written as

$$J_i = \sum_{\text{all } k} L_{ik} X_k \quad (1)$$

where $L_{ik} = f(X_k)$ are called phenomenological coefficients and represent the interaction of species i with k . In the case of the electrochemical cell shown in Figure 1, the main force acting in the system is the applied field gradient. The current efficiency for electrolysis is given by

$$\text{CE} = \frac{Z_{\text{Na}} J_{\text{Na}}}{\sum_i Z_i J_i} \quad (2)$$

where Z is the charge on the species.

Obviously the smaller the hydroxyl ion flux the greater the current efficiency (since $J_{\text{OH}} \simeq 0$). The likely variation of the phenomenological coefficients with the applied force implies that the ratio $J_{\text{Na}}/J_{\text{OH}}$ - and hence current efficiency will alter with applied field.

Experimental

A 120-cm² piece of Nafion 390 was installed in an electrochemical cell using a TiO₂/RuO₂ coated titanium anode and a mild steel cathode. The current density of the cell was varied from 0.1 to 0.5 amps cm⁻² over a period of several days; the fluxes of the various components were measured at each current density. Figure 2 shows the variation of current efficiency with current density at constant external concentrations of sodium chloride and sodium hydroxide (that is, constant chemical potentials). It is evident that the flux of sodium ions increases relative to that of hydroxyl ions, with increasing current density. Figure 3 shows a dramatic change in the ratio of water flux to sodium ion flux, $J_{\text{H}_2\text{O}}/J_{\text{Na}}$.

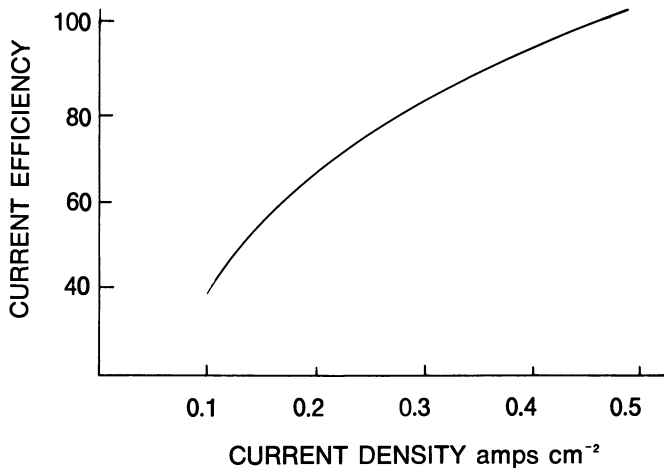


Figure 2. Current efficiency vs. current density for Nafion 390 at 7m NaOH

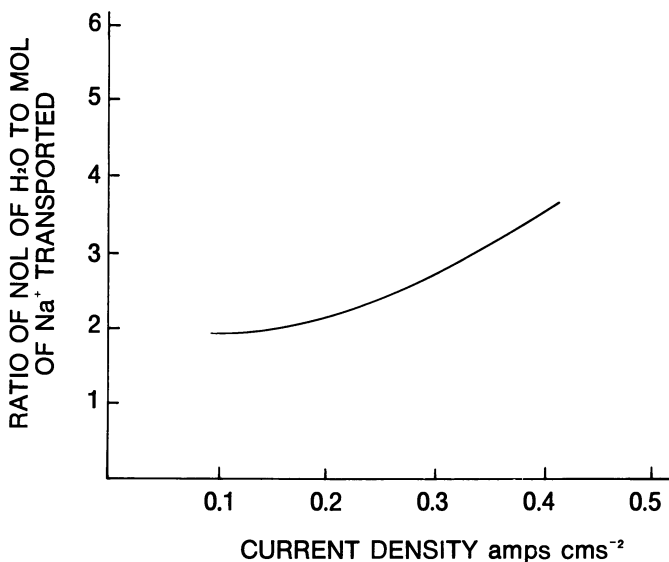


Figure 3. Ratio of moles of H₂O to moles of Na⁺ transported vs. current density for Nafion 390 at 7m NaOH

At low current density the degree of sodium ion hydration is small—about two water molecules for every sodium ion. The ratio $J_{\text{H}_2\text{O}}/J_{\text{Na}}$ remains steady until about 0.3 amps cm⁻² then rises with increasing current density. The dependence of cation transport number (5, 6) and electro-osmotic water fluxes (7, 8) on current density have been reported previously. In these cases the dependence of fluxes on current density can be explained by solution polarization phenomena alone.

The large increase in sodium ion hydration above 0.3 amps cm^{-2} , as shown in Figure 3, can be explained in terms of an increase in hydration in the side of the membrane facing the anode compartment. This is attributable to the increasing tendency of the sodium ions to drag their hydration sheaths into the membrane at higher field gradients. This phenomenon has the effect of increasing pressure gradients within the membrane, with the possibility of opening up alternative channels that are highly selective to sodium ion transport. In addition to pressure gradients within the membrane, which do alter the phenomenological coefficients, concentration profiles of components across the membrane show that significant concentration polarization of sodium hydroxide occurs in the side of the membrane facing the cathode. This effect will tend to increase with current density, leading to very high concentrations of sodium hydroxide in which ion pairs are formed, and reducing the tendency of hydroxyl ion back migration in the electrical field. While such ion pairs are formed in the case of sodium hydroxide, sodium ions associated with sulfonic acid groups still remain conductive and contribute to the overall increase in the fraction of sodium ion current. However, it should be noted that Mauritz et al. (9) find that with increasing water content the sodium ions become mobile and are no longer strongly associated with the sulfonate sites. This reasoning accounts for the observed membrane behavior in at least a qualitative manner.

The same experiment was carried out several times with different pieces of Nafion 390 cut from a large sheet; all data showed similar trends in current efficiency and electro-osmotic water with increasing current density. However, results from each membrane were nonidentical, presumably because of macroscopic inhomogeneities.

Operational Stability

Nafion 390 membranes operating at 0.5 amps cm^{-2} were unstable; current efficiency for a given caustic strength gradually decreased over a period of time, that is, increasing hydroxyl ion flux. This change in the transport properties can be attributed to a change in the membrane microstructure brought about by the heating effect of the electric current. Such transitions in membrane microstructure with concomitant changes in transport properties, brought about by boiling water, have been reported previously (10, 11).

Nafion membranes are composed of hydrophobic-hydrophilic comonomers. When the ionic form of Nafion is exposed to water, some swelling takes place. However, in order to minimize the free energy of the system, water will be taken up in such a way as to avoid contact with the hydrophobic TFE units of the copolymer. At equilibrium, for a fixed structure, there will be a balance between the free energy of dilution (osmotic swelling) and the free energy of hydration of the TFE units. As a result of these two opposing effects, water of hydration is contained in ion clusters which reduces the necessity of water-TFE interaction and yields a system of minimum energy. Several models

discussing the forces controlling ionic clustering in ionomers have also appeared recently (12, 13, 14). Since this hydrated polymer system is not chemically cross-linked, it is possible, by supplying sufficient energy, for the polymer chains to rearrange to yield a system of lower free energy. This is achieved by the formation of large hydrated ion clusters involving considerable molecular rearrangement to an expanded hydrated morphology. When the membrane is operated at high current density, sufficient energy is dissipated in the membrane to enable a transition to the expanded morphology. Similar changes can be achieved by heating the membrane to 170°C in water under pressure.

Upon drying out and heating to approximately 170°C for several hours, the membrane reverts to its original structure, which is most stable thermodynamically as the dehydrated form, since interaction energies of TFE and water are not present. An energy diagram of the polymer system is shown in Figure 4.

Evidence for these morphology changes can be obtained from low-angle x-ray diffraction (15).

Low-Angle X-Ray Diffraction. Experiments were carried out on unreinforced Nafion membranes (1100 equiv wt) kindly supplied by E. I. Du Pont de Nemours & Co. One piece of membrane was used as supplied, another was heated to 170°C in distilled water in an autoclave for 45 min; these membranes are referred to as 1100N and 1100E, respectively. Both samples were exchanged into the sodium form.

Diffraction patterns of these hydrated membranes were recorded with a linear position sensitive detector on a Kratky low-angle x-ray

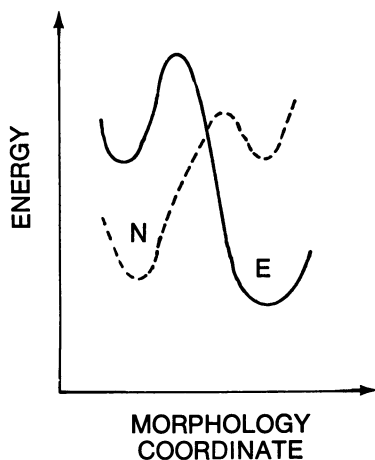


Figure 4. Energy vs. morphology coordinate for N- and E-type membranes. (—) hydrated; (---) dehydrated

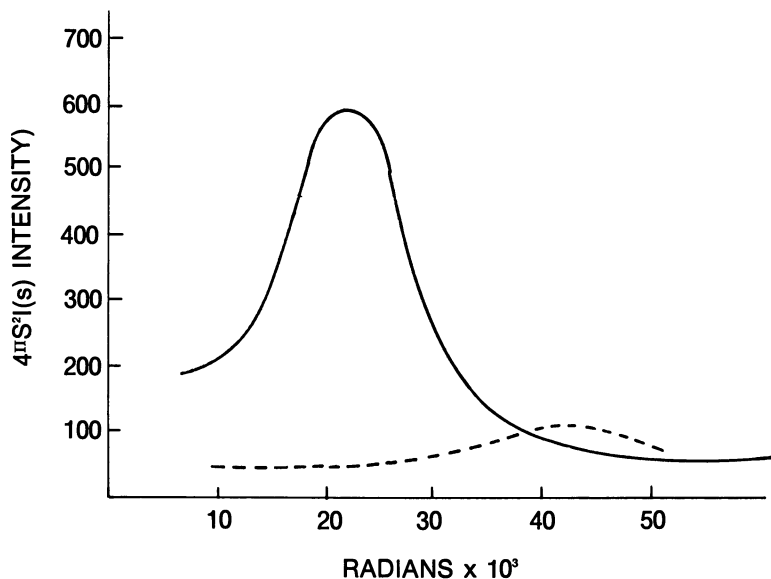


Figure 5. Plot of $4\pi S^2 I(S)$ vs. radians for N- and E-type membranes. (—) 1100E; (---) 1100N

camera. Figure 5 shows plots of $4\pi SI(S)$ (intensity) where $I(S)$ is the diffraction profile and S is the scattering variable $= 2 \sin \theta/\lambda$. It is evident from the data that the hydrated membranes consist of two distinct phases. In addition, considerable variation in both intensity and position of the diffraction peaks are observed for the N- and E-type membranes. Some basic structural parameters obtained from the x-ray data are shown in Table I.

Additional deductions can be made from the quantities L_p and $\langle \eta^2 \rangle$ provided the effective volume fraction ϕ of the two-phase structure is known. This can be deduced, to a first approximation, by assuming that

Table I.

Membrane	$t \text{ \AA}^a$	$\langle \eta^2 \rangle^b$	L_p^c	$d \text{ \AA}^d$	ϕ^e Re-duced	$d_s \text{ \AA}$	$d_r \text{ \AA}$	$d_i \text{ \AA}$
1100N	5	15.2×10^{-3}	14	38	0.075	40	46	101
1100E	5	44.4×10^{-3}	43	75	0.29	101	92	104

^a t = thickness of transition zone between phases.

^b $\langle \eta^2 \rangle$ = so-called invariant, which characterizes the degree of density contrast between the phases.

^c L_p = correlation length which characterizes the arrangement of the phases.

^d d = Bragg planar spacing, obtained by applying Bragg's Law to the position of the diffraction maxima.

^e ϕ = volume fraction of hydrated ionic phase.

the two-phase system includes pure water in a PTFE matrix of density 2.13 g mL⁻¹. This yields a phase electron-density difference $\Delta\rho_e$ of 0.466 mol electrons mL⁻¹, which can be used to calculate ϕ from the following equation

$$\langle \eta^2 \rangle = \Delta\rho_e \phi(1 - \phi) \quad (3)$$

Estimated values of ϕ together with correlation length can be used to calculate theoretical Bragg spacings (for three specific morphological models) which can be compared with observed spacings. The following models are:

1. Spherical: identical hydrated ionic spheres of Phase 1 arranged in a hexagonal lattice within the PTFE phase; planar spacings of the close-packed sphere d_s are shown in Table I.
2. Rods: Phase 1 consists of hydrated ionic rods arranged in a hexagonal lattice within the PTFE phase; planar spacings are d_r (*see* Table I).
3. Infinite hydrated ionic lamella; planar distance given by d_l (*see* Table I).

Comparison of interplanar distances for all three models with d in Table I indicates that the hydrated spherical ionic clusters are representative of Phase 1 in the N-type membrane, good agreement being obtained for the observed and theoretical Bragg spacings. However, with the E-type membrane there is a vague indication that the rod model tends to agree more with the observed Bragg spacings. The marked difference in the values of L_p and d between the N- and E-type membranes indicates that there has been a gross molecular rearrangement to a more expanded structure; it is not just a simple swelling phenomenon.

The difference in structure between the N- and E-type membranes has been substantiated further by transmission electron micrographs of these membranes in the UO_2^{2+} form. These show that the dimensions (~ 100 Å) of the ionic domains in the E-type membrane are roughly twice those of the domains in the N-type membrane (~ 50 Å). This agrees well with the x-ray data.

Conclusion

The transport properties of hydrophobic-hydrophilic ion-exchange membranes such as Nafion are likely to alter with time when operated at high current densities. The thermodynamic tendency of the system to form large hydrated ionic clusters is realized by increasing the molecular energy (kT) of the polymer chains to such an extent that the activation

energy barrier to morphology change is overcome. This change in membrane microstructure results in reduced cation selectivity, attributable to greater membrane hydration and to a change in the coupling or phenomenological coefficients of transporting species.

When chlor-alkali membrane cells are operated on an industrial scale it is desirable that the membrane be cross-linked so that the activation energy barrier to microstructure transition becomes extremely high. This will ensure that the transport properties of the membrane are invariant with time, even at high current densities.

Literature Cited

1. Adams, B. A.; Holmes, E. L. *J. Soc. Chem. Ind. (London)* 1935, 54, 1T.
2. Walter, J. Ionacs Inc., U.S. Patent 2 636 851.
3. Staverman, A. J. *Trans. Faraday Soc.* 1952, 48, 176.
4. Kirkwood, J. G. In "Ion Transport Across Membranes"; Clarke, H. T., Ed.; Academic: New York, 1954; p. 119.
5. Gregor, H. P.; Peterson, M. A. *J. Phys. Chem.* 1964, 68, 2201.
6. Bethe, A., Toropoff, T. *Z. Physik. Chem.* 1914, 88, 686.
7. *Ibid.* 1915, 89, 597.
8. Tombalakian, A. S. *J. Phys. Chem.* 1962, 66, 1006.
9. Lakshminarayanaiah, N. *Desalination* 1967, 3, 97.
10. Mauritz, K. A., Lowry. *Polym. Prepr., Am. Chem. Soc., Div. Polym. Chem.* 1978, 19.
11. Paterson, R.; Gardner, C. R. *J. Chem. Soc. A* 1971, 2254.
12. Munn, G. E. "Nafions Membranes—Factors Controlling Performance in the Electrolyses of Salt Solutions," *Proc. Electrochem. Soc., 152nd, Atlanta, 1977.*
13. Eisenberg, A. D. *Macromolecules* 1970, 3, 147.
14. Gierke, T. D. "Ionic Clustering in Nafion Perfluorosulfonic Acid Membranes and Its Relationship to Hydroxyl Rejection and Chlor-Alkali Current Efficiency," *Proc. Electrochem. Soc., 152nd, Atlanta, 1977.*
15. Hopfinger, A. J.; Mauritz, K. A.; Hora, C. J. "Prediction of the Molecular Structure of Nafion under Different Physicochemical Conditions," *Proc. Electrochem. Soc., 152nd, Atlanta, 1977.*
16. Yeo, S. C.; Eisenberg, A. D. *J. Appl. Polym. Sci.* 1977, 21, 875.

RECEIVED October 20, 1978.

Postscript

Regretably, S. Cutler passed away while his chapter was being refereed. Thus, it could not be handled in the usual manner. Minor corrections in the text were made without changing the thrust of the paper in any way. However, the referees had several reservations about the interpretation of the small-angle x-ray data. These were:

1. The calculation of the invariant does not appear to take into account the electron density of the anion.

2. The justification in assuming a hexagonal lattice is not substantiated and the question of how sensitive the results are to the choice of lattice is not discussed.
3. The wording of the last paragraph before the conclusion section seems to imply that the ionic domains in both the E- and N-type membranes are geometrically similar. This is in contrast to the model presented in the preceding paragraphs.

In spite of these discrepancies, the referees and editors agreed that this chapter represents a significant contribution to the symposium which, without a doubt, merited incorporation in the proceedings. Once again, we would like to take this opportunity to express our deep sorrow at the passing of S. Cutler.

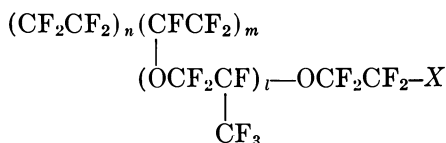
A Multinuclear Fourier Transform NMR Study of Perfluorosulfonate Ionomers

RICHARD A. KOMOROSKI¹

T. R. Evans Research Center, Diamond Shamrock Corporation,
P. O. Box 348, Painesville, OH 44077

Sodium-23 NMR was used to study cation binding in perfluorosulfonate ion exchange resins as a function of water content, temperature, and equivalent weight. A large chemical shift change (~ 130 ppm) and line width increase are seen upon decreasing the water content from 30 to 1%. These effects are reversed with increasing temperature. The data can be interpreted in terms of a fast equilibrium between bound and unbound, but loosely associated, cations in the hydrophilic regions of the material. A larger fraction of cations is bound with decreasing water content and temperature. The large change in chemical shift points to the formation of contact ion pairs. The data suggest the presence of three or four water molecules in the first hydration sphere of the sodium ions. Preliminary results for other alkali metals and water of hydration are presented.

Several authors in this volume (1, 2, 3) deal with the experimental and theoretical characterization of Nafion (a Du Pont registered trademark) ion-exchange resin, which has the general structure below.



¹ Current address: B. F. Goodrich Company, Research and Development Center, 9921 Brecksville Road, Brecksville, OH 44141.

Here, $X = \text{SO}_2\text{F}$, $\text{SO}_3\text{-H}^+$, $\text{SO}_3\text{-Na}^+$, etc. and l is small. The material possesses exceptional chemical, thermal, and mechanical stability, and can serve as an effective membrane separator in electrochemical cells (4).

Small-angle x-ray scattering studies (5) suggest that swollen Nafion exists as a biphasic structure, consisting of hydrated ionic clusters embedded in the surrounding fluorocarbon phase. Such a structure resembles a reversed micelle (Figure 1). Little is known about the structure of hydrated Nafion at the molecular level. Questions remain concerning the nature of the aqueous regions and their resemblance to typical electrolyte solutions. Information concerning polymer chain conformation and the relationship between structural variables, such as equivalent weight and microscopic structure, is also lacking.

It is desirable to have additional evidence, particularly at the molecular level, for the structure in Figure 1. Because the ion transport properties of a membrane separator are critical for its effective performance, an understanding of ionic mobility in the system is essential. Moreover, mathematical models (1, 3) devised to explain the behavior of Nafion must rest on a firm foundation of experimental evidence gath-

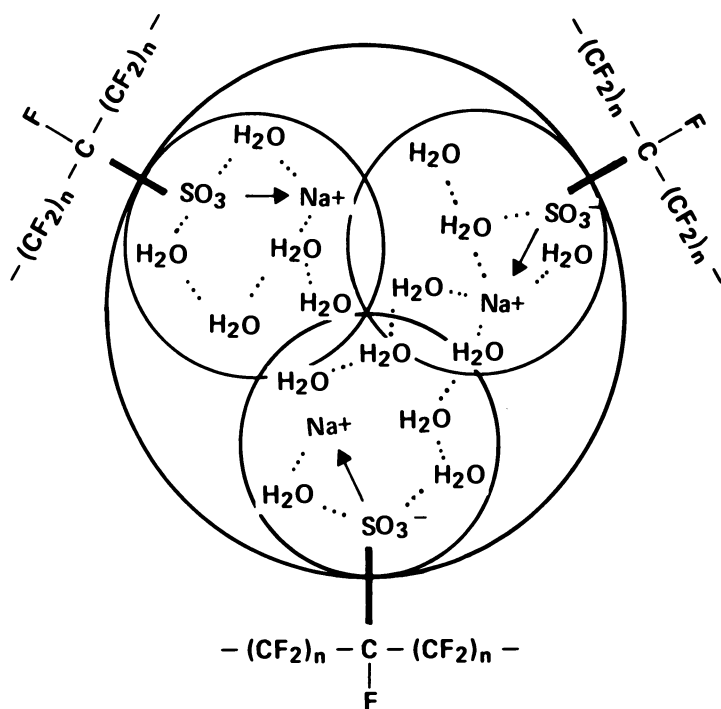


Figure 1. Schematic of the reversed micelle model of Nafion

ered using techniques sensitive to the motional and electronic environments of ions and solvent associated with the system.

Nuclear magnetic resonance (NMR) can provide detailed information on structure, electronic environment, and mobility of molecules and electrolyte solutions. NMR signals, arising from both the solvent or swelling agent (6,7) and the dissolved ions (6,7,8,9), can be used to probe interactions in the system of interest. Typical high resolution NMR (10) can be used to study polymeric molecules in solution, or in bulk, if the experiments can be conducted well above the glass transition temperature of the material (11). Glassy or highly crystalline materials are amenable to study by standard pulsed NMR techniques (12) or by recently developed high resolution techniques (13).

Nafion does not yield typical high resolution spectra for nuclei (^{19}F and ^{13}C) in the fluorocarbon phase at interesting temperatures ($\leq 90^\circ\text{C}$), even in the presence of water of swelling. In contrast, one can observe NMR signals of alkali metal counterions and water of swelling, even in the presence of small amounts of water. Thus it is possible to study aqueous regions of Nafion directly and to obtain information on the polymer structure indirectly.

Alkali metal NMR is a sensitive probe of both the immediate chemical environment and the mobility of these metal ions in aqueous and nonaqueous solvents (8,14). Table I is a list of isotopes of alkali metals that possess nuclear spins and, hence, should yield NMR signals. Some characteristics that relate to sensitivity are also given. It can be seen from Table I that the ^{23}Na nucleus is particularly attractive from a sensitivity point of view. However, all of the nuclei in Table I should be observable under favorable NMR conditions using Fourier transform techniques (15).

The chemical shifts of alkali metal nuclei are a very direct probe of ionic solutions and related systems (6,7,8,9). Perturbations of the

Table I. NMR Parameters of Alkali Metal Cations

<i>Element</i>	<i>Isotope</i>	<i>Spin</i>	<i>Per Nucleus Sensitivity (Relative to ^1H)</i>	<i>Natural Abundance (%)</i>	<i>Resonance Frequency (MHz) at 23.4 kG</i>
Li	6	1	8.5×10^{-3}	7.4	14.72
	7	3/2	2.9×10^{-1}	92.6	
Na	23	3/2	9.2×10^{-2}	100	26.46
	39	3/2	5.1×10^{-4}	93.1	
K	41	3/2	8.4×10^{-5}	6.9	9.65
	85	5/2	1.0×10^{-2}	72.8	
Rb	87	3/2	1.8×10^{-1}	27.2	13.12
	133	7/2	4.7×10^{-2}	100	

electronic environment of the ions will give rise to chemical shift changes. Since alkali metals do not usually participate in covalent bonding, the chemical shifts are sensitive only to the immediate environment of the cation. The simple electronic structure and small size of the sodium cation lead one to expect a relatively small range of chemical shifts. The magnitudes of the chemical shift ranges increase greatly from lithium through cesium (6). However, the sensitivity of the chemical shift to solvent decreases with increasing ionic size (6).

Sodium-23 chemical shifts depend linearly on concentration in aqueous solution (14). A dependence on the counterion has also been found at high concentrations (14). A good deal of effort has been directed toward the study of ^{23}Na shifts in nonaqueous solvents. Previous studies have revealed that ^{23}Na chemical shifts depend on the Lewis basicity of the solvent (8, 16, 17). With poor electron donors, the ^{23}Na resonance of a dissolved electrolyte occurs upfield of the same resonance in more basic solvents. Thus, the ^{23}Na chemical shift of NaI in a solvent such as acetic acid is upfield of its value in a solvent such as pyridine (16). A good correlation between solvating ability and chemical shift has been established (8). No correlation has been found between the polarity of the solvent and the ^{23}Na chemical shift of a dissolved electrolyte (8).

Nuclei with spin I greater than $1/2$ possess quadrupole moments (produced by asymmetries in the electronic environment) that interact with electric field gradients at the nucleus. Fluctuations in this interaction arising from translational or rotational diffusive motions in the liquid can provide an efficient mechanism of nuclear spin relaxation. Equation 1 governs this relaxation for ^{23}Na (18, 19).

$$\frac{1}{T_2} = \pi\Delta\nu = \frac{1}{10} \left(\frac{e^2qQ}{\hbar} \right)^2 f(\tau_R, \tau_{ex}) \quad (1)$$

Here, T_2 is the spin-spin relaxation time; $\Delta\nu$ is the linewidth; eq is the electric field gradient at the nucleus; eQ is the nuclear quadrupole moment; and $f(\tau_R, \tau_{ex})$ is some function of the correlation times τ_R and τ_{ex} , for rotational motion and exchange of the ions, respectively. An asymmetry parameter of zero is assumed (18).

Sodium-23 resonances in aqueous solutions of electrolytes are relatively narrow (14) since the aqueous environment is, on the average, highly symmetric (small electric field gradients), with only minor distortions attributable to collisions with, or exchange of, solvent molecules. Binding of a sodium ion to an anionic site on a polymer will produce a broadened resonance. This broadening can arise from distortion of the sodium electronic environment by the anionic group (increased electric field gradient) and decreased mobility attributable to the influence of the

polymer (increased τ_R). Electronic distortion created by binding produces an increase in the strength of the interaction (e^2qQ/\hbar), causing spin relaxation and, hence, the linewidth. Reduced mobility weights the spectral distribution of molecular motions toward components more efficient in producing relaxation.

The amount of broadening experienced by alkali metal ions upon binding to a polymer such as Nafion will depend on several factors including nuclear spin, electric quadrupole moment, stability of the hydrated ion, and electronic polarizability. This last factor relates to the ease with which electric field gradients can be produced by binding to an anionic site. More will be said later concerning the linewidth of alkali metal resonances in the presence of Nafion.

The present study uses ^{23}Na NMR to probe ionic mobility, binding, and electronic environment in hydrated Nafion. Data that bear on the development of theoretical models (1,3) are obtained. Preliminary results for other alkali metals and for water of hydration are presented.

Experimental Section

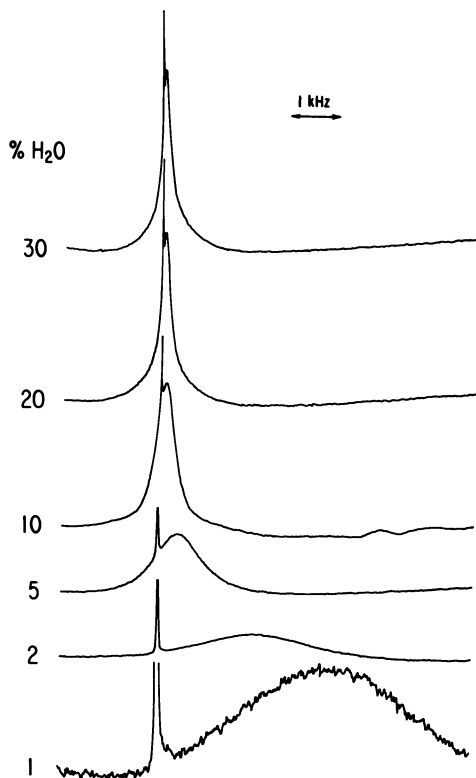
Alkali metal NMR spectra were observed at the appropriate resonance frequencies listed in Table I, using 12-mm tubes and a Varian XL-100 spectrometer with Gyrocode Observe capability. External ^{19}F or internal ^1H field-frequency lock was used. Depending on the linewidth of the resonance being observed, spectral widths of 256 Hz to 12 kHz in 8192 frequency domain points were used. For ^{23}Na and ^{85}Rb , 90° pulses of 50 μsec and a 0.1-sec repetition rate were used. For ^6Li and ^{133}Cs , the approximately 55° pulses were 30 μsec , and the pulse repetition rates for the Nafion samples were 60 sec and 1 sec, respectively.

Nafion samples (1100 equiv wt and in powder form) with rubidium and cesium as counterions were prepared by repeatedly equilibrating Nafion (Na form) with excess RbOH or CsOH . The lithium sample was prepared similarly using LiCl . All samples were washed repeatedly with distilled water. Details of the preparation of the sodium samples have been given elsewhere (20).

The ^1H NMR spectra were obtained at 100 MHz using Nafion spheres approximately 6.5 mm in diameter that were held between two Teflon vortex plugs in a 12-mm tube. The spheres were centered in the rf coil and were covered with benzene- d_6 .

^{23}Na NMR

In Figure 2 are the ^{23}Na spectra of Nafion- Na^+ as a function of water content at 30°C . The chemical shifts and linewidths are given in Table II, along with some results at elevated temperatures. Only a single resonance is observed in each case. At large swelling (30% water and above), the ^{23}Na linewidth is more than an order of magnitude broader than usually observed in concentrated aqueous electrolytes (14) at comparable



Journal of the American Chemical Society

Figure 2. Sodium-23 spectra of Nafion- Na^+ as a function of H_2O content at 30°C and 26.46 MHz. The narrow resonance arises from external 0.1M NaCl (20).

water-to-salt molar ratios. This fact is evidence for a significant interaction between the sodium ions and the polymer. As the amount of water is decreased at constant temperature, the ^{23}Na resonance broadens increasingly, reaching a value of about 4 kHz at 1% water, while the resonance shifts about 130 ppm upfield. This shift change is substantially larger than is typical for the ^{23}Na resonance, even in the presence of organic solvents and under a variety of conditions (8, 14, 16, 17). With increasing temperature at a given water concentration, both reduced linewidths and chemical shift changes are seen (Table II).

The data in Table II can be interpreted in terms of an equilibrium between bound and unbound (totally hydrated) sodium ions, with a fast exchange between populations. Such an approach is common in NMR studies of ion binding and ionic solutions, has been generally successful

Table II. ^{23}Na Chemical Shifts and Linewidths for Nafion SO_3Na^+ as a Function of Water Content and Temperature^a

% H_2O^b	T ($^\circ\text{C}$)	δ (ppm) ^c		$\Delta\nu$ (Hz) ^d
Saturated	30	—		220
Saturated	55	—		130
Saturated	92	—		100
30	30	$-2.2 \pm$	0.1	230
20	30	$-2.4 \pm$	0.1	260
10	30	$-3.6 \pm$	0.3	460
5	30	$-14.6 \pm$	1	1100
5	90	\sim	-4	600
2	30	$-73 \pm$	4	2500
2	90	\sim	-34	1900
1	30	$-130 \pm$	10	4000
1	90	\sim	-100	3000

^a At 26.46 MHz and 1100 equiv wt (20).

^b As weight percent of dry polymer.

^c Relative to external 0.1M NaCl, except for the values at 90° which were measured using the value found for 30% H_2O .

^d Estimated accuracy $\pm 10\%$. Not corrected for field inhomogeneity or bulk susceptibility effects.

Journal of the American Chemical Society

(7, 8, 9), and is physically realistic as a first approximation. The observed chemical shift and linewidth will be the weighted average of these values for the bound and unbound species. As the temperature or the amount of water is reduced, a larger fraction of sodium ions is bound at a given instant. This causes the resonance to broaden and shift upfield toward the position for the totally bound species. Assuming such a two-state model, it is possible to estimate the fraction of bound cations under a given set of conditions from the data in Table II.

As a model for the ^{23}Na shift changes in Nafion, the salt $\text{CF}_3\text{SO}_3\text{Na}$ was investigated as a function of concentration in aqueous solution. The results are in Table III. Upfield shift changes are observed with increas-

Table III. ^{23}Na Chemical Shifts and Linewidths of Aqueous $\text{CF}_3\text{SO}_3\text{Na}^a$

Conc. (M)	Approx. $\text{H}_2\text{O}/\text{Na}$ Molar Ratio	δ (ppm) ^b	$\Delta\nu$ (Hz)
0.1	540	0.0	—
1.0	50	-0.7	16
4.5	8	-2.3	33

^a From Ref. 20.

^b Relative to external 0.3M NaCl. Positive shifts are downfield. Not corrected for bulk susceptibility effects, which are estimated to be on the order of 0.1 ppm.

Journal of the American Chemical Society

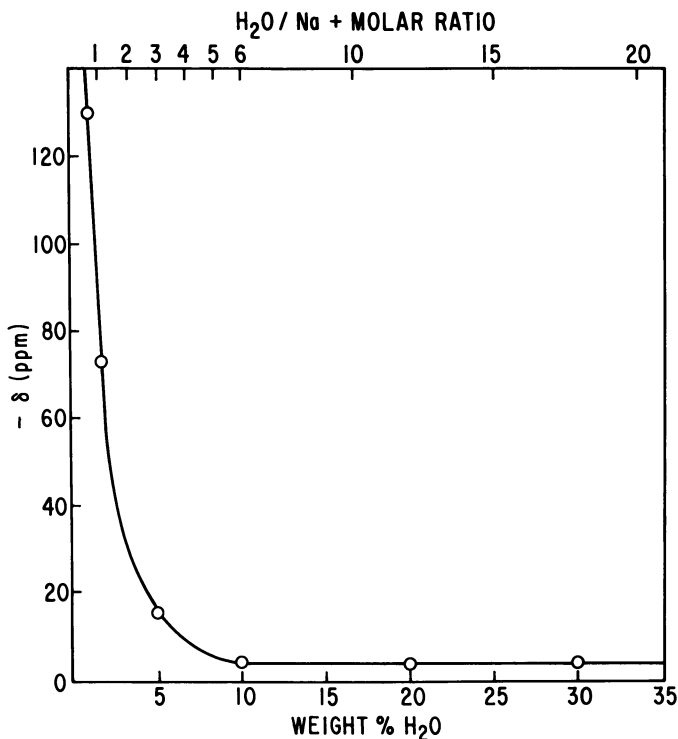
ing salt concentration (i.e., decreasing water) as for Nafion- Na^+ . At saturation, Nafion- Na^+ (1100 equiv wt) absorbs about 35% water (4), corresponding to an aqueous electrolyte concentration of about 2.6M. Hence, the shift changes for the model salt are of the same magnitude and direction as for Nafion (over the comparable concentration range). Unfortunately, solubility limitations prevent observation of larger shift changes for the model salt.

The correlation of the directions and magnitudes of the shift changes of Nafion and the model salt strongly suggest that the mode of binding is the same in the two cases, namely, the anion-cation electrostatic interaction. Since the $-\text{CF}_2\text{SO}_3$ moieties of Nafion are undoubtedly weakly basic and poor electron donors relative to water, the upfield shifts observed here with increased ion binding are consistent with previous observations (16, 17). The sodium nucleus experiences an increased shielding as water molecules are replaced by SO_3 groups in the neighborhood of the ion.

The large shift changes seen at low water contents are strong evidence for the formation of contact ion pairs. The amount of water present at these levels is not enough to effectively provide for solvent-separated ion pairs. This behavior also explains why only relatively small shift changes are seen in both aqueous and nonaqueous electrolyte solutions as a function of concentration. At the concentrations of electrolyte normally obtainable, the overwhelming majority of ions are solvent-separated, with only a small contribution from contact ion pairs. It is also true that because of its chemical nature, the Nafion system (i.e., perfluorosulfonate) might be expected to yield larger cationic shift changes compared with other anionic types under similar conditions.

Figure 3 is a plot of the ^{23}Na chemical shift change for Nafion (1100 equiv wt) vs. % water and the water-to-sodium molar ratio. Since changes in the first hydration sphere of the cation would be expected to cause the largest chemical shift changes, it is possible to estimate the number of water molecules in the first hydration sphere of Na^+ (more properly, a $\text{Na}^+-\text{SO}_3^-$ ion pair) in Nafion. One obtains an estimate of 3-4 water molecules per Na^+ ion from the plot in Figure 3. Essentially the same value can be obtained from a similar plot for the linewidth data (Figure 4). Similar behavior has been observed recently for the ^{23}Na linewidth in the sodium diisooctyl sulfosuccinate/water/heptane reversed micellar system (21) and in the caprylic acid/sodium caprylate/water system (22). Hence, the results obtained here provide support for the presence of hydrated ionic clusters in Nafion.

It should be pointed out that little can be learned concerning the detailed geometry of the ion pairs in Nafion at low water contents. The electronic distribution around the sodium cation attributable to the

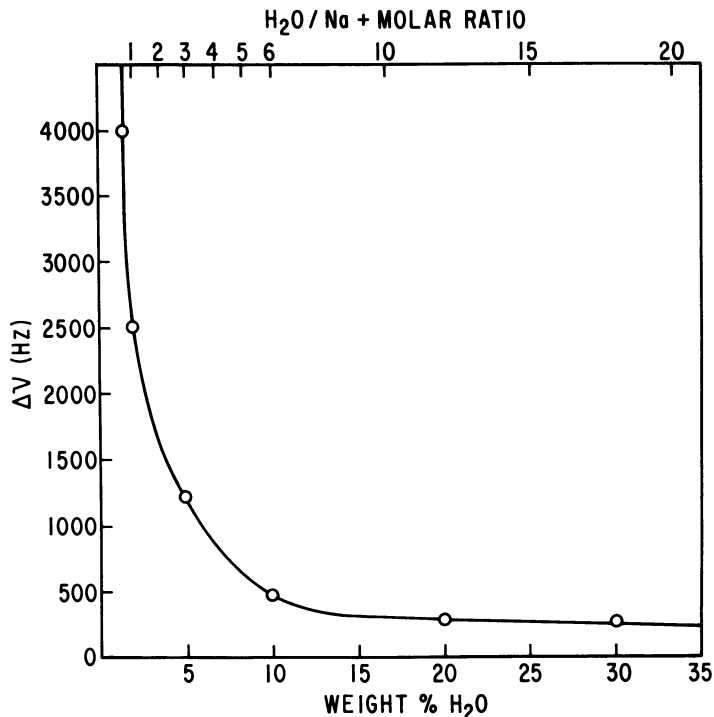


Journal of the American Chemical Society

Figure 3. Plot of the ^{23}Na chemical shift of Nafion (1100 equiv wt) vs. % H_2O and the $\text{H}_2\text{O}/\text{Na}$ molar ratio (20)

neighboring SO_3 group(s) is almost certainly highly anisotropic. No evidence for this can be seen in the spectra in Figure 2—most probably because of the rapid averaging between free and bound states that gives rise to the equilibrium spectra.

Comparison of the data in Figures 3 and 4 shows that while the chemical shift approaches that of the model salt, the linewidth approaches a value one order of magnitude higher. This behavior suggests that Na^+ ions in saturated Nafion are substantially restricted relative to the small molecular weight electrolyte, even when the contribution to the linewidth attributable to bound ions is taken into account. This result bears on the theoretical treatment of Nafion dissociation in terms of a four-state model (3). The bulk of the ions appears to be partially restricted (States 2 and 3 of Ref. 3), with a very small percentage bound as contact ion pairs (State 4 of Ref. 3). It is not known if any of the Na^+ ions can be considered totally free.



Journal of the American Chemical Society

Figure 4. Plot of the ^{23}Na resonance linewidth of Nafion (1100 equiv wt) vs. % H_2O and the $\text{H}_2\text{O}/\text{Na}$ molar ratio (20)

In Table IV is a comparison of the ^{23}Na NMR parameters vs. water for Nafion samples of three different equivalent weights. Excluding total saturation, only low water contents were chosen since the maximum amount of water absorbed decreases with increasing equivalent weight. The data in Table IV show that the ^{23}Na NMR parameters are not substantially affected by equivalent weight in the range of water contents where comparisons can be made validly. That is, essentially the same upfield shift changes and line broadening are seen at low water contents. For the saturated samples, a small upfield shift and a slight resonance broadening are expected because of the reduction in the maximum amount of water absorbed at higher equivalent weights.

In Table V is the temperature dependence of the ^{23}Na linewidths of Nafion- Na^+ for a number of equivalent weights. At all equivalent weights the resonance narrows with increasing temperatures. This behavior is indicative of exchange which is fast on the NMR time scale. With two exceptions (27° and 47°C at 1347 and 1500 equiv wt), the linewidth

Table IV. ^{23}Na NMR Parameters vs. Water Content at Several Equivalent Weights^a

<i>Equiv Wt</i>	% H_2O	$\Delta\delta(\text{ppm})^b$	$\Delta\nu(\text{Hz})^c$
1100	Sat.	-2.2	220
	5	-14.6	1100
	2	-74	2500
1347	Sat.	-4.5	340
	5	-10	810
	2	-61	2000
1500	Sat.	-3.2	360
	5	-10	880
	2	-53	2200

^a At 30°C and 26.46 MHz.^b Measured relative to an external frequency reference and given relative to external 0.1M NaCl.^c Estimated accuracy $\pm 10\%$.

increases slightly with increasing equivalent weight. This broadening approximately parallels that expected because of decreased water absorption (4). No evidence is seen for any additional effects arising from potential structural variations. It is not known how important bulk susceptibility effects, arising from an irregular sample configuration, are for the films of 1500 and 1800 equiv wt. It is highly unlikely that the differences seen between these samples and those of lower equivalent weight can be attributed entirely to this factor.

Arrhenius plots of the linewidth for the various equivalent weights are approximate straight lines for all except 1500 equiv wt. The cause for the different behavior of the latter sample is not known; it may stem from some problem in preparing the sample. An activation energy of 3.2 kcal/mol was obtained from the plot for the sample of 1100 equiv wt. The slopes of the plots for other equivalent weights (except 1500) were approximately the same as for the 1100-equiv wt sample.

It is difficult to assess the relative importance of the specific dynamic processes that give rise to the measured activation energy. Clearly, the

Table V. ^{23}Na Linewidth^a of Water-Saturated Nafion vs. Equivalent Weight and Temperature

<i>Equiv Wt</i>	<i>Temperature (°C)</i>			
	27	47	70	96
1100	220	160	112	80
1347	340	260	180	130
1500	330	230	190	170
1800	370	270	220	170

^a Estimated accuracy $\pm 10\%$. Not corrected for bulk susceptibility effects. In Hz.

motion of solvent molecules in and out of the ionic hydration sphere and the binding of the cation to an anionic site(s) will be involved. Calculations of the energetics involved in the dissociation equilibrium of bound and unbound cations yield activation barriers in reasonable agreement with this number (1). Previous NMR studies (23) on pure water yielded a value of 3.5 kcal/mol between 40° and 100°C. Using ^{23}Na NMR, a somewhat lower value (2.5 kcal/mol) was obtained for the reorientational process of water molecules in the hydration shell of Na^+ in aqueous NaCl (23).

^6Li , ^{85}Rb , and ^{133}Cs NMR

In Table VI are the results of some preliminary experiments used to determine the feasibility of observing NMR signals arising from other alkali metals bound to Nafion. Unfortunately, it was not possible to observe ^{39}K , ^7Li , or ^{87}Rb on the equipment available. From Tables I and VI it is apparent that the NMR properties of the nucleus in question are critical for observing its resonances when associated with Nafion. For ^6Li and ^{133}Cs , the Nafion resonances are narrow enough to be observed. This fact could be predicted from the very narrow linewidths of the model electrolytes, or from the spin relaxation behavior of the nuclei (24). On the other hand, the large ^{85}Rb linewidth seen for aqueous RbOH leads one to predict a very large linewidth for Rb-Nafion . This is indeed the case, since no resonance could be observed under high resolution conditions.

The larger linewidths observed for the alkali metal forms of Nafion relative to the corresponding model electrolytes indicate that ionic mobility is restricted because of ion binding to the polymer in the aqueous regions. Without additional studies it is not possible to obtain an estimate of relative binding strength from the data in Table VI. However, experiments identical to those for ^{23}Na are possible in order to probe the hydration properties of these other ions in Nafion.

Table VI. Linewidths^a of Several Alkali Metal Resonances of Electrolyte Solutions and Saturated Nafion (1100 Equiv Wt)

<i>Nucleus</i>	<i>Model^b</i>	<i>Nafion</i>
^6Li	< 0.2°	1.5
^{85}Rb	225	Not Observed (> 5 kHz)
^{133}Cs	1	145

^a In Hz at 30°C. Not corrected for field inhomogeneity or bulk susceptibility effects.

^b Approximately 4M solution of LiCl , RbOH , or CsOH .

^c Limited by magnetic field inhomogeneity.

^1H NMR

Proton (^1H) NMR has proved to be a sensitive method for studying hydrogen bonding in liquids and electrolyte solutions (6,7). Formation of a hydrogen bond causes the resonance of the bonded proton to move downfield. Hence, an upfield shift can be correlated with the breaking up of hydrogen bonds. This behavior has led to the characterization of ions in terms of their effect on water structure (7).

In Table VII are the relative ^1H chemical shifts of water in Nafion at several water contents. The experiments were conducted on specially prepared Nafion spheres in order to eliminate bulk susceptibility effects. These spheres behaved the same as the corresponding Nafion films and powders in limited ^{23}Na NMR experiments. The ^1H linewidths are sufficiently narrow to allow accurate measurement of the chemical shift. With decreasing water content, the resonance shifts upfield, suggesting the breakup of water-hydrogen bonding as for NaCl. The relative shift of pure water and water in saturated Nafion is not known at this time. The increased linewidth indicates decreased water mobility, as seen for the sodium ions. Additional experiments using model electrolytes and a chemical shift standard are warranted.

Table VII. ^1H Shifts and Linewidths of Water in Nafion- Na^+ Spheres (1100 Equiv Wt)^a

% H_2O	$\delta(\text{ppm})^b$	$\Delta\nu(\text{Hz})$
15	0.0	25
5	-0.5	35
1	-0.9	130

^a At 100 MHz and 30°C.

^b Relative to the value at 15% water.

Acknowledgments

I thank K. A. Mauritz for his stimulating discussions and other contributions to this work and N. J. Baldwin of the Major Analytical Instrument Facility at Case Western Reserve University for help in obtaining many of the spectra. I am also grateful to J. J. Chang and P. Meakin of Du Pont for providing the Nafion spheres for the ^1H NMR experiments.

Literature Cited

1. Mauritz, K. A.; Hora, C. J.; Hopfinger, A. J., chapter 8 in this book.
2. Cutler, S. G., chapter 9 in this book.
3. Mauritz, K. A.; Lowry, S. R. *Am. Chem. Soc., Polym. Prepr.* **1978**, *19*(2), 336.

4. Grot, W. G. F.; Munn, G. E.; Walmsley, P. N., presented at the 141st Electrochemical Society Meeting, Houston, TX, May 1972.
5. Yeo, S. C.; Eisenberg, A. *J. Appl. Polym. Sci.* **1977**, *21*, 875.
6. Burgess, J.; Symons, M. C. R. *Q. Rev., Chem. Soc.* **1968**, *22*, 276.
7. von Goldammer, E. *Mod. Aspects Electrochem.* **1975**, *10*, 1.
8. Popov, A. I. *Pure Appl. Chem.* **1975**, *41*, 275.
9. Laszlo, P. *Angew. Chem., Int. Ed. Engl.* **1978**, *17*, 254.
10. Bovey, F. A. "High Resolution NMR of Macromolecules"; Academic: New York, 1972.
11. Komoroski, R. A.; Mandelkern, L. In "Applications of Polymer Spectroscopy"; Brame, Jr., E. G., Ed.; Academic: New York, 1978.
12. McCall, D. W. *Acc. Chem. Res.* **1971**, *4*, 223.
13. Schaefer, J.; Stejskal, E. O.; Buchdahl, R. *Macromolecules* **1977**, *10*, 384.
14. Templeman, G. J.; Van Geet, A. L. *J. Am. Chem. Soc.* **1972**, *94*, 5578.
15. Farrar, T. C.; Becker, E. D. "Pulse and Fourier Transform NMR"; Academic: New York, 1971.
16. Greenberg, M. S.; Bodner, R. L.; Popov, A. I. *J. Phys. Chem.* **1973**, *77*, 2449.
17. Bloor, E. G.; Kidd, R. G. *Can. J. Chem.* **1968**, *46*, 3425.
18. Abragam, A. "The Principles of Nuclear Magnetism"; Clarendon: Oxford, 1961.
19. Marshall, A. G. *J. Chem. Phys.* **1970**, *52*, 2527.
20. Komoroski, R. A.; Mauritz, K. A. *J. Am. Chem. Soc.* **1978**, *100*, 7487.
21. Wong, M.; Thomas, J. K.; Nowak, T. *J. Am. Chem. Soc.* **1977**, *99*, 4730.
22. Lindman, B.; Ekwall, P. *Kolloid Z. Z. Polym.* **1969**, *234*, 1115.
23. Hertz, H. G. *Prog. Nucl. Magn. Reson. Spectros.* **1967**, *3*, 159.
24. Wehrli, F. W. *J. Magn. Reson.* **1978**, *30*, 193.

RECEIVED October 11, 1978.

Asphalt Ionomers

L. CIPLIJASKAS, M. R. PIGGOTT, and R. T. WOODHAMS

Department of Chemical Engineering and Applied Chemistry,
University of Toronto, Toronto, Ontario, Canada M5S 1A4

Shell Venezuelan asphalt [85–100 Penetration Index] was modified chemically with maleic anhydride or sulfur trioxide to produce carboxylated or sulfonated asphalts that could be neutralized with basic metal oxides such as calcium or magnesium. The resultant asphalt ionomers, when mixed with sand or traprock, produced composites that retained their strength when wet; however, the unmodified asphalt mix lost over 80% of its strength when immersed in distilled water. The neutralization step can be delayed to produce a post-thickening reaction after paving so that the surface remains dimensionally stable. The use of asphalt ionomers as binders in road paving materials should produce more durable road surfaces that are less subject to rutting, raveling, cracking, and pothole formation.

Asphaltic bitumen is used widely as a binder in road surfacing, caulking and sealing materials, adhesives, roofing shingles and membranes, impregnated papers, felts and fabrics, protective coatings, and as an extender for elastomers and plastics. Although asphalt is composed largely of carbon and hydrogen, the ratio of these elements may vary so that the physical and chemical properties depend on the relative proportions of aliphatic, aryl, alkene, or polynuclear aromatic structures comprising each particular sample. The viscosity of asphalt depends on the chemical composition and the molecular weight. Chemical analysis reveals that many asphalts contain minor proportions of oxygen, sulfur, or nitrogen that may be combined as carbonyl, phenolic, sulfonyl, or quinolone moieties (1).

It is known that many asphalts disintegrate slowly in water, and even though combined with aggregates such as sand or traprock, these asphalts will lose most of their strength when exposed to moisture (2, 3).

In the case of asphalt paving materials this phenomenon is referred to as water-stripping, debonding, or moisture damage, and is attributable to readsorption of water at the asphalt–aggregate interface and a catastrophic loss of adhesion. It has been shown by several investigators that the addition of minor amounts of basic oxides such as calcium oxide (lime), calcium hydroxide (hydrated lime), portland cement, or limestone helps to maintain adhesion in the presence of water (2). Cationic adhesion promoters such as organic amines may delay the loss of adhesion but cannot prevent the eventual loss (4). The decrease in composite strength (or modulus) in the presence of moisture depends on the type of aggregate (sand, traprock, granite, limestone, etc.), the quantity and type of basic additive, the type of asphalt, the temperature, the salinity, the relative humidity, and the length of exposure. Directly or indirectly, this decrease in strength leads to cracking and raveling with the eventual formation of potholes. In 1977, for example, there were an estimated 160 million potholes produced in nearly 4 million miles of roads and streets in the United States which required nearly one billion dollars for repairs (5). The failure of asphaltic membranes is also a major cause of the disintegration of reinforced concrete overpasses, bridges, and elevated highways. Clearly there is a need to improve the quality of asphalt paving materials in North America to reduce the costs of maintenance and extend the lifetime of roads and protective membranes.

The annual consumption of asphalt in North America is nearly 30 million metric tons of which 74% is used in road construction, 15% in roofing, and 11% in coatings, adhesives, and miscellaneous applications. At about 10 cents/kg, asphalt is evidently one of the cheapest and most abundant thermoplastics available in the world today.

A typical asphaltic road surfacing mix in the metro Toronto area comprises 56% traprock (orthoclase, $K_2Al_2Si_6O_{16}$), 38% sand (SiO_2), and 6% Venezuelan asphalt (Shell product, 85–100 penetration). Normally the surface is applied as a hot mix in a 5–15-cm thick layer over a concrete base. Cracks usually begin to appear in the fresh surface after a few months so that caulking and patching become necessary. Topcoats may be applied every few years to further prolong the lifetime of the road (which in the metro area averages 12–14 years before total replacement becomes necessary).

In 1975 the University of Toronto began an investigation of the factors affecting the performance and durability of asphaltic roadways including the evaluation of asphalt mixes containing powdered reclaim rubber (6). A parallel investigation was aimed at improving the interfacial adhesion between asphalt and the aggregate, particularly in the presence of moisture, so that problems caused by stripping or debonding could be eliminated (7).

Since it is well known in plastics technology that polymeric materials containing ionic substituents exhibit excellent adhesion to inorganic substrates, attempts were made to graft ionic substituents onto asphalt. Such modified asphalts will be designated herein as "asphalt ionomers." In the first series of experiments, maleic anhydride was observed to have a profound effect on asphalt, a phenomenon characterized by a gradual increase in viscosity and a corresponding increase in cohesive strength. Initial experiments also indicated that the modified asphalt retained its strength and adhesion when fully immersed in water for long periods of time. Unfortunately maleic anhydride is extremely toxic (hence its name, toxic anhydride) and its high vapor pressure at elevated temperatures precluded its direct use in the hot-mix process for safety reasons.

Sulfonation was next examined as an alternate method of introducing ionic substituents. In both maleic anhydride treatment and sulfonation, the acidic substituents were neutralized with basic oxides such as calcium or magnesium. This step was usually necessary to prevent the loss of adhesion to the aggregate in the presence of water, except when the aggregate itself insolubilized the acidic components (for example, limestone).

Although these results are preliminary and will require further evaluation by more conventional test procedures, there is good evidence to suggest that asphalt ionomers are capable of eliminating the problems caused by water-stripping and may help to maintain the tensile strength of asphaltic compositions in moist environments. Since most roads in North America are exposed to moisture, either from condensation, humidity, or ground water, wet-strength retention is important to protect the roads during seasonal changes when they are most susceptible to damage (through frost heave, thermal contraction, or embrittlement). Other factors affecting road performance include rutting (stress-induced flow), low-temperature brittleness, skid resistance, self-healing characteristics, toughness, and wear resistance. The acceptability of any new material for road surfacing is governed by cost, ease of application via conventional road laying techniques, and traffic safety.

Experimental

The asphalt (Shell Venezuelan, 85–100 penetration) was modified chemically by heating with a small quantity of maleic anhydride or, in the case of sulfonation, with a sulfur trioxide–tertiary amine salt. The reaction with maleic anhydride appears to be slow but spontaneous even at 23°C, and apparently is catalyzed by Lewis acids (aluminum trichloride, for example). In some preparations the maleic anhydride was dissolved in the warm asphalt and heated with 0.5% dicumyl peroxide

for 30 min at 150°C. When the reaction was complete, a stoichiometric excess of calcium oxide or magnesium oxide was added and the mixture allowed to cool.

Sulfonation was carried out by heating the asphalt with sulfur trioxide-trimethyl amine complex or sulfur trioxide-pyridine complex at temperatures near 135°C. Sulfamic acid treatment was also included in this series. Many other reagents were evaluated such as methyl methacrylate, 2-acrylamido-2-methylpropanesulfonic acid, 2-dimethyl-aminoethyl methacrylate, 2-vinylpyridine, 4-vinylpyridine, tetrahydrophthalic anhydride, norbornene dicarboxylic anhydride, and phthalic anhydride.

The lap-shear test was used to determine the room-temperature cohesive strength of the modified asphalts and to follow the thickening process in both air and water. Two aluminum strips 1 mm thick and 2.5 cm wide were overlapped 2.5 cm and firmly bonded together with a drop of molten asphalt. The test pieces were held in this position with alligator clips until ready for shear testing. In a few experiments pieces of traprock were polished and similarly bonded together as shown in

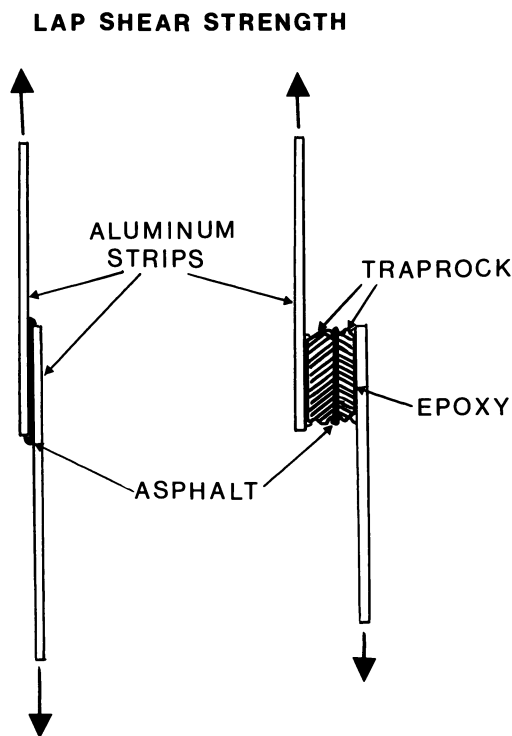


Figure 1. Lap-shear tests performed with thin strips of aluminum. In a few experiments traprock was used as the adherend. In the latter case, adhesion to the traprock approached zero when the assembly was placed in water for a few days.

Figure 1. In this manner the cohesive properties of a large number of asphalt ionomers could be measured.

A simplified test procedure was followed to evaluate the performance of asphalt ionomers in mixtures with sand and traprock. The sand and traprock were finely ground and sieved to -200 mesh (Tyler screen size) in order that small specimens could be prepared for flexural testing. Appropriate quantities of the ground fillers were added to the heated asphalt and subsequently hot-pressed into rectangular test bars at 172 MPa for 30 sec at 140°C . A standard 50-ton compression-molding press with a matched die cavity was used to mold these rectangular specimens (dimensions $2.54 \times 5.08 \times 0.77$ cm). Under these conditions of molding the void content was less than 1% for mixtures containing 6 wt % asphalt. This concentration of asphalt gave the strongest samples and is the same quantity of asphalt normally used in Metro roads. All comparisons were carried out at this asphalt concentration.

The miniature test bars were evaluated by a modified ASTM flexural test procedure using 3-point loading at a crosshead speed of 2 cm/min. The span-to-depth ratio was normalized at 6.62 so that the values of breaking load could be compared. Both the maximum load to fracture and the total strain energy were recorded. In most experiments an average of five measurements was determined for each condition.

The flexural test specimens were stored for long periods of time in air, water, and 5% aqueous sodium chloride solution to determine the effect of an aqueous environment on the mechanical properties.

A limited number of fracture energy measurements were carried out using a twin cantilever beam (8). This is a useful technique for estimating the crack propagation force and total energy to fracture for the various modified asphalts over a range of temperatures.

Viscosity measurements were determined with a rotating spindle viscometer (Haake Model VT23) in a temperature-controlled medium.

Results

Figure 2 shows the dramatic increase in viscosity that results when maleic anhydride is added to asphalt. This increase occurs even in the absence of any added catalyst or peroxide initiator. Other anhydrides such as phthalic anhydride and 5-norbornene-2,3-dicarboxylic anhydride were not as effective. Note that there is no noticeable change in the viscosity of the unmodified asphalt.

This pronounced increase in viscosity is also reflected in the lap-shear strength (*see* Figure 3). In this case the unmodified asphalt also shows a moderate increase in shear strength attributable to some form of slow association or thickening with time. Note that 0.1% aluminum chloride (a Diels-Alder catalyst) appears to accelerate the reaction with maleic anhydride. This increase in lap-shear strength occurs even when the test specimens are fully immersed in distilled water or in a 5% aqueous solution of sodium chloride. The addition of magnesium oxide (Michigan 1725) to asphalt also produced a marked increase in lap-shear strength

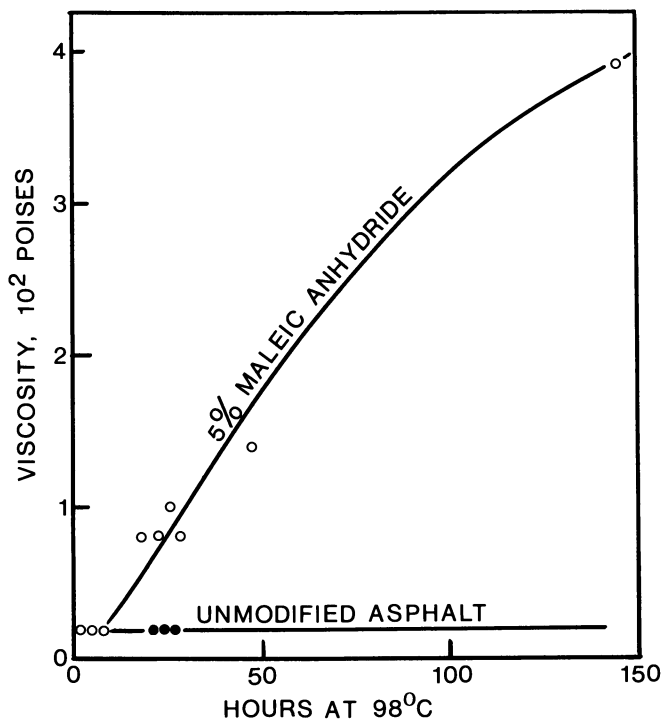


Figure 2. Asphalt containing maleic anhydride shows a pronounced increase in viscosity over a period of time. This thickening reaction occurs even at room temperature and without any added catalyst.

over a period of days at room temperature. The effect of a basic metal oxide on the lap-shear strength is shown in Figure 4. Starting at Point *a*, 26.8 g of maleic anhydride were ground cryogenically at -70°C (dry ice temperature) with 400 g of asphalt. No change was apparent after this treatment, so the mixture at Point *b* was heated for 3 hr at 120°C with 2 g of dicumyl peroxide initiator. A slight increase in lap-shear strength was observed (Point *c*) which continued to increase slowly over a period of several days. The mixture was then reheated at Point *d* and 28 g of hydrated lime were dispersed quickly. Thereafter a rapid increase in lap-shear strength occurred until the tests were discontinued at Point *e*. The lack of any change during cryogenic grinding suggests that the thickening reaction is not radical in nature and is probably cationic (9).

The compression-molded bars were placed in polyethylene bags that were filled with distilled water or a 5% saline solution. At periodic intervals several test bars were removed and tested in flexure to determine the apparent loss of strength. These results are summarized in

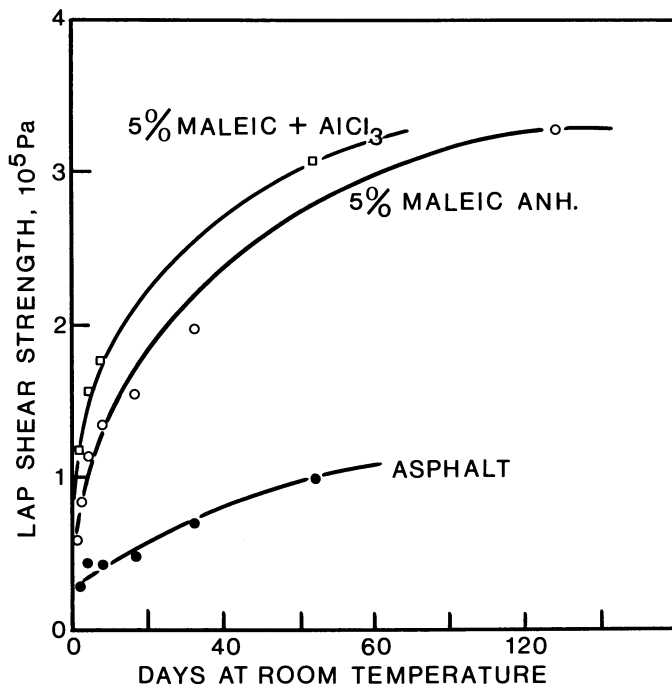


Figure 3. Unmodified asphalt shows a slight increase in shear strength with time but the rate of thickening is much more pronounced when maleic anhydride is present. This reaction is probably cationic (acid catalyzed) since a trace of aluminum chloride increases the rate.

Figures 5 and 6. Surprisingly the magnesium maleate-modified asphalt did not show any improvement in wet-strength retention with traprock (see Figure 5). Note that unmodified asphalt also loses most of its strength after 100 days immersion in water. However, complete wet-strength retention is obtained when sand is used as a filler. In air, even the magnesium maleate asphalt/sand mixture showed a gradual increase in strength.

The results with the magnesium sulfonate asphalt were precisely opposite those of the magnesium maleate asphalt (see Figure 6). In this series full wet-strength retention was obtained using traprock but not with sand. In all these experiments distilled water was more aggressive than the saline solution, which would tend to indicate that salting of roads in the winter months is less harmful than rainfall.

In the majority of molded samples the maximum load to fracture was found to be roughly proportional to the area under the stress-strain curve at 23°C. This stress-strain behavior was very sensitive to temperature as is evident in Figure 7. Brittle fracture was common at

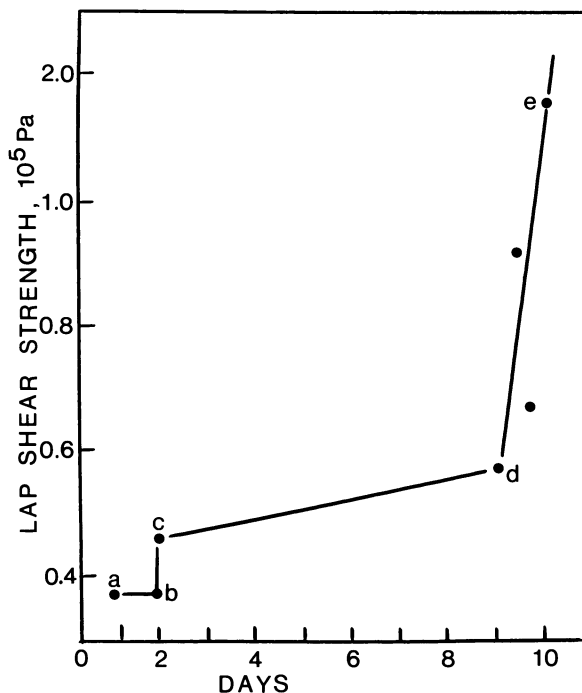


Figure 4. Cryogenic grinding of maleic anhydride with asphalt does not produce any change in lap-shear strength. After heating the mixture at 120°C with 0.5% dicumylperoxide the shear strength increased from Point b to Point c. Over a period of several days at room temperature the modified asphalt showed a gradual increase in lap-shear strength until at Point d the asphalt was mixed with 7% hydrated lime. A rapid increase in lap-shear strength was observed until the test was discontinued at Point e. (a) initial; (b) after cryogenic grinding; (c) after maleization; (d) after storage at 23°C; (e) after CaO addition.

temperatures below 0°C, and at -16°C there was no detectable difference in the flexural strengths of the modified and unmodified asphaltic composites.

From crack propagation tests with the double cantilever beam it was found that the failures were mostly cohesive and the crack initiation force was greatest for the maleated asphalts (300 ± 70 N vs. 200 ± 70 N for the untreated asphalt). These experiments were conducted on the modified asphalts prior to neutralization with metal oxides. No measurements were made with the metal salts of the acidified asphalts.

The rotating spindle viscosity followed the normal Arrhenius temperature relationship with a slightly higher activation energy for the maleated and sulfonated asphalts (without added metal oxide). The viscosity-temperature relationships of two of the modified asphalts are compared with that of the unmodified asphalt (*see* Figure 8).

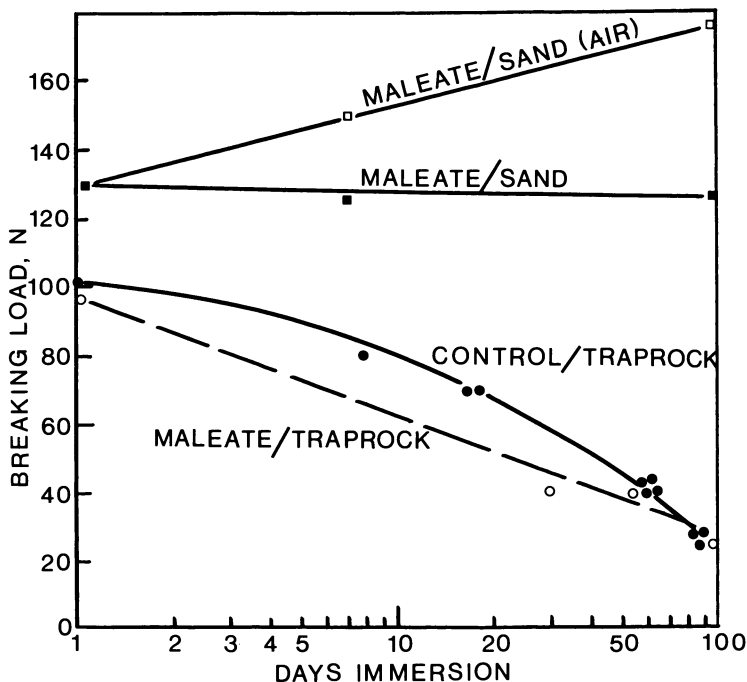


Figure 5. With powdered traprock, the asphalt control loses most of its strength after 100 days immersion in water. However, the wet-strength retention of the asphalt maleate (magnesium salt) is excellent in the case of sand and even shows an increase in air.

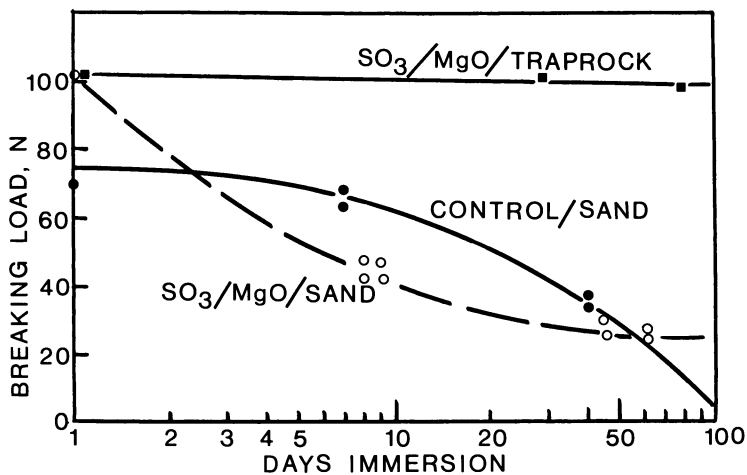


Figure 6. The behavior of the asphalt sulfonate (magnesium salt) is quite the opposite of the behavior shown in Figure 5. In this series the wet-strength retention was best with traprock and was almost zero with normal asphalt.

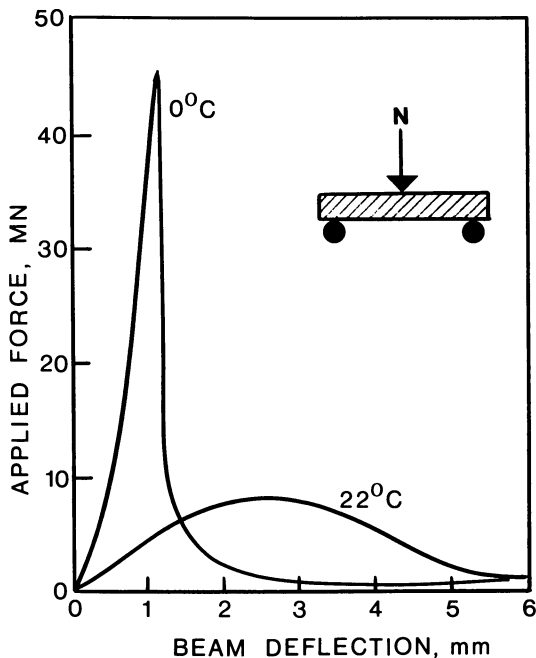


Figure 7. The typical low-temperature brittle fracture of 6% asphalt mixtures is clearly evident from stress-strain measurements using 3-point bending tests.

Discussion

Previous investigators have drawn attention to the beneficial effect of lime when added in small quantities to asphaltic bitumen. The lime helps retard oxidative hardening (13) and reduces the tendency towards water-stripping (4, 11, 12). Most asphalts are slightly acidic because of the presence of phenolic or carboxylic substituents and would therefore react with basic oxides to form insoluble salts. For example, Fromm (10) has described the use of iron salts of naphthenic acids as adhesion promoters to improve the water resistance of asphalt concretes. This promising approach is now undergoing commercial trials. The literature also describes methods of chemically modifying asphalt with maleic anhydride or acrylic acid (14), sulfur trioxide (15), sulfur dioxide (16), acetyl sulfate (17–21), and sulfuric acid (20). (For a recent review of the interfacial phenomena in asphaltic compositions see Ref. 4.)

In the present investigation asphalt was modified chemically to introduce acidic substituents and thereafter neutralized with a basic metal oxide to form a salt. The intention was to provide sufficient ionic content to ensure an interfacial bond with the aggregate strong enough

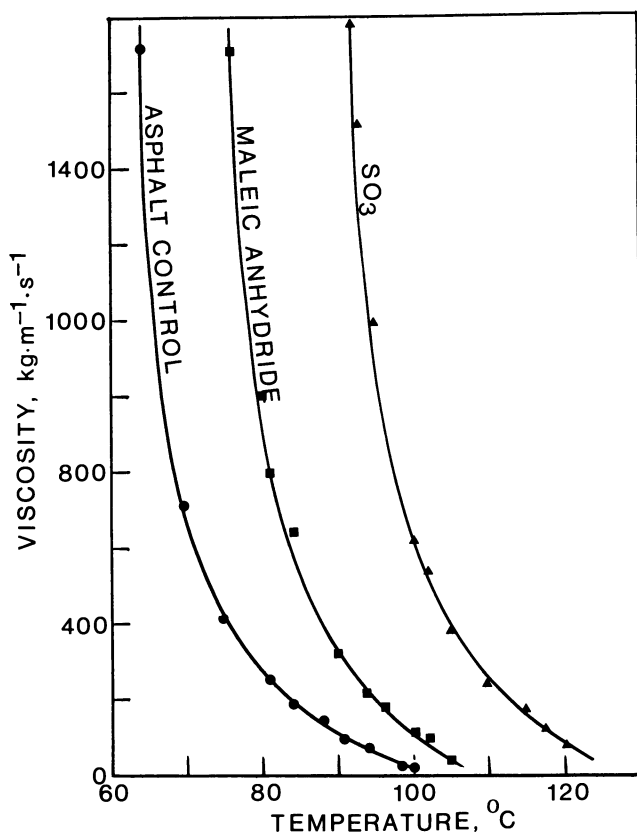


Figure 8. The maleation or sulfonation of asphalt increases the viscosity substantially as is evident from these viscosity measurements taken over a range of temperatures. As a result, higher mixing temperatures may be necessary with chemically modified asphalts.

to resist debonding by water molecules. The term ionomer, which was originally a Du Pont trade name applied to poly(ethylene comethacrylate) salts, has been adopted here to designate asphaltic materials containing ionic or salt substituents. Ionic substituents, unlike polar substituents, have relatively powerful long-range interactions. To minimize swelling and emulsification, the insoluble metal salts are preferred, such as those derived from calcium, magnesium, barium, zinc, chromium, and iron. Such metal ions may be introduced as lime, limestone, portland cement, asbestos, or various metal oxides. The surprising feature of this investigation was the unpredicted specificity of the magnesium maleate modification for the silica filler. Note for example in Figure 5 the strength retention of magnesium maleate-modified bitumen with sand and the

relatively poor retention in the case of traprock after prolonged immersion in water. On the other hand, magnesium sulfonate groups promote good strength retention with traprock and poor retention with sand. The weakly acidic surface of silica appears to be attracted more strongly to a salt of a weak acid (maleate) whereas the basic traprock is attracted more strongly to a salt of a strong acid (sulfonate). In a separate experiment an asphalt grafted with vinyl pyridine exhibited good wet-strength retention with sand but not with traprock. These observations tend to confirm an acid-base interaction at the interface. However, failure to neutralize the acid groups with a metal oxide resulted in very poor wet-strength retention (not shown). These observations emphasize the importance of maintaining a strong positive interaction with the aggregate surface to prevent loss of adhesion through the ingress of water and consequent desorption of the surface-active components. Therefore, the combined use of both acidic and basic aggregates in an asphaltic road mixture may require two different types of surface-active molecules for best results, that is, both carboxylated and sulfonated molecules.

A second interesting property of asphalt ionomers is their post-thickening behavior. The neutralization reaction may be carried out slowly or rapidly according to the conditions of the reaction. The maleated asphalt may be mixed with a minor proportion of a particulate metal oxide such as calcium or magnesium and the asphaltic mixture allowed to thicken slowly at ambient temperature, over a period of several days. This post-thickening reaction is analogous to the thickening of polyester resins for use in sheet molding compounds. Hence high-penetration (low viscosity) asphalts could be post-thickened to much greater viscosities after the admixture has been applied to a road surface, for example. The rate of thickening can be controlled by temperature, solubility, humidity, particle size, choice of neutralizing agent, or reagent concentration.

Whereas the approach taken in this investigation has been to create insoluble hydrophobic surface-active reagents by the in situ chemical treatment of asphalt, future researchers may find it more convenient to use readily available petroleum sulfonates or carboxylates as additives. The use of low molecular weight carboxylic elastomers, for example, may permit improved wet-strength retention as well as increased toughness at low temperatures (22, 23, 24).

Economic Considerations

The asphalt paving industry in North America involves an annual expenditure of about 60 billion dollars (U.S.). The average cost of the asphalt binder in a typical hot-mix paving contract in Ontario is about

five percent of the total contract. Any increase in the cost of this asphalt binder must be weighed against potential savings in terms of low maintenance costs and prolonged lifetime of the road surface. Obviously a doubling of the useful lifetime of an asphalt road would justify a considerable increase in the cost of the binder, and it would be unwise to use an inferior binder if frequent repairs or shortened lifetimes were incurred.

While it is quite possible that asphalt ionomers or suitable additives can be developed to permit good wet-strength retention, the tendency for asphalt to become brittle at temperatures below 0°C inevitably will lead to cracking; thermal shrinkage exerts tensile forces well beyond the fracture limit of asphalt concretes. Thus low-temperature plasticizers, such as liquid rubbers, must be used to permit some plastic flow or stress relaxation at sub-zero temperatures (22).

The use of post-thickening techniques is important since it permits the asphalt concrete to sustain greater loads at elevated temperatures without producing rutting, washboarding, and sagging. Such post-thickening behavior can be delayed until after mixing and paving are complete, so that no special mixing or paving procedures need be anticipated. When hot-mix asphalt paving materials are formulated properly to maintain strength when in the presence of moisture, to remain ductile at low temperatures, and to resist flow at elevated temperatures, asphalt roads should remain serviceable for more than a century.

Conclusion

It has been demonstrated that chemically modified asphalts are capable of retaining high cohesive strength and excellent adhesion in the presence of water. Therefore, such asphalt ionomers may have merit as binders in asphaltic road compositions, caulking and sealing materials, adhesives, roofing membranes, shingles, impregnated felts and papers, protective coatings, and low cost processing aids and extenders for filled thermoplastics.

Post-thickening reactions may be used to enhance the strength and toughness of asphalt ionomers after application, thereby avoiding high viscosities during the processing stages, and permitting normal road paving procedures to be employed.

The use of such asphalt ionomers in road surfacing should help reduce the incidence of rutting, raveling, bleeding, pothole formation, and cracking, thereby reducing road maintenance and extending the useful lifetime of roadways. Further studies are needed to develop suitable low-temperature flexibilizers for asphalt in order to eliminate cracking that is induced by embrittlement and thermal shrinkage.

Acknowledgments

The authors are particularly indebted to Joseph D. George of the Toronto Metro Roads and Traffic Department for his frequent advice and support, and to Val Raponi of Repac Construction Ltd. for his patience and generosity in supplying the road materials free of charge. These investigations were supported by a National Research Council of Canada Grant number A4873.

Literature Cited

1. Plancher, H.; Dorrence, S. M.; Petersen, J. C. *Proc. Annual Meeting Association Asphalt Paving Technologists, San Antonio, Feb. 21-23, 1977.*
2. Ishai, I.; Craus, J. *Proc. Annual Meeting Association of Asphalt Paving Technologists, San Antonio, Feb. 21-23, 1977.*
3. Fromm, H. J. *Asphalt Paving Technology* 1974, 43, 191.
4. Scott, J. A. N. *Proc. Annual Meeting Association Asphalt Paving Technologists, Florida, Feb. 13-15, 1978.*
5. Cronkite, Walter, CBS Television News, February 21, 1978.
6. George, J. D.; Ng, T. W.; Piggott, M. R.; Woodhams, R. T. *Proc. Annual Meeting Association Asphalt Paving Technologists, San Antonio, Feb. 21-23, 1977.*
7. Ciplijauskas, L.; Piggott, M. R.; Woodhams, R. T. *Ind. Eng. Chem. Prod. Res. Rev.* 1979, 18(2).
8. Anderson, G. P. "Analysis and Testing of Adhesive Bonds"; Academic: New York, 1977.
9. Casale, A.; Porter, R. S. "Advances in Polymer Science, Polymerization"; Springer-Verlag: New York, 1975; Vol. 17, p. 1.
10. Fromm, H. J. "The Mechanism of Asphalt Stripping from Aggregate Surfaces," Downsview, Ontario, Canada, 1974, Report RR190, Ministry of Transportation and Communications.
11. "Composite Materials"; Holliday, Leslie, Ed.; Elsevier: 1966; Chapter 9.
12. Craus, J.; Ishai, I.; Sides, A. *Proc. Annual Meeting Association Asphalt Paving Technologists, Florida, Feb. 13-15, 1978.*
13. Plancher, H.; Green, E. L.; Petersen, J. C. *Proc. Annual Meeting Association Asphalt Paving Technologists, New Orleans, Feb. 16-18, 1976.*
14. Grosmanin, J.; Verschave, A.; Marvillet, J. French Patent 2 201 336, 1974.
15. Plummer, M. A.; Schroeder, D. E.; Zimmerman, C. C. Canadian Patent 1 011 759, 1977.
16. Boca, Pier L.; Pacor, P. Canadian Patent 1 010 390, 1977.
17. Makowski, H. S.; Lundberg, R. D.; Singal, G. U.S. Patent 3 870 841, 1975.
18. Cantor, N. H. U.S. Patent 3 642 728, 1972.
19. Lundberg, R. D.; Makowski, H. S.; Westerman, L. U.S. Patent B 487 467, 1976.
20. Lundberg, R. D. *Polym. Prepr., Am. Chem. Soc., Div. Polym. Chem.* 1978, 19(1), 455.
21. *Ibid.*, 1978, 19(2), 287-313.
22. Ciplijauskas, L.; Piggott, M. R.; Woodhams, R. T. *J. Rubber Chem. Technol.*, in press.
23. Alexander, J. A. M.S. Thesis, Massachusetts Institute of Technology, Cambridge, MA, 1968.
24. B. F. *Goodrich Chemical Division New Product News (Elastomers)* 1969, 4(1).

RECEIVED October 2, 1978.

Water-Soluble Polyester Adhesives

JOHN M. NOONAN and ROBERT C. McCONKEY

Research Laboratories, Eastman Kodak Co., Rochester, NY 14650

Novel ionic polyesters that are soluble in water and that display very strong adhesive properties over the range 25°–120°C were synthesized using high-temperature melt-condensation polymerization. The polyester compositions contained the glycol 1,4-bis(2-hydroxyethoxy)cyclohexane and the diesters diethyl succinate and dimethylsodioimino-bis(sulfonyl-m-benzoate). Several nonionic diesters could be used in place of or in conjunction with diethyl succinate to give very strong adhesives. A UV-sensitive diester was incorporated into the polyester composition. The UV-sensitive polyester showed very strong adhesive strength; however, exposure of the adhesive to UV radiation caused a dramatic decrease in the adhesive strength.

There are many advantages in preparing polyester resins via high-temperature melt condensation, for example, (a) the polyesters are easily prepared in large-scale operations, (b) the desired molecular weight is easily achieved, (c) the monomers used are usually innocuous, and (d) the cost and potential pollution problems normally associated with organic solvents used during the synthesis and isolation steps of other polymerization techniques do not apply.

Many functional groups can survive the high temperatures used in melt-condensation polymerization, but only a few will directly render these polyesters truly hydrophilic. In fact, the literature reveals only two such functional groups: sulfonic acid salts (1, 2) and iminosulfonyl salts (3). Usually these groups are attached to the ring of an aromatic diester. However, the sodium salt of 1,3-dicarboxycyclohexane-5-sulfonic acid (4) easily survived the polymerization conditions.

We wish to report the synthesis of water-soluble ion-containing polyesters that were prepared by standard high-temperature melt-con-

densation procedures. These ionic polyesters are characterized by having a glycol component comprising one or more diols, a diester monomer that has an iminosulfonyl salt moiety, and one or more nonionic diesters. In addition, when the correct combination and ratio of the above monomers were used, the resulting polymers displayed excellent adhesive properties.

In an attempt to increase the cohesive strength of the polyesters at high temperatures, the polyesters were cross-linked. This was accomplished by incorporating a UV-sensitive diester into the polymer backbones and then effecting cross-linking with UV radiation. Unexpectedly, cross-linking caused a dramatic deterioration in the bond strength of the adhesives.

Experimental

Polymerization. The ionic polyesters were prepared by standard high-temperature melt-condensation procedures (3).

Viscosity Measurements. Viscosities were determined using an Ostwald-Fenske capillary viscometer. Measurements were made at 25°C and at a concentration of 2.5 mg/mL in 1:1 phenol-chlorobenzene.

Molecular Weight Determinations. Number-average (\bar{M}_n) and weight-average (\bar{M}_w) molecular weights were determined with a Waters gel-permeation chromatograph (GPC model 200) on diazomethylated polymer samples that were dissolved in tetrahydrofuran. The columns were 10^3 – 10^6 Å pore diameter. The molecular weights were reported as polystyrene equivalent weights.

Calorimetry. The glass transition temperatures (T_g 's) of the ionic polyesters were determined under nitrogen on a Du Pont 990 thermo-analyzer. Heating and cooling rates were 10°C/min.

Melt Viscosity. The melt viscosities were measured on a Rheometrics mechanical spectrometer with a cone-and-plate configuration under steady shear.

Substrates Sealed. Aqueous polymer solutions were coated on Estar base, which had been precoated with a subbing layer (5), to produce a 0.5-mil dry film thickness, then sealed to cellulose acetate, which had been precoated with another subbing layer (6). These subbing layers were vinyl terpolymers which were synthesized from acrylonitrile, vinylidene chloride, and acrylic acid.

Sample Sealing. Half-inch-wide substrate strips were sealed on a heated drum at 120°C using a roller with a 3-kg load weight (7).

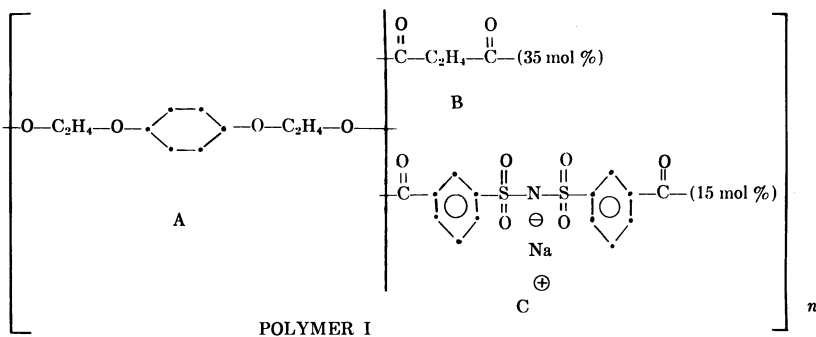
Peel Force Determinations. Peel force was measured on an Instron drum apparatus (7). The Estar substrate was peeled from the cellulose acetate substrate, and a 90° angle of peel was maintained at all times. The peel force measurements were made over the range 25°–120°C at two different rates: 0.1 in./min and 12 in./min.

Monomers. The following monomers were obtained from Eastman Organic Chemicals and used as received: diethylene glycol, ethylene glycol, hexamethylene glycol, diethyl succinate, diethyl malonate, diethyl adipate, and 1,4-cyclohexane dimethanol. The following monomers were

obtained from the Tennessee Eastman Company and used as received: 1,4-bis(2-hydroxyethoxy)cyclohexane, dimethyl sodioiminobis(sulfonyl-*m*-benzoate), and diethyl *p*-phenylenebis(acrylate).

Results and Discussion

Polymer I was an amorphous water-soluble polymer with an inherent viscosity of 0.33 and a T_g of 26°C. The \bar{M}_n and \bar{M}_w were 6,419 and 15,546 respectively. The ionic polyester displayed excellent adhesive properties as shown in Figure 1. Absolute peel force values could not be obtained



at most temperatures, regardless of peel rate, because the bond strength was great enough to cause the Estar base to break before bond failure occurred. The adhesive strength was very dependent on the structure of the ionic polyester.

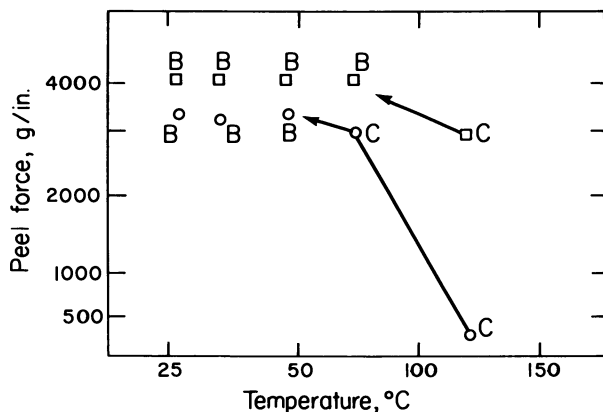


Figure 1. Temperature dependence of peel force for Polymer I: (○) peel rate at 0.1 in./min, (□) peel rate at 12 in./min; (A) adhesive failure, (B) Estar base broke, (C) cohesive failure

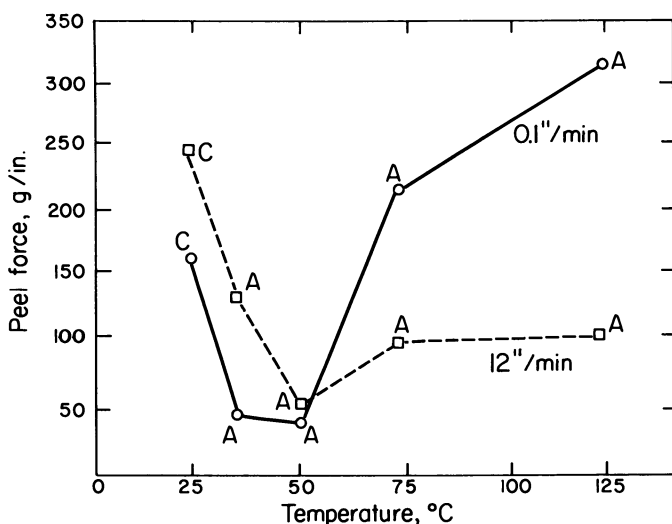


Figure 2. Temperature dependence of peel force for Polymer II: (—) peel rate at 0.1 in./min, (---) peel rate at 12 in./min; (A) adhesive failure, (B) Ester base broke, (C) cohesive failure

Diols. When the diol 1,4-bis(2-hydroxyethoxy)cyclohexane (A) was replaced with either 1,4-cyclohexanedimethanol (Polymer II) or ethylene glycol, the resulting polymers were much less soluble in water and their adhesive strength dropped drastically. In fact, the polymer with hexamethylene glycol was insoluble in water. (The peel force results of Polymer II are shown in Figure 2.) However, if only 25 mol % of 1,4-bis(2-hydroxyethoxy)cyclohexane was replaced with one of the above glycols, the resulting polymers were much more soluble in water and displayed very high peel strengths. Figure 3 shows the peel forces when the glycol component contained 25 mol % of A and 25 mol % of hexamethylene glycol (Polymer III).

When Diol A was replaced with diethylene glycol or tetramethylene glycol, the resulting polymers were readily soluble in water and showed peel forces equal to those of Polymer I. Therefore, to ensure high adhesive peel forces at least 50 mol % of the glycol content should be a diol having ether linkages.

Nonionic Diesters. The homologous series of diesters from oxalate to sebacate were individually substituted for the succinate moiety in Polymer I. With the exception of the malonate- and adipate-containing polymers, the resulting polymers displayed very low peel strengths. The bond strengths of the malonate- and adipate-containing polymers were almost equal to that of Polymer I as shown in Figure 4.

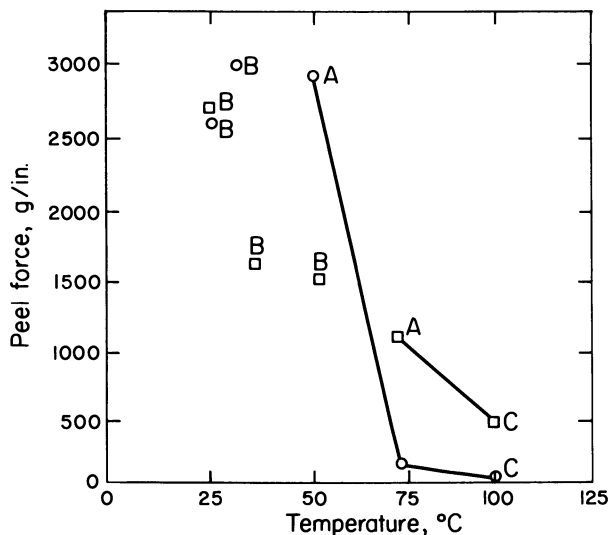


Figure 3. Temperature dependence of peel force for Polymer III: (○) peel rate at 0.1 in./min, (□) peel rate at 12 in./min; (A) adhesive failure, (B) Estar base broke, (C) cohesive failure

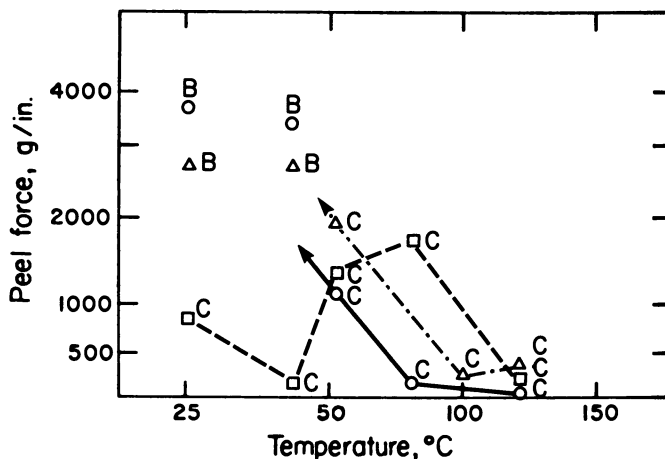


Figure 4. Temperature dependence of peel force for polymers containing 35 mol % malonate (□), 35 mol % adipate (○), and 17.5 mol % adipate (▽) at a peel rate of 0.1 in./min; (A) adhesive failure, (B) Estar base broke, (C) cohesive failure

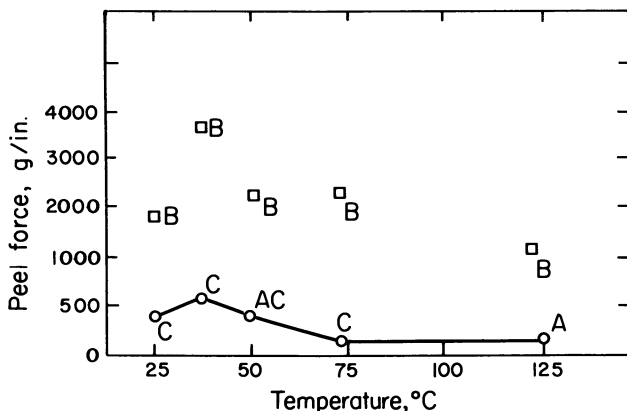


Figure 5. Temperature dependence of peel force for Polymer I modified with 10 mol % ethylene glycol vs. protonated form at a peel rate of 12 in./min: (□) Polymer I modified, (○) protonated Polymer I modified; (A) adhesive failure, (B) Estar base broke, (C) cohesive failure ($T_g = -7^\circ\text{C}$; $\{\eta\} = 0.32$)

However, when only 17.5 mol % of the succinate moiety in Polymer I was replaced with either the malonate or adipate moiety, the bond strengths of the resulting polymers were greater than those of polymers containing 35 mol % of the malonate or adipate moieties (Figure 4).

Dimethyl Sodioiminobis(sulfonyl-*m*-benzoate). The content of the sodioiminobis(sulfonyl-*m*-benzoate) (8,9) moiety (C) in Polymer I was varied from 5 to 50 mol %, with the appropriate corresponding change in the succinate content. We determined that 12–15 mol % of C was necessary to give maximum peel force values such as those shown in Figure 1. When the concentration of C was greater than 15 mol %, a semicrystalline polymer that had very low bond strength was obtained. When the content of C was less than 12 mol %, the T_g of the resulting polymers ranged from -10° to 10°C , and as a result these polymers had very low peel forces above 35°C .

Protonation of Polymer I. The sodium cation associated with Polymer I was replaced with the hydrogen ion by acidifying an aqueous solution of Polymer I with 1N hydrochloric acid. The protonated polymer was insoluble in water but soluble in organic solvents, especially chlorinated solvents. The bond strength of the protonated polymer was very poor (Figure 5).

When the sodium cation of Polymer I was replaced with the potassium cation, the T_g of the resulting polymer decreased to 8°C . In addition, the bond strength was very low, especially in the range 25° – 50°C .

Melt Viscosity. The steady shear viscosities of Polymer I representing the Newtonian flow region at four temperatures are shown in Figure 6. The melt viscosity drops precipitously between 150° and 200°C .

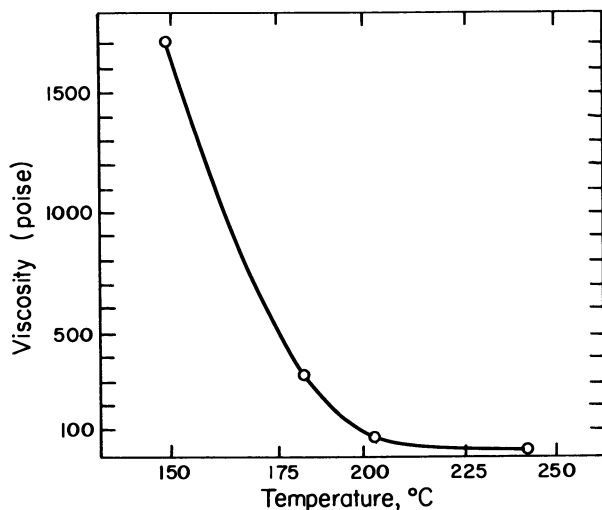
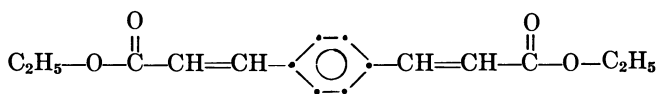


Figure 6. Steady shear viscosities representing the Newtonian flow region

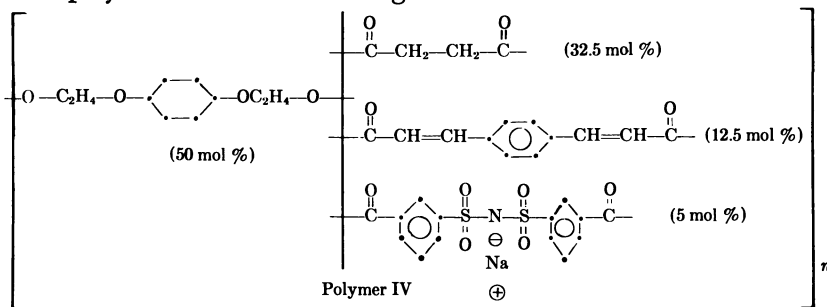
Effect of Cross-Linking on Peel Force. The bond strength of Polymer I was low at temperatures above 100°C (Figure 1). In an attempt to increase the bond strength, a few potentially cross-linkable sites were incorporated into the structure of Polymer I. A change in the viscoelastic properties of the polymers should result upon cross-linking the polymer matrix with UV radiation and provide higher cohesive bond strengths.

The UV-sensitive diester diethyl *p*-phenylenebis(acrylate) (D) (3)



D

was chosen as the potentially cross-linkable site and was incorporated into a polyester with the following structure:



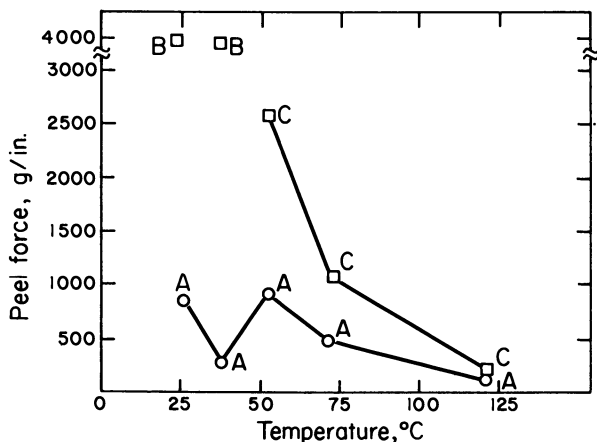


Figure 7. Temperature dependence of peel force for Polymer IV at a peel rate of 12 in./min: (□) unexposed Polymer IV, (○) exposed Polymer IV; (A) adhesive failure, (B) Estar base broke, (C) cohesive failure

Polymer IV was an amorphous polymer with an inherent viscosity of 0.44 and a T_g of 11°C. It was coated from water, and the film was sealed in the usual manner. The polyester displayed very high peel forces (see Figure 7). However, when the resulting film was sealed and then exposed to UV radiation for 20 min before peeling, the subsequent peel forces were very low (Figure 7). If the UV-sensitive polyester film was first exposed to UV radiation and then sealed between the substrates, the

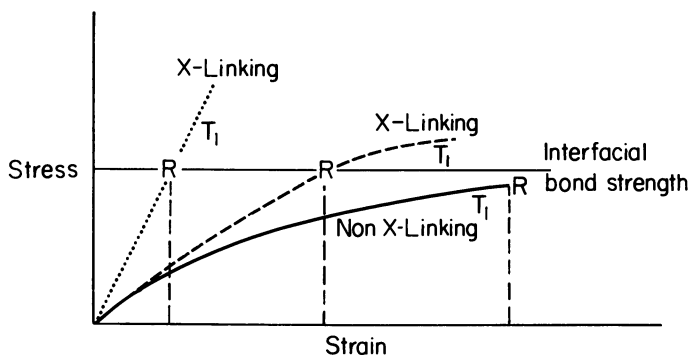


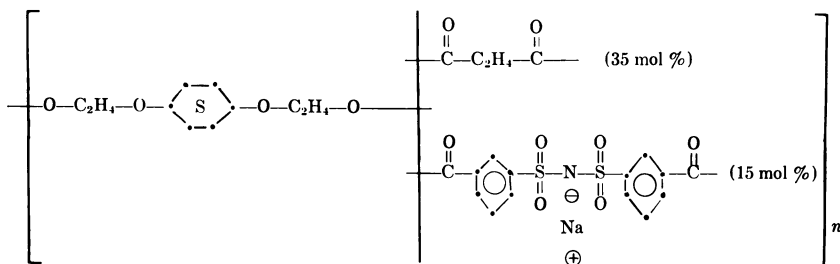
Figure 8. Schematic stress-strain relations for a noncross-linked (I), lightly cross-linked (II), and highly cross-linked (III) polymer. The horizontal line denotes a possible level of the interfacial bond strength; the dashed lines denote the limiting strain attainable in each case. R represents bond rupture.

peel strength looked almost the same as if the exposure had taken place after the sealing operation.

The mode of bond failure in the unexposed films was mainly cohesive. However, when a cross-linked polymer matrix was formed with UV exposure, the mode of bond failure was interfacial at all testing temperatures. We believe that by cross-linking the polymer with UV radiation, the modulus of the polyester was increased. This in turn caused the cohesive strength to be much greater than the interfacial bond strength. As a result, the mode of bond failure became interfacial, or adhesive (10) (Figure 8).

Conclusions

We synthesized a new class of water-soluble polyester adhesives. We demonstrated that to ensure very strong adhesive properties certain compositional boundaries must be maintained. The optimal composition is the following:



We also incorporated a UV-sensitive diester into the preferred adhesive composition. The adhesive properties were destroyed when this polyester was cross-linked by exposure to UV radiation.

Acknowledgments

We are grateful to R. Dann and E. Tytler for determining the peel force data, to R. W. Connelly for determining the melt viscosity data, and to J. L. R. Williams for many helpful discussions.

Literature Cited

1. Griffing, J. M.; Remington, W. R. U.S. Patent 3 018 272, 1962.
2. Heiberger, P. U.S. Patent 3 563 942, 1971.
3. Arcesi, J. A.; Rauner, F. J. U.S. Patent 3 929 489, 1975.
4. Garforth, J. D. U.S. Patent 3 682 866, 1972.
5. Nadeau, G. F.; Starck, C. B.; Jacoby, F. J. U.S. Patent 3 143 421, 1964.
6. Hannie, D. E.; Ducharme, G. L. U.S. Patent 4 061 496, 1977.

7. Parsons, W. F.; Faust, M. A.; Brady, L. E. *J. Polym. Sci., Polym. Phys. Ed.* **1978**, *16*, 775.
8. Caldwell, J. R.; Jones, G. C. U.S. Patent 3 546 180, 1970.
9. DeChristopher, P. J.; Adamek, J. P.; Lyon, G. D.; Klein, S. A.; Baumgarten, J. *J. Org. Chem.* **1974**, *39*, 3525.
10. Gent, A. N.; Petrich, R. P. *Proc. R. Soc. London, Ser. A* **1969**, *310*, 433.

RECEIVED January 29, 1979.

Polymeric Quaternary Ammonium Borohydride Reducing Agents

M. M. COOK, P. R. DEMKO, S. E. WAGNER,
R. A. MIKULSKI, and J. G. CLEMENTS

Ventron Corp., Chemicals Division, Congress St., Beverly, MA 01915

Strong base anion-exchange resins containing borohydride counterions are a convenient source of insoluble, polymer-supported reducing agents. These materials have enhanced solvolytic stability and, in selected cases, increased reactivity (particularly in nonpolar solvents) over sodium or tetraethylammonium borohydride. Commercial anion-exchange resins in the borohydride form provide unique features in applications such as solvent purification, metal reduction, or arsine generation, where the introduction of soluble cations or anions is undesirable or where ultrapure borohydride is required. The preparation and regeneration of these polymeric borohydride reducing agents are based on standard ion-exchange methods.

The high level of interest in polymer-bound reagents is evidenced by the numerous publications on this topic in the past ten years. Despite the attractive potential for polymer-bound reagents, the expense involved in preparing a custom-synthesized resin and the frequent lack of regenerability has severely limited their practical use. To overcome these limitations we have examined the use of commercially available ion-exchange resins as polymeric supports for synthetic reagents. Specifically, we have examined strong base anion-exchange resins containing borohydride counterions as insoluble, polymer-supported reducing agents. The results of several studies on the use of these polymer-bound borohydrides are presented in this chapter.

Polymer-bound borohydride reagents were first reported in 1961 by two independent groups (1, 2). More recently other authors have reported on polymer-bound borohydride attached to ion-exchange resins

(3) and to derivatized cellulose (4, 5). Several other workers have investigated polymeric reducing agents containing borane groups covalently attached to the polymer backbone: polymeric amine boranes (6, 7) and polymeric sulfide boranes (8).

We have investigated the solvolytic stability and reactivity of polymer-bound borohydrides and have evaluated these materials in several applications such as solvent purification, arsine generation, and metal reduction. These polymer-bound borohydrides offer several advantages over sodium or tetraethylammonium borohydride. The primary advantages are the convenience of use and the minimal introduction of ionic species or organic by-products into the treated bulk media. With the polymer-bound borohydrides, the cation is bonded covalently to the insoluble resin while the borohydride anion or its oxidation product (borate) is retained by ionic bonding. Typically, boron at levels of less than 5 ppm is the only impurity introduced into the treated medium.

Both the preparation and regeneration of the polymeric borohydrides are quite straightforward. Since borohydride is a stronger anion than either chloride or borate, simply passing a borohydride solution through the resin bed serves to convert the anion-exchange resin to the borohydride form (*see* Figure 1). The detailed procedure given in the experimental section includes a pre- and postpurification of the chloride and borohydride forms of the resin to assure maximum purity of the polymer-bound borohydride.

We evaluated both gel and macroreticular types of styrene-divinylbenzene (DVB) and acrylate-DVB strong base anion-exchange resins, all having quaternary ammonium groups attached to the polymer backbone. We used commercially available resins, specifically those of Rohm and Haas: Amberlyst A-26, Amberlite IRA-400, Amberlyst XE-279, and Amberlite IRA-458 (all in the chloride form). The A-26 and IRA-400 resins contain styrene-DVB skeletal structures, with IRA-400 being a gel-type resin and A-26 the macroreticular resin. Resins IRA-458 and XE-279 contain acrylate-DVB skeletal structures, where IRA-458 is a gel-type resin and XE-279 a macroreticular resin. These studies compare the properties of the borohydride form of these resins with sodium and tetraethylammonium borohydride.

Experimental

Procedure for Preparing the Polymer-Bound Borohydride Reducing Agent. The following procedure is recommended for preparing polymer-bound borohydride from commercially available, strong base anion-exchange resins. The procedure has been used and found effective with the IRA-400, A-26, XE-279, and IRA-458 anion-exchange resins, all commercially available from Rohm & Haas Corporation (chloride form).

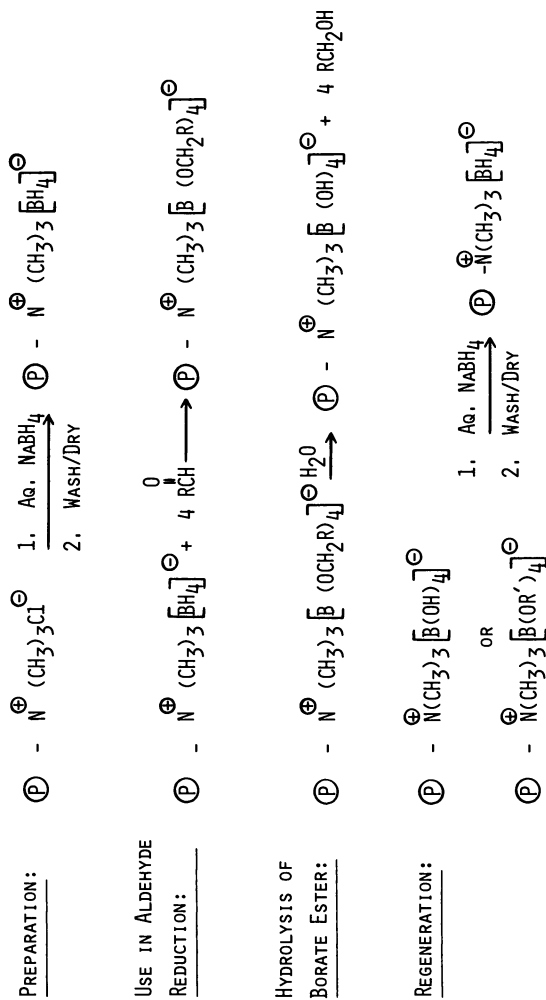


Figure 1. Preparation, use, and regeneration of polymer-bound borohydride

This procedure assures quantitative conversion to the resin-borohydride form, obtained as a purified dry resin. Quantities of polymer-bound borohydride of up to 500 g have been prepared successfully by this procedure.

The procedure consists of the following steps:

- A. *Prepurification of the Chloride-Form Resin.* The desired quantity of commercial chloride-form wet resin was charged to a column of suitable size. Purification of the resin was accomplished by conversion from the chloride to hydroxide form and back to the chloride form with 1N NaOH and 1N HCl, respectively.
- B. *Conversion of Resin Chloride to Polymer-Bound Borohydride.* The resin was converted to the borohydride form by washing twice with aqueous 1N NaBH₄ solution stabilized with a small amount of sodium hydroxide (< 1.0 wt %). (Each wash used twice the theoretical quantity of NaBH₄ based on the total resin capacity of the column.) During use in chemical reductions, polymer-bound borohydride is oxidized to the borate form. Exhausted resin may be regenerated directly from the borate to the borohydride form by washing with the NaBH₄ solution as described previously.
- C. *Postpurification of Polymer-Bound Borohydride.* The polymer-bound borohydride is washed with either deionized water or ethanol, depending on the media of intended use. Washing with anhydrous ethanol was used when essentially water-free resin was desired. Washing volumes were approximately two to three times the resin volume. In the case of Resin A-26 or IRA-400, washing was continued until a colorless effluent was obtained, signifying essentially complete removal of impurities present in the commercial resin. The polymer-bound borohydride may be used directly at this point for the purification of organic chemicals by column treatment.
- D. *Drying of Polymer-Bound Borohydride and Analysis for Hydride Content.* Residual solvents were removed from the polymer-bound borohydride for hydride content analysis. For this purpose, a sample (2–3 g) of the polymer-bound borohydride was transferred to a suitable vessel and dried in a vacuum desiccator under a pressure of about 20 torr at ambient temperature. Percent hydride of the dry polymer-bound borohydride was determined by measuring the volume of hydrogen evolved on hydrolysis of the borohydride with acid.

Reduction of Aldehydes and Hydroperoxides. Stock solutions of approximately 100–200 ppm of 2-ethylhexanal in 95% ethanol, hexane, and 2-ethylhexanol were prepared. Accurate carbonyl assays were conducted (ASTM method E411-70, "Trace Quantities of Carbonyl Compounds with 2,4-Dinitrophenylhydrazine"); initial carbonyl levels were

reported in parts per million. All aldehyde reduction studies were conducted using these stock solutions. Analogous solutions containing cumene hydroperoxide were prepared. Peroxides (as H_2O_2) were detected by iodine liberation/titration with $Na_2S_2O_3$ and reported in parts per million. Batch methods were used for all reduction studies.

For each solvent, aldehyde and hydroperoxide reductions via the A-26, IRA-400, XE-279, and IRA-458 borohydride-form resins were investigated. Amorphous sodium borohydride and tetraethylammonium borohydride were used for comparison. Studies were run at both ambient temperature and at $45^\circ C$. Percent hydride of each resin was determined immediately prior to use.

To a three-neck, 250-mL round-bottomed flask equipped with a water-jacketed condenser and nitrogen inlet and outlet lines were charged 75 g of ethanol, hexane, or 2-ethylhexanol solution. Magnetic stirrers were used to maintain constant agitation. In cases where reductions were accomplished at an elevated temperature ($45^\circ C$), flasks were immersed in constant-temperature oil baths. Solutions were allowed to equilibrate with the surroundings before appropriate reducing agents were introduced.

Samples were treated with 1000 ppm borohydride for 4 hr; reducing agents were added directly to the reaction flask. For 1000 ppm BH_4^- treatment of 75 g of sample, 0.075 g BH_4^- are required. Appropriate quantities of $NaBH_4$ and $(C_2H_5)_4NBH_4$ were determined from formula weights. Resin quantities were calculated from hydride percentages (determined daily).

Reactions were quenched after 4 hr. In cases of treatment with resin, simple gravitation filtering was sufficient to isolate the resin from the sample. Subsequent assays for aldehyde (or peroxide) and boron were effected. When $NaBH_4$ or $(C_2H_5)_4NBH_4$ were used, samples were neutralized with excess aqueous hydrochloric acid. Organic and aqueous phases were separated when possible and both were subsequently analyzed for aldehyde (or peroxide). Weights of analyzed samples were noted; percent reduction was calculated.

Purification of 95% Ethanol with Polymer-Bound Borohydride. A 90-cm³ bed (height = 17.8 cm; area = 5.1 cm²) was charged with A-26 resin, borohydride form. A solution of 95% ethanol spiked with crotonaldehyde (initial aldehyde level = 82 ppm as CO, mol wt 28) was pumped continuously through the bed in an upflow manner. Aliquot samples were removed at various times and analyzed for aldehyde (ASTM Method E411-70). Contact time was calculated by dividing the empty bed volume by the flow rate. Several runs were made at various face velocities (i.e., flow rate/cross-sectional area) to determine the effect of face velocity on the aldehyde reduction/contact time relationship.

Reduction of Silver. A 100-mL sample of a silver salt solution containing 5000 ppm of silver at a pH of 4.5 was stirred with 1 g of borohydride-form A-26 anion-exchange resin in a beaker for 30 min. The reduced silver powder and the resin were filtered from the solutions. An analysis of the filtrate showed 0.05 ppm silver. The above reduction was also carried out efficiently over a pH range of 4.5–8.5.

Reduction of Copper. A 100-mL solution containing 500 ppm of copper sulfate was stirred with 1 g of borohydride-form A-26 anion-exchange resin for 30 min. The reduced copper along with the resin was

filtered from the solution. The filtrate contained less than 0.05 ppm of copper.

Reduction of Cadmium. A 100-mL solution containing 500 ppm of cadmium nitrate was stirred with 1 g of borohydride-form A-26 anion-exchange resin for 30 min. The reduced cadmium and resin were filtered and the filtrate was found to contain less than 0.05 ppm of cadmium.

Application of Polymer-Bound Reducing Agents for Silver Recovery from Photographic Fixer. Several 10-mL aliquots of a spent photographic fixer solution containing 0.55% silver were diluted to 100 mL and adjusted to 5 different pH levels: 4.5, 5.5, 6.5, 7.5, and 8.5. One gram of borohydride-form A-26 anion-exchange resin was added to each sample. The samples were stirred and allowed to stand at 20°C for 30 min.

The precipitated silver powder and the resin were filtered. The filtrate was analyzed by atomic absorption spectroscopy and was found to contain less than 0.05 ppm of silver.

Results and Discussion

Aldehyde Reduction. The results of 2-ethylhexanal reduction in 95% ethanol, 2-ethylhexanol, and hexane with the various types of polymer-bound borohydrides, sodium borohydride, and tetraethylammonium borohydride are shown in Table I.

In 95% ethanol, the polymer-bound borohydrides, sodium borohydride, and tetraethylammonium borohydride are equally effective for

Table I. Reduction

Temperature	Borohydride Source					
	A-26		IRA-400		XE-279	
	Final Aldehyde Level	% Reduction	Final Aldehyde Level	% Reduction	Final Aldehyde Level	% Reduction
A. 95% Ethanol (Initial)						
Ambient	0	100	20	81	<1.0	99.3
45°C	0	100	3.0	97.1	<1.0	99.3
B. 2-Ethylhexanol (Initial)						
Ambient	41.0	79.9	113	44.6	106.5	47.8
45°C	5.7	97.2	88	56.9	108.5	46.8
C. Hexane (Initial)						
Ambient	1.8	98.3	83.0	22.4	89.5	16.4
45°C	1.5	98.6	97.5	8.1	84.0	21.5

* In all cases, 1000 μg borohydride (BH_4^-)/g solution were used. Final aldehyde levels measured after batch treatment of the solution for 4 hr under a nitrogen atmosphere.

the reduction of aldehydes. At the levels used (1000 ppm BH_4^-), both sodium and tetraethylammonium borohydride are soluble in aldehyde-spiked 95% ethanol. Since good contact with the hydrophilic resin would be expected, good reduction would be anticipated in all cases.

However, in the 2-ethylhexanol, the sodium and tetraethylammonium borohydrides are, in general, more reactive than the polymer-bound borohydrides. Of the resins, those polymers having the styrene-DVB skeletal backbone (A-26 and IRA-400) offer some advantage over the acrylate-DVB-based resin (XE-279 and IRA-458). Of the styrene-DVB resins, the macroreticular resin (A-26) gives the best reduction, particularly at an elevated temperature. Both sodium borohydride and tetraethylammonium borohydride appeared to have limited solubility at this level in 2-ethylhexanol. However, since 2-ethylhexanol is more viscous and less polar than ethanol, reactions involving the porous ion-exchange resins would be somewhat slower than the corresponding reduction with soluble borohydrides.

In nonpolar solvents such as hexane, the macroreticular styrene-DVB (A-26) polymer-bound borohydride was substantially more effective in aldehyde reduction than the other reducing agents.

Hydroperoxide Reduction. The results of the cumene hydroperoxide reductions are shown in Table II. These results differ significantly from the aldehyde reduction studies.

of Aldehydes^a

<i>Borohydride Source</i>					
<i>IRA-458</i>		<i>NaBH₄</i>		<i>(C₂H₅)₄NBH₄</i>	
<i>Final Aldehyde Level</i>	<i>% Reduction</i>	<i>Final Aldehyde Level</i>	<i>% Reduction</i>	<i>Final Aldehyde Level</i>	<i>% Reduction</i>
<i>Aldehyde Level = 105 ppm)</i>					
< 0.5	99.8	< 1.0	99.3	< 1.0	99.3
< 0.5	99.8	< 1.0	99.3	< 1.0	99.3
<i>Aldehyde Level = 204 ppm)</i>					
177	13.2	0	100	2	99
113	44.6	0	100	4.7	97.7
<i>Aldehyde Level = 107 ppm)</i>					
77.0	28	72.5	32.2	46.5	56.6
76.0	29	61.9	42.1	67.0	37.4

Table II. Reduction

Temperature	<i>Borohydride Source</i>					
	<i>A-26</i>		<i>IRA-400</i>		<i>XE-279</i>	
	<i>Final Peroxide Level</i>	<i>% Reduction</i>	<i>Final Peroxide Level</i>	<i>% Reduction</i>	<i>Final Peroxide Level</i>	<i>% Reduction</i>
	<i>A. 95% Ethanol (Initial</i>					
Ambient	0	100	0	100	20.4	32.7
45°C	8.2	72.9	1.5	95	15.0	50
	<i>B. 2-Ethylhexanol (Initial</i>					
Ambient	5.1	88.1	36.0	15.7	42.7	0
45°C	1.4	96.7	32.8	23.2	42.7	0
	<i>C. Hexane (Initial</i>					
Ambient	0	100	27.1	49.5	34.9	35
45°C	0	100	9.7	81.9	38.7	27.9

* In all cases, 100 μg borohydride (BH_4^-)/g solution were used. Final hydroperoxide levels measured after batch treatment of the solution for 4 hr under a nitrogen atmosphere.

In 95% ethanol, sodium borohydride and the acrylate-DVB-based polymer-bound borohydrides (XE-279 and IRA-458) were not as reactive as tetraethylammonium borohydride or the styrene-DVB-based polymeric borohydrides (A-26 and IRA-400). In the 2-ethylhexanol and hexane evaluation, the macroreticular styrene-DVB polymer-bound borohydride (A-26) was, in general, more reactive than the other resins or sodium or tetraethylammonium borohydrides.

The physical structure of the IRA-458 resin appeared unaltered after reduction, however, visible breakdown of the A-26, IRA-400, and XE-279 resins was quite noticeable.

Solvolytic Stability. Solvolytic stability of all four polymer-bound borohydrides was investigated in 100% ethanol as a function of temperature and in water as a function of pH. Comparative studies for sodium borohydride and tetraethylammonium borohydride were conducted. Solvolytic decomposition of the borohydride group results in the generation of hydrogen gas. Stability measurements were obtained by observing volume of hydrogen gas evolved as a function of time. Percent loss of hydride as a function of time was calculated from resin weight and initial hydride content.

Figures 2 and 3 depict percent loss of hydride vs. time for the A-26, IRA-400, XE-279, and IRA-458 resins in 100% ethanol at 40°C and

of Hydroperoxide*

<i>Borohydride Source</i>					
<i>IRA-458</i>		<i>NaBH₄</i>		<i>(C₂H₅)₄NBH₄</i>	
<i>Final Peroxide Level</i>	<i>% Reduction</i>	<i>Final Peroxide Level</i>	<i>% Reduction</i>	<i>Final Peroxide Level</i>	<i>% Reduction</i>
<i>Peroxide Level = 30.3 ppm as H₂O₂)</i>					
24.2	20.1	30.3	0	0	100
19.5	35.6	30.3	0	0	100
<i>Peroxide Level = 42.7 ppm as H₂O₂)</i>					
42.7	0	42.7	0	42.7	0
40.7	4.7	34.9	18.3	4.8	88.8
<i>Peroxide Level = 53.7 ppm as H₂O₂)</i>					
37.1	30.9	36.7	31.7	17.5	67.4
45.2	15.8	45.1	16	23.1	57

ambient temperature, respectively. Figure 3 illustrates stability of sodium borohydride and tetraethylammonium borohydride in 100% ethanol at ambient temperature. As would be anticipated from reduction study data, the more reactive macroreticular styrene-DVB polymer-bound borohydride (A-26) was substantially less stable solvolytically than the other three borohydride resins. All four resins were more stable than either sodium or tetraethylammonium borohydride. Solvolytic stabilities of the resins were inversely proportional to temperature. The initial apparent pH of the ethanol used was approximately 4.8; pH values following stability studies were generally in the 9–11 range. The observed leveling-off effect would therefore be expected since the borohydride solvolysis rate is known to be related directly to the acid concentration (9).

Figure 5 illustrates comparative stabilities of the A-26, IRA-400, XE-279, and IRA-458 resins in water of about pH 7.0. Comparative studies for sodium borohydride and tetraethylammonium borohydride are also shown in Figure 4. The styrene-DVB resins (A-26 and IRA-400) appear to have somewhat greater stabilities than the acrylate-DVB resins; in all cases, the stabilities of the resins were greater than those of either sodium or tetraethylammonium borohydride. Again, final pH values were greater (generally 8–9) than the initial value of 7.0.

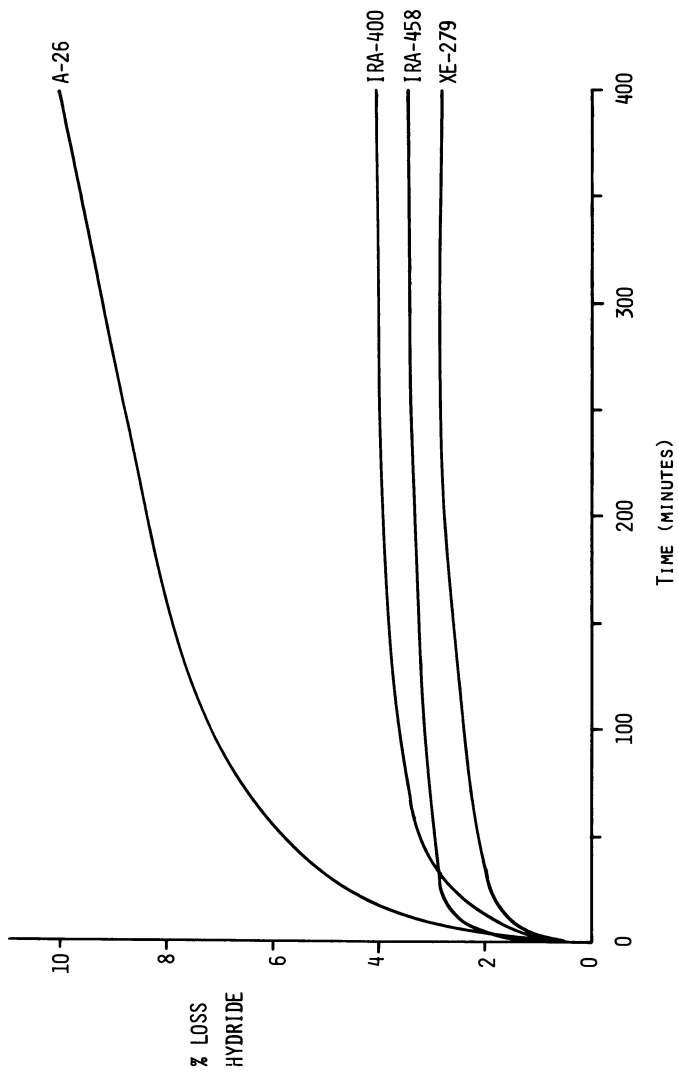


Figure 2. Stability of polymer-bound borohydride in 100% ethanol at 40°C: percentage loss hydride vs. time ($[BH_4^-] = \text{ca. } 0.025M$)

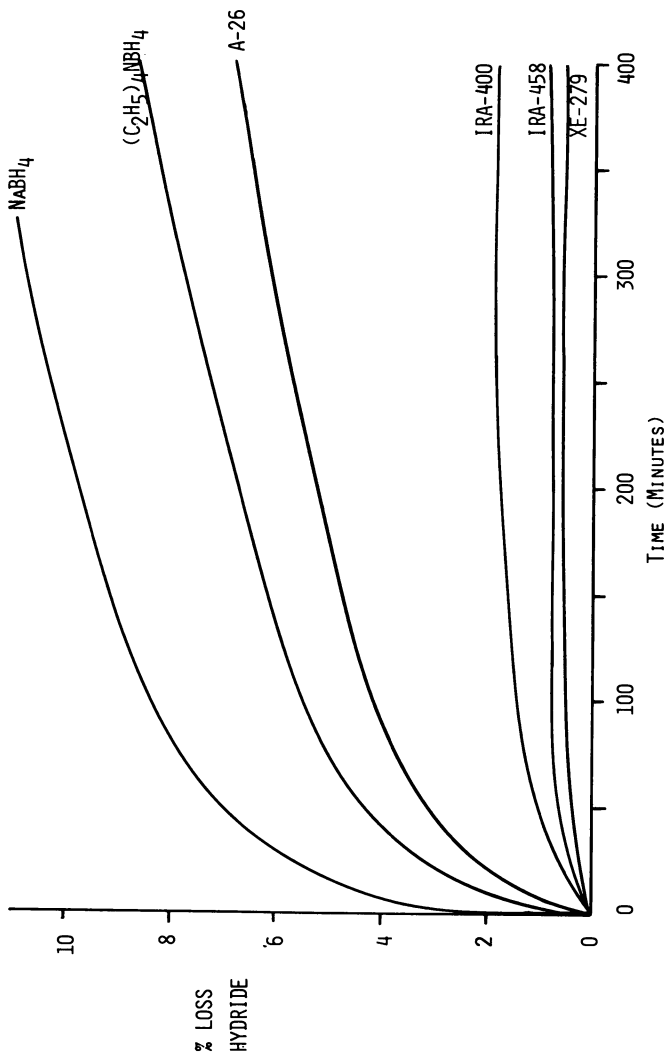


Figure 3. Stability of polymer-bound borohydride in 100% ethanol at ambient temperature: percentage loss hydride vs. time ($[BH_4^-] = \text{ca. } 0.025M$)

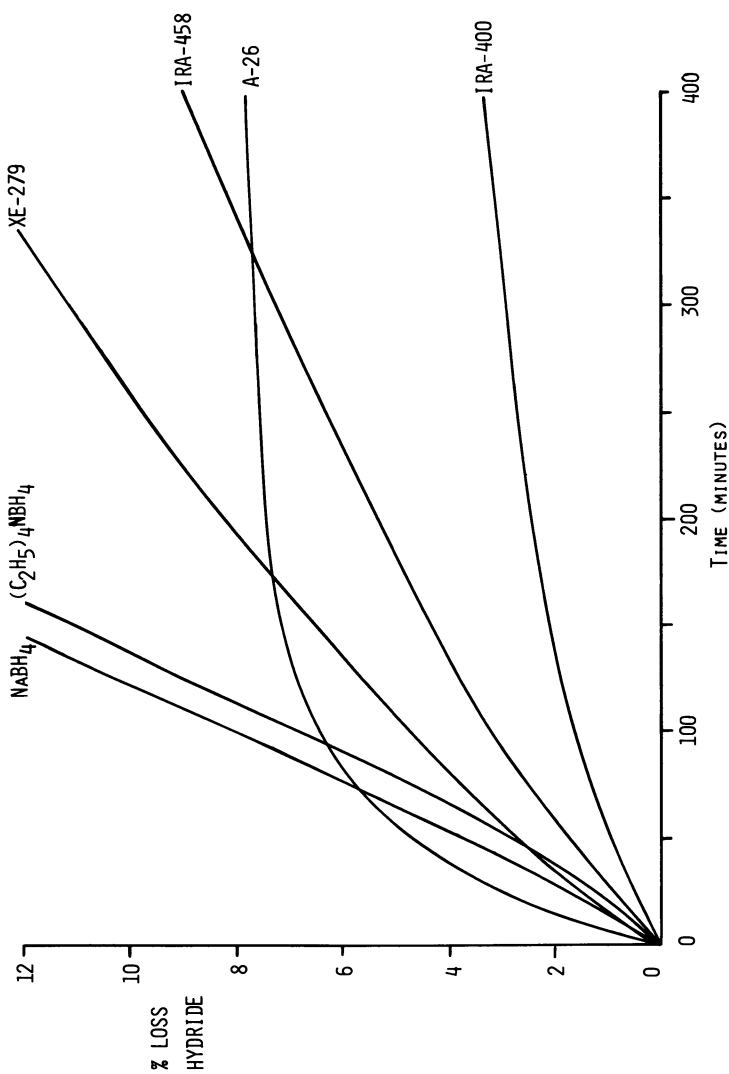


Figure 4. Stability of polymer-bound borohydride in H_2O at $pH = 7$: percentage loss hydride vs. time (ambient temperature, $[BH_4^-] = ca. 0.025M$)

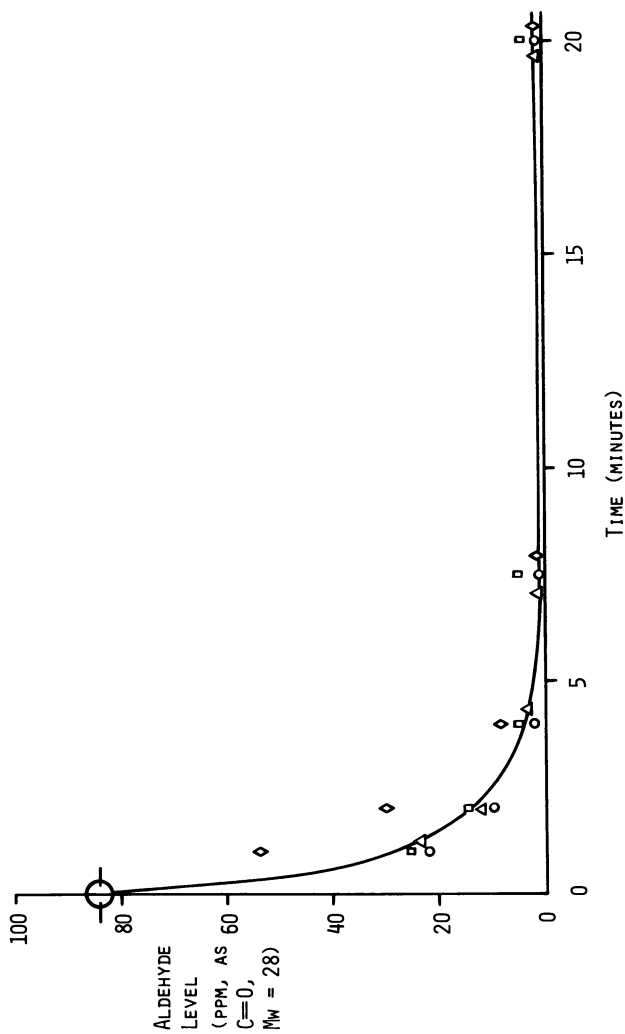


Figure 5. Aldehyde level vs. contact time for 95% ethanol through a bed of polymer-bound borohydride (A-26) at 27°C. Face velocity: (◇) = 0.32 ft/min (9.7 cm/min); (□) = 0.99 ft/min (30.2 cm/min); (○) = 1.65 ft/min (50.3 cm/min); (△) = 2.59 ft/min (78.9 cm/min)

Based on the stability and aldehyde and hydroperoxide reduction studies, the macroreticular borohydride-form styrene-DVB resin (A-26) appears to be the most reactive reducing agent of those investigated. This polymer-bound borohydride reagent was thus selected for investigation of several application areas of interest.

Other Applications

Solvent Purification (10). Several analytical tests in our laboratories, particularly those involving low-level aldehyde and peroxide analyses, require solvents that are essentially aldehyde-free. Achieving the required purity, in the case of ethanol, usually meant a rather time-consuming, tedious distillation. We found that by purifying ethanol with polymer-bound borohydride the distillation step was no longer necessary. Passing the ethanol to be purified through a column containing the polymer-bound borohydride removes any impurities that can be reduced with sodium borohydride. As can be seen in Figure 5, a contact time of 10 min is usually sufficient to remove most impurities.

This procedure is generally effective for the purification of other solvents. However, depending on the solvent or specific impurity, it may be necessary to alter the contact time and/or flow rate.

In addition to offering convenient and effective removal of borohydride-reducible impurities, this system offers several unique advantages over sodium borohydride. First, the polymer-bound borohydride is remarkably stable in alcohols (with the exception of methanol). Second, since the hydride capacity is on the order of 12 meq of hydride per gram of dry resin, a small amount of polymer-bound borohydride will remove trace carbonyl impurities from a substantial volume of alcohol. Third and most importantly, no new contaminants such as Na^+ or BO_2^- are added to the alcohol since the borate ion remains bonded to the resin.

Presently we are evaluating further the use of these polymer-bound borohydrides for purification of beverage ethanol as a supplement to existing purification methods.

Generation of Volatile Hydrides (11). The use of commercial sodium borohydride as a reducing agent for the generation of volatile arsine (AsH_3) in trace arsenic analysis is often complicated by trace (ppb) arsenic impurities in the borohydride. The following procedure using polymer-bound borohydride has eliminated these problems:

A 25-mL solution containing 500 ppb of arsenic (Ag^{3+}) was stirred with 1 g of borohydride-form A-26 anion-exchange resin. The reaction vessel was connected to an absorption tube filled with a solution to absorb the volatile hydride of arsenic (i.e., arsine, AsH_3). The absorption solution is made by dissolving 1 g of silver diethyldithiocarbamate (SDDC) in 200 mL of pyridine. The volatile arsine is complexed with the SDDC solution to give a colored solution, whose absorbance is

Table III. Concentration of Metal Ion Before and After Treatment with Polymer-Bound (A-26) Borohydride

<i>Ionic Species</i>	<i>Concentration (ppm)</i>	
	<i>Initial</i>	<i>Final</i>
Ag ⁺¹	500	< 0.05
Cu ⁺²	500	< 0.05
Cd ⁺²	500	< 0.05

Table IV. Concentration of Silver Ion in a Photographic Fixer Before and After Treatment with Polymer-Bound (A-26) Borohydride

<i>pH</i>	<i>Concentration</i>	
	<i>Initial (%)</i>	<i>Final (ppm)</i>
4.5	0.55	< 0.05
5.5	0.55	≤ 0.2
6.5	0.55	< 0.05
7.5	0.55	< 0.05
8.5	0.55	< 0.05

measured at a suitable wavelength. This technique is useful in the analysis of low levels of arsenic in the part-per-billion range.

Reduction of Metal Ions. In terms of metal reduction, these polymer-bound borohydrides react analogously to sodium borohydride. Several examples of this reduction are shown in Table III. In most cases, the reduced metal was attached quite strongly to the resin beads.

We further evaluated these polymer-bound borohydrides for recovery of silver from spent photographic fixer. Samples of photographic fixer containing 0.55% ionic silver were diluted and adjusted to various pH's. The resulting levels of silver after the polymer-bound borohydride treatment are shown in Table IV. Based on these results we further evaluated a cartridge system containing polymer-bound borohydride to remove low levels of heavy metal ions. Although this technique could be feasible for once-through treatment, there are some practical disadvantages: separation of the reduced metal from the resin proved difficult, and in streams with high ionic strength, displacement of borohydride by other ionic species could be a problem.

Summary

Based on the results of these studies we feel that polymer-bound borohydrides offer several advantages in the treatment of systems where introduction of ionic species is undesirable. These borohydrides are

extremely simple to prepare and very convenient for many laboratory purifications.

We are continuing more detailed studies on the use of polymer-bound borohydrides for solvent and ethanol purification.

Acknowledgments

The authors wish to thank Ramesh S. Hegde for his helpful suggestions and contributions to this chapter. We also graciously acknowledge the support work of Ventron's Analytical Department, in particular that of Jill Rider.

Literature Cited

1. Taylor, F. M., Imperial Chemical Industries Limited, British Patent 876 034, 1961.
2. Sansoni, B.; Sigmond, D. *Naturwissenschaften* **1961**, *18*, 598.
3. Gibson, H. W.; Bailey, F. C. *J. Chem. Soc. Chem. Commun.* **1977**, 815.
4. Perrier, D. M.; Benerito, R. R. *Appl. Polym. Symp.* **1976**, *29*, 213.
5. Perrier, D. M.; Benerito, R. R.; Steele, R. H. U.S. Patent 4 032 293, 1977.
6. Cernia, E.; Gasparini, F. *J. Appl. Polym. Sci.* **1975**, *19*, 917.
7. Hallensleben, M. L. *J. Polym. Sci., Polym. Symp.* **1974**, *47*, 1.
8. Crosby, G. A. U.S. Patent 4 029 706, 1977.
9. Davis, R. E.; Swain, C. G. *J. Am. Chem. Soc.* **1961**, *82*, 5949.
10. Demko, P. R., "Alfa Bits," unpublished data.
11. Hedge, R. S., U.S. Patent 4 107 099, 1978.

RECEIVED October 13, 1978.

Cyclopolymerization of *N*-Substituted Diallylamines

J. H. HODGKIN and S. DEMERAC

Division of Applied Organic Chemistry, CSIRO, P.O. Box 4331,
G.P.O. Melbourne, Victoria, 3001, Australia

New diallylaminomonomers were prepared with a wide variety of complex polar groups attached to the nitrogen atom. These were evaluated as monomers for cyclopolymerization to multifunctional polypyrrolidines. A majority of the monomers homopolymerized readily to soluble polymers of molecular weights between $2-8 \times 10^3$ with considerable structural perfection. Cocyclopolymerization of some monomers with small quantities of a tetrallyldiamino monomer yielded cross-linked resins suitable for ion-exchange testing. Structural studies on both types of polymers (cross-linked and soluble) were carried out using ^{13}C -NMR techniques.

Our interest in the synthesis of functional polymers for use as polymeric chelating agents, catalysts, and drugs has led to the synthesis of many new monomers based on diallylamine (1, 2). These have been cyclopolymerized to pyrrolidine chains with relatively perfect and well characterized structures. The materials range from soluble, low molecular weight oils to highly cross-linked resins, depending on the monomer functionality and polymerization conditions.

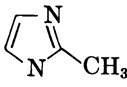
This type of polymerization method has the potential to give more complex polymer structures with less defects than the normal practice of carrying out reactions on preformed polymers. Therefore we have continued with the synthesis and cyclopolymerization of new complex monomers. Most of the previously synthesized monomers were made by a one-step Mannich reaction using a diallylamine and either a phenol or an aromatic amine. This chapter describes the synthesis and attempted polymerization of a much wider variety of monomer structures.

Discussion

Monomer Synthesis. As the Mannich reaction provided a simple and convenient method for synthesizing previous monomers, its application was continued with a number of the new monomers (I to VI, Table I). A range of active hydrogen starting materials was used so the reaction conditions had to be changed in each case. There is extensive and detailed literature on the reaction conditions needed for each type of compound (3, 4, 5) and our methods were identical to those described previously for similar reagents. Different, but generally one-step synthetic methods were chosen for producing monomers VII to XIV. Only representative samples of the types of monomers made have been shown in Table I; other monomers and a more detailed list of synthetic methods and polymer applications will be described in a following report.

The starting materials were chosen partly for their simplicity and cheapness and partly for their possible application in the final polymer—as either chelating groups (for example, V and VII) or polymeric drugs (VI). Structures such as the nitro compound (I) offer a simple method for obtaining primary amino groups on a polymer chain. This may have applications in the attachment of amino acid chains in protein synthesis.

Table I. Monomer

<i>Starting Material</i>	<i>Reaction Method</i>	<i>Ref.</i>
$\text{O}_2\text{N}-\text{CH}_2-\text{CH}_2-\text{CH}_2-\text{CH}_3$	Mannich Reaction	(6)
$\text{CH}_3-\overset{\text{O}}{\underset{\parallel}{\text{C}}}-\text{CH}_3$	Mannich Reaction	(5)
$\text{CH}_3-\overset{\text{O}}{\underset{\parallel}{\text{C}}}-\text{C}_6\text{H}_5$	Mannich Reaction	(5)
	Mannich Reaction	(7)
$\begin{array}{c} \text{H} \quad \text{COOEt} \\ \diagdown \quad / \\ \text{C} \\ / \quad \diagdown \\ \text{C}_2\text{H}_5 \quad \text{COOEt} \end{array}$	Mannich Reaction	(5)

Because of polymerization problems with the ketone monomers (II and III) and with monomers containing free carboxylic acid groups (IX), simple derivatives such as (X to XII) were synthesized instead.

The monomers generally were obtained in high yield with none of the problems of multiple substitution evident in the preparation of phenolic Mannich monomers (2). The reaction of acetone with excess diallylamine and formaldehyde could be made to yield a disubstituted product, but this was difficult to isolate in a highly purified form. Monomers such as VII could be obtained from α -picoline by a Mannich reaction but the yields were much lower than those obtained with the 2-vinylpyridine/diallylamine reaction.

Although all of these monomers appeared to be quite stable at room temperature in air, polymerization yields were always increased greatly when the monomers were freshly purified (generally by distillation under vacuum) and stored under nitrogen at 0°C. The structures of these new monomers were verified by NMR and IR spectroscopy (Table III, experimental), except for monomer III which could not be obtained analytically pure because of the presence of small amounts of amine elimination products. However, spectroscopy and the synthesis of a derivative (XII) confirmed the structure proposed.

Preparation

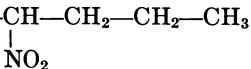
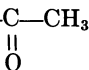

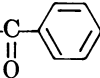
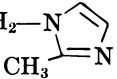
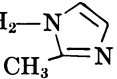
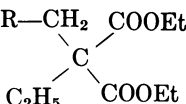
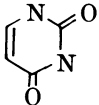
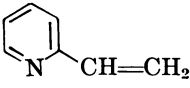
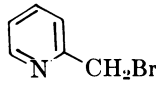
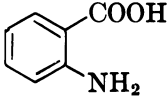
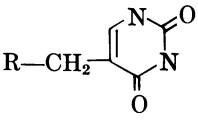
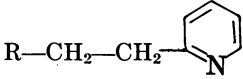
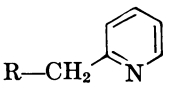
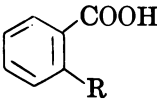
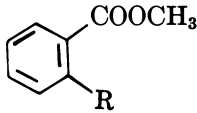
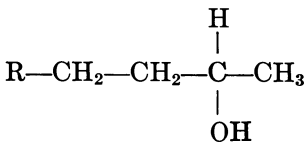
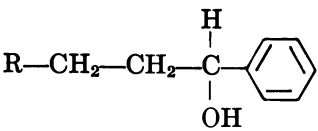
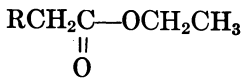
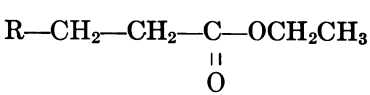
<i>R</i> — <i>N</i> (CH ₂ —CH=CH ₂) ₂	Product	Yield (%)	Purification and Properties
<i>R</i> —CH ₂ —CH—CH ₂ —CH ₂ —CH ₃ (I)		73	Colorless liquid; bp 82°–84°C/0.5 mm
<i>R</i> —CH ₂ —CH ₂ —C—CH ₃ (II)		81	Colorless liquid; bp 62°–65°C/0.5 mm
<i>R</i> —CH ₂ —CH ₂ —C—  (III)		63	Chromatography and distillation; pale yellow oil; bp 102°–104°C/0.2 mm
<i>R</i> —CH ₂ —N—  (IV)		77	Colorless liquid; bp 95°–97°C/0.1 mm
<i>R</i> —CH ₂ —C—COOEt (V)		52	Chromatography; undistillable; brown viscous oil

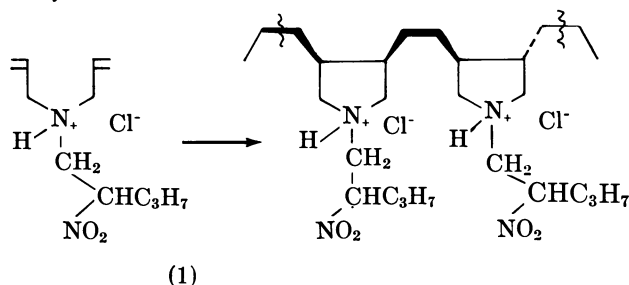
Table I.

<i>Starting Material</i>	<i>Reaction Method</i>	<i>Ref.</i>
	Mannich Reaction	(8)
	Reaction with diallylamine	(9)
	Reaction with diallylamine	
	Reaction with allylbromide	(10)
IX	Esterification with diazomethane	
II	Reduction with sodium borohydride	(11)
III	Reduction with sodium borohydride	
$\text{BrCH}_2\text{—}\overset{\text{O}}{\parallel}\text{C—OCH}_2\text{CH}_3$	Reaction with diallylamine	
$\text{BrCH}_2\text{—CH}_2\text{—}\overset{\text{O}}{\parallel}\text{C—OCH}_2\text{CH}_3$	Reaction with diallylamine	

Continued

<i>Product</i> $R-N(CH_2-CH=CH_2)_2$	<i>Yield</i> (%)	<i>Purification and Properties</i>
	(VI)	65 Recrystallized from ethanol; white needles; mp 196°C
	(VII)	52 Colorless oil; bp 66°-69°C/0.02 mm
	(VIII)	51 Light yellow oil; bp 126°-128°C/10 mm
	(IX)	69 Recrystallization from ether as colorless plates; mp 92°C
	(X)	75 Colorless oil; bp 90°-93°C/0.02 mm
	(XI)	89 Colorless oil; bp 50°-51°C/0.5 mm
	(XII)	85 Colorless oil; bp 102°-108°C/0.05 mm
	(XIII)	69 Pale yellow oil; bp 108°-110°C/25 mm
	(XIV)	74 Colorless oil; bp 110°-112°C/15 mm

Polymerization. The cyclopolymerization of substituted diallyl-amino monomers has been described in a number of previous papers (1, 2, 12, 13) and the polymerization mechanisms and polymer structures have been worked out in considerable detail (14). The monomers with a single diallylamino substituent such as I (Equation 1) form relatively perfect polypyrrolidene structures with cis substituted rings predominating over trans by a ratio of about 5:1.



These polymers are generally low molecular weight (not more than 10,000), chloroform-soluble solids. However, use of different comonomers with more than one diallylamino unit per molecule can (and has been used to) increase the molecular weights to highly cross-linked, insoluble gels (15, 16). In the latter materials the degree of structural perfection is more difficult to determine.

With the present series of monomers, described in Table I, the polymerization methods studied were the same as those described in previous work (2). Again, polymerization of concentrated aqueous solutions of the amine hydrochlorides using the titanous chloride/hydrogen peroxide initiation system provided the best polymerization method. Where this technique did not yield polymers, other free-radical initiation systems were equally unsuccessful. Table II gives some examples of the results of these polymerization experiments.

There were great differences in the ease and type of polymerization for the different types of monomer structures. The aliphatic nitro compounds, exemplified by I, polymerized in good yield to pale yellow solids with the simple polypyrrolidene structure (Equation 1), and there were no noticeable unsaturated end groups in the ^{13}C NMR (Figure 1) or IR spectra. In contrast, the ketone-substituted monomers formed brown oily solids which cross-linked on standing to insoluble gels. The ^{13}C NMR spectra of these polymers before they became heavily cross-linked (Figure 2) showed that they had only a partial pyrrolidene structure and a considerable number of unreacted double bonds. The results indicate that a high proportion of single allyl groups had reacted initially in a noncyclic polymerization and the remaining unsaturated group of the diallyl pair then reacted slowly to cross-link the polymer.

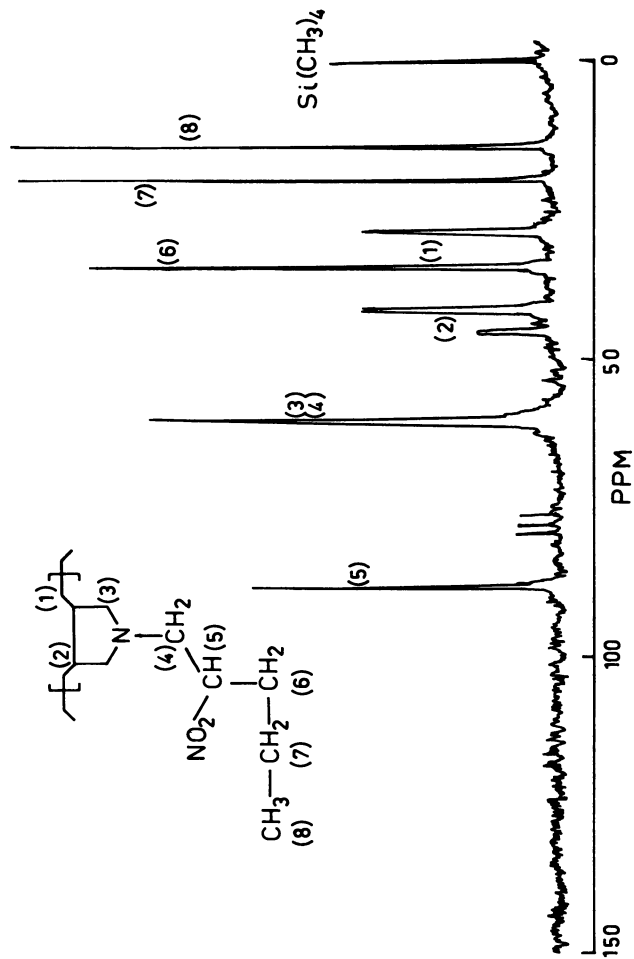
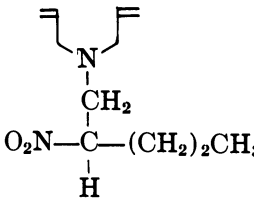
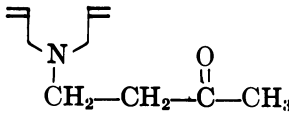
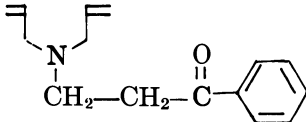
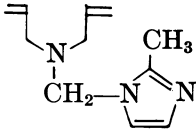
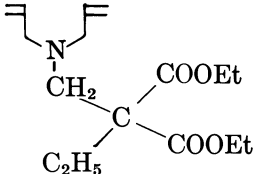
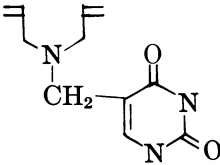
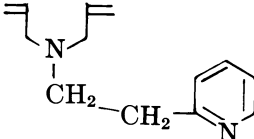


Figure 1. Proton-decoupled natural abundance ^{13}C NMR spectrum of cyclopolymerized monomer I in CDCl_3 .

Table II. Homopolymerization

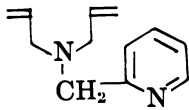
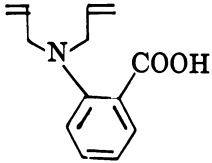
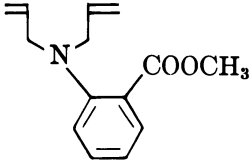
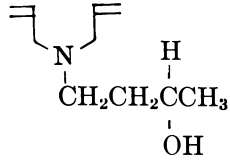
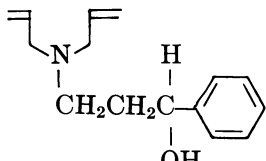
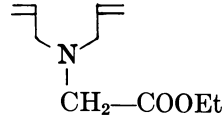
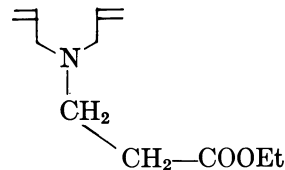
<i>Monomer</i>		<i>% Conversion</i>
	I	75
	II	50
	III	40
	IV	No significant polymerization
	V	60
	VI	No polymerization
	VII	33

of Diallylamino Monomers

<i>Polymer Properties</i> ^a	<i>Polymer Structure</i> (¹³ C NMR and IR results)
Pale yellow solid; mp 74°–77°C; mol wt 5.8×10^3	Relatively perfect polypyrrolidine, IR 1370, 1565 cm ⁻¹ (nitro)
Pale brown solid, initially soluble in chloroform but cross-linked on standing to a rubbery gel	Only partially cyclized, very im- perfect structure
Pale brown solid, initially soluble in chloroform but cross-linked on standing to a rubbery gel	Only partially cyclized, very im- perfect structure
—	—
Cream solid; mp 122°–128°C; mol wt 6.0×10^3	Relatively perfect polypyrrolidine, IR 1255, 1760 cm ⁻¹ (ester)
—	—
Light brown glassy solid; mol wt 4.6×10^3	Some indication of double bonds by ¹³ C (< 5%) but mainly poly- pyrrolidine, IR 756, 1600 cm ⁻¹ (pyridine)

^a Except where noted all polymers were soluble in chloroform and insoluble in petroleum ether.

Table II.

<i>Monomer</i>		<i>% Conversion</i>
	VIII	32
	IX	No polymerization
	X	50
	XI	55
	XII	64
	XIII	90
	XIV	75

Continued

<i>Polymer Properties^a</i>	<i>Polymer Structure (¹³C NMR and IR results)</i>
Light brown glassy solid; mol wt 2.7×10^3	Some unsaturation but mainly poly- pyrrolidine, IR 755, 1600 cm^{-1} (pyridine)
—	—
White solid; mp 120°–124°C; mol wt 2.9×10^3	Pure polypyrrolidine, IR 1245, 1725 cm^{-1} (ester); 752 cm^{-1} (aromatic)
White solid; mp 70°–75°C; mol wt 7.7×10^3	Pure polypyrrolidine, IR 1160, 3440 cm^{-1} br (hydroxyl)
White solid; mp 68°–75°C; mol wt 6.8×10^3	Pure polypyrrolidine, IR 1220, 3200 cm^{-1} br (hydroxyl)
Cream solid; mp 155°–160°C; mol wt 5.6×10^3	Polypyrrolidine but some hydrolysis of ester, IR 1225, 1755 cm^{-1} (ester)
White solid; decomp. \approx 210°C; mol wt 4.7×10^3	Polypyrrolidine but ester almost completely hydrolyzed, IR very broad hydroxyl and acid peaks

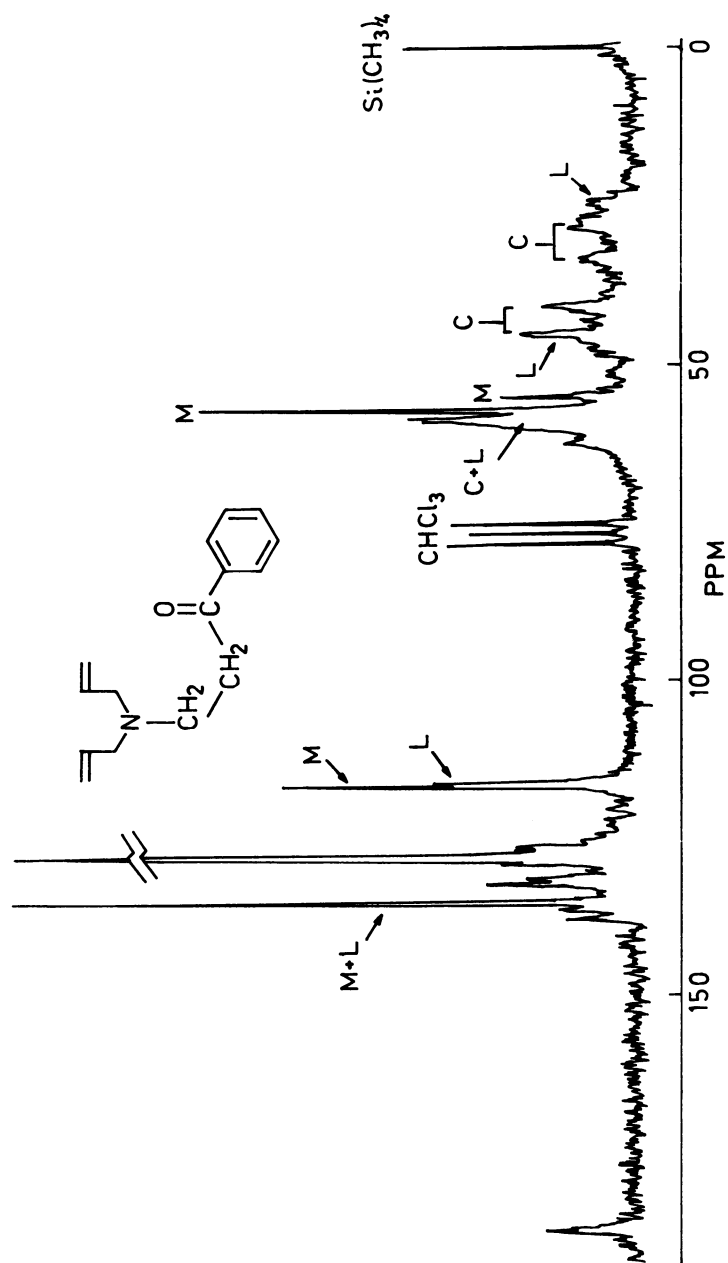


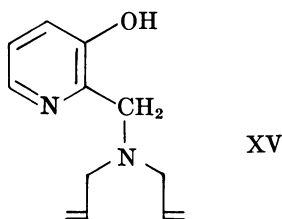
Figure 2. The ^{13}C NMR spectrum of cyclopolymerized monomer III in CDCl_3 : (M) monomer; (C) cyclopolymer; (L) linear polymer

Figure 2 is a ^{13}C NMR spectrum of polymer III contaminated with monomer to highlight the different types of structures present. The large peaks at about 117 and 135 ppm are attributable to allyl groups in different environments, and the major peak at 128 ppm results from various aromatic carbon atoms.

Reduction of the ketone groups of monomers II and III to alcohols gave monomers XI and XII, which readily polymerized to polypyrrolidines in high yield and purity. Figure 3 is a ^{13}C NMR spectrum of a low molecular weight ($> 2 \times 10^3$) sample of polymer XII and is included to highlight the presence of CH_3 end groups in this short chain. The higher mobility of such chain ends could be distinguished by spin-lattice relaxation experiments.

A number of the monomers (IV, VI, and IX) did not polymerize at all in spite of repeated attempts under different conditions, and only the unreacted monomer was recovered. For the amino acid monomer IX it was initially thought that its unusually strong chelating power for the metal salts used in the redox initiators was the reason for the problem. However, experiments with other nonchelating amino acids and different types of initiators indicate that none of the diallylaminomonomers containing free acid groups yield polymers. Blocking the acid group by esterification, for example, monomers X and V, again gave monomers that polymerized readily to well-characterized polypyrrolidine structures.

Monomers VII and VIII were designed to provide highly chelating structures for metal ions such as nickel and cobalt. Previous efforts to obtain significant quantities of polymers from similar monomers, such as XIV (2) and its acetyl derivative (16), were unsuccessful. However, the two new compounds polymerized to give a reasonable yield of polypyrrolidine polymer. The ^{13}C NMR spectra of these materials showed a



noticeable amount of free allyl groupings (indicating approximately 5% unsaturation) but no other impurities. Problems were encountered in purifying the polymers for ^1H NMR spectroscopy because of their strong affinity for paramagnetic metal ions.

Polymer Properties. All the soluble polymers were purified by repeated precipitation from chloroform using petroleum ether, and most were fine white or cream solids with reasonably high melting points

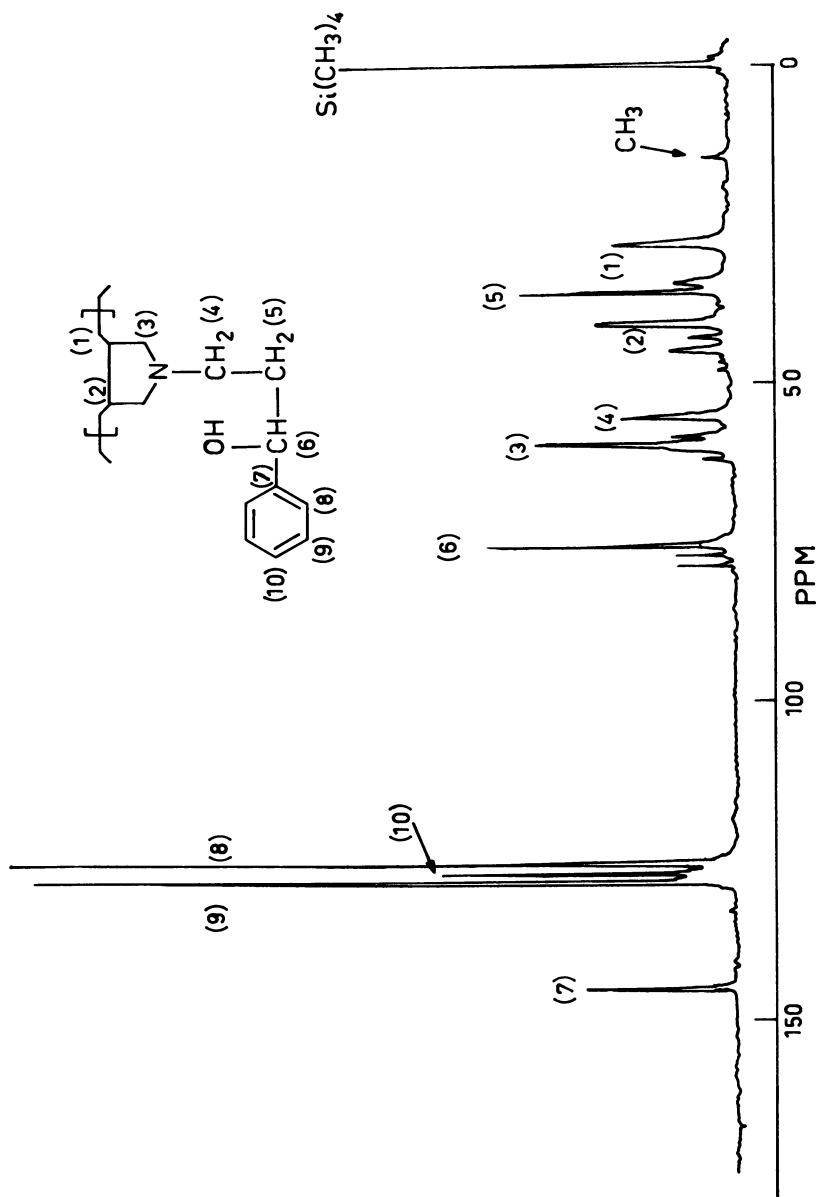


Figure 3. The ^{13}C NMR spectrum of cyclopolymers of monomer XII in CDCl_3 .

(Table II). However, the two pyridine-containing polymers remained as light-amber, glassy materials even after repeated precipitations.

The polymer solubilities varied with the polarity of the monomer structure as expected—the nitro polymer I being soluble in nonpolar solvents such as benzene and the highly polar amino acid XIII being soluble in polar solvents such as ethanol.

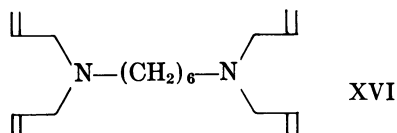
These polymers all retained solvents very strongly, which made the elemental analysis extremely unreliable as a guide to polymer structure. For example, the polymer from diallylaminoethylpyridine (VII) contained more than 6% chlorine even after vacuum drying at room temperature for 48 hr. This could only be reduced below 1% by prolonged vacuum treatment at 60°C, conditions under which polymer decomposition occurred.

The polymer molecular weights were determined by vapor-phase osmometry in chloroform using polystyrene standards of molecular weight 6×10^2 , 2.9×10^3 , and 3.6×10^3 . The results are also shown in Table II and range from 2×10^3 to 8×10^3 , which is the general range for this type of cyclopolymerization (2, 17) unless multifunctional monomers are present.

In general, the ^{13}C NMR peak positions in Figure 4 and the IR spectra in Table III were very similar to those of the equivalent monomers except for those groups directly associated with, or very closely connected to the pyrrolidine ring. This confirmed that the functional groups attached to the diallylamine unit have not taken part in the polymerization.

No detailed experiments have been carried out yet to determine the usefulness of these polymers as chelating agents or drug carriers. However, preliminary tests with ethanolic solutions of metal acetates show that polymers VII, VIII, and XIV give colored complexes with some of the common transition elements. In the case of VIII, a green complex is formed with cupric acetate and a yellow complex with cobaltic acetate. More complete experiments will be reported in a latter communication.

Cross-Linked Polymers. Apart from the soluble polymers, insoluble resins with unusual functional groups are of interest in areas such as metal-chelating resins. The most promising monomers of Table I were studied as potential resins. To obtain cross-linked polymers without adding new interfering groups, 1,6-diallylaminohexane (XVI) was used in 5–10 mol % quantities as the cross-linking monomer.



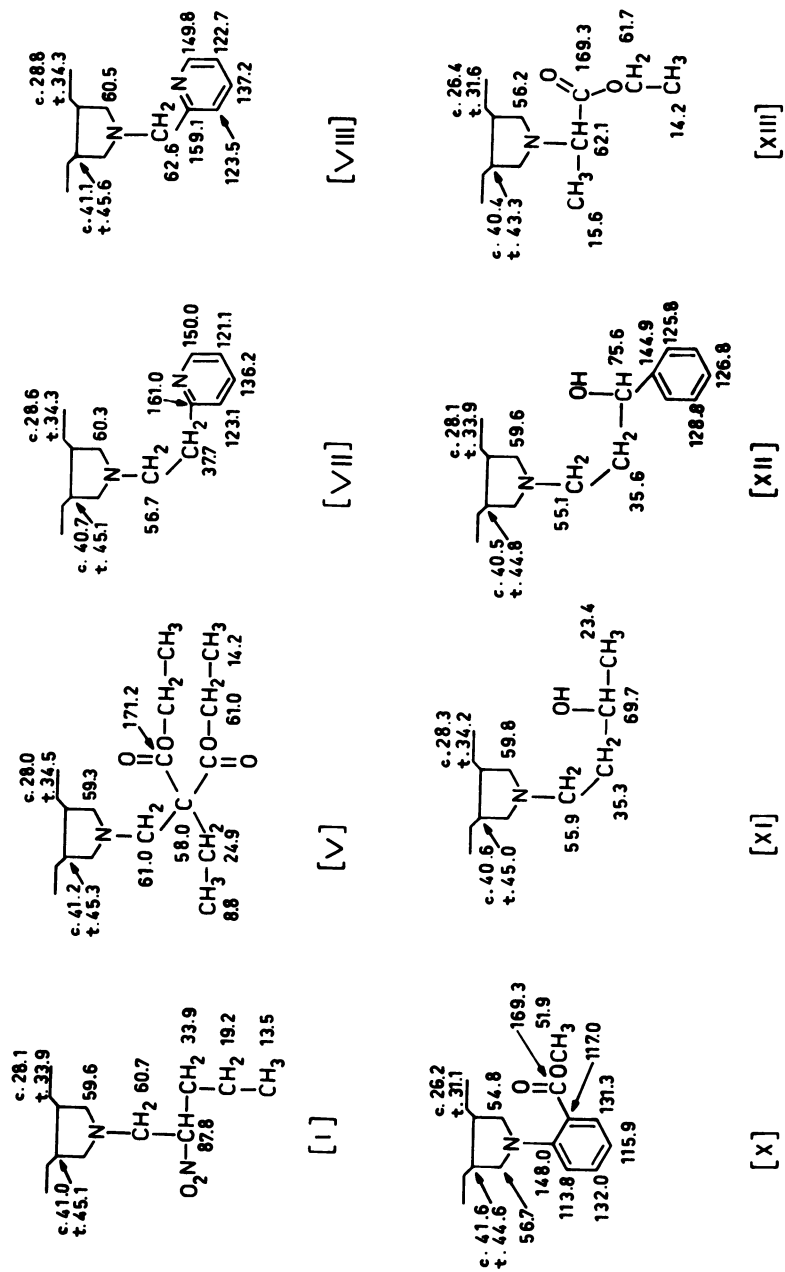
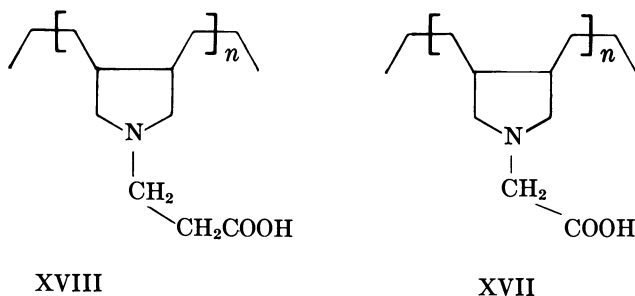


Figure 4. The ^{13}C NMR results for soluble polypyrrolidines (ppm from TMS)

Monomers V, VII, X, XIII, and XIV copolymerized readily to give high yields (70–90%) of cross-linked resins. The ^{13}C NMR spectra showed that they had the polypyrrolidine structures expected with a minimum of uncyclized groups. Only low yields of cross-linked resin could be obtained from the diallylaminomethylpyridine monomer VIII.

Polymer Properties. Preliminary studies are being carried out with the various cross-linked polymers using ^{13}C NMR spectroscopy to determine the changes in structure that occur with different pH changes and with different metal ions present. Of particular interest have been samples of cross-linked resins XIII and XIV that have been hydrolyzed to the amino acid polypyrrolidines XVII and XVIII, respectively. In these cases there are extensive changes in the ^{13}C NMR spectra of the water-swollen polymers depending on whether the conditions are acidic, basic, or neutral (Figure 5).



Experimental

Materials and Instrumentation. Diallylamine and the various starting materials for monomer synthesis were readily available commercial materials of the highest available purity and were used without further treatment. The formaldehyde used was either BDH analytical reagent solution with 37–40% w/v formaldehyde and 11–14% w/v methanol or BDH analytical reagent paraformaldehyde.

The elemental analyses were carried out by the Australian Micro-analytical Service, CSIRO, Melbourne. IR spectra were recorded on a Unicam SP200 spectrophotometer in potassium bromide discs (for solids) and as thin films between sodium chloride plates (for liquids). Proton magnetic resonance (PMR) spectra of the monomers were recorded on a Varian HA100 instrument and ^{13}C NMR spectra on a Varian CF7/20. In both cases the chemical shifts (δ) are quoted in ppm with tetramethyl silane as the internal standard.

Monomer preparations were carried out by methods similar to those described in the references listed in Table I, and the monomer yield and properties are described in this table and Table III.

1-Diallylamino-2-butane (I) was prepared by the addition of diallylamine (10 g, 0.103 mol) to 10 mL of formalin; then,

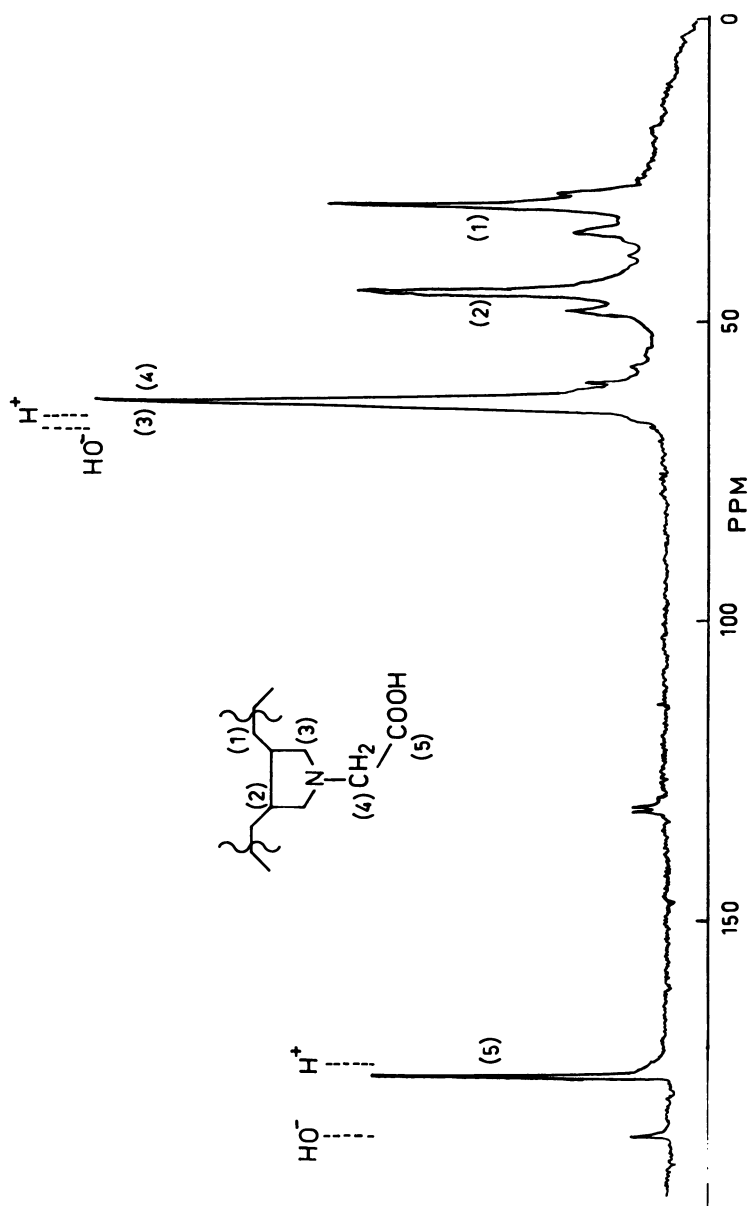


Figure 5. The ^{13}C NMR spectrum of cross-linked resin XVII swollen in D_2O

1-nitrobutane (10 g, 0.097 mol) was added with stirring. The mixture was stirred for 5 hr with slight warming, and the product was extracted with ether and then distilled.

1-Diallylamino-3-oxobutane (II) was synthesized from diallylamine (20 g, 0.206 mol), acetone (29 g, 0.5 mol), paraformaldehyde (4 g, 0.13 mol), and concentrated hydrochloric acid (30 mL)—all combined in 50 mL of ethanol and refluxed for 3 hr. Then a further 4 g of paraformaldehyde was added and the mixture refluxed for 8 hr. The solution was concentrated, then basified with aqueous sodium bicarbonate and extracted with chloroform. The product was purified by distillation.

1-Diallylamino-3-oxo-3-phenylpropane (III) was prepared as II using acetophenone instead of acetone.

N'-(N,N-Diallylaminomethyl)-2-methylimidazole (IV) was prepared from diallylamine (24.2 g, 0.25 mol) and imidazole (19 g, 0.25 mol) dissolved in 100 mL of ice water and acidified with 50 mL of concentrated hydrochloric acid. Formaldehyde (25 mL, 0.25 mol) was added slowly to the solution with stirring and left for 24 hr. The product was extracted from the aqueous solution with chloroform after basification with sodium hydroxide. The product was purified by distillation.

1-Diallylamino-2,2-biscarbethoxybutane (V) was synthesized from diallylamine (20 g, 0.206 mol) in ethanol to which formaldehyde (22 mL, 0.22 mol) was added slowly with stirring, followed by ethyldiethyl malonate (37.5 g, 0.2 mol). The mixture was heated at reflux for 48 hr and then the excess ethanol removed and replaced with water. The product was purified by extraction of unchanged ethyldiethylmalonate and then repeated chromatography on alumina.

5-Diallylaminomethyl uracil (VI) was prepared from a mixture of uracil (22.4 g, 0.2 mol), paraformaldehyde (11 g, 0.36 mol), and diallylamine (33 g, 0.34 mol) in 200 mL of ethanol refluxed for 24 hr. The resulting solid product was crystallized from ethanol.

2-Diallylaminomethylpyridine (VIII) was prepared from 2-bromomethylpyridine hydrobromide (10 g, 0.04 mol), diallylamine (12 g, 0.12 mol), and 80 mL of ethanol heated in an autoclave at 120°C for 15 hr. The mixture was cooled and made alkaline before extraction with ether/petroleum (40/60). The product was purified by distillation.

2,2-Diallylaminomethylpyridine (VII) was made from 2-vinylpyridine (15 g, 0.14 mol), diallylamine hydrochloride (15 g, 0.14 mol), 10 mL of water, and 60 mL of glacial acetic acid stirred under gentle reflux for 8 hr. The mixture was then made alkaline and extracted with diethylether. The product was purified by distillation.

N,N-Diallylanthranilic acid (IX) was prepared from anthranilic acid (24.6 g, 0.2 mol) and allylbromide (25 g, 0.20 mol) dissolved in 40 mL of ethanol and refluxed for 8 hr. The solution was basified by an equivalent amount of aqueous

Table III. Analysis and Spectral

Com- pound	Analysis				Major IR ^a Peaks (cm ⁻¹)
	C	H	N		
I	60.59	9.15	14.12	Calc	1555 (NO ₂)
	60.89	9.19	14.08	Found	
II	71.81	10.25	8.38	Calc	1718 (C=O)
	72.07	10.27	8.53	Found	
III	78.56	8.35	6.11	Calc	1690 (C=O)
				Found	695 } (Ar) 749 }
IV	69.07	8.95	21.97	Calc	750 } (Ar) 1423 }
	68.89	8.66	22.33	Found	
V	64.62	9.15	4.71	Calc	1738 (C=O)
	64.41	8.95	4.85	Found	1240 (C=O)
VI	59.71	6.83	18.99	Calc	1720 } br (C=O) 1680 }
	59.75	6.68	19.16	Found	
VII	77.18	8.97	13.85	Calc	749 } (Ar) 1598 }
	77.3	8.8	14.10	Found	
VIII	76.55	8.56	14.88	Calc	1598 } (Ar) 757 }
	76.3	8.6	15.0	Found	
IX	71.83	6.96	6.55	Calc	1660 br (C=O) 1602 } (Ar) 1460 }
	71.8	6.7	6.5	Found	
X	72.70	7.41	6.06	Calc	1732 (C=O) 752
	72.59	7.12	6.04	Found	
XI	70.96	11.31	8.28	Calc	3400 br (OH)
	70.46	11.10	8.08	Found	
XII	77.87	9.15	6.06	Calc	3400 br (OH)
	77.89	8.76	5.80	Found	
XIII	65.54	9.35	7.65	Calc	1748 (C=O)
	65.67	9.60	7.67	Found	

^a All compounds had diallylamino peaks at $\approx 920, 995, \text{ and } 1645\text{m}^{-1}$.

Results for Diallylaminomonomers

<i>¹H NMR (ppm)</i>			
<i>Allyl</i>	<i>N-Methylene</i>	<i>Aromatic</i>	<i>Other</i>
6.2–5.6 m (CH)	3.11 m		4.60 m (CHNO ₂)
5.4–4.9 m (CH ₂)	2.52 d, 2.68 d ≈ 3.06 m		0.95 t (CH ₃) 1.9–1.1 m (CH ₂ —CH ₂)
6.2–5.6 m (CH)	2.78 m		2.08 s (CH ₃)
5.4–4.9 m (CH ₂)	(CH ₂ —CH ₂)		
6.1–5.5 m (CH)	3.10 m	7.55–7.35 m	
	(—CH ₂ —CH ₂)		
	(N—CH ₂)	8.10–7.7 m	
5.3–4.9 m (CH ₂)			
6.2–5.6 m (CH)	4.61 s	6.93 m	2.45 s (CH ₃)
5.3–5.0 m (CH ₂)	3.19 m		
6.2–5.5 m (CH)	3.18 s		0.78 t (CH ₃) 4.18 q (CH ₃) 1.22 t (CH ₃) 2.10 q (CH ₂)
5.35–4.95 m (CH ₂)	3.22 d		
6.2–5.6 m (CH)	3.28 s	7.22 s	10.55 br s (NH)
5.4–5.0 m (CH ₂)	3.11 d		
6.2–5.58 m (CH)	3.17 m	8.52 m (αCH)	
5.17–4.98 m (CH ₂)	2.90 m (CH ₂ CH ₂)	7.45 m (γCH) 7.10 m (βCH)	
6.3–5.6 m (CH)	3.79 s	8.56 m (αCH)	
	3.18 d	7.52 m (γCH)	
5.4–5.0 m (CH ₂)	3.18 d	7.10 m (βCH)	
6.2–5.6 m (CH)	3.72 d	7.8–7.3 m	
5.4–5.0 m (CH ₂)		8.5–8.3 m	
6.2–5.6 m (CH)	3.72 d	7.75–6.8 m	3.88 s (CH ₃)
5.4–5.0 m (CH ₂)			
6.2–5.6 m (CH)	3.4–2.6 m		1.16 d (CH ₃) 1.8–1.3 m (—CH ₂) 4.15–3.6 m (CH)
5.4–5.0 m (CH ₂)			
6.2–5.6 m (CH)	3.4–2.6 m		
5.4–5.0 m (CH ₂)			
6.1–5.6 m (CH)	3.27 d 3.30 s		1.29 t (CH ₃) 4.17 q (—CH ₂ —O)
5.3–5.0 m (CH ₂)			

Table III.

Com- pound	Analysis				Major IR ^a Peaks (cm ⁻¹)
	C	H	N		
XIV	66.97	9.71	7.10	Calc	1758 (C=O)
	66.67	9.48	7.11	Found	

sodium bicarbonate solution. The resulting crystals of mono-allylanthranilic acid were separated out and retreated with allylbromide (25 g, 0.206 mol) in refluxing ethanol. The solution was rebasified after 8 hr of refluxing and extracted with chloroform. The product was purified by crystallization from diethylether.

N,N-Diallylmethylanthranilate (X) was prepared from the acid (IX) by esterification with diazomethane.

1-Diallylamino-3-hydroxybutane (XI) was obtained from the 3-oxo compound (II) by reduction with sodium borohydride in refluxing methanol. It was purified by distillation.

1-Diallylamino-3-hydroxy-3-phenylpropane (XII) was obtained from the 3-oxo-3-phenyl compound III by reduction with sodium borohydride as for XI.

Ethyl-3-diallylamino propionate (XIV) was synthesized from ethyl 3-bromopropionate (20 g, 0.111 mol) to which diallylamine (29 g, 0.3 mol) was added slowly with stirring and heating at 100–105°C. After complete addition, heating was continued for another 15 min. The mixture then was cooled and water was added. The solution was basified with ammonia and the product extracted with chloroform and purified by distillation.

Ethyl diallylaminoacetate (XIII) was obtained from ethyl-bromoacetate by reaction with diallylamine as before.

1,6-Diallylamino hexane (XVI) was obtained from ICI Australia Ltd. and purified by vacuum distillation.

Polymer preparation was as described in Ref. 2.

Literature Cited

- Hodgkin, J. H.; Solomon, D. H. *J. Macromol. Sci., Chem.* **1976**, *A10*(5), 887.
- Hodgkin, J. H.; Allen, R. J. *J. Macromol. Sci., Chem.* **1977**, *A11*(5), 937.
- Thompson, B. B. *J. Pharm. Sci.* **1968**, *54*, 715.
- Tramontini, M. *Synthesis* **1973**, 703.
- Blicke, F. F. In "Organic Reactions"; Wiley: New York, 1942; Vol. 1, pp. 303–341.
- Blomquist, A. T.; Shelley, T. H. *J. Am. Chem. Soc.* **1948**, *70*, 147.
- Stocker, F. B.; Kurtz, J. L.; Gilman, B. L.; Forsyth, D. A. *J. Org. Chem.* **1970**, *35*, 883.

Continued

¹ H NMR (ppm)			
<i>Allyl</i>	<i>N-Methylene</i>	<i>Aromatic</i>	<i>Other</i>
6.2–5.6 m (CH)	2.60 m (CH ₂ —CH ₂)		1.20 t (CH ₃) 4.07 q (CH ₂ —O)
5.4–4.9 m (CH ₂)			

8. Delia, T. J.; Scovill, J. P.; Munslow, W. D. *J. Med. Chem.* **1976**, *19*, 344.
9. Reich, H. E. *J. Am. Chem. Soc.* **1955**, *77*, 4913.
10. Carnahan, F. L.; Hurd, C. D. *J. Am. Chem. Soc.* **1930**, *52*, 4586.
11. Vrma, R. S.; Nobles, W. L. *J. Pharm. Sci.* **1967**, *56*, 328.
12. Johns, S. R.; Willing, R. I.; Middleton, S.; Ong, A. K. *J. Macromol. Sci., Chem.* **1976**, *A10*(5), 875.
13. Hawthorne, D. G.; Johns, S. R.; Solomon, D. H.; Willing, R. I. *Aust. J. Chem.* **1976**, *29*, 1955.
14. Solomon, D. H.; Hawthorne, D. G. *J. Macromol. Sci., Rev. Macromol. Chem.* **1976**, *C15*, 143.
15. McLean, C. D.; Ong, A. K.; Solomon, D. H. *J. Macromol. Sci., Chem.* **1976**, *A10*(5), 857.
16. Hodgkin, J. H., unpublished data.
17. McLean, C. D.; Ong, A. K.; Solomon, D. H. *J. Macromol. Sci., Chem.* **1976**, *A10*, 851.

RECEIVED September 21, 1978.

How Cationic Polymer Structure Relates to Dewatering Efficiency of Waste-Activated Sludges

J. E. MORGAN, M. A. YORKE, and J. E. BOOTHE

Calgon Corporation, Calgon Center, Box 1346, Pittsburgh, PA 15230

The efficiency of a cationic polymer in dewatering waste-activated sludge or blends thereof depends upon the relationship between polymer structure and the sludge characteristics. "Branched" structures were found to be most effective on waste-activated or predominately waste-activated sewage sludges. An "optimum degree of branching" was found to produce the best filtration rates in each series of polymers tested (presumably because the branched structures reduce the compressibility of the biofloc). The data collected on 100% raw primary sludge indicate that polymer dewatering efficiency is not greatly enhanced with branching for this sludge type. The coarse fibrous nature of this sludge reduces the compressibility of the sludge floc and facilitates dewatering, therefore lessening the importance of the flocculant structure.

Polymer treatment of municipal wastes is common practice. Numerous papers have been published relating sludge characteristics to dewaterability (1-7). Little has been done to correlate polymeric flocculant characteristics with the ability to dewater activated sludges.

Raw waste water enters a waste treatment plant, flows through a rough preliminary screen to remove coarse materials, then flows into a primary sedimentation basin. Raw primary sludge is collected from the primary sedimentation basin. This sedimentation process removes approximately 40% of the suspended solids and approximately 35% of

0-8412-0482-9/80/33-187-235\$05.00/0
© 1980 American Chemical Society

the biological oxygen demand (BOD). Raw primary sludge is anaerobic, consisting of raw organic material in an active state of bacterial decomposition. Primary sludges dewater rapidly because of the fibrous and coarse nature of the solids.

The effluent from a primary sedimentation basin contains 50% or more suspended solids and BOD. It can be treated by a secondary process such as waste activation to remove approximately 90% suspended solids and BOD. This waste activation process consists of biological oxidation and sedimentation steps. The sludge obtained from the secondary sedimentation is known as waste-activated sludge. It is composed of fine cellular biofloc that, when subjected to filtration, forms a highly compressible cake and, consequently, dewateres poorly.

Most municipal waste treatment plants dewater blends of waste-activated and raw primary sludges. A mixture of the two types of sludges facilitates concentration of solids and disposal by conventional dewatering methods. Cationic polymers are widely used in the waste treatment industry as dewatering aids.

As a means of increasing polymer efficiency, the effect of polymer branching was investigated. Homopolymers of diallyldimethyl ammonium chloride (DADMAC), copolymers of DADMAC and acrylamide (Figure 1), and homopolymers of 3-acrylamidomethylbutyltrimethyl ammonium chloride (AMBTAC) (Figure 2) were synthesized using both emulsion and solution polymerization techniques. Known branching or cross-linking agents such as methylenebisacrylamide (MBA) and triallylmethyl ammonium chloride (TAMAC) (Figure 3) were added to the monomer solutions before polymerization to alter the structures of the resultant polymers. The abilities of "branched" structures to increase the dewatering rates were compared with their "linear" counterparts on a wide range of waste-activated and raw sludge blends.

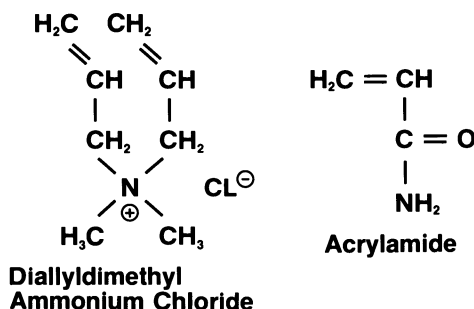
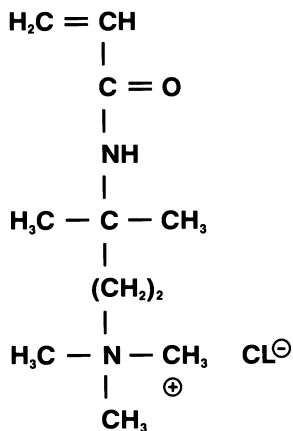
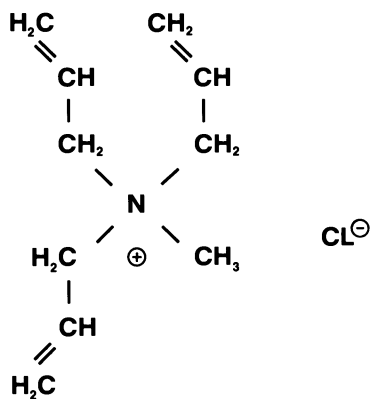


Figure 1.

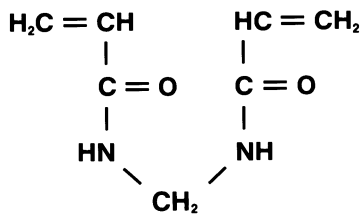


**3-Acrylamidomethylbutyl
Trimethyl Ammonium Chloride**

Figure 2.



Triallylmethyl Ammonium Chloride



Methylenebis Acrylamide

Figure 3.

Experimental

Materials. DADMAC, AMBTAC, and TAMAC monomers were produced internally by Calgon Corporation. The acrylamide monomer, received in bulk, was purchased from American Cyanamid. The MBA used was reaction grade from Aldrich Chemical. All monomers were used as received without further purification.

The benzene was histological grade and the ferrous ammonium sulfate and Na₄ EDTA were ACS certified grade. All were purchased from Fisher Scientific Company. The sodium octyl phenoxyethoxy-2-ethanol sulfate (20% aqueous solution) was used as received from Rohm & Haas. The *t*-butylperoxypivalate, also used as received from the Lucidol Division of Pennwalt Corporation, was a 75% solution in mineral spirits. The nitrogen gas was purified grade from Union Carbide. De-ionized water was used in all polymerizations.

Measurements. The monomer to polymer conversion for the DADMAC and AMBTAC homopolymers was measured by liquid chromatography. The DADMAC content in the precipitated DADMAC/acrylamide copolymers was measured by Cl⁻ titration.

Polymerizations. HOMOPOLYMER DADMAC-SOLUTION POLYMERIZATION. To a 1-L four-neck resin pot equipped with a mechanical stirrer, thermometer, condenser, purge tube, and heat regulating device were added 492 g of 55% aqueous DADMAC monomer. The pH was adjusted to 6.0 with dilute hydrochloric acid, heated to 50°C, and purged with nitrogen for 1 hr while stirring. Then, 0.05% Na₄ EDTA (based on weight reaction mix) was added followed by 1.5×10^{-2} mol *t*-butylperoxypivalate/mol monomer. The temperature was maintained at 50°C ± 2°C for 18 hr, at which time the monomer conversion to polymer leveled off at 95%. The polymer was isolated via acetone precipitation.

HOMOPOLYMER DADMAC-EMULSION POLYMERIZATION. The equipment setup outlined in the solution polymerization was used to prepare the emulsion polymer. To the resin pot 321.5 g benzene, 138.5 g of 72.2% aqueous DADMAC monomer, and 40 g of 20% aqueous sodium octyl phenoxyethoxy-2-ethanol sulfate were added. The mixture was stirred at 170–180 rpm with a paddle stirrer and heated to 50° ± 1°C. The suspension was purged with nitrogen gas for 1 hr. Then, 7 ppm Fe⁺² (added as Fe(NH₄)₂(SO₄)₃ · 6H₂O) were added, followed by 2×10^{-3} mol *t*-butylperoxypivalate/mol monomer. The reaction mixture was stirred for 20 hr at 50° ± 1°C under a nitrogen blanket. The polymer conversion after 20 hr was 90 ± 2%. The product was isolated by adding the benzene emulsion to acetone, filtering the product, and drying.

HOMOPOLYMER AMBTAC-SOLUTION POLYMERIZATION. The equipment setup was the same as in the previous sections. After adjusting the pH to 9.5, a 35% aqueous solution of AMBTAC monomer was added to the reactor. The monomer solution was heated to 35 ± 1°C and purged with nitrogen gas for 1 hr. Then, 1.5×10^{-3} mol *t*-butylperoxypivalate/mol monomer was added. The solution was maintained at 35 ± 5°C for 4 hr, at which point more than 95% conversion was achieved. The product was isolated by acetone precipitation.

HOMOPOLYMER AMBTAC-EMULSION POLYMERIZATION. The following were added to an 8 oz pop bottle: 62 g benzene, 20 g AMBTAC dissolved in 10 g deionized H₂O, and 8 g 20% aqueous solution of sodium octyl phenoxyethoxy-2-ethanol sulfate. The bottle was sealed with an airtight septum, placed in a constant temperature bath set at 50° ± 2°C, and agitated by shaking. The suspension was purged with N₂ gas using a syringe needle as the inlet; another needle served as the vent. After 1 hr, the needles were removed. Then, 7 ppm Fe⁺² were added followed by 2 × 10⁻³ mol *t*-butylperoxypivalate. The bottle was agitated in a constant temperature bath for 20 hr, after which time the polymer conversion was measured at more than 95%. The product was isolated by adding the benzene emulsion to acetone, filtering the product, and drying.

DADMAC/ACRYLAMIDE COPOLYMER (75/25 WT %)–EMULSION POLYMERIZATION. The following were added to the reaction vessel: 64.4 parts benzene, 15 parts DADMAC, 5 parts acrylamide, 13.5 parts deionized H₂O, and 2 parts sodium octyl phenoxyethoxy-2-ethanol sulfate. The vessel was purged for 1 hr with N₂ at 50° ± 1°C after which 5 ppm Fe⁺² and 2 × 10⁻³ mol *t*-butylperoxypivalate/mol monomer were added. The temperature was held at 50° ± 1°C for 20 hr. The product, isolated via acetone precipitation, was found to be a DADMAC/acrylamide copolymer (60/40 wt %).

DADMAC/ACRYLAMIDE COPOLYMER (75/25 WT %)–SOLUTION POLYMERIZATION. This product was synthesized in a manner similar to the solution homopolymerizations of DADMAC and AMBTAC. The product, isolated via acetone precipitation, was found to contain 60% DADMAC and 40% acrylamide.

Results and Discussion

A set of DADMAC homopolymers was synthesized via inverse emulsion. Concentrations of TAMAC ranging from 0 to 5.0 mol % (based on monomer concentration) were added to the monomer solutions before polymerization to induce branching. All polymerizations were initiated with the same concentration of a conventional free-radical catalyst. These samples were evaluated for their ability to dewater 100% activated sewage sludge. The filtration rate served as a measure of a sample's dewatering ability.

This filtration rate was determined by a Buchner Funnel procedure where a preconditioned sludge sample was filtered through a prewetted Whatman No. 40 filter paper at a pressure of 15 in. Hg. Brookfield viscosities were measured on 0.5% aqueous solutions prepared from precipitated polymer using an LVF viscometer. The data displayed in Figure 4 show a tremendous decrease in filtration rate and rise in Brookfield viscosities with increasing TAMAC concentrations until the polymer becomes so highly branched that its complete solubility is questionable.

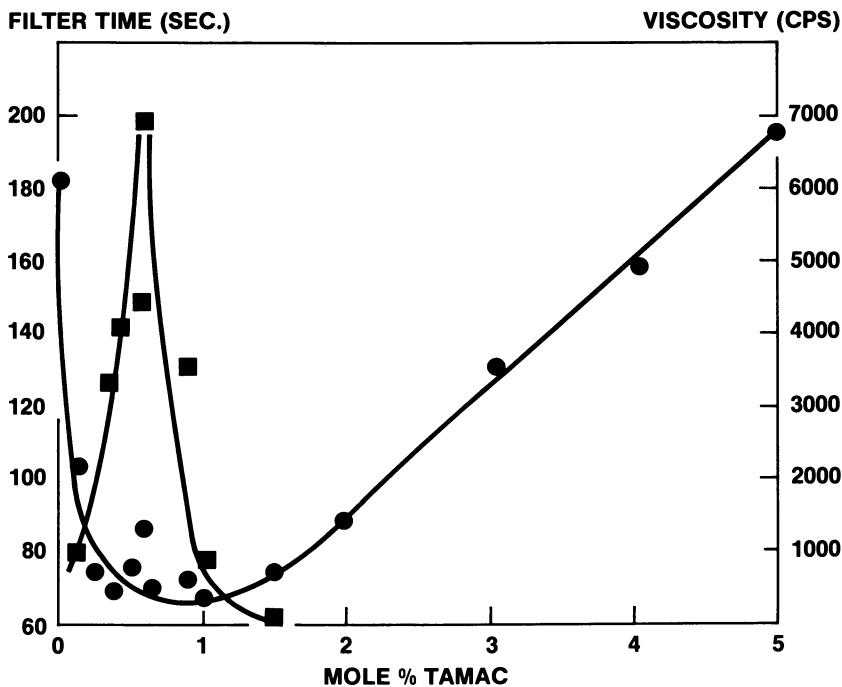


Figure 4. Emulsion DMDAAC homopolymer filter time and viscosity vs. mol % TAMAC: (●) filter time; (■) viscosity

A similar experiment was conducted on polyDADMAC samples polymerized in aqueous solution. TAMAC concentrations higher than 0.035 mol % produced polymers containing insoluble gel. The data given in Figure 5 show decreasing filtration times and increasing solution viscosities with increasing TAMAC concentration until insolubility occurred. The ordinate in Figure 5 serves as an axis for both filtration and viscosity responses.

Another series of DADMAC emulsion homopolymers was synthesized containing 0–0.5 mol % MBA. Data given in Table I indicate the same phenomenon of decreasing filtration rate with increasing MBA concentration as was observed for the series containing TAMAC. Hence, the enhanced dewaterability is independent of the type of branching agent employed.

The effect of branching on the performance of 75% DADMAC/25% acrylamide copolymers in dewatering 100% waste-activated sludge was also investigated. A series of copolymers was prepared by an inverse emulsion method adding up to 0.5 mol % TAMAC (based on DADMAC

FILTER TIME (SEC.) & VISCOSITY (CPS)

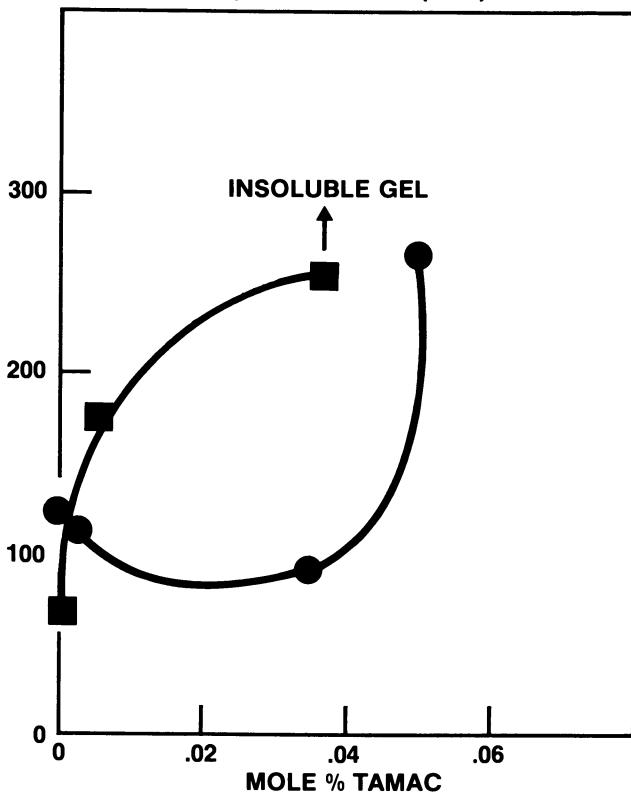


Figure 5. DMDAAC solution homopolymer filter time and viscosity vs. mol % TAMAC: (●) filter time; (■) Brookfield viscosity

Table I. Effect of MBA Addition to DADMAC Emulsion Polymers for Dewatering 100% Waste-Activated Sludge

Sample	Mol % MBA	400-mL Filter Time (sec)
A	0	567
B	0.01	505
C	0.01	465
D	0.03	358
E	0.05	186
F	0.10	157
G	0.20	145
H	0.30	128
I	0.50	114

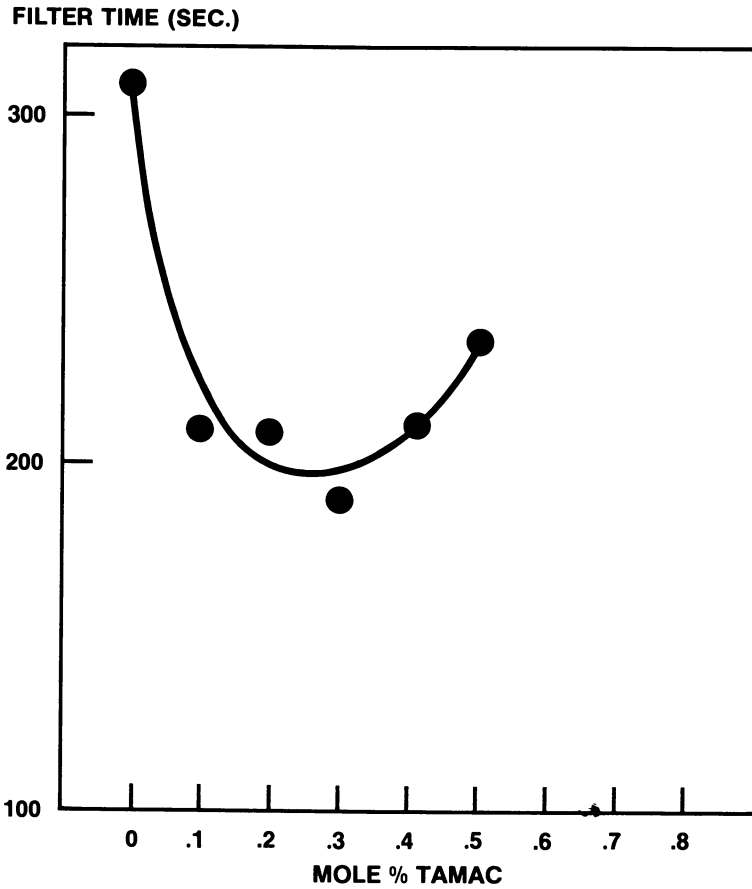


Figure 6. Plot of 75/25 DMDAAC/acrylamide mol % TAMAC vs. filter time

concentration). Figure 6 indicates that the filtration times proceed through a minimum with increasing TAMAC concentration. There appears to be an optimum degree of branching which produces the best filtration performance for dewatering waste-activated sludge.

The above data indicate that branching dramatically increases polymer efficiency in the treatment of activated sewage sludge. This effect was found to be independent of both polymerization technique (emulsion vs. solution) and polymer composition (homopolymer vs. copolymer). In all cases, filtration time decreases to a minimum and then increases with increasing concentrations of branching agents.

To insure that this effect was not limited to DADMAC homopolymers and copolymers, a second cationic monomer was included in this study. A series of AMBTAC homopolymers was polymerized by an inverse emulsion technique adding 0–0.7 mol % MBA. Three solution polymers were also prepared containing 0–0.05 mol % MBA, two of which contained small amounts of insoluble gel. All samples were evaluated on 100% waste-activated sludge. The data indicate that the branching effect is also independent of cationic monomer type. An optimum degree of branching was found to produce the best dewatering rates. Minimum filtration times were also observed for the solution polymers with increasing MBA concentration even though insoluble gel was present (*see* Figure 7).

These studies demonstrate that the dewatering efficiency of a polymer for treatment of waste-activated sludge depends upon the degree of branching for a given polymer. An optimum degree of branching is desirable regardless of the type of monomer or polymerization technique used. Data up to this point find basis only in treatment of 100% waste-activated sludge. Is the efficiency of the branched polymer structure dependent upon the type of sludge treated? Does the optimum degree of branching change as the sludge composition varies?

To address these questions, another series of DADMAC/AM copolymers (75/25 wt %) was prepared by an inversion emulsion method using 0, 0.2, and 0.4 mol % TAMAC. This series was evaluated on waste-activated and raw primary sludge blends combined in varying proportions. The evaluation of this series for dewatering waste-activated sludge is depicted in Figure 8. It shows that the sample prepared with 0.2 mol % TAMAC produces the lowest filtration time over the widest dosage range of all the samples tested on this particular sludge. The linear-emulsion polymer dewatered this sludge very poorly in comparison with the branched versions. Similarly, the sample prepared with 0.4 mol % TAMAC dewatered this sludge more slowly than the sample containing 0.2 mol %. This, again, confirms that an optimum degree of branching will rapidly flocculate and dewater waste-activated sludge.

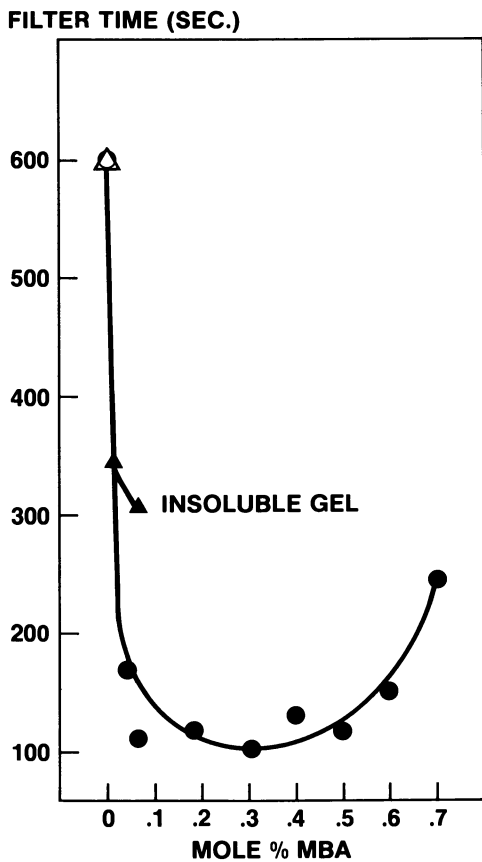


Figure 7. AMBTAC homopolymer mol % MBA vs. filter time: (●) emulsion polymerized; (▲) solution polymerized

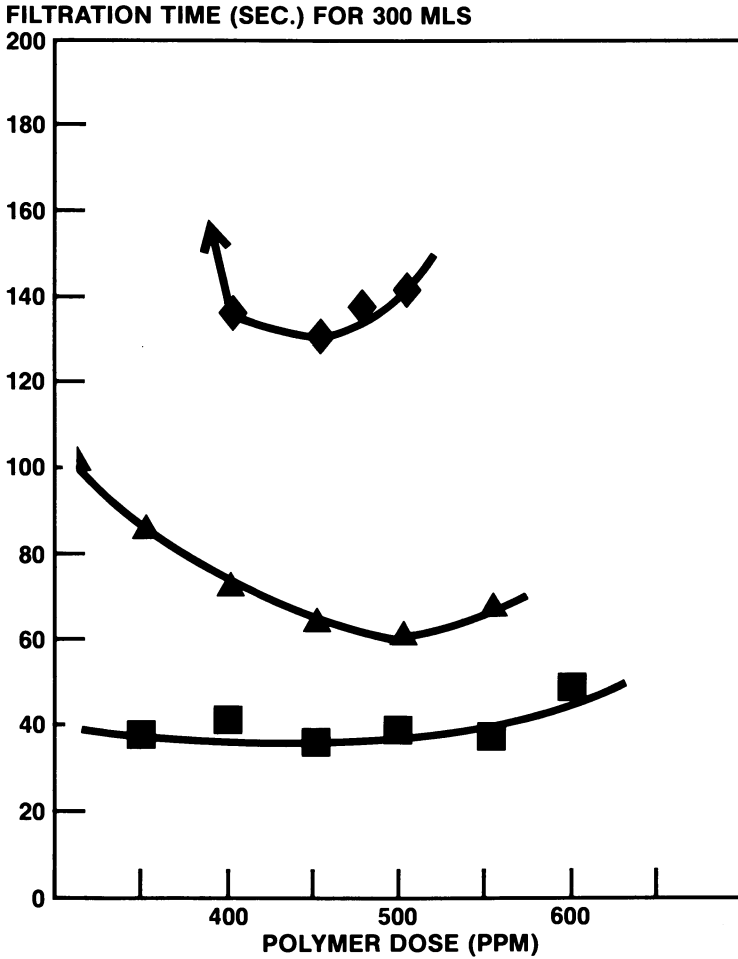


Figure 8. Buchner Funnel evaluation of emulsions on waste-activated sludge (emulsions: (◆) no TAMAC; (■) 0.2 mol % TAMAC; (▲) 0.4 mol % TAMAC)

The 10% cake times of the same copolymer series were compared for dewatering efficiency of raw primary sludge. The 10% cake time denotes the amount of time, in seconds, required to produce a sludge cake containing 90% moisture, or 10% solids. Figure 9 illustrates that all of the polymers produce nearly the same filtration time. Because of its fibrous nature, this sludge forms a noncompressible cake and is dewatered easily. Polymer structure has a minimal effect for this type of sludge.

With blends of the two types of sludge, the differences between samples increase with increasing proportions of waste-activated sludge (*see* Figures 10–12). Again, more rapid dewatering occurs with sludges treated with the polymer containing 0.2 mol % TAMAC than with any other sample. This implies that the dependence of polymer performance on structural properties is specific to waste-activated sludge.

Since dewatering rate appears to correlate with the floc properties, we decided to use an empirical method to define these properties. This method was developed independently from this study by J. Boothe and R. Stong (private correspondence). The filtration rates at the optimum dosage were fitted to an asymptotic curve of the form $V = A - Br^t$ using nonlinear least squares where:

V = Volume of filtrate at given time (t)

A = Maximum filtrate volume obtainable

$B = A$ at $t = 0$ for a perfect fit of the equation

r = Dewatering rate parameter—dependent upon the polymer sludge floc characteristics (as well as ionic strength, pH media viscosity, and temperature, all of which would remain constant for a given sludge blend during a specific evaluation period). It is defined as $0 < r < 1$.

t = Time expressed in seconds

The term “floc properties” includes cake compressibility, pressure changes with increasing cake thickness, binding to filter media, etc. Plotting the dewatering rate parameter r against the sludge blend composition in Figure 13 shows similarities in floc properties between the linear-solution polymer and the linear-emulsion polymer. The polymer prepared with 0.2 mol % TAMAC produces the best floc properties and, therefore, the fastest filtration rates (in all the sludge blends evaluated) as indicated by the low r values obtained.

This same technique could be applied to the linear and branched homopolymers. Time did not permit evaluation of these samples on the various sludge blends.

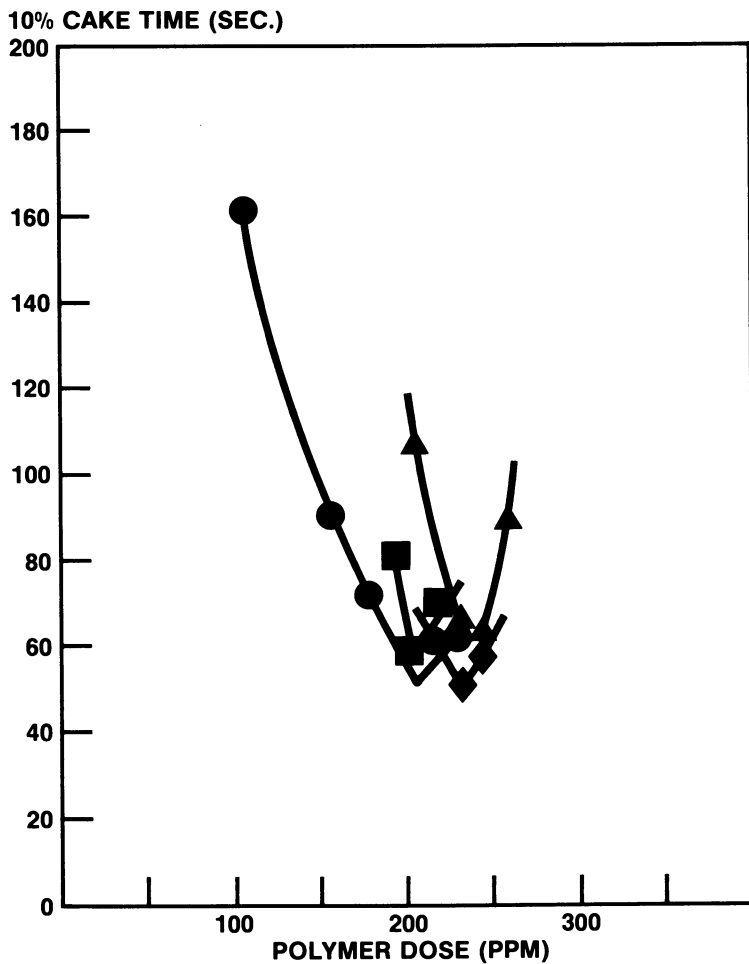


Figure 9. Buchner Funnel evaluation of emulsions on raw sludge ((●) no TAMAC—solution; emulsions: (◆) no TAMAC; (■) 0.2 mol % TAMAC; (▲) 0.4 mol % TAMAC)

American Chemical
Society Library

1155 16th St. N. W.

In *Ions in Polymers*; Eisenberg, A.; American Chemical Society: Washington, DC, 1980.

Washington, D. C. 20036

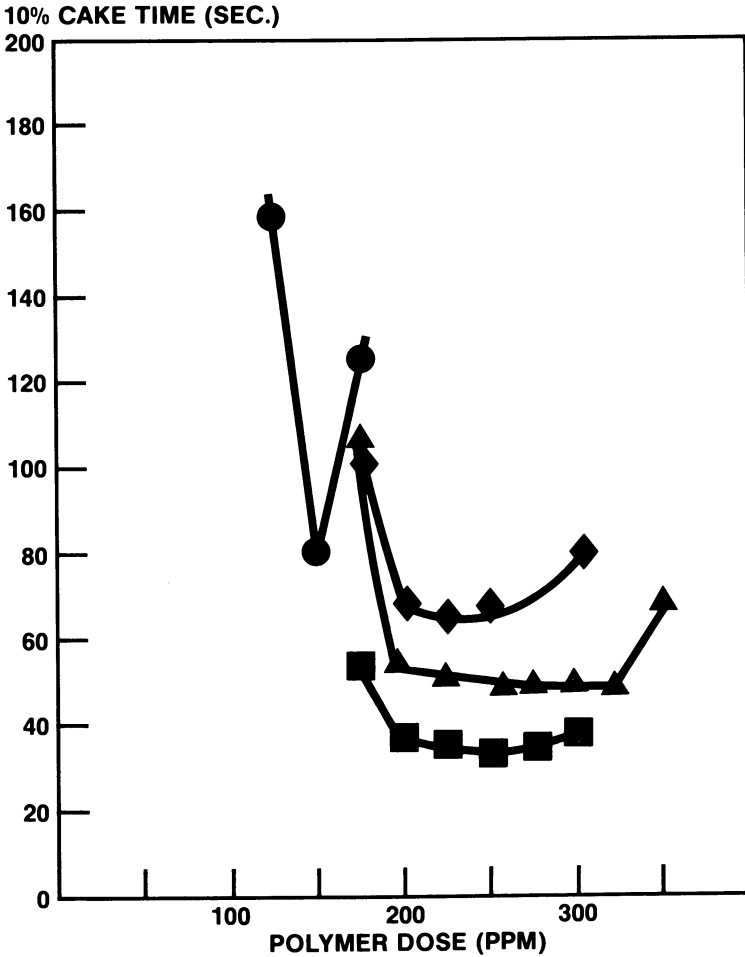


Figure 10. Buchner Funnel evaluation of emulsion copolymers on 75% raw/25% waste-activated sludge blend ((●) no TAMAC—solution; emulsions: (◆) no TAMAC; (■) 0.2 mol % TAMAC; (▲) 0.4 mol % TAMAC)

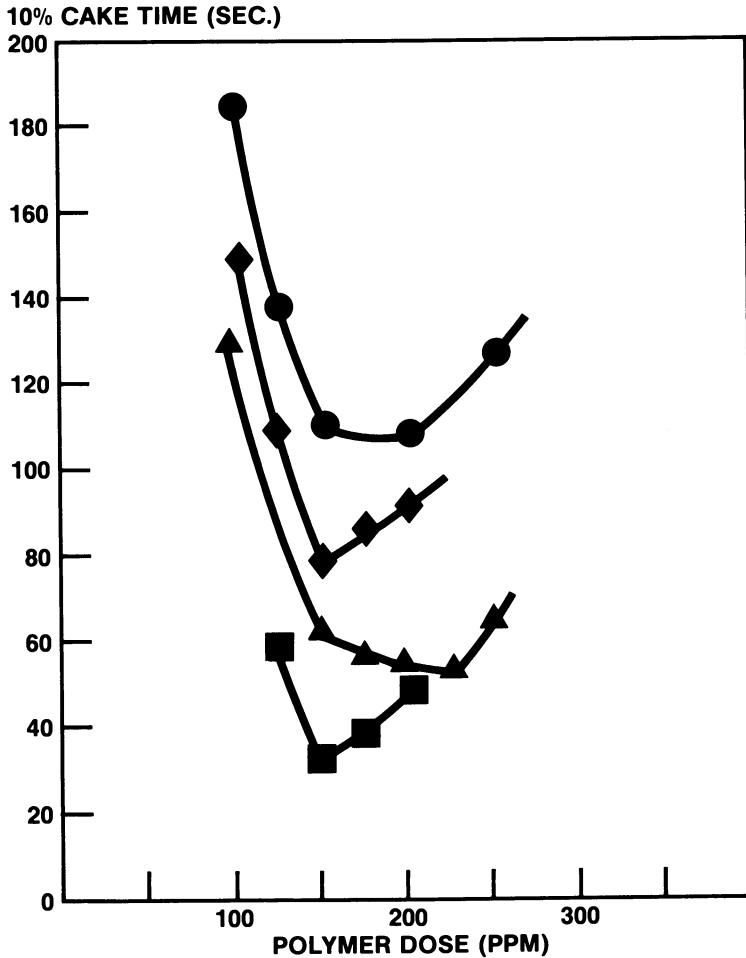


Figure 11. Buchner Funnel evaluation of emulsion copolymers on 50% raw/50% waste-activated sludge blend ((●) no TAMAC—solution; emulsions: (◆) no TAMAC; (■) 0.2 mol % TAMAC; (▲) 0.4 mol % TAMAC)

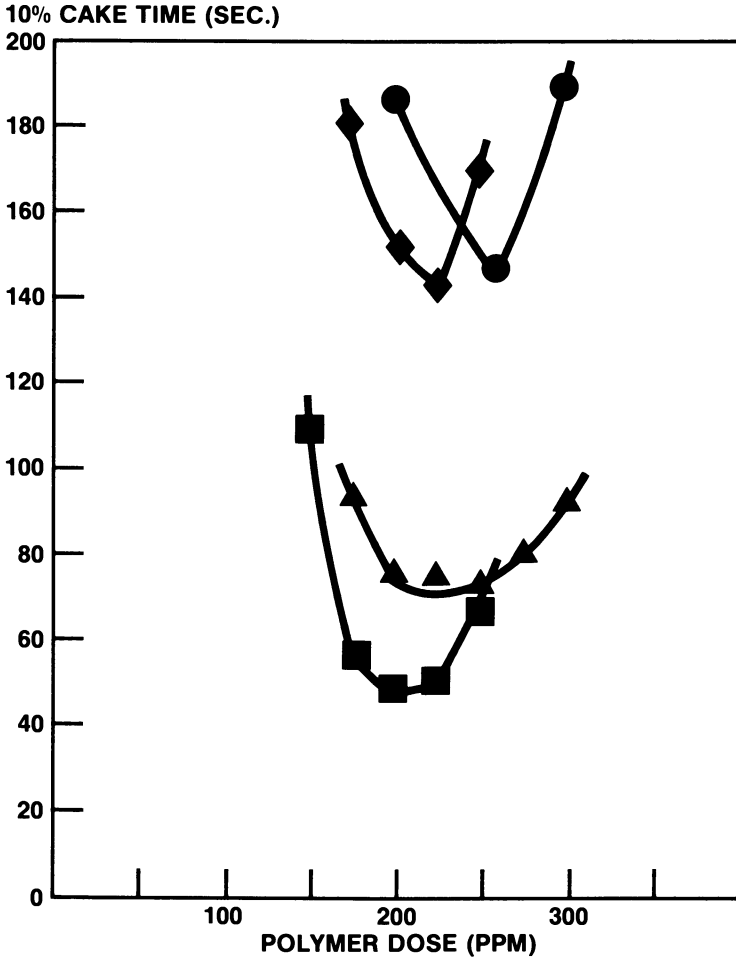


Figure 12. Buchner Funnel evaluation of emulsion copolymers on 25% raw/75% waste-activated sludge blend ((●) no TAMAC—solution; emulsions: (◆) no TAMAC; (■) 0.2 mol % TAMAC; (▲) 0.4 mol % TAMAC)

DEWATERING RATE PARAMETER

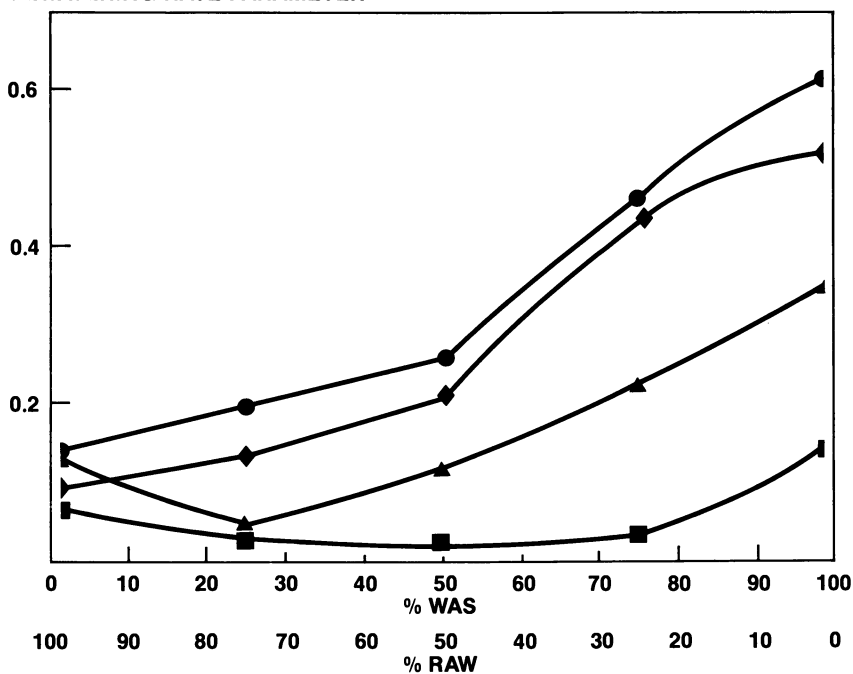


Figure 13. Dewatering rate parameter vs. sludge composition ((●) no TAMAC—solution; emulsions: (◆) no TAMAC; (■) 0.2 mol % TAMAC; (▲) 0.4 mol % TAMAC)

Summary

Therefore, we can state that branching enhances polymer efficiency in dewatering activated sludges. An optimum degree of branching produces the best dewaterability. This effect is specific to waste-activated sludges.

The branching phenomenon is independent of both polymer type—polyDADMAC vs. polyAMBTAC and polymer composition—homopolymer vs. copolymer. In addition, it is also independent of the type of branching agent used.

Acknowledgment

We wish to thank Roger Sigler and John Wiernik for conducting all performance testing and Randel Stong for his work in the development of the empirical filtration model.

Literature Cited

1. Karr, P. E.; Keinath, T. M. "Influence of Particle Size on Dewaterability," *J. Water Pollut. Control Fed.* 1978, 50(8), 1911–1930.
2. Novak, J. T.; Becker, H.; Zurov, A. "Factors Influencing Activated Sludge Properties," *J. Environ. Eng. Div. Am. Soc. Civ. Eng.* 1977, 103, EE 5, 815–828.
3. Parker, D. S.; Kaufmann, W. J.; Jenkins, D. "Physical Conditioning of Activated Sludge Flocc," *J. Water Pollut. Control Fed.* 1971, 43(9), 1817–1833.
4. Randall, C. W.; Turpin, J. K.; King, P. H. "Activated Sludge Dewatering Factors Affecting Drainability," *J. Water Pollut. Control Fed.* 1971, 43(1), 102–120.
5. Ryssov-Nielson, Henning M. SC. "The Role of Natural Extracellular Polymers in the Bioflocculation and Dewatering of Sludge," *Vatten* 1975, 31(1), 33–39.
6. Process Design Manual for Sludge Treatment and Disposal, U.S. Environmental Protection Agency Technology Transfer, EPA 621/1-74-006, Chapters 3, 6, and 7.
7. Flock, H. G.; Rausch, E. G. In "Water Soluble Polymers," *Polym. Sci. Technol.* 1973, 2, 21–73.

RECEIVED October 16, 1978.

Dielectric Properties and Electret Behavior of Complexed Polyethers

R. E. WETTON and D. B. JAMES

Department of Chemistry, Loughborough University,
Loughborough, Leicestershire, U.K.

F. P. WARNER

Polymer Laboratories Ltd., Church Stretton, Salop, U.K.

Polyethers were found to form complexes with many simple metal salts. The resulting materials are tough thermoplastics if the starting polymer molecular weight is high. High dielectric constant (~ 1000) and loss values (~ 300) are exhibited by some of these systems in appropriate temperature ranges. Detailed results of audio frequency bridge measurements and thermal discharge current measurements are reported for the polypropylene oxide/zinc chloride systems. A rearranging complex model is proposed to fit the established facts, and uses of these materials are discussed.

We have found that a wide range of metal salts will coordinate and chelate with polyethers to give single-phase thermoplastics. A common occurrence (1, 2) in these systems is for the glass transition (T_g) to be highly elevated—up to 140°C in some cases. This aspect of the subject of molecularly dispersed salts in polymers can be found in Ref. 2.

High molecular weight polymers combined with the appropriate salt are tough materials capable of forming into films. One of a number of interesting phenomena exhibited by these systems is their high dielectric constant (ϵ') and loss (ϵ'') values over certain temperature regions. These properties together with their areas of application are the main focus of this chapter.

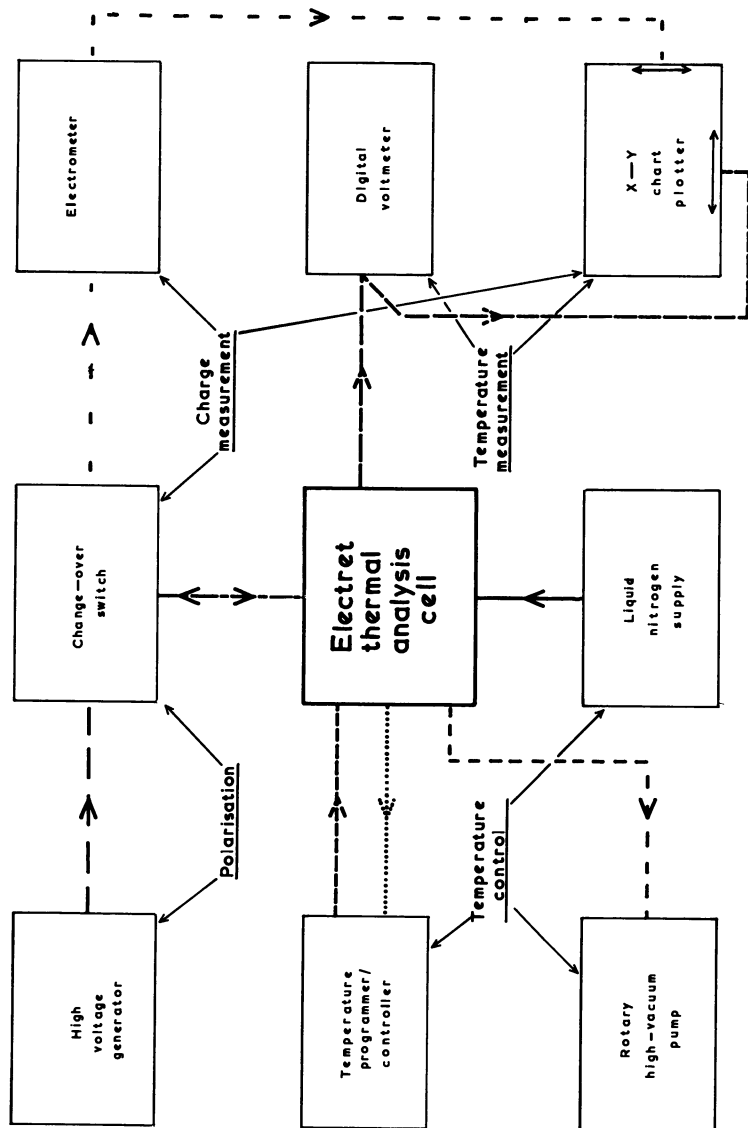


Figure 1. Block layout of electret thermal analysis instrument. The sample is polarized at high temperature, cooled, and the thermal discharge current monitored at a programmed rate of heating.

Experimental

Complexes of the appropriate polymer/salt systems were produced by dissolving the salt and polymer in a common solvent (for example, methanol) or solvent mixture. The polyether used in the present work was commercial poly(propylene oxide) (PPO) manufactured by Hercules Powder Co. under the name Parel 58. It had a M_n of 350,000 and was noncrystallizable because of approximately 40% head-head linkages and 5% allyglycidyl ether comonomer in the chain. The two solutions were mixed, and thin sheets (≈ 1 mm thick) were prepared by casting onto Teflon plates with solvent removal under dry nitrogen/vacuum. When necessary the temperature was raised to preserve mutual solubility throughout the solvent-removal stage. All chemicals and solvents used were free of water. The anhydrous conditions are necessary because water will generally coordinate to the metal salt in preference to the ether oxygens.

Dielectric measurements on discs cut from these sheets were performed under dry nitrogen or vacuum in a three-terminal, temperature-variable cell, based on the commercial Wayne Kerr Cell and using the Wayne Kerr Universal Transformer Ratio Arm Bridge with External Audio Frequency Oscillator and Detector as described by us previously (4). Thermal discharge current measurements are reported on a thermal scanning prototype (5) of an instrument shown schematically in Figure 1. The polymer disc is subjected to a polarizing voltage V_p at a polarization temperature T_p , which is normally above ambient. The sample is cooled with the field "on" until a suitable low temperature is reached when it is shorted through a sensitive picoammeter. Thermal discharge currents are recorded as the temperature of the sample is scanned upwards.

Results and Discussion

The basic features of the dielectric behavior of these polyether systems at 2 kHz can be seen in Figure 2 where $\log \epsilon'$ is plotted vs. temperature for the case of PPO with zinc chloride as the chelated salt. Unmodified PPO at this frequency exhibits a β relaxation at low temperatures (-110°C) and a step related to the α process (T_g) at about -50°C . Thereafter the dielectric constant decreases with temperature in accordance with the Debye term ($\mu^2/3kT$) for dipolar polarization, with added effects attributable to restricted chain conformations as discussed by Williams (6). This simple behavior is modified dramatically by the introduction of coordinated salts; the behavior at the 4% level is attributable to the following factors. Between -50° and 10°C a protracted α process is observed ending in a rather indefinite first plateau in ϵ' between 10° and 40°C . This is the T_g relaxation of chains containing 9% of nearest neighbor oxygens chelated to zinc chloride, but with these units dispersed randomly in positions along the chain to give an overall chain that is effectively a random copolymer of chelated and unchelated units. This concept explains the temperature dependence of T_g rather

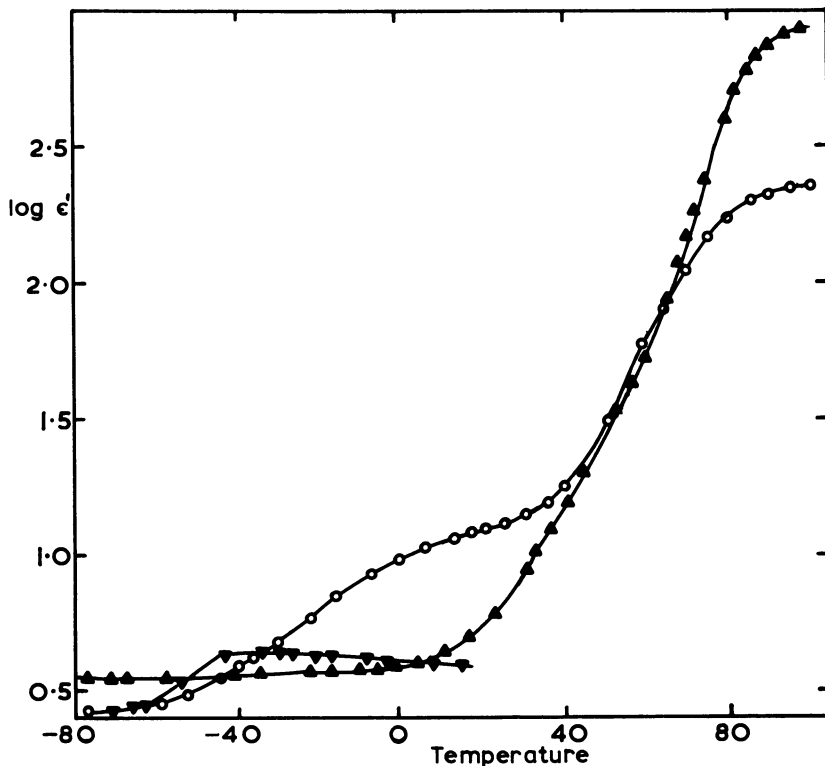


Figure 2. Log (dielectric constant) vs. temperature for selected PPO-ZnCl₂ systems. The normal T_g process can be seen at lower temperatures and the α' process at higher temperatures: (▼) 0 mol %; (○) 4.4 mol %; (▲) 18.0 mol %.

neatly and is supported by a mass of other evidence such as IR spectra, x-ray diffraction, and dynamic mechanical data. The dielectric constant value in the first plateau region is substantially greater than 10 and reflects the high dipole moment of the coordinated units. Using the Fröhlich equation (7), the resultant dipole moment of the coordinated unit, shown in Figure 3, may be evaluated from the relaxed and unrelaxed dielectric constant values shown in Table I.

At low concentrations of chelated units a consistent value of 7.5 D is obtained for the dipole moment. However, above 8.7 mol % of added salt the value falls, presumably because of strong dipole interaction effects as these highly dipolar units become more closely spaced along the chain.

Referring again to Figure 2, it is seen that the dielectric constant finally climbs to a plateau value of approximately 600 in what we have

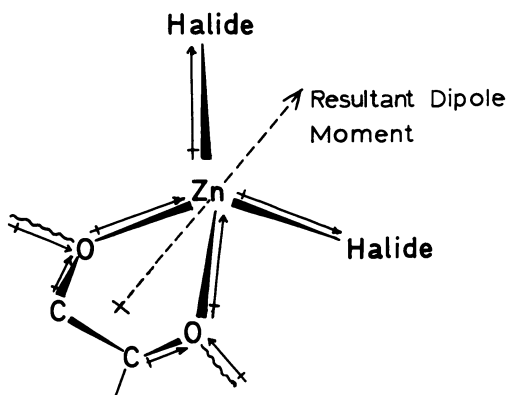


Figure 3. Chelate formed between two neighboring main-chain oxygens and $ZnCl_2$ showing direction of resultant dipole

Table I. Dipole Moment of Chelate Structure

Mol % $ZnCl_2$	ϵ_V	ϵ_R	$Ng\mu^2 \times 10^{14}$ (erg)	$N \times 10^{-20}$ (dipolar groups/cm ³)	$\mu(D)$
2.20	4.50	8.30	1.29	2.27	7.5
4.40	4.50	12.6	2.54	4.58	7.5

termed the α' process. An exhaustive investigation of the system by small- and wide-angle x-ray diffraction techniques indicates that these chelated systems are single phase above 5 mol % of added salt. We have also verified that field strength has no effect on the relaxation process and that changing the electrode type produces only small effects. For reasons that will be discussed later, it is believed that this process originates from additional polarization of the chelated structures attributable to localized migration of the other ligand, in ionized form, that is, Cl^- in the present case. Such a mechanism is suggested in Figure 4.

Progressive changes in the dielectric behavior are found with increasing metal salt concentration, with the α process rapidly increasing in its temperature location until at 18% it is amalgamated completely with, or obscured by, the α' process which then dominates the dielectric response. Frequency plane data for this α' relaxation in the 18 mol % zinc chloride sample are shown in Figure 5. The relaxation is much sharper than a normal main-chain relaxation with the data giving excellent Cole-Cole (8) circular arc plots with the breadth parameter = 0.14. This reflects

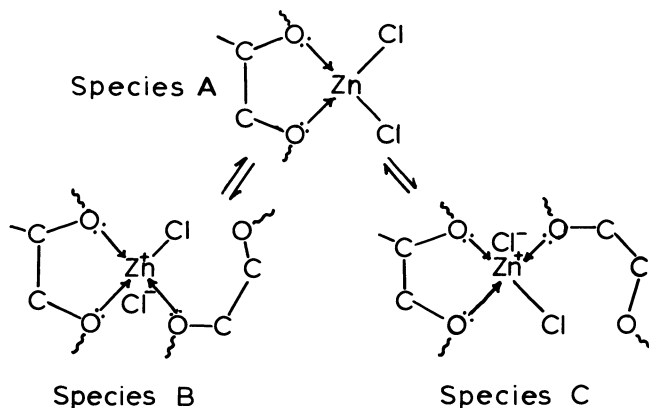


Figure 4. Possible rearrangement mechanism for ionized form of complex giving rise to the α' relaxation

that the curves are getting close to the Debye limit, when the breadth parameter is zero. The values of dielectric loss observed in the peak regions are higher than normally observed in single-phase polymers by a factor of several hundred.

In considering the mechanism for this extremely large polarization process the following observations are pertinent. The strength of the α' process reaches a maximum at about 20 mol % of added zinc chloride as shown in Figure 6, despite the fact that 30 mol % of salt can be accommodated before a second phase is formed. Low levels of water absorption destroy the relaxation process and produce conductivity effects at low frequency. This together with the lack of field and thickness dependence indicates fairly strongly that this relaxation is not a disguised conductivity effect. It is related to a configurational rearrangement of ionic forms of the complexes. One possible process involving localized displacement of Cl^- is shown in Figure 4. The process, as shown, requires the cooperation of an additional ether group, and a mechanism such as this would explain two curious facts, namely, (a) that the α' relaxation strength peaks before complete coordination has been achieved and (b) that the activation energy for the process increases continuously with concentrations of metal salt. The activation energy starts at a very low value for a cooperative process on the order of 60 kJ mol^{-1} and increases to 170 kJ mol^{-1} at 30 mol % zinc chloride, which is the level of complete coordination. The concentration of possible polar species will decline as the system is depleted of uncoordinated oxygens. Similarly, the activation energy for rearrangement will increase since the necessary additional oxygen has to come from further afield to coordinate.

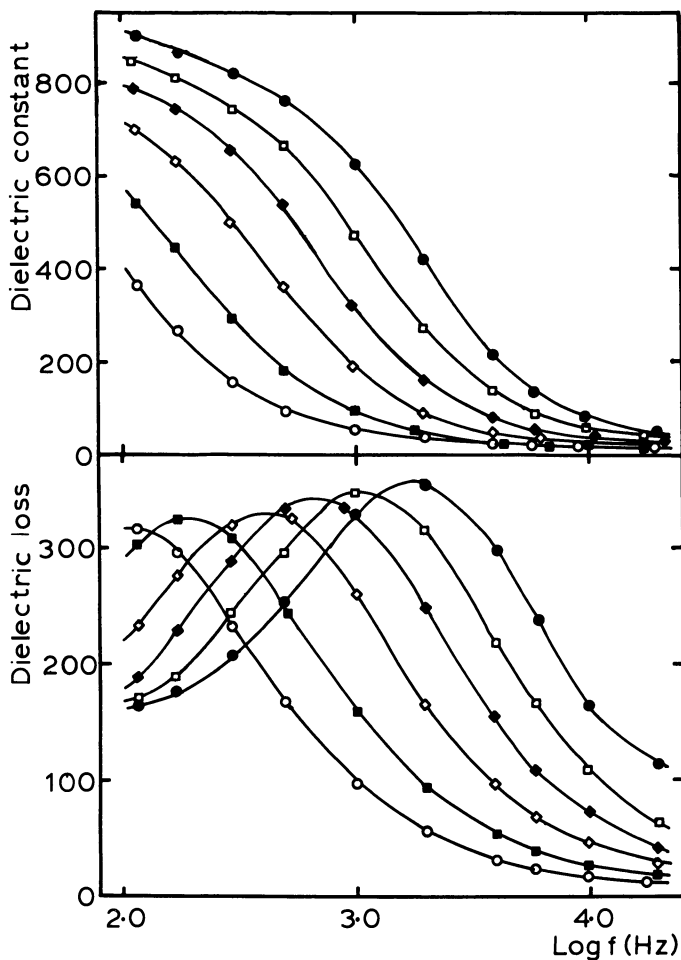


Figure 5. Dielectric constant (ϵ') and loss (ϵ'') in the frequency plane in the region of the α' relaxation (PPO + 18.0 mol % ZnCl_2 ; α' relaxation—(○) 55.0°C; (■) 60.0°C; (◇) 65.0°C; (◆) 70.0°C; (□) 75.0°C; (●) 80.0°C)

Thermal discharge currents exhibit behavior parallel to low-frequency dielectric loss as a function of temperature. This is shown clearly in Figure 7 for the case of the 2 mol % zinc chloride content PPO. Both i and ϵ'' show three relaxation regions, with the temperature locations normally displaced to lower values in the case of the current curve because of the dc nature of this measurement. However, this generalization is not always true as can be seen from a comparison of Tables II and III. At low salt concentrations the lowest temperature relaxation

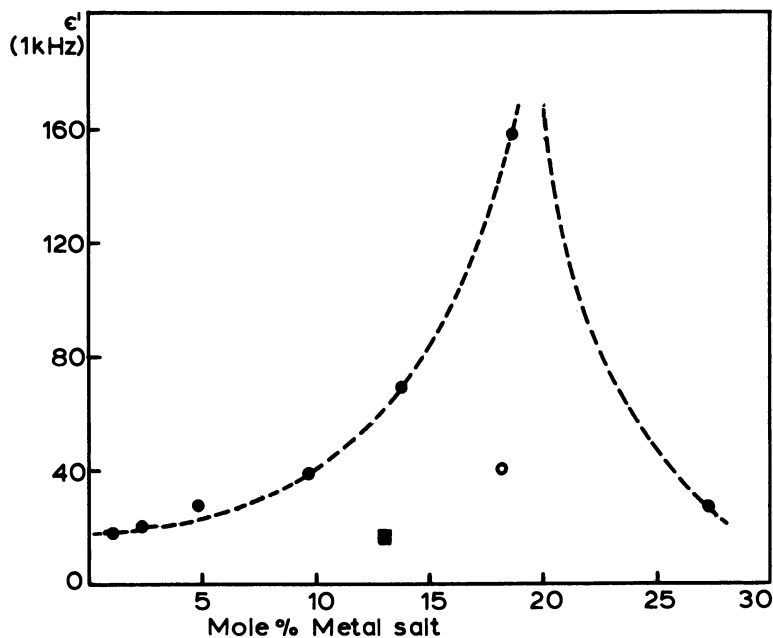


Figure 6. Dielectric constant values corresponding to the peak values of $\tan \delta$ in the T plane (as an approximate relaxation strength variable) as a function of salt concentration: (●) ZnCl_2 ; (○) ZnBr_2 ; (■) ZnI_2 .

Table II. T_g Relaxation

Mol % ZnCl_2	$T(\text{electret})^\circ\text{C}$ ($5^\circ\text{C}/\text{min}$)	$T_g(\text{DSC})^\circ\text{C}$ ($15^\circ\text{C}/\text{min}$)	$T_g(\text{dielectric})^\circ\text{C}$ (1 kHz)
0	-71	-64	-54.8
1.09	-68	-62	-53.3
2.22	-64	-61	-52.3

Table III. High-Temperature Relaxation

Mol % ZnCl_2	$T(\text{electret})^\circ\text{C}$ ($5^\circ\text{C}/\text{min}$)	$T_g(\text{dielectric})^\circ\text{C}$ (1 kHz)
4.40	65	41.9
8.72	67	40.9
13.3	73	47.4
18.0	88	57.5
27.0	83	68.8

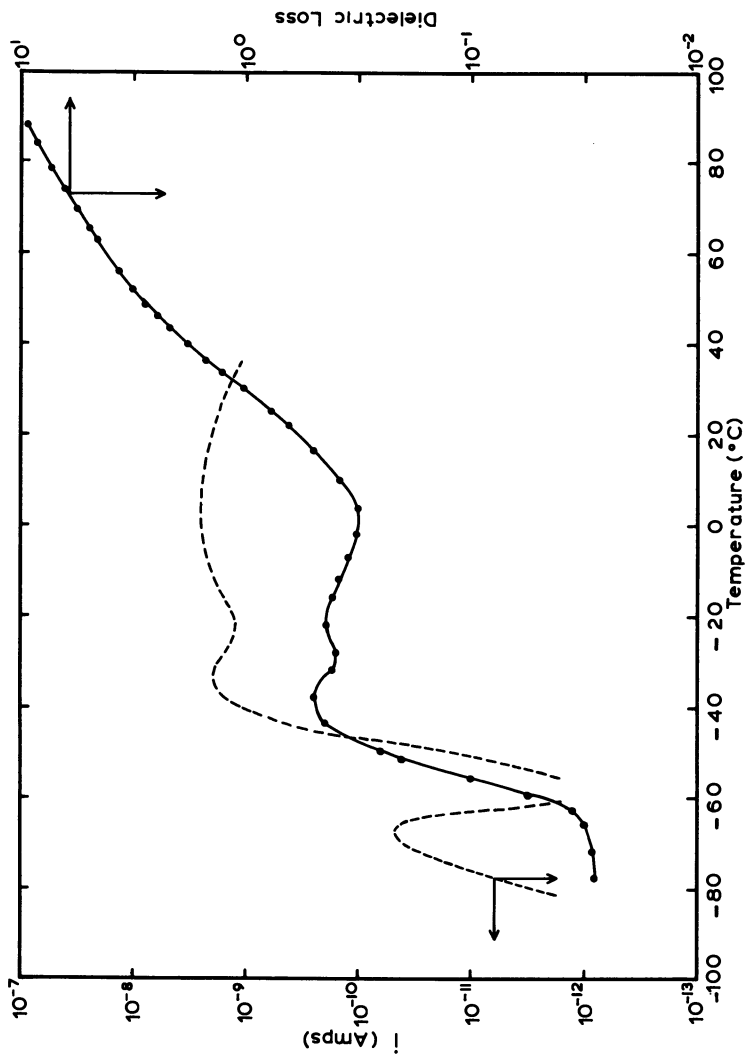


Figure 7. Comparison of thermal discharge currents (---) with ϵ'' for PPO containing 2% $ZnCl_2$:
 (---) electret; (●—●) dielectric

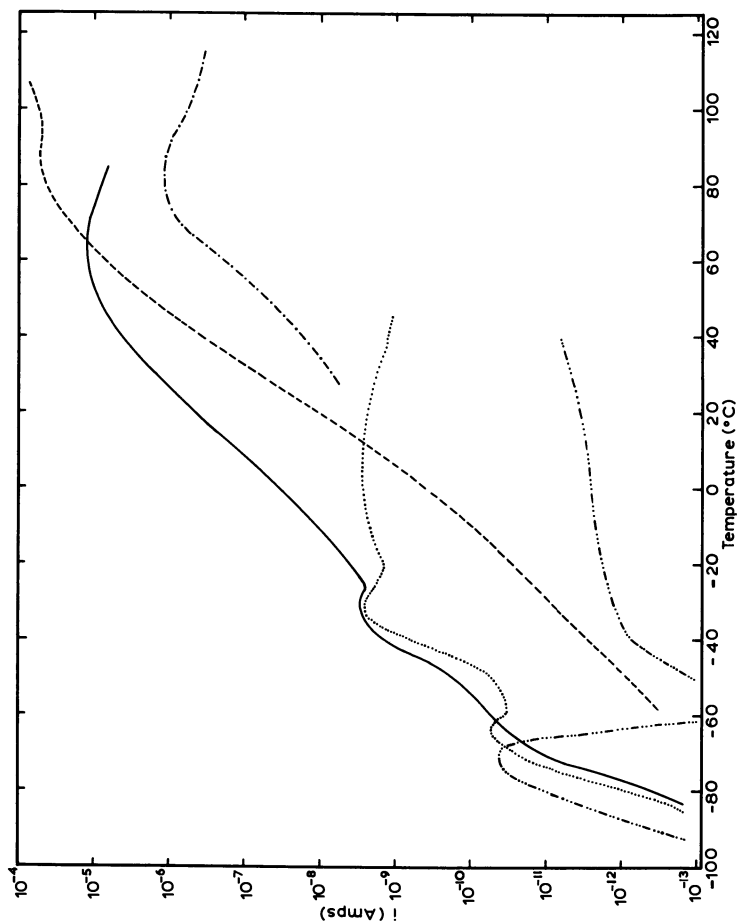


Figure 8. Thermal discharge currents for a series of ZnCl_2 -containing PPO samples. Comparison of relaxation locations are given in Tables II and III. Field strength 2 kV/cm; $T_p = 40^\circ\text{C}$; heating rate $5^\circ\text{C}/\text{min}$; mol % ZnCl_2 : (— \cdot - \cdot -) 0; ($\cdot \cdot \cdot$) 2.2; (—) 4.4; (---) 18.0; (- \cdot - \cdot -) 27.0.

process is still that of uncomplexed chains (Table II), the central process is attributable to motion of the complexed units, and the high temperature relaxation is associated with complex breakdown (Table III).

In thermal discharge measurements the time integral $\int_0^\infty i dt$ represents the total charge stored in the electret at the moment of shorting. As this is a constant for a given sample and given polarization conditions, the current magnitude is proportional to the rate of thermal scanning in the same way that DTA peaks are rate sensitive. All data reported in this chapter were taken at a standard $5^\circ\text{C}/\text{min}$ heating rate. The overall picture of thermal discharge behavior as a function of metal salt concentration is shown in Figure 8. The maximum discharge current is exhibited by the 18 mol % zinc chloride sample and an increase of salt then reduces the peak maximum, again parallel to the magnitude of dielectric relaxation strength. All data in Figure 8 were obtained for discs polarized under constant conditions of $T_p = 40^\circ\text{C}$ and $V_p = 200\text{ V}$ (field = $2\text{ kV}/\text{cm}$). Thus it is premature to state that the discharge current maximum will lie always at the 18 mol % zinc chloride level. Figure 9, for example, indicates, as expected, that increasing polarization temperature at these relatively low temperatures increases the total polarization

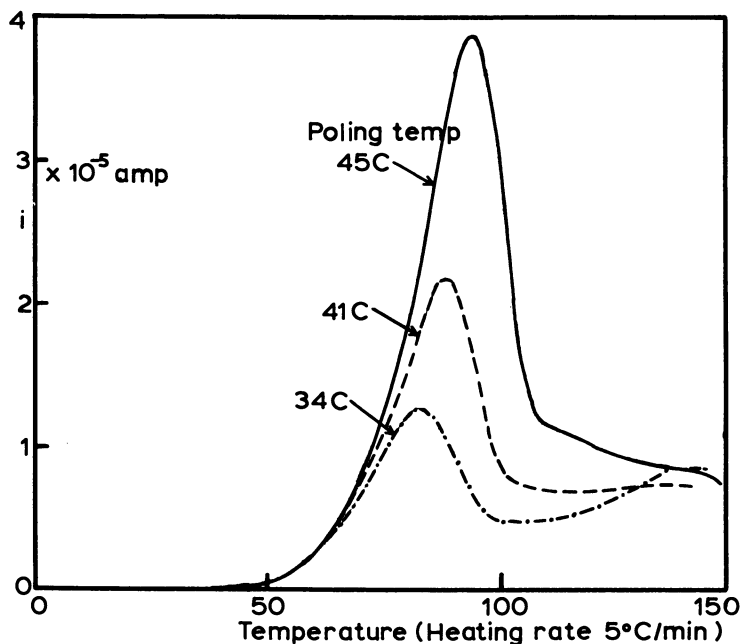


Figure 9. Effect of poling temperature on thermal discharge currents for the 16-mol % ZnCl_2 in PPO (field strength $2\text{ kV}/\text{cm}$, heating rate $5^\circ\text{C}/\text{min}$)

Table IV. Charge Storage/Lifetimes of Some Polymer Electrets

	<i>Charge</i>	<i>Half-Life (20°C)</i>
18% ZnCl ₂ in PPO	.072 C	10 ⁵ min 69 days
27% ZnCl ₂ in PPO	.0029 C	1.3 × 10 ⁴ min 9 days
PVF ₂	2.1 μC	25 mins

and hence the discharge current peak. This enhancement with increased polarization temperature eventually gives rise to a decline when the samples become significantly conductive (typically ~ 100°C).

It is not our intention to enter into a detailed discussion of the thermal discharge current data at this stage, but rather to point out the broader significance of these results. The data in Figure 8 indicate that at the higher salt loadings the major part of the charge should be stable at room temperature. In related salts this effect can be enhanced to give powerful polymer electrets. The major drawback in the development of this material for commercial use is its water sensitivity. Table IV compares the lifetime and charge storage capabilities of similarly sized polymer discs of a number of relevant polymers under ambient conditions.

Polymer Laboratories Ltd. (U.K.) is developing applications of related complexed material to capacitors and dielectric heating.

Acknowledgment

Financial support from the Science Research Council for part of this work is gratefully acknowledged.

Literature Cited

1. Wetton, R. E.; James, D. B.; Whiting, W. *J. Polym. Sci., Polym. Lett. Ed.* **1976**, *14*, 577.
2. James, D. B.; Wetton, R. E.; Brown, D. S. *Polymer* **1979**, *20*, 187.
3. James, D. B.; Wetton, R. E.; Brown, D. S. *Polym. Prepr., Am. Chem. Soc., Div. Polym. Chem.* **1978**, 358.
4. Fielding-Russell, G. S. *Ph.D. Thesis, Loughborough University*, 1967.
5. Wetton, R. E. Electret Thermal Analyses of Polymers, *Society of Chem. and Ind. Meeting, Bradford, U.K.*, 1979.
6. Williams, G. *Trans. Faraday Soc.* **1965**, *61*, 1564.
7. Fröhlich, J. G. "Theory of Dielectrics"; Oxford University Press: London, 1958.
8. Cole, K. S.; Cole, R. H. *J. Chem. Phys.* **1941**, *9*, 341.
9. U.K. Patent Application 35 990/76; U.S. Patent Application 828 607.

RECEIVED December 8, 1978.

The Viscosity Enhancement of Polyethers by Salts

A. EISENBERG, K. OVANS, and H. N. YOON

Department of Chemistry, McGill University, 801 Sherbrooke St. W.,
Montreal, Quebec, Canada H3A 2K6

The viscosity enhancement in low molecular weight poly(ethylene oxide) and poly(propylene oxide) resulting from dissolution of LiClO_4 was measured as a function of molecular weight and salt content. It is shown that on a $\log \eta$ vs. temperature plot, the viscosities for various salt contents yield lines of identical shape that can be superimposed by simple shifts along the temperature axis to yield a master curve for each molecular weight. Furthermore, by additional vertical shifting one can obtain a single master curve for all molecular weights and salt contents studied here, for each of the two families of polymers. Between about 3 and 13 mol % the increase in viscosity is attributable mainly to the increase in the glass transition temperature. Below that region another mechanism must be operative, since the glass transition rises only very slowly while the viscosity rises appreciably.

In the past few years considerable effort has been devoted to the investigation of the structure and properties of ion-containing polymers. This effort has been manifested in a substantial upswing in the number of publications and symposia dealing with this field. Undoubtedly, this high level of interest is attributable not only to the many industrial applications of these materials, but also to the fact that they present a range of challenging problems to the polymer chemist, quite aside from their potential applications. Because of the recent appearance of two books (1, 2) dealing with ion-containing polymers, no review of the subject will be presented here. Suffice it to say that the ions tend to

aggregate in media of low dielectric constant, and that this aggregation leads to a profound modification of the properties of the parent polymers, even at low ion contents, both in solution and in bulk.

To date, much of the effort in this field has been devoted to a study of ionic copolymers based on ethylene, styrene, or the rubbers (1, 2). More recently, other families of ionomers have come under study, for example, the aromatic (3) or asphalt ionomers (4) as described in this symposium, or those based on the ethyl acrylates (5) or the ionenes (6), to mention just a few. In all of these materials the ionic groups are attached by covalent bonds to the chain. However, there is another way of incorporating ions into polymeric materials, that is, by dissolving salts of relatively low lattice energy, such as LiClO_4 , in polyethers. It was recognized quite early that these mixtures exhibit polyelectrolyte properties in methanol solutions (7, 8), and that their properties are very different from those of the bulk parent polymer (9) in that the glass transition temperature (T_g) is elevated by the presence of the salt, and the rheological properties are influenced profoundly. More recent studies (10, 11, 12) have confirmed these findings.

More specifically, in the work of Moacanin and Cuddihy (9), which centered on the poly(propylene glycol)–lithium perchlorate system and which forms one of the points of departure for this work, it was shown that T_g rises with the addition of the salt—initially linearly at the rate of about $5.5^\circ/\text{mol } \%$, with the rate increasing at about 20 mol % of the salt. The dynamic mechanical properties of these systems were very different for polymers of different molecular weights. Thus, for the low molecular weight materials (mol wt \simeq 2000), both the modulus and the loss tangent reflect primarily the increase in the glass transition, while for the polymer of high molecular weight, behavior typical of a phase-separated (or clustered) system was observed. The densities were found to be nonadditive, suggesting a strong interaction between the small ions and the chain dipoles.

In the study of Hannon and Wissbrun (10), which forms another point of departure for this work, a range of properties was investigated for the phenoxy–calcium thiocyanate system. The glass transition was observed to increase at a rate of $1.8^\circ/\text{mol } \%$ salt; this, and the absence of negative deviations from additivity of specific volume, suggests that the interactions here are weaker than those in the systems studied by Moacanin and Cuddihy. The viscosity behavior reflected exclusively the increase in T_g . A strong shear-rate dependence of the viscosity was observed over the entire 40° range (170° – 210°C) studied, and even at the lowest shear rates ($3 \times 10^{-1}\text{sec}^{-1}$) the curves did not approach zero shear behavior. The samples could not be studied above 210°C because of incipient decomposition.

A very recent study by Wetton, James, and Whiting (12) focused on

the glass transition behavior of poly(propylene glycol) with transition metal chlorides. In contrast to the behavior found by Moacanin and Cuddihy, the glass transition was found to rise only very slowly at low salt contents, with the rate increasing considerably at intermediate loadings; at relatively high salt concentrations the rate of increase of T_g dropped again quite appreciably. More recent efforts by the same group are presented elsewhere (13, 14).

While it has been known for a long time that the addition of salts to polyethers enhances the viscosity of the solution, aside from the work of Hannon and Wissbrun on a weakly interacting and non-Newtonian system, no quantitative information has been available on that effect in the strongly interacting materials like the PPO-LiClO₄ solutions. Therefore, the present work focuses on a study of the viscosity-temperature behavior of a polymer-salt system that was not complicated by non-newtonian behavior or by thermal decomposition (as shown by the reproducibility of the results on cooling from high temperature). The interactions in this system were known to be strong, and the viscosity enhancement could be studied over wide ranges as a function of the salt content, the polymer molecular weight, and the oxygen to carbon ratio of the host polymer. For this purpose, the low molecular weight oligomers of poly(ethylene oxide) (PEO) and poly(propylene oxide) (PPO) were selected, the salt being LiClO₄. The variation in the number of carbon atoms along the chain between the oxygen atoms has been explored already (13, 14), and thus is not addressed in this work. Furthermore, in order to explore the tie-in between the rise in the glass transition and the viscosity, the T_g 's of the noncrystalline polymers were studied also, that is, those based on PPO. This chapter reports the first phase of this investigation, that is, the study of the viscosity and the glass transition. Theoretical aspects of the work are left for the future.

It is worth recalling that polymer-salt interactions in systems other than the polyethers also have been explored, primarily in highly crystalline materials. However, they will not be reviewed here because of the dissimilarity of those polymers and the preliminary nature of this report. It should also be mentioned that the effect of salts in increasing the viscosity of the polyethers has been described in the commercial literature on these materials, but the information is of a qualitative nature only.

Experimental

Sample Preparation. The polymers used in this study were obtained from Union Carbide (Carbowax 400 (PEO) and poly(propylene glycol) 400 and 1000), from Polyscience (poly(ethylene oxide) 1500 and poly(propylene glycol) 4000), and from J. T. Baker (poly(ethylene glycol) 4000 and 6000). For the sake of simplicity, all the polymers based on

ethylene oxide will be referred to as PEO while those from propylene oxide will be designated PPO. The polymers were dried under vacuum at 80°C for 2 hr before adding the LiClO₄. The latter had been dried for 24 hr at 125°C and stored under vacuum at 60°C prior to use. The dissolution process was carried out by mixing the salt directly with the polymer at 80°C under vacuum. While this procedure is somewhat more difficult than codissolution in a common solvent followed by evaporation of the solvent, it was preferable since no complications resulting from residual solvent would be present. Furthermore, no evidence of incomplete dissolution was encountered. If a sample had to be stored prior to the viscosity measurement, then it was vacuum dried again at 80°C.

Density Determinations. All densities were measured pycnometrically. Since the density and viscosity are related directly to each other, and since the technique used for viscosity measurements (see next section) did not yield data of a precision higher than about 1–3%, no attempt was made to keep the precision of the density measurement to better than 0.1%. Densities of the PPO system were not measured since they had been obtained by Moacanin and Cuddihy (9).

Viscometry. Two types of capillary viscometers were used throughout this work. One consisted of a bulb of known volume that was filled through a capillary of known dimensions under partial or high vacuum. This instrument was used in the range of 0.1–10 poise.

The other viscometer consisted of a straight capillary tube that was filled with the fluid, again under partial or complete vacuum. The height as a function of time was plotted logarithmically, and yielded a slope of 2. The latter technique represents a slight modification of the method used by Fox and Flory (15), the modification consisting of the abandonment of predetermined heights at which the times were measured. Another modification consisted of the calculation of a gravity correction, which was sometimes necessary if a partial vacuum was used to fill the capillary. The equations that give the height as a function of time for the capillary filling process are given in the Appendix, both with and without the gravity correction. The method was used in the range of 1–10⁵ poise.

Dynamic Mechanical Data. The T_g 's were determined using a vacuum torsional braid instrument, with 4-in. long fiberglass braids. The dry samples were deposited onto the braids and stored in PTFE containers under vacuum at 70°–80°C for 24–48 hr, depending on the salt content. After mounting in the instrument, the samples were again kept under vacuum for 12–18 hr prior to the start of the run. The samples were cooled to well below T_g and studied while they were warming up to room temperature at their natural heating rate (0.5°–2°C/min, depending on the temperature).

Results

Densities. Figure 1 shows the densities for several PEO–salt mixtures as a function of temperature. Within an accuracy of better than 1%, both $(\partial\rho/\partial T)_c$ and $(\partial\rho/\partial c_s)_T$ (ρ = density, c_s = salt content in mol %) were linear and independent of molecular weight over the entire

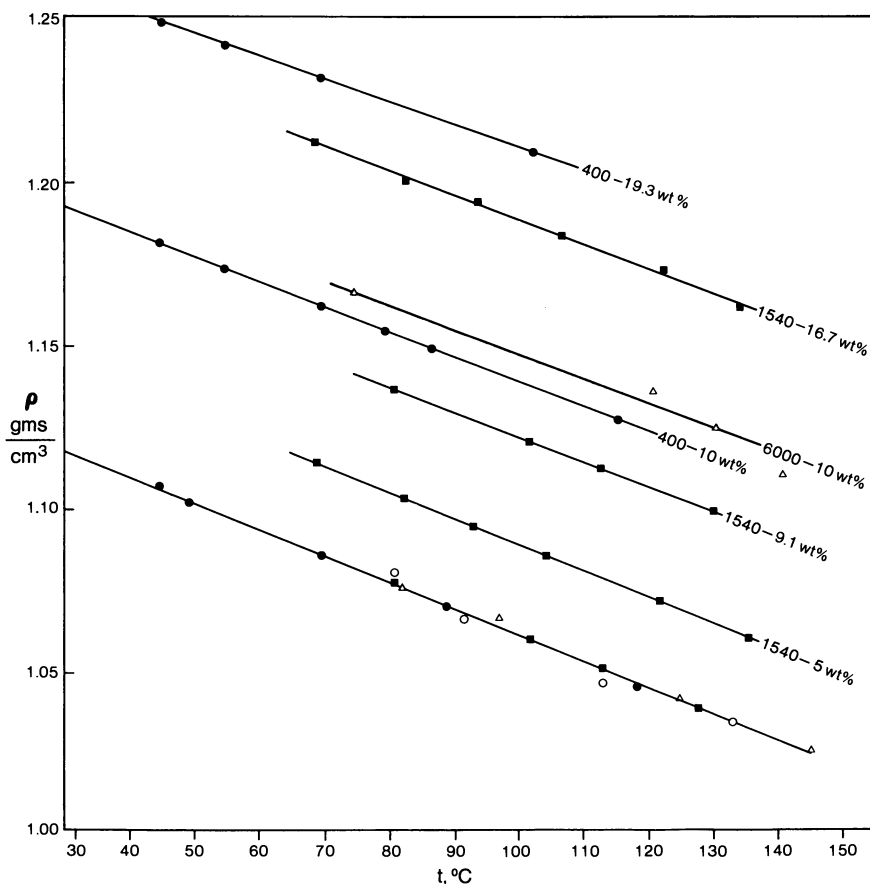


Figure 1. Density vs. temperature for the PEO samples. The bottom line gives the results for the pure polymer of various molecular weights: (●) 400; (■) 1540; (○) 4000; (△) 6000.

range studied so that interpolations could be used. Thus, it was not necessary to determine the density of each polymer at every salt content as a function of temperature. For the PPO system, the densities obtained by Moacanin and Cuddihy were used.

Viscosities. Figure 2 shows the viscosities as a function of temperature of the various PPO's studied. It was found that a simple vertical shift could superimpose all the graphs. The bottom curve for PPO 400 shows this superposition, since all the experimental points have been shifted arbitrarily down to it. The shift factors relative to the 400 sample (that is, η/η_{400}) are shown in Figure 3.

Figure 4 shows the viscosity as a function of temperature for the PPO 4000 sample containing 0, 2.9, 6.1, 9.6, and 13.6 mol % LiClO_4

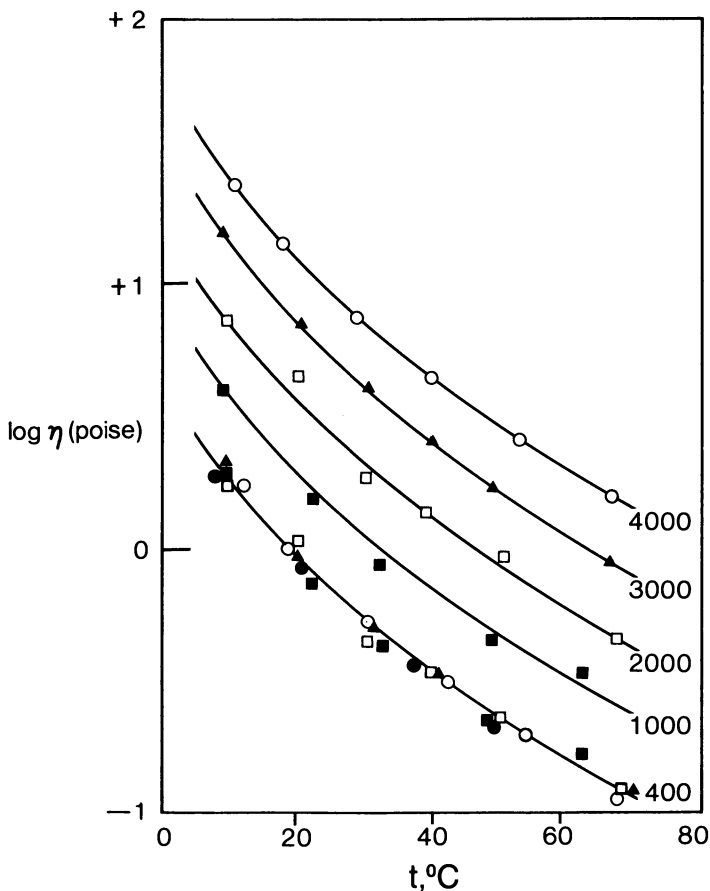


Figure 2. Viscosity vs. temperature for the pure PPO polymers of various molecular weights and the master curve for the system superimposed onto the curve for the pure polymer by vertical shifting

(based on 1 mol of the propylene oxide repeat unit, the weight percentages being 0, 5, 10, 15, and 20) in the temperature range of 10° – 80°C . Again it was found that shifting could bring about superposition. However, in this case the shifting had to be horizontal. The pure material was used as the reference state, and all the other curves were shifted relative to that one. The master curve is shown as the dotted line extending toward the low temperature region. This type of superposition was also observed to hold for the other salt samples, each of which generated a master curve. All of these master curves, in turn, could be superimposed by vertical shifting as described earlier for pure polymers. Thus, one single curve represents the viscosity–temperature relationship of the PPO samples of all molecular weights between 400

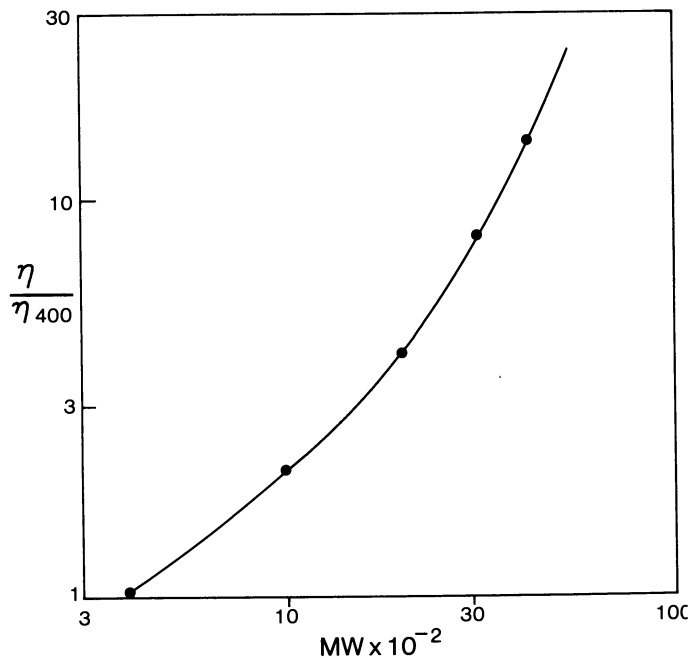


Figure 3. Plot of η/η_{400} (or vertical shift factor) vs. molecular weight for the PPO polymers

and 4000 and salt contents of 0–13.6 mol %. The shift factors for materials of different molecular weight were given already in Figure 3, while the horizontal shift factors for variations in salt content are shown in Figure 5.

In general, the observations made for the PPO system apply to the PEO system also, although the effects are smaller. Furthermore, since the materials remain crystalline up to about 50°C, viscosity data below that temperature could not be obtained. Figure 6 shows the results for the pure polymers, while Figure 7 gives the data for PEO 4000 for various salt concentrations as well as the master curve. The horizontal shift factors for the PEO system are given in Figure 8. Finally, a comparison of the PEO and PPO system is shown in Figure 9 in which the viscosities of the polymers of 4000 mol wt are plotted at 60°C as a function of the salt content. The same figure also shows the plot for PPO 4000 at 40°C for the sake of comparison.

Dynamic Mechanical Data. Figure 10 shows the loss tangent as a function of temperature for the PPO-400 samples with various salt contents, while Figure 11 shows the peak positions vs. salt content for PPO 4000, 2000, and 400. The results of Moacanin and Cuddihy for the 2000 sample are also shown as the dotted line.

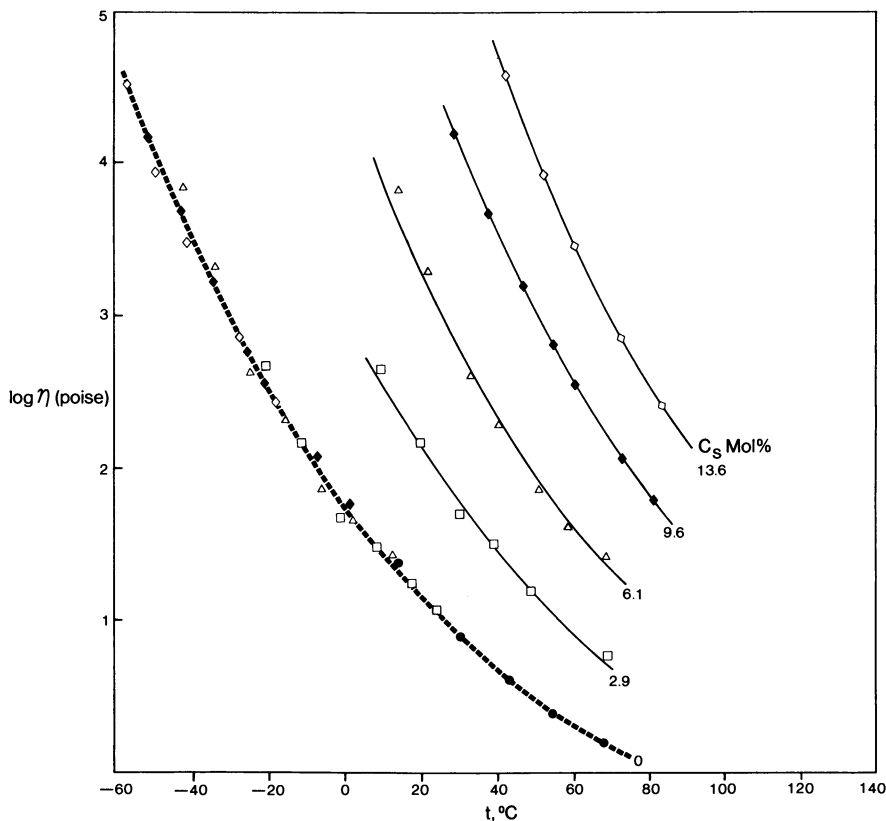


Figure 4. Viscosity vs. temperature for the PPO-4000 polymers with various LiClO_4 contents and the master curve for the system superimposed onto the curve for the pure polymer by horizontal shifting

Calculations and Discussion

Calculation of WLF Constants. Using the values of the glass transition obtained from the peak positions (Figure 11) along with the viscosity data (Figure 4) one can calculate the WLF constants (16) assuming that the viscosity at the T_g is 10^{13} poise. The numbers obtained in that way are given in Table I for PPO 4000, for which the most extensive data were assembled.

It is clear that the C_1 value is essentially constant over the entire salt concentration range. By contrast, the C_2 value for the pure polymer is considerably lower than that of the salt solutions, the latter showing only a relatively small change with salt content. Therefore, it seems reasonable to inquire whether, at least for the four salt solutions, the viscosity enhancement is attributable primarily to the increase in the glass transi-

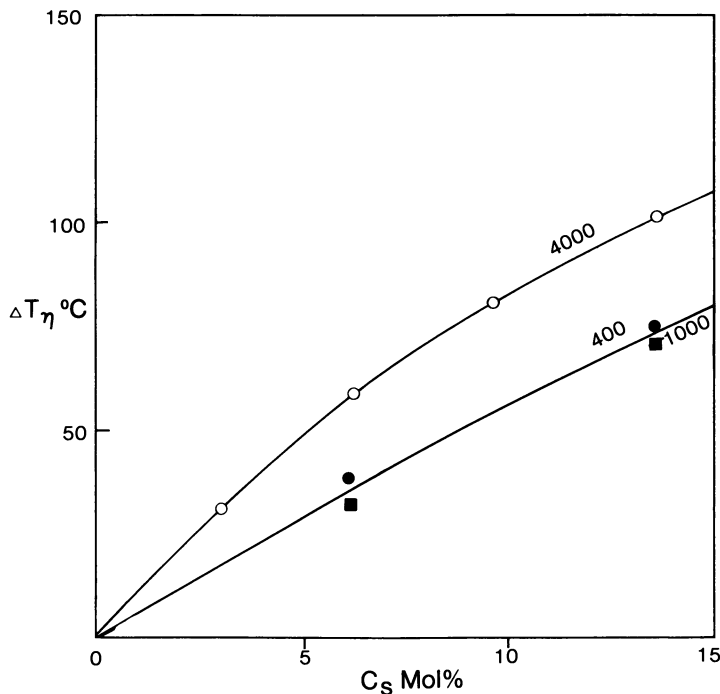


Figure 5. Shift factors vs. salt content for the PPO samples of various molecular weights

tion, or whether other effects predominate. The relation between the viscosity increase and the change in the glass transition can be seen best in a plot of ΔT_η (Figure 5) vs. ΔT_g (the difference in the glass transition of the salt solution and the pure polymer) for the same salt content. This comparison is shown in Figure 12. It is clear that for the salt solutions the increase in the viscosity is attributable primarily to the rise in T_g , just as it is for the phenoxy polymers (10, 11). However, this is not the case for the first few percent of salt since in changing C_s from 0 to 2.9 mol %, the increase in T_g is negligible, while ΔT_η rises by about 30°C. Thus, another effect must be operative in that region. At this

Table I. Glass Transitions and WLF Constants for PPO 4000

C_s (wt %)	C_s (mol %)	T_g (°C)	$-C_1$ (°C)	C_2 (°C)
0	0	-61.5	14.7	19.8
5	2.9	-58	15.5	32.8
10	6.1	-35	15.0	30.4
15	9.6	-14	14.7	29.2
20	13.6	+6.5	14.4	28.1

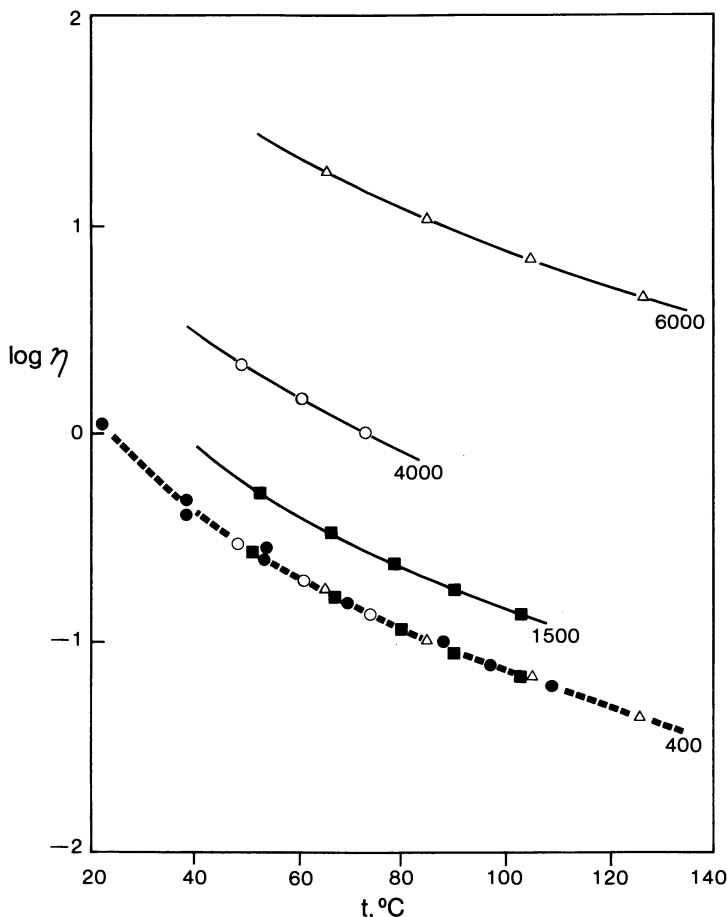


Figure 6. Viscosity vs. temperature for the pure PEO polymers of various molecular weights and the master curve for the system superimposed onto the curve for the pure polymer by vertical shifting

time, no definitive statements can be made concerning that effect. It is noteworthy that in spite of the existence of at least two factors which affect the viscosity (one of these being the increase in T_g), the superposition effect discussed previously seems to be operative over the entire salt concentration range.

Dynamic Mechanical Properties. The shapes of the curves in Figure 10 are characteristic of all the other materials for which they were measured in the course of this work. Most notably, the height of the peak for the 2.9-mol % sample (5 wt %) was always lower than that for any other salt content, and the curve for the 9.6-mol % sample (15 wt %) was always the broadest.

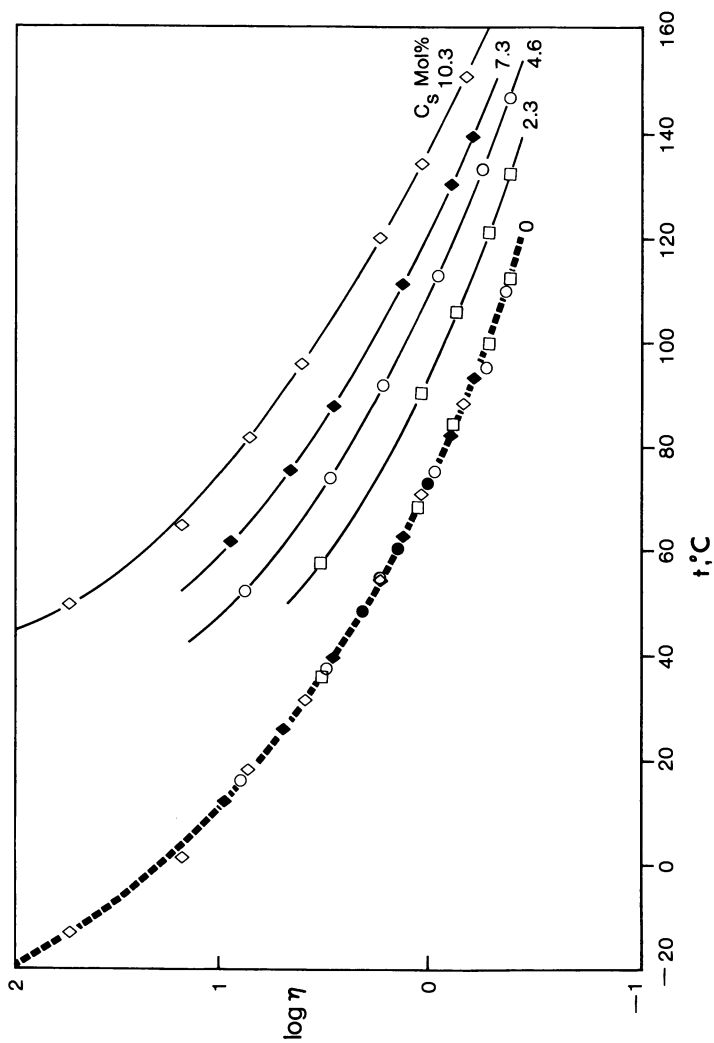


Figure 7. Viscosity vs. temperature for the PEO-4000 polymers with various LiClO_4 contents and the master curve for the system superimposed onto the curve for the pure polymer by horizontal shifting

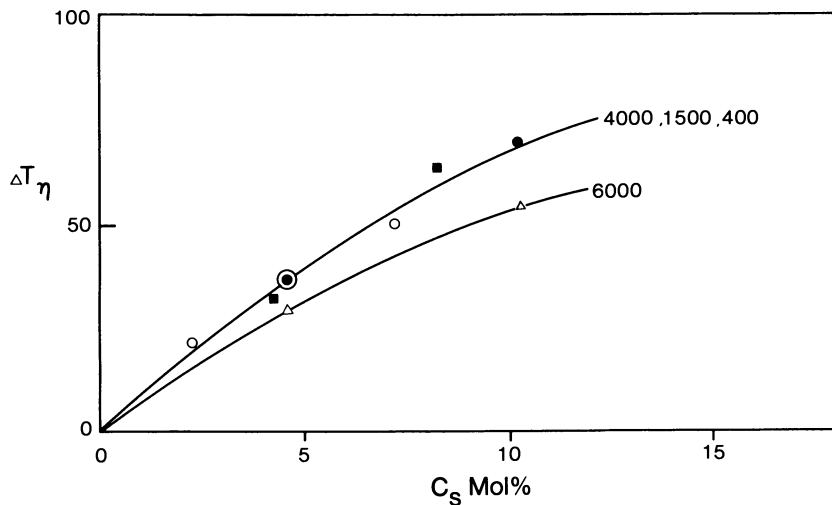


Figure 8. Shift factors vs. salt content for the PEO samples of various molecular weights

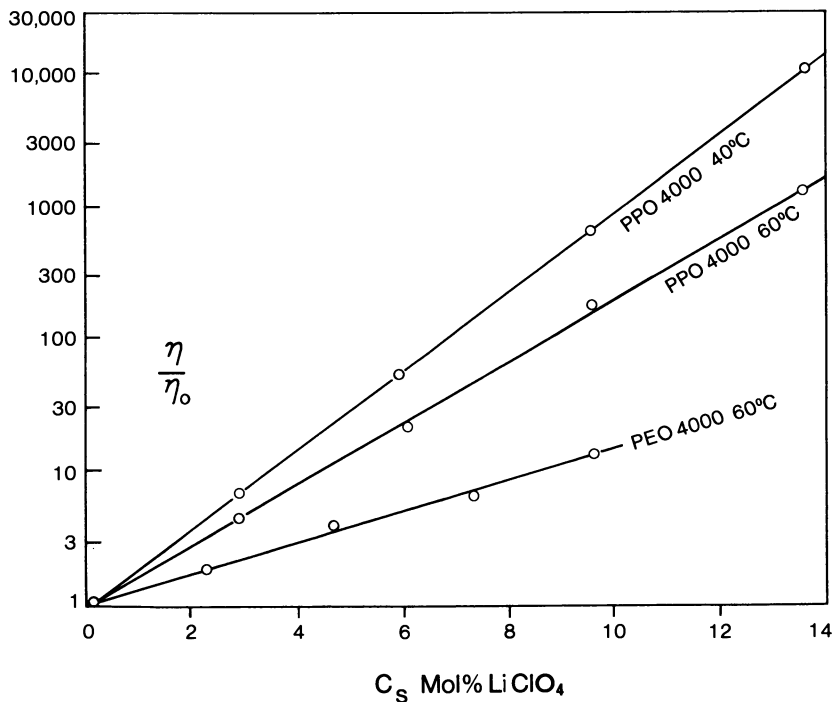


Figure 9. Plot of η/η_0 vs. salt content for PPO 4000 at 40°C and 60°C and for PEO 4000 at 60°C

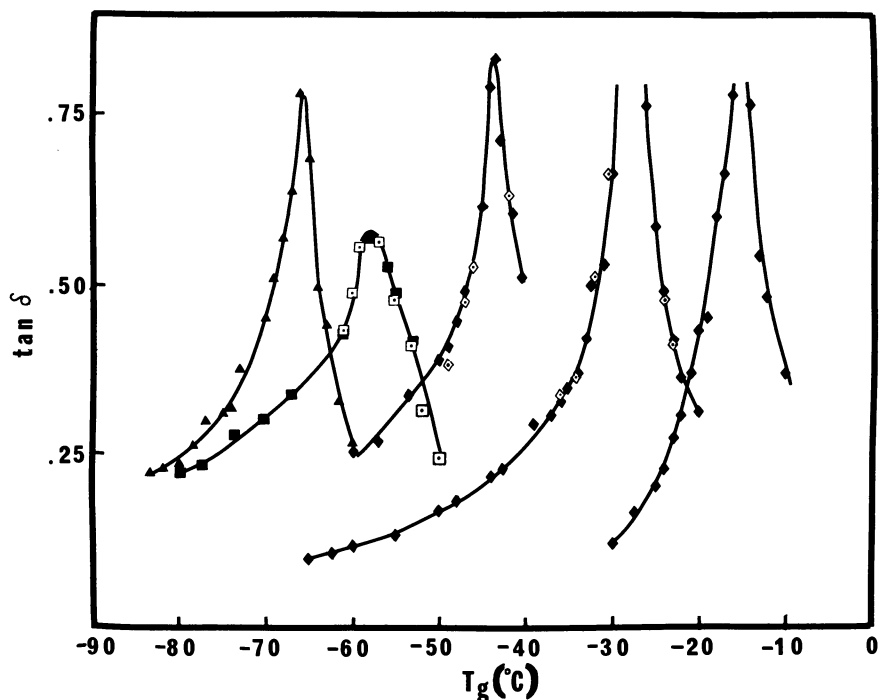


Figure 10. Plot of $\tan \delta$ vs. temperature for PPO-400 samples with increasing salt contents (left to right: 0, 2.9, 6.1, 9.6, and 13.6 mol %)

A comparison of the present results with those of Moacanin and Cuddihy for a polymer of the same molecular weight shows that the values are essentially in agreement, except for a sizable discrepancy (about 7°) for the pure material. The trend, however, is quite different, that is, the data of Moacanin and Cuddihy fall on a straight line in the range of 0–15 wt % salt, with the rate increasing above that value. By contrast, in this study, the initial rate of increase in T_g with salt content is negligible until about 5 wt %, but above that point it becomes linear up to 20 wt %. The discrepancies between these two studies are within experimental error in the range of 5–20 wt %; the lower value for the pure material may be attributable to a somewhat higher moisture content in the pure polymer in the case of the earlier study. It is worth pointing out that the trends found in this work are the same as those found by Wetton et al. (12) for low salt contents. In any case, the discrepancies between Moacanin and Cuddihy and this work are, numerically speaking, quite small.

Finally, it is worth noting that the glass transitions in the PEO systems were not measured in the course of this work. For the pure

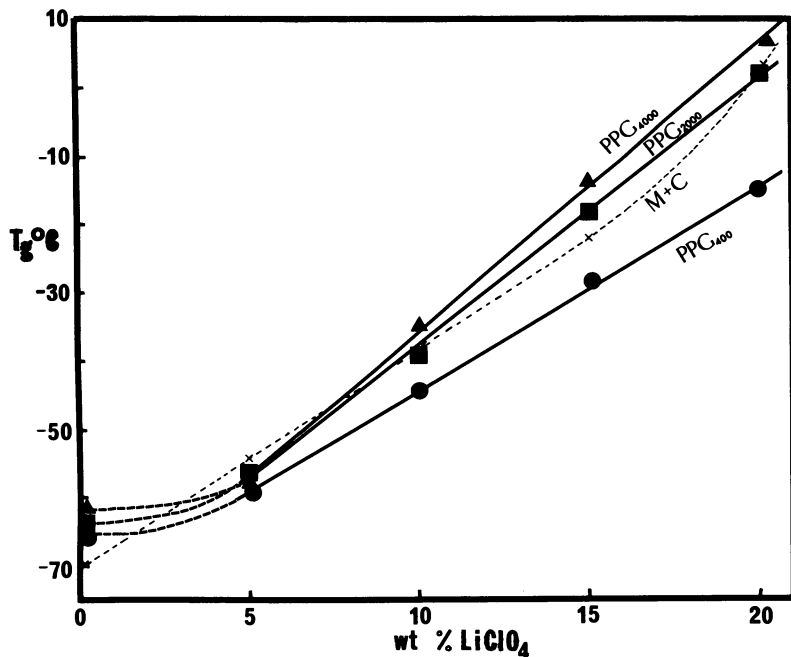


Figure 11. Plot of T_g (from peak maxima) vs. salt content for PPO samples of various molecular weights. The curve of Moacanin and Cuddihy for the PPO-2000 sample is also included ($\cdot \cdot \cdot$).

materials they were measured by Faucher et al. (17), but because of the high crystallinity of the pure PEO samples the values obtained in that study are not applicable directly to the present work. However, the smaller effect of the salt on the viscosity enhancement in PEO argues for a lower T_g of that material than of the PPO system.

Acknowledgments

It is a pleasure to acknowledge that this work was supported, in part, by the U.S. Army Research Office. A valuable discussion with R. F. Landel also is acknowledged with gratitude.

Literature Cited

- Holliday, L., Ed. "Ionic Polymers"; Applied Science Publishers: London, 1975.
- Eisenberg, A.; King, M. "Ion-Containing Polymers"; Academic Press: New York, 1977.

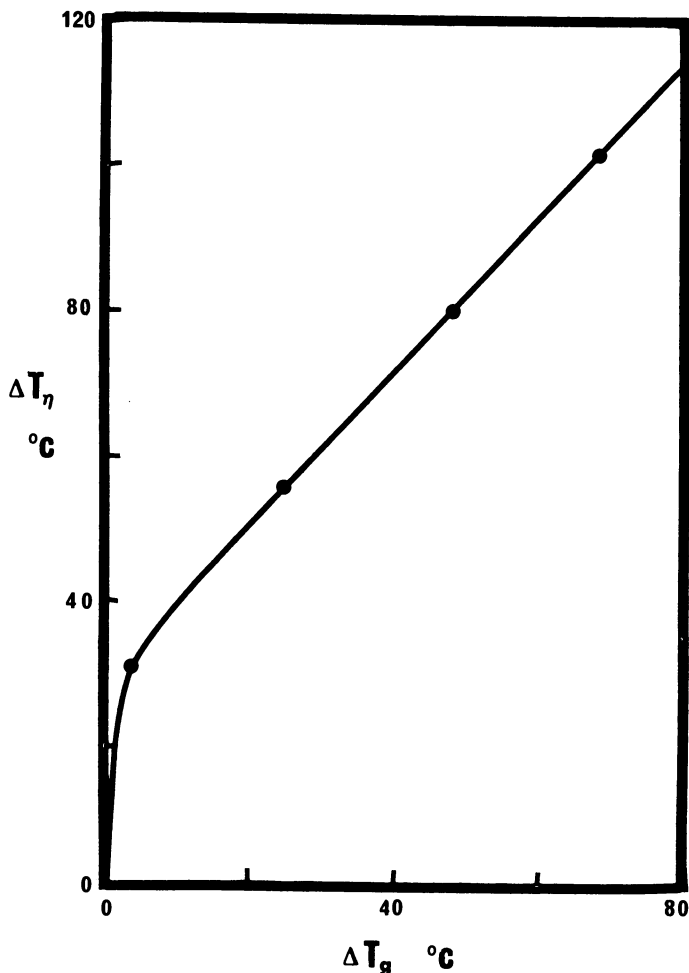


Figure 12. Plot of ΔT_η vs. ΔT_g for PPO-4000 samples of various salt contents

- Harris, F. W.; Reinhardt, B. A.; Case, R. D. *Polym. Prepr., Am. Chem. Soc., Div. Polym. Chem.* 1978, 19(2), 394.
- Woodhams, R. T.; Cipiljauskas, L. T. *Polym. Prepr., Am. Chem. Soc., Div. Polym. Chem.* 1978, 19(2), 401.
- Matsura, H.; Eisenberg, A. *J. Polym. Sci., Polym. Phys. Ed.* 1976, 14, 1201.
- Rembaum, A.; Baumgartner, W.; Eisenberg, A. *J. Polym. Sci., Polym. Lett. Ed.* 1968, 6, 159, and subsequent publications.
- Lundberg, R. D.; Bailey, F. E.; Callard, R. W. *J. Polym. Sci., Polym. Chem. Ed.* 1966, 4, 1563.
- Liu, K. J.; Anderson, J. E. *Macromolecules* 1969, 2, 235.
- Moacanin, J.; Cuddihy, E. F. *J. Polym. Sci., Polym. Symp.* 1966, 14, 313.

10. Hannon, M. J.; Wissbrun, K. F. *J. Polym. Sci., Polym. Phys. Ed.* **1975**, *13*, 113.
11. *Ibid.*, p. 223.
12. Wetton, R. E.; James, D. B.; Whiting, W. *J. Polym. Sci., Polym. Lett. Ed.* **1976**, *14*, 577.
13. James, D. B.; Wetton, R. E.; Brown, D. S. *Polym. Prepr., Am. Chem. Soc., Div. Polym. Chem.* **1978**, *19*(2), 347.
14. Wetton, R. E.; James, D. B.; Warner, F. P. *Polym. Prepr., Am. Chem. Soc., Div. Polym. Chem.* **1978**, *19*(2), 353.
15. Fox, T. G.; Flory, P. J. *J. Am. Chem. Soc.* **1948**, *70*, 2384.
16. Williams, M. L.; Landel, R. F.; Ferry, J. D. *J. Am. Chem. Soc.* **1955**, *77*, 3701.
17. Faucher, J. A.; Koleske, J. V.; Santee, E. R., Jr.; Stratta, J. J.; Wilson, C. W. *J. Appl. Phys.* **1966**, *37*, 3962.

Appendix

Without the gravity correction, the equation is

$$t = (4\eta/P_0 a^2) l^2$$

where t is the time, η the viscosity, P_0 the superposed pressure, a the capillary radius, and l the height of the liquid at time t . Under conditions where the gravitational correction term becomes larger, the effective pressure P is

$$P = P_0 - \rho g l$$

where ρ is the density of the liquid and g the acceleration attributable to gravity. The complete equation becomes

$$t = (8\eta/a^2 \rho g) \{ (P_0/\rho g) \ln [P_0/(P_0 - \rho g l)] - l \}$$

RECEIVED October 30, 1978.

Clustering in Ion-Containing Polymers: Preliminary Small-Angle Neutron Scattering Experiments

M. PINERI

Centre d'Etudes Nucléaires de Grenoble, Département de Recherche
Fondamentale, Section de Physique du Solide,
85 X—38041 Grenoble Cedex France

R. DUPLESSIX

Institut Laue Langevin, BP 156—38041 Grenoble Cedex France

S. GAUTHIER and A. EISENBERG

Department of Chemistry, McGill University, 801 Sherbrooke Street West,
Montreal, PQ, Canada M3A 2K6

Small-angle neutron scattering test experiments were performed on two ion-containing polymer systems—the styrene–sodium methacrylate copolymers and the Nafions (copolymers based on the perfluoroethylene backbone with side chains containing a terminal sulfonic acid group) developed by Du Pont de Nemours. Evidence for ion aggregation was found in the styrene copolymers for ion concentrations of 3.8, 7.2, and 10 mol %. No appreciable changes in the radius of gyration were observed in the acid and salt copolymers; however, for the 10% salt sample extrapolation to zero concentration was found to be impossible. Clustering of absorbed water was observed in the hydrated Nafion samples in both the acid and sodium salt forms.

The phenomenon of ion clustering in polymers containing ionic comonomers has received considerable attention recently, primarily in materials based on styrene, ethylene, or butadiene backbones containing a small concentration of pendant carboxylic acid groups randomly distributed along the chain. These materials have been reviewed in two

recent books (1, 2). More recently, materials with sulfonic acid groups have been the subject of several studies. These new polymers include the Nafions (3–7), a polymer system with a perfluoroethylene backbone and sulfonic acid groups on a short side chain, and the sulfonate-containing ethylene–propylene copolymers (8, 9, 10).

While several experimental approaches have been used in studying the phenomena associated with ion aggregation (1, 2), the most convincing experimental evidence for the existence of ionic clusters comes from small-angle x-ray experiments. These have been conducted most extensively in the ethylene ionomers (11), but one study has also been performed on the styrene-based systems (12). In the latter materials a low-angle peak appears in samples containing more than 6 mol % of the ionic comonomer (11). This peak, in a material devoid of crystallinity, can only be attributed to ionic cluster formation. While recent experiments (13) suggest that small ionic aggregates (multiplets) and large clusters coexist over wide concentration ranges, at approximately 6 mol % of ions it is the clusters that begin to dominate a wide range of properties—at this concentration their numbers begin to increase dramatically. Below this critical concentration, time–temperature superposition is obeyed with the ions acting merely to slow down the primary relaxation mechanism. However, above this concentration time–temperature superposition becomes invalid because of the dominance of ion clustering. Water absorption studies have shown that only one water molecule per ion pair is absorbed for ion concentrations below 6%, compared with 3–5 water molecules for concentrations above 6%. In Nafion samples clustering has been assumed not only from rheological measurements (7), but also because of the presence of a small-angle x-ray scattering peak at low angles in hydrated acid specimens. An average distance of about 50 Å between the ionic clusters has been proposed because of the position of this peak (3). A spherical cluster morphology was suggested on the basis of electron microscopy experiments. An estimate of the cluster size was possible with the assumption that all of the absorbed water was associated with the ionic clusters. A diameter of about 40 Å has therefore been suggested (3).

No information is available concerning the cluster size distribution, the structure of the clusters, or the percentage of ions inside the clusters for these materials. Such results have been obtained recently for only one system, a terpolymer with pyridine side groups complexed with iron chloride, using techniques such as Mössbauer spectroscopy and magnetic susceptibility experiments (14).

In spite of the wide range of efforts devoted to the ionomers to date, no investigation concerning the conformation of these polymer molecules in the bulk state has, as yet, been undertaken. Recently, a unique technique suitable for the investigation of this problem has become

available, that is, small-angle neutron scattering (SANS). Already interesting results have been obtained with it on polyethylene and polystyrene (15, 16). This technique involves a nuclear interaction between the neutrons and the specimen. The large differences of neutron scattering lengths between deuterium and hydrogen atoms permit one to label the whole chain or parts of it. It is therefore possible to study the conformation of a single labeled chain embedded in a matrix of unlabeled polymer (17). Furthermore, intermolecular organization can be studied by labeling only some specific sites along the chain (18). It has been shown (16) that deuteration does not affect the thermodynamic properties of an amorphous chain; therefore, complete compatibility exists between deuterated and protonated molecules, and the information from SANS using mixtures of protonated and deuterated chains is characteristic of the protonated polymers.

Wavelengths between 4 and 20 Å can be obtained from the Laue-Langevin Institute (I.L.L.) cold source (16, 17). These values are fairly well adapted to match the scattering vector q ($q = 4\pi/\lambda \sin \theta/2$, where θ is the scattering angle and λ the wavelength) with molecular dimensions between 20 and 500 Å, corresponding to usual polymer coil sizes. In comparison with x-rays, one has to note the wide range of q values which are accessible, especially on the small-angle side. The results that will be discussed in this publication concern only experiments performed on the D11 and D17 experimental setups in the I.L.L. in Grenoble. These two instruments have been described extensively in the literature (16, 17, 18, 19). The experiments reported here correspond to test experiments, which explains why, in some cases, the q domain is not well fitted. However, in spite of this factor the results were thought to be of sufficient interest to warrant this presentation of the preliminary conclusions.

The Purpose of the Experiments

Several different types of experiments are possible, depending on the specimens. For the styrene copolymers it is possible to determine if clustering is present from the behavior of the curve $I(\theta)$ vs. θ at very low angles. The differences in the coherent diffusion length between the sodium cations and the other atoms are, indeed, large enough to give a good contrast (16). The use of neutrons permits one to explore larger clusters and larger intercluster distances than is possible with x-rays. Furthermore, by deuteration of the methacrylate groups it is possible to determine if an association of the acid groups through hydrogen bonding exists because of the good contrast between hydrogen and deuterium. Another question of interest is the possible change of chain conformation when the concentration of ions is large enough for them to be subject to extensive clustering. If the clustering is predominantly intramolecular,

that is, if most of the ionic groups in a cluster come from the same chain, then one should expect a drastic change in the radius of gyration when compared with the value obtained in a θ solvent. Using SANS, it is possible to get the radius of gyration of these polymer chains by studying mixtures of completely deuterated chains in a protonated matrix (16).

Nafion samples can absorb several water molecules per acid or salt group. Because of the tetrafluoroethylene backbone structure, a good contrast exists between the water molecules and the polymer matrix. It is therefore possible to explore water clustering in these materials.

Samples

The samples were synthesized by the same techniques as those used for the styrene ionomers (12). The protonated styrene-methacrylic acid copolymers were prepared by thermal initiation. The polymerization took place in sealed glass tubes in the bulk at 80°C after several freeze-thaw cycles. A conversion of 10% was obtained after 19 hr. The polymer was precipitated in methanol and neutralized in a benzene-methanol solution. A similar procedure was used for the deuterated samples except that the unreacted deuterated styrene monomer was evaporated prior to the precipitation. The mixing of the deuterated and protonated styrene copolymers was performed in a benzene solution by stirring for 1 hr. The benzene used as the solvent contained a minimum amount of methanol necessary to dissolve the ionomer (approximately 5–10% for the samples of high ion content). The samples were freeze-dried, then dried further at 60°–80°C under vacuum, and finally compression-molded at $T_g + 30^\circ\text{C}$.

The Nafion samples were obtained from the Du Pont de Nemours Company. The equivalent weight of the samples studied here is 1200.

The hydration of the Nafion samples was accomplished in an oven through which air of a very well defined humidity level was allowed to flow. This hydration procedure has been described previously (20). Special small watertight cells were built to fit into the neutron beam. After hydration the specimens were stored inside the oven in the small tight cells until the experiment. In this way several samples corresponding to different humidity levels could be run at the same time.

Results and Discussion

Styrene-Methacrylic Acid Copolymers and Their Salts. Two different types of experiments were performed with these copolymers. A possible clustering of the ionic groups was studied with copolymers containing protonated styrene monomers and deuterated methacrylic acid groups. The radius of gyration measurements were studied from mixtures of all deuterated chains in a protonated matrix.

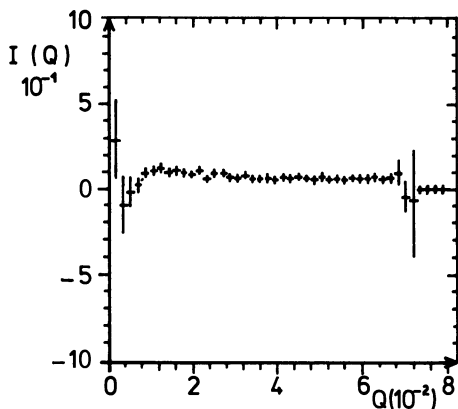


Figure 1. Intensity vs. angle for the copolymer of protonated styrene containing 7.2 mol % deuterated methacrylic acid

SAMPLES WITH DEUTERATED METHACRYLIC ACID GROUPS AND PROTONATED STYRENE MONOMERS. Three different copolymers were studied with the acid concentrations corresponding to 3.8, 7.2, and 10 mol %. Figure 1 shows the curve representing intensity vs. angle for the sample containing 7.2% deuterated acid after subtracting the intensity of a polystyrene reference used as a background sample; a similar curve was obtained for the 3.83% sample. One can observe that there is no scattered intensity over the entire q vector range, thus no long-range fluctuations exist in the samples. In contrast with these results, a large increase in the diffused intensity was observed at very small angles for the 10% acid copolymer, as shown in Figure 2. At this time no explanation can be offered to explain this behavior which may be characteristic of some kind of aggregation of the acid groups through hydrogen bonding at such high concentrations.

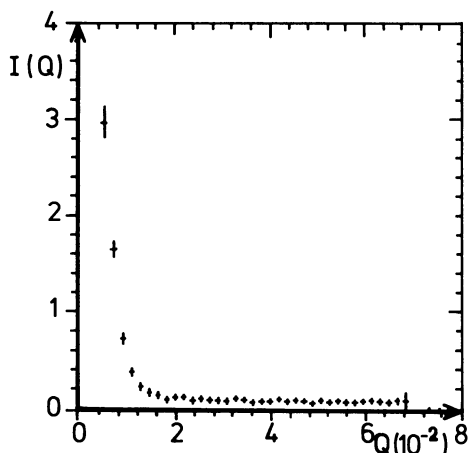


Figure 2. Intensity vs. angle for the copolymer of protonated styrene containing 10 mol % deuterated methacrylic acid

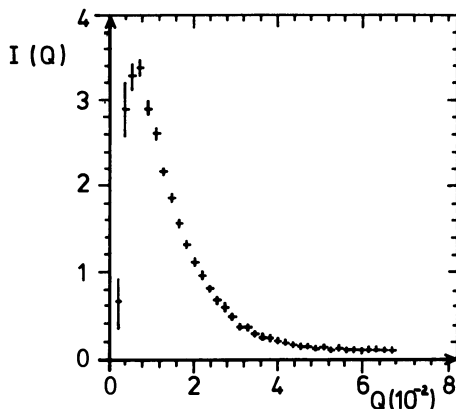


Figure 3. Same plot as in Figure 1 for the corresponding sodium salt

The sodium salt samples corresponding to the above acids gave diffusion curves similar to that shown in Figure 3. The characteristics of these curves can be summarized as follows:

1. A large increase in the intensity values is observed with decreasing θ values for all three sodium salts.
2. No Debye behavior characteristic of the Gaussian coil has been observed. Such a dependence can be studied by making a Zimm plot in the range $qR < 1$ with q the scattering vector and R the radius of gyration.
3. An asymptotic behavior was obtained on plotting $q^4 I(q)$ vs. q^4 . Such behavior is characteristic of the presence of a two-density system with a sharp range in the contrast between the two phases. Figure 4 shows such a curve for the 7.25% specimen.

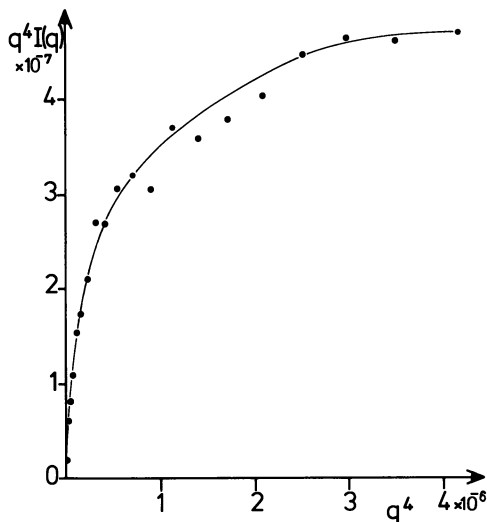


Figure 4. Plot of $q^4 I(q)$ vs. q^4 for the 7.2% styrene-sodium methacrylate copolymer

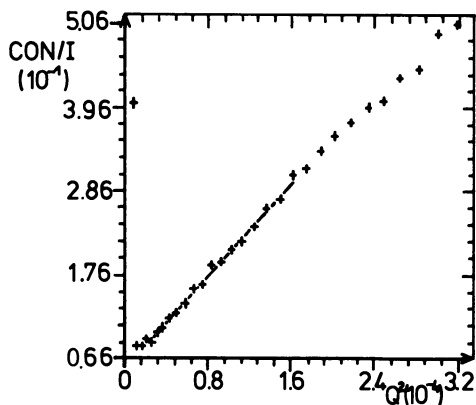


Figure 5. Zimm plot for the specimen corresponding to a mixture of 0.5% deuterated chains in a protonated matrix consisting of a styrene-methacrylic acid copolymer with 3.8 mol % acid

All of these observations suggest the presence of clusters with a large sodium salt concentration. It is important to note the existence of these clusters even at low salt concentration (3.25%). Quantitative experiments are underway to define the size, form, and concentration of the clusters.

RADIUS OF GYRATION MEASUREMENTS. The radii of gyration of the acid and salt samples of the completely deuterated styrene-methacrylic copolymers were measured. The ion concentrations studied were 3.8, 7.2, and 10 mol % methacrylic acid. For each sample two mixtures of 0.5 and 1% of deuterated chains in a protonated matrix were run. The radius of gyration corresponding to these 0.5 and 1% concentrations was obtained from a Zimm plot. By extrapolation to 0% concentration one obtains the radius of gyration corresponding to each concentration. Figures 5 and 6 represent two Zimm plots corresponding, respectively, to the acid and salt forms of a mixture of 0.5% deuterated chains in a protonated styrene copolymer matrix with each copolymer containing 3.8%

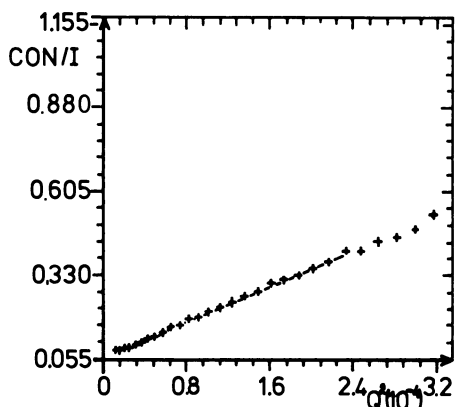


Figure 6. Same plot as in Figure 5 for the sodium salt form

methacrylic acid. The radii of gyration obtained from the values of the slope are 191 Å for the acid and 204 Å for the salt. Table I gives the extrapolated values of the radius of gyration for each sample. On the basis of these results, the following points can be made:

1. There is a systematic error in the radius of gyration measurement because high molecular weight samples (mol wt ~ 4 to 5×10^5) were used, and the extrapolation was done in a domain where qR is slightly larger than one. In spite of this limitation, the qR values are similar to the values obtained for polystyrene samples of similar molecular weight.
2. The qR values are very similar for all samples except the 10%-salt copolymer.
3. Extrapolation was not possible for the 10%-salt sample, probably because of extensive clustering.

Experiments scheduled for the future will involve lower molecular weight samples in order to have $qR < 1$. For each ion concentration, four different deuterated chain concentrations (0.25, 0.5, 1, and 1.5%) will be run in order to achieve a more reliable extrapolation. More samples with intermediate acid concentrations will be studied. It also seems interesting to investigate the changes in the radius of gyration when going from the ester to the acid and to the salt form of a chain.

Nafion Samples. Results showing the effect of hydration on Nafion acid samples are shown in Figures 7 and 8. The plots of relative scattered intensity as a function of Q correspond to samples dried at 23°C, samples hydrated at 14 and 74% relative humidity (R.H.), and to a sample soaked in water for 24 hr. From these curves, we can outline several points:

1. A scattering maximum is observed in the dry, 14 and 74% R.H. samples corresponding to a Bragg spacing of 130–150 Å. The maximum has largely disappeared for the soaked sample. Based on data previously reported on small-angle x-ray scattering studies by Du Pont, this maximum can be tentatively attributed to interference between regions of crystalline CF_2 groups. Based on this assignment, the data reported here indicate that water alters the structure of the samples by changing the spacing and alignment between the crystalline regions.
2. A very large increase in the overall intensity is observed on hydration in this region of Q . Such an increase is evidence for a clustering of water molecules since a uniform distribution of water would not lead to an intensity increase. On this basis one can say that in the dry sample, scattering contrast arises from mass density fluctuations between crystalline and amorphous regions. This contrast

Table I. Extrapolated Values of the Radius of Gyration Corresponding to Each Ion Concentration of the Acid and Salt Forms of Styrene-Methacrylic Acid Copolymers

Acid concentration	3.83%	7.25%	10%
Acid form	191	183	172
Salt form	204	180	no extrapolation

is small when compared with that between CF_2 regions and water-rich regions that are present after hydration.

A more thorough investigation at intermediate humidity levels is needed. In addition, it is clear that a number of other studies including scattering at larger Q , quantitative investigations of intensities, and a comparison of small-angle neutron and x-ray results are needed to understand the complex structure present in hydrated Nafions.

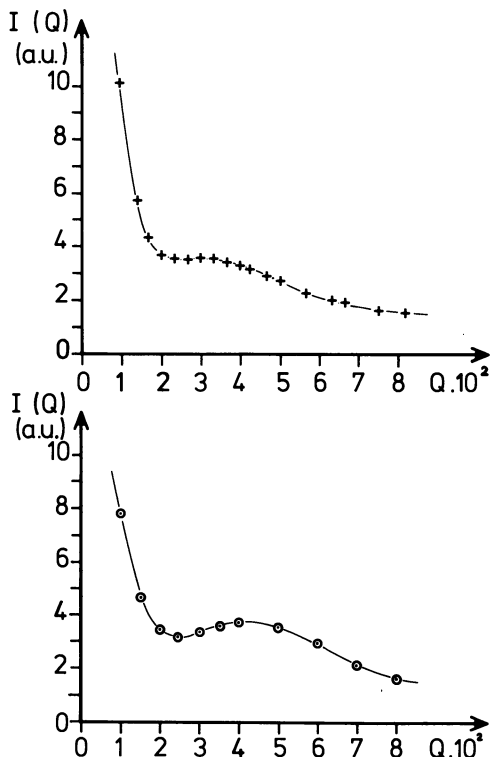


Figure 7. Diffused intensity vs. angle for the Nafion acid form in the dry state (+) and with water corresponding to 14% R.H. (O)

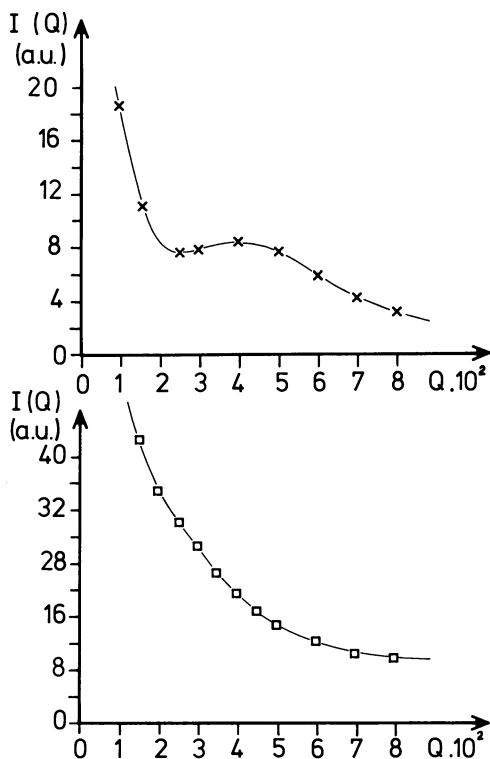


Figure 8. Same plot as in Figure 7 for samples corresponding to a 74% R.H. content (X) and to a 100% R.H. content soaked in water (\square)

Acknowledgment

A. Eisenberg and S. Gauthier are pleased to acknowledge that a part of this research was supported by the U.S. Army Research Office.

Literature Cited

- Holliday, L. "Ionic Polymers"; Halsted: 1975.
- Eisenberg, A.; King, M. "Ion Containing Polymers"; Academic: 1977.
- Gierke, T. D. 152nd National Meeting of the Electrochemical Society, Atlanta, GA, October 1977.
- Mauritz, K. A.; Hora, C. J.; Hopfinger, A. J. *Polym. Prepr., Am. Chem. Soc., Div. Polym. Chem.* 1978, 19(2), 324-329.
- Mauritz, K. A.; Lowry, S. R. *Polym. Prepr., Am. Chem. Soc., Div. Polym. Chem.* 1978, 19(2), 336-340.
- Komorowski, R. A. *Polym. Prepr., Am. Chem. Soc., Div. Polym. Chem.* 1978, 19(2), 341-346.
- Yeo, S. C.; Eisenberg, A. *J. Appl. Polym. Sci.* 1977, 21, 875.
- Makowski, H. S.; Lundberg, R. D.; Westerman, L.; Bock, J. *Polym. Prepr., Am. Chem. Soc., Div. Polym. Chem.* 1978, 19(2), 292-297.
- Neumann, R. M.; MacKnight, W. J.; Lundberg, R. D. *Polym. Prepr., Am. Chem. Soc., Div. Polym. Chem.* 1978, 19(2), 298-303.

10. Makowski, H. S.; Lundberg, R. D. *Polym. Prepr., Am. Chem. Soc., Div. Polym. Chem.* **1978**, *19*(2), 304–309.
11. MacKnight, W. J.; Taggart, W. P.; Stein, R. S. *J. Polym. Sci., Polym. Symp.* **1974**, *45*, 113.
12. Eisenberg, A.; Navratil, M. *Macromolecules* **1974**, *7*(1), 90–94.
13. Hodge, I.; Eisenberg, A. *Macromolecules* **1978**, *11*, 283.
14. Meyer, C. T.; Pineri, M. *J. Polym. Sci., Polym. Symp.* **1978**, *16*, 569–581.
15. Kirste, R. G.; Kruse, W. A.; Schelten, J. *J. Makromol. Chemie* **1972**, *162*, 299.
16. Cotton, J. P.; Decker, D.; Benoit, H.; Farnoux, B.; Higgins, J.; Jannink, G.; Ober, R.; Picot, C. *Macromolecules* **1974**, *7*, 863.
17. Picot, C.; Duplessix, R.; Decker, D.; Benoit, H.; Bone, F.; Cotton, J. P.; Daoud, M.; Farnoux, B.; Jannink, G.; Nierlich, M.; de Vries, A. J.; Pincus, R. *Macromolecules*, **1977**, *10*, 436.
18. Duplessix, R., unpublished data.
19. Neutron beam facilities, I.L.L. BP 156 Centre de Tri 38042 Grenoble.
20. Pineri, M.; Escoubez, M.; Roches, G. *Biopolymers*, in press.

RECEIVED October 13, 1978.

Structure Variation of Sulfonated Polystyrene Surfaces

R. W. BIGELOW, F. C. BAILEY, W. R. SALANECK, J. M. POCHAN, D. F. POCHAN, H. R. THOMAS, and H. W. GIBSON¹

Xerox Corporation, Webster Research Center, Webster, NY 14580

A type of angle-dependent x-ray photoemission spectroscopy was used to investigate the molecular orientation at the surface of sulfonated polystyrene as a function of reaction depth. A model based on these measurements indicates that at a critical sulfonation depth the aliphatic hydrocarbon backbone becomes exposed preferentially at the surface. These results are consistent with surface energy and triboelectric charging measurements, which also reveal the effects of associative interactions in the form of conversion dependencies.

The chemical modification of polymers is an established technique for the attainment of new and useful surface properties. In particular, there is considerable interest in surface modification as a means of controlling dyeability (1, 2), electrical charging (3,4), wettability (5, 6), and adhesion (7, 8), where presumably the functional group orientation becomes a critical factor in determining the interfacial characteristics. To date, however, direct analysis of such modified surfaces has been carried out in only a few instances (9-14). For example, in a recent study of the surface structure of potassium-exchanged sulfonated polystyrene using angle-dependent x-ray photoemission spectroscopy [XPS(θ)] (10), it was concluded that both the potassium and sulfur atoms reside below the surface in accordance with thermodynamic arguments requiring surface free energy minimization (15, 16). Also, using the XPS(θ) technique Briggs and coworkers (11) examined the surface structures of chromic acid-etched polyethylene and polypropylene, and correlated the relative

¹ Author to whom correspondence should be addressed.

atomic concentrations with surface energy measurements. However, each of these studies examined a limited number of samples. This chapter examines surface properties of a series of polystyrene (PS) films, modified to varying depths by sulfonation, using XPS(θ), surface energy measurements, and triboelectric charging. A model based on the results of these measurements indicates that at a critical sulfonation depth the heteroatoms become preferentially oriented into the bulk.

Experimental

Films of varying sulfonation depth were obtained by exposing free-standing 80- μm thick films of oriented PS (Dow Trycrite, Type 1000) to 99.7 \rightarrow 100.3% sulfuric acid at 25°C under dry conditions (\sim 100 ppm water) for selected periods of time up to 60 min. The films were then quenched in 96% sulfuric acid, washed with deionized water, dried, and stored in a dry nitrogen atmosphere. Sulfonation was confirmed independently by IR difference spectroscopy (17) and the XPS results. The degree of sulfonation was established by three independent techniques: (1) direct titration of the acidic protons; (2) measurement of visible absorption of companion films ion-exchanged with methylene blue (a cationic dye); and (3) interferometric estimation of reacted depth. These methods are described in detail elsewhere (18). In conversion from the number of moles of sulfuric acid per gram of film (Methods 1 and 2) to number of monolayers reacted, two assumptions were made: (1) an absolutely smooth surface and (2) 100% reaction of each layer in sequence, that is, a diffusion-controlled process (19). Above about 30 ideal monolayers the estimated accuracy is approximately \pm 5%. From zero to 30 monolayers the accuracy is less, on the order of 25 to 100%, being less for the lesser extents of reaction, of course.

The XPS(θ) characterization was accomplished with an AEI 200B photoelectron spectrometer. The instrumental conditions and geometrical constraints imposed in the present study have been described previously (10). Films were transferred from the storage containers to the instrument sample probe in a dry nitrogen atmosphere (typical residual oxygen concentration was \leq 40 ppm and water was removed by exposing the environment to \sim 200 cm^2 of copper tubing held at liquid nitrogen temperature) and inserted directly into the high vacuum of the instrument.

Surface tension measurements were made via the advancing contact-angle (γ_c) technique (15) with a Rame-Hart rheogoniometer. Values for γ_c are estimated to be accurate to \pm 1.0 dyn/cm.

Triboelectric charging data were accumulated on vacuum-dried ($>$ 2 weeks, \sim 1 torr) samples at zero humidity (\sim 100 ppm water) using the device of Figure 1 as described previously (20).

Results and Discussion

XPS(θ). To establish a standard for comparison of the XPS(θ) data, Figures 2 and 3 present the relevant photoemission intensities ($I(\theta)$) for an untreated sample and one sulfonated to a depth of approximately

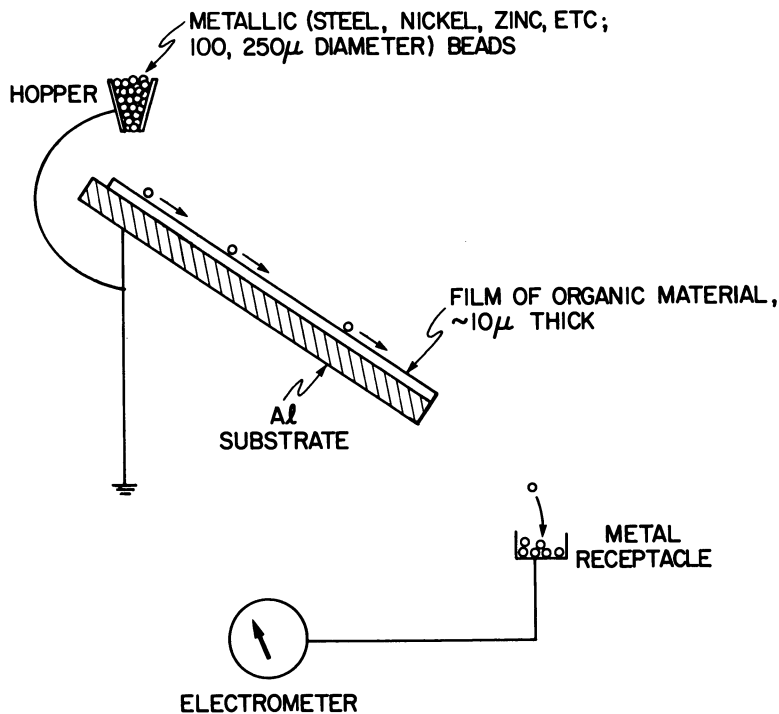


Figure 1. Cascade device for measurement of triboelectric charging (20, 38, 39)

600 monolayers, respectively. The details of the application of this technique have been discussed previously (10). Of particular importance to the ensuing arguments is the approximately constant ratio of intensities in Figure 2 between the main C(1s) core-level emission and the clearly resolved shake-up satellite structure at approximately 6.6 eV higher binding energy in going from $\theta \sim 10 \rightarrow 80^\circ$. Since these particular satellite features reflect $\pi^* \leftarrow \pi$ valence orbital excitation processes localized on the benzene chromophore (21, 22, 23, 24), their uniform magnitude relative to the primary peak intensities as a function of angle provides compelling evidence for the similarity in bulk and surface concentration of unperturbed pendent aromatic rings of the untreated polymer. The relatively insensitive angle dependence of the C(1s)/O(1s) intensity ratio indicates that the residual oxygen in the untreated film is distributed approximately uniformly throughout the bulk. Since a typical escape depth for detected electrons in these measurements is between 10 and 30 Å (25), the bulk sampling depth extends approximately 20 Å below the surface.

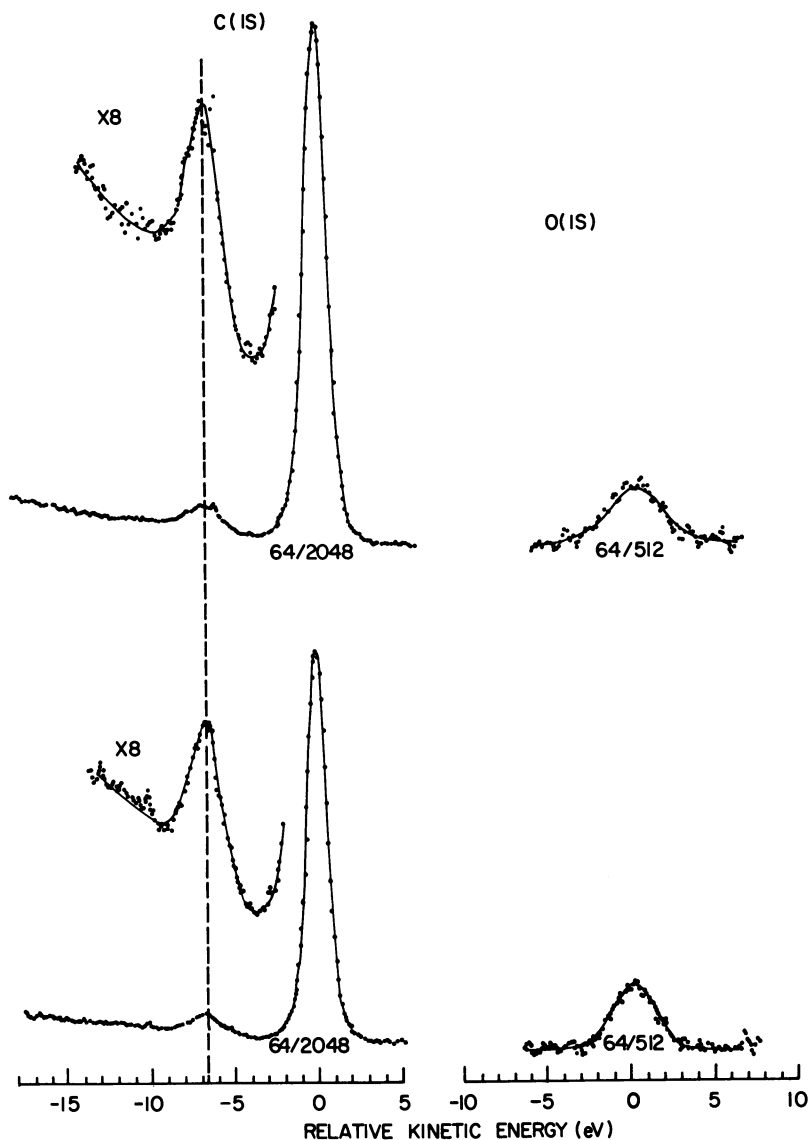


Figure 2. The C(1s) and O(1s) x-ray photoemission signals of a typical untreated PS film taken at $\theta \sim 10^\circ$, bulk mode (upper) and $\theta \sim 80^\circ$, surface mode (lower). The intensity (I_i) of a displayed signal is calculated by the relationship [(area of displayed signal)(sensitivity scale factor)/(number of scans required to produce the signal)]. The respective scan (A) and scale factors (B) are given below each signal (A/B). ($\cdot \cdot \cdot$) KE of -6.6 eV relative to the main C(1s) peak.

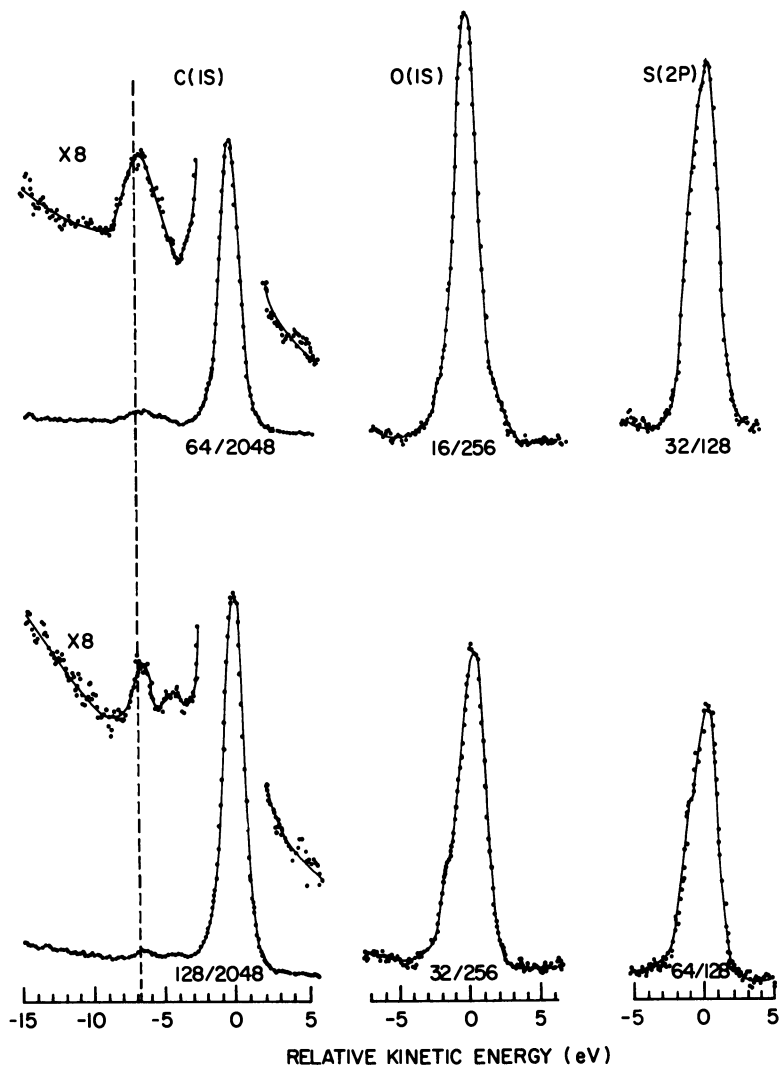


Figure 3. The C(1s), O(1s), and S(2p) emission signals at $\theta \sim 10^\circ$ (upper) and $\theta \sim 80^\circ$ (lower) for the most heavily sulfonated sample considered by XPS (see text). ($\cdot \cdot \cdot$) KE of -6.6 eV relative to the main C(1s) peak.

Figure 3 confirms, for example, that in the more strongly sulfonated samples the heteroatoms lie preferentially below the surface; the emission intensities for the O(1s) and S(2p) levels decrease more rapidly than the matrix C(1s) signal as the sample is rotated from $\theta \sim 10^\circ \rightarrow 80^\circ$. Although there are some important variations in the angle-dependent C(1s) heteroatomic intensity ratios as a function of sulfonation (this will be

addressed in greater detail later), profound increases in the matrix/heteroatom signal ratios in going from $\theta \sim 10 \rightarrow 80^\circ$ are observed beginning at approximately 10 monolayers sulfonation depth.

In addition to indicating a preferred interfacial structure, Figure 3 exhibits some interesting irregularities in the satellite structure of the C(1s) signal obtained at $\theta \sim 80^\circ$. To explore this problem in greater detail Figure 4 compares the C(1s) signal ($\theta \sim 80^\circ$) of representative samples from this study with the C(1s) spectrum of an oxidized film reported by Clark et al. (26). It should be noted that while corresponding measurements on Films A \rightarrow D of Figure 4 at $\theta \sim 10^\circ$ yielded some low-intensity satellite structures not present in the parent film, the shake-up features were clearly resolvable and of a magnitude comparable with that presented in Figure 2. At least a portion of the C(1s) satellite structures of Figure 4 may be attributed to chemical shifts arising from various oxidation states of the surface carbon atoms. However, it should be emphasized that the intensities of the satellite structures in Figure 4 do not increase with the degree of sulfonation. Comparison measurements conducted on solvent-cast PS films showed a shake-up structure comparable with the untreated free-standing film ($\theta \sim 10 \rightarrow 80^\circ$). However, relative to the free-standing untreated samples, much less residual oxygen was present. Although sulfonation of the solvent-cast films did not seriously perturb the shake-up features evident in the untreated film at $\theta \sim 10^\circ$, satellite maxima were absent at $\theta \sim 80^\circ$. These results indicate that prolonged exposure to the reagent merely alters the state of a limited number of carbon atoms that may initially exist in a lower oxidized form at the surface of the untreated free-standing films (26, 27).

The notable absence or decrease in the C(1s) shake-up intensity characteristic of the unsubstituted aromatic structure at $\theta \sim 80^\circ$ is more difficult to resolve. Two possibilities merit consideration. An obvious one is that sulfonation leads to a preferential ring opening of the surface phenyl groups, and that the $\theta \sim 80^\circ$ measurements are, therefore, sampling a polyethylene-like structure. Within this context Storp and Holm (28) attributed the decrease observed in PS shake-up intensity concomitant with ion bombardment as evidence of ring destruction. Such a mechanism in the present case, however, does not appear well-founded in the literature. A more plausible explanation is that the shake-up intensity is quenched because of strong intra- and/or intermolecular interactions. In a detailed study of para-substituted PS and appropriate model compounds, for example, Clark and co-workers (29) attribute the shake-up process at approximately 6.6 eV higher binding energy relative to the main peak as primarily attributable to two one-electron $\pi^* \leftarrow \pi$ excitations. The character of these excitations is shown in Figure 5 for a phenyl moiety para-substituted with both electron-donating and -accepting ele-

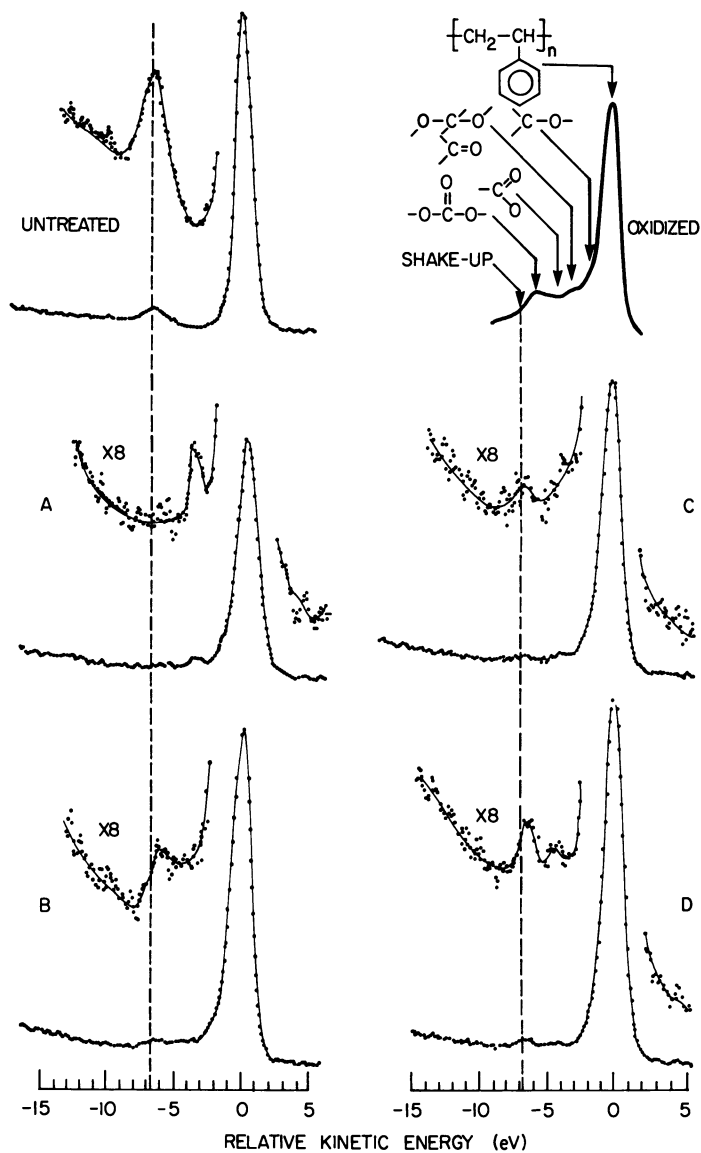


Figure 4. The C(1s) emission signals and high-energy satellite structure taken at $\theta \sim 80^\circ$ for an untreated PS film (taken from Figure 2) and four films of various exposure times to sulfuric acid, increasing in the order A \rightarrow D. These are compared with the highly oxidized PS film reported by Clark et al. (26).

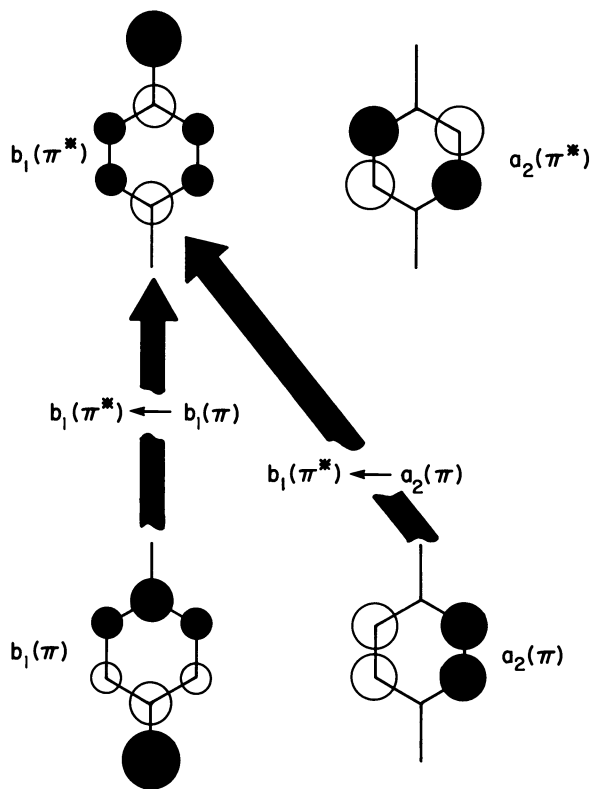


Figure 5. Representation of the $\pi^* \leftarrow \pi$ excitation processes of interest for a D-Ar-A configuration. The orbital lobes reflect the relative magnitudes of the atomic-orbital coefficients and are viewed from above the molecular plane.

ments (D-Ar-A). The probability of such shake-up processes accompanying core ionization is (21, 22, 23, 24):

$$P(j' \leftarrow i) = | \langle \Psi_n(i) | \Psi_{n-1}^*(j') \rangle |^2 \quad (1)$$

where $\Psi_n(i)$ are wave functions of the unperturbed ground state—the $b_1(\pi)$ and $a_2(\pi)$ orbitals of Figure 5, for example. $\Psi_{n-1}^*(j')$ are the final-state wave functions which can be approximated by the ground-state virtual levels (the $b_1(\pi^*)$ and $a_2(\pi^*)$ levels of Figure 5) modified by the presence of the appropriate core hole. Explicit computations of shake-up intensities have been conducted on model compounds of interest (21, 22, 23, 24, 29, 30, 31) using the sudden-approximation and equivalent-cores approach (32, 33). However, for our purposes the $\Psi_{n-1}^*(j')$ states may be viewed simply in terms of the unperturbed $b_1(\pi^*)$ and $a_2(\pi^*)$

levels, that is, $\Psi_{n-1}^*(j') \sim \Psi_n^*(j')$. Within the LCAO-ZDO approximation

$$P(j' \leftarrow i) \propto \left| \sum_A C_{A,n}^i C_{A,n}^{j'} \right|^2 \quad (2)$$

where $C_{A,n}^i$ and $C_{A,n}^{j'}$ are the atomic orbital coefficients of the atomic centers A in states i and j' , respectively. Therefore, Figure 5 and Equation 2 indicate that by decreasing or modifying the carbon atomic orbital coefficients in selected levels through appropriate substitution, the shake-up intensity associated with the C(1s) core-level ionization can be reduced dramatically. In accordance with correlations outlined by Clark et al. (29, 30, 31) and a spectroscopic moment of -40 ($\text{cm} \cdot \text{m}/1$)^{1/2} for the $-\text{SO}_3\text{H}$ group (34), one would expect, in the absence of additional interactions, that the phenyl C(1s) $\pi^* \leftarrow \pi$ shake-up intensity would be quenched significantly concomitant with sulfonation as described previously. However, because of the abundance of possible interactions, the electron-withdrawing characteristics of the $-\text{SO}_3\text{H}$ group could be neutralized, or even reversed. Within this context, XPS(θ) measurements on solvent-cast films of *p*-toluenesulfonic acid monohydrate exhibited C(1s) shake-up structure at $\theta \sim 10 \rightarrow 80^\circ$ similar to the unperturbed phenyl group. In addition, charge transfer in the ground state to or from the carbon atom connecting the phenyl group to the polymer backbone could lead to a D-Ar-A configuration. Chemically shifted carbons arising from these types of interactions were not resolved in the present XPS(θ) measurements. However, the asymmetry on the low binding energy side of the main C(1s) signal observed in the preliminary study of potassium-exchanged sulfonated PS at $\theta \sim 80^\circ$ (10) suggests the presence of negatively charged surface carbon atoms, that is, strong intermolecular interactions of a different nature than is evident in the bulk.

Arguments of the nature just presented imply the existence of an excited state $D \rightarrow A \pi^* \leftarrow \pi$ intramolecular charge-transfer transition at or near the surface, which in principle should be subject to optical detection. Experiments are underway to resolve these issues.

Assuming a continuous bulk distribution of atomic centers, the appropriate concentration ratios ($\theta \sim 10^\circ$) are obtained from the emission intensities (I) according to (35, 36):

$$\frac{n_i}{n_j} = \left(\frac{\sigma_j \lambda_j}{\sigma_i \lambda_i} \right) \frac{I_i}{I_j} \quad (3)$$

where σ is the photoemission cross section relative to C(1s) — $\sigma_{\text{O}(1s)} = 2.85$ and $\sigma_{\text{S}(2p)} = 1.75$ obtained as the sum of the $2p_{1/2}$ and $2p_{3/2}$ components (37). λ is the elastic mean-free path of the escaping photo-

electrons ejected with a kinetic energy KE. It has been shown that to a good approximation over small energy ranges $\lambda \propto (\text{KE})^{1/2}$ (35, 36). Substituting the emission intensities from Figure 3 ($\theta \sim 10^\circ$), and $\text{KE}_{\text{C}(1s)} = 970$ eV, $\text{KE}_{\text{O}(1s)} = 722$ eV, and $\text{KE}_{\text{S}(2p)} = 1089$ eV for the $\text{MgK}\alpha$ x-ray source into Equation 3 yields $n_{\text{C}(1s)}/n_{\text{O}(1s)} = 2.4$, $n_{\text{C}(1s)}/n_{\text{S}(2p)} = 7.5$, and $n_{\text{O}(1s)}/n_{\text{S}(2p)} = 3.1$, compared with the theoretical relative concentrations of 2.67, 8.0, and 3.0, respectively. These results are representative of films sulfonated to a depth ≥ 10 monolayers and are indicative of free oxygen centers (possibly water) in addition to some unreacted functional groups. However, the concentration of residual oxygen present in the untreated films appears insufficient to account for this excess. As sulfonation progresses past a depth of ≥ 10 monolayers, some variations are observed in the relative atomic concentrations at both $\theta \sim 10^\circ$ and 80° . In light of these variations we are hesitant to assume a specific model necessary for depth profiling. We have, however, profiled the gross relative carbon/oxygen content near the surface ($\theta \sim 80^\circ$) for a series of samples (see Figure 6a). Although variations in the gross C(1s)/O(1s) ratios at $\theta \sim 10^\circ$ and the C(1s)/S(2p) ratios at $\theta \sim 10 \rightarrow 80^\circ$ also were found for selected films, a direct correspondence with the results of Figure 6a was not obtained.

Triboelectric Charging. Triboelectric charging is sensitive to the chemical composition of the solid (20, 38, 39, 40, 41). Based on electrostatic arguments, the charging level, given in terms of the charge to mass ratio (Q/M), is expected to increase with the extent of reaction, assuming a homogeneous distribution of the newly formed groups (20, 40). However, Q/M is expected to decrease with the distance of a particular charging site from the surface up to a certain critical depth (several microns) beyond which the charging becomes invariant. On this basis the net effect is that Q/M is expected to increase, asymptotically approaching a constant value. The constant value in terms of the depth is several microns (41, 42).

As seen in Figure 6b, the charging data do not conform to expectations. The charging as a function of the extent of reaction increases to a maximum value and then decreases to an asymptotic value. Superimposed on this general curve are several smaller excursions.

Critical Surface Energy. The effect of sulfonation depth on the surface tension of sulfonated PS films is shown in Figure 6c. For comparison the result for an unconverted PS film is shown also. Increased sulfonation causes γ_c , in general, to increase to a sulfonation depth of approximately 10 monolayers and then decrease beyond this value. It is interesting to note that the untreated PS values for γ_c are slightly higher than those observed at very low sulfonation depths and at very high conversion ratios. The former data were taken for a PS film that had

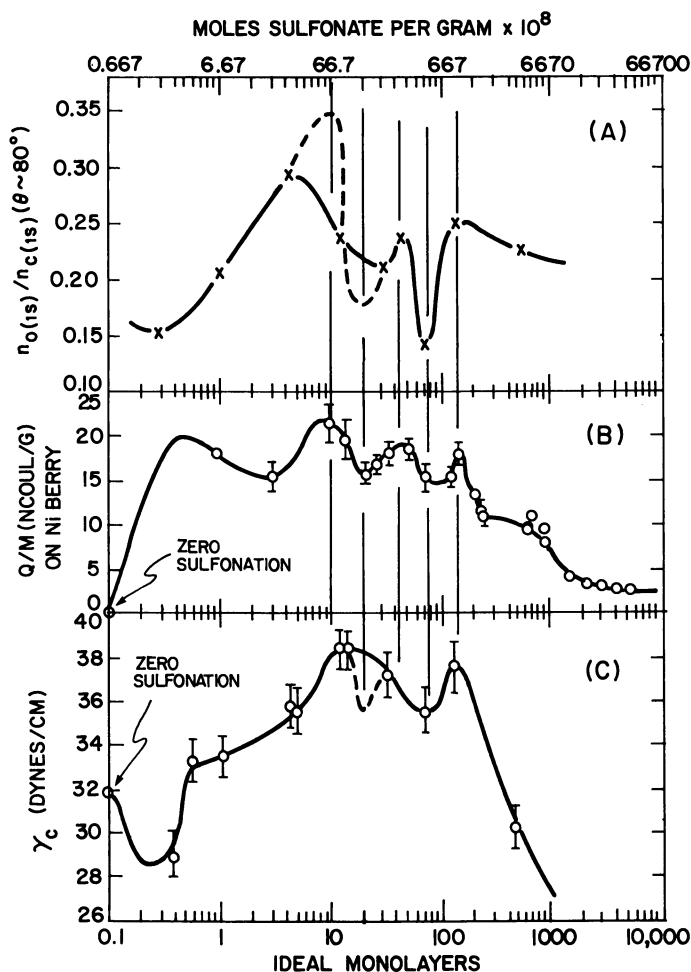


Figure 6. Comparison of results of the three experimental techniques. (A) The $n_{o(1s)}/n_{c(1s)}$ ($\theta \sim 80^\circ$) ratios obtained from the XPS(θ) measurements according to Equation 3 as a function of depth of sulfonation in monolayers and moles of sulfonate per gram, determined analytically: (---) emphasizes the correlation with the triboelectric charging data (Figure 6b) which extend over a larger number of samples; (—) point-to-point fit of data; (B) Q/M (ncoul/g) vs. sulfonation depth in monolayers and the number of moles in sulfonate per gram (C) γ_c (dyn/cm) vs. sulfonation depth in monolayers and the number of moles of sulfonate per gram: (---) emphasizes the correlation with the results of Figures 6a and 6b; (—) point-to-point fit of data

been pumped in a 10^{-3} -torr vacuum and then exposed to 40% RH and measured over a period of 24 hr. Within experimental error all values obtained from very short (2 min) to very long (24 hr) treatments were identical.

It should be noted that the zero sulfonation data displayed in Figure 6c are different from those recently published (10). A further examination of the earlier work revealed that the value of $\gamma_c = 36$ dyn/cm reported in Ref. 10 was obtained using a commercial sample of PS containing some chemical additives that apparently affected γ_c . Measurements on the PS used in the present experiments consistently produced values of $\gamma_c = 32 \pm 1$ dyn/cm.

Comparison of Methods. Figure 6 compares the results of the three experimental techniques. The solid curves in Figure 6 are drawn to connect the experimentally measured data, whereas the dashed lines in Figures 6a and 6c are drawn to correlate the XPS and surface energy measurements. Inflection points are resolved in the triboelectric data (Figure 6b). With the exception of the data below approximately a 2–3- μ conversion depth, such a comparison shows that the maxima and minima correlate. In view of the fact that the three methods probe widely varying depths (~ 30 Å for XPS, 1 monolayer for surface energy, and several microns for triboelectric charging) this surprising correspondence must be attributed to modulations in the orientation and association (aggregation) of the sulfonic acid groups induced by continued sulfonation.

The reason for these observations is not clear. We believe that the gross shape of the individual data curves is attributable to the inability of the sulfonated film to reorient during initial reaction stages (< 10 monolayers reaction depth), followed by reorientation and association of sulfonate groups at higher conversions. The modification of the gross features observed indicates the complex nature of the surface and bulk structures of these highly polar films and the need for further experimental investigation of the observed effects.

Summary

In summary, through the use of a simple type of XPS(θ), the molecular orientation at the surface of sulfonated PS films has been determined. In the more sulfonated films the sulfur and oxygen atoms reside preferentially below the surface, as their respective XPS(θ) core-level signals decrease with increasing θ faster than the matrix C(1s) signal. These results are corroborated by surface energy measurements that also indicate that the accessibility of the sulfonate groups depends on associative interactions in the solid. In particular, it appears that a preferential

surface alignment provides a less polar interface and that a critical sulfonation depth is necessary to overcome surface irregularities in the untreated films.

Literature Cited

1. Mittal, K. L. In "Adhesion Science and Technology"; Lee, L. H., Ed.; Plenum: New York, 1975; p. 129.
2. Takabayashi, F.; Maeda, S. Japanese Patent 7 316 709, 1973; *Chem. Abstr.* 1974, 80, 38286n.
3. Andrews, J. M.; Collins, A. H. *Appl. Chem.* 1966, 16, 139.
4. Diggwa, A. D. S. *Plast. Polym.* 1974, 43, 101.
5. Hradil, J.; Stamberg, J.; Kaganov, A. L. *J. Polym. Sci.* 1974, 47, 123.
6. Baszkin, A.; Ter-Minassian-Saraga, L. *J. Colloid Interface Sci.* 1973, 43, 190.
7. Nelson, J. A.; Vollmer, W. K. U.S. Patent 2 879 177, 1959; *Chem. Abstr.* 1959, 53, 11889f.
8. Zisman, W. A. *Ind. Eng. Chem.* 1963, 55, 19.
9. Rasmussen, J. R.; Bergbreiter, D. E.; Whitesides, G. M. *J. Am. Chem. Soc.* 1977, 99, 4746.
10. Salaneck, W. R.; Gibson, H. W.; Bailey, F. C.; Pochan, J. M.; Thomas, H. R. *J. Polym. Sci., Polym. Lett. Ed.* 1978, 16, 447.
11. Briggs, D.; Brewis, D. M.; Konieczko, M. B. *J. Mater. Sci.* 1976, 11, 1270.
12. Millard, M. M. *Anal. Chem.* 1972, 44, 828.
13. Millard, M. M.; Lee, K. S.; Pavlath, A. E. *Text. Res. J.* 1972, 42, 307.
14. Millard, M. M.; Pavlath, A. E. *Text. Res. J.* 1972, 42, 460.
15. Fox, H. W.; Zisman, W. A. *J. Colloid Sci.* 1952, 1, 109.
16. Osipow, L. I. "Surface Chemistry"; Reinhold: New York, 1962.
17. Hart, R.; Jannsen, R. *Makromol. Chem.* 1961, 43, 242.
18. Gibson, H. W.; Bailey, F. C. *Symp. Macromol., Internat., 26th* 1979, 1, p. 530.
19. Gibson, H. W.; Bailey, F. C. *Macromolecules*, 1980, 13, in press.
20. Gibson, H. W.; Pochan, J. M.; Bailey, F. C. *Anal. Chem.* 1979, 51, 483.
21. Ohta, T.; Fujikawa, T.; Kuroda, H. *Bull. Chem. Soc. Jpn.* 1975, 48, 2017.
22. Riga, J.; Pireaux, J. J.; Caudano, R.; Verbist, J. J. *Physica Scripta* 1977, 16, 346.
23. Riga, J.; Pireaux, J. J.; Verbist, J. J. *Mol. Phys.* 1977, 34, 131.
24. Salaneck, W. R.; Thomas, H. R. *Solid State Commun.* 1978, 27, 685.
25. Clark, D. T.; Thomas, H. R. *J. Polym. Sci., Polym. Chem. Ed.* 1977, 15, 2843.
26. Clark, D. T.; Cromarty, B. J.; Dilks, A. *J. Polym. Sci., Polym. Chem. Ed.* 1978, 16, 3173.
27. Dwight, D. W.; McGrath, J. E.; Wightman, J. P. *J. Appl. Polym. Sci. Appl. Polym. Sym.* 1978, 34, 35.
28. Storp, S.; Holm, R. *J. Electron Spectrosc. Relat. Phenom.* 1979, 16, 183.
29. Clark, D. T.; Dilks, A.; Peeling, J.; Thomas, H. R. *Trans Faraday Soc.* 1975, 60, 183.
30. Clark, D. T.; Dilks, A. *J. Polym. Sci., Polym. Chem. Ed.* 1976, 14, 533.
31. Clark, D. T.; Dilks, A. *J. Polym. Sci., Polym. Chem. Ed.* 1977, 15, 15.
32. Jolly, W. L.; Hendrickson, D. N. *J. Am. Chem. Soc.* 1970, 92, 1863.
33. Snyder, L. C. *J. Chem. Phys.* 1971, 55, 95.
34. Platt, J. R. *J. Chem. Phys.* 1951, 19, 263.
35. Carter, W. J.; Schweitzer, G. K.; Carlson, T. A. *J. Electron Spectrosc. Relat. Phenom.* 1974, 5, 827.

36. Cadman, P.; Gossedge, G.; Scott, J. D. *J. Electron Spectrosc. Relat. Phenom.* **1978**, *13*, 1.
37. Scofield, J. H. *J. Electron Spectrosc. Relat. Phenom.* **1976**, *8*, 129.
38. Gibson, H. W. *J. Am. Chem. Soc.* **1975**, *97*, 3832.
39. Gibson, H. W.; Bailey, F. C. *Chem. Phys. Lett.* **1977**, *51*, 352.
40. Gibson, H. W.; Bailey, F. C.; Mincer, J. L.; Gunther, W. H. H. *J. Polym. Sci., Polym. Chem. Ed.*, **1979**, *17*, 296.
41. Pochan, J. M.; Gibson, H. W.; Bailey, F. C.; Hinman, D. F. *J. Electrostatics*, **1980**, *7*, in press.
42. Fabish, T. J.; Saltsburg, H. M.; Hair, M. L. *J. Appl. Phys.* **1976**, *47*, 930.

RECEIVED August 3, 1979.

An Electrochemical Method for the Determination of the Effective Volume of Charged Polymers in Solution

PETER SLOTA and JACOB A. MARINSKY

Department of Chemistry, State University of New York at Buffalo,
Buffalo, NY 14214

An electrochemical method projected for the determination of the effective volume of a colloiddally dispersed polyelectrolyte phase in aqueous media was evaluated. Experiments with the highly flexible Sephadex (carboxymethyl-dextran) gel and the more rigidly cross-linked polymethacrylic acid resin were performed for this purpose. With the well-defined resin (gel) phase it was possible to measure the polymer volume as a function of every experimental condition used to test fully the fundamental concepts on which the method is based. The results substantiate the validity of concepts developed. Application of this method for estimating the effective volume of weakly acidic (basic) polymers in solution seems worthy of further consideration. However, some modification of the treatment of the electrochemical data is necessary for polymeric sols, and this aspect is discussed briefly.

The electrochemical method proposed here for the measurement of the effective volume of charged polymers dispersed as colloidal suspensions is based on an observation by Merle (1). In his recent study of the influence of the swelling of the weakly acidic Sephadex gel on its potentiometric properties during neutralization with standard base in the presence of a fully dissociated polyelectrolyte, sodium polyvinyl sulfate, he discovered that over the complete neutralization range

$$\text{pH} - \text{pNa} - \log \frac{\alpha^2}{1 - \alpha} - \log \frac{v}{V_p} = \text{Constant} \quad (1)$$

0-8412-0482-9/80/33-187-311\$05.00/0
© 1980 American Chemical Society

In this equation α represents the degree of neutralization, ν the number of repeating functional units in the polymer, and V_p the volume of the gel. We sought the origin of this constant term in the following theoretical analysis of Merle's observation.

At equilibrium, during each step of the potentiometric titration of a weakly acidic (or weakly basic) gel $(HA)_\nu$, in the presence of a simple electrolyte MX, the chemical potential μ of each diffusible component (HX, MX, and H_2O) is equal in both phases; for example,

$$\mu_{\text{HX}} = \bar{\mu}_{\text{HX}}$$

$$\mu_{\text{MX}} = \bar{\mu}_{\text{MX}}$$

and

$$\mu_{\text{H}_2\text{O}} = \bar{\mu}_{\text{H}_2\text{O}} \quad (2)$$

the bar placed above μ identifying the gel (resin) phase.

In the gel (resin) phase

$$\begin{aligned} \bar{\mu}_{\text{HX}} &= \mu^\circ_{\text{HX}} + RT \ln \bar{a}_{\text{HX}} + \Pi V_{\text{HX}} \\ \bar{\mu}_{\text{MX}} &= \mu^\circ_{\text{MX}} + RT \ln \bar{a}_{\text{MX}} + \Pi V_{\text{MX}} \end{aligned} \quad (3)$$

where μ° represents the chemical potential of each component in the standard state, Π the osmotic pressure of the water in the gel phase, and V the partial molar volume of the diffusible components. The osmotic pressure is related to the activity of water a_w in the two phases by

$$\Pi = -(RT/V_w) \ln (\bar{a}_w/a_w) \quad (4)$$

At equilibrium, the distribution of HX and MX during each step of the potentiometric titration is defined by the reaction



Recalling that the activity of each component in the solution phase is defined by

$$\mu = \mu^\circ + RT \ln a \quad (6)$$

we have chosen the standard state to be the same in both phases so that the sum of all μ° terms is zero; we obtain

$$RT \ln [(a_{\text{HX}} \bar{a}_{\text{MX}}) / (\bar{a}_{\text{HX}} a_{\text{MX}})] = \Pi / RT (V_{\text{HX}} - V_{\text{MX}}) \quad (7)$$

as the expression of this equilibrium.

In Merle's examination of carboxymethyldextran, polyvinyl sulfate (a fully dissociated polyelectrolyte) was used in place of a simple salt to control the ionic strength. Invasion of the gel phase by coion X was thus avoided. The electrochemical potential of the mobile counterions are equal throughout such a system at equilibrium and Equation 7 transforms to

$$\ln [(a_{\text{H}}\bar{a}_{\text{M}})/(\bar{a}_{\text{H}}a_{\text{M}})] = (\Pi/RT)(V_{\text{H}} - V_{\text{M}})$$

or

$$p\text{M} - p\text{H} = p\bar{\text{M}} - p\bar{\text{H}} + (\Pi/RT) 0.4343 (V_{\text{H}} - V_{\text{M}}) \quad (8)$$

At equilibrium the $p\bar{\text{H}}$ of the gel (resin) phase is given by Equation 9

$$p\bar{\text{H}} = p\bar{K}_{(\text{HA})\nu}^{\text{int}} + \log \frac{\alpha}{1 - \alpha} + \log \bar{y}_{\text{A}^-} \quad (9)$$

where

$$p\bar{\text{H}} = -\log \bar{C}_{\text{H}} - \log \bar{y}_{\text{H}} \quad (10)$$

$\bar{K}_{(\text{HA})\nu}^{\text{int}}$ is the intrinsic dissociation constant of the repeating acidic group in the macromolecule, α is the degree of neutralization, \bar{C}_{H} denotes the concentration of H^+ in the gel, and \bar{y}_{A^-} and \bar{y}_{H} are activity coefficients of the designated species in the gel phase. Correction for deviation from ideality of the associated species HA is considered negligible and activity coefficients are assigned only to the charged species H^+ and A^- . With this representation of $p\bar{\text{H}}$ Equation 8 becomes

$$p\text{M} - p\text{H} = p\text{M} - p\bar{K}_{(\text{HA})\nu}^{\text{int}} - \log \frac{\alpha}{1 - \alpha} - \log \bar{y}_{\text{A}^-} + \frac{\Pi}{RT} (0.4343) (V_{\text{H}} - V_{\text{M}}) \quad (11)$$

By definition

$$p\bar{\text{M}} = -\log \bar{C}_{\text{M}} - \log \bar{y}_{\text{M}} \quad (12)$$

and Equation 11 becomes

$$p\text{M} - p\text{H} = -\log \bar{C}_{\text{M}} - \log \bar{y}_{\text{M}} - p\bar{K}_{(\text{HA})\nu}^{\text{int}} - \log \frac{\alpha}{1 - \alpha} - \log \bar{y}_{\text{A}^-} + \frac{\Pi}{RT} (0.434) (V_{\text{H}} - V_{\text{M}}) \quad (13)$$

For each molecular unit of HA dissociated, one molecule of M^+ enters the gel (resin) phase and

$$\bar{C}_M = \alpha\nu/V_p \quad (14)$$

where ν denotes the number of ionizable groups in $(HA)_\nu$ and V_p is the effective volume of the gel domain. Substituting this definition of \bar{C}_M in Equation 13

$$\text{pH} - \text{pM} - \log \frac{\alpha^2}{1 - \alpha} + \log \frac{V_p}{\nu} + \frac{\Pi}{RT} (0.4343) (\bar{V}_M - \bar{V}_H) = \text{p}\bar{K}_{(HA)}^{\text{int}} + \log \bar{y}_{A^-} + \log \bar{y}_M \quad (15)$$

In the experiments of Merle, the pH, pNa, and V_p of carboxymethyl-dextran were measured as a function of α during titration with standard NaOH in the presence of sodium polyvinyl sulfate. We can therefore substitute Na for M in Equation 15. In addition, the Π/RT (0.4343) term is small enough in this system to neglect so that the following equation should adequately describe the potentiometric data.

$$\text{pH} - \text{pNa} - \log \frac{\alpha^2}{1 - \alpha} - \log \frac{\nu}{V_p} = \text{p}\bar{K}_{(HA)\nu}^{\text{int}} + \log \bar{y}_{A^-} + \log \bar{y}_{Na} \quad (16)$$

The left-hand side of this equation is identical to the left-hand side of Equation 1 found by Merle to yield a constant value of 3.76 ± 0.07 over the complete neutralization range of his study; the preceding analysis does not lead to prediction of the observed constancy. Instead, the right-hand side of the equation is equal to $\text{p}\bar{K}_{(HA)\nu}^{\text{app}}$, as shown later, and should vary with the degree of neutralization by increasing slowly in magnitude with increasing α .

There is experimental evidence to support the estimate that $\bar{y}_H = \bar{y}_{Na}$ in this system. In the research of Travers and one of the present authors (2), a study of the complexation of divalent metal ions by polymethacrylic acid (PMA) showed that deviation from ideality with α of the divalent ions exposed to the same potential as the H^+ ion was described exactly by the deviation term deduced from the potentiometric properties of the PMA. Additional evidence for this estimate is available in the ion-exchange literature (3, 4, 5). At a relatively low cross-linking percentage (2 wt % divinyl benzene) \bar{y}_H is about equal to \bar{y}_{Na} , as evidenced by the ion-exchange distribution of Na^+ and H^+ between a polystyrene sulfonate-based resin and a simple dilute electrolyte mixture of Na^+ and H^+ (Na^+ , H^+ , X^-). The selectivity coefficient measured over the complete composition range of the resin deviates very little from unity to demonstrate this as an experimental fact ($K_{H^{Na}} = 1.02 \pm 0.02$

at $\bar{X}_{\text{Na}} = 0$, $K_{\text{H}^{\text{Na}}} = 1.07 \pm 0.02$ at $\bar{X}_{\text{Na}} = 0.5$, and $K_{\text{H}^{\text{Na}}} = 1.12 \pm 0.03$ at $\bar{X}_{\text{Na}} = 1$) (6).

Since $\bar{y}_{\text{Na}} \approx \bar{y}_{\text{H}}$ the right-hand side of Equation 16 can be written as $p\bar{K}_{(\text{HA})\nu}^{\text{int}} + \log \bar{y}_{\Delta^-} + \log \bar{y}_{\text{H}}$. From Equations 9 and 10

$$p\bar{K}_{(\text{HA})\nu}^{\text{int}} + \log \bar{y}_{\text{H}} + \log \bar{y}_{\Delta^-} = p\bar{C}_{\text{H}} - \log \frac{\alpha}{1 - \alpha} \quad (17)$$

and

$$p\bar{K}_{(\text{HA})\nu}^{\text{int}} + \log \bar{y}_{\text{H}} + \log \bar{y}_{\Delta^-} = p\bar{K}_{(\text{HA})\nu}^{\text{app}} \quad (18)$$

Equation 16 can thus be rewritten as

$$\text{pH} - \text{pNa} - \log \frac{\alpha^2}{1 - \alpha} - \log \frac{\nu}{V_p} = p\bar{K}_{(\text{HA})\nu}^{\text{app}} \quad (19)$$

Since Merle's data indicate that deviation from ideality of the charged species is negligible in the gel, contrary to expectations derived from the preceding analysis, we reexamined the potentiometric properties of the flexible carboxymethyl-dextran gel system (Sephadex CM-50) studied by Merle. We also carried out a parallel investigation of the much more rigid PMA resin (IRC-50) cross-linked with approximately 5 wt % divinyl benzene. The titrations of these polymers with standard base were made in the presence of sodium polystyrene sulfonate. The pH and pNa of the solution phase and the volume (V_p) of the gel (resin) phase were measured at selected α values covering the complete neutralization range.

We have sought to demonstrate the validity of Equation 19 by showing that a plot of the sum of the terms on the left-hand side of that equation as a function of α yields an intercept value of the ordinate at $\alpha = 0$ which can be identified unambiguously with the $p\bar{K}_{(\text{HA})\nu}^{\text{int}}$ measured for the linear polyelectrolyte analog of the gel (resin).

With such a demonstration of the fundamental development presented it would be appropriate to propose this approach (with some modification) for the measurement in aqueous media of the effective volume of colloiddally dispersed polyacid over its complete neutralization range.

In the aqueous polyelectrolyte system the experimental measurement of pC_{H} can be used to evaluate $\bar{K}_{(\text{HA})\nu}^{\text{app}}$ directly since

$$pC_{\text{H}} - \log \frac{\alpha}{1 - \alpha} = p\bar{K}_{(\text{HA})\nu}^{\text{app}} = p\bar{K}_{(\text{HA})\nu}^{\text{int}} - 0.4343 \frac{\epsilon\psi(a)}{kT} + \log \bar{y}_{\text{H}} + \log \bar{y}_{\Delta^-} \quad (20)$$

This equation is based on the assumption that the Boltzmann distribution applies to these systems. With this assumption the $-0.4343 \epsilon\psi_{(a)}/kT$ term provides the local concentration of H^+ ion, with an electric potential energy of $\epsilon\psi_{(a)}$, at the polyion surface a , relative to its average concentration at the point of measurement. As before, the \bar{y}_H and \bar{y}_A parameters correct for the thermodynamic nonideality of the ions in these systems. Usually they are included arbitrarily in the $-0.434 \epsilon\psi_{(a)}/kT$ term.

With $p\bar{K}_{(HA)}^{app}$ directly accessible in this way, V_p can be calculated according to Equation 19.

Experimental

Both the Sephadex gel (C-50-120) received from the Sigma Chemical Company and the cross-linked PMA (Amberlite IRC-50) received from the Rohm and Haas Company were first treated with 1M HCl to convert them completely to their acid form. After complete removal of excess acid was assured by exhaustive washing with deionized water, the water was withdrawn from the Sephadex by filtration. The moist gel was then stored in a sealed polyethylene bottle. Reproducible sampling for an experiment from this source was demonstrated by the high precision obtained from capacity measurements of samples taken concurrently with those used in the potentiometric measurements program.

With the IRC-50, excess water was first removed by patting it dry with absorbent paper. The resin then was equilibrated isopiesticly with saturated ammonium chloride prior to storage in a sealed polyethylene bottle.

The sodium polystyrene sulfonate, average molecular weight approximately 50,000 and 500,000 (Versa-T1-50 and 500, respectively), was kindly donated by the National Starch and Chemical Corporation. It was prepared for use as described in an earlier paper (7). The standard NaOH was Fisher Certified Reagent.

Sephadex samples of approximately 1 g were weighed (1.000 g = .5154 \pm .0015 meq of H) into approximately 20–25 mL of 0.05M and 0.03M NaPSS solution (mol wt \approx 50,000 and 500,000, respectively). These samples, covered by a nitrogen gas atmosphere, were then neutralized with standard base to define an α range of study from 0.1 to 0.9.

With the resin, samples of 0.1 g were weighed (0.100 g = .819 meq \pm .002; water content = 23.69%) into approximately 83 mL of a 0.03M NaPSS (mol wt \approx 500,000) solution. An α range from 0.025 to 0.98 was covered in the examination of these materials.

In preparing all solutions, the distilled, deionized water was boiled to remove CO_2 prior to its use. All samples were then kept sealed to prevent any absorption of CO_2 during equilibration. For the Sephadex, a 3–4-day period was sufficient to achieve equilibrium; with the IRC-50, however, the equilibrium interval exceeded 2 weeks. At equilibrium, pH and pNa measurements at 25° \pm 0.1°C were made with the system under a nitrogen atmosphere. All pH measurements were made with a glass electrode using a Radiometer Model 4 pH meter. A sodium-ion selective electrode was used to measure pNa. A saturated calomel electrode was used as the reference electrode.

Prior to the potentiometric measurements the glass electrode was adjusted with the standard buffer solutions over the pH range of the samples encountered; the sodium electrode was calibrated using standard sodium chloride solutions. For study of the Sephadex-NaPSS system an additional calibration of both the sodium and the glass electrodes was made. With the Sephadex system, the ratio of Na^+ to H^+ did not exceed 1000 until α was greater than 0.6; below this Na^+ to H^+ ratio, H^+ interferes significantly with the Na^+ measurements. A quantitative estimate of the extent of this interference at the experimental concentration of the NaPSS (0.05M) was effected by measuring pNa as a function of pH (5.6 to 2.6) during controlled addition of HPSS (*see* Figure 1).

To evaluate the pH response of the glass electrode in the PSS⁻ solution, a 0.05M (0.03M) PSS⁻ solution (monomer basis) containing 0.01M H^+ and 0.04M (0.02M) Na^+ (100 mL) was titrated with 0.7556M NaOH. These data were compared with data from a parallel titration of

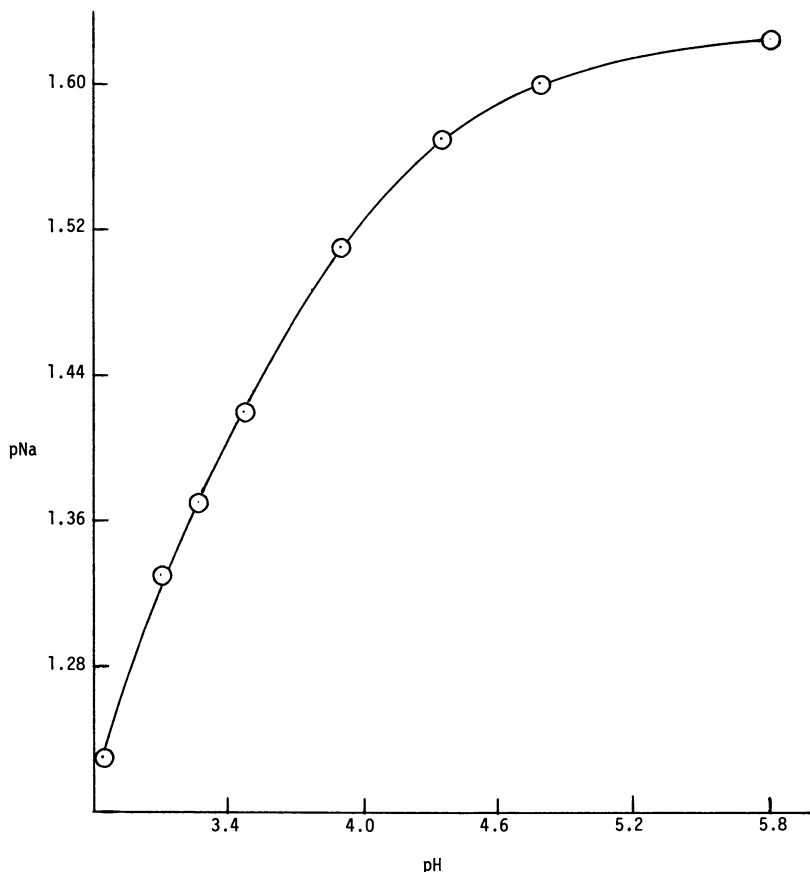


Figure 1. Response of Na^+ -ion selective electrode at different H^+ concentrations (0.05M NaPSS, XM HPSS)

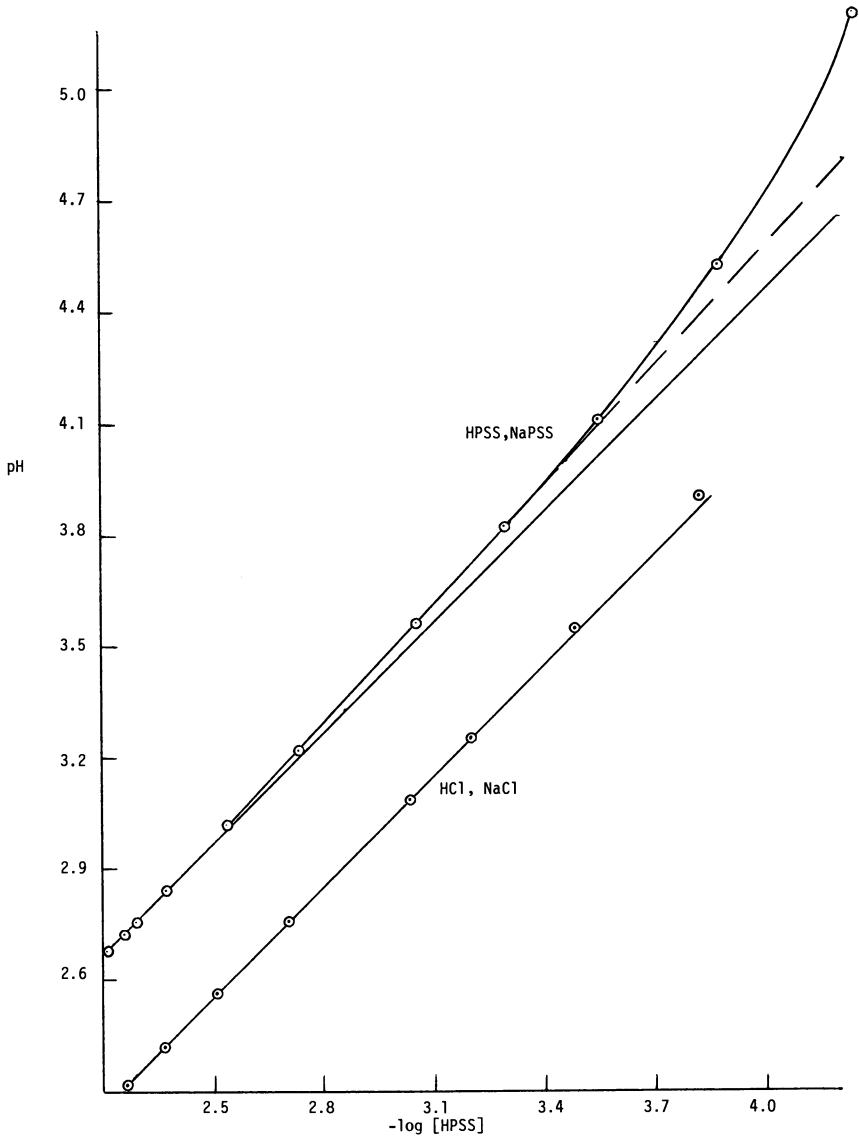


Figure 2. Glass electrode response in 0.05M Na-HPSS and 0.05M Na-HCl

0.01M HCl in 0.04M (0.02M) NaCl by plotting pH vs. pC_H (see Figure 2). Nernstian response of the glass electrode is obtained with the HCl-NaCl system, indicated by the slope of unity obtained from the plot of pH vs. pC_H . Deviation from Nernstian response of the glass electrode in the PSS systems can be estimated from the increase in the slope of the straight line obtained from similar plots of the PSS⁻, pH data; the correct pH is estimated from the pH value given by a straight line of

unit slope drawn from the lowest pH data points. In analyzing the Sephadex and IRC-50 data, deviation of the glass electrode from Nernstian response was presumed to continue to be given by extension of the straight line defined by the earlier experimental points. Curvature of the line indicated at higher pH in Figure 2 was disregarded. (Beyond a pC_H value of 4.0, estimate of the concentration of H^+ ion is based on an extremely small difference between the total acid and total base added (1.00–0.99), and a 0.1% error in either value already leads to an error of 10% in C_H at this point.)

To assist computation of the degree of dissociation of the Sephadex and IRC-50 at the lower pH values, the activity coefficient of hydrogen ion in the presence of the polystyrene sulfonate was determined by examining the potentiometric property of 0.001M reagent-grade acetic acid from Fisher in the presence of 0.03, 0.06, and 0.09M NaPSS (mol wt \approx 500,000). At each polystyrene sulfonate concentration a unique activity coefficient (0.300, 0.290, and 0.290, respectively, in 0.03, 0.06, and 0.09M NaPSS), essential for the resolution of the acid dissociation constant, was resolved by this approach.

To measure the volume of the Sephadex at equilibrium the equilibrated samples were contained in a calibrated tube (0.1 mL/division). An apparent volume was obtained from visual observation of the boundary defined by the layer; to obtain the true volume an aliquot of the equilibrated solution phase was analysed for sodium by flame photometry. Most of the supernatant solution was then removed until 2.0 ± 0.025 mL of solution remained above the gel-defined boundary. Exactly 1.00 mL of water was added and the mixture was stirred sufficiently to assure a homogeneous aqueous phase. The solution phase was sampled immediately for sodium analysis with the flame photometer. From the observed dilution of the aqueous phase the true volume of the Sephadex gel at equilibrium was obtained. A correction for the matrix volume was based on the monomeric molecular weight of the Sephadex ($\sim 220 \pm 25$; capacity of 4.5 ± 0.5 meq/dry g). In our samples, which contained about 88% water or 0.12 g acid/g sample, a volume of about 0.13/g is estimated for the matrix by assuming a density of approximately 0.9 for the dehydrated Sephadex.

To measure the volume of each equilibrated IRC-50 sample the resin was quantitatively transferred from the equilibrium solution to a sintered glass disc contained in a centrifuge tube. The tube was covered with parafilm to prevent any loss of water during the centrifugation performed to remove as much of the surface liquid as possible (4, 7). The resin was then transferred quantitatively to a portion of the original solution contained in a pycnometer. The volume of solution displaced by the resin yielded the volume of the resin phase including its organic matrix. To obtain the volume of the inert matrix for subtraction from this number, several resin samples whose gross volumes had been determined as described previously were once again separated from the solution for centrifugation. The centrifuged sample was weighed carefully and then dried at 105°C until constant weight was reached. The difference in the measured volume of the resin sample and the weight of the water removed was considered to yield the volume of the resin matrix. The correction term was subtracted from each of the gross resin volumes obtained.

Results

The data obtained for the several systems studied are presented in Tables I and II. These data, expressed as $\text{pH} - \text{pNa} - \log(\alpha^2 v / [(1 - \alpha)(V_p)])$, after correcting for deviation from Nernstian response of the glass electrode with the PSS solution (*see* Figure 2), have been plotted vs. α in Figures 3 and 4. (*Note*: 1. The osmotic pressure term $0.4343 (\Pi/RT)(V_M - V_H)$ is very small, even in the more inflexible resin system where it reaches a maximum value of less than 0.01 in the highest neutralization region, and has been neglected. 2. It was not possible to calibrate the glass electrode directly over the higher pH range encountered in the IRC-50-0.03M NaPSS system. The trend of discrepancy observed at the lower pH range was presumed to persist for the estimate of pH correction in this system. 3. In Figure 4 the value ordinarily assigned to pK^{app} by presuming $\text{pH} - \log \alpha / (1 - \alpha)$ to be a measure of this parameter has been included for comparison. However, such treatment of potentiometric data for this purpose is known to be inappropriate (5).) The resultant curves have been extrapolated, as shown, to intercept the ordinate axis at $\alpha = 0$. The $\text{pK}_{(\text{HA})_v}^{\text{int}}$ values of 3.25 and 4.83 so resolved for Sephadex and IRC-50, respectively, are in excellent agreement with the value of 3.25 observed for carboxymethyl dextran (8), the linear polyelectrolyte analog of Sephadex, and the value of 4.83 reported for both PMA (2,9), the linear analog of IRC-50, and isobutyric acid (10), its repeating monomer unit. Only the data for which the more precise

Table I. Potentiometric and Volume Measurement Data for the Sephadex-NaPSS System

<i>0.05M NaPSS</i>					
α	<i>pH</i>		<i>pNa</i>		$V_p(\text{mL})$
	<i>exp</i>	<i>corr</i>	<i>exp</i>	<i>corr</i>	
0.111	2.975	2.975	1.330	1.757	2.07
0.273	3.704	3.657	1.516	1.709	2.53
0.409	4.131	4.031	1.575	1.691	3.12
0.603	4.650	4.483	1.608	1.681	3.28
0.751	5.060	4.847	1.627	1.668	3.77
0.900	5.622	5.342	1.658	1.658	4.24
<i>0.03M NaPSS</i>					
0.111	3.058	3.033	1.561	2.050	1.85
0.190	3.533	3.463	1.735	2.027	2.27
0.270	3.882	3.757	1.827	1.994	2.77
0.407	4.350	4.205	1.916	1.984	3.11
0.602	4.922	4.697	1.928	1.964	3.87
0.900	6.016	5.630	1.962	1.962	4.31

Table II. Potentiometric and Volume Measurement Data for the IRC-50-0.03M NaPSS System^a

α	<i>pH</i>		<i>pNa</i>	V_p (mL)
	<i>exp</i>	<i>corr</i>		
0.0287	5.033	4.839	1.964	0.0511 ^b
0.0512	5.549	5.298	2.002	0.0516 ^b
0.0755	5.852	5.578	2.010	0.0686 ^b
0.0995	6.068	5.778	2.005	0.0770 ^b
0.100	6.036	5.748	2.027	0.09 ^c
0.200	6.644	6.236	2.014	0.1128 ^b
0.200	6.655	6.245	2.044	0.10 ^c
0.300	6.917	6.488	2.065	0.13 ^c
0.349	7.162	6.717	2.060	0.14 ^c
0.400	7.352	6.891	2.070	0.15 ^c
0.400	7.279	6.853	2.026	0.1459 ^b
0.451	7.512	7.038	2.065	0.15 ^c
0.500	7.712	7.224	2.072	0.15 ^c
0.549	7.755	7.263	2.070	0.17 ^c
0.600	7.928	7.423	2.072	0.17 ^c
0.650	8.040	7.527	2.062	0.18 ^c
0.700	8.243	7.715	2.060	0.18 ^c
0.751	8.359	7.822	2.053	0.18 ^c
0.800	8.478	7.932	2.012	0.1704 ^b
0.849	8.833	8.261	2.065	0.20 ^c
0.899	9.093	8.501	2.072	0.19 ^c
0.985	10.166	9.486	2.053	0.20 ^c

^a 0.1 g PMA resin in approximately 83 mL 0.03M NaPSS.^b Volume displaced by the resin measured to ± 0.00005 mL.^c Measured to ± 0.005 mL.

volume measurements (*see* Table II) were obtained as described in the experimental section are used in Figure 4. The less precise data were obtained by measuring volume displacement in a 5.0-mL buret with 0.05-mL divisions. These samples were used to fix the time interval of 2 weeks found to be needed for their equilibration. They were opened several times to measure pH over a period of more than 4 weeks. Although precautions were taken to avoid absorption of CO₂, the possibility of such sample contamination is much greater in these measurements than those analyzed in Figure 4. In addition, the growth of bacteria in the samples was always a potential problem.

With the IRC-50-NaPSS system, the rigid matrix of the resin is resistant to the entry of solvent so that at equilibrium the concentration of counterions increases from 0.46 to 4.08M over the α range examined. At these resin-phase molarities it has been shown that the contribution of ion-solvent interaction to the deviation from ideal behavior of the counterions (*II*), while negligible at low concentration, is a factor to

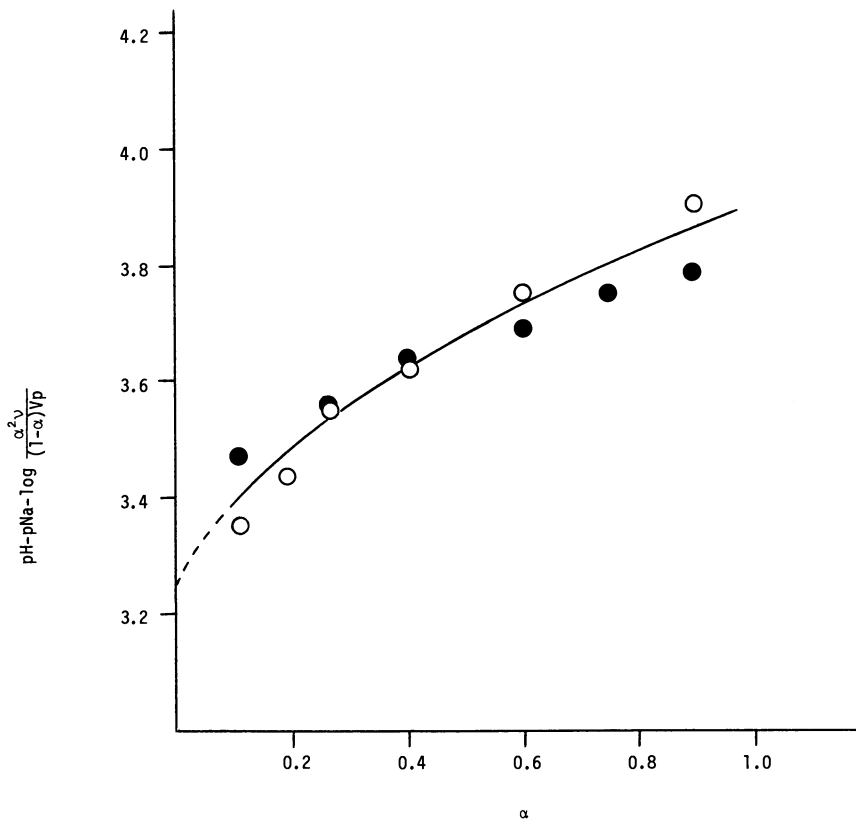


Figure 3. Potentiometric study of H Sephadex gel in 0.03M NaPSS solution (O) and 0.05M NaPSS solution (●)

consider. Therefore, one might expect that as \bar{C}_{Na} increased with α the identification of \bar{y}_{Na} with \bar{y}_H would be an increasingly incorrect estimate of the situation in this system. The net effect would be that \bar{y}_{Na} becomes smaller than \bar{y}_H so that the value of $pK_{(HA)_\nu}^{app}$, based on the assumption of their equality, is increasingly too small. This is not a serious problem since as α decreases, \bar{C}_{Na} decreases and \bar{y}_{Na} approaches \bar{y}_H in value. Extrapolation of the data as shown must yield $pK_{(HA)_\nu}^{int}$ as expected.

On the basis of the observed results there is no question that the fundamental interpretation of the left-hand side of Equation 1 is expressed correctly in Equation 19. The discrepancy between our results and those of Merle has to be a consequence of the greater accuracy of the g_{el} volume and potentiometric measurements performed in this research. Merle did not correct for the volume of solution contained between gel beads nor did he calibrate his glass electrode in the presence of the fully dissociated sodium polyvinyl sulfate medium that he used.

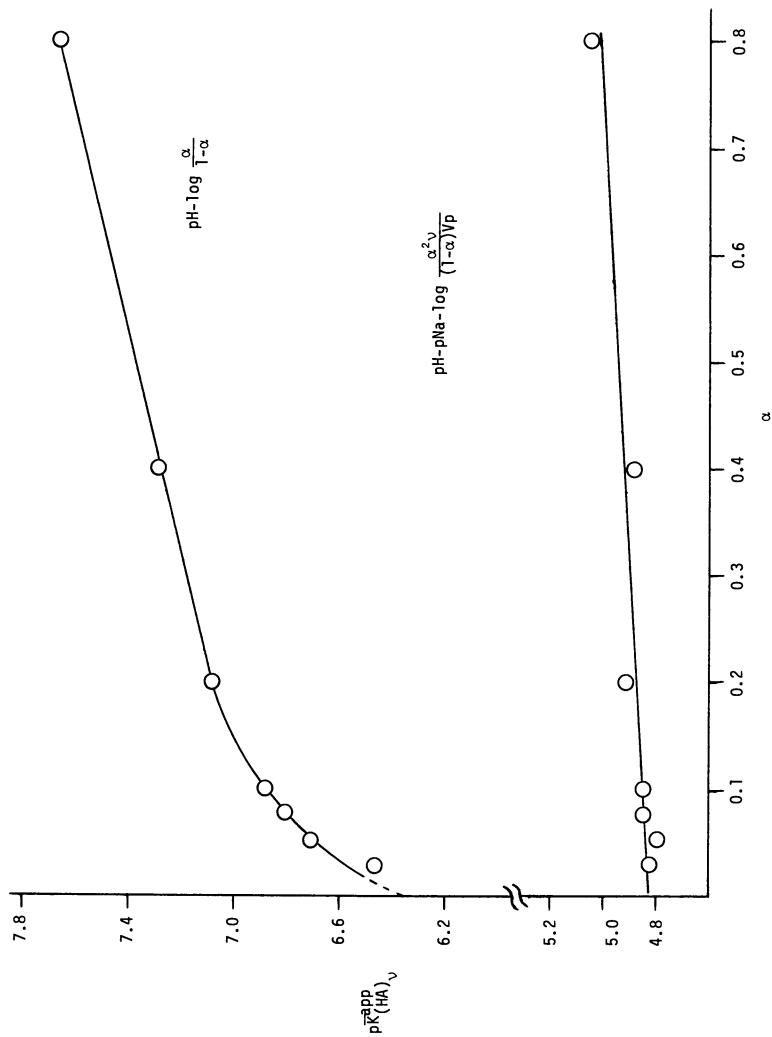


Figure 4. Potentiometric study of IRC-50 in 0.03M NaPSS solution

Thus a reliable experimental approach to the evaluation of the intrinsic pK values of highly swollen, weakly acidic (basic) gels and more rigidly cross-linked ion-exchange resins has been demonstrated fully in this study. It is the successful culmination of earlier studies in this direction by Nagasawa (12), Katchalsky (13), and Michaeli (14).

Discussion

We have shown already that the right-hand side of Equation 19 is experimentally accessible from the value of $p\bar{K}_{(HA)\nu}^{app}$ derived from measuring the pH of colloiddally dispersed polyacid during neutralization with standard base in the presence of a fully dissociated polyelectrolyte salt such as NaPSS. Since the concentration of counterions in a linear polymer domain is expected to be less than in even the minimally constrained Sephadex systems studied, the estimate that $\bar{y}_{Na} = \bar{y}_H$ is fully justified. As a consequence, potentiometric data, obtained as described for the gel and resin study to yield values of pH, pNa, α , and $p\bar{K}_{(HA)\nu}^{app}$, can, in principle, be used directly in Equation 19 to evaluate V_p , the effective volume of the polymer domain at every experimental condition used.

Unfortunately, a fundamental difference between a gel (resin) and a linear polyelectrolyte precludes this possibility. In resins and gels there is a well-defined physical boundary, each phase being essentially electrically neutral. However, in the case of a simple linear polyelectrolyte solution there is no discernible boundary, and the two phases, polymer and liquid, are not uncharged; a sizeable charge on the macromolecule is compensated by the presence of oppositely charged counterions in the liquid phase.

The phase boundary, as a consequence, must be defined arbitrarily. Those counterions with a thermal energy (kT) less than the energy of the electric field ($e\psi_{(a)}/kT$) can be assumed to define the boundary ($r = a$) of the polyelectrolyte for this purpose.

In colloidal suspensions of polyelectrolytes, where the existence of two phases is not discernible by visual observation, the concentration of Na^+ ions, \bar{C}_{Na} , is given by Equation 21 instead of by Equation 14.

$$\bar{C}_{Na} \sim \alpha \nu (1 - \phi_p) / V_p \quad (21)$$

where ϕ_p is the practical osmotic coefficient of the polyelectrolyte. The appropriate equation for the evaluation of V_p is then

$$pH - pNa - p\bar{K}_{(HA)\nu}^{app} - \log \left[\left(\frac{\alpha^2}{1 - \alpha} \right) (1 - \phi_p) \right] = \log (\nu / V_p) \quad (22)$$

We arrive at this estimate with the cell model proposed by Lifson and Katchalsky (15) for the analysis of the colligative properties of salt-free polyelectrolytes.

Literature Cited

1. Merle, Y. *J. Polym. Sci., Polym. Phys. Ed.* **1976**, *14*, 1317.
2. Travers, L.; Marinsky, J. A. *J. Polym. Sci., Polym. Phys. Ed.* **1974**, *47*, 285.
3. Helfferich, F. "Ion Exchange"; McGraw-Hill: New York, 1962; Chapter 5, p. 183.
4. *Ibid.*, Chapter 5, p. 231.
5. *Ibid.*, Chapter 4, p. 88.
6. Myers, G. E.; Boyd, G. E. *J. Phys. Chem.* **1956**, *60*, 521.
7. Reddy, M. M.; Marinsky, J. A. *J. Phys. Chem.* **1970**, *74*, 3844.
8. Gekko, K.; Noguchi, H. *Biopolymers* **1975**, *14*, 2555.
9. Arnold, R.; Overbeek, J. Th. G. *Rec. Trav. Chim.* **1950**, *69*, 192.
10. Lange, N. A. "Handbook of Chemistry," 6th ed.; Handbook Publishers, Inc.: Sandusky, Ohio, 1946; p. 1377.
11. Marinsky, J. A.; Reddy, M. M.; Amdur, S. *J. Phys. Chem.* **1973**, *77*, 2128.
12. Nagasawa, M.; Ishigai, H.; Kagawa, I. *Mem. Fac. Eng., Nagoya Univ.* **1958**, *10*, 105.
13. Michaeli, I.; Katchalsky, A. *J. Polym. Sci.* **1957**, *23*, 683.
14. Michaeli, I.; Kinrot, K. *Isr. J. Chem.* **1973**, *11*, 271.
15. Katchalsky, A. "Polyelectrolytes," *IUPAB Symposium on Macromolecules, Leiden, 1970*.

RECEIVED October 23, 1978.

Cooperative Silver Ion Binding by Synthetic Polycarboxylic Acids

ULRICH P. STRAUSS and A. JAMES BEGALA

Department of Chemistry, Rutgers University, The State University of New Jersey, New Brunswick, NJ 08903

The interactions of silver ion with polyacrylic acid and two copolymers of maleic acid were found to exhibit characteristics strikingly different from normal polyelectrolyte behavior. Potentiometric titrations with silver nitrate showed that most of the silver ion binding occurred over a narrow range of the silver ion activity. The location of this critical range depended strongly on the extent of polyacid protonation. Dilatometry data indicated that the volume changes accompanying the silver ion binding were remarkably insensitive to the extent of polyacid ionization. The intrinsic viscosity of polyacrylate was depressed significantly more sharply by silver than by hydrogen ion. The cooperativity is ascribed to silver-carboxylate cluster formation caused by the bridging of nonadjacent chain portions by linear two-coordinate argentous ion complexes.

Cooperative effects associated with the binding of metal ions by certain proteins (1) and polynucleotides (2) are significant in that they allow the biological activity of the macromolecules to be modulated by small changes in the thermodynamic activity of the metal ion. It seems likely that considerable progress in our understanding of the molecular basis of such cooperative phenomena would result from their study in synthetic polyelectrolyte systems. However, the binding of metal ions by synthetic polyelectrolytes is generally anticooperative, a behavior which may be ascribed to the electrostatic repulsions between bound metal ions (3). We have now discovered that the binding of silver ion by polyacrylic acid as well as by two other polycarboxylic acids exhibits pro-

0-8412-0482-9/80/33-187-327\$05.00/0
© 1980 American Chemical Society

nounced cooperativity. We report here the results of exploratory potentiometric, dilatometric, and viscosimetric studies carried out with these systems.

Experimental

Materials. Two samples of polyacrylic acid, PAA-1 (4) and PAA-2, were obtained as gifts from S. C. Johnson Company. Their degrees of polymerization were 3090 and 4420, respectively, as calculated from the intrinsic viscosities of their sodium salts in 0.10*N* NaBr at 15°C using the appropriate relation of Takahashi and Nagasawa (5). The samples of the hydrolyzed copolymers of maleic anhydride with ethylene (HEMA) and with methyl vinyl ether (HVMEMA) have been described previously (4).

Ion Binding Determinations. The binding of hydrogen and silver ions was determined by emf measurements under nitrogen at $30 \pm 0.05^\circ\text{C}$ with a Radiometer model 25 pH meter. Details concerning the methods used for hydrogen ion have been given earlier (4). For convenience a few definitions are restated here. The degree of neutralization, α , of the polyacids is given by the expression

$$\alpha = ([\text{TMAOH}] + [\text{H}^+] - [\text{OH}^-])/C_p \quad (1)$$

where $[\text{TMAOH}]$, $[\text{H}^+]$, and $[\text{OH}^-]$ are the molarities of added tetramethylammonium hydroxide, free hydrogen ion, and free hydroxyl ion, respectively, and C_p is the concentration of polyacid expressed in monomoles per liter. In the case of the maleic acid copolymers, one monomole contains one maleic acid residue and one ethylene or vinyl methyl ether residue so that $\alpha = 2$ at complete neutralization. An alternative measure of the degree of neutralization, α' , useful for comparisons between the polyacids, is given by the relation

$$\alpha' = ([\text{TMAOH}] + [\text{H}^+] - [\text{OH}^-])/n_p \quad (2)$$

where n_p is the normality of total polyacid. Thus, $\alpha' = \alpha$ for PAA, $\alpha' = \alpha/2$ for HEMA and HVMEMA, and $\alpha' = 1$ at complete neutralization for all three polyacids.

For silver ion a Radiometer P401 silver electrode and a Radiometer K601-saturated $\text{K}_2\text{SO}_4/\text{HgSO}_4$ reference electrode were used. The degree of binding of silver ion (θ_{Ag}) is given by the relation

$$\theta_{\text{Ag}} = ([\text{Ag}^+] - [\text{Ag}^+]_f)/n_p \quad (3)$$

where $[\text{Ag}^+] - [\text{Ag}^+]_f$ are the molarities of total and free silver ion, respectively. The molarity of free silver ion was determined from a calibration curve of the emf as a logarithmic function of the silver ion concentration. The calibration curve was linear and had a slope of 60 mV/decade. In all work involving the silver ion care was taken to avoid unnecessary exposure to light and to keep the pH and silver ion concentration low enough to prevent exceeding the solubility product constant of silver hydroxide ($K_{\text{sp}} = 1.52 \times 10^{-8} \text{ mol}^2 \text{ L}^{-2}$).

Other Methods. The procedure used for determining volume changes resulting from mixing two solutions in Linderstrom-Lang dilatometers at 30°C has been described previously (4). Viscosities were measured at 30°C using a Cannon-Ubbelohde dilution viscosimeter immersed in a bath thermostated to within 0.01°C.

Results and Discussion

Binding Isotherms. The degree of binding of silver ion θ_{Ag} by polyacrylic acid at various initial values of the degree of proton dissociation α is presented in Figure 1 as a function of the molarity of free silver ion $[Ag^+]_f$. Both samples of polyacrylic acid are represented: PAA-1 at $\alpha = 0.805$ and PAA-2 at $\alpha = 0.410, 0.615, \text{ and } 0.910$. The polyacid concentrations were 0.06 monomolar, with the solvent in these as well as in the other experiments reported here being an aqueous 0.2M TMANO₃ solution.

The striking feature of the curves in Figure 1 is the sharp inflection arising from a large increase in θ_{Ag} over a very small range of $[Ag^+]_f$. In contrast, a corresponding increase in hydrogen ion binding by polyacrylate occurs over a more than thousand-fold increase in the free hydrogen ion concentration (6, 7), and a corresponding increase in silver ion binding by polyphosphate occurs over a more than hundred-fold increase in the free silver ion concentration (7). The results indicate that the interaction between silver ion and polyacrylate is highly cooperative and specific.

The experiments exhibited several additional peculiarities. In the composition ranges corresponding to the steeply rising portions of the curves equilibrium was approached very slowly after each addition of the silver ion titrant. Times on the order of 1 hr were necessary for the emf values to attain constancy. As the addition of silver ion was continued beyond the steeply rising regions of the curves, gel-like precipitates appeared. The arrows in Figure 1 indicate the compositions at which gel formation was first detected in the titration runs. However, in several instances turbidity was observed at compositions corresponding to somewhat lower silver ion contents than those indicated by the arrows in solutions that had been set aside for one or more days.

Changes in the polyacid concentration from 0.009 to 0.06 monomoles/L had no effect on the binding isotherms. By following the pH as silver ion was added to the polyacrylate solutions it was found that no significant amounts of bound hydrogen ion were displaced by the silver ion binding. This finding is consistent with the observation that θ_{Ag} never exceeded the initial value of α , as is evident from the curves in Figure 1. It is also apparent from these curves that the silver activity at which the sharp rise in θ_{Ag} takes place increases with increasing protonation of the polyacrylate.

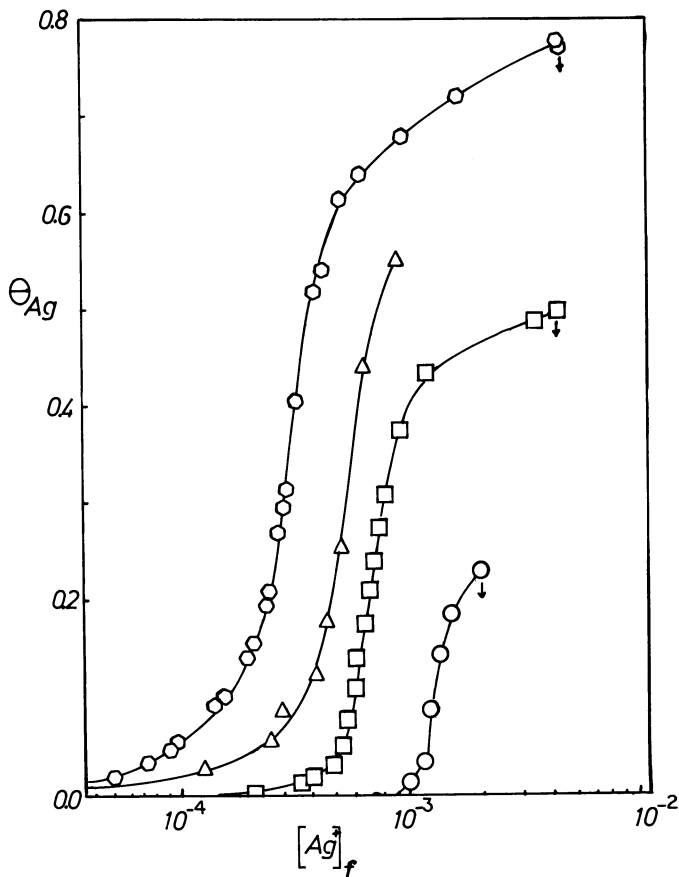


Figure 1. Silver ion binding by TMA salts of polyacrylic acid in 0.20M TMANO₃ at 30°C. The ordinate θ_{Ag} denotes mol of bound silver ion/equiv of total polyacid; the abscissa, $[Ag^+]_f$, the molarity of free silver ion. (\diamond) PAA-2 at $\alpha = 0.910$; (\triangle) PAA-1 at $\alpha = 0.805$; (\square) PAA-2 at $\alpha = 0.615$; (\circ) PAA-2 at $\alpha = 0.410$.

As can be seen from the binding isotherms shown in Figure 2, the interactions of silver ion with HEMA and HVMEMA are also cooperative. However, the rise in θ_{Ag} at the inflection point is less steep for these copolymers than for the polyacrylic acid; the steepness decreases in the order PAA > HEMA > HVMEMA.

Dilatometry. The volume changes observed on adding silver nitrate to the TMA salts of PAA-1 at $\alpha' = 0.805$, HEMA at $\alpha' = 0.70$, and HVMEMA at $\alpha' = 0.67$ in 0.2M TMANO₃ are shown in Figure 3. The abscissa n_{Ag} represents the moles of added Ag⁺ bound per mole of neutralized carboxylate groups, that is, $n_{Ag} = \theta_{Ag}/\alpha'$, and the ordinate ΔV represents the corresponding volume change. The points for PAA define

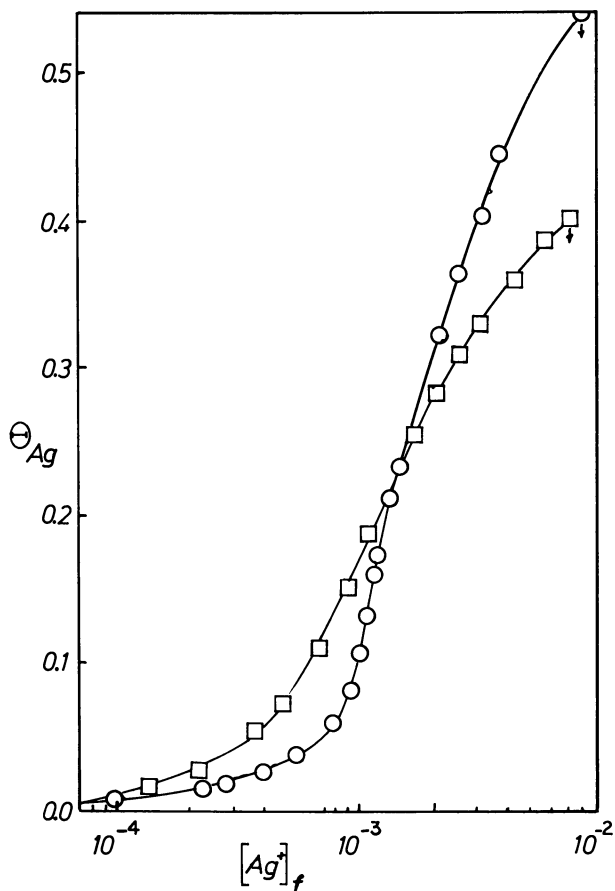


Figure 2. Silver ion binding by TMA salts of copolymers of maleic acid in 0.20M TMANO₃ at 30°C. Notation of abscissa and ordinate as in Figure 1. (○) copolymer with ethylene at $\alpha' = 0.70$; (□) copolymer with methyl vinyl ether at $\alpha' = 0.67$.

a straight line, yielding a value of 21.7 mL/mol of bound silver ion for the differential molar volume change, ΔV_D , defined as $d\Delta V/dn_{Ag}$ (4). The points for the two maleic acid copolymers fall quite close to the PAA line. The constancy of the value of ΔV_D over the whole binding range distinguishes the interactions of silver ion from those of hydrogen and magnesium ions for which ΔV_D decreased with increasing binding (4). The unusual behavior of silver ion is brought out further by a series of three experiments concerning the interaction of silver ion with PAA-2 as a function of the degree of proton dissociation α . The results of these experiments, each carried out in duplicate, are presented in Table I. The volume change per mole of silver ion bound, given in the third

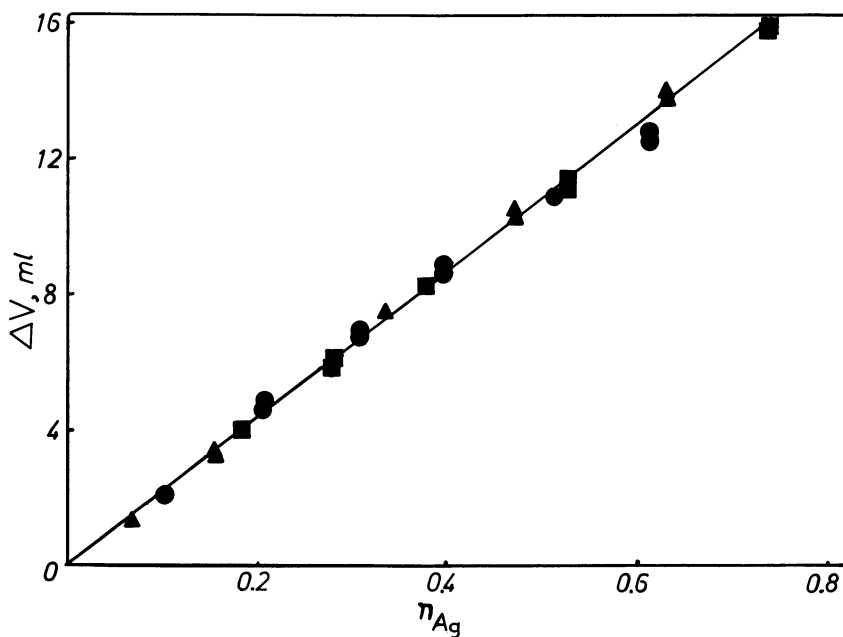


Figure 3. Volume change on the addition of silver nitrate to the TMA salts of the polyacids in 0.2M TMANO₃ at 30°C. The abscissa η_{Ag} denotes mol of added Ag⁺ bound/equiv of neutralized carboxylate groups; the ordinate, the corresponding volume change. A straight line has been drawn through the points for PAA-1. (■) PAA-1 at $\alpha = 0.805$; (▲) HEMA at $\alpha' = 0.70$; (●) HVMEMA at $\alpha' = 0.67$.

Table I. Volume Changes for the Binding of Silver Ion by Polyacrylic Acid (PAA-2) as a Function of the Degree of Neutralization

α	θ_{Ag}	ΔV (mL/mol Ag ⁺ bound)	ΔV_D (mL H ⁺)	Estimated Maximum Values of ΔV (mL/mol Ag ⁺ bound)	
				Ag(COO)	Ag(COO) ₂ ⁻
0.910	0.160	22.3			
0.910	0.160	21.3	22.3	21.2	33.7
0.615	0.146	22.8			
0.615	0.146	22.6	20.0	19.4	30.1
0.410	0.124	23.1			
0.410	0.124	23.6	17.4	18.1	27.5

column, increases slightly with decreasing α . In contrast, the values of ΔV_D for hydrogen ion, obtained from a previous paper (4) and given in the fourth column, exhibit a significant decrease with decreasing α . This decrease has been shown to indicate that the average electrostriction volume per unprotonated carboxylate group diminishes with increasing hydrogen ion binding, an effect which is ascribed to a cooperative enhancement of the hydration of adjacent ionized carboxylate groups (4, 8). It is therefore surprising that such a decrease in hydration does not result also in a decrease in the volume change brought about by silver ion.

It is noteworthy that in all instances the observed volume changes were complete within 30 min of mixing the initial solutions. Although the dilatometers were left in the thermostated bath for over 24 hr, no further volume changes were observed, even in those solutions in which gels appeared.

Viscosity. To estimate the effect of the silver ion binding on the molecular dimensions of polyacrylate, the intrinsic viscosity of PAA-2 at $\alpha = 0.910$ was determined as a function of θ_{Ag} . The results are shown in Figure 4. The effect of bound hydrogen ion on the intrinsic viscosity is included in the same graph. The abscissa is given as θ_{total} , defined as $(\theta_{Ag} + \theta_H)$, so that the results may be compared at equal values of the degree of total cation binding. It is evident that the silver ion depresses the intrinsic viscosity more sharply than does the hydrogen ion. It is worth noting that the calculated θ -solvent intrinsic viscosity for sample PPA-2 is 7.52 L/equiv (5). This value was attained at $\theta_{Ag} = 0.50$ under the conditions corresponding to the results shown in Figure 4. The solutions at $\theta_{Ag} = 0.70$, for which the intrinsic viscosity is below the θ -solvent value, were clear at the time when the viscosities were measured. However, a gelatinous phase was visible on the following day.

Discussion. In the preceding sections we presented experimental evidence indicating that the binding of silver ion by certain polycarboxylates exhibits positive cooperativity. In this section we shall consider the molecular basis for this exceptional behavior. The most likely cause appears to be the formation of silver carboxylate clusters which can be rationalized in the following manner. The most stable complexes of the argentous ion are of the two-coordinate linear type, a relevant example being the silver diacetate complex (9). The bond angle of 180° makes it impossible for the silver ion, in contrast to most other multiply bound cations, to be chelated to two adjacent carboxylate groups on the polyacid chain. Therefore, the silver ion will be complexed by two randomly located carboxylate groups, thereby forming a bridge between two chain portions. The free energy of this process contains an unfavorable entropy contribution associated with the loss of chain mobility attributable to the bridge formation. The complexing of additional silver ions near the

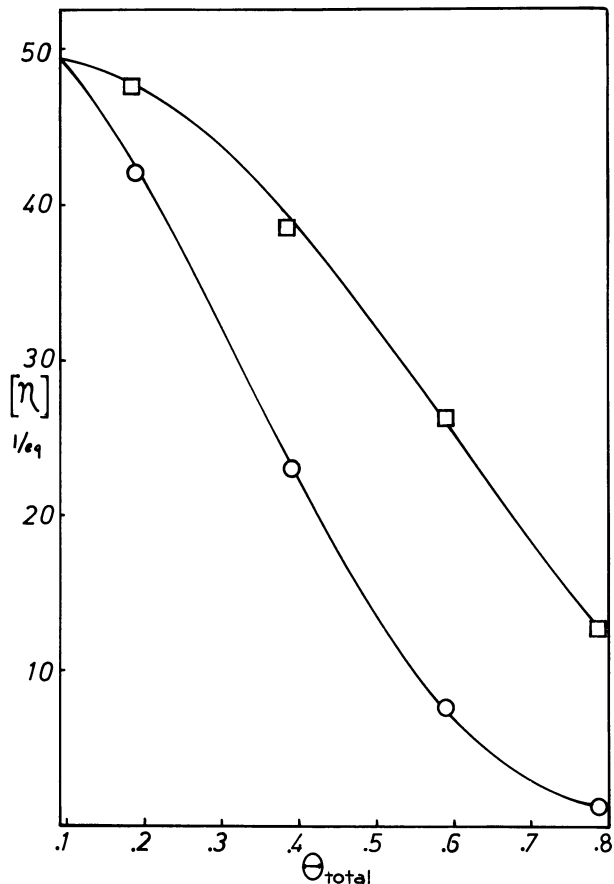


Figure 4. Effects of bound silver and hydrogen ions on the intrinsic viscosity of the TMA salt of polyacrylic acid in 0.2M $TMAO_3$ at 30°C. The abscissa θ_{total} denotes the sum of θ_H and θ_{Ag} . (○) silver ion bound to PAA-2 initially at $\alpha = 0.910$; (□) hydrogen ion bound to PAA-2 initially at $\alpha = 0.910$.

initial bridge causes comparatively little additional chain immobilization and is therefore favored over the initiation of new bridges. A cluster of uninegative silver dicarboxylate complexes formed in this way would be unstable because of its high negative charge density, unless it attracted still further silver ions into its domain. Thus the cluster may be expected to contain a significant proportion of electroneutral silver carboxylate complexes. In line with this expectation, the observation that in three of the four binding isotherms for PAA shown in Figure 1, the ratio of bound silver ions to unprotonated carboxylate groups (θ_{Ag}/α) substantially exceeds the value of 0.5 before the ends of the steeply rising portions are

reached indicates that at least some, if not all, of the complexes must be electroneutral. Additional evidence for the presence of electroneutral complexes, based on dilatometric results, will be presented later. In the absence of direct structural information concerning the complexes and the clusters formed by them, we can only present a few speculations. Thus, a structure in which a pair of silver ions bridge two carboxylate groups, reported for a related compound (10), could well apply to our electroneutral complexes. Regarding the clusters, the type of bridging domain described previously, consisting of pairs of chain portions cross-linked by a number of silver ions, is only the simplest of a number of models. Quasicrystalline clusters formed by elements from a greater number of chain portions would also yield the observed cooperativity.

The delays in reaching constancy in the emf values, which were observed in all parts of the transition region, may be ascribed to a slow rearrangement of inefficiency packed, initially formed bridging clusters. The slowness in the rearrangement indicates that substantial free energy barriers oppose the change from one set of clusters to another.

While the cooperativity would result from both intra- and intermolecular clusters, there is evidence that the clusters are predominantly intramolecular. The insensitivity of the binding isotherms to the polyacid concentration and, in contrast, their strong sensitivity to the degree of proton dissociation, indicate that it is the intramolecular concentration of ionized carboxylate groups that controls the silver ion binding. The sharp depression of the intrinsic viscosity of PAA by silver ion, shown in Figure 4, is a further piece of evidence. Even at high values of θ_{Ag} where the viscosimetrically determined molecular dimensions fall below the estimated θ -solvent value, and where phase separation is expected on theoretical grounds (11), the initial effects on the addition of silver ion appear to be intramolecular. The long delays experienced in observing turbidity and gelation in such solutions indicate that the rearrangement from intra- to intermolecular clusters must be a slow one.

The dilatometry results give further information about the nature of the silver carboxylate complexes. By procedures discussed previously (4, 12) one can estimate the molar volume change that would occur if the association of one carboxylate group and one silver ion were to result in the complete elimination of electrostricted water from the hydration layers of these species. Based on previous dilatometry results involving the protonation of our polycarboxylates (4), and on electrostriction volumes of 5.4 and 8.4 mL for hydrogen and silver ions, respectively (12, 13, 14), the predicted molar volume changes for such an association of silver ion with PAA, HEMA, and HVMEMA are 20.5, 19.6, and 19.4 mL, respectively, for the conditions leading to the results presented in Figure 3. The corresponding estimates for the case where one silver ion associ-

ates with two carboxylate groups with complete loss of electrostriction are 32.3, 30.5, and 30.1 mL. The experimental value of 21.7 mL obtained for all three polyacids from the slope of the line in Figure 3 is much closer to the first set of estimates. In fact, the deviations from these estimates is less than the uncertainty limits of ± 2.4 mL within which the electrostriction volume of hydrated silver ion can be estimated (12). Thus, the results given in Figure 3 are consistent with an interpretation of the complexes being equimolar in silver ions and carboxylate groups, although they do not exclude the possibility that a substantial number of the complexes are of the 1-2 type. In contrast, the results given in Table I indicate that as the degree of protonation of PAA is increased, the experimental values of ΔV for the binding of silver ion cannot be made to fit an interpretation entirely in terms of equimolar complexes. Estimates for equimolar as well as for 1-2 complexes, consistent with the decrease in the average electrostriction volume per $-\text{COO}^-$ group and computed from the $\Delta V_D(\text{H}^+)$ values, are presented in the last two columns of Table I. A comparison of these estimates with the experimental values in the third column points to an increasing proportion of 1-2 complexes as α decreases. This finding may be rationalized in light of the previous discussion—with increasing protonation of the PAA, the electrostatic potential near the $\text{Ag}(\text{COO})_2^-$ bridges becomes less negative, thereby lessening the tendency to attract additional silver ions.

Acknowledgment

Support of this research by the U.S. Public Health Service (Grant No. GM12307) is gratefully acknowledged.

Literature Cited

1. Voordouw, G.; Roche, R. S. *Biochemistry* 1974, 13, 5017.
2. Lynch, D. C.; Schimmel, P. R. *Biochemistry* 1974, 13, 1841.
3. Armstrong, R. W.; Strauss, U. P. *Encycl. Polym. Sci. Technol.* 1969, 10, 781.
4. Begala, A. J.; Strauss, U. P. *J. Phys. Chem.* 1972, 76, 254.
5. Takahashi, A.; Nagasawa, M. *J. Am. Chem. Soc.* 1964, 86, 543.
6. Gregor, H. B.; Luttinger, L. B.; Loebel, E. M. *J. Phys. Chem.* 1955, 59, 34.
7. Begala, A. J., Ph.D. Dissertation, Rutgers University, New Brunswick, NJ, 1971.
8. Ikegami, A. *J. Polym. Sci., Part A*: 1964, 2, 907.
9. MacDougall, F. H.; Peterson, S. *J. Phys. Chem.* 1947, 51, 1346.
10. Blakelese, A. E.; Hoard, J. L. *J. Am. Chem. Soc.* 1956, 78, 3029.
11. Flory, P. J. "Principles of Polymer Chemistry"; Cornell University Press: Ithaca, NY, 1953; Chapters 12-14.
12. Hen, J.; Strauss, U. P. *J. Phys. Chem.* 1974, 78, 1013.
13. Zana, R.; Yeager, E. *J. Phys. Chem.* 1966, 70, 954.
14. Millero, F. J. *Chem. Rev.* 1971, 71, 147.

RECEIVED October 16, 1978.

Synthesis and Aqueous Solution Viscosity Behavior of Polyampholytes from Cationic–Anionic Monomer Pairs

J. C. SALAMONE, C. C. TSAI, A. P. OLSON, and A. C. WATTERSON

Polymer Science Program, Department of Chemistry,
University of Lowell, Lowell, MA 01854

This chapter reports the syntheses and viscosity behavior in aqueous salt solution of two recently prepared polyampholytes. These polymers, derived from cationic–anionic vinyl monomer pairs, exhibit viscosity behavior in salt solution that is contrary to that of normal polyelectrolytes. The intrinsic viscosity is found to increase with increasing salt concentration for one of the samples and remain virtually unchanged for the other. Also, a modified form of the Einstein–Simha equation is observed to correlate especially well with the experimental data, where, in some cases, the Huggins equation apparently is not appropriate. In the context of these findings, some previous results with regard to the behavior of a polyvinylimidazolium sulfobetaine are discussed.

It is recognized that numerous studies have been conducted on the aqueous solution properties of polyelectrolytes. These studies have generally dealt with ion-containing polymers possessing a low molecular weight mobile counterion (1–10). In recent years our group has become interested in the synthesis and solution properties of polyampholytes that contain no mobile counterions, as very few studies of this unusual class of polymers have been reported. Our initial studies of this type of ion-containing polymer were obtained from a polyvinylimidazolium sulfobetaine (see Figure 1) in which the cationic and anionic charges were on one pendant group. Surprisingly, it was found that this homopolymer, which was insoluble in water and existed as a hydrogel, was very soluble

0-8412-0482-9/80/33-187-337\$05.00/0
© 1980 American Chemical Society

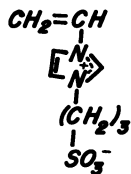


Figure 1.

in certain salt solutions. In addition, it was found to increase in intrinsic viscosity $[\eta]$ and in the second virial coefficient A_2 (from light scattering) in solutions with increasing salt concentration for a particular salt. Through comparison of different salts, it was observed that apparently there is an increase in the same two parameters as the site-binding ability of either the cationic or anionic gegenion increases (11, 12).

We investigated the syntheses and viscosity behavior of polyampholytes derived from cationic-anionic monomer pairs of the type shown in Figure 2. It should be noted that the cationic-anionic monomer pairs that are under consideration contain no nonpolymerizable ions.

Experimental

The syntheses of the monomers 3-methacrylamidopropyltrimethylammonium 2-acrylamido-2-methylpropanesulfonate (Figure 2a) and 3-methacrylamidopropyltrimethylammonium 2-methylpropanesulfonate (Figure 2b), and their corresponding polymers are reported here. The preparations of 1-vinyl-3-(3-sulfopropyl)imidazolium hydroxide inner salt and its homopolymer have been reported previously (11).

Monomer Preparations. 3-METHACRYLAMIDOPROPYLDIMETHYLAMMONIUM 2-ACRYLAMIDO-2-METHYLPROPANESULFONATE (MPDMA · AMPS). To 3.73 g (18 mmol) of 2-acrylamido-2-methylpropanesulfonic acid (AMPS) (mp 185.5°dec) in 100 mL of anhydrous tetrahydrofuran (THF) at -10°C was added dropwise with stirring a solution of 3.40 g (20 mmol) of methacrylamidopropyltrimethylamine (MPDMA) (bp $93^\circ\text{C}/0.2$ mm) in 80 mL of anhydrous THF. After a few hours the precipitate was filtered and washed thoroughly with cold THF. Then the precipitate was recrystallized from an anhydrous THF solution. The resulting crystals of MPDMA · AMPS have a melting range from 65.0° to 66.0°C , and are very hygroscopic. An NMR of this substance in D_2O showed: $\delta 6.24\text{--}6.15(\text{m}, 3\text{H}, \underline{\text{CH}}_2=\text{CH}-\text{CO}-\underline{\text{NH}}-\text{C}(\text{CH}_3)_2-\text{CH}_2-\text{SO}_3^-)$, $\delta 5.69$ (d of

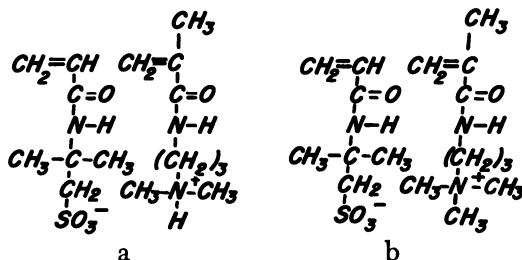


Figure 2.

a

b

d,1H,CH₂=CH—CO—NH—), J_{cis} = 3.6 Hz, J_{trans} = 8.3 Hz, J_{gem} = 0 Hz, δ5.71–5.48(m,3H, CH₂=C(CH₃)—CO—NH—(CH₂)₃—N(CH₃)₂—H), δ3.35(s,2H,CH₂=CH—CONH—C(CH₃)₂—CH₂—SO₃⁻), δ3.24(t,2H, J = 6.8 Hz, CH₂=C(CH₃)—CONH—CH₂—CH₂—CH₂—N(CH₃)₂), δ3.08(t,2H, J = 6.8 Hz, CH₂=C(CH₃)CONH—CH₂—CH₂—CH₂—N(CH₃)₂), δ2.89(s,6H,CH₂=C(CH₃)—CONH—(CH₂)₃—N(CH₃)₂), δ1.93(d of d,3H,CH₂=C(CH₃)—CONH—(CH₂)₃—), δ1.70(m,2H,CH₂=C(CH₃)—CONH—CH₂—CH₂—CH₂—N(CH₃)₂), δ1.51(s,6H,CH₂=CH—CONH—C(CH₃)₂—CH₂—SO₃⁻). Calculated analysis of C₁₆H₃₁N₃O₅S: C, 50.91%; H, 8.28%; N, 11.13%; experimentally determined: C, 50.03%; H, 8.35%; N, 10.76%.

3-METHACRYLAMIDOPROPYLTRIMETHYLAMMONIUM 2-ACRYLAMIDO-2-METHYLPROPANESULFONATE (MPTMA · AMPS). Ten mL of methacrylamidopropyltrimethylammonium chloride solution (ca. 50 wt %) were diluted with 90 mL of distilled water. The diluted solution was passed through a column (i.d. 1.5 cm) containing 40 g of Dowex 1-X4 (2.5 meq/g) anion-exchange resin (OH⁻ form). Then the eluent, which was free of chloride ions, was titrated with an aqueous solution containing 5 wt % AMPS to a pH of 6.8. The neutralized solution was then freeze-dried, followed by recrystallization from chloroform solution to obtain crystals of MPTMA · AMPS. The crystals were hygroscopic and had a melting range from 146° to 147.2°C. The NMR of this substance in D₂O showed: δ6.24–6.15(m,3H,CH₂=CH—CONH—C(CH₃)₂—CH₂—SO₃⁻), δ5.69 (d of d, CH₂=CH—CONH—C(CH₃)₂—CH₂—SO₃⁻), J_{cis} = 3.6 Hz, J_{tran} = 8.3 Hz, J_{gem} = 0 Hz, δ5.71(m,1H,trans proton of methacrylamido group), δ5.48(m,1H as proton of methacrylamido group), δ3.41(s,2H, methylene group of AMPS), δ3.36(t,2H, J = 6.8 Hz, CH₂=C(CH₃)—CONH—CH₂—CH₂—CH₂—N(CH₃)₃), δ3.27(t,2H, J = 6.8 Hz, CH₂=C(CH₃)—CONH—CH₂—CH₂—CH₂—N(CH₃)₃), δ3.12(s,9H, protons of trimethylammonium group), δ2.14(m,2H,CH₂=C(CH₃)—CONH—CH₂—CH₂—N(CH₃)₃), δ1.93(d of d,3H, CH₂=C(CH₃)—CONH—), δ1.51 (s,6H, CH₂=CH—CONH—C(CH₃)₂—CH₂—SO₃⁻). Calculated analysis of C₁₇H₃₃N₃O₅S: C, 52.15%; H, 8.50%; N, 10.73%; experimentally determined: C, 51.78%; H, 8.20%; N, 10.41%.

Polymer Preparations. PREPARATION OF POLY(3-METHACRYLAMIDOPROPYLDIMETHYLAMMONIUM 2-ACRYLAMIDO-2-METHYLPROPANESULFONATE. Ten mL of an aqueous solution composed of 1.89 g (ca. 5 mmol) of MPDMA · AMPS (mp 65.0–66.0°C) and 2.8 mg (0.2 mol %) of 4,4'-azobis-4-cyanovaleric acid (ACVA) were prepared. The solution was degassed, sealed, and placed in a thermostated bath at 55°C.

After 10 hr the cloudy gel that appeared was dissolved in distilled water and dialyzed exhaustively against distilled water. The purified polymer was obtained by lyophilization (yield 1.18 g). Calculated analysis of C₁₆H₃₁N₃O₅S: C, 50.91%; H, 8.28%; N, 11.13%; experimentally determined: C, 50.13%; H, 8.20%; N, 10.80%.

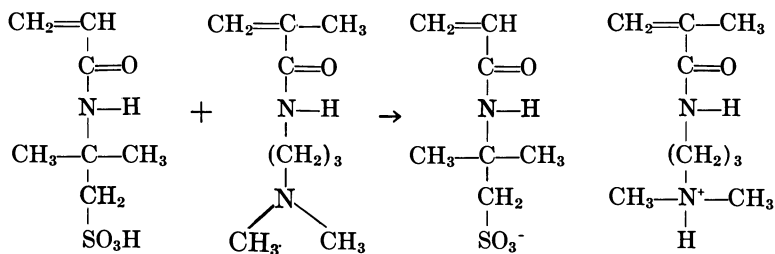
PREPARATION OF POLY(3-METHACRYLAMIDOPROPYLTRIMETHYLAMMONIUM-2-ACRYLAMIDO-2-METHYLPROPANESULFONATE. Ten mL of an aqueous solution composed of 1.96 g (ca. 5 mmol) of MPTMA · AMPS (mp 146.0–147.2°C) and 2.8 mg (0.2 mol %) of ACVA were prepared. The solution was degassed, sealed, and placed in a thermostated bath at 55°C. After 10 hr the cloudy gel was dissolved in 200 mL of distilled water.

The solution was dialyzed exhaustively against deionized water, followed by lyophilization to obtain the polymer (yield 1.05 g). Calculated analysis of $C_{17}H_{33}N_3O_5S$: C, 52.15%; H, 8.50%; N, 10.73%; experimentally determined: C, 51.62%; H, 8.30%; N, 10.51%.

Viscosity Determinations. The viscosity determinations were made using an Ubbelohde dilution viscometer maintained in a bath at a constant temperature of $25^\circ \pm .02^\circ C$.

Discussion

The preparation of cationic-anionic monomer pairs (MPDMA · AMPS and MPTMA · AMPS) is best considered as the neutralization of a strong acid and a strong base, that is, AMPS and MPDMA, respectively (*see* Reaction 1).



Reaction 1

AMPS is a water-soluble monomer; it is also soluble in polar organic solvents such as methanol, dimethyl formamide (DMF), and dimethyl sulfoxide (DMSO). MPDMA is soluble in similar polar solvents. Because of the solubility characteristics of these two species, the reactions (that is, the formation of the ion pairs) were conducted in water, methanol, or DMF. The product, MPDMA · AMPS, was very hygroscopic and apparently had a tendency to polymerize spontaneously during the course of isolation (solvent stripping and precipitation by non-solvents). The preferred medium for preparation was found to be anhydrous THF which also had been used for other ionic monomer pairs (13). In addition, a slight excess of MPDMA was used to ensure complete reaction of AMPS. The excess base, MPDMA, was removed using cold THF (which did not dissolve the product).

In the preparation of MPTMA · AMPS, the ionic moieties seemed to be stable in dilute solution at room temperature. Thus, the lyophilization of a 5% solution yielded the cationic-anionic monomer pair directly. The NMR spectrum of MPTMA · AMPS showed the same chemical shifts as those shown by MPDMA · AMPS except for the methyl groups on the quaternized nitrogen. The quaternized ammonium group (of MPTMA) showed a slightly more deshielded effect on its methyl groups ($\delta 3.12$)

than did the protonated ammonium group (of MPDMA) on its methyl groups ($\delta 2.89$). A similar observation pertained to the methylene group adjacent to the ammonium ion, that is, $\delta 3.27$ of the former and $\delta 3.08$ of the latter.

An alternative method of preparation for MPTMA · AMPS involved the use of a cation-exchange resin, IRA-120 (Na⁺ form). The resin was saturated with methacrylamidopropyltrimethylammonium chloride, washed thoroughly with deionized water, and then washed with a dilute solution of AMPS. Lyophilization of the neutral eluent yielded the crude product. Some contamination of this product with sodium 2-acrylamido 2-methylpropanesulfonate was expected; this species was removed with methylene chloride using soxhlet extraction, followed by recrystallization from chloroform to yield pure MPTMA · AMPS.

In the polymerization of the ion monomer pairs (which is carried out in aqueous solution) the cationic moieties (MPTMA⁺ or MPDMA⁺) and the anionic moiety (AMPS⁻) could have similar Q and e values, since they are the derivatives of acrylamide, resulting in a random incorporation of these units into the chain. Under these circumstances, a resulting network of ionically cross-linked chains seemed possible. Indeed, initially, hydrogels were formed in the polymerization of the monomer pairs of MPTMA · AMPS and MPDMA · AMPS.

The elemental analyses of the polymers formed from the ion pairs indicate equimolar amounts of cationic and anionic units; however, this does not necessarily lead to the conclusion that the polymers are alternating, nor is it necessary that each individual polymer chain contain equal numbers of cationic and anionic units. If the individual polymer chains are not neutral, unpolymerized species that act as counterions could be present. To determine whether or not this is the situation, proton NMR spectroscopy was used. The polymers were dissolved in D₂O containing 1 wt % NaCl (to aid in solubilization). The polymer solutions were studied with a JEOL PFT-100 NMR spectrometer. An accumulated spectrum (100 scans) did not show the existence of any unpolymerized vinyl groups for either ion (methacrylamido or acrylamido). A similar sample that had been doped with 0.5 mol % (with respect to polymer) of monomer clearly showed the existence of the vinyl groups. These results indicate that the polymers prepared here do not contain unpolymerized monomer as counterions in any substantial amount. Thus, the resulting bulk polymer samples are composed of equimolar amounts of cationic and anionic units. Each type of charge is balanced by a charge of opposite sign that is located on the same chain or another chain. One plausible result of this situation is, as previously mentioned, a network structure stabilized by coulombic forces of attraction that could be considered as ionic cross-links (either inter- or intra-

Table I. Comparison of Results Obtained from the

Sample	[KCl]	Huggins	
		Corre	Slope
MPDMA · AMPS	0.5M	0.98	2.5
MPDMA · AMPS	1.0M	0.52	0.93
MPDMA · AMPS	2.0M	0.88	3.1
MPTMA · AMPS	1.0M	1.0	1.1
MPTMA · AMPS	2.0M	1.0	1.1

chain). The viscosity studies that are presented here may also be interpreted so as to lend support to an ionically cross-linked network picture of these ion-containing polymers.

Preliminary viscosity studies in KCl solution have been conducted for poly(MPTMA · AMPS) and poly(MPDMA · AMPS). The results are reported in Table I. The results shown came from treating the data in two ways: using the Huggins equation (Equation 1) and plotting

$$\eta_r = 1 + [\eta]c + k'[\eta]^2c^2 \quad (1)$$

reduced viscosity vs. concentration, and using a modified form of the Einstein–Simha equation (Equation 2) by plotting relative viscosity vs.

$$\eta_r = 1 + [\eta]c \quad (2)$$

concentration. In the former method, the limiting viscosity number (intrinsic viscosity $[\eta]$) is the intercept on the viscosity axis. In the latter case, it is the slope of the line obtained. As can be seen from Table I, the polymers exhibited different behavior. In the case of the polymer derived from MPDMA · AMPS, the Huggins equation does not adequately represent the experimental data. This was first recognized in the study of this polymer in 1.0M KCl. If the data obtained are treated using the Huggins equation, the correlation coefficient is very poor (*see* Table I). In addition, the value for the Huggins constant, k' , is significantly outside the typical values allowed from theoretical considerations. On the other hand, a plot of relative viscosity vs. concentration (modified Einstein–Simha) agrees very well with the data obtained (*see* Figure 3b). For poly(MPTMA · AMPS) either equation produces a linear plot that fits the data very well. However, treating the data with Equation 2 results in an intercept that deviates substantially from the theoretically predicted value of 1. The same situation is observed for the remaining KCl solutions (*see* Table I and Figures 4a and 4b).

The observation that a modified Einstein–Simha equation may be used to represent the viscosity data for poly(MPDMA · AMPS) suggests

Huggins Equation and the Einstein–Simha Equation

<i>Huggins</i>		<i>Einstein–Simha</i>		
$[\eta](dl/g)$	k'	<i>Corre</i>	<i>Slope (dl/g)</i>	<i>Intercept</i>
1.9	0.71	1.0	2.4	0.98
2.2	0.19	1.0	2.4	1.0
2.0	0.78	1.0	2.5	0.98
1.8	0.35	1.0	3.3	0.61
1.9	0.30	1.0	3.3	0.67

that this polymer may be behaving as a suspension rather than as a dissolved, flexible coil. In light of these findings, the behavior of one of our previously prepared polyampholytes, poly(1-vinyl-3-(3-sulfopropyl)imidazolium hydroxide inner salt), has been reconsidered to determine whether the suspension behavior was applicable also. Indeed, as is shown in Figure 5 and Table 2, the modified Einstein–Simha equation produces a linear plot with the expected intercept throughout the concentration range studied whereas the Huggins equation is less suitable. Figure 6 shows the sulfobetaine behavior as a function of KCl concentration using Equation 2.

In most cases the viscosity behavior of these materials may be rationalized on the basis of almost negligible particle–particle interactions, even at polymer concentrations of 1% (by weight to volume), with the

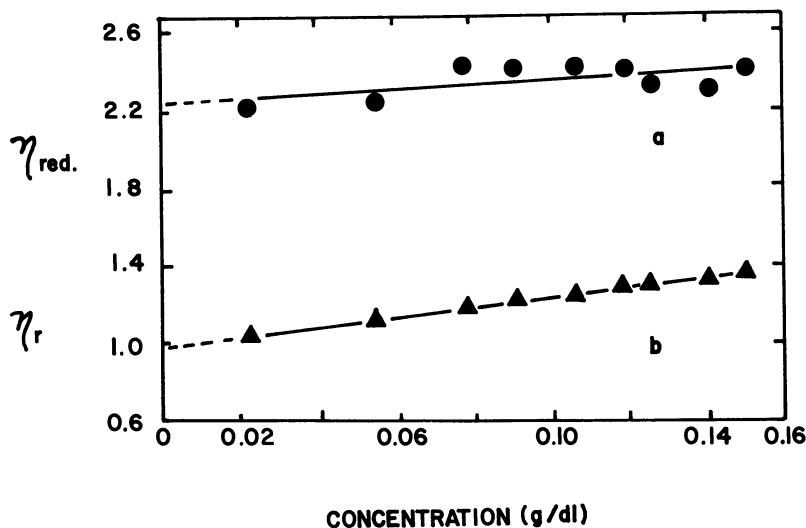


Figure 3. (a) Reduced viscosity as a function of MPDMA · AMPS concentration in 1.0M KCl; (b) relative viscosity as a function of MPDMA · AMPS concentration in 1.0M KCl

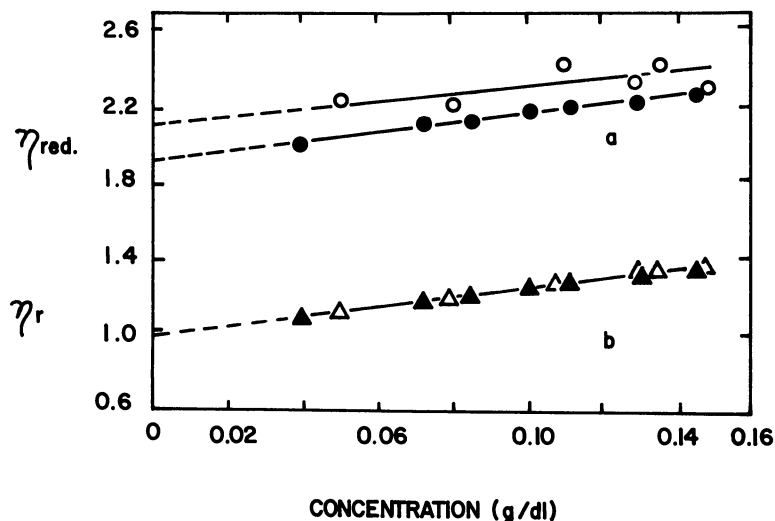


Figure 4. Reduced (●) and relative (▲) viscosity as functions of MPDMA · AMPS concentration in 0.5M KCl; reduced (○) and relative (△) viscosity as functions of MPDMA · AMPS concentration in 2.0M KCl

importance of the interactions being related to the nature of the inorganic salt present. The greater the site-binding ability of the anion, the more normal the viscosity behavior as predicted by Equation 1, which includes a term for particle-particle interactions. Apparently, an anion with good site-binding capabilities (low charge/radius ratio) is effective at neutralizing the ionic cross-links that are present. Thus, the anion aids in the solvation of large portions of the polymer molecules, resulting in a more flexible dissolved chain (as compared to a cross-linked microgel). The relative abundance of cross-links (or flexibility and abundance of loops) may help to determine which viscosity equation applies. In the case where there are numerous cross-links and resulting short lengths of flexible chain, the polymer solution is perhaps best considered as a suspension rather than as a flexible coil. On the other hand, if the cross-links

Table II. Comparison of Results Obtained from the Huggins

Solvent	Huggins		
	Corre	Slope	$[\eta]$ (dl/g)
0.5M KI	0.99	0.089	0.52
0.5M KBr	0.91	0.059	0.40
0.5M KCl	0.53	0.020	0.22
0.5M LiCl	0.94	0.041	0.11
0.5M NaCl	0.97	0.037	0.21

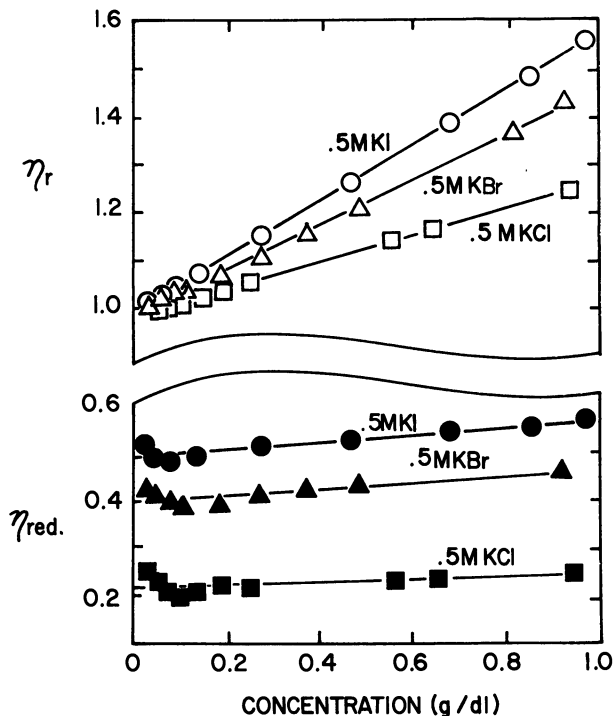


Figure 5. Reduced viscosity as a function of PVISB concentration in 0.5M KI (●), 0.5M KBr (▲), and 0.5M KCl (■); relative viscosity as a function of PVISB concentration in 0.5M KI (○), 0.5M KBr (Δ), and 0.5M KCl (□)

are neutralized effectively in the process of dissolution (11, 12), relatively few of them will remain, so treating the polymer solution as being composed of flexible coils may be more correct. Two factors that might influence the abundance of cross-links are the density of the charges involved and the availability of the charges (exposed or not exposed).

In the near future we hope to report on further studies of these unusual ion-containing polymers.

Equation and the Einstein-Simha Equation for PVISB

Huggins	Einstein-Simha		
k'	Corre	Slope	Intercept
0.39	1.0	0.58	0.99
0.37	1.0	0.46	0.99
0.41	1.0	0.24	1.0
3.3	1.0	0.15	0.99
0.81	1.0	0.25	1.0

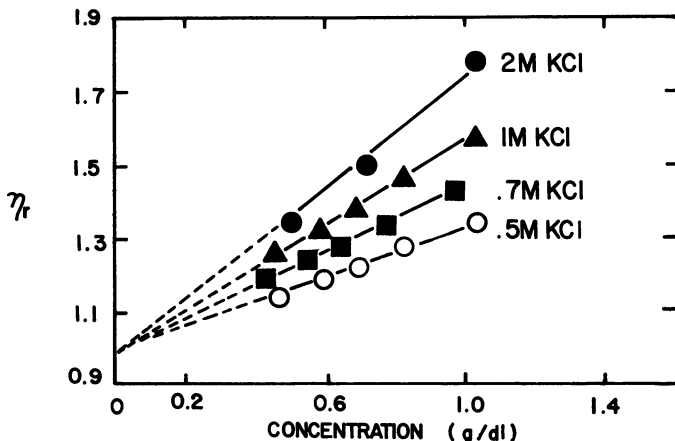


Figure 6. Relative viscosity as a function of PVISB concentration in KCl solutions of various concentrations

Acknowledgment

This research was carried out with the financial support of the National Science Foundation, Grant DMR 76-23624.

Literature Cited

- Hart, R.; Timmerman, D. *J. Polym. Sci.* **1958**, *28*, 118.
- Oth, A.; Doty, P. *J. Phys. Chem.* **1952**, *56*, 43.
- Huggins, M. L. *J. Am. Chem. Soc.* **1942**, *64*, 2716.
- Fuoss, R. J.; Strauss, V. P. *J. Polym. Sci.* **1948**, *3*, 246, 602.
- Katchalsky, A.; Lifson, S. *J. Polym. Sci.* **1953**, *11*, 409.
- Nagasawa, M.; Izumi, M.; Kagawa, I. *J. Polym. Sci.* **1959**, *37*, 375.
- Katchalsky, A.; Alexandrowicz, Z.; Kedem, O. In "Chemical Physics of Ionic Solutions"; Conway, B. V., Barrados, R. G., Eds.; Wiley: New York, 1966.
- Strauss, V. P.; Ander, P. *J. Am. Chem. Soc.* **1958**, *80*, 6494.
- Strauss, V. P.; Leung, Y. P. *J. Am. Chem. Soc.* **1965**, *87*, 1476.
- Hen, J.; Strauss, V. P. *J. Phys. Chem.* **1954**, *78*, 1013.
- Salamone, J. C.; Volkens, W.; Israel, S. C.; Olson, A. P.; Raia, D. C. *Polymer* **1977**, *18*, 1058.
- Salamone, J. C.; Volkens, W.; Olson, A. P.; Israel, S. C. *Polymer* **1978**, *19*, 1157.
- Salamone, J. C.; Watterson, A. C.; Hsu, T. H.; Tsai, C. C.; Mahmud, M. U. *J. Polym. Sci. Polym. Lett. Ed.* **1977**, *15*, 487.

RECEIVED October 18, 1978.

Heparin

L. B. JAUQUES

Hemostasis–Thrombosis Research Unit, Department of Physiology,
University of Saskatchewan, Saskatoon, Sask., CANADA S7N 0W0

Heparin is an important biological anionic polyelectrolyte consisting of chains of 2 to 23 units of 2x(2,6-disulfoglucosamine-2-sulfiduronic acid)–(2,6-disulfoglucosamine-glucuronic acid). It complexes a wide range of electrolytes, producing metachromasia of dyes, inhibition or activation of enzymes and hormones, and increased negative electrostatic charge on membranes and cells. It is used in surgery and medicine with cardiovascular devices and for treatment of thromboembolism, is taken up rapidly by the reticuloendothelial system, and provides protection by increasing the negative charge of the endothelial surface. Heparin counteracts various toxic amines, is important in fat metabolism by releasing lipoprotein lipase and diamine oxidase, and with histamine, constitutes the granules of the mast cell. These provide ion-exchange control of the composition of tissue fluid, and their disruption is responsible for sensitivity reactions.

Heparin is an essential drug for cardiovascular surgery and medicine. Approximately ten metric tons were produced in the United States in 1978 which, with an average of 1 g per patient, means it will be used for about a million patients. It is extracted commercially from beef lung and pork intestine and is issued as the sodium salt of a highly sulfated mucopolysaccharide (1). Much new information on its chemical nature has been obtained recently by using more specific chromatographic (electrophoretic) methods together with a series of enzymes separated after induction in *Flavobacterium heparinum* with a radioisotopically labeled heparin as substrate, and by using NMR techniques (2). This information has resulted in a much improved understanding of the nature

of the biological actions of heparin and its clinical effectiveness (3, 4, 5, 6) and in an improved procedure for its administration to patients (inhalation).

Figure 1 shows the structural formula for the major form of the heparin hexasaccharide, 2x(2,6-disulfoglucosamine-2-sulfoiduronic acid)-(2,6-disulfoglucosamine-glucuronic acid). This hexasaccharide is repeated in a chain from 2 to 22 (23, 24?) times to give 22 separate chains of molecular weights from 3,500 to 35,000 daltons. There are also side-to-side associations, dimers, etc. Variants within the hexasaccharide (unsulfated iduronic acid, sulfated glucuronic acid) are important in determining biological activity.

This complex composition was demonstrated by successive electrophoresis in agarose, acrylamide, and ampholyte (see Figure 2). In agarose gel, heparin migrates electrophoretically with an overall charge of an ester sulfate, with beef-lung heparin giving one band and pork-intestinal heparin, two bands, the second band being slower. In acrylamide gel, the two heparin preparations show a smear over a range equivalent to 6,000 to 37,500 daltons of reference compounds. Electrophoresis with an ampholyte buffer mixture present (as in electrofocusing proteins) shows 21 or 22 distinct bands in place of the smear. When the individual components obtained by cutting the gel with LKB ampholyte are eluted and again subjected to electrophoresis with beef-lung heparin, a single line is obtained in both agarose and acrylamide. In the acrylamide gel, the positions of the individual bands are sequential, covering the whole distance of the smear of the original heparin. With pork-intestinal heparin, when each individual fraction from electrophoresis with LKB ampholyte is subjected to electrophoresis in acrylamide, two bands are obtained, with one at half the distance of the other, indicating that a dimer of each of the chains in beef-lung heparin is present in pork-intestinal heparin. In acrylamide gel, each fraction bears a simple relationship to the preceding and succeeding members of the series, differing by a molecular weight of 1,700 or one octosulfated hexasaccharide. Each fraction combines with toluidine blue and is degraded with the specific enzymes of *Flavobacterium heparinum* like heparin. Hence, beef-lung heparin consists of at least 21 components of the same charge density with molecular weights from 3,000 to 37,500 (chains of 2-22 hexasaccharides), while pork-intestinal heparin contains a large proportion of dimers of these chains.

Heparin, then, consists of a series of highly sulfated compounds, identical in carbohydrate composition but separated by complexing with LKB ampholyte (with progressive adjustment of pH), into a large number of separate chains. These chains are flexible molecules, probably in a Gaussian coil, and are characterized by a shell of negative charges

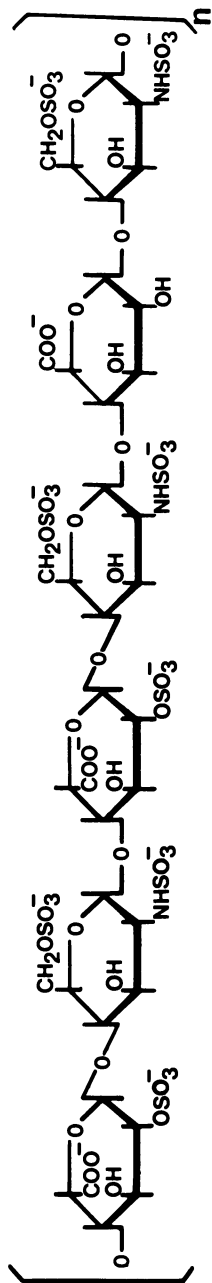
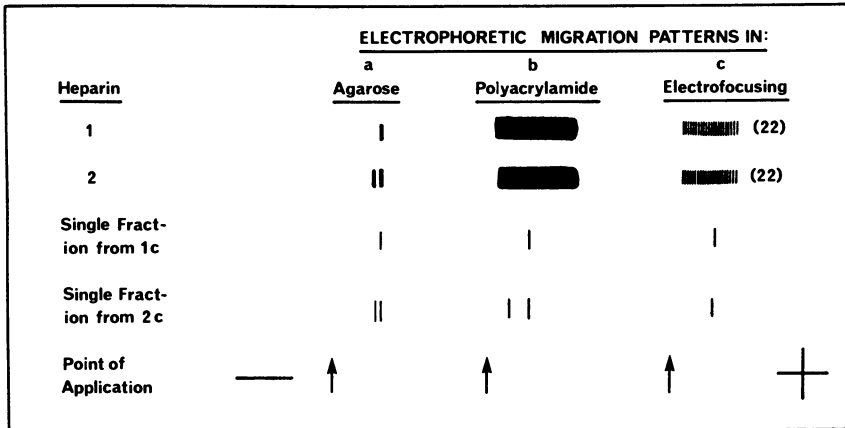


Figure 1. Heparin hexasaccharide—the major constituent of commercial heparin as obtained by enzymatic degradation



Seminars in Thrombosis and Hemostasis

Figure 2. Electrophoretic migration patterns of commercial heparins. The cathode and the point of application are considerably to the left of each pattern, the anode is to the right. Separation in agarose on the basis of charge density, in polyacrylamide on the basis of molecular size, and in LKB ampholyte on the basis of pH and chain length, producing a specific insoluble complex with ampholyte. (2)

produced by the high concentration of different anionic groups (iduronic and glucuronic carboxyl), and three types of sulfate radicals (substituted on amine (sulfamino), and secondary and primary alcohol groups). This gives a high proportion of sulfate per hexose unit; hence the compounds are multisulfated (7). Usually heparin is prepared as the sodium salt, although ammonium, potassium, calcium, and barium salts are sometimes prepared. The usual preparations contain about 12% sodium. A pH value in the physiological range will influence the dissociation of the two uronic acid residues differently, while the iduronic acid can form a lactone. There is strong binding of counterions of sodium, potassium, ammonium, quaternary ammonium radicals, and coions such as sulfate, phosphate, and acetate. The structure provides an effective ion-exchange vehicle. The high negative charge and flexible, complex carbohydrate chain provide for strong, highly specific binding of proteins and dyes. The strong metachromatic color produced with toluidine blue (and Azure A) is characteristic. Heparin and related sulfated mucopolysaccharides form a very distinct group of biological polymers since they are not neutral like polysaccharides, and unlike other biological polymers, their molecules do not have a rigid structure. Their strong acidity makes them unique in biology. They appear to be biological equivalents of the anionic detergents or surfactants of industrial chemistry.

As a drug, heparin is standardized by biological assay using a blood coagulation system (1). One International Unit of heparin is 1/130 mg of the International Standard Heparin Preparation (prepared for and held by the World Health Organization—Division for Biological Standards). As shown in Figure 3 (assay of heparin Preparation 1 against heparin Preparation 1), coagulation tests are highly reproducible (variability $\ll 5\%$) when a single heparin preparation is compared with itself. When two heparin preparations are compared (Preparation 1 with Preparation 2 in Figure 3), a wide variation in relative activity is found ($\pm 50\%$). This phenomenon is related to the multiple chains found in heparin on electrophoresis in ampholyte, as shown in Figure 4. The upper figure (by circles) shows the relative anticoagulant activity of the individual chains separated by electrophoresis in LKB ampholyte. The lower part of the figure shows the distribution of heparin found in the different chains (this is the distribution pattern for this particular lot of commercial heparin). Only one-third of the chains have anticoagulant activity in the USP assay, and two of the chains account for 35% of the total activity. A significant part of the anticoagulant activity of heparin is attributable to binding with the plasma protein inhibitor, Antithrombin-III. Again only one-third of the commercial heparin combines with

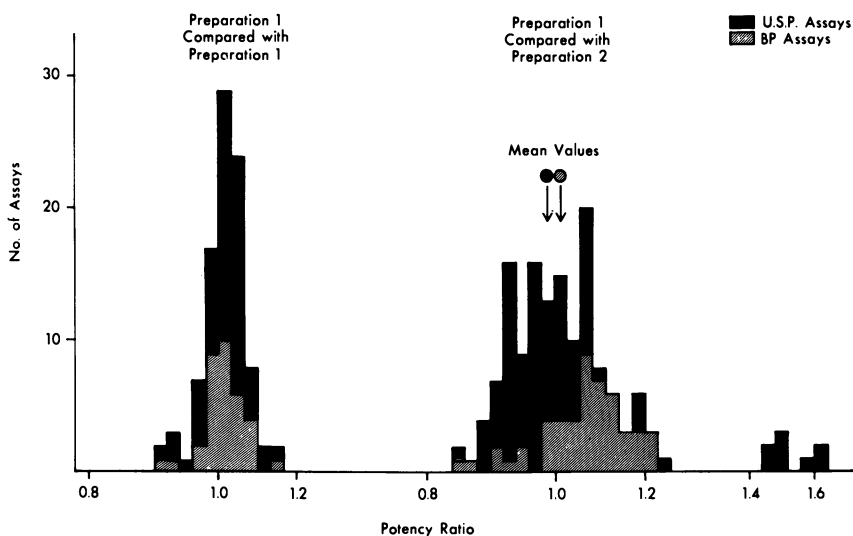
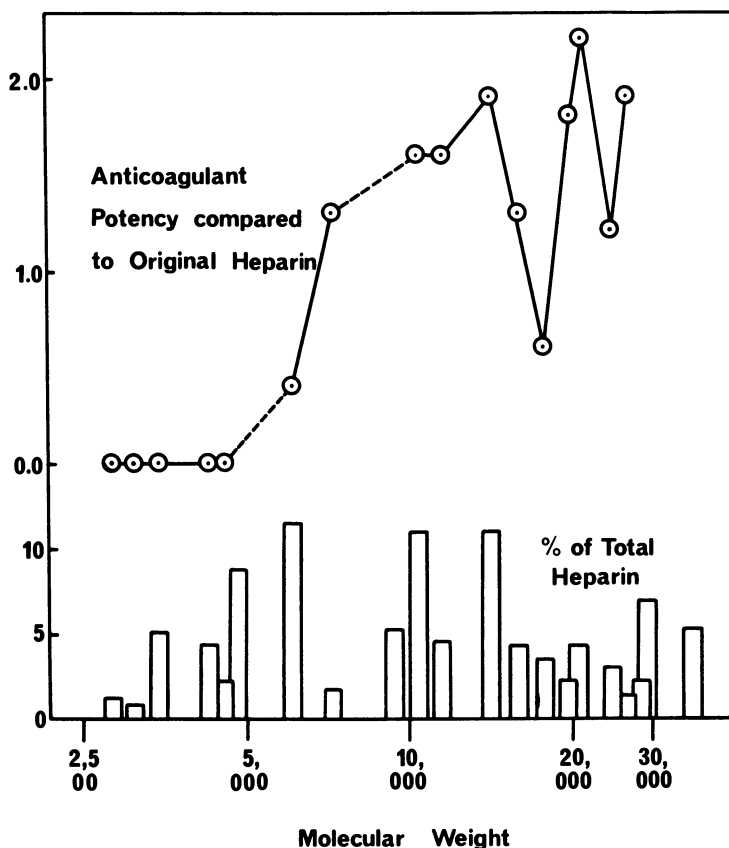


Figure 3. Assay of heparin (data from WHO International Collaborative Study (9)). Frequency distribution for the potency ratio for two heparin preparations tested on different days, in different laboratories, and by different tests: 1 = preparation from porcine intestinal mucosa; 2 = International Standard Heparin # 2 (1958).



Seminars in Thrombosis and Hemostasis

Figure 4. Anticoagulant activity of individual heparin chains of beef-lung heparin. Chains were separated by electrophoresis of Upjohn beef-lung heparin Lot #517-042 with LKB carrier ampholine batch #18. The apparent molecular weights were obtained from electrophoresis in acrylamide by the technique of Hilborn and Anastasiadis (10). The anticoagulant activity was determined by the USP procedure comparing the individual fraction with the original heparin. The quantity was estimated by optical density of toluidine blue-stained band on gel. (2)

Antithrombin-III (11) and only a portion of this, probably only one or two chains, converts Antithrombin-III into an immediate inhibitor of the enzyme thrombin (14). The chains optimal for this do not appear to be identical to those optimal for USP anticoagulant activity or to those optimal for production of inhibitor activity against other important plasma serine proteases (coagulation Factor Xa, etc.).

The 21 or more bands observed give a pattern distinctive for a given commercial heparin, almost constituting a fingerprint. No single chain

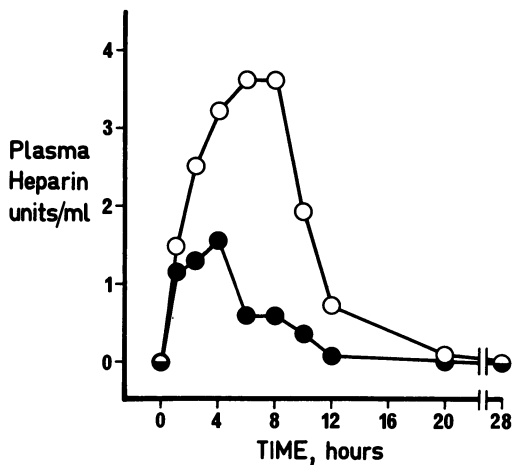
more than 10% of the total is found in any of the 21 components. The pattern is different with different tissue sources and following different extraction and purification procedures. Heparin preparations showing marked differences in ampholyte pattern also show great differences in various coagulation test systems (15). Since the preparations are all effective clinically, it is evident that biological standardization is of limited value and that physicochemical specifications will be more useful.

Heparin is used medically to prevent blood coagulation in cardiovascular surgery and to prevent and treat thromboembolism. Where plastic devices are inserted in the cardiovascular system as valves, shunts, and catheters, heparin has been found to be most effective when ionically held on the surface of the plastic (16). This is accomplished by incorporating an alkylamine, tridodecyl methylammonium chloride (TDMAC), which takes up heparin from solution. It has been shown that heparin, when administered, is taken up by the blood vessel lining (the endothelium). Since the concentration of heparin taken up by the endothelium is two to three orders of magnitude greater than that in blood (*see* Table I), even at low blood concentrations, the uptake mechanism is very effective; heparin increases the negative charge of the endothelium (18) and thus provides protection. The heparin taken up by the endothelium is later returned to the circulatory system as antithrombin-active chains (*see* Figure 5). A dog was injected subcutaneously with 100 mg of sodium heparin (1120 units by antithrombin and color test with toluidine blue). Blood samples were taken and the heparin was extracted and tested at the times shown. The ratio of antithrombin activity to heparin concentration (measured by toluidine blue) was 1.0 for injected heparin, and 3.2 for heparin in blood, 8–17 hr after injection.

Table I. Heparin Concentration in Blood and Endothelium^a
(units/mL)

<i>Intravenous Injection (min after)</i>	<i>Blood</i>	<i>Endothelium</i>	<i>Endothelium Blood</i>
5	17.1	583	34
15	10.9	600	55
30	5.6	1400	250
60	1.5	700	156
<i>Subcutaneous Injection (min after)</i>			
5	0.2	500	?
30	0.2	300	1500
60	0.34	700	2059

^a Data from (18).



Thrombosis Research

Figure 5. Increased antithrombin activity of heparin after injection: (O—O) antithrombin activity as equivalent units of heparin; (●—●) concentration of heparin in units by toluidine blue (20). (For the heparin injected, 1 unit by AT equals 1 unit by toluidine blue.) (24)

In forming complexes with cations such as dyes and proteins, heparin changes their properties, for example, the metachromatic color of dyes. When injected, heparin activates and releases a clearing factor—two groups of lipolytic enzymes that are not normally present in the blood—from tissues. The enzymes of one group, released from endothelium (including liver) and adipose tissue, preferentially catalyze hydrolysis of triglycerides from lipoprotein, particularly low density lipoprotein, and hence are lipoprotein lipases (LPL). The other group released from the liver carries out a much more extensive degradation of lipids—phospholipase, monoglyceride hydrolase, diglyceride lipase, and triglyceride lipase. These enzymes are also released by other sulfated mucopolysaccharides and heparinoids (with some variation in proportion of enzymes). The lipoprotein lipase is attached to endothelium by a sulfated mucopolysaccharide (hence is displaced by heparin) and supplies triglyceride to the endothelial cell. It is believed that this activity in the vascular bed represents the major pathway by which triglyceride fatty acid is cleared from the plasma and made available to the peripheral tissues. Heparin also releases histaminase (diamine oxidase, DAO). It is a competitive inhibitor for many enzymes, for example, smooth muscle myosin ATPase, DNA and RNA ribonucleases, pepsin, and trypsin, and changes the surface charge of proteins on cell surfaces.

Large quantities of heparin and histamine are present in granules of mast cells (*see* Figure 6). The heparin is frequently in the form (macro-

molecular heparin) of a lipoprotein-lipase inhibitor. The mast cells are found widely dispersed in tissues. The insoluble granules consist of the complex heparin-histamine-basic protein. They thus provide an ion exchanger (21) for control of tissue fluid composition for ions (including protein antibodies). This process also provides histamine as a chemical messenger. Thyroid-stimulating hormone releases histamine to increase blood flow in the thyroid (22); hypertonicity in tissues releases histamine to elicit the thirst reflex (23). If granules escape from mast cells into intracellular fluid, the high sodium ion concentration dissociates and releases histamine, etc. from the granule. This accounts for symptoms observed in anaphylaxis and sensitivity reactions (*see* Figure 7).

Significant physiological functions not occurring in mast cells have been found for heparin and histamine (3, 4, 5, 6). In this form the agents are synthesized and released as required. Thus, in the intestine, in response to a meal of fat, secretion of histamine causes increased vessel permeability and fat transport, while secretion of heparin causes release of DAO to destroy the histamine in a negative feedback cycle (*see* Figure 8).

The extraordinary properties of heparin as a mixture of biological anionic polyelectrolytes are important in understanding its action as a drug. These properties are: (1) chemically it consists of multiple chains

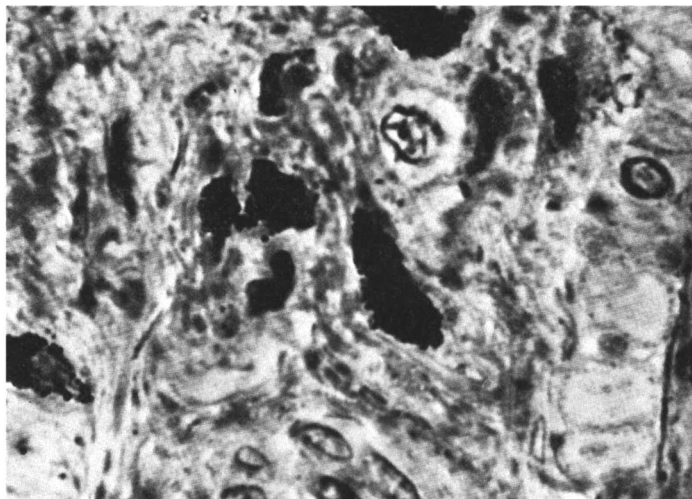


Figure 6. Mast cells from pig intestinal mucosa (the main source of commercial heparin). The tissue section was stained with toluidine blue; the mast cell is characterized by the many granules stained with the dye. (magnification = 1000X)

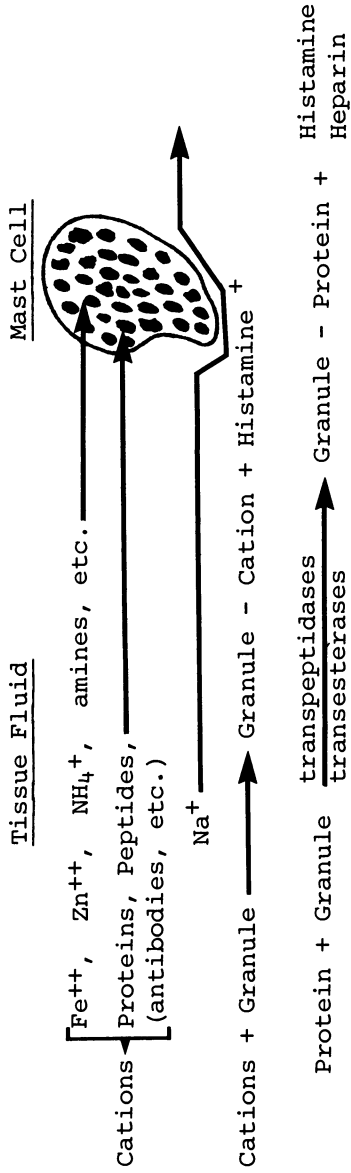
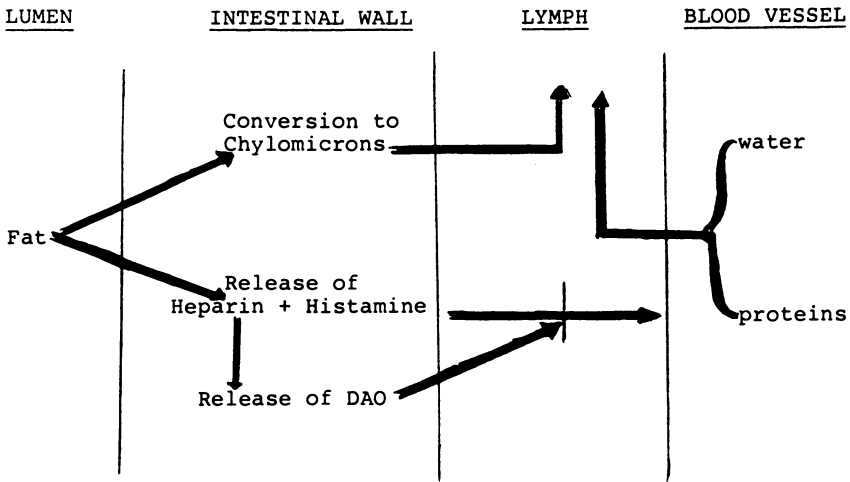


Figure 7. Ion exchange by mast cells in tissues (21)



Seminars in Thrombosis and Hemostasis

Figure 8. Release of heparin and histamine in the intestinal wall with a fat meal (5)

with a very high negative charge to complex effectively a wide range of electrolytes and increase the negative charge of membranes; (2) pharmacologically it has a special affinity for endothelium and for the reticulo-endothelial system and thus is effective clinically as an antithrombotic agent that is metabolized; and (3) biologically it occurs in a wide variety of polymer sizes with corresponding variety in biological activities and functions in different tissues.

For current reviews with extensive references see Refs. 1-6.

Literature Cited

1. Jaques, L. B. *Methods Biochem. Anal.* 1977, 24, 203, 312.
2. Jaques, L. B.; McDuffie, N. M. *Semin. Thromb. Hemostasis* 1978, 4(4), 277-297.
3. Jaques, L. B. *Semin. Thromb. Hemostasis* 1978, 4(a), 275-276.
4. Jaques, L. B.; Mahadoo, J. *Semin. Thromb. Hemostasis* 1978, 4(a), 298-325.
5. Jaques, L. B. *Semin. Thromb. Hemostasis* 1978, 4(a), 326-349.
6. *Ibid*; 350-353.
7. Jaques, L. B. *Medical Hypotheses* 1978, 4(2), 123-135.
8. Jaques, L. B. *Artery* 1978, 4(2), 144-156.
9. Bangham, D. R.; Woodward, P. M. *Bull. W.H.O.* 1970, 42, 129.
10. Hilborn, J. C.; Anastassiadis, P. A. *Anal. Biochem.* 1971, 39, 88-92.
11. Danishefsky, I.; Tzeng, F.; Ahrens, M.; Klien, S. *Thromb. Res.* 1976, 8, 131-140.
12. Höök, M.; Bjork, I.; Hopwood, J.; Lindahl, U. *FEBS Lett.* 1976, 66, 90-93.
13. Andersson, L. O.; Barrowcliffe, T. W.; Holmer, E.; Johnson, E. A.; Sims, G. E. C. *Thromb. Res.* 1976, 9, 575-583.

14. Lam, L. H.; Silbert, J. E.; Rosenberg, R. D. *Biochem. Biophys. Res. Commun.* **1976**, *69*, 570–577.
15. Bianchini, P.; Osima, B.; Rimini, V.; Macchi, M. *European Symposium on Advances in Coagulation, Fibrinolysis, Platelet Aggregation and Atherosclerosis, Palermo, 1976*, Comm. #9.
16. Gott, V. L. *Adv. Exp. Med. Biol.* **1975**, *52*, 351–374.
17. Falb, R. D.; Leininger, R. I.; Grode, G.; Growley, J. In “Heparin Structure, Functions and Clinical Usage”; Bradshaw, R. A.; Wessler, S., Eds.; Plenum: New York, 1975; pp. 365–374.
18. Hiebert, L. M.; Jaques, L. B. *Thromb. Res.* **1976**, *8*, 195–204.
19. Sawyer, P. N.; Stanczewski, B.; Pomerance, A.; Lucass, T.; Stoner, G.; Srinivasan, S. *Surgery* **1973**, *74*, 263–275.
20. Levy, S. W., Ph.D. Thesis, University of Saskatchewan, Saskatoon, Sask., Canada, 1951.
21. Jaques, L. B. *General Pharmacology* **1975**, *6*, 235–245.
22. Melander, A.; Westgren, U.; Fundler, F.; Ericson, L. E. *Endocrinology* **1975**, *97*, 1130–1137.
23. Goldstein, D. J.; Halperin, J. A. *Nature* **1977**, *267*, 250–252.

RECEIVED October 17, 1978.

INDEX

A

Acetate, zinc14-15
 neutralization of sulfonated
 EPDM with 6, 7t
 Acetyl sulfate 5
 Acids, free polymeric 8
 Acids, saturated fatty 39
 2-Acrylamido-2-methylpropane-
 sulfonic acid (AMPS) 338
 solubility of 340
 3-Acrylamidomethylbutyltrimethyl
 ammonium chloride
 (AMBTAC)236-252
 -emulsion polymerization,
 homopolymer 239
 -solution polymerization,
 homopolymer 238
 Acrylate-DVB anion exchange
 resins 196
 stability of 203
 Acrylic acid-based ionomers,
 ethylene-54, 114
 Acrylonitrile copolymers, car-
 boxylated butadiene- 54
 Additives, polymer37-51
 Adhesion between asphalt and
 aggregate, interfacial 172
 Adhesion promoters of asphalts 172, 180
 Adhesives, cross-linking 186
 Adhesives, water-soluble
 polyester185-193
 Adipate-containing polymers ..188, 189f
 Aldehydes by borohydrides,
 reduction of200t-201t
 Alkali
 and chlorine using Nafion, elec-
 trolysis for the production
 of145-153
 metal cations, NMR parameters
 of 157t
 metal nuclei, chemical shifts
 of157-159
 metal resonances of electrolyte
 solutions and saturated
 Nafion, linewidths of 166t
 Amine-neutralized ethylene-meth-
 acrylic acid copolymers 54
 Ammonium borohydride reducing
 agents, polymeric quater-
 nary195-209
 Ammonium ions, quaternary 56
 AMBTAC (*see* 3-Acrylamido-
 methylbutyltrimethyl ammo-
 nium chloride)236-252

AMPA (2-acrylamido-2-methyl-
 propanesulfonic acid) 338
 Ampholyte 350
 AMPS (*see* 2-Acrylamido-2-methyl-
 propanesulfonic acid) 338
 Anhydride, maleic 173
 Anion
 -cation electrostatic interactions. 162
 -exchange resins
 acrylate-DVB196, 203
 with borohydride counterions. 195
 styrene-DVB 196
 site-binding ability 344
 Anionic monomer pairs, poly-
 ampholytes derived from
 cationic-337-346
 Anionic polyelectrolyte, biological. 349
 Antithrombin-III353-354
 Asphalt (s)
 adhesion promoters of172, 180
 and aggregate, interfacial
 adhesion between 172
 binders, cost of 183
 concretes, improving water
 resistance of 180
 effect of water on171-172
 grafting ionic substituents onto . 173
 ionomers171-183
 post-thickening behavior of .. 182
 wet-strength retention of 173
 modified 173
 crack propagation tests of ... 178
 lap-shear strength tests
 of ...174f, 175-176, 178f-179f
 stress-strain behavior
 of177-178, 180f
 viscosity of ...175, 176f, 178, 181f
 wet-strength retention
 of177, 179f, 181-182
 paving industry, economic con-
 siderations of182-183
 resistance to debonding by
 water molecules 181
 roads (moisture damage),
 water-stripping in 172
 Asphaltic bitumen171, 180
 Asphaltic roadways, factors
 affecting the performance
 and durability of 172
 Atomic-orbital coefficients 303

B

Backbone plasticizers70, 75
 Barium stearates 42

Binders, cost of asphalt	183
Binding in liquids and electrolyte solutions, hydrogen	167
Biological oxygen demand (BOD)	236
Bitumen, asphaltic	171, 180
Blood coagulation prevention	355
Blood and endothelium, heparin concentration in	355 <i>t</i>
BOD (biological oxygen demand)	236
Bond failure in ionic polyesters	192–193
Borohydride counterions, anion-exchange resins with	195
2-ethylhexanal reduction by	200–201
polymer-bound generation of volatile hydrides by	208
preparation, use, and regeneration of	197 <i>f</i>
reducing agents	195–209
solvent purification by	208
solvolytic stability of	196, 202–203, 204 <i>f</i> –207 <i>f</i>
reducing agents, polymeric quaternary ammonium	195–209
reduction of aldehydes by	200 <i>t</i> –201 <i>t</i>
reduction of hydroperoxide by	202 <i>t</i> –203 <i>t</i>
sodium	200
tetraethylammonium	200
Bragg spacing	152
Butadiene–acrylonitrile copolymers, carboxylated	54
Butadiene–styrene methacrylic acid copolymers	55
C	
Calcium thiocyanate system, phenoxy–	268
Carboxylate(s) clusters, formation of silver	333–336
ionomers, comparison of sulfonate and	21–35
as plasticizers	75
butadiene–acrylonitrile copolymers	54
polyethylene ionomers	54
Carboxylated butadiene–acrylonitrile copolymers	54
polyethylene ionomers	54
polystyrene (C-PS)	3
behavior(s) rheological	27, 28 <i>f</i>
softening	26, 27 <i>f</i>
solution viscosity	27–34
effect of temperature on the solution	34 <i>f</i> , 35
preparation of	21–35
viscosity–concentration relations for PS and	24, 25 <i>f</i>
Carboxylic acid copolymers, ethylene–	53

Carboxymethyl dextran gel system, potentiometric properties of	313
Cation(s) electrostatic interactions, anion–	162
–exchange membranes	145
transport phenomena and morphology changes associated with Nafion	145–153
on flow and physical properties of EPDM, effect of	11–17, 14 <i>t</i> –15 <i>t</i>
NMR parameters of alkali metal and zinc stearate on flow and physical properties of metal sulfonate EPDM, effect of	46, 48 <i>t</i> –49 <i>t</i>
Cationic adhesion promoters of asphalts	172
–anionic monomer pairs, polyampholytes derived from	337–346
polyelectrolytes	54
polymers in dewatering waste-activated sludges, efficiency of	235–252
Cells from pig intestinal mucosa, mast	357 <i>f</i>
Cells in tissues, ion exchange by mast	357, 358 <i>f</i>
Chelated salt, zinc chloride as a	255
Chelating resins, metal	225
Chelating structures	223
Chlor–alkali production	145, 146
Chloride, plasticized polyvinyl (PVC)	68
Chlorine using Nafion, electrolysis for the production of alkali and	145–153
Cluster(s) existence of ionic	284
formation, mechanism of	125–131
application to Nafion	131–137
formation of silver carboxylate structure in Nafion	333–336
structure in Nafion	136
Clustering in ion-containing polymers, ion	283–292
in Nafion, water	286, 290–292
in styrene–methacrylic acid copolymers and their salts, ionic	286–292
Cole–Cole circular arc plots	257
Colloidal suspensions of polyelectrolytes	324
Comonomers, hydrophobic–hydrophilic	149
Copolymers acid ethylene–carboxylic	53
ethylene–acrylic	54
methacrylic amine–neutralized ethylene–butadiene–styrene	54
butadiene–styrene	55
ethylene–	111–112

Copolymers (*continued*)

- butadiene-styrene (*continued*)
 radius of gyration measurements of deuterated styrene 289-292
 carboxylated butadiene-acrylonitrile 54
 with deuterated methacrylic acid groups and protonated styrene monomers 287
 ionic clustering in 287-289
 neutron scattering in 287
 α relaxation in ethylene-based 113-115
- Counterion(s)
 divalent 54
 ethylene bistrioctylphosphonium 60-63
 on the melt-flow properties of sulfonated EPDM, effect of quaternary phosphonium .. 56
 metal 55
 and metal stearates on flow and tensile properties of EPDM ionomers, effects of 42*t*-43*t*
 on the physical properties of an ionomer, effect of 60
 polyvalent quaternary 61
 quaternary
 alkyl-substituted 62
 divalent 60
 effect of *n*-alkyl chain lengths of substituents of 58
 monovalent 60
 tetralkyl phosphonium 58
 structure on ionomer properties, effect of 53-65
 in sulfonated EPDM, quaternary phosphonium 53-65
 comparison of divalent and monovalent 61*t*
 tetradecamethylene bistriethylphosphonium 60-63
 tetraethylphosphonium 62
 on the tensile properties of sulfonated EPDM, effect of quaternary phosphonium .. 56
 triethylheptylphosphonium 62
 triethyloctadecylphosphonium .. 64
- C-PS (*see* Carboxylated polystyrene) 344-345
- Cross-links 344-345
- Cross-linked ion-exchange resins, intrinsic pK values of 311-324
- Cross-linked polymers 225, 227
 ionically 70
- Cross-linking
 adhesives 186
 monomer 225
 on peel force of ionic polyesters, effect of 191-193
- Crystallinity, polyethylene 9, 11
- Crystallinity, polymer backbone .. 92
- Crystallization theories 112

D

- DADMAC (*see* Diallyldimethyl ammonium chloride)
- DAO (diamine oxidase) 356
- DBP (Dibutyl phthalate) 72
- Debonding by water molecules, asphalt resistance to 181
- Debye term for dipolar polarization 255
- Diallylamine(s)
 cyclopolymerization of *N*-substituted 211-232
 monomers
 aliphatic nitro 216, 217*f*
 amino acid 223
 analysis and spectral results for 230*t*-233*t*
 homopolymerization 218*t*-221*t*
 ketone-substituted 216, 222*f*
 preparation 212*t*-215*t*
 polymerization methods 216
 polymers, properties of .. 223, 225, 227
- 1-Diallylamino-2,2-biscarbethoxybutane, preparation of 229
- 1-Diallylamino-2-butane, preparation of 227, 229
- 1-Diallylamino-3-hydroxy-3-phenylpropane, preparation of 232
- 1-Diallylamino-3-oxo-3-phenylpropane, preparation of 229
- 1-Diallylamino-3-oxobutane, preparation of 229
- 1,6-Diallylaminohexane 225
- 5-Diallylaminoethyl uracil, preparation of 229
- N'*-(*N,N*-Diallylaminoethyl)-2-methylimidazole, preparation of 229
- 2-Diallylaminoethylpyridine, preparation of 229
- 2-2-Diallylaminoethylpyridine, preparation of 229
- N,N*-Diallylanthranilic acid, preparation of 229, 232
- Diallyldimethyl ammonium chloride (DADMAC) 236-252
 acrylamide copolymer-emulsion polymerization 239
 /acrylamide copolymer-solution polymerization 239
 -emulsion polymerization, homopolymer 238
 -solution polymerization, homopolymer 238
- N,N*-Diallylmethylanthranilite, preparation of 232
- Diamine oxidase (DAO) 356
- Dibutyl phthalate (DBP) 72
- Dielectric
 behavior of PPO complex ... 255, 256*f*
 measurements of hydrogenated, sulfonated PP's 104-109

- Dielectric (*continued*)
 properties of complexed
 polyethers253-264
 properties of hydrogenated
 sulfonated PP's117-118
 Diester diethyl *p*-phenylene-
 bis(acrylate), UV-sensitive .. 191
 Diesters, nonionic 188
 Diethyl *p*-phenylenebis(acrylate),
 UV-sensitive diester 191
 Differential scanning calorimetry
 (DSC) 79
 -determined glass transitions
 (T_g 's) of sulfonated
 PP's79, 80f, 81f, 87-89
 traces of hydrogenated,
 sulfonated PP's94-96
 Dilatometry of silver ion binding 330-333
 Diluents 70
 Dimethyl formamide (DMF) 92
 Dimethyl sodioiminobis(sulfonyl-
m-benzoate) 190
 Dioctyl phthalate (DOP)71-75
 Diols 188
 Dipolar polarization, Debye term
 for 255
 2x(2,6-Disulfoglucosamine-2-
 sulfoiduronic acid)-(2,6-
 disulfoglucosamine-glucu-
 ronic acid) 350
 Divinyl benzene (DVB) 196
 anion-exchange resins, acrylate-
 stability of 203
 anion-exchange resins, styrene .. 196
 stability of 203
 DMF (dimethyl formamide) 92
 Domaines, ionic 3
 DOP (*see* Dioctyl phthalate)
 Du Pont's inert perfluorosulfonic
 acid membranes 146
 DSC (*see* Differential scanning
 calorimetry)
 DVB (*see* Divinyl benzene)

E

- E-type membranes150f-151f, 152
 energy vs. morphology coordi-
 nate for N- and 150f
 Economic considerations of asphalt,
 paving industry182-183
 Einstein-Simha equation .342-345, 343t
 Elastomer(s)
 ion-containing 91
 metal sulfonate-containing
 EPDM 4
 thermoplastic 3, 39
 Electret
 behavior of complexed poly-
 ethers253-264
 charge storage/lifetimes of
 polymer 264t
 thermal analysis instrument 254f

- Electrochemical
 cell, current efficiency for
 electrolysis in 147
 cells, membrane separator in .145-153
 method for the determination of
 the effective volume of
 charged polymers in
 solution311-324
 Electrolysis in an electrochemical
 cell, current efficiency for ... 147
 Electrolysis for the production of
 alkali and chlorine, using
 Nafion145-153
 Electrophoretic migration pat-
 terns of heparins350, 352f
 Electrostatic interactions,
 anion-cation 162
 Emulsion polymerization
 DADMAC/acrylamide copoly-
 mer- 239
 homopolymer AMBTAC- 239
 homopolymer DADMAC- 238
 ENB (5-ethylidene-2-norbornene). 4
 Endothelium, heparin concentra-
 tion in blood and 355t
 Enzymes, lipolytic 356
 EPDM (*see* Ethylene-propylene-
 diene monomer terpolymer)
 Equilibrium studies311-316
 Ethyl acrylate-based ionomers ... 87
 Ethyl diallylaminoacetate, prepa-
 ration of 232
 Ethyl-3-diallylaminopropionate,
 preparation of 232
 Ethylene
 -acrylic acid-based
 ionomers54, 114
 -based copolymers, α relaxation
 in113-115
 -based ionomers110-111
 bistrioctylphosphonium counter-
 ion60-63
 -carboxylic acid copolymers ... 53
 maleic anhydride with
 (HEMA) 328
 -methacrylic acid copoly-
 mers111-112
 amine-neutralized 54
 2-Ethylhexanal reduction by
 borohydrides200-201
 Ethylene-propylene-diene mono-
 mer terpolymer
 (EPDM)3-19, 37-51, 53-65
 effect of cation on flow and
 physical properties
 of11-17, 14t-15t
 effect of Mooney viscosity and
 sulfonate content on melt
 viscosity and tensile prop-
 erties of15, 17t
 ionomers, effects of metal
 counterion and metal
 stearates on flow and
 tensile properties of42t-43t

- Ethylene-propylene-diene monomer
terpolymer (EPDM) (*continued*)
metal sulfonate-containing 3-19
plasticization of 37-51
metal sulfonate(s), effect of
cation and zinc stearate on
flow and physical prop-
erties of 46, 48t-49t
stearic acid on melt index
of 39, 40f
stearic acid on tensile strength
of 39, 41f, 42, 43f
zinc stearate on the melt
index of 44f
zinc stearate on the tensile
strength of 45f, 47f
properties of 4t-5t, 9
sulfonated
comparison of divalent and
monovalent quaternary
phosphonium counterions
in 61t
effect of quaternary phos-
phonium counterions on
the tensile and melt-flow
properties of 56
ionomers, preparation of 56-57
neutralization of 5-6
with zinc acetate 6, 7t
neutralized with quaternary
phosphonium ion(s)
effect of water uptake on 64t
physical properties of 59t
tensile properties of 58t, 63t
quaternary phosphonium
counterions in 53-65
rheological and tensile prop-
erties of 7
synthesis and properties of 3-19
sulfonate content, effect of
on elongation 11, 13f
on melt viscosity 9-11
on modulus 11, 13f
on tensile strength 11, 12f
sulfonation of 5
on water absorption, effect of
cation on 17, 18f
5-Ethylidene-2-norbornene
(ENB) 4

F

- Fatty acids, saturated 39
Filtration rate as a measure of
polymer dewatering
ability 239, 240f-242f, 243
Flory equation for melting-point
depression 110, 118
Floc properties 246, 251f
Formamide, dimethyl (DMF) 92
Fourier transform NMR study of
perfluorosulfonate ionomers,
multinuclear 155-167

G

- Gel(s)
at equilibrium, volume of
Sephadex 319
intrinsic pK values of swollen,
weakly acidic (basic) 311-324
potentiometric titration of a
weakly acidic 312
(resin)-phase kinetics 311-316
system, potentiometric properties
of carboxymethyl-dextran 315
Glass transition (T_g 's) 115
behavior of poly(propylene
glycol) 269
effect of plasticizer level on the
PS 72, 73f
of a semicrystalline system 116
of sulfonated PP's, DSC-
determined 79, 80f, 81f, 87, 89
Glycerol 71-75
Gums, effect of various metal stea-
rates on zinc sulfonate 46, 48t-49t

H

- HEMA, interactions of silver
ion with 330
HEMA, maleic anhydride with
ethylene 328
Heparin 349-359
anticoagulant activities of 353
chains of beef-lung 354f
assay of 353f
beef-lung 350
concentration in blood and
endothelium 355t
electrophoretic migration pat-
terns of 350, 352f
hexasaccharide structural
formula of 351f
and histamine in the intestinal
wall, release of 357, 359f
preparation of 352
pork-intestinal 350
uses of 355
Histaminase 356
Histamine 356, 357
in the intestinal wall, release
of heparin and 357, 359f
Homopolymerization of diallyl-
amino monomers 218t-221t
Huggins equation 342-345
HVMEMA (*see* Maleic anhydride
with methylvinyl ether)
Hydration model, four-state
ion-counterion 130, 131f
Hydration shell 129
ion-dipole 134, 137
Hydrides by polymer-bound boro-
hydrides, generation of volatile 208
Hydrocarbon
backbone, polystyrene 21-35
-phase relaxations in sulfonated
PP's, amorphous 88-89
polymers, ionic groups in 3

- Hydrogels 341
 Hydrogen bonding in liquids and electrolyte solutions 167
 Hydroperoxide by borohydrides, reduction of202t–203t
 Hydrophilic ion-exchange membranes, transport properties of hydrophobic-145–153
 Hydrophobic-hydrophilic ion-exchange membranes, transport properties of145–153

I

- Inhibitor, lipoprotein-lipase 357
 Inhibitor, plasma protein 353
 Ionically cross-linked polymers ... 70
 Ionic
 associations, plasticizers for 38
 clustering in styrene-methacrylic acid copolymers and their salts286–292
 clusters 88
 existence of 284
 in Nafion 284
 hydrated 162
 relaxation mechanism in microphase-separated ... 114
 in sulfonated PP's 87
 domain(s) 3
 plasticizer39, 70, 175
 groups in hydrocarbon polymers 3
 -phase relaxation 92
 in sulfonated PP's 88
 hydrogenated114–115
 polyesters185–193
 bond failure in192–193
 peel force of 186
 effect of cross-linking on 191–193
 stress-strain relations for a noncross-linked and cross-linked 192f
 substituents onto asphalt, grafting 173
 Ionomers
 asphalt171–183
 post-thickening behavior of .. 182
 wet-strength retention of 173
 carboxylated polystyrene 54
 comparison of sulfonate and carboxylate21–35
 dual plasticization of sulfonated polystyrene67–76
 effect of counterion on the physical properties of 60
 effects of metal counterion and metal stearates on flow and tensile properties of EPDM42t–43t
 ethyl acrylate-based 87
 ethylene-acrylic acid-based ... 114
 ethylene-based110–111
 multinuclear Fourier transform NMR study of perfluoro-sulfonate155–167

- Ionomers (*continued*)
 parameters affecting the mechanical and flow properties of 9–17
 phase separation of 124
 preparation of sulfonated EPDM56–57
 properties, effect of counterion structure on53–65
 PS-based sulfonate67–76
 structures, theoretical model for123–143
 Ion(s)
 clustering in ion-containing polymers283–292
 -containing elastomers 91
 -counterion hydration model, four-state130, 131f
 -dipole hydration shell134, 137
 effect of water uptake on a sulfonated EPDM neutralized with quaternary phosphonium 64t
 exchange
 by mast cells in tissues ...357, 358f
 membranes, transport properties of hydrophobic-hydrophilic145–153
 resin(s)
 intrinsic pK values of cross-linked311–324
 structure of Nafion 155
 physical properties of sulfonated EPDM neutralized with quaternary phosphonium 59t
 by polymer-bound borohydrides, reduction of metal 209
 quaternary ammonium 56
 silver
 binding
 dilatometry of330–333
 on the molecular dimensions of PAA, effect of 333
 by synthetic polycarboxylic acids, cooperative ..327–336
 cluster, quasicrystalline 335
 degree of binding of 328
 depression of the intrinsic viscosity of PAA by 333, 334f, 335
 electrostriction volume of hydrated335–336
 with HEMA, interactions ... 330
 with HVMEMA, interactions of 330
 by PAA acid as a function of the degree of neutralization, volume changes for the binding of 332t, 333, 336
 by PAA, isotherms of degree of binding of ...329, 330f, 331f
 substituents in quaternary phosphonium 56

Ion(s) (*continued*)

- tensile properties of sulfonated EPDM neutralized with quaternary phosphonium .58t, 63t
- transport through membrane cube, schematic of computer simulation of 141f
- transport through Nafion 139–143
- computer model of 138–143

K

- Kinetics, gel (resin)-phase 311–316
- Kinetics, solution 311–316

L

- Lamellae, chain-folded 112
- LCAO-ZDO approximation 303
- Lime to asphaltic bitumen, addition of 180
- Lipases, lipoprotein 356
- Lipolytic enzymes 356
- Lipoprotein lipase(s) 356
- inhibitor 357
- Lithium perchlorate system, poly(propylene glycol)- 268

M

- Magnesium
 - maleate-modified asphalt, wet-strength retention of 177, 179f, 181–182
 - stearates 42
 - sulfonate-modified asphalt, wet-strength retention of 177, 179f, 181–182
- Maleate-modified, sulfonate-modified, and unmodified asphalts, viscosity-temperature relationships of 178, 181f
- Maleic anhydride 173
 - with methyl vinyl ether (HVMEMA) 328
 - interactions of silver ion with 330
 - with ethylene (HEMA) 328
 - modified asphalt, viscosity of 175, 176f
- Malonate containing polymers .188, 189f
- Mannich reaction 212
- Mast cells from pig intestinal mucosa 357f
- Mast cells in tissues, ion-exchange by 357, 358f
- Maxwell-Wagner effect 117
- MBA (*see* Methylenebisacrylamide)
- Melt
 - condensation polymerization, high-temperature 186
 - flow improvers 46
 - flow properties of sulfonated EPDM, effect of quaternary phosphonium counterions on 56

Melt (*continued*)

- index of metal sulfonate EPDM, effect of stearic acid on . .39, 40f
- index of metal sulfonate EPDM, effect of zinc stearate on 44f
- viscosity on the level of neutralization, dependence of S-PS 68, 69f
- Melting-point depression, Flory equation for 110–118
- Membrane(s)
 - cation-exchange 145
 - Du Pont's inert perfluorosulfonic acid 146
 - E-type 150f–151f, 152
 - energy vs. morphology coordinate for N- and E-type 150f
 - N-type 150f–151f, 152
 - Nafion, operational stability of 149–150
 - separator in electrochemical cells 145–153
 - transport phenomena and morphology changes associated with Nafion cation-exchange 145–153
 - transport properties of hydrophobic-hydrophilic ion-exchange 145–153
- Metachromatic color of dyes 356
- Metal
 - alkali
 - NMR 157
 - nuclei, chemical shifts of . .157–159
 - resonances of electrolyte solutions and saturated Nafion, linewidths of 166t
 - carboxylates as plasticizers 75
 - chelating resins 225
 - counterion(s) 55
 - and metal stearates on flow and tensile properties of EPDM ionomers, effects of 42t–43t
 - ions by polymer-bound borohydrides, reduction of 209
 - ions by polymethacrylic acid (PMA), complexation of divalent 314
 - neutralized styrene-methacrylic acid copolymers 54
 - salts 181
 - stearates 42
 - on flow and tensile properties of EPDM ionomers, effects of metal counterion and 42f–43f
 - on zinc sulfonate gums, effect of various . .46, 48t–49t
 - sulfonate(s) 8
 - containing EPDM 3–19
 - effects of cation and zinc stearate on flow and physical properties of 46, 48t–49t

- Metal (*continued*)
 sulfonate(s) (*continued*)
 effects of stearic acid on
 melt index of 39, 40*f*
 effects of stearic acid on
 tensile strength
 of 39, 41*f*, 42, 43*f*
 effects of zinc stearate on
 the melt index of 44*f*
 functions of zinc stearate
 in 46
 water absorption, effect of
 cation and zinc
 stearate 46, 50*f*
 zinc stearate on the
 tensile strength of . . 45*f*, 47*f*
- Methacrylamidopropylidimethyl-
 amine (MPDMA) 338
 solubility of 340
- 3-Methacrylamidopropylidimethyl-
 ammonium 2-acrylamido-2-
 methylpropanesulfonate
 (MPDMA · AMPS) 338
 preparations of 338–339
 polymerization of
 MPTMA · AMPS and 341
- 3-Methacrylamidopropyltrimethyl-
 ammonium 2-acrylamido-2-
 methylpropanesulfonate
 (MPTMA · AMPS) 339
 alternative method of preparation
 for 341
 and MPDMA · AMPS,
 polymerization of 341
 NMR spectrum of 340
- Methacrylic
 acid copolymers
 butadiene–styrene 55
 ethylene– 111–112
 amine-neutralized 54
 metal-neutralized styrene– 54
 and their salts, ionic clustering
 in styrene– 286–292
 acid groups and protonated
 styrene monomers, copoly-
 mers with deuterated 287
 ionic clustering in 287–289
 neutron scattering in 287
 copolymers, radius of gyration
 measurements of deuterated
 styrene– 298–292
- Methyl vinyl ether, maleic anhy-
 dride with (HVMEMA) 328
- Methylenebisacrylamide
 (MBA) 236–252
 addition to emulsion polymers
 for dewatering waste-
 activated sludge, effect of . . 241*t*
- Microbrownian segmental motion 88, 115
- Monomer(s)
 cross-linking 225
 diallylamine
 aliphatic nitro 216, 217*f*
- Monomer(s) (*continued*)
 diallylamine (*continued*)
 amino acid 223
 homopolymerization . . . 218*t*–221*t*
 ketone-substituted 216, 222*f*
 preparation 212*t*–215*t*
 polyampholytes derived from
 cation–anionic 337–346
- Monte Carlo simulation calculations 125
- Mooney viscosity 9, 15
 and sulfonate content on melt
 viscosity and tensile prop-
 erties of EPDM, effect of . 15, 17*t*
- MPDMA (*see* Methacrylamido-
 propylidimethylamine)
- MPTMA · AMPS (*see* Methacryl-
 amidopropyltrimethylammonium)
- Mucopolysaccharides, sulfated 352
- N
- N-type membranes 150*f*–151*f*, 152
 and E-type membranes, energy
 vs. morphology coordinate
 for 150*f*
- Nafion 123–143
 acid samples, effect of hydration
 on 290, 291*f*, 292*f*
 cation-exchange membranes,
 transport phenomena and
 morphology changes asso-
 ciated with 145–153
 cluster structure in 136
 computer model of ion transport
 through 138–143
¹³³Cs NMR of 166
 current efficiency vs. current
 density for 148
 electrolysis for the production of
 alkali and chlorine using . 145–153
 equilibrium density and water
 absorption properties of . . . 136
¹H chemical shifts and linewidths
 of water in 167
¹H NMR of 167
 hydrated ionic clusters in 162
 ion-exchange resin, structure of . 155
 ion transport through 139–143
 ionic clusters in 284
⁶Li NMR of 166
 linewidth(s)
 of alkali metal resonances of
 electrolyte solutions and
 saturated 166*t*
 -Na⁺, ²³Na chemical shifts and
 temperature dependence of the
²³Na 164, 165*t*
 mechanism of cluster formation
 applied to 131–137
 membranes, operational stability
 of 149–150
 molecular organization in 127

- Nafion (*continued*)
 molecular organization of the dry
 and hydrated structures
 for132*f*–133*f*
 -Na⁺ as function of water content,
²³Na spectra of159–160*f*
 Na⁺ ions in saturated 163
²³Na NMR of159–166
 parameters vs. water for ..164, 165*t*
 as a probe of ionic mobility,
 binding and electronic
 environment of hydrated 159
⁸⁵Rb NMR of 166
 schematic of the reversed
 micelle model of 156*f*
 separators, current efficiency vs.
 caustic concentration 142*f*
 water clustering in 290–292, 296
 Nernstian response of glass electrode 318
 Neutron scattering in copolymers
 with deuterated methacrylic
 acid groups and protonated
 styrene monomers 287
 NMR (*see* Nuclear magnetic
 resonance)
 Nuclear magnetic resonance (NMR)
 alkali metal 157
 of Nafion
¹³³Cs 166
¹H 167
⁶Li 166
²³Na159–166
⁸⁵Rb 166
 parameters of alkali metal cations
 parameters vs. water for Nafion,
²³Na164, 165*t*
 as a probe of ionic mobility,
 binding and electronic
 environment in hydrated
 Nafion, ²³Na 159
 study of perfluorosulfonate
 ionomers, multinuclear
 Fourier transform155–167
 Nuclear spin relaxation 158
- O**
- Olefins 7
- P**
- PAA (*see* Polyacrylic acid)
 Paving industry, economic consid-
 erations of asphalt182–183
 Paving materials, asphalt 172
 PEO (*see* Poly(ethylene oxide))
 Perfluorosulfonate ionomers, multi-
 nuclear Fourier transform
 NMR study of155–167
 Perfluorosulfonic acid membranes,
 Du Pont's inert 146
 Phase separation of ionomers 124
 Phenoxycalcium thiocyanate
 system 268
- Phosphonium, quaternary
 counterions in sulfonated EPDM 53–65
 on the melt-flow properties,
 effect of 56
 comparison of divalent and
 monovalent 61*t*
 on the tensile properties of,
 effect of 56
 counterions, tetralkyl 58
 ions, substituents in 56
 ions, sulfonated EPDM
 neutralized with
 effect of water uptake on 64*t*
 physical properties of 59*t*
 tensile properties of58*t*, 63*t*
- Photographic fixer, application of
 polymer-bound reducing
 agents for silver recovery .200, 209*t*
- Phthalate plasticizers, plasticization
 of S-PS with 74
 Plasma protein inhibitor 353
 Plasma serine proteases 354
 Plasticization
 ionic domain 75
 of metal sulfonate-containing
 EPDM37–51
 of S-PS ionomer, dual67–76
 of S-PS with phthalate
 plasticizers 74
 Plasticizing polyvinyl chloride (PVC) 68
 Plasticizer(s) 68
 backbone70, 75
 for ionic associations 38
 ionic domain39, 70
 level on the PS glass transition,
 effect of72, 73*f*
 low-temperature 193
 metal carboxylates as 75
 plasticization of S-PS with
 phthalate 74
 on S-PS tensile properties and
 flow behavior, effect of DOP
 and zinc stearate 75*t*
 stearate 38
 Plasticizing action 70
 PMA (*see* Polymethacrylic acid)
 Polarization, Debye term for dipolar 255
 Polyacids, degree of neutralization
 of328
 Polyacrylic acid (PAA) 327–336
 as a function of the degree of
 neutralization volume
 changes for the binding of
 silver ion by332*f*, 333, 336
 effect of the silver ion binding
 on the molecular dimensions
 of 333
 isotherms of degree of binding
 silver ion by 329, 330*f*, 331*f*
 protonation of 336
 by silver ion, depression of the
 intrinsic viscosity of 333, 334*f*, 335
 Poly(AMPDMA · AMPS), viscosity
 studies for342*f*, 343, 344*f*

- Polyampholytes derived from
 cationic-anionic monomer
 pairs, synthesis and aqueous
 solution viscosity behavior
 of 337-346
- Polycarboxylic acids, cooperative
 silver ion binding by
 synthetic 327-336
- Polyelectrolyte(s)
 biological anionic 349
 cationic 54
 colloidal suspensions of 324
 linear 324
- Polyester adhesives, water-
 soluble 185-193
- Polyesters, ionic 185-193
 bond failure in 192-193
 effect of cross-linking on peel
 force of 191-193
 peel force determinations 186
 stress-strain relations for non-
 cross-linked and cross-
 linked 192f
- Polyethers
 dielectric properties of
 complexed 253-264
 electret behavior of com-
 plexed 253-264
 by salts, viscosity enhancement
 of 267-280
- Poly(ethylene comethacrylate)
 salts 181
- Polyethylene
 ionomers, carboxylated 54
 oxide (PEO) 269
 polymers
 densities of 270-271
 dynamic mechanical prop-
 erties of 276, 279-280
 viscosities 273, 276f, 277f, 278f
 vs. temperature
 for 273, 276f, 277f
 salt mixtures, density vs.
 temperature for 270, 271f
 α relaxation in 113-116
- Polyethylenic crystallinity 9, 11
- Polymer
 additives 37-51
 adipate-containing 188, 189f
 backbone crystallinity 92
 -bound borohydrides
 generation of volatile
 hydrides by 208
 preparation, use, and
 regeneration of 197f
 reactivity of 196
 reagents 195-209
 reducing agents, preparation
 of 196-198
 reduction of metal ions by ... 209
 solvent purification by 208
 solvolytic stability of 196, 202-203,
 204f-207f
- bound reducing agents for silver
 recovery from photographic
 fixer, application of ... 200, 209t
- Polymer (*continued*)
 cross-linked 225, 227
 densities of PEO 270-271
 densities of PPO 270-271
 dewatering
 ability, filtration rate as
 a measure of 239, 240,
 240f-242f, 243
 efficiency of raw primary
 sludge 246, 247f
 efficiency of waste-activated
 sludges, effect of degree
 of branching on ... 242f, 243,
 244f, 245f
 waste-activated sludge, effect
 of MBA addition to
 emulsion 241f
 electrets, charge storage/
 lifetimes of 264t
 ion-clustering in ion-
 containing 283-292
 ionic groups in hydrocarbon ... 3
 ionically cross-linked 70
 malonate-containing 188, 189f
 molecular weight, effect of PS
 functionalization on the
 backbone 23-26
 properties of diallylamine 223, 225, 227
 -salt interactions 269
 in solution, electrochemical
 method for the determina-
 tion of the effective volume
 of charged 311-324
 treatment of municipal wastes .. 235
- Polymeric acids, free 8
- Polymeric quaternary ammonium
 borohydride reducing
 agents 195-209
- Polymerization
 emulsion
 DADMAC/acrylamide
 copolymer- 239
 homopolymer AMBTAC- ... 239
 homopolymer DADMAC- ... 238
 high-temperature melt-
 condensation 186
 methods, diallylamine 216
 of MPTMA · AMPS and
 MPDMA · AMPS 341
 solution
 DADMAC/acrylamide
 copolymer- 239
 homopolymer AMBTAC- ... 238
 homopolymer DADMAC- ... 238
- Poly(3-methacrylamidopropyl-di-
 methylammonium 2-acryl-
 amido-2-methylpropanesul-
 fonate, preparation of 339
- Poly(3-methacrylamidopropyltri-
 methylammonium-2-acryl-
 amido-2-methylpropanesul-
 fonate, preparation of 339-340
- Polymethacrylic acid (PMA)
 complexation of divalent metal
 ions by 314

- Polymethacrylic acid (PMA)
(*continued*)
-NaPSS system, potentiometric
and volume measurement
data for the cross-linked .. 321f
potentiometric properties of 314
potentiometric study of
cross-linked 323f
resin 315
- Polymethylene, conformational
energy map for 126f
- Poly(MPTMA · AMPS), viscosity
studies for 342
- Poly(pentamers (PP's) 77
- sulfonated 78
amorphous hydrocarbon-phase
relaxations in 88-89
characterization data for 79f
DSC-determined glass transi-
tions (T_g 's) of ... 79, 80f, 81f,
87-89
- DSC results for 79-80
- hydrogenated
characterization data for ... 94f
dielectric measurements
of 104-109
dielectric properties of .. 117-118
DSC traces of 94-96
dynamic mechanical
measurements of 97-104
dynamic mechanical
properties of 113-117
effect of water on ... 103f, 104
ionic-phase relaxation in .. 114-115
preparation of 93
 α relaxation in 113-115
 γ and γ' relaxation in ... 116-117
temperatures of mechanical
relaxations in 102f
thermal, dynamic mechan-
ical, and dielectric
properties of 91-118
ionic clusters in 87
ionic-phase relaxations in 88
 γ relaxation in 80-89
 β relaxation in ... 80-88, 115-116
temperature dependencies of
the tensile storage and
loss moduli for 80-86
thermal and dynamic mechan-
ical properties of 77-89
sulfonation of 78
- Poly(propylene glycol), glass
transition behavior of 269
- Poly(propylene glycol)-lithium
perchlorate system 268
- Poly(propylene oxide) (PPO) .255, 269
chelate structure, dipole
moment of 257f
dielectric behavior of 255, 256f
polymers
densities 270-271
dynamic mechanical prop-
erties of ... 273, 276, 279-280
glass transitions and WLF
constants for 274, 275f
- Poly(propylene oxide) (PPO)
(*continued*)
viscosities of 271f-273f, 274f,
275f, 278f
viscosities vs. temperature
for 271, 272f, 274f
temperature dependence of T_g
of 255, 256f
thermal discharge currents
for 259, 261f, 263f
thermal discharge behavior as a
function of metal salt con-
centration 262f, 263
- Polypyrrolidene structures 216
- Polystyrene (PS) 22
-based sulfonate ionomers 67-76
and C-PS, viscosity-concentra-
tion relations for 24, 25f
carboxylated (C-PS) (*see*
Carboxylated polystyrene)
- films
triboelectric charging of .. 304, 305f
cascade device for measur-
ing 297f
XPS (θ) data of ... 296-304, 298f,
299f, 301f
x-ray photoemission signals
and high-energy structure
for 300, 301f
x-ray photoemission signals
of untreated 298f
- functionalization on the back-
bone polymer molecular
weight, effect of 23-26
glass transition, effect of
plasticizer level on 72, 73f
hydrocarbon backbone 21-35
softening behaviors of 26, 27f
and S-PS, modulus-temperature
relationship for 68-69, 70f
and S-PS, viscosity-concentra-
tion relation for 24, 26f
sulfonate, sodium 316
sulfonated (S-PS) (*see*
Sulfonated polystyrene) ... 3
- Polyvalent quaternary counterions . 61
- Polyvinyl chloride, (PVC)
plasticized 68
- Polyvinyl chloride (PVC) and
S-PS, stress-strain relation-
ships for plasticized 74f
- Polyvinylimidazolium sulfo-
betaine 337, 338f
- Polyvinyl sulfate 313
- Poly(1-vinyl-3-(3-sulfopropyl)-
imidazolium hydroxide inner
salt) 343, 345f, 346f
- Potentiometric studies 311-324
- Potentiometric titration of a
weakly acidic gel 312
- Potholes, formation of 172
- PP's (*see* Poly(pentamers))
- PPO (*see* Poly(propylene oxide))
- Proteases, plasma serine 354
- Protein inhibitor, plasma 353
- PVC (*see* Polyvinyl chloride)

Q

- Quaternary ammonium borohydride reducing agents, polymeric195-209
 ammonium ions 56
 counterion(s)
 alkyl-substituted 62
 divalent 60
 effect of *n*-alkyl chain lengths of substituents of 58
 monovalent 60
 phosphonium
 in sulfonated EPDM53-65
 comparison of divalent and monovalent ... 61*t*
 effect on melt-flow properties of 56
 effect on tensile properties of 56
 tetraalkyl 58
 polyvalent 61
 phosphonium ions, substituents in 56
 phosphonium ions, sulfonated EPDM neutralized with
 effect of water uptake on 64*t*
 physical properties of 59*t*
 tensile properties of58*t*, 63*t*

R

- Radius of gyration measurements of deuterated styrene-methacrylic copolymers ...289-292
 Reducing agents
 polymeric quaternary ammonium borohydride195-209
 preparation of polymer-bound borohydride196-198
 for silver recovery from photographic fixer, application of polymer-bound 200, 209*t*
 ionic-phase 92
 mechanism in microphase-separated ionic cluster 114
 nuclear spin 158
 Resin(s)
 anion-exchange acrylate-DVB 196
 with borohydride counterions . 195
 styrene-DVB 196
 gel-type 196
 -phase kinetics, (gel)311-316
 intrinsic pK values of cross-linked ion-exchange311-324
 ion-exchange 195
 macroreticular 196
 metal chelating 225
 PMA 315
 stability of acrylate-DVB 203
 stability of styrene-DVB 203
 Rheological behavior (*see also* Viscosity, melt) 27
 of C-PS27, 28*f*
 of S-PS27, 28*f*

- Road surfacing mix, asphaltic 172
 Roadways, factors affecting the performance and durability of of asphaltic 172

S

- Salt(s)
 interaction, polymer- 269
 metal 181
 poly(ethylene comethacrylate) . 181
 viscosity enhancement of polyethers by267-280
 zinc chloride as a chelated ... 255
 Sand 172
 SANS (small-angle neutron scattering) 285
 Scattering vector *q* 285
 Sedimentation basin of raw primary sludges, primary ...235-236
 Sephadex gel311-324
 at equilibrium, volume of 319
 on its potentiometric properties during neutralization, influence of the swelling of the weakly acidic 311
 potentiometric study of 322*f*
 Sephadex-NaPSS system, potentiometric and volume measurement data 320*t*
 Serine proteases, plasma 354
 Silver
 carboxylate clusters, formation of333-336
 diacetate complex333-336
 ion
 binding
 degree of 328
 dilatometry of330-333
 on the molecular dimensions of PAA, effect of 333
 by PAA acid as a function of the degree of neutralization, volume changes for ... 322*t*, 333, 336
 by PAA, isotherms of degree of329, 330*f*, 331*f*
 by synthetic polycarboxylic acids, cooperative ..327-336
 cluster, quasicrystalline 335
 depression of the intrinsic viscosity of PAA by 333, 334*f*, 335
 electrostriction volume of hydrated335-336
 with HEMA, interactions of . 330
 with HVEMA, interactions of 330
 Site-binding ability, anion 344
 Sludge, raw primary 235
 polymer dewatering efficiency of246, 247*f*
 primary sedimentation basin of235-236
 Sludge(s), waste-activated
 effect of degree of branching on polymer dewatering efficiency of ...242*f*, 243, 244*f*, 245*f*

- Sludge(s), waste-activated
(*continued*)
effect of MBA addition to emul-
sion for dewatering 241*t*
efficiency of a cationic poly-
mer in dewatering 235–252
- Small-angle neutron scattering
(SANS) 283–292
- Sodium
borohydride 200
ions in saturated Nafion 163
polystyrene sulfonate 316
polyvinyl sulfate 311
- Sodium-23
chemical shift(s) 158
and linewidth for Nafion–Na⁺ 161*t*
change for Nafion 162, 163*f*
linewidth of Nafion, tempera-
ture dependence of ... 164, 165*t*
NMR, Nafion 159–166
parameters vs. water for ... 164, 165*t*
as a probe of ionic mobility,
binding and electronic
environment in hy-
drated 159
resonances in aqueous electro-
lyte solutions 158
spectra of Nafion–Na⁺ as a func-
tion of water content ... 159, 160*f*
- Solution
behavior of C-PS, effect of tem-
perature on 34*f*, 35
behavior of S-PS, effect of tem-
perature on 34*f*, 35
kinetics 311–316
polymerization
DADMAC/acrylamide copoly-
mer- 239
homopolymer AMBTAC- ... 238
homopolymer DADMAC- ... 238
viscosity behavior of C-PS 27–34
viscosity behavior of S-PS ... 27–34
- Solvent purification by polymer-
bound borohydrides 208
- Spectroscopy, x-ray photoemission
angle-dependent XPS(θ) ... 295
- S-PP (*see* Sulfonated polypentana-
mers)
- S-PS (*see* Sulfonated polystyrene)
- Sulfate, acetyl 5
- Sulfobetaine, polyvinylimidazo-
lium 337, 338*f*
- Sulfonate(d)
and carboxylate ionomers, com-
parison of 21–35
content on melt viscosity and
tensile properties of
EPDM, effect of Mooney
viscosity and 15, 17*t*
- EPDM
comparison of divalent and
monovalent quaternary
phosphonium counter-
ions in 61*t*
effect of content on
elongation 11, 13*f*
- Sulfonate(d) (*continued*)
EPDM (*continued*)
effect of content on (*continued*)
melt viscosity 9–11
modulus 11, 13*f*
tensile strength 11, 12*f*
ionomers, preparation of ... 56–57
metal 3–19
effect of
cation and zinc stearate
on flow and physical
properties of ... 46, 48*t*–49*t*
stearic acid on melt index
of 39, 40*f*
stearic acid on tensile
strength of .39, 41*f*, 42, 43*f*
zinc stearate on the melt
index of 44*f*
zinc stearate on the ten-
sile strength of ... 45*f*, 47*f*
functions of zinc stearate in 46
plasticization of 37–51
water absorption, effect of
cation and zinc stearate
on 46, 50*f*
neutralization of 5–6
with zinc acetate 6, 7*t*
neutralized with quaternary
phosphonium ion(s)
effect of water uptake on .. 64*t*
physical properties of 59*t*
tensile properties of 58*t*, 63*t*
properties of
effect of quaternary phos-
phonium counterions
on the melt-flow 56
effect of quaternary phos-
phonium counterions
on the tensile 56
rheological and tensile 7
synthesis and 3–19
quaternary phosphonium
counterions in 53–65
- gums, effect of various metal
stearates on zinc 46, 48*t*–49*t*
- ionomers, PS-based 67–76
metal 8
-modified and unmodified as-
phalts, viscosity tempera-
ture relationships of male-
ate-modified 178, 181*f*
- polypentamers (sulfonated
PP's) 78
characterization data for ... 79*t*
DSC-determined glass transi-
tions (T_g 's) of ... 79, 80*f*, 81*f*,
87–89
- DSC results for 79, 80*f*
hydrogenated
characterization for 94*t*
dielectric measurements
of 104–109
dielectric properties of ... 117–118
differential scanning calo-
rimetry (DSC) traces
of 94–96

- Sulfonate(d) (*continued*)
- polypentanamers (sulfonated)
 - PP's (*continued*)
 - hydrogenated (*continued*)
 - dynamic mechanical
 - measurements of97-104
 - properties of113-117
 - effect of water on behavior of103f, 104
 - preparation of 93
 - relaxations in114-115
 - ionic-phase114-115
 - α 113-115
 - γ and γ' 116-117
 - temperatures of mechanical relaxations in .. 102t
 - thermal properties of .110-113 and dynamic, mechanical and dielectric .91-118
 - ionic clusters in 87
 - relaxation(s) in
 - amorphous hydrocarbon-phase88-89
 - ionic-phase 88
 - α 80-88
 - β 80-88, 115-116
 - γ 80-86, 89
 - thermal and dynamic mechanical properties of77-89
 - temperature dependencies of the tensile storage and loss moduli for 80-86
 - polystyrene (S-PS)3, 67-76
 - behavior of
 - effect of temperature on the solution34f, 35
 - rheological27, 28f
 - softening26, 27f
 - solution viscosity27-34
 - characteristics of 68
 - film(s)
 - critical surface
 - energy304, 306
 - effect of sulfonation depth on surface tension of304, 305f, 306
 - x-ray photoemission signals of 299f
 - ionomer, dual plasticization of67-76
 - melt viscosity on the level of neutralization, dependence of68, 69f
 - modulus-temperature relationship for PS and68-69, 70f
 - with phthalate plasticizers, plasticization of 74
 - preparation of21-35, 68
 - stress-strain relationships for plasticized PVC and 74f
 - surface structure of potassium-exchanged 295
 - surfaces, structure variation of295-306
- Sulfonate(d) (*continued*)
- surface structure of potassium-exchanged (*continued*)
 - tensile properties and flow behavior, effect of DOP and zinc stearate plasticizers on 75t
 - viscosity-concentration relation for PS and24, 26f
 - Sulfonation
 - of asphalts 173
 - of EPDM 5
 - of PP 78
 - reagents 5
 - Sulfonic acids 4
 - Surfaces, structure variation of sulfonated polystyrene ...295-306
 - Stearates
 - barium 42
 - magnesium 42
 - on the melt index of metal sulfonate EPDM, effect of . 44f
 - metal 42
 - on flow and tensile properties of EPDM ionomers, effects of metal counterion and42t-43t
 - plasticizers 38
 - zinc42, 44-51, 75
 - in metal sulfonate EPDM, functions of 46
 - on metal sulfonate EPDM water absorption, effect of cation and46, 50f
 - sulfonate gums, effect of various metal46, 48t-49t
 - on the tensile strength of metal sulfonate EPDM, effect of45f, 47f
 - Stearic acid 39
 - on melt index of metal sulfonate EPDM, effect of ...39, 40f
 - on tensile strength of metal sulfonate(s) EPDM, effect of39, 41f, 42, 43f
 - Stress-strain behavior of modified asphalts177, 178, 180f
 - Styrene
 - DVB anion-exchange resins ... 196
 - stability of 203
 - methacrylic acid copolymers
 - butadiene- 55
 - metal-neutralized 54
 - and their salts, ionic clustering in286-292
 - radius of gyration measurements of
 - deuterated289-292
 - monomers, deuterated methacrylic acid groups and protonated
 - copolymers with 287
 - ionic clustering in287-289
 - neutron scattering in 287

- T**
- TAMAC (*see* Triallylmethyl ammonium chloride)
- TDMAC (*see* Tridodecyl methylammonium chloride)
- Tensile properties of EPDM, effect of Mooney viscosity and sulfonate content on melt viscosity and15, 17*t*
- Tensile properties of a sulfonated EPDM neutralized with quaternary phosphonium ions56, 58*t*, 63*t*
- Tensile strength
effect of EPDM sulfonate content on11, 12*f*
of metal sulfonate EPDM, effect of stearic acid on39, 41*f*, 42, 43*f*
of metal sulfonate EPDM, effect of zinc stearate on45*f*, 47*f*
- Termonomers 7
- Terpolymers, ethylene-propylene-diene monomer (EPDM) 3-19, 37-51, 53-65
- Tetradecamethylene bistriethylphosphonium counterion ... 60-63
- Tetraethylammonium borohydride. 200
- Tetraethylphosphonium counterion 62
- Tetrahydrofuran (THF) 340
- T_g 's (glass transitions) of sulfonated PP's, DSC-determined 79, 80*f*, 81*f*, 87-89
- Thermodynamics, theory of irreversible 147
- Thermoplastic(s)67, 172
elastomer 3, 39
single-phase 253
- THF (Tetrahydrofuran) 340
- Thromboembolism 355
- Tissues, ion exchange by mast cells in357, 358*f*
- p*-Toluenesulfonic acid monohydrate, XPS(θ) measurements on solvent-cast films of. 303
- Transport phenomena and morphology changes associated with Nafion cation-exchange membranes145-153
- Transport properties of hydrophobic-hydrophilic ion-exchange membranes145-153
- Traprock 172
- Triallylmethyl ammonium chloride (TAMAC)235-252
- Triboelectric charging of PS film(s)304, 305*f*
cascade device for measuring .. 297*f*
- Tridodecyl methylammonium chloride (TDMAC) 355
- Triethylheptylphosphonium counterion 62
- Triethyloctadecylphosphonium counterion 64
- Triethylphosphonium counterion, tetradecamethylene, *bis*-60-63
- Triocylphosphonium counterion, ethylene, *bis*-60-63
- V**
- Venezuelan asphalt 172
- Viscosity
behavior of C-PS, solution27-34
behavior of S-PS, solution 27-34
-concentration relations for PS and C-PS24, 25*f*
-concentration relation for PS and S-PS24, 26*f*
enhancement of polyethers by salts267-280
melt (*see also* Rheological behavior) 27
effect of EPDM sulfonate content on 9-11
on the level of neutralization, dependence of S-PS ...68, 69*f*
and tensile properties of EPDM, effect of Mooney viscosity and sulfonate content on15, 17*t*
- Mooney 9, 15
and sulfonate content on melt viscosity and tensile properties of EPDM, effect of15, 17*t*
of unmodified asphalt175, 176*f*
- W**
- Waste
-activated sludges
effect of degree of branching on polymer dewatering efficiency of ..242*f*, 243, 244*f*, 245*f*
effect of MBA addition to emulsion polymers for dewatering 241*t*
efficiency of a cationic polymer in dewatering235-252
activation process 236
polymer treatment of municipal. 235
treatment plants, municipal ... 236
- Water clustering in Nafion .286, 290-292
- Water-stripping in asphalt roads (moisture damage) 172
- X**
- X-ray photoemission
signals of sulfonated PS film ... 299*f*
signals of untreated PS film ... 298*f*
spectroscopy, angle-dependent
XPS(θ) 295
data of PS films296-304, 298*f*, 299*f*, 301*f*

- X-ray photo emission (*continued*)
 spectroscopy, angle-dependent
 XPS(θ) (*continued*)
 measurements on solvent-cast
 films of *p*-toluenesulfonic
 acid monohydrate 303
 XPS(θ) (*see* X-ray photoemission
 spectroscopy, angle-dependent)

Z

- Zimm plot 289
 Zinc
 acetate 14-15
 neutralization of sulfonated
 EPDM with 6, 7*t*
 chloride as a chelated salt 255

- Zinc (*continued*)
 stearate(s) 42, 44-51, 75
 on flow and physical proper-
 ties of metal sulfonate
 EPDM, effect of cation
 and 46, 48*t*-49*t*
 on the melt index of metal
 sulfonate EPDM, effect of 44*f*
 in metal sulfonate EPDM,
 functions of 46
 on metal sulfonate EPDM
 water absorption, effect
 of cation and 46, 50*f*
 plasticizers on S-PS tensile
 properties and flow be-
 havior, effect of DOP and 75*t*
 on the tensile strength of
 metal sulfonate EPDM 45*f*, 47*f*
 sulfonate gums, effect of vari-
 ous metal stearates on 46, 48*t*-49*t*

*Jacket design by Joan Wolbier.
 Editing and production by Susan Moses.*

*The book was composed by Service Composition Co., Baltimore, MD,
 printed and bound by The Maple Press Co., York, PA.*